GEOGRAPHY
ENVIRONMENT
SUSTAINABILITY

Special Issue «Urban environmental
geography: Moscow and other megacities»

CONTENTS

CONTENTS

Pavel L. Kirillov¹, Alla G. Makhrova¹, and Tatiana G. Nefedova²
¹ Lomonosov Moscow State University, Leninskie Gory 1, Moscow, 119991, Russia
² Institute of Geography, Russian Academy of Sciences, Staromonetniy pereulok 29, Moscow, 119017, Russia
* Corresponding author: trene12@igras.ru

CURRENT TRENDS IN MOSCOW SETTLEMENT PATTERN DEVELOPMENT: A MULTISCALE APPROACH

ABSTRACT. The article studies current trends in Moscow population in context of socio-economic polarization strengthening between the capital city and other regions of the country. The study applies multiscale approach covering Moscow influence on Central Russia and other regions, interaction with the Moscow oblast and the level of internal population distribution within Moscow and particular settlements and villages in New Moscow territories. The gap in development is significantly noticeable for expanding Moscow and Moscow oblast against the background of depopulation in Central Russia regions and cities. Within the boundaries of Moscow the continuing model of extensive spatial growth of population has led to the most rapid growth of its periphery zone. Areas similar to bedroom communities in Old Moscow are forming in the municipalities of New Moscow located along the Moscow ring road (MKAD) and main radial highways, while large part of the new territories remain a typical countryside with villages and summer residents. Analysis of New Moscow suburban areas reveals the actual land use mosaics obscured by the official delimitation of Moscow and Moscow oblast and the formal division of population into urban and rural.

KEY WORDS: population, Moscow, Moscow region, Central Russia

INTRODUCTION

Contrasts between major cities and the rest of the territory are a typical feature of Russia. No wonder the words of the poet Afanasy Fet, written 150 years ago, have not lost their relevance: "People in the capitals, who are accustomed to huge, incessant capital flows, have no desire to understand how the whole immense terrain, without distinction of classes, for months lives without a penny" (Fet 1871). In the late Soviet times, there were attempts to smoothen these contrasts by locating industrial enterprises in small towns and improving wages and living conditions in small settlements. However, this was only partly successful in suburbs and in the South, and after the market returned at the turn of the millennium, the contrast of the Russian space increased.

Russia, like other countries with a late start of urbanization, experienced the

urban revolution in the twentieth century, turning from a rural and agrarian country into urban and industrial. From 1913 to 2000, the urban population increased almost sevenfold, and the proportion of city dwellers reached 70%. And although in the early 1990s, due to political transformations and the economic crisis, the urban population ceased to grow, in the late 1990s Russia returned to the stage of active urbanization (Nefedova and Treivish 2019). Under the influence of agglomeration effects, the concentration of population and economy in the largest centers leads to increased socio-economic polarization not only between cities and rural areas but also between cities, which manifests itself at various levels in strengthening gradients between cities of different sizes in terms of income, investment in fixed capital, housing development, retail trade turnover, and average life standards.

While a significant number of country's regions and especially regions of Central Russia are characterized by depopulation, Moscow shows a continuous growth (amounted to 965.5 thousand people which only for the period from 2010 to 2018). At the same time, during the last two intercensal periods, current statistics reveal a decline or stabilization of Moscow population, while the censuses show a sharp increase, which is mainly due to undercounting of migrations by current population registration.

MATERIALS AND METHODS

The purpose of this study is to identify main trends in the population of Moscow and its zone of influence in the twenty-first century, including those of the latest administrative changes of 2012, when the city area was increased almost 2.5 times. This requires research at several levels: from studying the regions of the country and Central Russia and the influence of Moscow on them, through the interaction of Moscow with Moscow oblast to the analysis of the internal structure of population distribution in Moscow, and down to individual settlements and

villages in the new territories of Moscow. This investigation is based on the use of official statistics on for subjects of the Russian Federation, cities, municipalities, settlements, as well as cartographic information, data from mobile network operators, and field studies.

Moscow has been studied from various angles in the works of multiple scholars. It was considered as an emerging global city (Kolossov et al. 2002), other studies focused on the development of its budget and social sphere (Zubarevich 2018), ethnic migration (Vendina 2005; Todd 2018), the impact of migration on housing market (Kashnitsky and Gunko 2016), the transformation of Moscow from the main city into the mega-region (Argenbright 2013), urban planning, place-based protest, and civil society (Argenbright 2016), features of its development policy (Büdenbender and Zupan 2017), and others. Several papers considered problems of its development in Moscow agglomeration and the Central Russia context (Kurichev and Kuricheva 2018; Kuricheva 2017; Makhrova et al. 2017; Brade et al. 2014; Makhrova et al. 2016).

The expansion of the city's territory and the emergence of New Moscow in 2012 caused a surge of interest in Moscow and a rise of works both in Russia and abroad (Cox 2012; How to Build... 2015; Argenbright 2018; Kolosov 2013; Makhrova et al. 2013; Shuper and Em 2013). At the same time, an array of works has been developed that analyzed general patterns of development of post-Soviet cities and growth of spatial heterogeneity as one of the main features of their development (Golubchikov et al. 2014; Golubchikov 2016; Ferencuhova and Gentele 2016). The novelty of this study lies in the fact that it carries out a multiscale analysis of Moscow's development using the population dynamics, an available indicator of socio-economic polarization and space compression processes, in the scale of regions and cities of the whole country (macro level), in one of its most developed parts, Central Russia (meso level), and within the boundaries of the Moscow metropolitan region and within Moscow itself (micro level).

RESULTS AND DISCUSSION

1. Moscow Compared to the Country and Its Regions

In the 2000s, against the background of the depopulation of a significant part of regions, Moscow shows a continuous growth of its demographic potential associated with the significant advancing of social and economic development of the city compared to the rest of the territories, which led to a sharp increase in its attractiveness and rapid population growth. While the population of about 70% of Russia's cities decreased, Moscow continued to grow at a high rate, as a result its share in the country's population increased even more, emphasizing the global trend of greater spatial development heterogeneity. The proportion of the capital in the Russian population in 2018 reached 8.5%, which together with Moscow oblast made 13.6%, while the proportion of St. Petersburg was 3.6% with a stable share of Leningrad oblast (Table 1).

In the 2010s, the population growth rates in Moscow slowed down, especially towards the end of the period under review, when the capital began to give way not only to some of the North Caucasus republics but also to several other territories attractive to migrations (Tyumen and Moscow oblasts,

St. Petersburg, Khanty-Mansi Autonomous okrug, and Krasnodar krai), by 2018 falling outside the top twenty regions with the fastest growing population. The main contribution to the increasing population of the city is made by migration, although its rate is falling. In general, the 2002–2017 period was characterized by a natural decrease in population, although in recent years the natural growth coefficient increased, reaching 1.1 per 1000 people in 2017. Nevertheless, the capital continues to lag behind both the national republics with an incomplete demographic transition and the regions with a younger population age structure (Tyumen oblast and its oil and gas okrugs) (Fig. 1).

2. Moscow in Central Russia

As a capital, Moscow occupies a unique position, mustering resources of the whole country and producing economic, social, and political innovations, which initially spread to neighboring areas (Zubarevich 2018). Moscow oblast, thanks to its advantageous position near the capital, and Moscow itself make up the territory of maximum population growth within Central Russia (within the borders of the Central Federal District). In fact, apart from these two regions, which form the Moscow Capital Region, population growth in 2002–2018 in the district was only due to relatively prosperous Belgorod oblast. The absolute

Table 1. Population dynamics of Moscow and Moscow oblast

Territory	Population (thousand people)			Share in the total population of Russia, %		
	2000	2010	2018	2000	2010	2018
Moscow	8537	11541	12507	5.9	8.1	8.5
Moscow oblast	6464	7106	7503	4.4	5.0	5.1
Moscow and Moscow oblast	15001	18647	20010	10.3	13.1	13.6
St. Petersburg	4661	4899	5352	3.2	3.4	3.6
Leningrad oblast	1687	1719	1814	1.1	1.2	1.2
St. Petersburg and Leningrad oblast	5662	6618	7166	4.3	4.6	4.8

Source: Rosstat data.
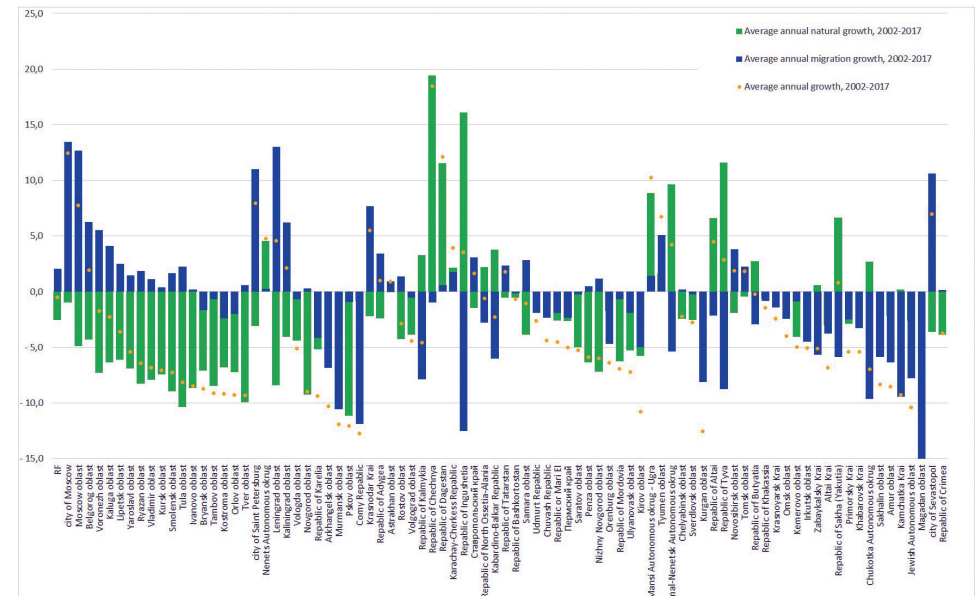
Fig. 1. Population dynamics by regions of the Russian Federation in 2002–2018.

amount of migration inflow to the Moscow Capital Region allowed the district as a whole to compensate not only for natural but also migration loss in several other regions

The comparison to socio-economic indicators between Central Russia regions reveals that along the leadership of Moscow in many respects, the gap between Moscow and the Moscow oblast in 2000-2018 decreased, and the gap between the Moscow oblast and its neighboring regions did not change (Table 2). At the same time, the standard of living of the population in

the regions surrounding Moscow and the Moscow oblast remains below the average level.

The spatial polarization observed within Central Russia, where the higher distance from Moscow implies lower employment, wages, and retail turnover per capita, all of which increase only in the metropolitan agglomerations of neighboring regions, is well reflected in the migration growth rate. The highest population flow was expectedly characteristic of the Moscow region centers (15.3 per 1000 people). In the

Table 2. Comparison of socio-economic indicators for Moscow, Moscow oblast, and adjacent regions, and the Russian Federation 2001 to 2017.
(Moscow oblast = 1)

	Personal income			Gross regional product per capita			Retail turnover per capita		
	2001	2010	2017	2001	2010	2017	2001	2010	2017
Moscow oblast	1	1	1	1	1	1	1	1	1
Moscow	4.5	2.0	1.5	5.2	3.0	2.4	5.5	1.7	1.4
Regions adjacent to Moscow oblast	0.7	0.6	0.6	0.9	0.6	0.6	0.6	0.6	0.6
Russian Federation average	1.2	0.8	0.8	1.4	1.0	1.0	1.1	0.8	0.7

Source: compiled according Rosstat data

agglomerations of the territories adjacent to the Moscow region, this rate decreased almost three-fold (4.5 per 1000 people), and the urban settlements located outside the agglomerations and distant from the capital and the centers of neighboring regions, were already losing population (–1.9 per 1000 people).

Labor migrations are much more widely practiced: commuting and "otkhod" for work in Moscow and Moscow oblast from other regions for on weekly or monthly basis. Many residents of the Moscow oblast work in Moscow, and labor migrants from adjacent regions replace them. With the desire to work in Moscow or closer to capital along with housing prices beyond reach, the population often retains the official registration in their region. The return mobility of population with labor, social and recreational (including dachas) purposes has become the important factor that greatly affects on real population in Moscow and on the surrounding area, including the countryside (Between Home… 2016).

In the framework of Central Russia, typical Russian dachas ("second housing") model of

urban dwellers in countryside is most clearly implemented, embodying the tradition of combining the advantages of urban and rural lifestyle. There many types of dachas: old dachas of the beginning-the middle of the XX century, and garden associations, and the houses bought or inherited by urban dwellers in villages, and the new cottages interspersed in areas of garden and country building or organized in separate settlements (Between Home… 2016). Old dachas are located closer to Moscow. Gardening associations with cheaper housing are concentrated in more remote areas of Moscow oblast and in adjacent regions at the distance of 200-250 km from Moscow. In these regions Muscovites buy rural houses and use them seasonally as dachas. Despite the active growth of cottage settlements around Moscow, mostly common are traditional country and garden villages. Seasonal migration favorably still, determines the specification of suburbanization in the megalopolis. In the Moscow region and adjacent municipal districts of Yaroslavl' oblast the urban population of the country in summer season exceeds the number of rural residents (Fig. 2).
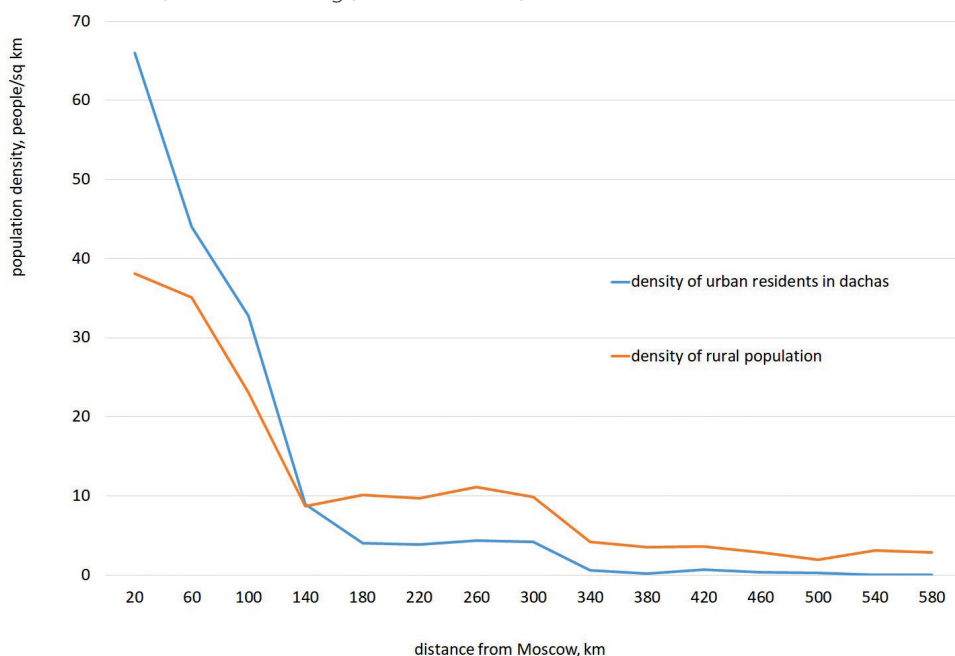
Fig. 2. The change in the density of rural population and urban gardeners in different distance from Moscow (MKAD), North East sector (Yaroslavl, Ivanovo, Kostroma regions), people/sq.km

Pavel L. Kirillov et al.   CURRENT TRENDS IN MOSCOW ...

04|2019

11 GES

3. Moscow and Moscow Oblast

The very first question is about the real population size of Moscow and Moscow oblast. Typical official statistics, for several reasons, and the sharp fluctuations of the population with daily, weekly and seasonal rhythms distort the real picture of the distribution of the resident population throughout the city and its immediate surroundings. Comparison of the total size of the resident population in the statistics and the population size estimates accordance to the data of mobile network operators on a winter weekday night, which are as close as possible to the real population size, give a rather unexpected result. They show that official statistics significantly overstate the population of Moscow but underestimates the figures for Moscow oblast. The population of the capital on a winter weekday night is less than that in the statistics by 1.6 million people, amounting to 10.7 million against 12.5 million people. The population size of Moscow oblast, according to mobile network operators, reaches almost 8.5 million people against the "official" 7.5 million people (Makhrova and Babkin 2018). At the same time, as shown by the data of mobile network operators, even on a winter weekday day, when the real population size of the capital is maximum primarily due to work- and education-related commuters, it is more than 600 thousand people less than shown in the statistics.

Such discrepancies are difficult to explain and may be due to various causes. First, it is the fact that Muscovites share two homes: keeping their capital registration, they also live in their dachas in Moscow oblast, which reduces the capital population and increases that of the oblast (Between Home… 2016). In addition, some Muscovites constantly live in the oblast, solving their housing problem by acquiring cheaper accommodation in Moscow oblast while retaining their registration in Moscow and all the related "capital goods" (supplements to pensions, Moscow health care, etc.). However, sociological polls show that there are quite few of those, about 300 thousand people.

A significant part of the discrepancies in the population estimates of Moscow and Moscow oblast may be associated with errors in the census. Such deviations were detected during the 2002 census when the registered population exceeded the real one. Thus, current statistics showed that in 2002, the capital population was 8.6 million, but the census estimated it at 9.9 million people. Similar discrepancies were also characteristic of the 2010 census when the population increased from 10.6 to 11.4 million people (Mkrtchyan 2011). As a rule, these discrepancies are attributed to undercounting of migrations, which raises doubts about the correctness of the population census methodology.

4. Moscow and Its Internal Structure of Settlement

The Russian capital has always been a city with a high population density, where decompression was each time achieved by expanding the boundaries of the city and not as a result of suburbanization processes, as was the case in the agglomeration cores of economically developed countries. On its own, the high population density is not a particular problem. The classic of modern urbanism, J. Jacobs (2011) calls a high population density one of the principles of urban diversity, which is exactly what attracts people to cities. However, comparing the population density of Moscow with other cities considered to be similar to the capital, this indicator is often rated as dangerously high (this was cited as one of the arguments in favor of the last expansion of the city). The size of the city's territory represents a bigger problem. Among other cities, including the largest ones, Moscow stands out for its atypically large size for a city, which makes the authorities to ensure that its territory is accessible by city standards to all residents of the capital, including in loosely populated affiliated territories.

In the 2010s, as in previous decades, the population of the capital was increasing and so was the population size of all administrative districts of the city, although the dynamics of this growth was uneven (Table 3). In recent years, the composition of the three leading

okrugs in terms of population size has not changed: these are the Southern, Eastern and South-Western okrugs, the population of each exceeding or approaching 1.5 million people. The population of another five okrugs of the capital is also higher than 1 million: almost all of their territory is located within the Moscow Ring Road, representing a fairly densely built-up area. For a long time, Zelenogradsky okrug (previously the city of Zelenograd) located 20 km away from the ring road, which was created as a Soviet analog of Silicon Valley, is characterized by the smallest population density and the highest growth rates. After another large-scale expansion of the city in 2012, which occurs about every 25 years, two okrugs of New Moscow have the smallest population size with the highest growth rates.

The latest expansion of Moscow's territory has led to significant changes in the population distribution within the district zones[1]. While the specific weight of the Moscow districts

[1] *For a detailed analysis of changes in the distribution population proportions in the context of administrative districts of the city, six zones of districts were distinguished: central (all districts of the Central Administrative okrug); sub-central (12 districts that are first-order neighbors of central districts, that is, districts that share borders with central districts); middle (third- and fourth-order neighbors of central districts); peripheral (depending on the territorial size of districts and their configuration, these are one or three "layers" of the districts located on the inner side of the Moscow Ring Road); the near outer zone (districts beyond the Moscow Ring Road until the borders of the Small Concrete Ring); and the far outer zone (districts beyond the borders of the Small Concrete Ring).*

Table 3. Population distribution in administrative okrugs of Moscow

Administrative okrugs	Population, thousand people		Share in population, %		Population size change over 2016–2018, %
	2016	2018	2016	2018	
Central	768.3 (9)	775.9 (9)	6.2	6.2	101.0
Northern	1158.5 (7)	1176.6 (7)	9.4	9.4	101.6
North-Eastern	1413.7 (4)	1424.9 (4)	11.5	11.4	100.8
Eastern	1505.8 (2)	1515.9 (2)	12.2	12.1	100.7
South-Eastern	1380.7 (5)	1405.7 (5)	11.2	11.2	101.8
South-Western	1426.2 (3)	1437.2 (3)	11.6	11.5	100.8
Southern	1774.4 (1)	1785.3 (1)	14.4	14.3	100.6
Western	1362.7 (6)	1382.5 (6)	11.1	11.1	101.5
North-Western	988.4 (8)	1001.3 (8)	8.0	8.0	101.3
Zelenogradsky	237.9 (10)	243.1 (10)	1.9	1.9	102.2
Novomoskovsky	200.1 (11)	234.2 (11)	1.6	1.9	117.0
Troitsky	113.4 (12)	124.7 (12)	0.9	1.0	110.0
Moscow as a whole	12330.1	12506.5	100.0	100.0	101.1

*parentheses indicate the position of the okrug on the corresponding date.
Source: Mosgorstat official data.

located on the inner side of the Moscow Ring Road (MKAD) is decreasing at different rates, the share of the near outer zone increased, which is represented by districts beyond the ring road. Due to active housing development the population is growing rapidly, having grown over the past three years by almost 90 thousand (Table 4). However, the density of residents remains to be low here, second only to municipalities of the far outer zone (all within the borders of Troitsky okrug), which, despite their capital status, resemble the typical periphery of Moscow oblast (Fig. 3). These are the districts that concentrate the primary resource for prospective housing development and the related increase in the amount and proportion of the population in the future. However, the proportion of the population of all the zones varies very little, which indicates steady major proportions in the population distribution of Moscow.

Important changes in the population distribution, which are not reflected by statistics, are associated with the emerging trends of greater social segregation along the west-east direction, which are superimposed on the inherited center-peripheral differences. The overall differences between

the center and the periphery, as well as the west and east, are relatively stable, but as the modern geography of prestige is forming and the processes of social-spatial polarization are growing, districts of the central and western okrugs become more prestigious, and most districts of the North-Eastern, Eastern and Southern okrugs are more and more clearly positioned as non-prestigious with marginal population (Vendina 2005). The attractiveness of the Eastern okrugs, as well as Southern okrug, is significantly reduced by the fact that they increasingly concentrate migrants, including non-Russian ethnicities from the former republics of Central Asia and Transcaucasia (Vendina 2005; Immigrants 2009).

Moscow, as well as other major capitals of the world, is characterized by a significant excess of the population concentrated here during the daytime over the resident population[2]. At the same time, due to the seasonal nature of Russian suburbanization and the dacha migration during the warm season, a specific feature of Moscow consists of significant population size differences associated with the effect of seasonal and weekly rhythms in the life of the population. A winter weekday

[2] The daytime population of Moscow, like any other megapolis, consists of residents and additional population, where the latter includes people coming from towns and districts of Moscow Oblast and neighboring regions with work-related, cultural and everyday goals, as well as temporary population (tourists, visitors to the city, transit passengers, patients of various medical institutions, etc.).

Table 4. Change of population size, share, and density by zones of Moscow districts

District zone	Population, thousand people		Share in total population, %		Population density, people/km^2	
	2016	2018	2016	2018	2016	2018
Central	734.1 (5)	775.9 (5)	7.5 (4)	7.5 (5)	11543 (2)	11715 (2)
sub-central	906.9 (4)	957.6 (4)	7.6 (3)	7.6 (4)	9310 (4)	9830(4)
Middle	3174.4 (2)	3184.9 (2)	25.2 (2)	25.1 (2)	12192 (1)	12233 (1)
Peripheral	5844.6 (1)	5891.3 (1)	46.6 (1)	46.5 (1)	11523 (3)	11615(3)
near outer	1553.2 (3)	1641.4(3)	12.7 (5)	12.9 (3)	2288 (5)	2417(5)
far outer	50.7 (6)	55.4 (6)	0.4 (6)	0.4 (6)	53 (6)	58 (6)
Moscow as a whole	12263.9	12506.5	100.0	100.0	4785	4882

Source: compiled according to Mosgorstat data.

Population density, people/km², 2018.

- < 1
- 1 - 5
- 5 - 10
- 10 - 15
- 15 - 20
- > 20

District zone

- I   Central
- II   Sub-central
- III Middle
- IV   Peripheral
- V   Near outer
- VI   Far outer
- ──── zone boundaries

Administrative okrugs
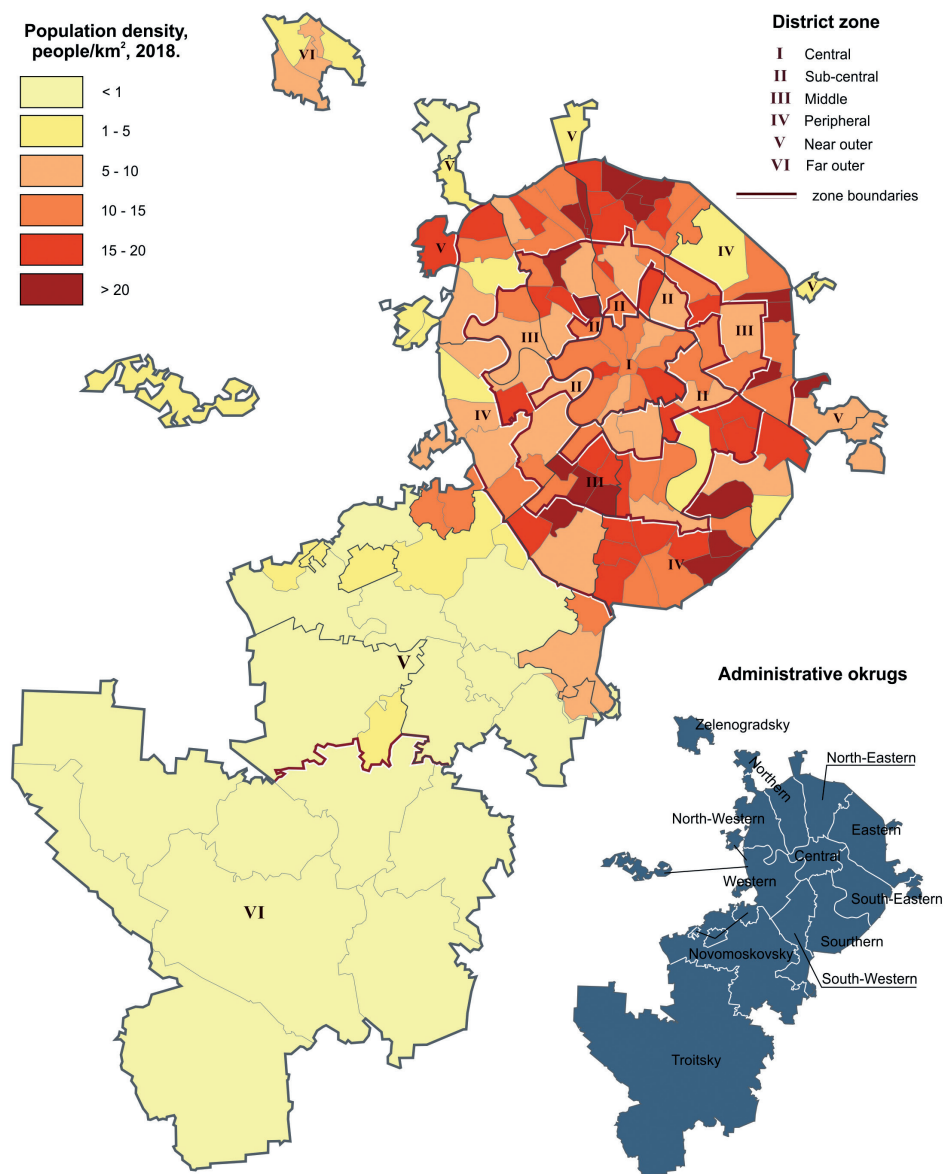
Fig. 3. Population density of Moscow municipalities, 2018, people/sq.km

is a period of maximum concentration of the population in Moscow and "pull-up" of the population to the center, while on a summer day off a significant part of the city's population spreads out over dachas. Taking seasonal changes into account, this leads to a 30% difference between a summer day off and a winter weekday. In general, in the summer months, the population of Moscow does not exceed 10 million, "shrinking" by about 15% at the weekend (Makhrova and Babkin 2018).

The daily dynamics is most pronounced in the city center, which concentrates a significant part of the capital's workplaces and shopping, entertainment, and leisure facilities, and the population difference between the daytime maximum and the nighttime minimum on a winter weekday is 2.8 times. This territory is also characterized by pronounced seasonality: the population size on a winter weekday is 2.1 times higher here than on a summer day off.

The sub-central zone, consisting of the Moscow districts adjacent to the Central okrug, is also subject to daily population fluctuations, which are less pronounced despite noticeable decentralization of office and shopping centers: weekly population drops are 1.5 times and seasonal 1.8 times. In the middle zone of Moscow, which serves as a kind of transition between the attractor districts of the center and sub-center dormitory areas on the periphery, daily fluctuations are poorly pronounced, amounting to only 5%. Weekly and seasonal changes play a more significant role, but they reach only 1.2–1.4 times.

In the rest of Moscow's periphery districts within the Moscow Ring Road, daily fluctuations are also only 5%, but the daytime population is less than the night one, that is, the majority of these districts are common dormitory areas. For the districts of Moscow located beyond the ring road (except for New Moscow), the dormitory character determines a significant excess of the nighttime population over the daytime one (by almost 40%). At the same time, the daytime population in some of those districts (Mitino, Vykhino-Zhulebino, Nekrasovka, Yuzhnoye Butovo, Solntsevo, and Novo-Peredelkino) reaches only 60–70% of the nighttime one (Makhrova and Babkin 2018).

5. New Moscow and Its Interaction with Old Moscow and Moscow Oblast

In 2012, the expansion of Moscow by 2.5 times at the expense of sparsely populated territories in the south-south-west of Moscow oblast split the Moscow suburbs up to the borders of Kaluga oblast. Two hundred fifty thousand people in the least populated areas of the Leninsky, Podolsky and Naro-Fominsky districts are now part of New Moscow. Three towns, two urban-type settlements, 234 villages, 52 settlements, and 652 gardeners' and dacha partnerships of residents of Moscow and towns of Moscow oblast were transferred to Moscow. Now the Moscow territory statistics report more than 150 thousand rural residents, which in principle contradicts the very concept of a city. For example, St. Petersburg, despite the presence of suburbs within the city limits, has no rural population.

The official concepts for the development of the vast southern territories of New Moscow have changed several times over the past five years. The previously proposed projects for construction of ministries and business and specialized centers in New Moscow have not been implemented. The supposed development similar to Korotishchi (almost merged cities of Korolev, Mytishchi, and Pushkino in Moscow oblast) also could not be realized due to the vast territory of New Moscow and the relative weakness of its cities (How to Build… 2015). And although federal officials abandoned initial plan of moving to the southern territories of New Moscow, the changes that have taken place in these territories over six years are great. The population of New Moscow has almost doubled, and about 11 million square meters of real estate has been developed here (New Moscow 2017).

Towns in the territory of New Moscow grew exceptionally fast from 2012 to 2018: Moskovsky, from 20.3 to 53.4 thousand people; Shcherbinka, from 35.3 to 51 thousand people; Troitsk, from 44 to 60.9 thousand people. The rural population was increasing slower, which indicates the ongoing processes of concentration in urban areas. However, this applies only to the resident population and its official registration. Huge discrepancies between official data and the real population, as evidenced by various sources, indicate a significant proportion of labor migrants in the capital region, as well as those Muscovites who live in dachas in the territory of New Moscow.

The expansion of Moscow did not change the trend for the Moscow oblast's population concentration closer to the Moscow Ring Road[3]. The population size was growing in different directions, mainly due to migration growth, and remained the largest in the first and second zones of remoteness from the Moscow Ring Road (Fig. 4). At the same time, the migration increase in Moscow oblast's districts adjacent to New Moscow in the first zone[4] did not exceed the average for this entire zone. However, after the expansion of Moscow, districts and city okrugs of the second and third zones of Moscow oblast in

the south and south-west began to attract many more migrants (Nefedova 2018). The fact that migrants even outside the southern sector were still rushing to the zone closest to Moscow indicates that the spread of Moscow's territory continues in all directions even after the accession of new territories. At the same time, in the south and south-west of Moscow oblast, this spread beyond the Moscow Ring Road turned out to be greater.

Construction of residential buildings in the territory of Moscow oblast was also more active around New Moscow. The construction business, which became one of the main

stimulus for expanding the capital's territory, involved not only the nearest territories joined to Moscow but also Moscow oblast's territories adjacent to New Moscow, becoming a driver of increasing migration to suburbs of the capital (Kurichev and Kuricheva 2018). As a result, the attractiveness of the southwestern sections of Moscow oblast turned out to be about the same and even greater closer to the Moscow Ring Road, as compared to the newly joined territories of New Moscow. This is due to the relatively cheaper real estate outside of Moscow, complete infrastructure in cities and rural settlements, as well as in some cases better accessibility of the capital's

[3] To identify and analyze the internal differentiation of Moscow Oblast, the previously applied grouping of municipalities into four zones in terms of their distance from the Moscow Ring Road is used. The first (closest) zone includes districts and urban okrugs bordering Moscow, the second (middle) zone includes municipalities that are second-order neighbors of Moscow, and the third zone includes third-order neighbors. The radius of the first zone generally reaches 20–30 km, with the only exception of Odintsovsky District, which is very prominent to the west. The second zone is 20–60 km away from the Moscow Ring Road, and the third zone is 60–100 km away. The far fourth zone includes western and eastern margins of the oblast, which do not form a continuous ring. In 2016, more than 70% of the population of Moscow Oblast lived in the first and second zones, where 6% of the first zone territory accounted for 34% of the population.
[4] These are Leninsky and Odintsovsky districts; in the second belt, city okrugs Naro-Fominsk, Podolsk, and Domodedovo; in the third zone, Chekhovsky District.
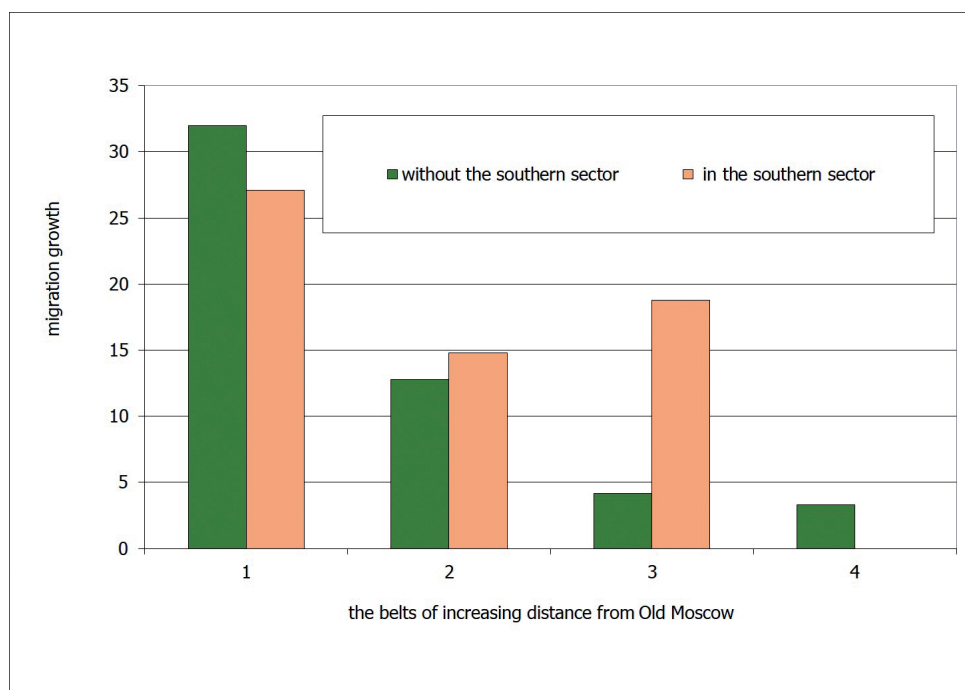
Fig. 4. Migration growth in Moscow oblast per 1000 inhabitants in 2014–2015 in terms of distance from the old territory of Moscow. Compiled according to Mosoblstat data.

center from Moscow oblast than from New Moscow.

Before they were removed from the oblast, the territories that comprised New Moscow were built up with multi-storey and low-rise housing. In 2012, the government announced low-rise development as a priority in the new territories of Moscow. However, it became unprofitable to build family houses, townhouses, and cottages on the capital's land, and such housing began to gradually give way to multi-story residential complexes. At the same time, developers of multi-storey housing became noticeably more active in the areas of Moscow oblast close to the Moscow Ring Road near New Moscow (Figs. 5 and 6). As a result, the vast territory south of the Moscow Ring Road is almost identical in both New Moscow and Moscow oblast, representing a complex mosaic of multi-storey and one-storey buildings, gardeners' partnerships, fields and forests.

Fig. 5. New buildings in Novodrozhzhino in Leninsky District of Moscow oblast (Photo by T.G. Nefedova).

Fig. 6. New Vatutinki in Desenovsky Settlement of New Moscow (Photo by T.G. Nefedova).

A noticeable increase in the rate of population growth outside the three towns that comprised New Moscow, before and after joining to Moscow, is a typical settlement of Novomoskovsky District (List of Settlements 2018). This is especially true for the Vnukovo settlement, sandwiched between Moscow's enclaves Solntsevo and Vnukovo, as well as of Sosenskoe, which is adjacent to the Moscow Ring Road (Fig. 7). A less pronounced response to the expansion of Moscow was observed for those settlements where new development started before joining Moscow, for example, in the Mosrentgen settlement, which lies right next to

the Moscow Ring Road. Due to such significant transformations very close to the Moscow Ring Road, the new territories of the capital include typical villages.

After the expansion of Moscow, the population growth in Troitsky District outside the town of Troitsk has been much smaller (Fig. 8) than in Novomoskovsky District. In the settlement farthest from the Moscow Ring Road (60 km), Rogovskoe, which borders Kaluga oblast, forests are interspersed with fields, small dacha villages, and gardeners' partnerships, which is not like a city at all. Nevertheless, the population is also growing there,
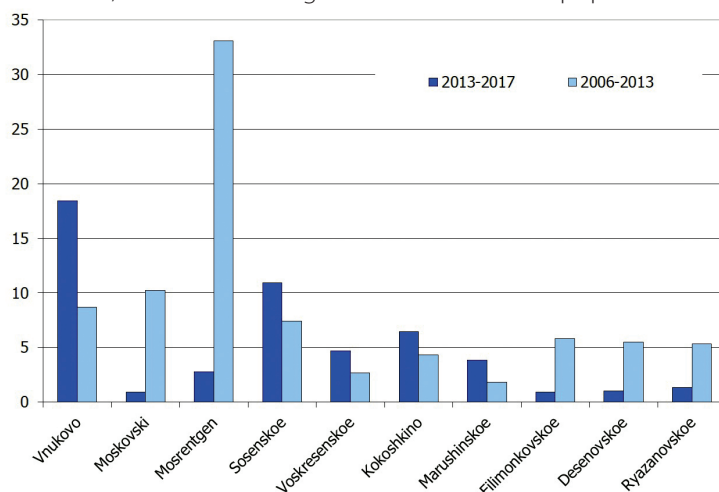
(A) Novomoskovsky District
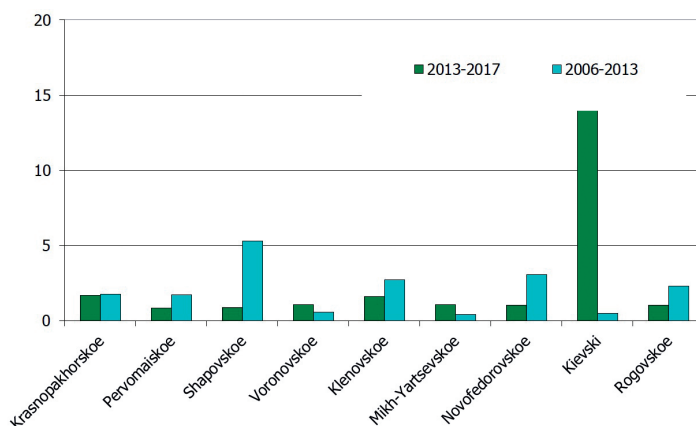
(B) Troitsky District

Fig. 7. A-B. Average annual population growth rates outside the towns of Moskovsky, Troitsk, and Shcherbinka in settlements of New Moscow before and after its formation, %. Compiled according to List of settlements (List of settlements... 2012)

mainly due to external migrants, who, registering on the outskirts of New Moscow, in fact live and work within or near the Moscow Ring Road.

Thus, against the extremely high population density in the Center of Moscow, the new remote territories of the capital are characterized by typical rural areas with many small villages, dacha settlements, and the prevalence of rural population in these formally urban regions.

In addition to rural residents in New Moscow, there are more than 600 gardeners' and dacha partnerships (All-Russian… 2017) of not only Muscovites but also residents of Podolsk and Naro-Fominsk, sometimes with shabby wooden houses without any amenities. Each of these partnerships includes from a few dozen to more than a hundred plots with houses, which in the summer are able to host several hundred people. In general, the population in the summer season increases by hundreds of thousands of people, which is comparable to a population of a dispersed city. They also include numerous dachas in villages, inherited or bought by Muscovites and residents of the oblast.

There is a pronounced seasonal population growth here: in Novomoskovsky District, the closest to Moscow, it is about 30%, reaching almost 90% in the more distant Troitsky District, which brings it closer to certain poorly urbanized rural municipalities of the oblast (Makhrova and Babkin 2018).

The fate of second, dacha housing owners, who now became part of New Moscow, remains unclear. Perhaps some of them will want to get a permanent registration here to secure their rights to the expensive land. Many gardeners' non-commercial partnerships are gradually turning into economy class cottage settlements. A trend of registering elderly parents in these houses has already been observed. But the vast majority of owners continue to live in two houses (Between Home… 2016). The Moscow authorities set the task of transforming houses in gardeners' partnerships into homestead properties of good quality with permanent residence, although very few Muscovites are ready to give up apartments within the Moscow Ring Road. Moreover, this will require not only significant individual investments of citizens, which is far from what everyone can do, but also creating a social infrastructure that is very costly with

**Fig. 8. Forests and fields in Rogovsky Settlement of New Moscow
(photo by T.G.Nefedova).**

such a dispersed population and discrete patterns of development.

CONCLUSIONS

1. The center of Russia, Moscow and its surroundings, is a place of the strongest spatial socio-economic contrasts in the country. At the same time, these contrasts are characteristic not only of the vast territory of the Central Russian megalopolis but also of Moscow itself, especially after the addition of the so-called New Moscow with its poorly developed rural areas lying far from the Moscow Ring Road.

2. Moscow, together with Moscow oblast forming the Moscow metropolitan region, became the main center of gravity in the post-Soviet space, actively increasing its demographic potential and importance both within the country and Central Russia. At the same time, the population dynamics, which serves as an accessible integral indicator of the level of socio-economic development and attractiveness of the territory for the population and business, shows how spatial heterogeneity was increasing during the last two decades.

3. The discrepancy in the development trajectories of Moscow and the surrounding Moscow oblast is particularly noticeable against the background of the depopulation of a significant part of slowly modernizing regions and cities of Central Russia with an inherited industrial burden. The gradient of polarization of the Central Russian megalopolis space between the cities of Moscow oblast and adjacent regions in terms of migration growth reaches three times, while the outflow of population from cities located beyond the boundaries of the megalopolis runs almost two times faster than in cities of the megalopolis, satellites of the capital and centers of neighboring oblasts.

4. The population estimates for Moscow and Moscow oblast, published by official statistics and those made using data from mobile network operators, significantly differ, showing serious distortions of the real picture of the resident population distribution. The population of Moscow is overestimated, and the population of Moscow oblast is underestimated, which is due to methodological problems of migration accounting and population censuses, as well as strong population fluctuations caused by massive centripetal flows of work-related commuters and centrifugal streams of dacha residents in the summer.

5. Within Moscow itself, the steadily growing population shifts towards the outer zone of the districts that increase at maximum rates, which leads to the decentralization of its internal distribution. At the same time, the newly attached territories are distinguished by a low population density, preserving the inherited features of development. Important changes are associated with increased social segregation of the capital along the west-east and center-periphery directions. Districts of the center and western okrugs are becoming increasingly prestigious. At the same time, most of the peripheral districts of the North-Eastern, Eastern and Southern okrugs are perceived as non-prestigious outskirts with a high level of concentration of non-Russian migrants.

6. Moscow is characterized by pronounced population fluctuations. On a summer day off, its population size is 30% less than on a winter weekday, not exceeding 10 million people in the summer months. Different parts of the city have their own fluctuation rhythms. Central and sub-central districts are dominated by daily fluctuations, while in the municipalities surrounding the city center the amplitude of fluctuations is smaller. The median and peripheral zones are characterized by seasonal fluctuations with an even less pronounced gradient. The outer zone of Moscow's districts outside the Moscow Ring Road is characterized by significant daily fluctuations due to work-related commuters. New Moscow is dominated by weekly and seasonal fluctuations with smoother daily dynamics, while areas of the outer periphery, closer to the borders of Kaluga oblast, have especially pronounced seasonal rhythms due to dacha specialization of these territories.

7. The authorities have always underestimated the unity of the Moscow region, which is mainly occupied by the metropolitan agglomeration. Its unity is defined both by the territorial closeness of Moscow's core and suburbs and by the stable links between them. The general infrastructure, powerful flows of population, capital, and information require this urban formation to be approached as a system or organism, where impacts on some parts inevitably affect the rest. Dissection of this "body" by administrative boundaries does not change the nature of its evolution and functioning. Analysis of non-urban areas within New Moscow shows that with such a mosaic pattern of land use the official division not only into Moscow and Moscow oblast but also into urban and rural populations becomes almost meaningless.

8. Over the past seven years after the new territories were joined to Moscow, there is still a question about the exact position of the boundary of the urban "capital landscape" in New Moscow. Areas that can be redeveloped have been added, and their migration inflow of younger and more active population has increased. But in case of acute land use conflicts, "lack of oxygen" for small business, low qualification of migrant workers, and poor quality of the

infrastructure environment, the metropolitan effect is limited to a small area in settlements of the first and second zones of distance from the Moscow Ring Road and along major highways, where discrete urbanized territories are formed. The transformation of New Moscow into a "garden city" gets delayed. For the time being, New Moscow is mostly represented by typically rural areas with villages, half-ruined agriculture, locals and dacha residents who are not certain about their future, and islands of multi-storey buildings that get denser towards the old territories of Moscow.

ACKNOWLEDGMENT

REFERENCES

All-Russian agricultural census of 2016, (2017). Vol. 2. Moscow: Statistics of Russia. (in Russian).

Argenbright R. (2013). Moscow on the Rise: From Primate City to Megaregion. The Geographical Review, 103 (1), pp. 20-36.

Argenbright R. (2016). Moscow under Construction: City-Building, Place-Based Protest, and Civil Society. Lanham, MD: Lexington Books.

Argenbright R. (2018). The evolution of New Moscow: from panacea to polycentricity. Eurasian Geography and Economics, 59 (3-4), pp. 408-435.

Between Home and …. Home. The Return Spatial Mobility of Population in Russia (2016). Ed.: Nefedova, T.G., Averkieva, K.V. and Makhrova, A.G. Moscow: Novyi Khronograf (in Russian). http://ekonom.igras.ru/data/bhah2016.pdf.

Brade I., Makhrova A. and Nefedova T. (2014). Suburbanization of Moscow s Urban Region. Confronting Suburbanization: Urban Decentralization in Postsocialist Central and Eastern Europe. Edited by K. Stanilov and L. Sykora. Chichester, West Sussex, UK: Wiley-Blackwell, pp. 97-132.

Büdenbender M. and Zupan D. (2017). The Evolution of Neoliberal Urbanism in Moscow, 1992-2015. Antipode, 49(2), pp. 294-313.

Cox W. (2012). The Evolving Urban Form: Moscow's Auto-Oriented Expansion. New Geography. 22/02. [online]. Available http://www.newgeography.com/content/002682-the-evolving-urban-form-moscows-auto-oriented-expansion. [Accessed 1 September 2017].

Ferencuhova S., Gentele M. (2016). Introduction: Post-Socialist cities and urban theory. Eurasian Geography and Economics, 57 (4-5), pp. 483-496.

Fet A. (First published: 1871). Stepanovka's Life, or Lyrical economy. Zarya, 6, pp. 3-86 (in Russian). http://ruslit.traumlibrary.net/book/fet-stepanovka/fet-stepanovka.html#work007

Golubchikov O., Badyina A. and Makhrova A. (2014). The Hybrid Spatialities of Transition: Capitalism, Legacy and Uneven Urban Economic Restructuring. Urban Studies, 51(4), pp. 617-633. DOI: 10.1177/0042098013493022

Golubchikov O. (2016). The urbanization of transition: ideology and the urban experience. Eurasian Geography and Economics, 57 (4-5), pp. 607-623.

How to build the New Moscow, (2015). Ed. G. Revzin. Part 2. Moscow: Strelka. (in Russian) [online] Available at: http://2016.mosurbanforum.ru/files/2015/issledovanie/1504_new_moscow_book_part_2.pdf [Accessed 20 January 2018]. (in Russian).

Immigrants in Moscow, (2009). Ed. J. A. Zaionchkovskaya. Moscow: Kennan Institute (in Russian).

Jacobs J. (2011). Death and life of big cities. Moscow: New publishing house (in Russian).

Kashnitsky I. and Gunko M. (2016). Spatial variation of in-migration to Moscow: testing the effect of housing market. Cities, 59, pp. 30-39.

Kolossov V., Vendina O. and O'Loughlin J. (2002). Moscow as an emergent word city: international links, business development, and the entrepreneurial city. Eurasian Geography and Economics, 43 (3), pp. 170-196.

Kolosov V. (2013). Will city limits expansion solve Moscow's problems? Ukrainian Geographical Journal, 3, pp. 3-8.

Kurichev N. and Kuricheva E. (2018). Relationship of Housing Construction in the Moscow Urban Agglomeration and Migration to the Metropolitan Area. Regional Research of Russia, 8 (1), pp. 1–15.

Kuricheva E.K. (2017). Housing construction in Moscow agglomeration: spatial consequences. Vestn. Mosk. un-ta. Ser. 5. Geogr. ;(3), pp. 87-90. (In Russian with English abstract)

List of settlements that became part of Moscow on July 1, 2012. (2012). (in Russian) [online]. Available at: https://ru.wikipedia.org/wiki_spisok_naselennyh_punktov_voshedshih_v_sostav_moskvy_1_iyulya_2012 #cite_note-MosObl-1 [Accessed 15 January 2018]

Makhrova A. and Babkin R. (2018). Analysis of Moscow agglomeration settlement system pulsations based mobile operators data. Regional Research of Russia, 2 (60), pp. 68–78. (in Russian).

Makhrova A., Kirillov P. and Bochkarev A. (2017). Work Commuting of the Population in the Moscow Agglomeration: Estimating Commuting Flows Using Mobile Operator Data. Regional Research of Russia, 7(1), pp. 36-44. 10.1134/S2079970517010051

Makhrova A., Nefedova T. and Treivish A. (2013). Moscow Agglomeration and 'New Moscow': The Capital City-region Case of Russia's Urbanization. Regional Research of Russia, 3, pp. 131-141. DOI: 10.1134/S2079970513020081.

Makhrova A., Nefedova T. and Treyvish A. (2016). Central Russian megalopolis: space polarization and population mobility. Vestnik Mosk. Univ., Ser. 5, 2, pp. 64–74 (in Russian).

Mkrtchyan N. (2011). Population dynamics in Russian regions and the role of migration: a critical assessment based on the 2002 and 2010 censuses. Izvestiya of the Russian Academy of Sciences, 5, pp. 28-41 (in Russian).

Nefedova T. (2018). New Moscow outside its towns. Old and New Moscow: the trends and problems of development. Moscow: Russian Geographical Society, pp.184-219 (in Russian).

New Moscow: how the new territories have changed in five years, (2017). PBC June 30. (in Russian) [online]. Available at: https://realty.rbc.ru/news/5956020a9a7947724f9d14e6 [Accessed 30 January 2018].

Shuper V. and Em P. (2013). Moscow city expansion: an alternative based on central place theory. Regional Research of Russia 3(4), pp. 376-385.

Todd M. (2018). The political geographies of religious sites in Moscow's neighborhoods. Eurasian Geography and Economics, 58 (6), pp. 642-669.

Vendina O. (2005). Migrants in Moscow: is Moscow beading forwards ethnic segregation. Migration segregation in regions of Russia. Vol. 3. Moscow: Migration Research Center. (in Russian).

Zubarevich N. (2018). Economic and budgetary advantages of Moscow: how they are formed and used. Old and New Moscow: the trends and problems of development. Moscow: Russian Geographical Society, pp. 25-37 (in Russian).

04|2019

23 GES

Viacheslav I. Vasenev[1], Alexey M. Yaroslavtsev[1,2], Ivan I. Vasenev [1,2], Sofiya A. Demina[1], Elvira A. Dovltetyarova[1]

[1]People's Friendship University of Russia, Miklukho-Maklaya str.6, Moscow, 117198, Russia
[2] Russian State Agrarian University – Moscow Timiryazev Agricultural Academy, Timiryazevskaya st., 49, Moscow,127550, Russia
* Corresponding author: vasenev-vi@rudn.ru

LAND-USE CHANGE IN NEW MOSCOW: FIRST OUTCOMES AFTER FIVE YEARS OF URBANIZATION

ABSTRACT. Urbanization coincides with remarkable environmental changes, including conversion of natural landscapes into urban. Moscow megapolis is among the largest urbanized areas in Europe. An ambitious New Moscow project expanded the megapolis on extra 1500 km^2 of former fallow lands, croplands and forests. The research aimed to monitor land use changes in New Moscow between 1989 and 2016 years. Landsat 5 and Landsat 8 images (30 m spectral resolution) and Sentinel – 2 images (10 m spectral resolution) were analyzed. All the images were collected for the similar summer period (from June to August). The images were preprocessed and classified by Semi-Automatic Classification Plugin in open source QGIS software to derive land cover maps. The following land cover classes were identified: water, built-up areas, bare soils, croplands and forested areas, and the total area covered by each class was estimated. The following land-use change pathways were reported: 1) reduction of the forested areas by 2.5% (almost 2000 ha) between 1989 and 1998; 2) partial reforestation (more than 1000 ha) and abandonment of croplands (more than 3000 ha) between 1998 and 2010 and 3) intensive urbanization (more than 11000 ha) between 2010 and 2016. New build-up areas and infrastructures were constructed on former forested areas and croplands. Although, some uncertainties in the absolute estimates are expected due to the classification errors, the general urbanization trend can be clearly distinguished as a principal outcome after the five years of New Moscow project.

KEY WORDS: land use and land cover change, deforestation, supervised classification, satellite images, Landsat, urban planning, sustainable development

INTRODUCTION

Global urban population increases continuously and about 70 percent of the world's population will live in cities by 2050 (FAO 2009). Urbanization coincides with remarkable environmental, social and economic consequences (Turner 2002; Foley et. al., 2005). Conversion of the former agricultural and forested lands into urban

Viacheslav V. Vasenev et al.   LAND-USE CHANGE IN NEW MOSCOW: ...

04|2019

25 GES

areas is one of the main outcomes. An intensive urbanization in coming decades is projected in the developing countries and regions (FAO 2002). As a result, these countries will face numerous challenges in meeting the needs of the growing urban populations, including the demands for housing, infrastructure, transportation, energy, and employment, as well as for basic services such as education and health care (U.N. 2014).

The urban expansion occurs on former natural and forested areas and often coincides with deforestation. The rate of deforestation process is increasing every year and it brings a big change in the earth's physical and chemical environments (Kumar 2017). The tree canopies perform as barriers for dust, noise and pollution (U.N. 2014) and maintain the temperature regime of the forest ecosystem (FAO 2018). Tree roots help to hold soil particles together and mitigate soil erosion (Bond, Hughes 2013). Forests contribute to water balance by controlling the precipitation distribution between surface run-off and ground waters (Kalnay, Cai 2003). Cutting the forests down decreases this protective service, disturbs nutrient cycles and increases greenhouse gases' emission (Hendesron-Sellers 2009; Bond, Hughes 2013). Deforestation of the suburbs results in substantial changes in the urban climate and contributes to urban heat island (Kalnay, Cai 2003; Oke 1982; Voogt, Oke 2003). Urban heat island decreases the comfort and quality of life in cities and causes the extra costs for cooling (Sarrat et.al. 2006; Tan et.al. 2010; Kolokotroni et. al., 2006; Chen et. al. 2016).

Urban green spaces include places with 'natural surfaces' or 'natural settings', but may also include specific types of urban greenery, such as street trees and green lawns. Typical green spaces in urban and sub-urban areas are public parks and urban forests; other definitions may also include private gardens, woodlands, children's play areas, riverside footpaths, beaches, and so on (WHO 2014). Under the condition of growing or even stable population, deforestation would reduce the total area of green spaces per capita (Gracey 2003). Decreasing of the green

areas per capita below minimal thresholds can create health risks for population (SniP II-60-75 Russian Federation). The most likely negative consequences for human health are insufficient physical activity, depression, respiratory diseases and allergic reactions (WHO 2014).

Monitoring land-use changes and studying their consequences are especially interesting and relevant in the regions with ongoing urbanization. New Moscow is a unique area, which has been experiencing a rapid urbanization during last five years since 2012. Remarkable development of new urban infrastructure in New Moscow coincides with conversion of fallow, agricultural and forested lands into build-up areas. The aim of the research was to analyze the land-use changes dynamics in the current New Moscow area between 1989 and 2016 and to investigate the land-use change and environmental consequences of New Moscow project.

MATERIAL AND METHODS

Deforestation of suburban areas is a continuous non-linear process, that shall be considered to select a relevant monitoring approach. Federal State Statistics Service provides information about land-use change annually but lacks spatial explicitness and doesn't allow following rapid changes occurring in short time periods. Similarly, land-use change studies based on the existing cartographic maps will not catch up with the ongoing rapid land-use changes like urbanization (Sivtsov 2014). In comparison to census data and cartographic maps, a remote sensing approach and GIS-based solutions give a considerable advantage to obtain more detailed information with an appropriate frequency (Frelinger, Gabriele 1999; Lurie et al. 2017). Open access to data is available from many official sources, which provide satellite imagery free of charge, e.g USGS Earth Explorer, NOAA CLASS; NASA; EOLi. Remote sensing data is widely used for land use monitoring and agricultural purposes (Hadjimitsis et.al. 2010; Liang et.al. 2008). Implementing remote sensing approaches to monitor urbanization and estimate its environmental consequences is getting increasingly relevant

Research area. New Moscow extends from 54º55'N to 55º61'N latitudes and from 36º42' to 37º71' longitudes Southwest of the Moscow city and covers an area of more than 148 thousand hectares, which was officially included into the Moscow city boundaries in 2012 (Fig. 1). The climate is temperate continental, summer is warm, winter is moderately cold. Before 2012, less than 10% of the New Moscow areas was urbanized, whereas forests and croplands had covered 51 and 17% of the areas respectively. New Moscow forests mainly belong to the category of mixed forest. Birches (Betula pendula, Betula alba), alders (Alnus inana), firs (Picea abies), pines (Pinus sylvestris), maples (Acer platanoides), oaks (Quercus robus), lindens (Tilia cordata) and aspens (Populus tremula) are the most spread species (Vasilev and Chistov 2016). Grain, row and vegetables are the most spread crops in the region. Soils in the region are dominated by Retisols (Shishov and Voitovich 2002; FAO 2006).

As a result of the New Moscow Project, the area of Moscow city increased by almost 2.5 times. In 2012-2018, more than 8 million m^2 of housing, 2.8 million m^2 of non-residential property objects, 47 public facilities and 2 metro stations have been constructed and completed. The development potential is estimated as 63.9 million m^2 for new working places, 89.8 million m^2 for residences

and 1156 km for the construction and reconstruction of roads. By 2035, it is planned to build 65 km of metro tracks and to open 29 new metro stations (Privezentseva and Tesler 2015). Established infrastructure and created working places attract labor migration and lead to redistribution of population inside Moscow, especially parts of the New Moscow neighboring old Moscow boundaries (Makhrova and Kirillov 2018). With all these achieved and planned activities, New Moscow is for sure the most ambitious urbanization project in Russia.

Datasets. The datasets used in the study was derived from a sequence of satellite images from 1989, 1994, 1998, 2007, 2010, 2015 and 2016 taken by Landsat 5, Landsat 8 or Sentinel 2 (Table 1). The resolution of images allows to detect land use and land cover (LULC) categories of the study area.

Image Classification methods. The supervised classification approach was used to classify the land-use types. The following research steps were taken: 1) the pre-processing operations (including atmospheric correction and clipping); 2) supervised classification of images; 3) classification accuracy evaluation and 4) estimation of the forested areas. Supervised classification algorithm is presented on Fig. 2.
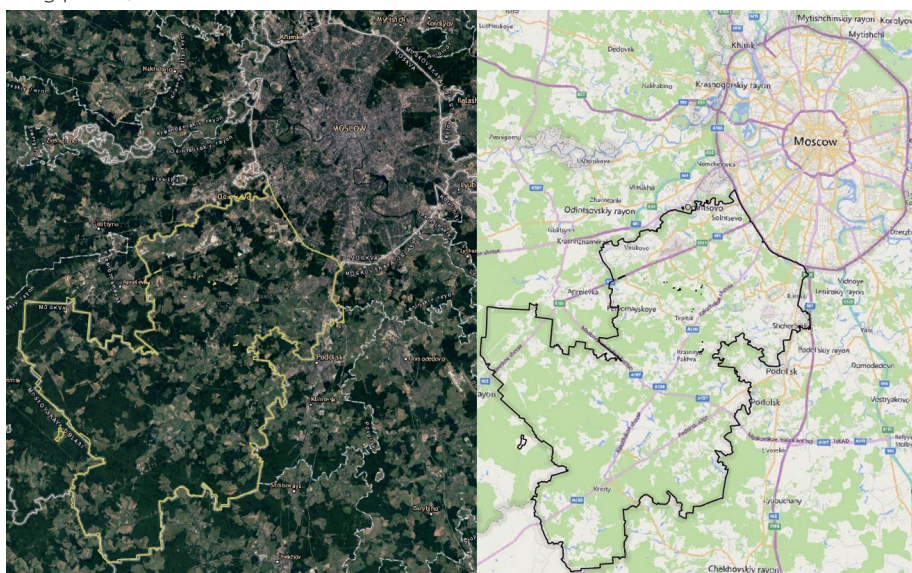
Fig. 1. Geographic location of study area (QGIS, Quick Map Services plugin, Google Satellite, ESRI Boundaries & Places, Bing Map)

Table 1. Comparative characteristics of satellite images (Images taken from USGS official website)

Satellite	Sentinel-2	Landsat-5	Landsat-8
Date	07/24/2016	03/06/1989 30/07/1998 24/08/2007 15/07/2010	26/05/2015
Spatial resolution (meters)	10 m	30 m	30 m
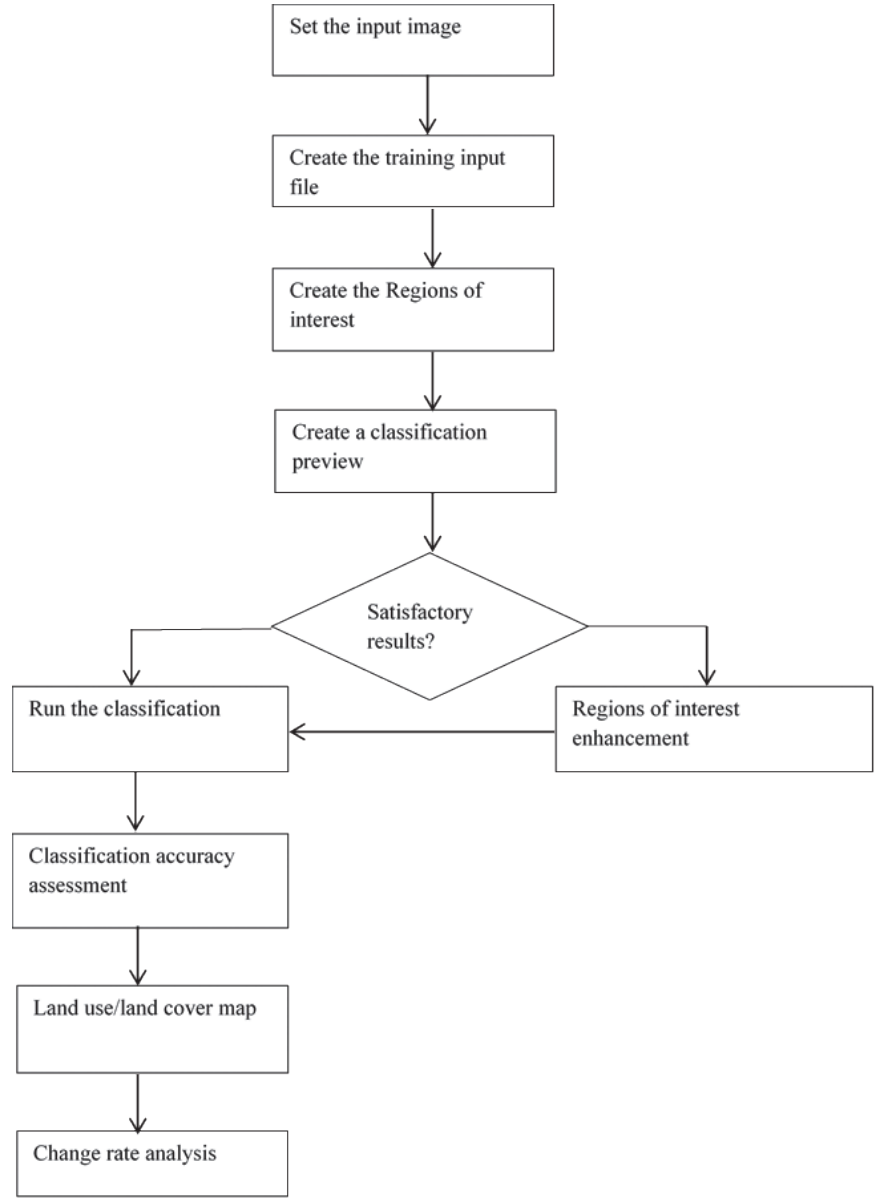
Fig. 2. Supervised classification workflow

Atmospheric correction of remote sensing data was used to decrease jamming and deterioration of images by smoothing and minimizing distortion, cloudiness and the effect of water vapor (Fallati et. al., 2017). Only the images collected during the similar period (growing season) were used to increase the comparability between the years. Correction and classification were performed using Semi-Automatic Classification Plugin. Land cover for selected the time periods between 1989 and 2016 was classified into 4 categories – forested, built-up, agricultural (including bare soils) and water bodies. The adopted classification is hierarchical with two levels of detail: Level I (macro-classes) and Level II (micro-classes). The images for each observation period were classified into 4 macro-classes: water, built-up, crops (including bare soil area) and forest. Classification was performed using Minimum Distance algorithm. The spatial accuracy of the classified maps was checked using Error Matrix by creating randomly scattered 100 points for every observation period. These points were overlaid on the classified images. All preprocessing operation, Error Matrix creation and classifying raster maps conversion to shape files were performed using Semi-Automatic Classification Plugin.

We assume that 1) the rate of urbanization expansion could increase considerably from 2012 to 2016 compared to the other time periods; 2) deforestation and urbanization processes in New Moscow are interrelated.

RESULTS AND DISCUSSION

Land-use change pathways in New Moscow in 1989-2016. Land-use maps were derived from the satellite images for each of the observation periods and an overlay between the maps from different periods allowed illustrating the major land-use change pathways. Three land-use categories – forested areas, croplands and urban (build-up) areas experienced the most considerable changes during the entire observation period and the land-use

structure of the New Moscow territory in 2016 is considerably different compared to the first observation period in 1989. Urban expansion was obviously the dominating trend in the area. The total build-up area increased almost two times – from 1.3 to 2.4 km^2. The major part of new build-up areas was developed within approximately 30 km from the Moscow city (boundaries before 2012), whereas urban expansion in the remote parts of the region were less intensive. The forested area in 2016 was 0.26 km^2 less than in 1989, evidencing that 3.5% of the initial forest resources were lost during this period. Cropland areas also decreased on 0.2 km^2, which is more than 4% of the arable lands in 1989 (Fig. 3).

Comparison between 1989 and 2016 highlights the major land-use change outcomes but does not describe land-use dynamic inside this period, which is important to understand the drivers behind land-use change in the region. When the maps derived for all the observation periods were compared, the following land-use change pathways were found: 1) forested areas converted to built-up areas; 2) forested areas converted to croplands; 3) croplands converted to built-up areas (fig.4) . None of these land-use change pathways remained linear for the whole observation periods but increased or decreased the intensity or even changed to a reverse land-use change in result of social-economic impacts and political decisions. Several periods with different dominating land-use change pathways can be distinguished. During the period between 1989 and 1998, cropland increased on more than 1.1 km^2, whereas the forested areas decreased on approximately 0.1 km^2. This can be an evidence of the intensification of agriculture in the Moscow region by 1998 after its collapse in the beginning on 1990s, which could partly occur on former forested areas (e.g., non-protected forests). In 1998-2010 the opposite trend was observed – forested areas increased on 0.1 km^2 and cropland decreased on comparable 0.33 km^2. Partly, this outcome can be explained by reforestation of the abandoned croplands, which profitability in the Moscow region
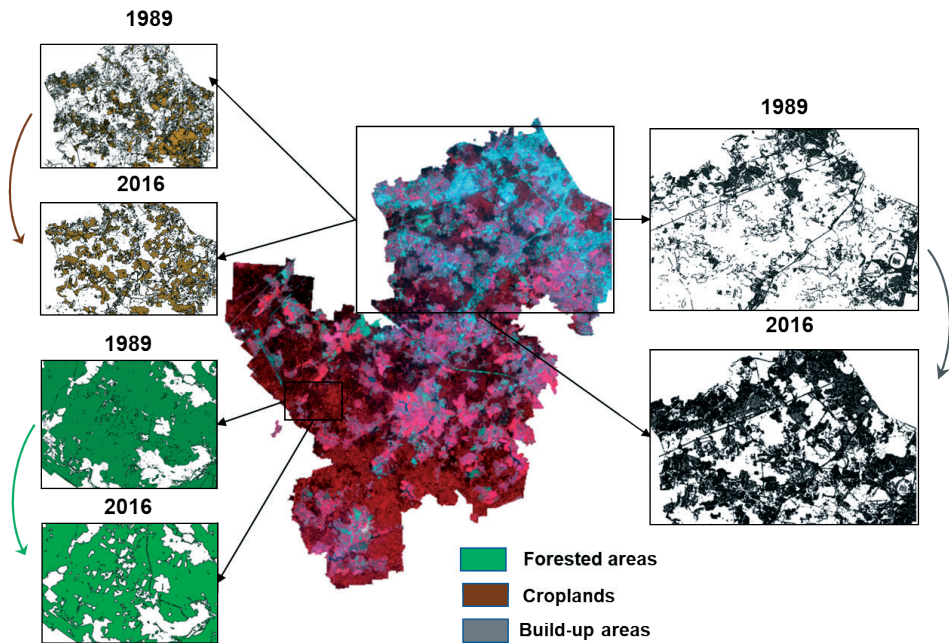
Fig. 3. Changes in forested areas, croplands and build-up areas in New Moscow between 1989 and 2019
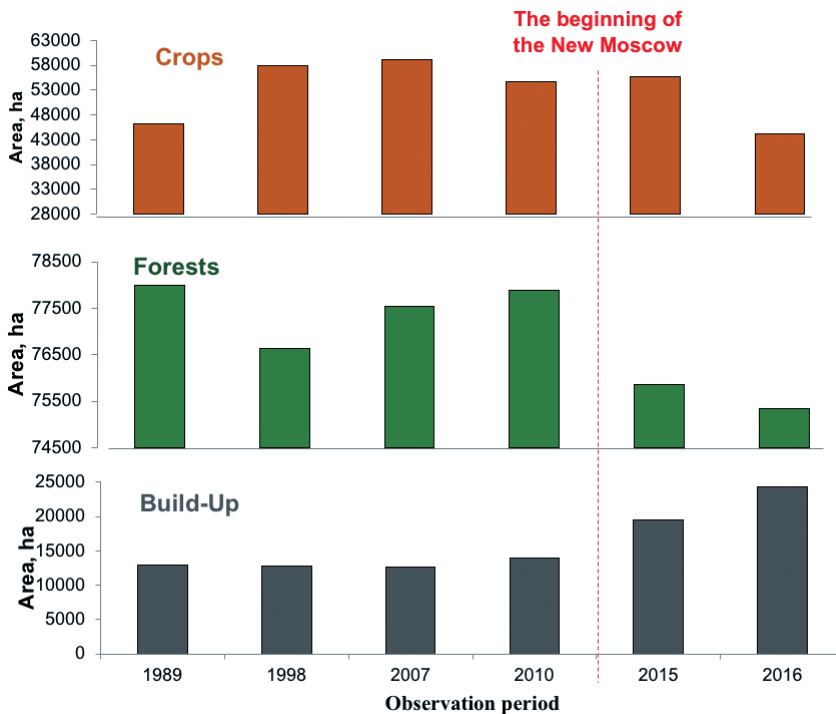
Fig. 4. Land-use change dynamics in New Moscow during the period 1989-2019

is rather low. Interestingly, during twenty years between 1989 and 2010 the extent of build-up areas increased just on 0.09 km² or by 7% from the initial urban area.

However, the next period between 2012 and 2016 showed a rapid urbanization on more than 1.1 km² (86% of build-up areas in 2010). Apparently, this urbanization

occurred on former forested areas and croplands, which extent decreased on 0.25 and 1.0 km^2 correspondingly during this time period.

Data accuracy and uncertainties of projections. Several sources of uncertainty of the obtained estimates could be expected. The primary one is the classification error. To check the classification accuracy was checked by a routine procedure based on the Kappa hat criteria measured based on the comparison between observed and expected estimates. The output table (Table 2) includes overall accuracy, producer and user accuracy for each established macro-classes. Overall classification accuracy 2007, 2010, 2016 classification exceeds 85 %, that is minimum level of interpretation accuracy in the identification of land use and land cover categories from remote sensor. Further, the outcomes of the remote sensing analysis were compared to the census data to validate and explain the found land-use changes. One of the main indicators for the building construction sphere is the established dwellings (mln. square meters of total floor space of dwellings). This indicator characterizes a housing stock development at the end of the year. We compared this indicator to the extents of build-up areas projected by remote-sensing approaches and obtained a significant correlation (r = 0.89) between the values. This confirms that the reported urbanization trend was correct.

Besides, the approach we used is focused on the land conversion between the macro-classes (forested areas, croplands and build-up areas), whereas changes in micro-classes were estimated with less accuracy and therefore could cause additional errors. For example, in the period between 1998 and 2010 an increase in the total area of the forests was reported. However, a detailed study of the high-resolution images available from the resource Google Earth Pro space images, explained this outcome by the gradual "reforestation" of felling sites. The figure 5 gives an example of a specific forest site which was cut down in the 80-s and abandoned afterwards. They stood out against the background of a common array, young shoots were rare and crown not lush enough. Considering these properties and the spatial resolution of satellite images (30 m per pixel), the algorithm did not classify such areas to the "forest" macro-class until 2007. Only the results of the classification for 2010 showed that these areas were recognized as forested again (Fig.5).

Finally, the negative consequences of urbanization are not limited to the decrease in the quantity of forested areas, but also alter the quality of forests, change their structure and deplete the ecosystem services they provide (DeFries and Pandey 2010; Lyu et al. 2018). Defragmentation of the forested areas activates the "edge erosion" when the forested areas

Table 2. Classification accuracy (Error Matrix)

Observation period	Overall classification accuracy [%]	Macroclass 'Forest' producer accuracy [%]	Macroclass 'Forest' user accuracy [%]	Macroclass 'Crops' producer accuracy [%]	Macroclass 'Crops' user accuracy [%]	Macro-class 'Forest' Kappa hat	Macro-class 'Crops' Kappa hat
1989	78.84	92.31	80.00	95.65	88.00	0.73	0.78
1998	77.98	91.79	84.40	65.10	64.14	0.59	0.49
2007	87.50	99.70	83.33	77.78	87.00	0.71	0.80
2010	95.71	99.80	99.80	91.18	81.58	0.98	0.79
2015	94.15	93.84	99.05	95.93	89.11	0.98	0.83
2016	93.80	86.90	95.77	97.59	93.70	0.94	0.80

Viacheslav V. Vasenev et al.   LAND-USE CHANGE IN NEW MOSCOW: ...

04|2019

31 GES

08/08/2004   07/23/2008   07/13/2014

08/28/2016   05/22/2017   05/22/2017 – zoomed image
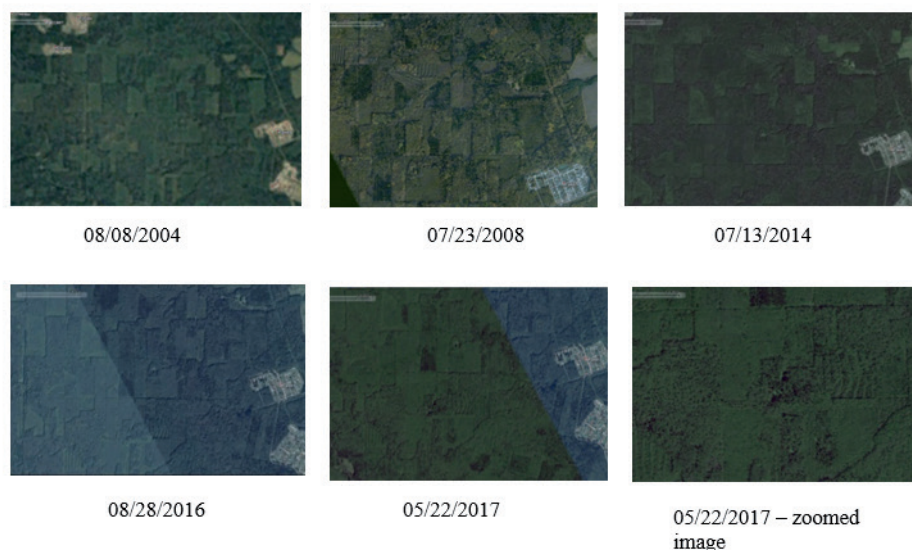
Fig. 5. Regeneration of the cutting area in the South-Western part of the study region (images are taken using Google Earth Pro service).

neighboring urban areas get exposed to high anthropogenic load resulting in biodiversity loss and simplification of the vertical structure (Rysin et al. 2004). Deforestation followed by intensive development of urban infrastructure (i.e., building construction, development of roads and railways) creates further risks for air quality (Belyakov and Koldobskaya, 2018), soil degradation (Romzaykina et al. 2020), biodiversity loss (Demina et al. 2019) and erosion (Daykovskaya 2014). All these multiple consequences shall be taken into consideration for sustainable urban development in New Moscow.

CONCLUSION

Ongoing urbanization alters land-use structure globally and regionally. New buildings and infrastructures are developed on former agricultural and forested lands to satisfy the demand of growing population in place for settlement. New Moscow projects is a unique case of the tremendous increase of urbanization intensity by a political decision. Land-use change dynamics observed in the region between 1989 and 2010 changed considerably in 2010-2016 when the New Moscow project was started. The build-up area remaining invariable for almost twenty years increased two times during the following six years. The extent of the agricultural and forested areas decreased to a total 1.25 km^2 for the same period. Although some uncertainties in the absolute estimates are expected due to the errors in semi-Automatic Classification and land cover dynamics inside the distinguished land-use classes, the general tendency of an intensive urbanization is clear and confirmed by a strong correlation with a census data on the new dwellings put in place. A rapid urbanization on former croplands and forested areas can result in depletion of important ecosystem services, which shall be considered for such ambitious projects as New Moscow.

ACKNOWLEDGEMENTS

REFERENCES

Bityukova V.R., Koldobskaya N.A. (2018). Environmental factors and constrains in the development of the new territory of Moscow (so-called "New Moscow"). Geography, Environment, Sustainability, 11(2), 46-62. DOI: 10.24057/2071-9388-2018-11-2-46-62

Bond T., Hughes C. (2013). O-level Biology Challenging Practice Solutions (Yellowreef). London: Yellow reef Limited.

Chen L., Huang L., Mendez-Garcıa C., Kuang J., Hua Z., Liu J., and Shu W. (2016). Microbial communities, processes and functions in acid mine drainage ecosystems. Current Opinion in Biotechnology, 38, 150–158, DOI: 10.1016/j.copbio.2016.01.013.

Daykovskaya T.S. (2014). Assessment of gully network current state in the New Moscow area. Geomorphology, 4, 39-47, DOI: 10.15356/0435-4281-2014-4-39-47.

DeFries R., Pandey D. (2010). Urbanization, the energy ladder and forest transitions in India's emerging economy. Land Use Policy, 27 (2), 130-138, DOI: 10.1016/j.landusepol.2009.07.003.

Demina S., Vasenev V., Ivashchenko K., Ananyeva N., Plyushchikov V., Hajiaghayeva R., Dovletyarova E. (2018). Microbial properties of urban soils with different land-use history in New Moscow. Soil Science, 4, 132-140, DOI: 10.21657/tsd.47684.

Fallati L., Savini A., Sterlacchini S., Galli P. (2017). Land use and land cover (LULC) of the Republic of the Maldives: first national map and LULC change analysis using remote-sensing data. Environmental Monitoring and Assessment, 189(8), 417, DOI: 10.1007/s10661-017-6120-2.

FAO. (2002). Urbanization - Linking Development Across the Changing Landscape. Axel W. Drescher, David Iaquinta, Julio Dávila, Adriana Allen, Fred Kruger and the Comparative Agricultural Development Service (ESAC), http://www.fao.org/fileadmin/templates/FCIT/PDF/sofa.pdf).

FAO. (2006) World reference base for soil resources 2006. World Soil Resources Reports, 103, Rome.

FAO. (2009). Population and development review, 35 (4), 837–839.

FAO. (2018). FRA team-Lead author Monica Garzuglia. Seventy years of FAO's Global Forest Resources Assessment (1948-2018), Roma, Italy.

Foley A.J. et al. (2005). Global consequences of land use. Science 309, 570-574, DOI: 10.1126/science.1111772.

Frelinger D. R., Gabriele M. (1999). Remote Sensing Operational Capabilities: Final Report. RAND.

Gracey M. (2003). Child health implications of worldwide urbanization. Rev Environ Health, 18(1), 51, DOI: 10.1515/reveh.2003.18.1.51.

Hadjimitsis D. G., Papadavid G., Agapiou A., Themistocleous K., Hadjimitsis M. G., Retalis A., Michaelides S., Chrysoulakis N., Toulios L. and Clayton C. R. I. (2010). Atmospheric correction for satellite remotely sensed data intended for agricultural applications: impact on vegetation indices. Natural Hazards and Earth System Sciences, 10, pp. 89-95, DOI: 10.5194/nhess-10-89-2010.

Henderson-Sellers A., Dickinson R. E., Wilson M. F. (2009) Tropical deforestation: important processes for climate models, Climate change, 13(1), 43-67, DOI: 10.1007/BF00140161.

Kalnay E., Cai M. (2003). Impact of urbanization and land-use change on climate. Nature 423 (6939), 528–531, DOI: 10.1038/nature01675.

Kolokotroni M., Giannitsaris I. and Watkins R. (2006). The effect of the London urban heat island on building summer cooling demand and night ventilation strategies. Solar Energy, 80. 383-392, DOI: 10.1016/j.solener.2005.03.010.

Kumar D. (2017). Monitoring and assessment of land use and land cover changes (1977 - 2010) in Kamrup district of Assam. India using remote sensing and GIS techniques, 15 (3), 221-239, DOI: 10.15666/aeer/1503_221239.

Liang T., Zhang X., Xie H., Wu C., Feng Q., Huang X. and Chen Q. (2008). Toward improved daily snow cover mapping with advanced combination of MODIS and AMSR-E measurements. Remote Sensing of Environment, 112, 3750–376, DOI: 10.3390/rs5115463.

Lurie I.K., Prokhorova E.A., Semin V.N., Sakirkina M.A. (2017). Provision of web-cartographic support for the ecological and geographical assessment of the New Moscow territory development. Vestnik Moskovskogo universiteta, ser. Geografiya, 5, 49–57 (in Russian).

Lyu R., Zhang J., Xu M., Li J. (2018). Impacts of urbanization on ecosystem services and their temporal relations: A case study in Northern Ningxia, China. Land Use Policy, 77, 163-173, DOI: 10.1016/j.landusepol.2018.05.022.

Makhrova A.G., Kirillov P.L. (2018). New Moscow: old and new features of social-economic development. In Old and New Moscow: tends and problems of development. IP Matushkin I.I. Publisher, 89-119.

Oke, T.R. (1982). The Energetic Basis of the Urban Heat Island. Quarterly Journal of the Royal Meteorological Society, 108, 1-24, DOI: 10.1002/qj.49710845502.

Privezentseva S.V., Tesler K.I. (2015). Features of Public Transport Availability Organization for Big Cities (on the Example of "New Moscow"). Proceedings of Moscow State University of Civil Engineering, 6, 115—123 (In Russian).

Romzaykina O., Vasenev V., Andrianova D., Neaman A., Gosse D. (2020). The Effect of Sealing on Soil Carbon Stocks in New Moscow. Springer Geography, 29-36, DOI: 10.1007/978-3-030-16091-3_5.

Rysin L.P., Saveleva L.I., Rysin S.L. (2004). Forest monitoring in urbanized areas. Russian journal of ecology, 4, 209-213.

Sarrat C., Lemonsu A., Masson V. and Guedalia D. (2006). Impact of urban heat island on regional atmospheric pollution. Atmospheric Environment, 40, 1743-1758.

Shishov L., Voinovich N. (2002). Soils of Moscow Region and Their Use. Dokuchaev Soil Science Institute, Moscow.

Sivtsov I.A. (2014). Economic approval behind establishing boundaries and extents of new territories of Moscow city. PhD thesis in economy and land planning, Moscow.

SniP II-60-75**. Building codes and regulations. Design standards. Planning and construction of cities, towns and rural settlements.

Tan D. S. H., Ang Y., Lim G. S., Ismail M. R. B. and Meier R. (2010). From 'crypticspecies' to integrative taxonomy: an iterative process involving DNA sequences, morphol-ogy, and behaviour leads to the resurrection of Sepsis pyrrhosoma (Sepsidae: Diptera). Zoologica Scripta, 39, 51–61, DOI:10.1111/j.1463-6409.2009.00408.x.

Turner BL II. (2002). Toward integrated land-change science: Advances in 1.5 decades of sustained international research on land-use and land cover change. Challenges of a Changing Earth. Berlin: Springer, 21–26.

U. N., Department of Economic and Social Affairs, Population Division (2014). World Urbanization Prospects: The 2014 Revision, Highlights (ST/ESA/SER.A/352).

Vasilev O.D., Chistov S.V. (2016). The study and mapping of environmental functions of forests in New Moscow. Izvestiya vysshih uchebnyh zavedenij Geodeziya i aehrofotosemka, 60(5), 128–133 (in Russian).

Voogt J.A., Oke T.R. (2003). Thermal remote sensing of urban climates. Remote Sensing of Environment, 86, 370–384, DOI: 10.1016/S0034-4257(03)00079-8.

World Health Organization. (2014). Global status report on noncommunicable diseases. town-planning policy and construction complex of Moscow city. https://stroi.mos.ru/new-moscow

Tatiana V. Chernenkova[1]*, **Ivan P. Kotlov[2]**, **Nadezhda G. Belyaeva[1]**,
Olga V. Morozova[1], **Elena G. Suslova[3]**, **Michail Yu. Puzachenko[1]**,
Alexander N. Krenke[1]

[1] Institute of Geography, Russian Academy of Sciences, Staromonetniy pereulok 29,
Moscow, 119017, Russia
[2] Severtsov institute of ecology and evolution, Russian Academy of Sciences,
Leninsky ave. 33, Moscow, 119071, Russia
[3] M.V. Lomonosov Moscow State University, Leninskie Gory, Moscow, 119991,
Russia
* Corresponding author: chernenkova50@mail.ru

SUSTAINABLE FOREST MANAGEMENT TOOLS FOR THE MOSCOW REGION

ABSTRACT. The paper presents an inventory of current forest formations and a map of forest vegetation in the Moscow region. To assess current forest formations, an approach integrating both ground- and remote sensing data was applied. The transformation of forests in the Moscow region was evaluated by the criteria of changing the quality, quantity and spatial configuration of forests, in accordance with the model SLOSS (Single Large or Several Small). The conceptual model "Pressure-State-Response" (hereinafter PRS) was used to develop appropriate tools for sustainable environmental management in the region. The use of this model made it possible not only to assess the state of forests but also to determine the main impacts affecting them, as well as the effectiveness of measures aimed at optimizing environmental management regimes in order to maintain forest biodiversity. Complex assessment of sets of indicators for each group of PRS criteria is performed for the integrated multicriteria assessment of sustainable forest management within the boundaries of urban districts. The average normalized score was calculated for each group of criteria. Correlation between the scores of the groups of criteria evaluated and classification of administrative units according to the ratio of groups of the K-means method criteria performed. As a result of component-by-component evaluation, the values of indicators are presented in form of tables and map charts. Benchmarking of Specially Protected Natural Area (SPNA) system and reforestation activities is performed regarding to the forest biodiversity conservation in the urban districts. It is shown that single integrated assessment of the ecological value of the territory (the "State" criterion), an integrated assessment of impact factors (the "Load") and appropriate actions to maintain forest biodiversity (the "Response" criterion) can be considered as an expression of generalized information directly used in decision-making and assessment of current trends for a particular region.

KEY WORDS: Moscow region, forest biodiversity, sustainable management, anthropogenic impact, specially protected natural areas, reforestation

INTRODUCTION

The problem of a sustainable combination of anthropogenic activities with the environment for the Moscow region is extremely urgent. Sustainable forest management means the management of forests in such a way as to ensure their biological diversity, productivity, renewal, viability, as well as environmental, economic and social functions (Ministerial conference 1993). The proximity to large urban clusters inevitably leads to a change in the natural properties of forests, while their importance for the city is extremely high. In general, the transformation of forests in conditions of long-term economic impact in accordance with the SLOSS model (Single Large or Several Small) occurs in different directions (Diamond 1975; Ovaskainen 2002; Ovaskainen 2012) (Fig 1).

Forest ecosystems of the Moscow region have been affected by deep anthropogenic transformations since the 16th century, and the decline in the quality of forest cover in the region occurred in all directions with different intensity for different periods of its history. Zonal broad-leaved and coniferous forests have been replaced by secondary mostly small-leaved forests, thus there has occurred a change in biodiversity and a decrease in the resistance of ecosystems to external damaging factors. Recently, the region has been characterized by massive outbreaks of bark beetle in spruce plantations, intensive urban development, cottage construction, and recreation. As a result, active economy, including widespread forest plantation practice, has significantly changed the ecological and coenotic range[1] of zonal[2] coniferous and broad-leaved forest communities. Today's forests in the Moscow region are distinguished by a number of features: a significant recreational pressure due to the high population density; limited purpose use of forests (in accordance with the Forest Code of the Russian Federation forests belong to the protection group); poor sanitary condition and unstable ecological situation caused by a lack of regulatory sanitary measures.

The wide experience in studying of typological diversity of forest communities and their dynamics is saved up for the forests
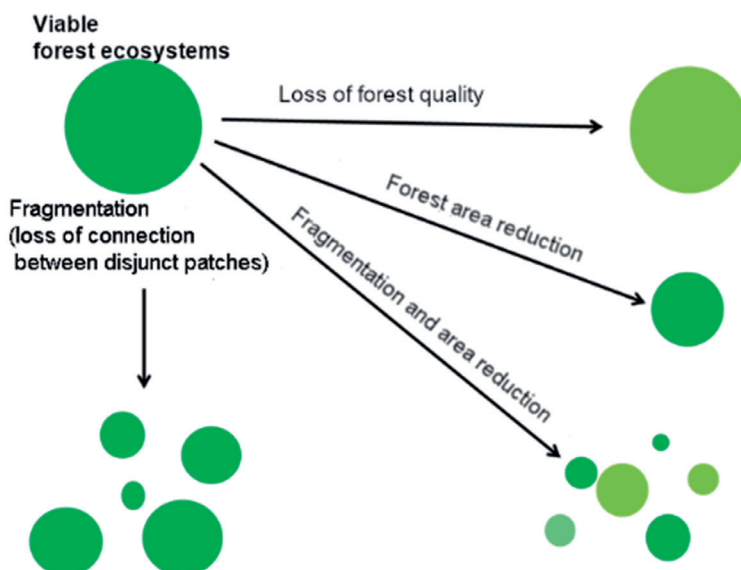
Fig. 1.Trends of forest changes at the regional level (Ovaskainen 2002; Ovaskainen 2012 as modified)

[1]Coenotic range – belonging to a typological unit
[2]Zonal – communities which occupy uplands natural areas (well-drained plains or watersheds) on soils of medium grain-size composition (sandy loam or loam).

Tatiana V. Chernenkova, Ivan P. Kotlov et al.   SUSTAINABLE FOREST MANAGEMENT ...

04|2019

37 GES

of the Moscow region (Konovalov 1929; Byazrov et al. 1971; Kurnaev 1968; Forests 1982; Forests 1987; Forests 1985; Dynamics 2000; Rysin and Savelieva 2007). The map of vegetation of the Moscow region is developed (1:200 000 scale, ed. by Ogureeva 1996) which is based on the materials of forest inventory data and field research. Later, the list of community types used for the "Explanatory text and map legend" (Ogureeva 1996) was significantly revised and supplemented (Suslova 2019).

A number of papers dedicated to the environmental and socio-economic prospects of New Moscow development are known (Komarova 1997; Golubchikov 2012; Makhrova et al. 2013; Kuricheva 2014; Lurie et al. 2015; Ataev-Troshin 2017; Nefedova 2017). Economic assessments of ecosystem services in the strategies of socio-economic development in the implementation of individual megaprojects are known (Economy of biodiversity conservation 2002; Ecological and economic index... 2012). The existing losses of ecosystem services of natural landscapes are calculated for the territory of Moscow (New Moscow with an area of about 160 thousand hectares) which amount to about 10 trillion rubles (Tishkov 2014).

Despite the long history of studies in the region, the assessment of the current state of forests in the Moscow region is still not developed, and there are questions unanswered left in relation to the dynamics of forests and the possibility of forecasting their environmental and recreational potential. Available information is limited to the Forestry Committee of the Moscow region's annually updated data on the areas covered by the main types of forest stands of different age classes on designated forest lands and lands of defense and security. The lack of up-to-date information on the structure and composition of the Moscow region forest cover makes it impossible to assess the current state of forests and their respective socio-environmental functions. This information should also include regularly updated digital maps of typological forest diversity.

The purpose of this work is to inventory the current typological forest compositions and to develop tools for sustainable environmental management in the Moscow region. The first part of the study is performed with modern digital technologies, including modeling. The second part is based on the conceptual model "PRS" (OECD 1993).

Present study is the follow-up of the approach based on the system of indicators of forest state assessment of the Moscow region (Levitskaya and Chernenkova 2012). It is also follow-up of studies on the identification of the forests typological composition in the region performed by Chernenkova et al. (2015; 2018; 2019).

MATERIAL AND METHODS

In selecting the best tools for sustainable environmental management, the PSR model not only assesses the state of forests, but also determines the main impacts on them, as well as the effectiveness of measures aimed at optimizing environmental management regimes to maintain forest biodiversity. In accordance with the criteria of the model, we propose to perform a component-by-component assessment of the main indicators in relation to urban districts of the Moscow region – units of municipal management according to the reform of 2019. Table 1 contains the list of criteria and indicators for forest management, used to assess forest condition and processes – the pressure and response measures to maintain forest biodiversity. Finding the relationship between the Pressure, State and Response components of the model forms a mechanism to maintain a certain quality of forest cover.

When formulating a set of indicators, we proceeded from the following requirements: 1) consistency with the list of the main criteria and indicators generally accepted in national and international practice;
2) the possibility of obtaining official statistics;
3) the possibility of obtaining data and processing them using independent sources (field- and remote sensing data);
4) the possibility of obtaining quantitative

Table 1. Criteria and indicators of forest management in the Moscow region

Criteria	Indicators
Pressure – effects of natural and anthropogenic factors on forest cover	The area of forest- and tree cover loss (ha) as a result of construction, logging, fires, pest and forest diseases, adverse weather conditions, etc.
	Built-up area (ha)
	The overall impact on the forest (the ratio of human population to the area of urban district (persons/km^2))
	Agricultural land area (ha)
	Environmental pollution (emissions (tonnes))
State of forest cover	Typological diversity (the proportion of nominally primary forests (%))
	Forest area (ha)
	Spatial structure of forest cover (fragmentation metrics of area (ha), shape, proximity (m))
Response – measures to maintain forest biodiversity	Area (ha) and number of SPNA
	Reforestation (ha) (natural and plantation)

estimates and calculating complex indicators of environmental value for the territory.

The resulting list of the main forest cover indicators corresponds well with the conceptual approach of assessing their transformation in three main areas – changes in their quality, quantity and spatial configuration reflected in the SLOSS model (Fig. 1).

The values of the indicators were evaluated within the urban districts, with the estimated values of the parameters converted into a unit area or presented in absolute units. All variables are given equal weight because there are no generally accepted priorities in ranking the parameters.

Condition of forest cover

Inventory of typological diversity of the forest composition is an important step towards identifying the conditions of sustainable environmental management. To assess the current composition of forest cover, an approach integrating ground and remote sensing data was applied.

The analysis used the results of field descriptions (about 1500 geobotanical descriptions on the area of 400 m^2). The localization of the points is related to the surface coverage of habitats, heterogenity in vegetation composition, soil composition and origin of rock material. Land cover types not presented in the descriptions (agriculture fields, water bodies, human settlements) were added to the training sample, based on visual analysis of the remote sensing data. Thus, about 2500 more points used in the training sample were obtained.

The analysis of spatial distribution patterns of selected syntaxons and their cartographic mapping, consisted in interpolation of vegetation classes to the upper-scale levels, by relating the training sample to remote sensing data and a digital elevation model (DEM) (Puzachenko et al. 2014; Chernenkova et al. 2018). The forest formation[3] was the basic unit to be mapped, and was used as a grouping variable for multivariate analysis

[3]*Formation - the unit of classification, which is defined by the edificator of the tree layer and it includes indication dominant species of trees.*

of multispectral images. Data from Landsat satellites (TM, ETM+, OLI and TIRS sensors) and SRTM v3 data, as DEM, were used. The methodology used is covered in more detail in earlier publications (Puzachenko at al. 2014; Chernenkova et al. 2015; Puzachenko and Chernenkova 2016).

On the basis of the developed forest cover map, the area and the proportion of nominally primary forests were estimated within the urban districts.

Informative indicators of the quality of forest cover are landscape-ecological metrics of fragmentation of forest stands (McGarigal et al. 2012). To determine effective indicators the metrics were calculated by urban district. A comparative study of their correlation tables was carried out. As a result, for further analysis, three most simple and informative indicators were selected – the metric of the patch (an area of homogenous forest type located on relatively homogenous soil type and homogenous form of relief) area, the diversity of the patch shape, and the patch isolation.

The average patch area is the basic indicator of fragmentation for any spatial units. To calculate the metric in the context of urban districts, the area-weighted average was used. Emphasizing the importance of larger patches, the weighted average calculation of the metrics focuses on the characteristics of the forest area as a whole, rather than forest patches (with simple averaging) (Jaeger 2000).

A number of studies have shown that shape metrics (shape index, perimeter/area ratio, contiguity etc.) are indicators of many environmental processes, in particular, the intensity of seed propagation and overgrowth (Hardt and Forman 1989), affect the migration and foraging strategies of forest animals (Forman 1986; Buechner 1989). The main feature of the shape metrics is the indication of quantity and quality of ecotones, edges and boundary habitats. Shape index (SI) is the most simple and straightforward indicator of complexity of the contours (Fridland 1972; Patton 1975).

$$SI = \frac{0.25\, p_{ij}}{\sqrt{a_{ij}}}$$

where p_{ij} is the perimeter of the patch; m, a_{ij} is the area of the patch, m². The metric value varies from 1 (for a square shape) to infinity. In contrast to the simple perimeter/area ratio, the shape index is not sensitive to the size of patches.

Aggregation metrics show the degree of fragmentation and mutual mixing of different classes of vegetation among themselves – formations in our case. In particular, isolation of forest patches is the simplest metric associated with the theory of island biogeography (MacArthur and Wilson 1967) and the theory of metapopulations (Levins 1970). It is shown that isolation of local subpopulations affects the state of metapopulation and is critical for habitats of protected species (Lamberson at al. 1992; McKelvey et al. 1992). Isolation is measured as the euclidean nearest neighbor (ENN) distance between the closest to each other patches of the same type.
$ENN=h_{ij}$, where h_{ij} – distance (m) from patch $_{ij}$ to nearest neighboring patch of the same type (class), based on patch edge-to-edge distance, computed from cell center to cell center.

Pressure – effects of natural and anthropogenic factors on forest cover

To identify the main types of pressure on natural habitats (Table 1) official statistics for 2007-2018 (Federal State Statistics Service 2019), data obtained from remote sensing surveys were used as sources of information. In particular, information from large-scale global remote sensing survey (based on Landsat satellite data (Hansen et al. 2013) was used to estimate the area of forest cover loss and gain in the period 2000-2012). The main part of the study was carried out in 2013, but the clarification and annual update occurs annually.

Response – measures to maintain forest biodiversity

The size of SPNA is a priority parameter in assessing the sustainability of forest

management (The Ministerial… 1993; Montreal… 1995), because only protected areas provide possibility of effective conservation of species and ecosystem diversity, creating conditions for the spontaneous flow of natural environmental processes. In SPNA nominally primary and secondary forests of different types were described on 450 sample plots. A comprehensive assessment of sets of indicators for each group of criteria PSR was performed for an integrated multicriteria assessment of sustainable forest management within the borders of the urban districts. Each indicator in the group was normalized to scores from 0 to 1, and the average normalized score was calculated for each group of criteria. Correlation between scores of groups of criteria were estimated, classification of urban districts was performed on a ratio of groups of criteria by K-means method. The indicator values, resulting from component-by-component assessment, are presented in form of tables and map charts.

Multivariate statistical methods were employed in data processing using the software packages STATISTICA and IBM SPSS Statistics (correlation, regression and discriminant analyses). The standard ArcMap

software products were the means of geoinformation analysis and visualization of the results.

RESULTS

In accordance with the adopted methodological approach, reflecting the causal relationship between impacts and changes in forest cover, the following results were obtained on the main indicators of State, Pressure and Response.

State of forest cover

Typological composition of forests. The forests on the sample plots were classified to 18 syntaxons at the level of formations. The results of interpolation of forest vegetation classes by discriminant analysis allowed to estimate the diversity of forest cover throughout the region and to develop a map of vegetation cover (Fig. 2). Here and elsewhere according to the tradition of Russian geobotany, forestry and dendrology under small-leaved we mean birch, aspen, alder, and under broad-leaved we mean oak, lime, maple, ash.

51% of the Moscow region is forested, and 40% of the forest area is predominated

1 spruce forest (with isolated birch and aspen)
2 spruce forest with oak and lime
3 spruce forest with pine
4 spruce forest with small-leaves
5 pine-spruce forest
6 pine forest (with spruce and birch)
7 pine forest with lime, oak and hazel
8 oak forest with lime, spruce and birch
9 lime forest with oak
10 lime forest with spruce and birch
11 broad-leaved forest with spruce
12 birch forest with spruce and aspen
13 birch forest with oak and lime
14 aspen forest with spruce and oak
15 gray alder forest
16 black alder forest
17 small-leaved scrub
18 clearing
19 meadows
20 open land and wetland
21 willow shrub
22 agriculture
23 water bodies
24 settlements

Fig. 2. Map of forest formations in the Moscow region

by small-leaved species. The main forest forming small-leaved species are birch (*Betula pendula, B. pubescens*), aspen (*Populus tremula*), gray alder (*Alnus incana*), and willow (*Salix* spp.). The vast majority of small-leaved forests are secondary succession from coniferous, broad-leaved – coniferous and broad-leaved forests. Typological diversity of small-leaved forests is quite high, due to the variability of landscape conditions and a wide range of forests at different succession stages. Primary forest communities of alder (*Alnus glutinosa, A. incana*) and white willow (*Salix alba*) exist in riparian habitats, floodplains and in wetlands.

Spruce small-leaved communities are presented by a short-secondary succession of forests formed on-site from small-leaved forests. This type of community has very diverse understorey, including boreal species *(Oxalis acetosela, Rubus saxatilis, Gymnocarpium dryopteris, Maianthemum bifolium, Orthilia secunda, Pleurozium schreberi, Hylocomium splendens, Rhytidiadelphus triquetrus*) which combine in different proportions with nemoral species (*Carex pilosa, Galeobdolon luteum, Asarum europaeum, Pulmonaria obscura, Athyrium filix-femina, Ranunculus cassubicus, Aegopodim podagraria, Cirriphyllum piliferum, Eurhynchium angustirete*). The proportion of spruce – small-leaved forests within the total forest cover is 13%.

The compositions of spruce forests vary (combinations of spruce with birch, aspen, pine and broad-leaved species), and largely characterize the compositions of primary forests in the coniferous – broad-leaved zone. The proportion of plantations is high (mainly spruce mono cultivation). The understorey vegetation ranges from boreal to nemoral species compositions. The structure of spruce forest of the boreal group (small-herb-green-moss and green-moss) shows up a relatively small number of types of communities, while subnemoral (small-herb – broad-leaved herb) and nemoral (broad-leaved herb) groups of spruce forests have larger coenotic diversity. This is both due to the greater presence of other tree species, and to the diversity in ground cover

dominant species. The total area of spruce forests is 12%. The area of distribution of boreal small-herb – green-moss spruce forests is small (about 1.5%) with their predominance in the North-Western part of the region. Spruce forests with broad-leaved herb have the largest distribution and equals more than half of the total spruce forests area. This type also has a high proportion of plantation spruce trees.

Pine and pine-spruce forests on watershed surfaces are not fully primary communities and represent successional stages in in transition to more nature forests. The absence of pine regeneration in communities of automorphic (watershed[4] located) habitats indicates the origin of pine forests after fires and cutting, as well as in plantations. In one case, restoration is accompanied by active regeneration of spruce forests; in another case on rich soil – broad – leaved species, which supersede pine and pine-spruce communities within a few decades. A small proportion of pine forests will remain on the steep slopes of river valleys due to pine-friendly environmental conditions (light sandy soils with good drainage) with constantly maintained recreational effects, as well as in hydromorphic (peatbog) conditions. On the dry and poor sandy soils of Meshchera physiographical province (on the East of the region) there are areas of natural lichen-green-moss pine forests with *Calluna vulgaris, Convallaria majalis, Pulsatilla patents, Chimaphila umbellata, Jovibarba globifera, Veronica incana*. In the sub-latitudinal direction, as in the case of spruce-small-leaved, spruce-broad-leaved and spruce forests, there is a different ratio of communities with a predominance of plant species of the boreal, subnemoral and nemoral layer in the understorey. The total forest area with pine communities in the Moscow region is about 15%.

Forests with broad-leaved species retained the main features of pimary broad-leaved coniferous forests – mixed species composition, multi-storey forest structure and rich species composition. Spruce – broad-leaved forests with broad-leaved

---

[4] *Watershed is an elevated terrain that separates neighbouring drainage basins*

herb communities are characterized by a close proportion in the ratio of spruce and broad-leaved tree species (oak, lime and maple) in the upper understorey of the forest. The largest area of distribution of patches of broad-leaved – coniferous forests is located in the Central and Western parts of the study area, while the southern part is dominated by broad-leaved forests, which confirms the zonal transition on the Pakhra river (Petrov 1968) from broad-leaved – coniferous forests to broad-leaved ones. The latter are represented by oak, lime-oak and broad-leaved herb lime forests, often mixed with maple. Oak forests typically have a constant presence of *Corylus avellana* (coverage about 30%) in the understorey, other shrubs are rare. In the herb layer there are common broad-leaved herb species – *Galeobdolon luteum, Aegopodium podagraria, Asarum europaeum, Carex pilosa, Ajuga reptans, Geum rivale, Pulmonaria obscura*. In lime forests hazel is less frequent compared to oak forests in terms of presence cover (average 8%). *Euonymus verrucosa* is quite often occurs in lime forests. The herb cover is dominated by *Carex pilosa, Aegopodium podagraria, Galeobdolon luteum, Pulmonaria obscura*, rarely – *Mercurialis perennis*.

South of the Osetr river in the watersheds in several SPNA the primary broad forests are composed by oak, lime, maple, elm and ash, with shrubs (*Corylus avellana, Lonicera xylosteum, Euonymus verrucosa*) with broad-leaved herbs. In addition to the typical nemoral species here are also found *Corydalis marschalliana, Dentaria quinquefolia* and *Allium ursinum*. The undergrowth of *Acer campestre* is common in these forests. On the slopes of the river valleys the shrubby steppe oak forests with thorns and cherries occur.

In general, when a fairly arbitrary division of a nominally[5] primary and secondary forests is made, the secondary ones slightly dominate. The distribution of these two forest categories by area is presented in table Eq. (A. 1).

The number of forest species listed in the Red book of the Moscow region.

The third edition of the Red Data Book of Moscow region includes 675 species of flora and fauna which need special protection measures. This includes 300 objects of flora: 206 species of vascular plants, 25 species of moss, 3 species of algae, 40 species of lichens and 26 species of fungi (Red Data Book 2018). There are more than 400 forest dependent species – among them representatives of fauna, plants, fungi and lichens. The distribution of protected forest species among urban districts varies widely. It should be taken into account that the number of such species is related not only to the degree of preservation of species diversity in natural communities, including the rare and protected species, but also it is directly dependent on biotopic and consequently cenotic diversity. An example of this is the representation of the maximum number of protected forest species in the Serpukhov urban district (200 taxa), associated with the presence of complex pine forests, coniferous – broad-leaved and broad-leaved forests, wetlands and forest-steppe communities on the terraces of the Oka river and species protected within Prioksko-Terrasny state biosphere reserve. Good knowledge of protected ecosystems is also an important factor Eq. (A. 1).

The structure of forest cover (landscape metrics). The size of weighted average patch area in urban districts varies from 89.8 ha (Khimki) to 52966 ha (Serebryanye Prudy). The size of the region's weighted average patch area is equal to 606.9 ha.

The range of shape index is from 2.06 (Khimki) to 16.57 (Zaraisk). The weighted average shape index in the region is 3.39. Urban districts with the most fragmented forests (according to the shape index) are Naro-Fominsky, Solnechnogorsky, Shchelkovsky, Pushkinsky, Mytishchi, Istra, Ruzsky, Krasnogorsk and Odintsovsky. The most diverse shape index of forest patches are found in the urban districts Kashira and Serebryanye Prudy.

[5] *nominally primary community - human influenced in the past, but restored to its most essential properties (floral composition, storey structure, environmental conditions).*

Tatiana V. Chernenkova, Ivan P. Kotlov et al.   SUSTAINABLE FOREST MANAGEMENT ...

04|2019

43 GES

Isolation metric (the shortest distance between homogeneous forest stands) varies from 209 m (Zaraisky) to 257 m (Ruzsky). The smallest isolation is typical for urban districts of Kolomensky, Lukhovitsky and Serebryanye Prudy. The largest isolation is typical for the Istrinsky and Moscow. Weighted average isolation for the region is 233.5 m.

Pressure – effects of natural and anthropogenic factors on forest cover

Deforestation and natural disasters. Forests in the Moscow region are periodically exposed to natural disasters: fires, pests, adverse weather conditions and diseases according to Review of the forest pathology and sanitary condition of forests in the Moscow region (2009; 2010). Wood harvesting practiced by commercial felling in mature and overmature stands by sanitary cutting of dead and damaged forest stands; by clearing forest for construction of roads, pipelines, and so on. More than half of the wood volume is currently harvested through non-commercial fellings (mostly sanitary clear cuttings). In this regard, the issue of attributing the factor of "cutting" to the group of indicators "impact" becomes controversial, since the main purpose of cuttings should be aimed at maintaining the stability of forest ecosystems. In reality, mainly coniferous forests that have reached the age of technical maturity are subject to cutting. And overmature small-leaved trees are due to implementation difficulties not harvested, and remain as dying and dead wood in the forests, worsening their sanitary condition (Yakubov 2007). However, since the area of cuttings indirectly reflects the amount of damaged forests, the table Eq. (A. 1) gives the area of forest losses for the period 2001-2012.

Development and recreation. The negative impact of urban development (both civil and industrial) is primarily due to the direct rejection of natural land for economic needs, resulting in the disturbed continuity of natural space, destroyed habitats cenopopulations[6] of animals and plants. According to the dynamics of built-up areas

in the urban districts in 1992-2008 (The Nature 2009), the biggest increase (4-7%) was through cottage development near the capital, in the urban districts of the Central sector of the Moscow region.

Over the past five years since the expansion of its borders, the population density of Moscow has not changed, while in the Moscow region, as in the annexed territories, it has increased. In New Moscow, the population density increased by more than 30% (in Novomoskovsk – 37%, in the Troitsky district – almost 25%). The most significant growth was observed in the Moskovsky and Vnukovsky municipalities, which actively built up thanks to its proximity to the core of the region, the availability of territorial resources and the development of transport infrastructure. Less significantly, the population density increased in the settlements of Kievsky, Sosenskoye, Troitsk and Shcherbinka: the population of these territories increased by 30-50% (Makhrova and Kirillov 2018).

A relatively new type of anthropogenic impact on the natural habitats in the region is the lease of forest areas for recreational purposes. Leasable areas can be delimited by very solid fences that impede wildlife migration. In addition, the list of permitted construction projects on forest lease plots is wide and allows to doubt in the longlivety of the forest in the territory. The most attractive lease areas are those near Moscow city, where the proportion of leased forests is more than 8% of the total forest area in the urban districts. The total proportion of built-up land is shown in the table Eq. (A. 1).

The ratio of the human population to the area of the urban district indirectly characterizes the recreational pressure on forest ecosystems and is conventionally called the total impact on forests Eq. (A. 1). In the last decade, the overall impact on forests, through the population density, has been increasing consistently and in 2018 averaged 347 people/km^2 (Federal State Statistics Service 2019).

---

[6] *Cenopopulation – assemblage of individuals of a species within one phytocenosis occupying a certain habitat.*

Agricultural lands occupy almost 1 449 thousand hectares according to Rosstat in 2008 (1 585 thousand hectares according to our map of the formation composition), which is more than a third of the region. This figure includes abandoned agriculture fields in the early stages of overgrowth. The intensity of agricultural land use in the urban districts of the region can indirectly be estimated by the area of agricultural land. The proportion of agricultural land is biggest in the Southern and South-Eastern parts of the region, and smaller in the Eastern, Northern and South-Western parts of the region Eq. (A. 1).

Environmental pollution is characterized by the total amount of pollutants from all stationary sources in 2017 ('000 tonnes) (Federal State Statistics Service 2019). The distribution of the indicator is presented by urban districts in the table Eq. (A. 1).

Response – measures to maintain forest biodiversity

The area of SPNA. Intact forest ecosystems in the Moscow region are now preserved mainly in SPNA. Totally Federal SPNA occupy an area of 70.9 thousand hectares, which is 1.5% of the Moscow region, and regional SPNA – about 178.0 thousand hectares (3.9% of the Moscow region (Smirnova and Levitskaya 2018). SPNA of regional significance are located in all physiographic provinces in the territory of the Moscow region. SPNA are represented in almost all urban districts of the Moscow region, excluding Khimki and Kashira. Mainly undisturbed coniferous, deciduous-coniferous, deciduous and small-leaved forests are protected within the territory of 246 regional SPNA. The table Eq. (A. 1) shows the distribution of the ratio of the protected area of the total area of the urban district.

Over the years since the approval of the Layout of Development and Location of Specially Protected Natural Areas in the Moscow region in 2009, there have been several important events that led to changes in this document. In particular, the boundaries of the city of Moscow were expanded in 2012, in connection with which

7 regional SPNA located in the annexed territories were deprived of their protective status. Several new SPNA with a total area of about 12.5 hectares are included in the new edition of the Laouyt (resolution of the Government of Moscow region from 27.06.2017 No. 535/22 with changes in 28.01.2019). 20 new SPNA of previously planned are created during 2009 to 2019.

As a result of the planned reforms, including the creation of several large natural parks, the area of SPNA of regional importance will increase significantly: in the future 2020, together with Federal SPNA, it will occupy about 15.5% of the territory of the Moscow region.

Reforestation is a system of forest management activities that contributes to maintain sustainable forest management, especially for areas with active anthropogenic transformation of the natural environment. According to official statements (Federal State Statistics Service 2019), the forest cover increased with 53 000 ha from 2000 to 2009 (Levitskaya and Chernenkova 2012). An independent reforestation assessment based on remote sensing shows an increase of 50 000 ha from 2000 to 2009. Data from our study are generally consistent with the official statistics, and difference can be explained by unsufficient regeneration measures and, consequently, not full survival rate. At the same time, natural afforestation of meadows and arable lands tripled in recent decades, while the area of cropland decreased to half (Federal State Statistics Service 2019). On the first of January 2009, there were 288 thousand hectares of croplands in the region.

The highest rates of reforestation are observed in the urban districts of Dmitrovsky, Klin, Mozhaisk and Shatura (3.9 – 5.5 thousand hectares for the period 2000-2012). The urban districts'reforestation areas for the period 2001-2012 are reflected in table A. 1.

Integrated estimation

The integrated assessment of the state of forests in the urban districts of the Moscow region was carried out according to the following indicators: forest area, proportion of

Tatiana V. Chernenkova, Ivan P. Kotlov et al.   SUSTAINABLE FOREST MANAGEMENT ...

04|2019

45 GES

forest area in the urban district, the proportion of forest area that is nominally primary, weighted average indices: patch area, shape index and isolation.

Within the boundaries of the urban districts in the region, five classes of forest condition are allocated according to their ecological value, where 5 corresponds to the maximum ecological value and 1 is the value for minimum ecological value. Urban districts with the most valuable forests are concentrated on the North and East of the Moscow region. Egoryevsk, Shatura and Taldomsky have a maximum score of 5. Klin, Sergiev Posadsky and Dmitrovsky districts have a score of 4 (Fig. 3). The most disturbed (highly fragmented, small in area and represented by long-term small-leaved plantations) are forests of forest-steppe subzone and crop production – Zaraysk, Kashira, Serebrianye Prudy and Lukhovitsky. The unsatisfactory state is typical for urban districts adjacent to the axes of the South-Eastern transport corridors – Ryazan and Kashira roads – probably due to active urban development in the last decade. To this group the West-North-West part of the region – Volokolamsky, Lotoshinsky and

Shakhovskaya districts – historically the zone of meat and dairy cattle breeding.

"New Moscow" (# 40), as seen from the map (Fig. 3), has indicators of the integrated environmental value of forest cover which means quite good state of forest.

Pressure

The assessment of anthropogenic pressure on the forests was carried out by the following indicators: amount of pollutants released into the environment; recreational pressure; the proportion of built-up land; the proportion of farmland; loss of forest. 5 classes of intensity of pressure are allocated (Fig. 4), where 5 corresponds to the maximum forest pressure and 1 is the value for minimum pressure.

The most unfavorable situation is in urban districts of Lyubertsy, Khimki and Voskresensk. In Lyubertsy and Khimki the highest pressure factor is from the high population density for the region (about 2500 people/km^2). In Voskresensky district the reason for the high pressure is due to very high emissions of pollutants from chemical industry (653

1 Balashiha	11 Klin
2 Bogorodsky	12 Kolomensky
3 Volokolamsky	13 Krasnogorsk
4 Voskresensky	14 Leninsky
5 Dmitrovsky	15 Lotoshinsky
6 Domodedovo	16 Luhovitcky
7 Egoryevsk	17 Liubertsy
8 Zaraisk	18 Mozhaisk
9 Istra	19 Mytishchi
10 Kashira	20 Naro-Fominsky
	21 Odintsovsky
	22 Ozery
	23 Orehovo-Zuevo
	24 Pavlovskii Posad
	25 Podolsk
	26 Pushkinsky
	27 Ramensky
	28 Ruzsky
	29 Sergievo-Posadsky
	30 Serebrianye Prudy
	31 Serpukhov
	32 Solnechnogorsky
	33 Stupino
	34 Taldomsky
	35 Khimki
	36 Chekhov
	37 Shatura
	38 Shakhovskaya
	39 Shchelkovsky
	40 Moscow

Scores of state
- 1 - significantly disturbed
- 2 - disturbed
- 3 - average state
- 4 - good state
- 5 - most valuable

Fig. 3. Distribution of forest State indicators in the urban districts of the Moscow region

thousand tons). In the East – South-East part of the region (Lukhovitsky, Orekhovo-Zuyevo, and Shatura) the pressure is mainly due to significant losses of forest resources (10-15 thousand. ha for the period 2001-2012), which was probably caused by drought and fires in 2010, which were especially strong in this region. The lowest pressure is found in the Dmitrovsky district and in "New Moscow" (only the loss of forests was considered). Despite the increasing pressure on the ecosystems of the New Moscow in recent years (the growth of multi-storey and cottage housing, as well as a intensive road constructions), the "Pressure" indicator does not have the expected high value due to the fact that the territory of New Moscow stretches far in the South-West direction up to the borders with the Kaluga region. In general, most of the urban districts are exposed to medium or below average level of anthropogenic pressure.

Response

The response criterion contains information on the increase in forest area and presence of SPNA in urban districts (total area of SPNA, their number and the proportion of the total area). 5 classes of response were allocated (Fig. 5), where 5 corresponds to the highest response and 1 is the value for lowest response. Best response to pressure is found in Shatura district where almost close-to-maximum values are observed in all response indicators (more than 5 thousand hectares of the territory are reforested in 2001-2012, the highest area of SPNA (47 objects, which make up almost 20% of the urban district). Remote North-West urban districts have average or above average response scores: there are many active affoforestation processes and big area of SPNA.

Districts located near Moscow and within the strip to the South-East are characterized by the lowest level of response due to the small area of SPNA and little reforestation activities. One of the reasons for the little afforestation in this zone is the favorable cropping conditions, and thus less common to see abandoned agriculture fields. The area with high level of response is 5 times smaller than the area with low response.

Criteria interconnection

With the diversity and interaction of external factors affecting forest ecosystems in the region, it is important to assess the significance of their impact on the quality of forest cover.

1 Balashiha
2 Bogorodsky
3 Volokolamsky
4 Voskresensky
5 Dmitrovsky
6 Domodedovo
7 Egoryevsk
8 Zaraisk
9 Istra
10 Kashira
11 Klin
12 Kolomensky
13 Krasnogorsk
14 Leninsky
15 Lotoshinsky
16 Luhovitsky
17 Liubertsy
18 Mozhaisk
19 Mytishchi
20 Naro-Fominsky
21 Odintsovsky
22 Ozery
23 Orehovo-Zuevo
24 Pavlovskii Posad
25 Podolsk
26 Pushkinsky
27 Ramensky
28 Ruzsky
29 Sergievo-Posadsky
30 Serebrianye Prudy
31 Serpukhov
32 Solnechnogorsky
33 Stupino
34 Taldomsky
35 Khimki
36 Chekhov
37 Shatura
38 Shakhovskaya
39 Shchelkovsky
40 Moscow

Scores of pressure
1 - very low
2 - low
3 - average
4 - high
5 - highest

Fig. 4. Distribution of forest Pressure indicators in the urban districts of the Moscow region

Tatiana V. Chernenkova, Ivan P. Kotlov et al.   SUSTAINABLE FOREST MANAGEMENT ...

04|2019

47 GES

1 Balashiha
2 Bogorodsky
3 Volokolamsky
4 Voskresensky
5 Dmitrovsky
6 Domodedovo
7 Egoryevsk
8 Zaraisk
9 Istra
10 Kashira
11 Klin
12 Kolomensky
13 Krasnogorsk
14 Leninsky
15 Lotoshinsky
16 Luhovitcky
17 Liubertsy
18 Mozhaisk
19 Mytishchi
20 Naro-Fominsky
21 Odintsovsky
22 Ozery
23 Orehovo-Zuevo
24 Pavlovskii Posad
25 Podolsk
26 Pushkinsky
27 Ramensky
28 Ruzsky
29 Sergievo-Posadsky
30 Serebrianye Prudy
31 Serpukhov
32 Solnechnogorsky
33 Stupino
34 Taldomsky
35 Khimki
36 Chekhov
37 Shatura
38 Shakhovskaya
39 Shchelkovsky
40 Moscow

Score of response
- 1 - very low
- 2 - low
- 3 - average
- 4 - high
- 5 - highest

Fig. 5. Distribution of forest Response indicators in the urban districts of the Moscow region

To this purpose, the relationship between the main indicators of forest condition, pressure and response (Table 2) is considered. Pair correlations are calculated to assess the relationship between different criteria. Since not all distributions are normal according to the Kolmogorov-Smirnov criterion (the state and pressure criteria are rank type due to the nature of the measured parameters), Pearson and non pararametric Spearman correlations are used.

According to two correlation criteria, a significant relationship is observed between the state and response criteria (positive) and state and pressure (negative). The relationship between pressure and response is weak, unreliable, and has a negative sign.

Table 2. Pearson correlation coefficient and Spearman r between indicators of state, pressure and response

		Pearson correlation			Spearman r		
		Pressure	State	Response	Pressure	State	Response
Pressure	Correlation	1.0	-0.339*	-0.219	1.0	**-0.394****	-0.270*
	Significance		0.016	0.087		0.006	0.046
State	Correlation		1.0	**0.692****		1.0	**0.687****
	Significance			0.000			0.0
Response	Correlation			1.0			1.0
	Significance						.

* – significance level 0.05;
** – significance level 0.01

Integrated evaluation of the three groups of criteria

To rank urban districts according to the nature of the pressure, state and response ratio, the classification of administrative units was performed by the K-means method. Five classes and relationship of three groups of criteria are presented in Table 3 and Figure 6.

The calculated scores of the three criteria and the assignment to one of the 5 classes are given in Table 4.

Table 3. Classes of urban districts by three criteria

P-S-R class		Pressure	State	Response	Description
Class center	1	0.83	0.38	0.11	Low pressure. Average levels of state and response.
	2	0.51	0.18	0.06	Minimum pressure. Satisfactory state and response
	3	0.36	0.45	0.16	Average pressure. Highest level of state and response
	4	0.29	0.65	0.52	Low pressure. Average levels of state and response.
	5	0.55	0.83	0.86	Minimum pressure. Satisfactory state and response

1 Balashiha
2 Bogorodsky
3 Volokolamsky
4 Voskresensky
5 Dmitrovsky
6 Domodedovo
7 Egoryevsk
8 Zaraisk
9 Istra
110 Kashira
11 Klin
12 Kolomensky
13 Krasnogorsk
14 Leninsky
15 Lotoshinsky
16 Luhovitcky
17 Liubertsy
18 Mozhaisk
19 Mytishchi
20 Naro-Fominsky
21 Odintsovsky
22 Ozery
23 Orehovo-Zuevo
24 Pavlovskii Posad
25 Podolsk
26 Pushkinsky
27 Ramensky
28 Ruzsky
29 Sergievo-Posadsky
30 Serebrianye Prudy
31 Serpukhov
32 Solnechnogorsky
33 Stupino
34 Taldomsky
35 Khimki
36 Chekhov
37 Shatura
38 Shakhovskaya
39 Shchelkovsky
40 Moscow

Integral score
- 1 - very low
- 2 - low
- 3 - average
- 4 - high
- 5 - highest

Fig. 6. Distribution of integrated forest scores in the urban districts of the Moscow region

Tatiana V. Chernenkova, Ivan P. Kotlov et al.   SUSTAINABLE FOREST MANAGEMENT ...

04|2019

49 GES

Table 4. Urban districts ranking by three criteria

Urban districts	Criteria			Class
	Pressure	State	Response	
Balashiha	0.47	0.38	0.14	3
Bogorodsky	0.47	0.42	0.10	3
Volokolamsky	0.47	0.38	0.38	3
Voskresensky	0.94	0.26	0.11	1
Dmitrovsky	0.16	0.63	0.49	4
Domodedovo	0.43	0.28	0.02	2
Egoryevsk	0.48	0.81	0.72	5
Zaraisk	0.47	0.08	0.05	2
Istra	0.29	0.46	0.27	3
Kashira	0.71	0.02	0.02	2
Klin	0.37	0.66	0.59	4
Kolomensky	0.45	0.44	0.10	3
Krasnogorsk	0.55	0.32	0.04	2
Leninsky	0.49	0.26	0.01	2
Lotoshinsky	0.29	0.39	0.60	4
Lukhovitsky	0.63	0.11	0.22	2
Liubertsy	0.85	0.35	0.00	1
Mozhaisk	0.26	0.59	0.59	4
Mytishchi	0.36	0.42	0.12	3
Naro-Fominsky	0.40	0.51	0.19	3
Odintsovsky	0.73	0.53	0.14	1
Ozery	0.36	0.48	0.08	3
Orehovo-Zuevo	0.70	0.58	0.25	1
Pavlovskii Posad	0.35	0.41	0.12	3
Podolsk	0.38	0.21	0.03	2
Pushkinsky	0.32	0.45	0.07	3
Ramensky	0.51	0.32	0.07	2

Ruzsky	0.49	0.50	0.31	3
Sergievo-Posadsky	0.39	0.61	0.38	4
Serebrianye Prudy	0.41	0.00	0.11	2
Serpukhov	0.26	0.46	0.32	3
Solnechnogorsky	0.55	0.50	0.19	3
Stupino	0.25	0.51	0.09	3
Taldomsky	0.25	1.00	0.47	4
Khimki	1.00	0.18	0.00	1
Chekhov	0.25	0.42	0.05	3
Shatura	0.61	0.85	1.00	5
Shakhovskaya	0.74	0.39	0.17	1
Shchelkovsky	0.41	0.46	0.09	3
Moscow	0.40	0.51	0.16	3

In fact, the most optimal ratio of criteria is observed only in two urban districts – Egoryevsk and Shatura. Due to the remoteness and low pressure of the forest in the North and partly in the West – Dmitrovsky, Klin, Sergiev Posad, Taldom, Mozhaisk, and Lotoshinsky – are characterized by good integrated indicators, but for them there is already a decrease in the criteria of condition and response.

Separately, districts with the worst indicator values deserve attention. Among them there are adjacent to the Moscow district, Khimki, Liubertsy and Odintsovo, but also those in considerable distance to Moscow - Shakhovskaya and Orekhovo-Zuyevo.

In addition, unsatisfactory forest ranking is observed in other districts adjacent to Moscow – Krasnogorsk, Leninsky, Domodedovo, Podolsk and Ramensky. In the South similar forest ranking is obtained for Zaraysk, Kashira, Lukhovitsy and Serebrianye Prudy.

Drawing up the ratio of indicators in the form of a matrix of pressures and the state of forest ecosystems gives an idea of the forest distribution in the urban districts of the region, according to their state (environmental value), depending on the total pressure (Table 5). The districts with the most valuable forest ecosystems are located in the upper right corner of the matrix. It is in such forests that conditions are created for the preservation and functioning of intact forest ecosystems. The lower right corner of the matrix is occupied by Yegoryevsk and Shatura, whose forest ecosystems are characterized by high value and at the same time experience high anthropogenic pressures. In the lower left corner of the matrix there are districts, whose forests are subject to high anthropogenic pressures and severely damaged – Kashira, Lukhovitsky, Shakhovskaya, and Voskresensky.

Analyzing the matrix of correlation between the state of forest ecosystems and indicators of response (Table 6), it is possible to assess the effectiveness of the system of protection of natural areas and the need for other measures to maintain forest biodiversity in the urban districts of the Moscow region. In particular, in Sergiev Posad, located in the upper right corner of the matrix, where it is necessary to create new SPNA.

Table 5. Matrix of pressure and state of forest ecosystems in the urban districts of the Moscow region

Pressure	State				
	Significantly disturbed	Disturbed	Average state	Good state	Most valuable
Very low				Dmitrovskii	
Low		Lotoshinsky Podolsk	Istra Mozhaisk Mytishchi Moscow Naro-Fominskii Ozery Pavlovskii Posad Pushkinskii Serpuhov Stupino Chehov	Klin Sergievo-Posadskii	Taldomskii
Average	Zaraisk Serebrianye Prudy	Balashiha Volokolamskii Domodedovo Krasnogorsk Leninskii Ramenskii	Bogorodskii Kolomenskii Ruzskii Solnechnogorskii Shchelkovskii		Egorevsk
High	Kashira Lukhovitcky	Shahovskaia	Odintcovskii Orehovo-Zuevo		Shatura
Highest		Voskresenskii Liubertcy			

Reforestation activities are required in urban districts located in the upper left corner of the matrix. This is a fairly extensive list - urban district Zaraysk, Serebrianye Prudy, Kashira, Khimki, Podolsk, Balashikha, Domodedovo, Krasnogorsk, Leninsky, Ramensky, Shakhovskaya, Voskresensky, Lyubertsy and Lukhovitsky.

The system of SPNA effectively protects forest ecosystems in the urban districts of Dmitrov, Taldomsky, Klin, Yegoryevsk, and Shatura. These urban districts can be considered as model references.

To improve and maintain a proper quality of forest cover, the total area of SPNA should be increased in different natural provinces of the region, including large Natural parks in the West, North and East of the region. This includes also effective management of SPNA. Consolidation of existing SPNA and their component clusters, the identification of valuable forest communities and the creation of new SPNA, the organization of a network of ecological corridors, the real protection in the territory of zakazniks and nature monuments are also needed. It is not recommended to create high-density monocultures in SPNA during reforestation, and in existing middle-age plantations regular thinning is necessary for the introduction of other tree species, both small-leaved and broad-leaved. It is also recommended to identify areas where natural reforestation is preferable.

CONCLUSION

The assessment of current typological diversity of forests in the Moscow region and the territory of "New Moscow" on the basis of a joint analysis of both field- and remote sensing data is performed. As a result of the classification of forest vegetation of the study area, 18 syntaxons were allocated at the level of the formation composition of forests. An integrated assessment of the state of forest in the Moscow region and the territory of "New Moscow" using main forest management criteria and indicators, as well as the calculation of the dependence of indicators on different types of pressures for urban districts of the region carried out. The analysis of the efficiency of the existing system of SPNA and the process of reforestation in relation to the preservation of forest biodiversity in urban districts of the region is also performed.

It is shown that only two urban districts of the Moscow region have a balanced combination of state, pressures and response – Shatursky and Yegoryevsky. Another six districts, with minimal pressures, lack measures – reforestation and protection – to maintain forest biodiversity (the "response" criterion). These include Dmitrov, Klin, Lotoshinskiy, Mozhaisk, Sergiev Posad, and Taldomsky. The lack of response measures is observed not only for urban districts adjacent to Moscow, but also towards the West, East and especially the South of the region – Voskresensky, Shakhovskaya, Orekhovo-Zuevsky, Zaraysk, Kashira, lukhovitsky and Serebrianye Prudy.

The nature of the relationship between three forest management criteria was assessed. Positive relationship revealed between the indicators of "state" and "response", which shows up the trend of the conservation and rehabilitation of forests in forest-rich urban districts, while the most deforested regions are experiencing a shortage of measures for the protection of forests. This is confirmed by the nature of the relationship between pressure and response – weak negative and unreliable. A third set of criteria – the "state" and "pressure" is negatively connected. In fact, all three of the relationship suggests that the most valuable and intact forest areas have a minimum pressure and are secured by a network of SPNA and active process of forest regeneration. On the other hand, urban districts, whose forests are most fragmented and depleted, receive minimal conservation and reforestation support, and at the same time the burden on them obviously increases due to the pace of urban development and expansion of agricultural land. This fact shows a long-term imbalance in the management of forests and natural areas of the Moscow region. Among the likely short-term consequences there are the transition of forests from a state of natural forest to a more park-like state, which leads to the loss of natural stability and the ability of being sustained. This lead to an increase in the cost of their maintenance, which has to be paid by urban district budgets.

It is shown that a joint integrated assessment of the ecological value of the territory and an integrated assessment of the impact factors can be effective tool for decision support systems at the regional level. A characteristic feature of such system, built on the matrix of scores combination– neutralization of short-term market factors and focus on medium- and long-term planning of steps to manage the natural areas of a large region.

Assessment of factors of natural and anthropogenic impact, as well as their mutual combinations, there should be the main component of the regulatory measures on the environment with the justification of a maximum allowable value of the impact. However, due to far-from-complete elaboration of the relationship between definition of optimal ecological state of complex ecosystems and the allowable anthropogenic impact on them, it is hard to talk about finding the maximum allowable pressure loads (Yakovlev and Evdokimov 2011).

In the situation of multifactor impact on natural ecosystems the solution of this problem becomes much more complicated. In addition, there is no clear relationship between the degree of exposure to external factors and changes in biodiversity parameters. Moreover, examples of

increasing parameters of diversity in conditions of anthropogenic impact through allogeneic community's shifts were often recorded (Trubina and Vorobeychik 2012; Hansen et al. 1991; Ruotsalainen and Kozlov 2006; Zvereva et al. 2008; Diamond 1975; Ovaskainen 2002). Thus, within the framework of this study it is not possible to give a quantitative assessment of the maximum allowable pressure on forest ecosystems in the Moscow region without the developed criteria of the maximum allowable impact and the optimal state. The assessment of individual impact factors and their integrated values is a necessary step along the way. Therefore, an integrated assessment of the main factors impacting the forest in the region and an aggregation of these using the method of scoring is recommended.

ACKNOWLEDGEMENTS

REFERENCES

Ataev-Troshin V. (2017). New Moscow / V. Ataev-Troshin. Briansk: GUP «Briansk obl poligr obedinenie» (in Russian).

Buechner M. (1989). Are small-scale landscape features important factors for field studies of small mammal dispersal sinks? Landscape Ecology, 2, pp.191-199.

Byazrov L. G., Dylis N. V., Zhukova V. M., Nosova L. M., Solntseva O. N., Uspenskaia N. M., Utkin A. I. (1971). The main types of deciduous and spruce forests and their derivatives in Malinsky forestry Krasnopahor forestry Moscow region. In: N. Dylis ed. Biogeocenological studies in broad-leaved spruce forests. Moscow: Nauka, pp. 7-150 (in Russian).

Chernenkova T. V., Morozova O. V., Belyaeva N. G. and Puzachenko M. Yu. (2018). Actual organization of forest communities with broad-leaved trees in broad-leaved-coniferous zone (with Moscow region as an example). Vegetation of Russia. 33, pp. 107-130. DOI: 10.31111/vegrus/2018.33.107 (in Russian with English summary).

Chernenkova T. V., Morozova O. V., Puzachenko M. Yu., Popov S. Yu. and Belyaeva N.G. (2015). Composition and structure of spruce forests of the southwestern part of Moscow region. Contemporary problems of Ecology. 9(7), pp. 820-833. doi.org/10.1134/S1995425516070039

Chernenkova T. V., Puzachenko M. Yu., Belyaeva N. G., Kotlov I.P. and Morozova O. V. (2019). Characteristics and prospects of preserving the pine forests of the Moscow region. Lesovedenie. 5 (in print) (in Russian with English summary).

Diamond J. M. (1975). The island dilemma: Lessons of modern biogeographic studies for the design of natural reserves. Biol. Conserv., 7, pp. 129-146.

Dynamics of coniferous forests of the Moscow region. (2000). Moscow: Nauka (in Russian).

Ecological and economic index of Russian regions. Methods and indicators for calculation (2012). Moscow: RIA-Novosti, RGO, WWF.

Economics of biodiversity conservation. Handbook (2002) / A. A. Tishkov ed. Moscow: GEF project «Biodiversity Conservation», Institute of environmental Economics (in Russian).

Federal State Statistics Service / Municipal Indicators Database. Available at: http://www.gks.ru/dbscripts/munst/munst46/DBInet.cgi [Accessed 27.05.2019]

Forests of the Eastern part of the Moscow region. (1979). Moscow: Nauka (in Russian).

Forests of the Southern part of the Moscow region. (1985). Moscow: Nauka (in Russian).

Forests of the Western part of the Moscow region. (1982). Moscow: Nauka (in Russian).

Forman R. T. T. and Godron M. (1986). Landscape Ecology. New York: John Wiley & Sons.

Golubchikov S. N. (2012). What will the New Moscow be // Energy: economy, technology, ecology, 2, pp. 58–63 (in Russian)

Hansen A. J., Spies T., Swanson F., Ohmann J. (1991). Conserving biodiversity in managed forests. BioScience, 41 (3), pp. 382-392.

Hansen M. C., Potapov P. V., Moore R., Hancher M., Turubanova S. A., Tyukavina A., Thau D., Stehman S. V., Goetz S. J., Loveland T. R., Kommareddy A., Egorov A., Chini L., Justice C. O. and Townshend J. R. G. (2013). High-Resolution Global Maps of 21st-Century Forest Cover Change. Science, 342 (6160), pp. 850–853. Available at: http://earthenginepartners.appspot.com/science-2013-global-forest [Accessed 27.05.2019]

Hardt R. A. and Forman R. T. T. (1989). Boundary form effects on woody colonization of reclaimed surface mines. Ecology, 70, pp. 1252-1260.

Jaeger J. A. G. (2000). Landscape division, splitting index, and effective mesh size: new measures of landscape fragmentation. Landscape Ecol., 15, pp. 115-130.

Komarova N. G. (1997). The atmosphere and its pollution on the example of large cities of Russia // Life of the Earth. Issue 30. Earth science and ecology, pp. 142–157 (in Russian).

Konovalov N. A. (1929). Types of forests of Moscow region forestry. Proccedings on forestry experimental work. Central Forest Experiment Station. Issue 5. Moscow; Leningrad: "Selkhozgiz" (in Russian).

Kuricheva E. K. (2014). Territorial transformation of New Moscow under the influence of housing construction // Regional studies, 43(1), pp. 50–61 (in Russian).

Kurnaev S. F. (1968).The main forest types of the middle part of the Russian Plain. Moscow: Nauka (in Russian).

Lamberson R. H., McKelvey R., Noon B. R. and C. Voss. (1992). A dynamic analysis of northern spotted owl viability in a fragmented forest landscape. Conservation Biology, 6(4), pp. 1-8.

Levins R. (1970). Extinctions. In: M. Gertenhaber, ed., Some Mathematical Questions in Biology, Vol 2. Lectures on Mathematics in the Life Sciences. Amer. Math. Soc., Providence, Rhode Island, pp. 77-107.

Levitskaya N. N. and Chernenkova T.V. (2012). The Application of a Series of Indices for Assessing the State of Forests in Moscow Region. Lesovedenie. 6, pp. 14-29 (in Russian with English summary).

Lurie, I. K., Baldina, E. A., Prasolova, A. I., Prohorova, E. A., Semin, V. N. and Chistov, S. V. (2015). A series of maps of ecological and geographical assessment of land resources in the territory of New Moscow // Vestnik Mosk. Un., Series. 5. Geogr., no 4, pp. 49–58 (in Russian).

MacArthur R. H. and E. O. Wilson. (1967). The Theory of Island Biogeography. Princeton: University Press, Princeton.

Makhrova A. G., Tkachenko L. Ia. (2013). Plans and realities of New Moscow: continuation or change of development vector // Environmental planning and management, 1(14), pp. 37–50 (in Russian).

Makhrovoi A. G., Kirillova P.L. (2018). New Moscow: old and new features of social and economic development. Old and New Moscow: trends and problems of development. Collection of scientific articles: Izd. IP Matushkina I. I., pp. 89-119 (in Russian).

McGarigal K., Cushman S.A. and Ene E. (2012). FRAGSTATS v4: Spatial Pattern Analysis Program for Categorical and Continuous Maps. Computer software program produced by the authors at the University of Massachusetts, Amherst. Available at: http://www.umass.edu/landeco/research/fragstats/fragstats.html [Accessed 27.05.2019]

McKelvey K., Noon B. R. and Lamberson R. (1992). Conservation planning for species occupying fragmented landscapes: the case of the northern spotted owl. In: J. Kingsolver, P. Kareiva, and R. Hyey, eds. Biotic interactions and global change. Sinauer Associates, Sunderland, MA, pp. 338-357.

Ministerial conference on the protection of forest in Europe (MCPFE). Sound forestry – Sustainable development (1993). Helsinki: Ministry of Agriculture and Forestry.

Ministerial Conference on the Protection of Forests in Europe. (2015). Available at: http://www.foresteurope.org [Accessed 27.05.2019]

Nefedova T. G., Mkrtchian N. V. (2017). Migration of rural population and dynamics of agricultural employment in the regions of Russian // Vestnik Mosk Un. Series 5. Geography, no 5, pp. 58-67 (in Russian).

OECD environmental indicators – development, measurement and use. Reference paper. (2003). France, Paris: OECD.

Ovaskainen O. (2002). Long-term persistence of species and the SLOSS problem. J. Theor. Biol. 218, pp. 419-433.

Ovaskainen O. (2012). Strategies for Improving Biodiversity Conservation in the Netherlands: Enlarging Conservation Areas vs. Constructing Ecological Corridors. Helsinki.   Avaliable at: https://www.rli.nl/sites/default/files/u61/otso_ovaskainen_-_strategies_for_improving_biodiversity_conservation_in_the_netherlands.pdf [Accessed 27.05.2019]

Patton D. R. (1975). A diversity index for quantifying habitat "edge". Wildl. Soc. Bull. 3, pp. 171-173.

Puzachenko M. Yu., Chernenkova T. V. (2016). Definition of factors of spatial variation in vegetation using RSD, DEM and field data by example of the central part of Murmansk region. Current problems in remote sensing of the earth from space. 13 (5), pp. 167-191. DOI: 10.21046/2070-7401-2016-13-5-167-191 (in Russian with English summary).

Puzachenko Y. G., Sandlerskiy R. B., Krenke A. N., Puzachenko M. Y. (2014). Multispectral remote information in forest research. Lesovedenie. 5, pp. 13-29 (in Russian with English summary).

Red Data Book of Moscow region. (2018). Moscow region: "Verhove" (in Russian).

Review of the forest pathology and sanitary condition of forests in the Moscow region in 2008 and the forecast of the pathological situation for 2009. (2009). Pushchino (in Russian).

Review of the forest pathology and sanitary condition of forests in the Moscow region in 2009 and the forecast of the pathological situation for 2010. (2010). Pushchino (in Russian).

Ruotsalainen A. L. and Kozlov M. V. (2006). Fungi and air pollution: is there a general pattern? In: D. Rhodes ed. New topics in environmental research. Hauppauge: NY: Nova Science Publ., pp. 57-103.

Rysin L. P. and Savelieva L. I. (2007). Inventories of forest and biogeocenoses types. Moscow: KMK (in Russian).

Smirnova S. Iu., Levitckaia N. N. Features of development of system of especially protected natural territories in the Moscow region // Old and New Moscow: trends and problems of development. Moscow: Izd. IP Matushkina I.I., pp. 317-333 (in Russian).

Suslova E. G. (2019). Forests of Moscow region. Ecosystems: Ecology and Dynamics. 3 (1), pp. 119-190 (in Russian with English summary).

The Montreal Process. Criteria and indicators for the conservation and Sustainable management of temperate and boreal forests. (1995). Hull, Quebec: Canadian forest service.

The nature of the Moscow region: the loss of the last two decades. (2009). Moscow: Izd-vo TsODP (in Russian).

Tishkov A. A. (2014). Strategic resources for the development of New Moscow // Strategic resources and conditions for sustainable development of the Russian Federation and its regions. Moscow, pp. 134–143 (in Russian).

Trubina M. R., Vorobeychik E. L. (2012). Heavy industrial pollution increases the β-diversity of plant communities. Doklady AS USSR. 442(1), pp. 139-141 (in Russian).

Yakovlev A. S. and Evdokimova M. V. (2011). Ecological rationing of soils and their quality management. Pochvovedenie. 5, pp. 582-596 (in Russian).

Yakubov I. (2007). Around ten billion. Russian forest newspaper, 42. Available at: http://oldsite.zapoved.ru/press-service/publications/detail.php?ID=11108 [Accessed 27.05.2019]

Zvereva E., Toivonen E. and Kozlov M. V. (2008). Changes in species richness of vascular plants under the impact of air pollution: a global perspective. Global Ecol. Biogeogr, 17, pp. 305-319.

Viktoria R. Bityukova[1]*, Nikita A. Mozgunov[1]

[1] Faculty of Geography, Lomonosov Moscow State University; Leninskiye Gory; 119991 Moscow, Russia
*Corresponding author: v.r.bityukova@geogr.msu.ru

SPATIAL FEATURES TRANSFORMATION OF EMISSION FROM MOTOR VEHICLES IN MOSCOW

ABSTRACT. The article examines changing volumes of emission from vehicles by administrative and municipal districts of Moscow. In Moscow automobile transport is the general source of pollution, it produces more than 93% of allover, and this is the absolute maximum of impact for Russian cities and regions. In 2011-2017, it was the first time when the growth of motorization was noticed against background of reduce of pollution due to modernization of car park and new quality of petrol. Total gross emission from vehicles decreased four times. Shifts in the factors defining spatial specifics of distribution of pollution from vehicles are revealed. Assessments of air pollution based on information of all Moscow streets provides estimations for 93 thousand low-level city areas. One of the research result revealed a high correlation between changes of pollution density and changes in transport infrastructure including developing of public transportation, modernization of car park structure. Spatial uniformity of pollution from vehicles has become the main trend of recent years. Programs of the new housing construction and large-scale projects aimed at the transformation of the districts increase the transport connectivity of the city. Administrative decisions on the traffic intensity reduction in the central districts decrease territorial differentiation of pollution. Transport and planning structure at the level of the city, the district, and the area is the defining characteristic. An attempt to solve the transport problem through the transformation of the street road network complicates the application of innovative techniques for combatting air pollution in Moscow.

KEY WORDS: Moscow, vehicles, transport networks, emission, ecology, pollution areas, transport modelling, environment

INTRODUCTION

Greater polarization of society, growing social tension, and emerging territorial segregation have become crucial effects of Post-Soviet economic transformations in Russia in terms of intracity development. The development of Soviet cities based on the aspiration of unifying the space gave way to the development of cities under the market economy, significantly affected by the cost of urban land and real estate. Having first shown in the capital which is at the moment a "modernization outpost", a number of relatively new to Russia social and economic processes (territorial segregation of society, emerging ethnic quarters, gentrification of the center) have started to develop in the cities. This necessitates studying the transforming quality of urban environment in Moscow in order to foresee the development of other cities in the country. The Post-Soviet Moscow has experienced the period of structuring of the space, sharp polarization of the urban environment, new functions of many districts appearing (Vendina 1996).

Research of intracity differences in environmental quality is extremely relevant now and have significant applied value, first of all, in the context of studying trends in the development of real estate market and city lands, analyzing the best options of using city land plots, identifying problem urban areas and designing programs for their development. The environmental situation is a crucial component of urban environmental quality. The urbanized areas are the ones of deeply changed nature. High concentration of various activities in cities disrupts the dynamic balance in nature and deteriorates the ecological living conditions of people.

Vehicles have become the leading source of air pollution over the past decades: transport emissions exceed 50% of gross pollution in half of the regions and in three forth of the cities (Bityukova 2019). Atmospheric emissions from mobile sources account for 44.7% in Russia (2017) and over 93% in Moscow (980 thousand tons, an absolute maximum for Russian cities and regions). Vehicles are the source of highly toxic substances, emissions are localized and they form areas of high pollution density. However, transport is perceived by the population as a mobility factor, rather than a pollution factor and does not affect real estate prices (Bityukova, Makhrova, Sokolova 2007).

RELATED RESEARCH

The research of vehicle problems in the cities is at the intersection of social and natural sciences: geography, sociology, history, ecology, demography, and economics. Most of the environmental transport researches are devoted to technical aspects, i.e. improvement of cleaning system methods, reburning and fuel quality.

Socio-political aspects of development of communications, legal framework and social interpretation are generally viewed in the context of traffic flow optimization in the cities and agglomerations. Modelling of planning systems and assessing of the necessary level of development for roads and streets network in the cities always emphasize a special connection between transport system development and economic and social development (The concept of assessing 2016) with a specific demonstration of the changing role of the city centre falling into decay as city transport started to use long-distance highways which led to the formation of suburbs (case studies of Chicago, Detroit, Los Angeles) (Vuchik 2011). The Soviet town-planning practice, on the contrary, would form transport systems founded on the priority of public transport (Blinkin, Koncheva 2016).

The strategies of transport accessibility based on the assessment of direct and indirect costs with various planning goals, such as greater safety, unity of community, and environment protection provide maximum overall benefits (Isalou, Litman, Shahmoradi 2014). However, it is admitted that the state alone is able to implement a solution to transport problems of large cities in the context of Cost and Benefit Analysis and based on the need to internalize the outer effects of vehicles (Hovavko 2012). The monetized estimates of external and internal effects from transport show that in Moscow just as in US cities (Litman T. 2002) main potential damage is

connected with economic losses due to traffic jams (about 40 billion rub/year) while damage from air pollution, waste and water resources accounts for 15 billion rub/year (Kichendzhi, Katoyama 2011). Therefore, various political and planning reforms are needed, they can help both to increase cost efficiency, justice and to improve ecological situation since a car stuck in a traffic jam emits an average of 30% more pollutants.

Studies of environmental problems of transport are considered in various aspects:

– The impact of noise and pollution on people's health was studied, also health risk assessment for the population connected with functioning of vehicles facilities (Yakushev, Kurolap, Karpovich 2013). Special attention is paid to the impact analysis of solid particles, it is proved that up to 400 million people live under the pronounced impact of PM, transport being a key source of pollution (Revich 2018);

– Impact assessment for individual types of pollution was shown, especially for solid particles, in particular, the correlation coefficient between traffic intensity and concentrations of PM10 and PM2.5 are 0.36 and 0.39 respectively based on Tom-Tom index (Http://www.tomtom.com/en_gb/trafficindex) (Azarov, Kutenev, Stepanov 2012; Parsaev, Malyugin, Teterina 2018);

– Various environmental and geochemical researches were carried out, for example, salinization, pollution with heavy metals and metalloids near highways with various traffic intensity and in the courtyards with parking. All of them have demonstrated a rather uniform pollution of soils and of individual environments (Kosheleva, et al. 2018).

There is a large number of models of distribution and diffusion of emissions from mobile sources. However, there are almost no science works that would consider transformation of territorial structure of emissions from vehicles (Revich, Kuznetsova 2018).

Territorial structure of pollution is a set of orderly structured and interconnected elements

making an impact on the environment with inherent spatial coordination and symbiotic relations between them and with other structures – industry, environment, and settlements. Centers of impact with specific types and levels constitute elements of the structure, while impact areas form the network of relations. The territorial structure of pollution has significant methodical value since it is the proximity of areas of anthropogenic impact (AI) to certain natural complexes and population that creates a specific interaction which, at the extreme, turns into a conflict. Both the persistence of AI sources and the variability of areas cause changes in territorial proportions of pollution. Actual areas of impact were identified and used to calculate pollution density and to zone regions and cities, laying the basis for methodical developments in this work.

MATERIALS AND METHODS

The main problem in the research of changing territorial structure of vehicle pollution in Moscow is the development of a unified technique allowing to carry out the analysis of serial observations of transformations in traffic intensity, transport infrastructure and spatial patterns in Moscow transport. Since it is difficult to select one specific indicator reflecting the level of environmental stress to identify territorial differentiation of vehicle air pollution, the method of areas was applied (Bityukova 2019). The **density of harmful emissions** (CO, SO_2, NO_x, C, NH_3, CH_4, volatile organic compounds (VOC) other than methane (CH_4) man-made emissions only) (tons/sq.km per year) indicator is calculated for each street and areas with various density of atmospheric emissions are detected in order to assess atmospheric pollution within areas.

There were several steps of the research:

Traffic intensity assessment. A proprietary technique is used to assess the transport load allowing to calculate the intensity for motorways sections without direct measurements of the passing transport. The systems of transport monitoring in Moscow are widely used and problem of

the availability of these data has occurred a long time ago. Real-time monitoring and machine learning methods would make it possible to estimate environmental stress similarly to services of traffic congestion, e.g. Yandex.Probki. Currently, due to limited access to such systems, open data of Google and OSM cartographic services are used.

Transport intensity calculation is based on the formula:

$$G_K = \frac{v_{cp} \cdot t \cdot P}{2 \cdot l_{cp} + D} \cdot k_s \cdot k_r \cdot n$$

units/hour,

where:

V_{cp} – average daily speed of traffic flow, m/sec (based on Google geographic information system);

t – duration of allowing signal of traffic light, sec.;

P – number of allowing signal cycles per 60 minutes, units;

n – number of lanes for a specific section based on OSM API;

k_S – coefficient of distance from the road section to the city centre;

k_r – coefficient of the motor way class and the value of connectivity of the road section;

$2 \cdot l_{cp} + D$ – dynamic gauge – a minimum section of the road in meters required for safe movement in the traffic flow with the assigned speed (dynamic gauge) that includes the doubled average length of the vehicle and "effective distance", i.e. recommended minimum distance between moving cars in meters. Naturally, in reality high traffic intensity during rush hours does not allow this distance to be observed, while low intensity does not provide for the adequate number of moving cars for it to occur. Therefore, this condition is most relevant for the period which is characterized by traffic intensity close to its average daily value.

Reliable modelling of traffic load for roads of minimum and intraquarter significance is difficult which constitutes a disadvantage of this technique.

Calculation of atmospheric emissions. Running exhaust emissions from vehicles have reduced by 6 grams per km over the five years (2011-2017) and constitute 21 grams per km now (State Standard (GOST) 56162-2014, 2014).

Pollutant emission (g/sec) of moving vehicles flow on a motor way (or its section) with a fixed length of L (km) is determined by the formula:

$$M_{L,i} = \frac{L - L_0}{3600} \sum_1^K M_{K,i}^{\Pi} \cdot G_K \cdot k_C \cdot r_{V_{K,i}}$$

g/sec,

where:

$M_{K,i}^{\Pi}$ – specific running exhaust emission of i th harmful substance by K th group of cars for city service conditions, g/km

K – number of groups of cars;

G_K – average daily traffic intensity, i.e. the car number of each of K groups passing through the fixed section of the chosen part of the motorway per hour in both directions on all lanes, units/h;

K_C – correction factor taking into account climatic systems of the car, road conditions and gripping;

$r_{V_{k,i}}$ – correction factor taking into account average speed of traffic flow (V, km/h) on the chosen section of the motorway;

$1/3600$ – conversion coefficient (hours into seconds);

L – length of the section of the motorway, km;

L_0 – line of cars at a red light and length of the corresponding zone of the intersection, km.

Calculation of impact areas for vehicles. The most important proposed method component is the calculation of the surface area of pollution. It is necessary to take into account transport specificity and planning structure of the studied area which significantly impacts on territorial distribution of emission density around the city. For the most part, the planning is designed for the traffic of the mid 1980s and still has not undergone any significant changes. Therefore, problems connected with imperfect city planning exacerbate the impact of pollution from transport.

OND-86 (All-Union regulatory document) technique is quite suitable for visualization and interpretation of results. This technique identifies the fields of concentration equivalent to maximum allowable concentration – fields of concentration (fig. 1).
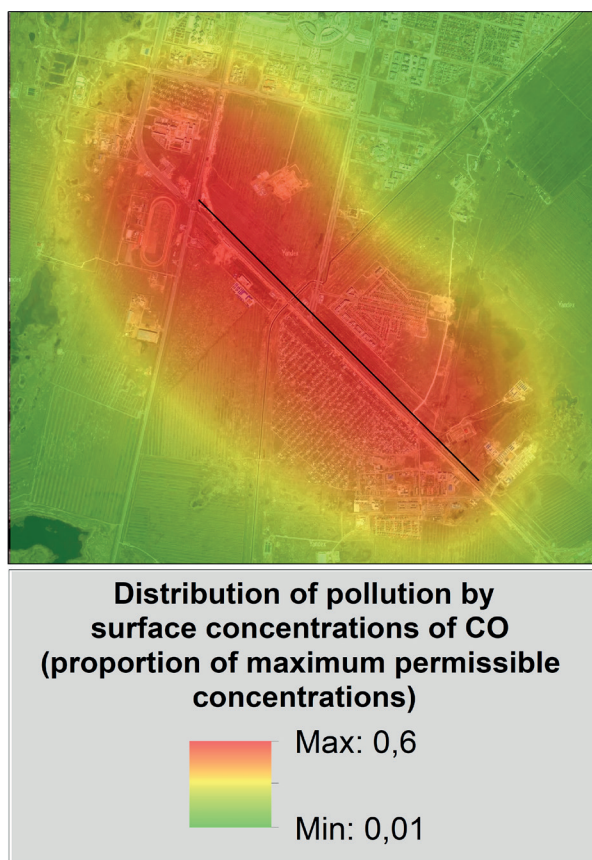
Fig. 1. An example of calculated area of pollution by surface concentrations of CO formed by automobile transport, exceeding the maximum permissible concentrations

Impact area for highways with traffic intensity of 10 thousand cars per day accounts for up to 400 meters, with the gas contamination and dust content showing up at a distance of up to 1-2 km downwind from the route in dry and clear weather. A persistent area of chemical impact (radius of 400 m) which is shown in continuously exceeded maximum allowable concentration is formed by large highways with traffic intensity of about 50 thousand cars per day.

Calculated data of specific running exhaust emissions of harmful substances for vehicles of various ecological classes and types of engine based on the fuel consumed is used to reflect emissions from different cars. These indicators are coincided with the current EMEP air pollutant emission inventory guidebook taking into account specific features of the structure and modes of vehicle movement.

Spatial impacts of traffic flows in the context of urban development is calculated as the product of the length of the road section multiplied by the impact area size (in sq.km). Thus, the impact area of vehicles flows (S) is calculated as the sum of products of the area of a rectangle (one side is equal to the length of the impact area interval (L_i), the other one is equal to the impact area ($2r$)) and the circle with the radius equal to the impact radius of r.

$$P = (V_i \cdot L_i \cdot 365 \cdot K) / (L_i 2_{\pi r}^2)$$

where

P – total value of emission density for vehicles flow in its impact area;
L_i – length of the calculated transport section (km);
V_i – a car traffic in the calculated section;
r – impact radius for vehicles flow on the adjacent territory (km);

K – emission volume for one car per 1 km per year (i.e. motor emission volume per year divided by total mileage for the whole city). Thus, the coefficient of impact for vehicle flows on the adjacent territory allowed defining and describing the total index of density of vehicle emission for the researched areas, the total number of which, as we allocated, was more than 93 thousand.

RESULTS AND DISCUSSION

Dynamics of air pollution from vehicles and its territorial proportions is the result of both *transformational* and *inherited factors*. Among the transformational factors are the intensify, for example the number of automobiles and the reduction of the anthropogenic impact such as fuels and engine improvement. *Inherited* conditions of development play a great role in the formation of areas with high emission density from vehicles: the planning structure, road network connectivity, the width of the roads, a number of bridges, relief features, the green belt and so on.

Impact level factors include the inherited technical quality of domestic cars. However, the majority of inherited development aspects boil down to *motor emission distribution across the territory:* the terrain, planning structure, bridges, road width, topology of the road network, low connectivity of the network, increased role of transit functions, etc.

The analysis of possible dependence of emissions volumes on vehicles and its dynamics showed that none of the indicators can be included in the equation of multiple linear regression. There are two main reasons for the absence of correlation between them. *First*, the static nature of the initial variables estimating only the registered population and the size of vehicle fleet. At the same time, the actual population and vehicle fleet are much more important for modern large cities with their strong daily, weekly and seasonal rhythmic. The use of indicators of the registered population and vehicle fleet lead to significant underestimation for the central districts of the city and possible overestimation for residential areas in the daytime. Second,
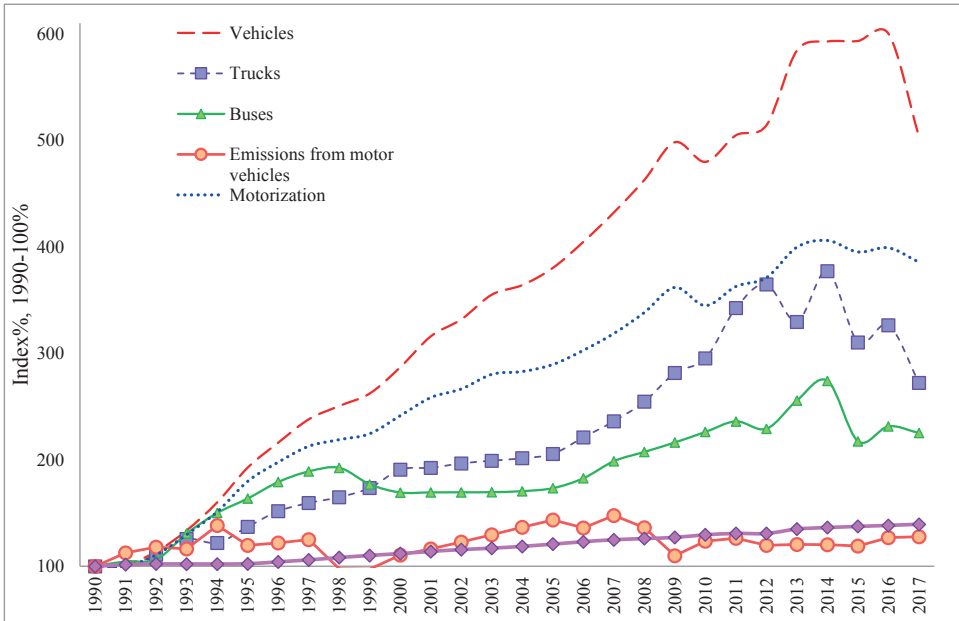
the various nature of independent and dependent parameters. The population, vehicle fleet size, parameters of planning structure of the territory, the housing stock are endogenous characteristics of the respective municipal districts. The emissions from vehicles today are much stronger connected with conditionally exogenous characteristics – first of all with transport geographical location, transit intensity of the district, capacity of the main highways crossing the district.

Since there are two groups of opposite factors, exacerbating air pollution and reducing it, no clear impact of the ***growing automobilization*** is observed. This trend had already been detected for Moscow earlier (Bityukova, 2008). Growing automobilization level became an important characteristic of the Post-Soviet period, Moscow became a leader in this process (second after Primorye and Sakhalin). Today Moscow concentrates 10% of the Russian vehicle fleet, over 4 million cars. Maximum annual increase in the number of cars (19.1%) was observed in the early 1990s, then the situation was more or less stable until the growth started to slow down in 1996. 2011-2013 saw an average annual decrease in vehicle fleet increase rates of 2-5% reflecting market saturation, and due to the fall in real income personal vehicle fleet reduced by 8%, and vehicle fleet of organizations by 6% after 2014 (fig. 2).

Until the mid-1980s atmospheric emission volume was growing at about the same rate as the automobilization level. Since 1986, with the vehicle fleet still growing, emission volume has started to decrease as the result of the introduction of the first exhaust control measures and measurements.

1990-1991 saw insignificant changes in the level of automobilization, but significant changes in the volume of emissions, a growth of 12%, which is, most likely, connected with a new pollution accounting technique. Until 1996 correlation coefficient between the level of automobilization and dynamics of emissions was still statistically significant (0.61), though slightly decreased by a cumulative effect of positive factors. Used cars prevailed in the structure of

Viktoria R. Bityukova and Nikita A. Mozgunov   SPATIAL FEATURES TRANSFORMATION OF ...

04|2019

63 GES

Fig. 2. Changes in the automobilization level in Moscow 1990-2017 (Main indicators, Transport in Russia, Demographic Yearbook)

growth during this period, high growth rates of the Moscow vehicle fleet did not affect the overall trend of its fast aging, and, therefore, the increase in specific emissions. 77% of cars in the structure of vehicle fleet had been used for more than 9 years. Therefore, 34% of the cars checked in 1998 were faulty based on emission indicators (Department of nature management and… 2002). Still in the context of the overall growth in the number of cars with petrol engines by 5%, consumption of gasoline reduced by 15% in 1999 demonstrating a decrease in specific fuel consumption.

Amidst economic growth and booming incomes of the population, the rapid growth of automobilization was in many respects guaranteed at the expense of quality cars. Construction of roads and reconstruction of transport network began (1997-2006), the correlation coefficient between the growing number of cars and atmospheric emission volume, for the first time, became statistically insignificant – 0.42, and at the present stage it is negative. 2009 to 2017 saw gross emission from mobile sources of pollution reduced by nearly 400 thousand tons (from 1342 to 982.4 thousand tons). At the same time the share of emissions from

mobile sources also reduced by 2 pp which could be a result of a statistical error since there was no growth of industrial production volume during the specified period.

The most important changes in the structure of influencing factors occurred during the post-industrial period of development of Moscow. While during the Soviet period despite the low level of automobilization and, as a result, low traffic intensity, the correlation coefficient between the growing automobilization and changing atmospheric emission level was 0.65, now the value of the correlation coefficient is decreasing to 0.13. According to FTS, the number of the registered privately owned vehicles per 1000 citizens varies 4 times by the districts of Moscow: 500-900 cars /1000 citizens are registered in the north and northwest of the capital; 380-500 are registered in the central districts, in the south and the southeast. However, interdistrict distinctions based on the total number of the registered cars are much higher, exceeding 25 times. Even given possible divergence between the registered and used cars, such a high level of concentration should be taken into consideration when planning parking spaces, outflows, etc.

Changes in the structure of the vehicle fleet have a complex and divergent nature. Along with the growing automobilization, Moscow witnesses an intensive implementation of higher ecological classes (EC) of the engine (approximately 2-3% per year) and a declining share of trucks (approximately twofold reduction in 1991-2006) that promote improvement of ecological parameters of vehicles. It is also connected with stricter requirements to environmental standards of fuel and cars. Changes in the structure of vehicle fleet also led to better quality of fuel promoted by the growth in environmentally oriented demand. At the same time, the formation of vertically integrated companies capable of supplying high-quality fuel to the market provided for investments in oil processing aimed at the production of gasoline of better quality. Standards below Euro-4 (with running exhaust emission, g/car*km, twice less than for Euro-3 and three times less than for Euro-2) were banned in 2013, standards below Euro-5 have been banned since January, 2016. Transition from motor fuels class 3 to class 4 caused reduction of emissions of sulphur dioxide by 79%, benz(a)pyrene by 22.7%, solid substances by 13.5%, nitrogen oxides and carbon oxide each by 4%. By 2014, up to 50% of motor fuels in Moscow corresponded to class 5. According to expert estimates based on the data on age structure of vehicle fleet by the beginning of 2014, passenger cars of ecological classes higher than 4 accounted for 50%, trucks – 30%, buses – 16% (Department of nature management and… 2017).

But at the same time fuel consumption is not decreasing quickly enough as the changes occurring in the structure of vehicle fleet of Moscow are very specific. The fleet has more cars with increased fuel consumption as compared to average Russian values (according to tax administration). The share of cars with the engine of 150-250 hp is 3 times higher than on average in the country and their growth values are maximum (47% of growth in 2011-2017 and even in recent years in the context of a 12% reduction of the fleet, the number of cars with an engine of 200-250 hp has grown by 12%) (fig. 3).

Thus, divergent trends have become the most important feature of formation of air pollution level in Moscow in recent years: automobilization is growing but pollution is reducing thanks to better quality of vehicle fleet and fuel. Periodic adjustments of emission accounting technique make it impossible to reveal more pronounced trends, but relative changes of these indicators allow to reveal specifics of the recent years.

However, once the planned level of motor fuel quality is reached, there will be almost no reserves to further decrease the emissions. *Improvement of gasoline quality and changes in the structure of vehicle fleet have reduced gross and specific (running exhaust emission has decreased by 4 times) emission from vehicles.* As a result, since 2007 the intensive growth of vehicle fleet in Moscow has not been followed by growing volumes of
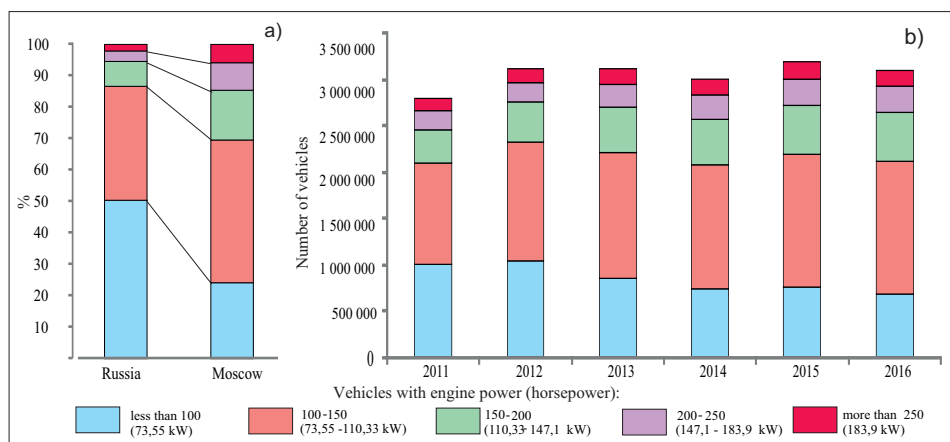
Fig. 3. The structure of passenger car fleet of Moscow by engine type (FTS data) a) as compared to Russia b) Dynamics in 2011-2016

Viktoria R. Bityukova and Nikita A. Mozgunov   SPATIAL FEATURES TRANSFORMATION OF ...

04|2019

65 GES

pollutants. At the same time, there was no significant decrease in the load on linear infrastructure, so it is impossible to reveal a significant improvement in ecological situation for a number of districts.

Density of the street road network (SRN) is the most important factor of changes in ecological situation. Impact of SRN density is one of the most contradictory factors: on the one hand, construction of roads creates new areas of emission, on the other hand, motor emission volume decreases if there are no traffic jams which increase running exhaust emission by 30%, therefore, the development of road network reduces motor emission volume (Bityukova, Kasimov, Vlasov 2011).

Intensive reconstruction of city transportation routes is a distinctive feature of the past decade significantly improving ecological situation in a number of districts. The reconstruction of MKAD has decreased emission volume by 76.6 thousand tons/year, an equivalent of decrease in specific fuel consumption for each car by 0.4 l / 100 km, i.e. a transition to a different class of cars. The most large-scale recent endeavour in the development of the transport system of Moscow is the construction of the Third Ring Road (TRR). TRR has decreased the polluting emissions by 14.5% by 2000 and changed the territorial structure. The new ring road has temporarily lessened the load on transportation routes of the city centre, reducing the surface area of areas with the maximum emission by 1% and with high emission by 18%.

However, decrease in traffic intensity and traffic jams in the centre, and a subsequent reduction in emission volumes owing to the construction of TRR was only a temporary phenomenon, since due to the further growth of vehicle fleet in the city TRR was no longer able to cope with this task. TRR has hardly changed the length of transport network of the city (only a 1% increase), so there was no reduction in the specific density of cars per 1 km of the road network. Moreover, the new transportation route to a certain extent became an incentive for a more intensive use of vehicles by residents of the capital which in its turn led to further increase in negative impact of cars on the environment of the city.

Modern transport construction does nothing but preserves the above-mentioned radial and ring structure. Experts back in the 1970s understood the inadequacy of this scheme suggesting construction of a "chordate triangle" (powerful high-speed chordate highways on the peripheries of the city creating a "vacuum effect" for the city centre) envisaged by the Master plan of Moscow 1972 (Yakshin 1975). But, at the same time, there is an increase in SRN density in the districts with a slightly lower density as compared to the average level for the city. Planning and development of roads in problem zones of the centre, in the southwest of the middle belt (between Garden Ring Road and Third Ring Road), as well as and in northern districts adjacent to MKAD helped to reduce emissions in those areas. Thus, a greater uniformity of SRN across the city has also become a factor of decreasing emission volumes and ensuring a more uniform distribution across the city (fig. 4, c, d).

New transport construction in the context of the current planning structure and capacity of roads additionally increases load on MKAD and main radial highways. The Soviet town-planning norms were based on 60 cars per 1000 citizens, therefore, areas of mass construction of the 1960-80s are not designed to meet high western standards of automobilization.

In 2011-2017 in Moscow, in the borders of 2012, there were over 16 million sq.m[1] of housing put into operation, they were commissioned primarily in the districts with a relatively low density of population; also buildings which promote the uniformity of vehicles impact. But localization of large residential complexes stimulates the use of radial highways which, according to our calculations, are also characterized by a quite uniform distribution of density of emissions from mobile sources (figure 4). Average density of emissions on the TRR –
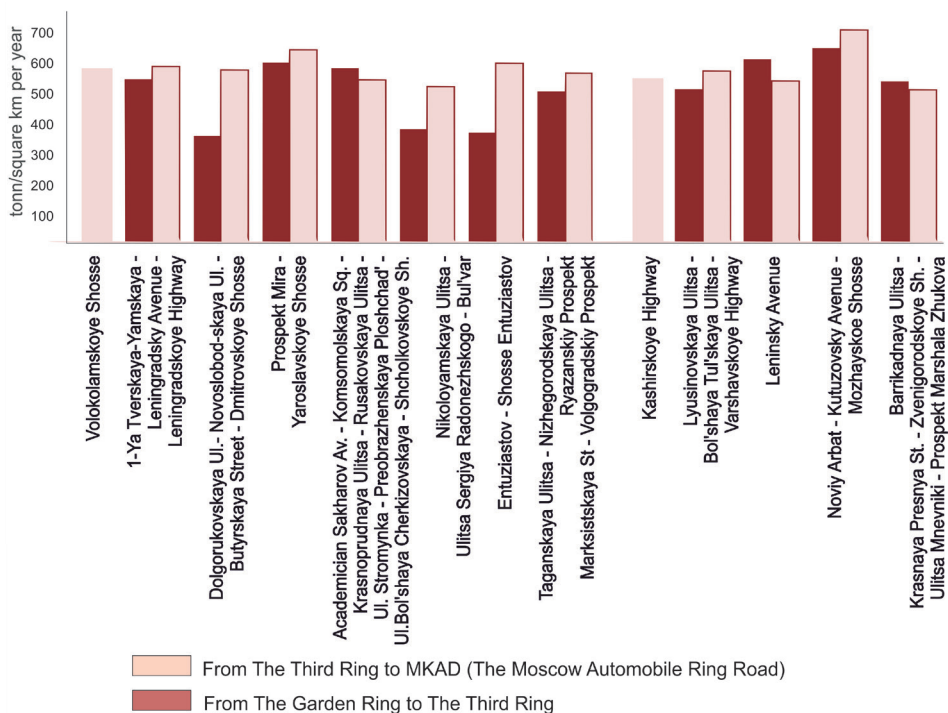
[1] Data by individual houses were provided by Popov A.A., the Head of CIAN Analytical Centre

MKAD interval has increased for the majority of motorways as compared to the Garden Ring – TRR interval. The only exceptions are Shchelkovskoye Highway, Leninsky Avenue and Marshal Zhukov Avenue where emission density decreases from the centre to periphery. This can be attributed to a considerable width of the route in the central part of the city as well as to specific features of traffic light regulation resulting in traffic jams while, as we approach MKAD, the problem is levelled.
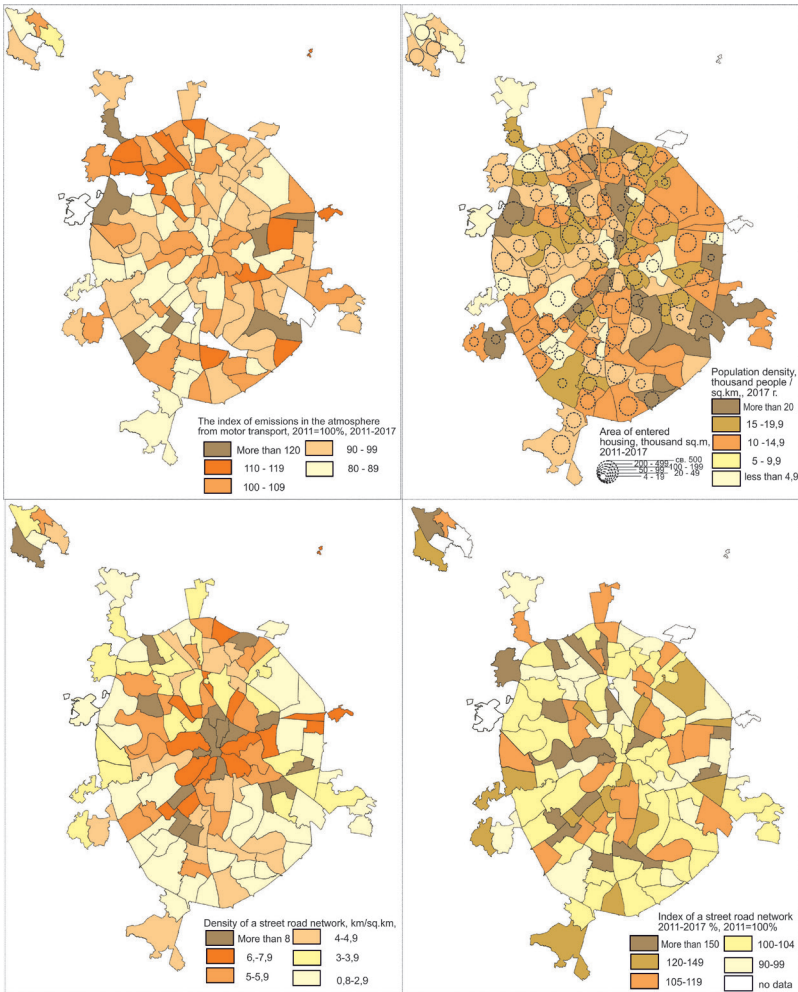
Population density of cities reflects the type of prevailing housing stock and impacts the forms of city transport organization. In cities with high population density trends, local authorities are choosing intermodal transport systems with the emphasis on public transport (Rodrigue 2017). Development of public transport in Moscow, due to a number of measures of economic and prohibitive nature, allowed to considerably lessen the load on the centre in recent years. As a result, the volume of emissions from vehicles has decreased by 10-20% in the central districts and in the districts where new lines of underground transport were constructed (MCC, new lines of the subway) (fig. 5, a, b).

Town-planning strategies of the Government of Moscow. Unfortunately, amidst intensive automobilization, Moscow did not use an important advantage, i.e. the experience of western cities which had undergone this stage thirty years earlier, first of all, in terms of the arrangement of parking spaces across the city. As a result, the width of even large highways is contracted by one third, and even twice in the centre, creating additional traffic jams and additional emissions. As it was mentioned above, TRR did not have any environmental effect. Experts are not too optimistic regarding the fourth ring either.

Changes in territorial proportions of emission from vehicles are almost more important for Moscow than the scale of vehicles impact itself. 2017, as compared to 2007, saw more uniformity in vehicles emissions density. The first and main difference is that for the first time in the Post-Soviet period areas with a density of emission more than 5 thousand tons/sq.km disappeared completely. Those areas used to be typical of almost the whole territory of the centre within the Garden Ring, and a considerable part within the Third Ring Road, along the

Fig. 4. Motor emission density by radial motorways tons/ sq.km per year.

Legend:
- From The Third Ring to MKAD (The Moscow Automobile Ring Road)
- From The Garden Ring to The Third Ring

Viktoria R. Bityukova and Nikita A. Mozgunov   SPATIAL FEATURES TRANSFORMATION OF ...

04|2019

67 GES

Fig. 5. Spatial differentiation of main factors and motor emission dynamics in 2011-2017

majority of the largest radial highways and MKAD, in the northeastern part of MKAD and along a part of Yaroslavskoye Highway. It happened despite the increase in traffic intensity and as a result of the effect of positive factors in the city: improvement of fuel quality and reduction of its specific consumption, improvement of car quality and reduction of the share of trucks causing decrease in specific atmospheric emissions. A part was also played by measures for the improvement of the road surface and the nature of traffic, over the five years (2011-2017) it saw transport construction and road reconstruction projects implemented, and vehicle fleet growing rates slowed down. The number of areas with a density of 3-5 thousand tons/sq.km declined though they

have already remained stable for a period of time. Most of these areas are still in the center. The share of areas with the lowest level of emission (up to 100 and 100-500 tons/sq.km), that used to be stable since the early 2000s, almost doubled as compared to 2007-2014. Motor emission density values were subject to averaging, i.e. anthropogenic impact on the territory becomes more uniform. This could have been viewed as a positive trend, but the reduction of "peaks" primarily around joining of radial highways with the Garden Ring was compensated by the growth of pollution in peripheral districts of the city that becomes especially evident in the absence of any significant differences between administrative districts of the city (Table 1).

Table 1. Distribution of areas by groups based on polluting emissions density, the share of the surface area of areas in the total area of Moscow

Density of emissions, (tons / square km)	The share of the surface area of areas in the total area, %													
	1992	2002	2007	2014	2017	Administrative districts								
						Central	North	Northeast	East	Southeast	South	Southwest	West	Northwest
<100	3	2	12	14	23	19	21	24	22	23	20	21	20	21
100-500	16	23	23	22	49	55	57	58	56	57	57	58	55	57
500-1000	18	25	32	34	14	13	14	12	14	12	14	15	16	15
1000-3000	37	43	28	25	8	6	6	5	6	5	6	5	7	5
3000-5000	22	5	5	4	6	9	2	1	2	2	3	2	2	2
>5000	4	3	1	0,5	0	0	0	0	0	0	0	0	0	0

Assessment of vehicles emissions in the South-East Administrative District.

Very interesting example of changing density emission because of roads networks modernization is on the Southeast part of Moscow. As the projects of road network reconstruction are being implemented in the South-East Administrative District (SEAD) there are positive shifts in the intensity and speed of traffic that, according to the Government of Moscow, is supposed to reduce the number of areas with maximum pollution. State of the Environment Report prepared by analytical services of the mayor's office confirms that the maximum concentration of complaints of the population about the condition of atmospheric air is in the South-East Administrative District. At the same time the number of the functioning enterprises in the territory of the district is reducing, and emission from stationary sources is declining. The presence of specific enterprises in the district, such as oil refinery, affects perception of the ecological situation as well. In terms of perception of the acoustic situation, vehicles accounts for more than a third of noise-related complaints.
Volgogradsky and Ryazansky Avenues and Lyusinovskaya Street are the main highways in the district which connect suburban districts with the central part of Moscow and are almost the sole communication route between TRR and MKAD in the South-East Administrative District.

A large infrastructure project was completed in the South-Eastern Administrative District in 2016, i.e. the reconstruction of Volgogradsky Avenue which included construction of the tunnel on Lyublinskaya Street aimed at lessening the load on this traffic intersection. Ostapovsky Drive was expanded to four lanes, a flyover at the crossing with Volzhsky Boulevard was constructed, several above-ground and underground crosswalks were put into operation.

Main works on the reconstruction of Ryazansky Avenue were completed in 2015, but the U-turn near Nizhegorodskaya Street MCC station has been built quite recently. The carriageway has been expanded, cycle infrastructure has been partially created, public transport lanes have been dedicated. The main traffic problems in the district are now related to active construction of Nekrasovskaya line and Big ring metro line. Nevertheless, it is estimated that transport infrastructure capacity of the South-East Administrative District at rush hours is insufficient resulting in frequent traffic jams and increasing environmental stress in the area (figure 7).

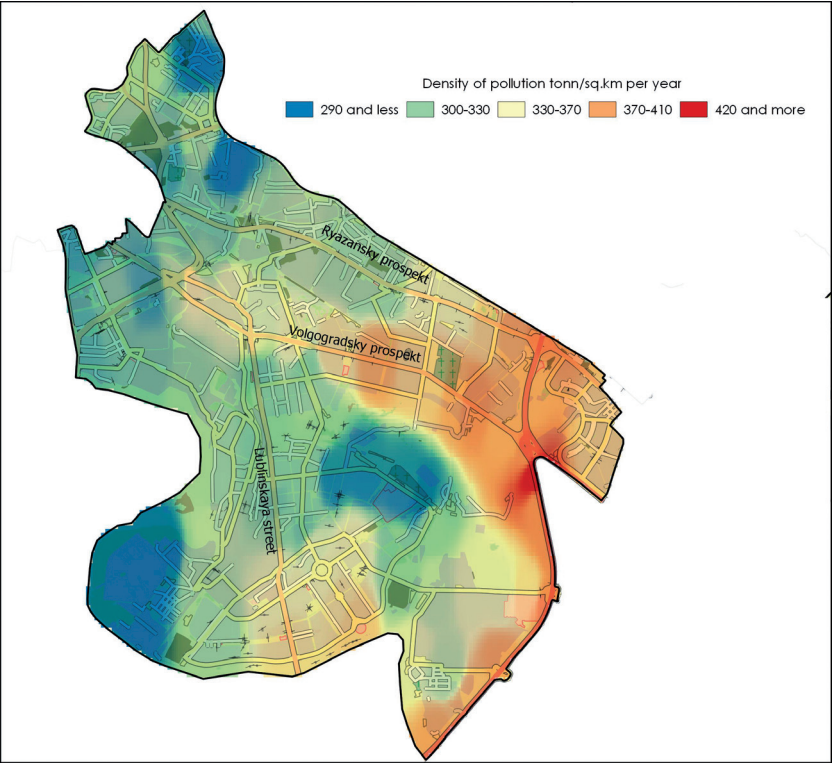**Fig. 6. Maximum road capacity in the South-East Administrative District (without Nekrasovka)**

Fig. 7. Emission density distribution in the South-East Administrative District (without Nekrasovka)

Outgoing highways of the district and the territories adjacent to MKAD are subject to the main average daily load. Despite the presence of natural emission reduction from MKAD to TRR, emission volumes do not differ significantly. Expansion of highways closer to the central part of Moscow up to TRR increases the average speed of traffic and decreases the duration of jams. Nevertheless, transformations of transport infrastructure in the district have not resolved the problem of road capacity in the South-East Administrative District. Ryazansky and Volgogradsky Avenues are still among the most loaded highways of the city at rush hours and the road from MKAD to TRR in the district can take up to 43-50 minutes.

CONCLUSIONS

The analysis of all the above-mentioned factors allows to reveal a number of trends in the dynamics of vehicles atmospheric emissions density over the past 7 years:

– the overall level of density of harmful substances emitted into the atmosphere of the city is decreasing in the entire territory of Moscow. Since the early 2000s the density of polluting emissions remained invariable for 40% of the territory, within 1000-3000 tons/sq.km per year, but over the past 7 years, large-scale road construction, development of public transport, improvement of the structure of vehicle fleet led to the situation when density of emissions does not exceed 500 tons/ sq.km per year for 70% of the territory of the city;

– currently, almost all areas with increased density of the pollutants emitted into the atmosphere are located only within the exposure limits of vehiclesation highways;

– the amplitude of fluctuations of atmospheric emission density has also decreased (by 1.5 times) suggesting the levelling of differences in pollution of the environment of the city. In general, a "blurring" of pollutants from vehicles across the territory of Moscow is observed for the reviewed period of 2011-2017. The previous periods witnessed a very high concentration of pollutants within the Garden Ring, while

2017 witnessed both the overall decrease in concentration of pollutants and a redistribution of harmful substances from vehicles between the territory of the Garden Ring and TRR. Thus, for the past 7 years a **more uniform environmental pollution** of the city is observed. On the one hand, anthropogenic impact is objectively moving from industrial and commercial areas to residential areas, with their hospitals, child care facilities, etc. Therefore, the number of people seriously affected by vehicle increases with a growing share of the most vulnerable demographic groups of population (children, the elderly, the sick and so forth).

On the other hand, this blurring of pollution areas reduces the sharpness of its perception, causes additional tolerance, unwillingness (and inability) to influence the authorities. The impact of environmental factor on the price of residential real estate which is quite low for a city with a high level of education can serve an example. According to realtors and buyer polls, there are more than fifteen factors influencing the price of residential real estate in the cities: quality of the object (house type, material of walls, condition of the apartment), size of housing and its location (proximity to the center, transport accessibility (first of all, subway)), prestige of the district, ecological situation, etc. (Bityukova et al. 2016).

Dynamics of air emission from vehicles is the result of both transformational and inherited factors. Impact level factors include the inherited quality of domestic cars. However, the majority of inherited development aspects boil down to motor emission distribution across the territory: the terrain, planning structure, bridges, road width, topology of the road network, low connectivity of the network, increased role of transit functions, etc.

REFERENCES

Azarov V.K., Kutenev V.F., Stepanov V.V. (2012). On the emission of particulate matter by vehicles, Ecology, №6 (77) pp. 55-58 (in Russian with English summary)

Basic Indicators of Environmental Protection--2017 (online) Federal State Statistics Service, http://www.gks.ru/bgd/regl/b_oxr17/Main.htm. [Accessed 02.12.2018]

Bityukova V., Sokolova E. (2008). On the brink of collapse Moscow's tangled traffic// Osteuropa: Zeitschrift fuer Gegenwartsfragen des Ostens. v. 58. № 4–5. P. 351-358+493

Bityukova V., Savoskul M., Kirillov P., Koldobskaya N. (2016). Transformation of environmental problems in Moscow: sociological dimension // GEOGRAPHY, ENVIRONMENT, SUSTAINABILITY, № 4, pp. 74-87

Bityukova V.R. (2019). Socio-environmental problems of the development of Russian cities. Moscow: Editorial URSS. (in Russian with English summary)

Bityukova V.R., Kasimov N.S., Vlasov D.S. (2011). Ecological Portraits of Russian Cities. Ecology and Industry of Russia, № 4, pp. 6-18 (in Russian with English summary)

Bityukova V.R., Mahrova A.G., and Sokolova E.P. (2006). Ecological situation as a factor in the differentiation of housing prices in Moscow, Moscow University Bulletin. Series 5. Geography.; 6, pp. 31-41. (in Russian with English summary)

Blinkin M., Koncheva E. (eds.), (2016), Transport systems of Russian cities: Ongoing transformation. Transformation research, economics and policy series. – Springer

Database of municipal indicators 2006-2018 (online) Federal State Statistics Service. http://www.gks.ru/free_doc/new_site/bd_munst/munst.htm [Accessed 02.12.2019]

Database on the forms of statistical tax reporting 2006-2018 (Report on the tax base and the structure of excise tax accruals on cars and motorcycles) (online) Federal tax service of Russia   https://www.nalog.ru/rn38/related_activities/statistics_and_analytics/forms/#t00 [Accessed 02.03.2019]

Demographic Yearbook. 2000-2018. (online) Federal State Statistics Service, http://www.gks.ru/free_doc/new_site/business/trans-sv/t3-4.xls [Accessed 02.03.2019]

Department of Natural Resources and Environmental Protection of Moscow (2002, 2018) Report on the state of the environment in the city of Moscow in 2002-2018. https://www.mos.ru/eco/documents/doklady/ [Accessed 02.03.2019]

Department of nature management and environmental protection of the city of Moscow State of the Environment Report in Moscow in 2017 (2018) (online) https://www.mos.ru/eco/documents/doklady/view/217165220/   [Accessed 11.07.2018]. (in Russian with English summary)

Department of nature management and environmental protection of the city of Moscow State of the Environment Report in Moscow in 2002 (2003) (online) https://www.mos.ru/eco/documents/doklady/view/217165220/ [Accessed 11.07.2018]. (in Russian with English summary)

Environmental protection in Russia —2016, 2017, 2018 (online) Federal State Statistics Service. http://www.gks.ru/bgd/regl/b16_54/Main.htm. [Accessed 02.12.2018]

GOST 56162-2014, 2014, (Emissions of pollutants into the atmosphere. Method of calculating emissions from motor vehicles when conducting summary calculations for urban settlements). Moscow: «Standartinform» (in Russian)

Hovavko I.Yu. (2012). Internalization of external effects of vehicles (on the example of Moscow) Moscow University Bulletin. Series 6. Economy. № 1, pp. 74-84 (in Russian with English summary)

Isalou A.A., Litman T., Shahmoradi B. (2014). Testing the housing and transportation affordability index in a developing world context: a sustainability comparison of central and suburban districts in qom, Iran TRANSPORT POLICY, Elsevier Science Publishing Company, Inc. pp. 33-39

Kichendzhi V., Khatoyama K. (2010). Moscow: transport problems of the metropolis. Moscow: Nauka (in Russian with English summary)

Kosheleva N.E., Dorokhova M.F., Kuzminskaya N.Y., Ryzhov A.V. and Kasimov N.S. (2018) Impact of motor vehicles on the ecological state of soils in the western district of Moscow. Moscow University Bulletin. Series 5. Geography. №2, pp. 16-27. (in Russian with English summary)

Litman T. (2002). Transportation Cost Analysis: Techniques, Estimates and Implications (online) Victoria Transport Policy Institute Website. June. URL: http:// www.vtpi.org/tca/tca00.pdf/ [Accessed 11.12.2018]

Parsaev E.V., Malyugin P.N. Teterina I.A. (2018). Metodology for the calculation of emissions for non-stationary transport flow, The Russian Automobile and Highway Industry Journal, vol. 15, № 5. , pp. 686-697.

Popov A A. (2007). Territorial differentiation of the quality of the urban environment in Moscow, Moscow University Bulletin. Series 5. Geography.; 4 pp. 29—36. (in Russian with English summary)

Regions of Russia. Annual Update (The number of owners of cars in the regions of the Russian Federation per 1000 people) 2000-2018. (online) Federal State Statistics Service, http://www.gks.ru/free_doc/new_site/business/trans-sv/t3-4.xls [Accessed 02.12.2018]

Revich B.A. (2018), Fine suspended particles in atmospheric air and their impact on the health of residents of megalopolises // PEMME, vol. XXIX, № 3, pp. 53-78 (in Russian with English summary)

Revich B.A., Kuznetsova O.V. (Ed.), (2018), Man in a megacity: the experience of interdisciplinary research. Moscow: LENAND. - 640 p. (in Russian with English summary)

Rodrigue J.-P. (2017) The Geography of Transport Systems. New York: Routledge.

The concept of assessing the level of development of urban agglomerations (2016) (online) The Institute for Urban Economics Foundation http://www.urbaneconomics.ru/sites/default/files/koncepciya_ocenki_urovnya_razvitiya_gorodskih_aglomeraciy_13.01.17.pdf [Accessed 02.03.2019]

Transport of Russia (2015) (online) Federal State Statistics Service, http://www.gks.ru/free_doc/new_site/business/trans-sv/t3-4.xls [Accessed 02.03.2019]

Vuchik V.R. (2011). Transportation in cities suitable for life. Moscow: Territoriya budushchego (in Russian with English summary)

Yakshin A.M. (1975) Prospects for the development of a network of urban highways. Moscow: Strojizdat (in Russian)

Yakushev, AB, Kurolap, SA, Karpovich, MA, (2013), Environmental Impact Assessment of Automobile Transport on the Air Basin of the Cities of the Central Black Soil Region - Voronezh: "Scientific Book"(in Russian with English summary)

**Mikhail I.Varentsov[1,2,3]*, Mikhail Y. Grishchenko[1]
and Hendrik Wouters[4]**

[1] Lomonosov Moscow State University, Faculty of Geography / Research Computing Center, Moscow, Russia

[2] A.M. Obukhov Institute of Atmospheric Physics, Moscow, Russia

[3] Hydrometeorological Research Center of Russia, Moscow, Russia

[4] Ghent University, Department of Forest and Water Management, Ghent, Belgium

*Corresponding author: mvar91@gmail.com

SIMULTANEOUS ASSESSMENT OF THE SUMMER URBAN HEAT ISLAND IN MOSCOW MEGACITY BASED ON *IN SITU* OBSERVATIONS, THERMAL SATELLITE IMAGES AND MESOSCALE MODELING

ABSTRACT. This study compares three popular approaches to quantify the urban heat island (UHI) effect in Moscow megacity in a summer season (June-August 2015). The first approach uses the measurements of the near-surface air temperature obtained from weather stations, the second is based on remote sensing from thermal imagery of MODIS satellites, and the third is based on the numerical simulations with the mesoscale atmospheric model COSMO-CLM coupled with the urban canopy scheme TERRA_URB. The first approach allows studying the canopy-layer UHI (CLUHI, or anomaly of a near-surface air temperature), while the second allows studying the surface UHI (SUHI, or anomaly of a land surface temperature), and both types of the UHI could be simulated by the atmospheric model. These approaches were compared in the daytime, evening and nighttime conditions. The results of the study highlight a substantial difference between the SUHI and CLUHI in terms of the diurnal variation and spatial structure. The strongest differences are found at the daytime, at which the SUHI reaches the maximal intensity (up to 10°C) whereas the CLUHI reaches the minimum intensity (1.5°C). However, there is a stronger consistency between CLUHU and SUHI at night, when their intensities converge to 5–6°C. In addition, the nighttime CLUHI and SUHI have similar monocentric spatial structure with a temperature maximum in the city center. The presented findings should be taken into account when interpreting and comparing the results of UHI studies, based on the different approaches. The mesoscale model reproduces the CLUHI-SUHI relationships and provides good agreement with *in situ* observations on the CLUHI spatiotemporal variations (with near-zero biases for daytime and nighttime CLUHI intensity and correlation coefficients more than 0.8 for CLUHI spatial patterns). However, the agreement of the simulated SUHI with the remote sensing data is lower than agreement of the simulated CLUHI with *in situ* measurements. Specifically, the model tends to overestimate the daytime SUHI intensity. These results indicate a need for further in-depth investigation of the model behavior and SUHI–CLUHI relationships in general.

KEY WORDS: urban heat island, UHI, SUHI, urban climate, mesoscale modelling, remote sensing, thermal satellite images, land surface temperature, Moscow, MODIS, COSMO

INTRODUCTION

An essential climatological feature of most urban environments is the positive temperature deviation from the rural surroundings, which is known as the urban heat island (UHI) effect (Oke 1982). The relevance of UHI studies is related to its impacts on ecosystems (Esau and Miles 2016), assets and services of human society such as damage to infrastructure and heating/cooling demands (Davies et al. 2008) and, most importantly, health and comfort of the urban population (Buechley et al. 1972; Dousset et al. 2011; Tan et al. 2010a). Nowadays, UHI studies mainly use three types of data: *in situ* temperature observations, remote sensing data (thermal satellite images) and climate model simulations, which are described below.

Regular *in situ* temperature observations are practiced at regular weather stations of national hydrometeorological services and other observational networks. They are usually made at the height of 2 m above the ground registering the near-surface air temperature (hereafter referred as SAT). SAT is one of the essential applied climate variables (GCOS 2010) used, apart from other calculations, in the calculation of biometeorological indices (Emelina et al. 2014). However, the regular weather stations are usually located outside of the urban areas or in urban parks that makes the data of such observations inappropriate for urban climate studies (Peterson 2003). Dense urban meteorological networks are created for scientific and monitoring purposes (e.g. Konstantinov et al. 2018), but only in a few dozens of cities around the world (Muller et al. 2013).

Remote sensing data is used to derive land surface temperatures (hereafter referred as LST) by the processing of thermal satellite images. In contrast to highly fragmented *in situ* measurements, satellite images provide a continuous and global spatial coverage. Such data can be subdivided into two types: high spatial resolution data recorded by ASTER, ETM +, TIRS imaging systems, and low resolution data obtained by MODIS, AVHRR and some others. Both data types have their advantages: the high-resolution data allows studying thermal structure of urban landscapes in more detail (Zhu et al. 2002; Sobrino et al. 2012; Baldina and Grishchenko 2014), whereas the low-resolution data offers a much higher sample frequency up to first dozens of minutes (Cheval and Dumitrescu 2017).

It is important to note that remote sensing and *in situ* data characterize different meteorological variables: the land surface temperature (LST) and the near-surface air temperature (SAT). These variables are generally different from each other, and their relationship is complex from a theoretical and empirical perspective (Yang et al. 2017). For example, on a hot summer day, LST can reach 60–70°C while SAT remains at about 30–35°C (Gornyy et al. 2016; Sobrino et al. 2012). The UHI effect is pronounced in the field of both variables, however the urban LST and SAT anomalies have different patterns of spatial and temporal (diurnal and seasonal) variations (Voogt and Oke 2003; Sheng et al. 2017; Sun et al. 2015). Due to such differences, the UHI signal in LST (hereafter referred as surface UHI or SUHI) and UHI signal in SAT (hereafter referred as canopy-layer UHI or CLUHI) are usually treated separately in modern urban climate studies (Voogt and Oke 2003).

Historically, the UHI has been discovered and studied for a long time as an anomaly of *in situ* observations of SAT at urban sites compared to rural areas. However, the rapid development of remote sensing technolo-

gies results in a recent exponential increase of SUHI studies (Zhou et al. 2018). Remote sensing data is now being used in a large number of SUHI studies, including the researches of the SUHI climatology (Choi et al. 2014; Miles and Esau 2017; Peng et al. 2012; Zhou et al. 2013) and spatial structure (Zhou et al. 2017) on the global or regional scale, and in more detailed theoretical and applied studies for specific cities. For example, Shen et al. (2016) and Gorny et al. (2016) used the high-resolution remote sensing data on LST to assess the urban climate change in Wuhan (China), Saint-Petersburg (Russia) and Kiev (Ukraine). Dousset et al. (2011) applied the remote sensing LST data to correlate environmental factors with a heat-related mortality for Paris during a heat wave. Another example is a series of urban climate studies for the city of Bucharest (Cheval and Dumitrescu 2015, 2017).

In most SUHI studies the authors note the significant differences between SUHI and CLUHI, but such difference does not prevent authors from making fundamental or applied conclusions on urban climatology. At the same time, the relationship between the SUHI and CLUHI still requires further detailed study (Zhou et al. 2018).

Rapid development of computing technologies and numerical methods for representing the processes occurring in the atmosphere have opened wide opportunities for application of the numerical modelling methods in urban climate studies. Mesoscale atmospheric models use a horizontal grid step of a few km. They are able to simulate the meteorological regime of a big city (see e.g. Martilli et al. 2002; Bohnenstengel et al. 2011; Wouters et al. 2016) with high spatial and temporal resolution, including the UHI effect and urban-induced mesoscale circulations, which are known as "urban breezes" (Lemonsu and Masson 2002). Such models could be used for assessing the urban climate change scenarios (Krayenhoff et al. 2018; Wouters et al. 2017). However, practical and scientific applications of such models require their accurate calibration and verification by comparing the results obtained from the models and from the observations. Remote sensing data al-

lows verifying the models for areas, including the urban ones that are not covered by *in situ* observations. However, the experience of using the remote sensing data for verification of the mesoscale models for urban areas is very limited due to a number of problems, which are related to the presence of clouds, to the LST dependence from the sensor view angle and to the anisotropy of a three-dimensional urban geometry (Hu et al. 2014).

Thus, *in situ* temperature observations, remote sensing data and modelling methods are actively used to study the UHIs. All of the approaches have benefits and shortcomings that are summarized in Table 1. Quite often, these approaches are used together (e.g. Konstantinov et al. 2015; Mariani et al. 2016; Sheng et al. 2017). However, there is a lack of studies focused on assessment of the contrasting behavior of the SUHI and CLUHI, and the models performance in reproducing such features. Moreover, such a comparison has never been carried out for Moscow megacity, despite the abundance of the UHI studies for Moscow within the framework of each of the considered approaches (e.g. Grishchenko 2012; Climate of Moscow… 2017; Lokoshchenko 2014).

Here, we present the simultaneous assessment of the surface UHI and canopy-layer UHI and their contrasting dynamics based on three quantitative methods, namely *in situ* observations, thermal satellite images and high-resolution regional climate modelling. We use the data on *in situ* SAT observations obtained from a dense network of weather and air-quality stations in the Moscow region to quantify the CLUHI and MODIS thermal satellite images to quantify the SUHI. We use the regional climate model COSMO-CLM (Rockel et al. 2008), coupled with the specific urban canopy scheme TERRA_URB (Wouters et al. 2016) to simulate the meteorological regime of the Moscow region, including the both types of the UHI, with a high (1 km) spatial resolution.

The aim of the study is the qualitative and quantitative comparison of the UHI features, which are evaluated according to the three considered methods, and analysis of their differences. We consider summer conditions, for

Table 1. A brief summary of the benefits and shortcomings of the three considered approaches to quantify the UHI

Approach to study the UHI	Analyzed variable and UHI type	Benefits	Shortcomings
In situ meteorological observations	SAT (other measured weather parameters are also available); CLUHI	The most precise data on air temperature with relatively high and regular temporal resolution, e.g. 3 hours for the most of regular weather stations	(1) irregular and discontinuous spatial coverage, which is usually especially poor in urban areas; (2) limited data access
Thermal satellite images	LST; SUHI	(1) continuous and near-global spatial coverage; (2) high spatial resolution, e.g. 1 km for MODIS system; (3) easy data access	(1) limited and irregular temporal resolution, e.g. 2 daytime and 2 nighttime images per day for MODIS system; (2) data is available only for cloud-free conditions
Mesoscale atmospheric modelling	SAT and LST (other modelled atmospheric, surface and soil variables are also available); CLUHI, SUHI and UHI in the ABL	(1) continuous spatial coverage; (2) high spatial and temporal resolution, e.g. 1 km and 1 hour; (3) an opportunity to access data on dozens modelled variables for different vertical levels; (4) an opportunity to change the model settings, land-use data, etc. in order to study the model responses to these changes	(1) the model simulations require the computational resources and the external data (initial and boundary conditions, land-use data, etc.); (2) high-resolution simulations are possible only for a limited area; (3) the models are not perfect and may strongly deviate from reality; (4) model verification is a necessary part of a model-based study

which the UHI studies are more relevant, due to the negative UHI impact on the biometeorological comfort. The summer of 2015 was selected because of the availability of the *in situ* data for the biggest number of sites, including several new automatic weather stations.

The study is structured as follows. The next section (Data and Methods) provides a detailed description of *in situ* observations, remote sensing data and modelling techniques. Section Results presents the results of the comparison of three quantitative methods. Section Discussion interprets and discusses the revealed differences between the methods. The last section (Conclusion) is the conclusion; it gives the practical recommendation for applied studies and actualizes the needs for further theoretical studies.

DATA AND METHODS

The study area and in situ observations

The city of Moscow is the biggest monocentric urban agglomeration in Russia and Europe with a population of about 16-17 million people (Cox 2018). The area of the city (administrative unit of Russia) is 2561 km², however it includes a wide area known as "New Moscow", which was joined to the city in 2011, but remains practically unbuilt. The actual area of the city (excluding the suburbs and satellite cities) is about 1000 km². Moscow is densely built with the midrise and high-rise block-houses. According to the popular classification of Stewart and Oke (2012), the prevailing types of local climate zones (LCZs) in Moscow are LCZ 5 (compact midrise) and LCZ

6 (open high-rise), while the historical city center is mostly covered by LCZ 2 (compact midsize) and several industrial areas (LCZ 10) are scattered within the city (Samsonov and Trigub 2018). There are a number of parks and urban forests in the city, including the two biggest ones, Losiny Ostrov National Park in the north-eastern part of the city and Bitsa Park in the southern part of the city. The area around the megacity is mostly covered by forests or croplands. The only big water bodies in the Moscow region are the water reservoirs located to the north of Moscow.

The city of Moscow serves as an optimal testbed for urban climate studies due its size, flat and homogeneous surrounding terrain, compact and relatively symmetric shapes. The dense meteorological network provides for *in situ* observations in the city and in its surroundings. Long-term meteorological observations are carried out at regular weather stations (hereafter referred as WSs) of the national hydrometeorological service (Roshydromet). Several WSs are located within the urban area, including Balchug WS in the city center and meteorological observatory of Lomonosov Moscow State University (MSU) in an urban park. More recent and denser networks include automatic weather stations (hereafter referred as AWSs) of the national hydrometeorological service and automatic air-quality stations (hereafter referred as AAQS) of Budgetary Environmental Protection Institution "Mosecomonitoring". The AWS network has been developed since 2012, whereas the AAQS network – since the 1990s. Meteorological observations at the AAQSs do not comply with the standards of the World Meteorological Organization (WMO) (e.g. the sensors are located at 4 m above the ground instead of 2 m as directed by WMO standards). Hence, AAQS data should be used with caution. However, previous studies have shown that AAQS observations are suitable for the analysis of the UHI in terms of the daily-mean or mean nighttime temperatures (Climate of Moscow… 2017).

In our study, we use regular SAT observations on 3-hourly intervals at 16 WSs (including 5 airport WSs), 11 AWSs and 37 AAQSs located in Moscow and its surroundings (Fig. 1). The basic study area is selected according to the location of these stations. It spans an area between 55.35 and 56.07 °N, and between 36.68 and 38.73 °E. Further comparison of three considered approaches is performed for this region. In addition, we use observations at 6 WSs located outside the central
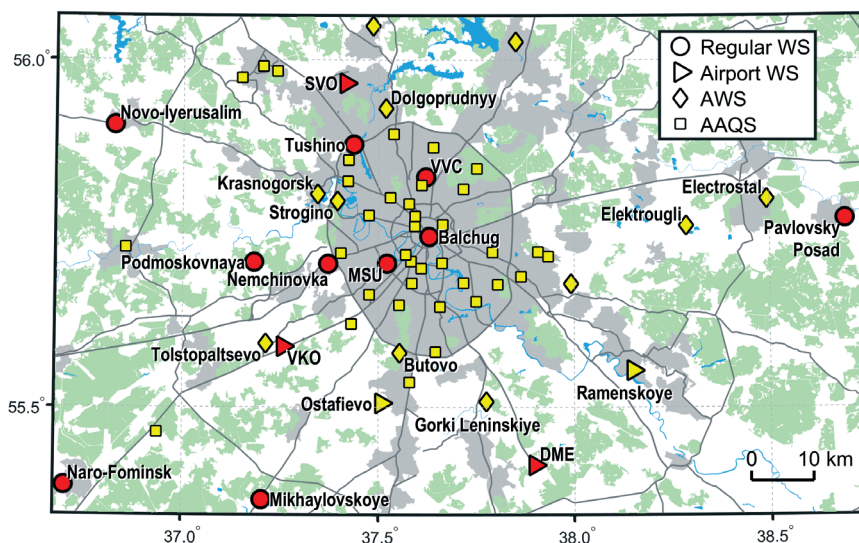
Fig. 1. Location of the weather stations, AWSs and AAQSs within the basic study area. Red color indicates the weather stations with long-term observation data, yellow color indicates the new observation sites (AWSs, AAQSs and two new airports). Urban areas, forests and primary highways are shown according to OpenStreetMap data

study region (Fig. 2) to evaluate the UHI intensity according to *in situ* observations. All observational data were collected in a single database and processed by quality control and gap filling routines; see details in (Climate of Moscow… 2017).

In situ LST observations are also carried out at the number of WSs. However, they are not carried out at the AAQSs. It should be noted that the measured LST characterizes the local conditions at the point of measurement and may not correspond to typical conditions of the surrounding landscape, especially for urban conditions. For these reasons, *in situ* data on LST is not used in our study.

Satellite images

As satellite data on the surface temperature, we use the data of the MODIS (Moderate Resolution Imaging Spectroradiometer) sensor operating on the Terra and Aqua satellites, namely the MOD11A1 and MYD11A1 rasters (data collection 6) with a grid spacing of 1 km. The MODIS sensor captures images in 36 channels of the visible, near infrared, short-wave infrared and thermal infrared ranges of the spectrum. The LST is determined from the channels 31 and 32 (10.78–11.28 and 11.77–12.27 µm, respectively) in the range that accounts for the maximum of the Earth's radiation (10–12 µm). This data is available on the NASA Earthdata web-portal (https://earthdata.nasa.gov/). The LST values for the daytime and nighttime images are contained in the LST_Day_1km and LST_Night_1km layers, respectively. For the Moscow region, the registration time of daytime (nighttime) Terra images is approximately 11:30 (21:50) MSK, for Aqua images – approximately 12:40 (02:30) MSK. Hence, MODIS data can be used for UHI studies for daytime (Terra and Aqua images), evening (Terra) and nighttime (Aqua) conditions. The zenith angle for the most of images is 25–30°.

For the further analysis, we selected images with a cloud cover less than 25% within the analyzed area, within a radius of 25 km and 10 km from the center of Moscow (three conditions must be fulfilled simultaneously). In total, we selected 21 daytime and 9

nighttime images from the Terra satellite, 19 daytime and 14 nighttime images from the Aqua satellite over the summer of 2015. Based on the selected images, the average LST was calculated. In order to avoid distortion of the average LST by gaps in the data, related with remaining cloud-covered pixels, data for such pixels was restored using the linear interpolation method from the data on the neighboring pixels.

Regional mesoscale modelling

We use the limited-area mesoscale model COSMO-CLM (Rockel et al. 2008) to simulate the meteorological regime of the Moscow region. The model is developed by the COSMO international consortium (Consortium for Small-scale Modelling, www.cosmo-model.org) and used for numerical weather prediction in many countries of the world, including Russia (Vil'fand et al. 2010). The COSMO-CLM version of the model is adapted for long-term simulations (Rockel et al. 2008). It is developed by the CLM community (www.clm-community.eu) and frequently used for regional climate studies. The model provides a numerical solution of nonhydrostatic thermo-hydrodynamical equations describing compressible flow in a moist atmosphere with given initial and boundary conditions. Thermal and humidity regime of the soil active layer is simulated by the TERRA module, which takes into account heat and humidity transport, evapotranspiration and other processes in the soil (Doms et al. 2011). Hence, the land surface temperature, which is important in our study, is a prognostic variable of the model.

The COSMO-CLM model is used in our study for a dynamic downscaling of the ERA-Interim reanalysis data (Dee et al. 2011) for the Moscow region. We use nested modelling domains D1, D2 and D3 (Fig. 2) with a grid spacing of 12, 3 and 1 km, respectively. These grids are designed in a rotated geographical coordinate system, where the origin (0 °N, 0° E) is moved to the center of Moscow. The inner model domain D3 covers the area of 180×180 km around Moscow center. A more detailed description of the simulations for Moscow is presented in previous studies (Varentsov et al. 2017a; 2017b;

2018). It includes the description of the calibrated configuration of the model reducing the systematic biases. The simulations are performed for the period from 1st May to 31st August 2015.

The urban canopy model (UCM) TERRA_URB (Wouters et al. 2016) is used to take into account the urban physics in terms of surface energy and moisture exchanges including the influence of street-canyon geometry. TERRA_URB scheme provides the corrections of the surface parameters (roughness length, albedo, emissivity, heat capacity, etc.) within the framework of TERRA module using the semi-empirical urban canopy dependences. In contrast to more complex UCMs such as TEB or BEM schemes (Martilli et al. 2002; Masson 2000), TERRA_URB scheme does not consider the road, roof and wall surfaces separately. Instead, the city is considered as a horizontal surface with radiative and thermodynamic properties that complies to the structure of the urban canopy. The anthropogenic heat flux (AHF) is parameterized according to (Flanner 2009)

(a)

(b)
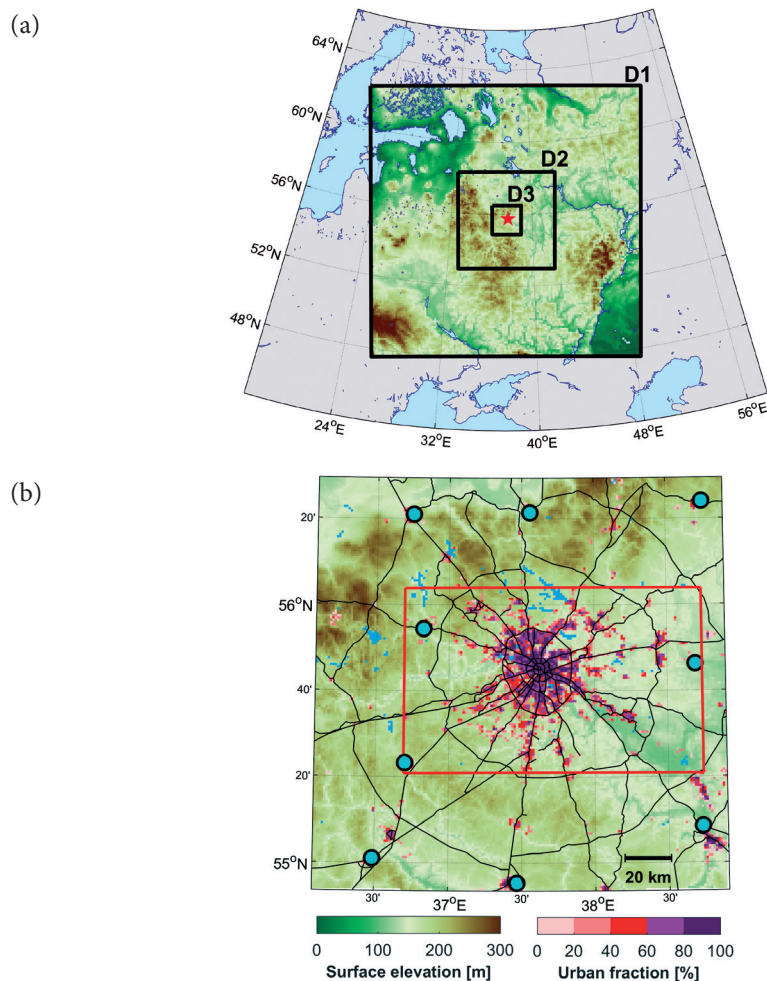
Fig. 2. The cascade-nested domains D1, D2 and D3 of the simulations with the COSMO-CLM model, with surface elevation is indicated by the color scale, and water surfaces – by the light-blue color (a). The detailed map of the inner D3 domain with urban fraction is indicated by an additional color scale (b). The cyan circles in (b) indicate the location of the WSs used for mean rural temperature assessment, the red rectangle indicates the basic study area that corresponds to Fig. 1. Black lines in (b) indicate the primary road network according to OpenStreetMap data

taking into account the annual-mean value together with its typical diurnal and annual variations and the dependence of its annual amplitude on the latitude. To describe the heterogeneity of the urban surface, TERRA_URB implements the so-called tile approach, for which urbanized and natural parts can coexist in each grid cell of the model. Hence, the LST and SAT values, heat fluxes and other soil or surface variables are simulated separately for natural and urban tiles in each grid cell of the model. The average values for each grid cell are calculated taking into account the area fraction of urban and natural tiles.

The application of the TERRA_URB scheme requires the definition of several urban canopy parameters for each grid cell of the model. These parameters are: urban area fraction (UF), annual-mean AHF, roof area fraction, mean building height (H) and H/W ratio, where W is mean street width. We use original method of GIS-based analysis of OpenStreetMap data to obtain these parameters (Samsonov et al. 2015; Varentsov et al. 2017b). The estimation of the mean annual AHF for each grid cell of the model is based on the estimate of its city-average value of 75 Wt/m^2 (Stewart and Kennedy, 2017). The spatial distribution of the urban fraction is shown in Fig. 2b. According to Wouters et al. (2016), thermal and radiative properties (albedo, emissivity, heat capacity and heat conductivity) of the urban materials are defined as constants over the urban area with minor changes (albedo of the urban substrate was set to 0.15; volumetric heat capacity was set to $1.6 \cdot 106$ J·K^{-1}·m^{-3}; heat conductivity to 0.8 W·K^{-1}·m^{-1}).

The model output contains dozens of meteorological parameters, related to the atmosphere, soil and land surface. In our study we use the modelled SAT and LST values, available on 1-km grid of D3 domain with 1-hour intervals.

Methodology for comparison of the three temperature data types

The comparison of the three considered approaches requires a geographical consistency between the two gridded datasets (MODIS images and COSMO-CLM simulations) and the *in situ* observations. Since the MODIS data and modelling results are available on different grids, we use bicubic interpolation to transfer MODIS data onto the projection and the grid used in the COSMO-CLM model. The further analysis uses the COSMO-CLM grid. In order to take into account possible discrepancies between the land-use data of the model grid and the actual location of the observational sites, a following method is applied. The comparison of the modelling results and *in situ* observations is performed for the model grid cells that are selected among 9 nearest grid cells taking into consideration the land use type (e.g. WS in urban environment was compared with a grid cell with a high urban fraction) (see details in Varentsov et al. 2017a). The same grid cells are used for the comparison of the *in situ* and remote sensing data. Modelling results available on hourly intervals and *in situ* data available on three-hourly intervals are interpolated in time for the registration time of MODIS satellite images.

RESULTS

Moscow UHI according to remote sensing data and in situ observations

In this section, the Moscow SUHI according to MODIS-derived LST data averaged over the selected cloud-free satellite images is analyzed and compared with *in situ* SAT observations. In order to quantify the SUHI, we define the LST anomaly (ΔLST) as departure from the mean LST value (T0), which is averaged over all rural grid cells within the study area. Grid cells are classified as rural if they are located outside of the 1 km (1 grid cell) buffer around the urban cells (with urban fraction > 0).

The intensive SUHI is clearly identified both for daytime, evening and nighttime conditions (Fig. 3). The mean maximum ΔLST reaches approximately 10°C at daytime, 5.5°C at evening and 6°C at night. However, there is a clear difference between the spatial structure of the daytime and evening/nighttime SUHIs. The daytime LST field is characterized by high spatial variability

(a)

(b)

(c)
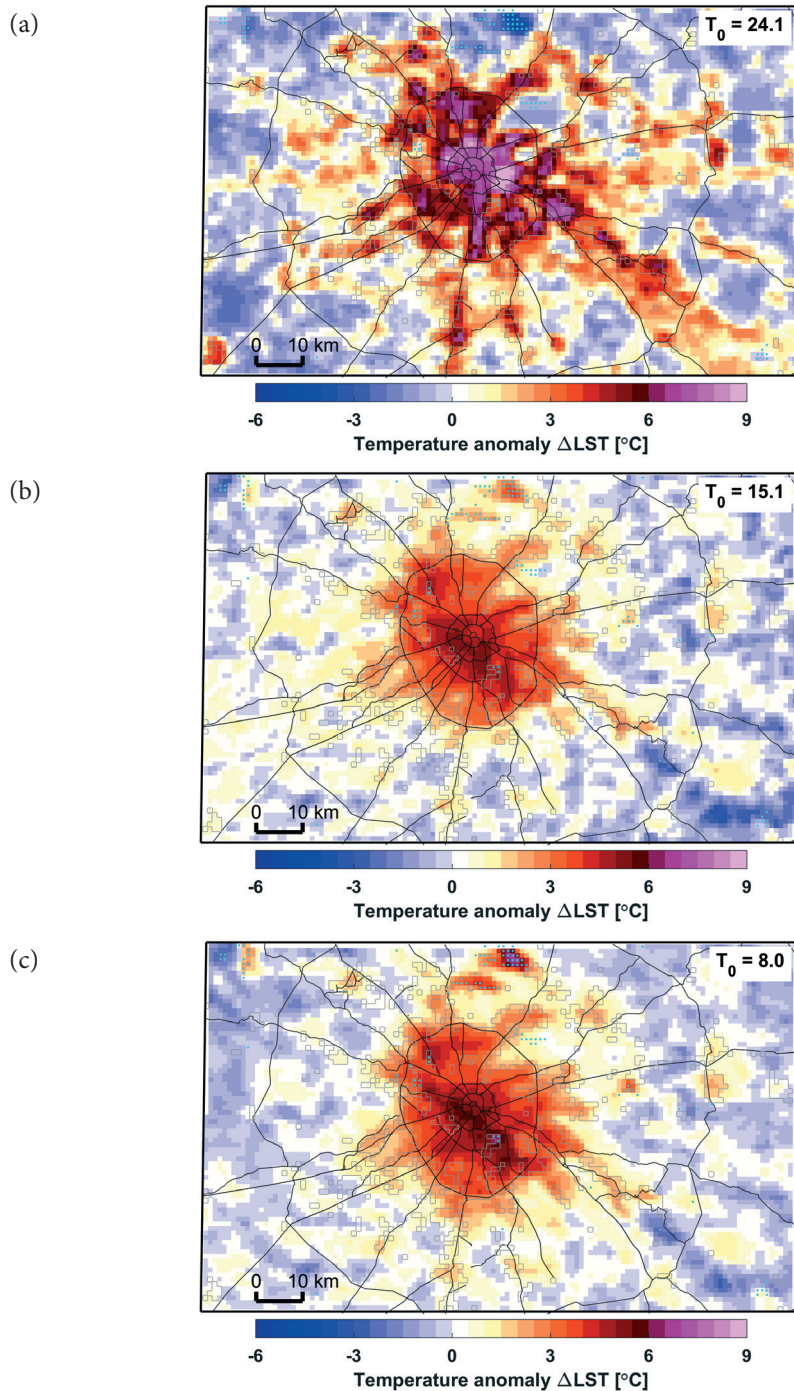
Fig. 3. Anomalies of the Land surface temperature (ΔLST) according to MODIS data, averaged over selected daytime (a) and evening (b) Terra images and nighttime Aqua images (c). Anomaly is defined as a difference between the LST and its mean rural value T0 (see details in text). Black lines indicate the primary highways according to OpenStreetMap data, gray contours indicate urban grid cells, cyan points indicate water grid cells

and sharp gradients between the urban and non-urban areas. The pronounced LST anomalies are found in all urban areas, including the city edges and small satellite towns around Moscow, and there are several isolated hotspots within the city. At the same time, the urban parks and green areas appear as cool as rural landscapes outside of the megacity. The evening/nighttime LST field is smoother. The nighttime SUHI is shaped as monocentric temperature anomaly, where the area of maximum temperatures is located in the central part of the city and extends from the northeast to the south-west. The city center is significantly warmer than urban periphery and satellite towns. Moreover, the positive anomaly is distributed over the few kilometers outside of the urban areas. In contrast to daytime conditions, the urban parks are warmer than rural areas outside of the city.

The principal difference between the daytime and nighttime conditions is also found in terms of relationship between the MODIS-derived SUHI and CLUHI, evaluated according to *in situ* data (Fig. 4). The spatial patterns of the evening/nighttime SUHI and CLUHI are highly correlated ($R^2 >$

0.7), and the range of urban-rural LST and SAT differences is quite similar. Indeed, the evening/nighttime SAT in the city center (Balchug WS and nearest AAQSs) is 5-6°C higher than in the rural areas, which is consistent with evening/nighttime ΔLST maxima. In contrast, the correlation between SAT and LST spatial patterns is much lower during the daytime ($R^2 \approx 0.4$), while the LST spatial variability is 2-3 times higher than SAT variability. The city center is only 1.5°C warmer than the rural areas (on average) during the daytime in terms of air temperatures, while the urban LST anomalies exceed 10°C.

Comparison of the modelling results, remote sensing and in situ data

The revealed difference between the daytime and nighttime SUHI-CLUHI relationships is based on the comparison of the MODIS LST data with a continuous spatial coverage and in situ SAT observations that are highly fragmented in space. We further use the modelling results to check the revealed SUHI–CLUHI relationships based on the data with a continuous spatial coverage. In addition,
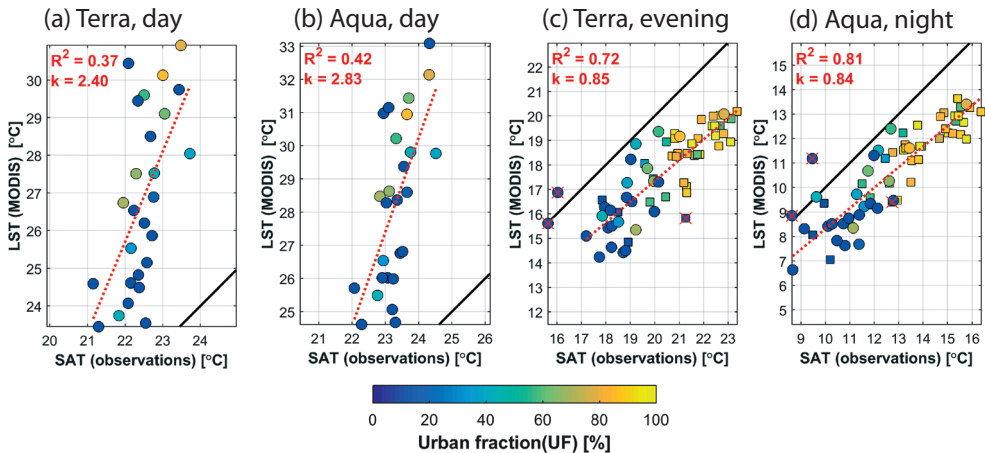
Fig. 4. Relation between LST and SAT values according to *in situ* observation and MODIS remote sensing data, averaged over selected daytime (a, b) and evening (c) and nighttime (d) Aqua/Terra images. Circle markers indicate AAQSs, square markers indicate WSs and AWSs. AAQS data is not used for daytime conditions. Color indicates the urban fraction in the corresponding model grid cells. Red lines indicate linear trends. The coefficient of determination (R^2) and slope (k) of the linear trends are shown for each panel. Red crosses indicate points that were excluded from linear regression due to the specific microclimatic features of corresponding sites. Solid black lines are one-to-one lines

we consider the opportunity to use MODIS LST data for the model verification as an additional verification to the one that is based on *in situ* observations.

Prior to comparison of the modelling results and MODIS data, it is important to highlight the key results of the model–observation comparison for air temperature and other meteorological parameters, which are presented in details in previous studies (Varentsov et al. 2017a, 2017b, 2018). Such comparison has shown that the model successfully reproduces the summertime meteorological regime of the Moscow region including the temporal variability of mean rural temperature and CLUHI intensity for the city center, including the diurnal and synoptic-scale variations and extremes of CLUHI intensity that reaches 8-9°C at calm and clear nights (Fig. 5). The model also adequately simulates the spatial structure of the CLUHI in field of mean summer temperature (Fig. 6). Approximately the same agreement is found between the observed and simulated SAT values, averaged over the specific moments of registration of the selected satellite images (not shown).

The fields of modelled SAT and LST, averaged over the moments of registration of
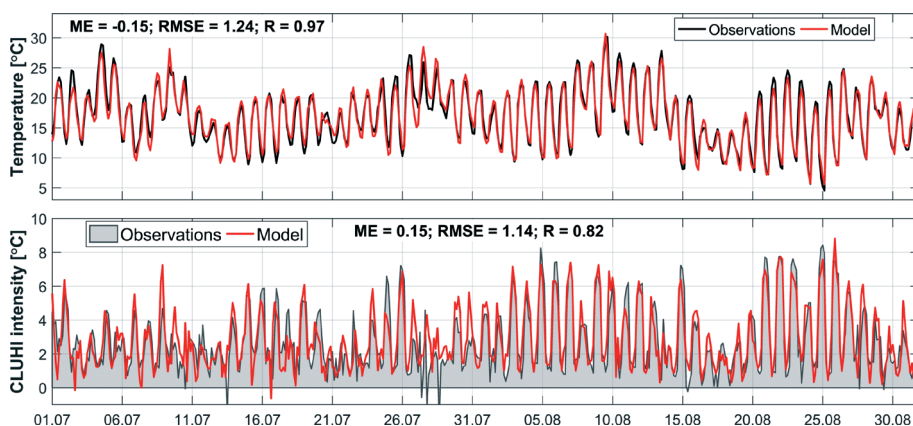
Fig. 5. Temporal variation of the mean rural air temperature (top panel) and CLUHI intensity for Balchug WS in the city center (lower panel) according to in situ observations and modeling results during July–August 2015. Mean rural temperature is averaged for each moment over nine rural WSs around Moscow (Fig. 2b); CLUHI intensity is defined as the difference between the temperature at the urban station and the mean rural value. The mean error (ME, °C), root-mean square error (RMSE, °C) and correlation coefficient (R) for model–observation comparison are shown for each panel
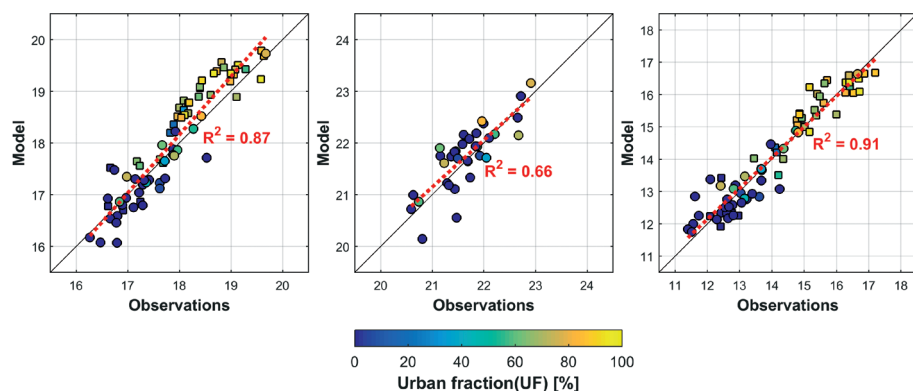
**Fig. 6. Comparison of the observed and modelled SAT values for daily-mean (left panel), daytime (15:00 MSK, center panel) and nighttime (03:00 MSK, right panel) values, averaged over the summer of 2015. Designations are similar to Fig. 4. The coefficient of determination of the linear trend (R^2) is shown for each panel. Solid black lines are one-to-one lines**

the selected Terra images, are presented in Fig. 7. Generally, the modelling results are consistent with MODIS remote sensing data (Fig. 3) in terms of spatial structure of LST fields and SUHI spatial patterns. The agreement is also found for the moments of registration of the selected Aqua images (not shown). However, the modelled SUHI intensity largely exceeds the MODIS-derived values: the modelled urban–rural LST differences exceed 16°C, while the urban LST anomaly according to MODIS data does not exceed 10°C. The modelled SUHI–CLUHI relationships confirm the results that are obtained based on MODIS data and *in situ* observations. The CLUHI and SUHI are almost equally intensive at evening and night, and their spatial patterns are strongly correlated. R^2 coefficient of the correlation between the modelled SAT and LST is higher than 0.85 both for considered mean nighttime and evening fields, both for urban and rural areas. At the daytime the pronounced SUHI is loosely correlated with a weak CLUHI, $R^2 < 0.3$. Moreover, the day-

time modelled CLUHI is weakly correlated with urban area fraction, since the warmest areas are shifted to the south-east of the city and further to the south-eastern rural areas.

In order to quantify the relationships between the modelling results and remote sensing data, we present a comparison of the MODIS-derived LST values versus modelled LST and SAT values (Fig. 8). In contrast to the very good agreement between the modelling results and *in situ* observations (Figs. 5, 6) and general agreement between the model and MODIS data on the CLUHI–SUHI relationships discussed previously, the agreement between the modelled and MODIS-derived LST values is lower. For the daytime conditions, in addition to significant overestimation of the SUHI intensity by the model, the spatial correlation between the modelled and observed LST values is quite weak ($R^2 \approx 0.6$ for all grid cells and only ≈ 0.4 for urban grid cells) that results in the significant scatter of points in
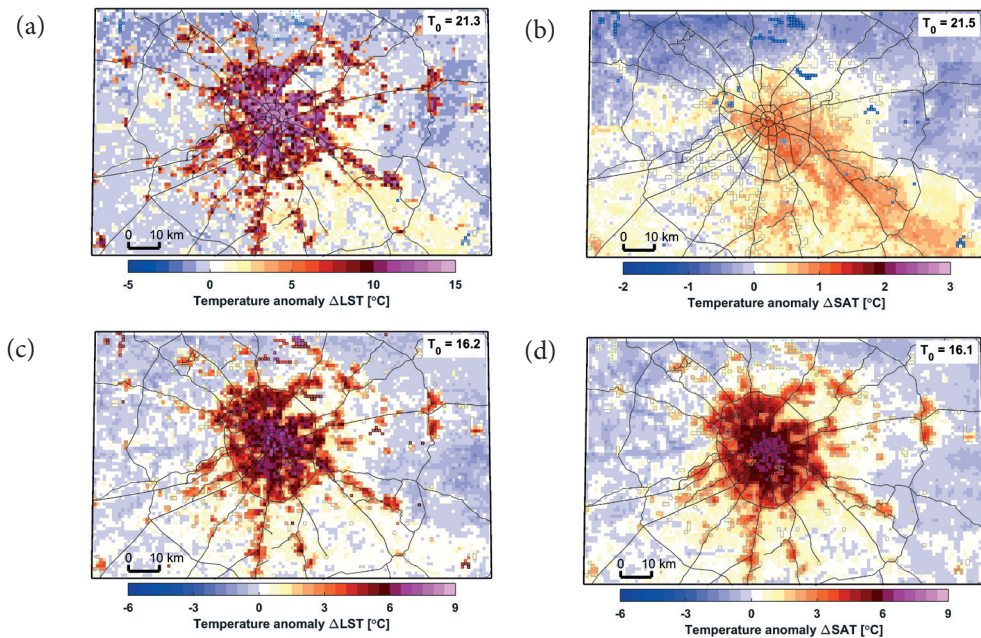
Fig. 7. Modelled fields of land surface temperature anomaly ΔLST (a, c) and surface air temperature anomaly ΔSAT (b, d), averaged over the moments of registration of the selected daytime (a, b) and evening (c, d) Terra images. Anomaly is defined as the departure from the mean rural LST/SAT value T_0 (see details in text). Black lines indicate the primary highways according to OpenStreetMap data, gray contours indicate urban grid cells, cyan points indicate water grid cells. Note that the color scale is different for daytime SAT and LST field

Fig. 8a. The correlation between modelled and MODIS-derived LST is stronger for the evening and nighttime conditions (Fig. 8b, c; $R^2 > 0.6$ both for rural and urban grid cells). However, the model slightly underestimates the LST spatial variability, especially for nighttime conditions (slope coefficient of the linear trend $k < 1$). Surprisingly, even better agreement is found between the MODIS-derived LST and modelled SAT (Fig. 8e, f) in terms of the correlation ($R^2 > 0.8$ for urban grid cells) and trend slope (k is closer to 1). In other words, the SUHI in the field

of the MODIS-derived LST is closer to the modelled CLUHI rather than the modelled SUHI. In contrast to nighttime conditions, the correlation between modelled SAT and MODIS-derived LST is very weak ($R^2 \approx 0.3$) for a daytime (Fig. 8d).

DISCUSSION

The presented results show substantial differences between CLUHI and SUHI, which are expressed in the diurnal course and spatial structure of the urban temperature
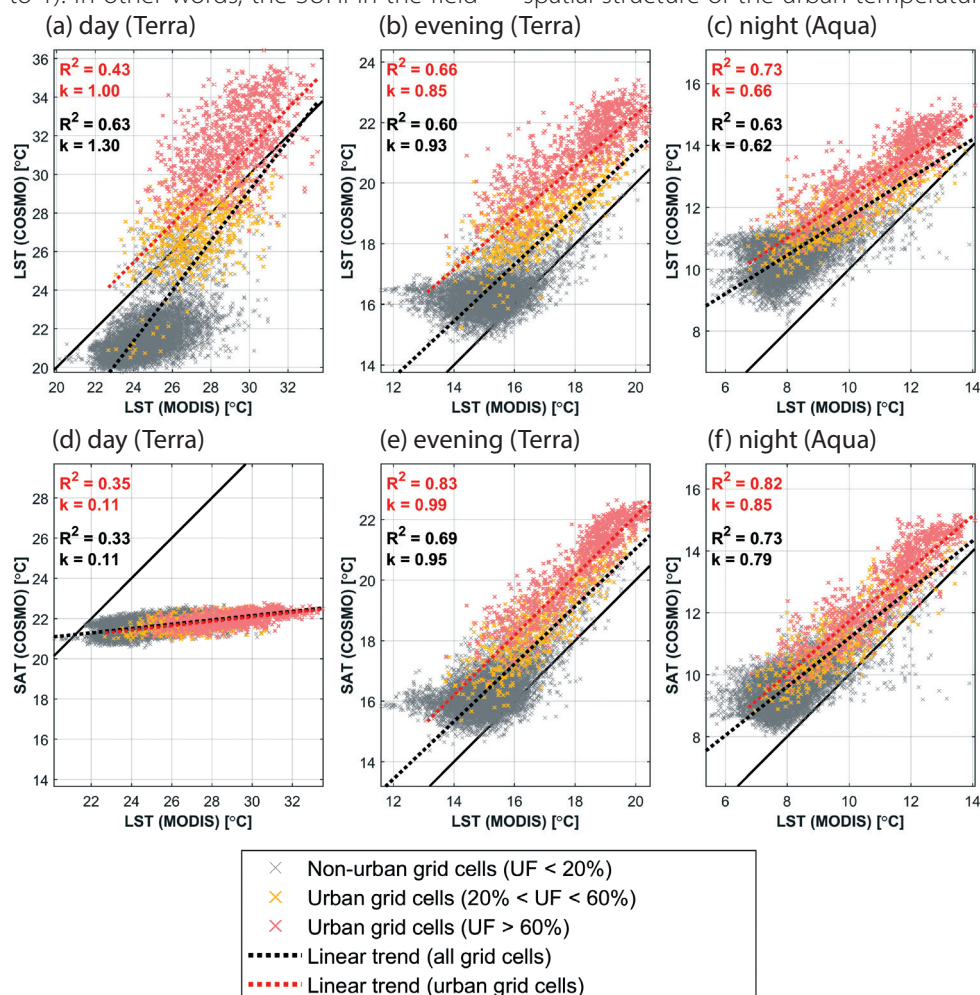
Fig. 8. Comparison of the MODIS-derived LST values and modelled LST (a-c) and SAT (d-e) values, averaged over the periods of registration of the selected satellite daytime (a, d) and evening (b, e) Terra images and nighttime Aqua images (c, e). Water grid cells are excluded from the analysis. Dotted lines indicate the linear trends, built for all grid cells (black line) and only for urban grid cells with urban fraction > 20% (red line). Determination (R^2) and slope (k) coefficients for these trends are shown in each panel. Solid black lines are one-to-one lines

anomalies. The SUHI is more pronounced during the day, while the CLUHI is more pronounced in the evening and night. The difference between CLUHI and SUHI was known before (Voogt and Oke 2003), however it is often not sufficiently considered in recent urban climate studies (see the literature review in the introduction). In addition, CLUHI–SUHI relationships are often considered separately from the physical processes in the atmospheric boundary layer (hereafter referred as ABL) and its lowest part, known as the surface layer.

The interpretation of the CLUHI–SUHI relationships with respect to the ABL processes is provided below. On a clear summer day, urban surfaces heat up more strongly in the countryside due to the smaller albedo, less heat consumption for evaporation, specific features of the urban geometry and other factors (Oke 1982; Ryu and Baik 2012), which determines a pronounced SUHI. However, in such conditions, atmospheric turbulence is well developed that determines the intensive mixing within the ABL, which reaches a height of 1–2 km during the day (Oke 1987). Intense vertical and horizontal turbulent mixing smoothens the local influence of various surface types on the thermal regime of the surface layer of the atmosphere, hence, weakens the CLUHI. At the same time, the intensive mixing leads to an intense redistribution of the daytime urban excess heating over the lower atmosphere up to 1 km above the ground (Wouters et al. 2013; Varentsov et al. 2018). Good mixing within a deep ABL results in the weakest correlation between the daytime SAT and LST values, which was also found beyond the UHI studies, e.g. in a regional study for Northeast China (Yang et al. 2017).

After sunset, the surface cools rapidly due to radiation cooling. The lower troposphere becomes stably stratified; the intensity of the vertical turbulent heat exchange between the surface-layer (canopy layer) and the upper atmosphere strongly decreases. The mixed-layer height is at least eight to ten times smaller during the night than during the day so that urban heat release is distributed over a significantly smaller

depth (Bohnenstengel et al. 2011). As a result, the nighttime UHI over a megacity typically extents to the lower troposphere for 100-150 m only (Wouters et al. 2013; Varentsov et al. 2018). Within the canopy layer the UHI is much more intense at nighttime than at daytime. In contrast to a stable nighttime surface layer over rural areas, the stratification remains neutral in a surface layer over the city (Wouters et al. 2013) that means the near-zero SAT-LST difference. This explains the significantly better match between the CLUHI and SUHI at evening and night.

At the same time, the role of horizontal transport increases in the thin stable ABL, which affects the UHI spatial structure. During the day, the SUHI is mainly determined by local properties of the underlying surface, first of all, by the presence of impervious urban surfaces or pervious green-covered surfaces. These features determine the sharp LST gradients and presence of the several isolated hotspots within the city. At night, the non-local effects established by atmospheric advection (transport of excessive heat within the city or further downwind to the suburbs) and horizontal turbulent mixing become larger and lead to smoother temperature gradients and monocentric SUHI spatial structure with a temperature maximum in the city center. Such differences between daytime and nighttime SUHI spatial patterns are consistent with MODIS-derived results for other cities (Cheval and Dumitrescu 2015; Sun et al. 2015; Zhou et al. 2015). The nighttime SUHI spatial patterns for Moscow are also consistent with spatial patterns of CLUHI according to the *in situ* observations (Climate of Moscow… 2017).

The modelling results are generally consistent with mechanisms described and are in a good agreement with *in situ* observations on the CLUHI spatiotemporal variations. However, the simulated daytime SUHI intensity substantially exceeds the corresponding MODIS-derived values. The agreement between remote sensing data and modelling results is much better for the nighttime and evening conditions, but surprisingly the MODIS-derived SUHI cor-

relates more strongly with the modelled CLUHI than with modelled SUHI.

A number of explanations could be proposed for such model behavior. Firstly, the remote sensing data for urban areas does not characterize the temperature of a horizontal Earth surface, but reflects the thermal conditions of the 3-dimensional urban canopy, which also includes shaded and unshaded walls, elements of street and yard greening, etc. Such objects are located above the surface that makes their temperatures closer to the surrounding air temperature. However, within the framework of the COSMO model and the TERRA_URB scheme, the simulated LST reflects the state of a uniform horizontal surface, the properties of which are adjusted in such a way as to ensure the adequate reproduction of the components of the surface thermal balance and SAT. Secondly, the model uncertainties may be related with thermal and radiative properties of urban materials. These properties may be crucial for the SUHI intensity, but in our study they were defined as constants over the urban area because of the lack of information on urban materials. Such inaccuracies may be combined with uncertainties of other parameters, which are important for simulation of the surface energy balance and which were not verified in detail in previous studies for TERRA_URB scheme and other UCMs (e.g. the surface layer resistances or roughness length for temperature). Finally, the deficiencies of remote sensing data may lead to discrepancies between the LST fields, particularly because of the possible uncertainties of the emissivity mask that is used for LST calculation (Hu et al. 2014).

In either case, the revealed discrepancies between the model and observations should be investigated in more detail in further research, also with application of additional alternative observational products (e.g. remote sensing data of higher resolution, airplane-based and tower-based radiative measurements, *in situ* LST observations).

CONCLUSION

In the presented study, we have analyzed the summertime UHI effect for the city of Moscow using three independent approaches and corresponding datasets: the dense *in situ* SAT observations, MODIS remote sensing LST data and high-resolution mesoscale modelling with the COSMO-CLM model and urban canopy parameterization TERRA_URB. Comparison of these three approaches was made for the city of Moscow for the first time. The results of the comparison revealed the principal difference between urban SAT and LST anomalies (known as CLUHI or SUHI respectively), and between the daytime and nighttime CLUHI–SUHI relationships. The differences between CLUHI and SUHI are consistent with a general understanding of the ABL processes and are confirmed by the modelling.

Generally, we found that the model and observations are in good agreement, particularly for daytime and nighttime CLUHI (in comparison with *in situ* observations), and for nighttime SUHI (in comparison with MODIS remote sensing data). However, the correspondence is substantially lower for the daytime SUHI, the intensity of which is substantially overestimated in the model. In addition, the modelled CLUHI corresponds to the observed SUHI surprisingly better than the modelled SUHI for evening and night.

The study appeals for further in-depth investigation of the feedbacks between the CLUHI, SUHI and ABL, including the development of the urban conceptual ABL models for investigation of the role of the ABL processes in the CLUHI-SUHI differences (e.g. Droste et al. 2018; Wouters et al. 2019); and for more comprehensive model verification studies for urban areas.

Finally, the presented results allow us to draw a number of recommendations about the applications of the considered temperature datasets in urban climate research and related fields.
1. The CLUHI is not equivalent to the SUHI, especially for daytime conditions. Accord-

ingly, remote sensing LST data cannot be a direct and universal replacement of *in situ* SAT observations data for urban climate studies. However, there is a stronger consistency between the nighttime CLUHU and SUHI. Hence, any comparison of climatological statistics on the CLUHI and SUHI intensities should be done with a great accuracy and taking into consideration the different CLUHI-SUHI relationships for the daytime and nighttime conditions.

2. The mesoscale model coupled with urban canopy models are able to successfully simulate the urban climate features for such a big city as Moscow. However, the good agreement between the modelling results and *in situ* observations on the CLUHI features does not automatically mean the same good agreement between modelling results and MODIS data on the SUHI features. Despite the very good agreement in CLUHI, presented results highlight potential misunderstanding of the urban-atmosphere interaction processes. Tackling these issues could offer great potential to further improve the urban atmosphere feedbacks in mesoscale atmospheric modelling and our understanding of the urban climate system.

3. The application of the remote sensing data for verification of the mesoscale modelling results for urban areas requires accuracy and careful consideration of the specific features of the model parametrizations and satellite images. Therefore, we recommend to focus on such tasks firstly in the nighttime conditions, since at night the agreement between remote sensing data, *in situ* observations and modelling results on both types of UHI is much better than in the daytime conditions. If possible, an integrated and comprehensive approach to model verification should be applied, based on both *in situ* and remote sensing data.

The above mentioned does not belittle the importance of remote sensing data as one of the important data sources for urban climatology. In addition to the SUHI studies and the model verification, remote sensing LST data could be used for regression modeling of SAT and biometeorological comfort indices as one of the predictors (Ho et al. 2016), for estimating anthropogenic heat fluxes (Chrysoulakis et al. 2018), for the diagnosis and monitoring of urbanization processes (Shen et al. 2016; Tan et al. 2010b; Weng and Lu 2008), for mapping the development and functional zones of urban areas (Grishchenko and Ermilova 2018) and for integrated analysis of local climatic features together with the *in situ* measurements (Konstantinov et al. 2015; Cheval and Dumitrescu 2017). Since the agreement between CLUHI and SUHI increases in the absence of intense solar heating, remote sensing LST data becomes especially valuable for urban climate studies in nighttime conditions and in the conditions of mid-latitude and Arctic winter. In either case, the joint use of *in situ*, remote sensing and modelling data could increase the value of UHI and urban climate studies if the relationships between the different methods are taken into consideration.

ACKNOWLEDGMENTS

Abbreviation list

ABL – atmospheric boundary layer
AWS – automatic weather station
AAQS　– automatic air quality station
CLUHI – canopy-layer urban heat island
COSMO – the atmospheric model, developed by Consortium for Small-Scale Modelling
COSMO-CLM – the version of the COSMO model adapted for long-term simulations

LST – land surface temperature
MODIS – Moderate Resolution Imaging Spectroradiometer
MSU – Moscow State University
SAT – surface air temperature
SUHI – surface urban heat island
UF – urban fraction
UHI – urban heat island
WMO – World Meteorological Organization
WS – regular (non-automatic) weather station

REFERENCES

Baldina E. A., Grishchenko M. Yu. (2014). Interpretation of multi-temporal space imagery in thermal infrared band. Moscow University Vestnik. Series 5. Geography, 3, pp. 35-42 (in Russian with English summary).

Bohnenstengel S. I., Evans S., Clark P. A., and Belcher S. E. (2011). Simulations of the London urban heat island. Quarterly Journal of the Royal Meteorological Society, 137(659), pp. 1625–1640, DOI: 10.1002/qj.855.

Buechley R. W., Van Bruggen J., and Truppi L. E. (1972). Heat island = death island? Environmental Research, 5(1), pp. 85–92, DOI: 10.1016/0013-9351(72)90022-9.

Cheval S. and Dumitrescu A. (2015). The summer surface urban heat island of Bucharest (Romania) retrieved from MODIS images. Theoretical and Applied Climatology, 121(3–4), pp. 631–640, DOI: 10.1007/s00704-014-1250-8.

Cheval S. and Dumitrescu A. (2017). Rapid daily and sub-daily temperature variations in an urban environment. Climate Research, 73(3), pp. 233–246. DOI: 10.3354/cr01481.

Choi Y.-Y., Suh M.-S., and Park K.-H. (2014). Assessment of Surface Urban Heat Islands over Three Megacities in East Asia Using Land Surface Temperature Data Retrieved from COMS. Remote Sensing, 6(6), pp. 5852–5867, DOI: 10.3390/rs6065852.

Chrysoulakis N., Grimmond S., Feigenwinter C., Lindberg F., Gastellu-Etchegorry J.-P., Marconcini M., Mitraka Z., Stagakis S., Crawford B., Olofson F., Landier L., Morrison W., and Parlow E. (2018). Urban energy exchanges monitoring from space. Scientific Reports, 8(1), p. 11498, DOI: 10.1038/s41598-018-29873-x.

Cox W. (2018). Demographia World Urban Areas (World Agglomerations). Wendel Cox Consultancy, Illinois (14th Annual Edition). Belleville, Illinois. URL: http://www.demographia.com/db-worldua.pdf.

Davies M., Steadman P., and Oreszczyn T. (2008). Strategies for the modification of the urban climate and the consequent impact on building energy use. Energy Policy, 36(12), pp. 4548–4551, DOI: 10.1016/j.enpol.2008.09.013.

Dee D. P., Uppala S. M., Simmons A. J., Berrisford P., Poli P., Kobayashi S., Andrae U., Balmaseda M. A., Balsamo G., Bauer P., Bechtold P., Beljaars A. C. M., van de Berg L., Bidlot J., Bormann N., Delsol C., Dragani R., Fuentes M., Geer A. J., Haimberger L., Healy S. B., Hersbach H., Holm E. V., Isaksen L., Kållberg P., Köhler M., Matricardi M., Mcnally A. P., Monge-Sanz B. M., Morcrette J. J., Park B. K., Peubey C., de Rosnay P., Tavolato C., Thepaut J. N., and Vitart F. (2011). The ERA-Interim reanalysis: Configuration and performance of the data assimilation system. Quarterly Journal of the Royal Meteorological Society, 137(656), pp. 553–597, DOI: 10.1002/qj.828.

Doms G., Förstner J., Heise E., Herzog H.-J., Mironov D., Raschendorfer M., Reinhardt T., Ritter B., Schrodin R., Schulz J.-P., and Vogel G. (2011). A description of the nonhydrostatic regional COSMO model. Part II: Physical parameterization. Deutscher Wetterdienst.

Dousset B., Gourmelon F., Laaidi K., Zeghnoun A., Giraudet E., Bretin P., Mauri E., and Vandentorren S. (2011). Satellite monitoring of summer heat waves in the Paris metropolitan area. International Journal of Climatology, 31(2), pp. 313–323, DOI: 10.1002/joc.2222.

Droste A. M., Steeneveld G. J., and Holtslag A. A. M. (2018). Introducing the urban wind island effect. Environmental Research Letters, 13(9), p. 94007. DOI: 10.1088/1748-9326/aad8ef.

Emelina S. V., Konstantinov P. I., Malinina E. P., and Rubinshtein K. G. (2014). Evaluation of the informativeness of several biometeorological indices for three areas of the European part of Russia. Russian Meteorology and Hydrology, 39(7), pp. 448–457, DOI: 10.3103/S1068373914070036.

Esau I. and Miles V. (2016). Warmer urban climates for development of green spaces in northern Siberian cities. Geography, Environment, Sustainability, 9(4), pp. 48–62, DOI: 10.24057/2071-9388-2016-9-4-48-62.

Flanner M. G. (2009). Integrating anthropogenic heat flux with global climate models. Geophysical Research Letters, 36(2), L02801, DOI: 10.1029/2008GL036465.

GCOS (2010). Implementation plan for the global observing system for climate in support of the UNFCCC (2010 update). GCOS Rep. 138, 186 pp. URL: https://library.wmo.int/doc_num.php?explnum_id=3851.

Gornyy V. I., Lyalko V. I., Kritsuk S. G., Latypov I. S., Tronin A. A., Filippovich V. E., Stankevich S. A., Brovkina O. V., Kiselev A. V., Davidan T. A., Lubsky N. S., and Krylova A. B. (2016). Forecast of Saint-Petersburg and Kiev thermal replies on climate change (on the basis of EOS and Landsat satellite imagery). Current Problems in Remote Sensing of the Earth from Space, 13(2), pp. 176–191, DOI: 10.21046/2070-7401-2016-13-2-176-191. (in Russian with English summary).

Grishchenko M. Y. and Ermilova Y. V. (2018). Mapping of the built-up areas of Russian Arctic biggest cities using satellite imagery of various spatial resolution. Geodesy and Cartography, 933(3), pp. 23–34, DOI: 10.22389/0016-7126-2018-933-3-23-34. (in Russian with English summary).

Grishchenko M. Y. (2012). ETM+ thermal infrared imagery application for Moscow urban heat island study. Current Problems in Remote Sensing of the Earth from Space, 9(4), pp. 95–101. (in Russian with English summary).

Ho H. C., Knudby A., Xu Y., Hodul M., and Aminipouri M. (2016). A comparison of urban heat islands mapped using skin temperature, air temperature, and apparent temperature (Humidex), for the greater Vancouver area. Science of The Total Environment, 544, pp. 929–938, DOI: 10.1016/j.scitotenv.2015.12.021.

Hu L., Brunsell N.A., Monaghan A.J., Barlage M., and Wilhelmi O.V. (2014). How can we use MODIS land surface temperature to validate long-term urban model simulations? Journal of Geophysical Research Atmospheres, 119(6), pp. 3185–3201, DOI: 10.1002/2013JD021101.

Kislov A.V., ed. (2017). Climate of Moscow in conditions of global warming. Moscow, Russia: Publishing house of Moscow University. 288 pp. (in Russian).

Krayenhoff E. S., Moustaoui M., Broadbent A. M., Gupta V., and Georgescu M. (2018). Diurnal interaction between urban expansion, climate change and adaptation in US cities. Nature Climate Change, 8(12), pp. 1097–1103, DOI: 10.1038/s41558-018-0320-9.

Konstantinov P. I., Grishchenko M. Y., and Varentsov M. I. (2015). Mapping urban heat islands of arctic cities using combined data on field measurements and satellite images based on the example of the city of Apatity (Murmansk Oblast). Izvestiya - Atmospheric and Ocean Physics, 51(9), pp. 992–998, DOI: 10.1134/S000143381509011X.

Konstantinov P., Varentsov M., and Esau I. (2018). A high density urban temperature network deployed in several cities of Eurasian Arctic. Environmental Research Letters, 13(7), p. 75007, DOI: 10.1088/1748-9326/aacb84.

Lemonsu A. and Masson V. (2002). Simulation of a summer urban breeze over Paris. Boundary-Layer Meteorology, 104(3), pp. 463–490, DOI: 10.1023/A:1016509614936.

Lokoshchenko M. A. (2014). Urban "heat island" in Moscow. Urban Climate, 10, Part 3, pp. 550–562, DOI: 10.1016/j.uclim.2014.01.008.

Mariani L., Parisi S. G., Cola G., Lafortezza R., Colangelo G., and Sanesi G. (2016). Climatological analysis of the mitigating effect of vegetation on the urban heat island of Milan, Italy. Science of the Total Environment, 569–570, pp. 762–773, DOI: 10.1016/j.scitotenv.2016.06.111.

Martilli A., Clappier A., and Rotach M. W. (2002). An urban surface exchange parameterization for mesoscale models. Boundary-Layer Meteorology, 104, pp. 261–304, DOI: 10.1023/A:1016099921195.

Masson V. (2000). A physically based scheme for the urban energy budget in atmospheric models. Boundary Layer Meteorology, 94(3), pp. 357–397, DOI: 10.1023/A:1002463829265.

Miles V. and Esau I. (2017). Seasonal and Spatial Characteristics of Urban Heat Islands (UHIs) in Northern West Siberian Cities. Remote Sensing, 9(10), p. 989, DOI: 10.3390/rs9100989.

Muller C.L., Chapman L., Grimmond C.S.B., Young D.T., and Cai X. (2013). Sensors and the city: A review of urban meteorological networks. International Journal of Climatology, 33(7), pp. 1585–1600, DOI: 10.1002/joc.3678.

Oke T.R. (1982). The energetic basis of the urban heat island. Quarterly Journal of the Royal Meteorological Society, 108(455), pp. 1–24, DOI: 10.1002/qj.49710845502.

Oke T. R. (1987). Boundary layer climates (2nd ed.). Routledge. 435 pp.

M.I. Varentsov, M. Yu. Grishchenko et al.   SIMULTANEOUS ASSESSMENT OF ...

04|2019

93 GES

Peng S., Piao S., Ciais P., Friedlingstein P., Ottle C., Bréon F.-M., Nan H., Zhou L., and Myneni R.B. (2012). Surface Urban Heat Island Across 419 Global Big Cities. Environmental Science and Technology, 46(2), pp. 696–703, DOI: 10.1021/es301245j.

Peterson T.C. (2003). Assessment of Urban Versus Rural In Situ Surface Temperatures in the Contiguous United States: No Difference Found. Journal of Climate, 16(18), pp. 2941–2959, DOI: 10.1175/1520-0442(2003)016<2941:AOUVRI>2.0.CO;2.

Rockel B., Will A., and Hense A. (2008). The regional climate model COSMO-CLM (CCLM). Meteorologische Zeitschrift, 17(4), pp. 347–348, DOI: 10.1127/0941-2948/2008/0309.

Ryu Y.-H., and Baik J.-J. (2012). Quantitative Analysis of Factors Contributing to Urban Heat Island Intensity. Journal of Applied Meteorology and Climatology, 51(5), pp. 842–854, DOI: 10.1175/JAMC-D-11-098.1.

Samsonov T.E., Konstantinov P.I., and Varentsov M.I. (2015). Object-oriented approach to urban canyon analysis and its applications in meteorological modeling. Urban Climate, 13, pp. 122–139, DOI: 10.1016/j.uclim.2015.07.007.

Samsonov T.E. and Trigub K. S. (2018). Mapping of local climate zones of Moscow city. Geodesy and Cartography, 936(6), pp. 4–25, DOI: 10.22389/0016-7126-2018-936-6-14-25 (in Russian with English summary).

Shen H., Huang L., Zhang L., Wu P., and Zeng C. (2016). Long-term and fine-scale satellite monitoring of the urban heat island effect by the fusion of multi-temporal and multi-sensor remote sensed data: A 26-year case study of the city of Wuhan in China. Remote Sensing of Environment, 172, 109–125, DOI: 10.1016/j.rse.2015.11.005.

Sheng L., Tang X., You H., Gu Q., and Hu H. (2017). Comparison of the urban heat island intensity quantified by using air temperature and Landsat land surface temperature in Hangzhou, China. Ecological Indicators, 72, pp. 738–746, DOI: 10.1016/j.ecolind.2016.09.009.

Sobrino J.A., Oltra-Carrió R., Sòria G., Bianchi R., and Paganini M. (2012). Impact of spatial resolution and satellite overpass time on evaluation of the surface urban heat island effects. Remote Sensing of Environment, 117, pp. 50–56, DOI: 10.1016/j.rse.2011.04.042.

Stewart I. D. and Kennedy C. A. (2017). Metabolic heat production by human and animal populations in cities. International Journal of Biometeorology, 61(7), pp. 1159–1171, DOI: 10.1007/s00484-016-1296-7.

Stewart I.D. and Oke T.R. (2012). Local climate zones for urban temperature studies. Bulletin of the American Meteorological Society, 93(12), pp. 1879–1900. DOI: 10.1175/BAMS-D-11-00019.1.

Sun H., Chen Y., and Zhan W. (2015). Comparing surface- and canopy-layer urban heat islands over Beijing using MODIS data. International Journal of Remote Sensing, 36(21), pp. 5448–5465, DOI: 10.1080/01431161.2015.1101504.

Tan J., Zheng Y., Tang X., Guo C., Li L., Song G., Zhen X., Yuan D., Kalkstein A. J., Li F., and Chen H. (2010a). The urban heat island and its impact on heat waves and human health in Shanghai. International Journal of Biometeorology, 54(1), pp. 75–84, DOI: 10.1007/s00484-009-0256-x

Tan K.C., Lim H.S., MatJafri M.Z., and Abdullah K. (2010b). Landsat data to evaluate urban expansion and determine land use/land cover changes in Penang Island, Malaysia. Environmental Earth Sciences, 60(7), pp. 1509–1521, DOI: 10.1007/s12665-009-0286-z.

Varentsov M.I., Samsonov T.E., Kislov A.V., and Konstantinov P.I. (2017a). Simulations of Moscow agglomeration heat island within framework of regional climate model COSMO-CLM. Moscow University Vestnik. Series 5. Geography, 6, pp. 25-37 (in Russia with English summary).

Varentsov M.I., Konstantinov P.I., and Samsonov T.E. (2017b). Mesoscale modelling of the summer climate response of Moscow metropolitan area to urban expansion. IOP Conference Series: Earth and Environmental Science, 96, p. 12009, DOI: 10.1088/1755-1315/96/1/012009.

Varentsov M., Wouters H., Platonov V., and Konstantinov P. (2018). Megacity-Induced Mesoclimatic Effects in the Lower Atmosphere: A Modeling Study for Multiple Summers over Moscow, Russia. Atmosphere, 9(2), p. 50, DOI: 10.3390/atmos9020050.

Vil'fand R. M., Rivin G.S., and Rozinkina I.A. (2010). COSMO-RU system of nonhydrostatic mesoscale short-range weather forecast of the hydrometcenter of Russia: The first stage of realization and development. Russian Meteorology and Hydrology, 35(8), pp. 503–514, DOI: 10.3103/S1068373910080017.

Voogt J. and Oke T.R. (2003). Thermal remote sensing of urban climates. Remote Sensing of Environment, 86(3), pp. 370–384, DOI: 10.1016/S0034-4257(03)00079-8.

Weng Q. and Lu D. (2008). A sub-pixel analysis of urbanization effect on land surface temperature and its interplay with impervious surface and vegetation coverage in Indianapolis, United States. International Journal of Applied Earth Observation and Geoinformation, 10(1), pp. 68–83, DOI: 10.1016/j.jag.2007.05.002.

Wouters H., De Ridder K., Demuzere M., Lauwaet D., and Van Lipzig N. P. M. (2013). The diurnal evolution of the urban heat island of Paris: A model-based case study during Summer 2006. Atmospheric Chemistry and Physics, 13(17), pp. 8525–8541. DOI: 10.5194/acp-13-8525-2013.

Wouters H., De Ridder K., Poelmans L., Willems P., Brouwers J., Hosseinzadehtalaei P., Tabari H., Vanden Broucke S., van Lipzig N. P. M., and Demuzere M. (2017). Heat stress increase under climate change twice as large in cities as in rural areas: A study for a densely populated midlatitude maritime region. Geophysical Research Letters, 44(17), pp. 8997–9007. DOI: 10.1002/2017GL074889.

Wouters H., Demuzere M., Blahak U., Fortuniak K., Maiheu B., Camps J., Tielemans D., and van Lipzig N. P. M. (2016). The efficient urban canopy dependency parametrization (SURY) v1.0 for atmospheric modelling: description and application with the COSMO-CLM model for a Belgian summer. Geoscientific Model Development, 9(9), pp. 3027–3054, DOI: 10.5194/gmd-9-3027-2016.

Wouters H., Petrova I.Y., van Heerwaarden C.C., Vilà-Guerau de Arellano J., Teuling A.J., Meulenberg V., Santanello J. A., and Miralles D.G. (2019). Atmospheric boundary layer dynamics from balloon soundings worldwide: CLASS4GL v1.0. "Geoscientific Model Development, 12 (12), pp. 2139-2153, DOI: 10.5194/gmd-12-2139-2019"

Yang Y.Z., Cai W.H., and Yang J. (2017). Evaluation of MODIS land surface temperature data to estimate near-surface air temperature in Northeast China. Remote Sensing, 9(5), p. 410, DOI: 10.3390/rs9050410.

Zhou B., Rybski D., and Kropp J.P. (2013). On the statistics of urban heat island intensity. Geophysical Research Letters, 40(20), pp. 5486–5491, DOI: 10.1002/2013GL057320.

Zhou B., Rybski D., and Kropp J. P. (2017). The role of city size and urban form in the surface urban heat island. Scientific Reports, 7(1), p. 4791, DOI: 10.1038/s41598-017-04242-2.

Zhou D., Xiao J., Bonafoni S., Berger C., Deilami K., Zhou Y., Frolking S., Yao R., Qiao Z., and Sobrino J. (2018). Satellite Remote Sensing of Surface Urban Heat Islands: Progress, Challenges, and Perspectives. Remote Sensing, 11(1), p. 48, DOI: 10.3390/rs11010048.

Zhou D., Zhao S., Zhang L., Sun G., and Liu Y. (2015). The footprint of urban heat island effect in China. Scientific Reports, 5, pp. 2–12, DOI: 10.1038/srep11160.

**Nikolay S. Kasimov[1], Natalia E. Kosheleva[1], Dmitry V. Vlasov[1]*,
Ksenia S. Nabelkina[1], Alexander V. Ryzhov[1]**
[1] Lomonosov Moscow State University, Leninskie gory 1, Moscow, 119991,
Russian Federation
*Corresponding author: vlasgeo@yandex.ru

PHYSICOCHEMICAL PROPERTIES OF ROAD DUST IN MOSCOW

ABSTRACT. Road dust is a composite substance formed due to wear of different components of transport infrastructure and motor vehicles. In 2017, 214 road dust samples were collected in Moscow to analyze pH, electrical conductivity (EC), and organic carbon (C_{org}) content that controls the ability of dust to fix pollutants. The road dust was dominated by sand and silt size particles (the share of PM_{10} particles varies from 2.3% to 39%) and had alkaline pH (6.4–8.1), high EC (33–712 μS/cm) and C_{org} (0.17–6.7%). The road dust is alkalinized by detergents and particles formed by abrasion of roadways and blown out from construction sites. A three-fold excess of the EC over the background values (dust in parks) is mainly due to the use of the de-icing agents and roadway maintenance. But the concentration of C_{org} in the Moscow's road dust is on average 2 times lower compared to the background values; the increased content of C_{org} in the courtyards is associated with the application of organic fertilizers. The most significant factor that determines the physicochemical properties of the dust was the type of a road. The dust on large roads including the Third Ring Road had higher pH (7.0–8.0) and EC (98–712 μS/cm); it contained higher proportions of the fine particle-size fractions compared to other roads. The C_{org} content in the road dust was minimum on Moscow's major radial highways due to the insignificant contribution of soil particles. The spatial trends in variability of the physicochemical properties of the dust in Moscow were not evident as they were to a large extent masked by other factors: proximity to industrial zones and large forest parks, differences in the de-icing agents used, unequal frequencies of road cleaning, and the various contribution of soil particles that vary in composition and genesis in different parts of Moscow.

KEY WORDS: megacity, urban pollution, particulate matter, accumulation potential, geochemical transformation, spatial variability

INTRODUCTION

Road dust is a multicomponent substance formed as a result of washing out and deflation of roadside soils, wear of different components of transport infrastructure and vehicles, crushing of solid waste and residues of de-icing agents (DIAs), and atmospheric precipitation of particulate matter (Ladonin and Plyaskina 2009; Nazzal et al. 2013; Prokofieva et al. 2015). Road dust originates from various sources and indicates pollution level of urban landscapes, since its particles are the carriers for many pollutants, including heavy metals and metalloids (HMMs). In turn, road dust itself may be a source of secondary pollution of the atmosphere and roadside soils. Road dust is lifted into the air by traffic and it is one of the six most important sources of suspended particulate matter (PM) in urban atmosphere (Belis et al. 2013; National Emissions Inventory 2017).

In the major cities of the world, road dust is increasingly being considered as an object of environmental and geochemical monitoring (Vlasov et al. 2015; Demetriades and Birke 2015; Jayarathne et al. 2017; Yang et al. 2017). Extensive literature is devoted to elemental composition of road dust; however, the physicochemical properties inherited from its different components have been studied to a much lesser extent, although they are the ones that determine the potential of the dust to fix pollutants. Usually, such parameters as pH, organic carbon content (C_{org}), electrical conductivity (EC), and particle size distribution are evaluated (Wang and Q_{in}, 2007; Al-Khashman 2007; Hu et al. 2011; Acosta et al. 2011). The studies of atmospheric dust focus on particles with an aerodynamic diameter of 10 μm or smaller (PM_{10}). This PM fraction is the most important indicator of air quality in many cities around the world, since it can penetrate the human respiratory tract, cause asthma in children and increase the risk of mortality from diseases of the cardiovascular system (Tager 2005; Fonova 2017; Report… 2017). The same particle size fraction is also important when studying road dust, since the particles PM_{10} contain up to 40–60% of the total amount of HMMs and the concentrations of Cd, Ag, Sb, Sn, Se, Cu, Bi,

Pb, Zn, Mo, and W in this fraction are 4–22 times higher than their abundances in the upper continental crust (Vlasov et al. 2015; Vlasov 2017).

When road dust settles on the surface of urban soils it changes their physicochemical properties. Road dust has a weak alkaline reaction and can form or increase the capacity of the existing alkaline geochemical barrier, which control the accumulation of many HMMs (Kosheleva et al. 2015). The presence of organic matter in dust causes the formation of organo-mineral geochemical barrier, and the occurrence of various-size dust particles leads to the appearance of sorption-sedimentation geochemical barriers.

In this study for the first time a comprehensive analysis of the road dust properties and their spatial distribution has been made for the entire urban area of Moscow, the largest megacity of Russia and Europe. Moscow has numerous industrial enterprises, heating power plants (HPPs), an extensive road and transport network, and over 4.6 million cars. Similar but limited in scope studies were previously conducted only for individual districts of Moscow (Ladonin and Plyaskina 2009; Vlasov et al. 2015; Prokofieva et al. 2015; Bityukova et al. 2016; Ladonin 2016). The purpose of this study was to evaluate the main physicochemical properties and the accumulation potential of the Moscow's road dust with respect to pollutants as its chemical composition is one of the important indicators of urban environment quality.

The specific objectives of the study were:

– to obtain a representative data set for the territory of Moscow that characterizes the dust on its roads in regard to various traffic intensity in different administrativedistricts (okrugs) of the city;

– to determine main physicochemical parameters of the road dust: pH, EC, C_{org}, and particle size distribution;

– to identify their spatial trends within the city;

– to assess the extent of technogenic geochemical transformation of the dust properties on the roads and to evaluate its accumulation potential with respect to inorganic pollutants (e.g., HMMs).

SOURCES OF ROAD DUST

Motor transport. It is the main source of air pollution in Moscow that presents up to 95% of total emissions, or 880–930 thousand tons per year (Report… 2017; Bityukova and Saulskaya 2017). The length of Moscow roads is 3,600 km, they occupy about 8% of its area (Fig. 1). The density of the road network is 4.2 km/km^2, including the main network 1.54 km/km^2 (Khusnullin 2013). At the beginning of 2017, the automobile fleet of Moscow was about 4.6 million units

of which 90.4% were passenger cars, 8.5% were trucks, and 1.1% buses. The number of vehicles is constantly increasing; the car ownership level is 340 per 1000 people.

Deposition of atmospheric aerosols resulting from anthropogenic emissions is one of the factors controlling the accumulation of road dust. Motor transport emissions consist of carbon monoxide (63%), nitrogen oxides (22%), and volatile hydrocarbons (13%) (Report… 2017). Particulate matter accounts for about 1% of the traffic emissions and non-exhaust emissions coming from abrasion of the road surface and road marking, break and tire wear, which ranges, according to various estimates, from 2.5 to > 5 thousand tons per year depending on traffic conditions – type, speed, and numbers of maneuvers (Nazzal

a   *b*
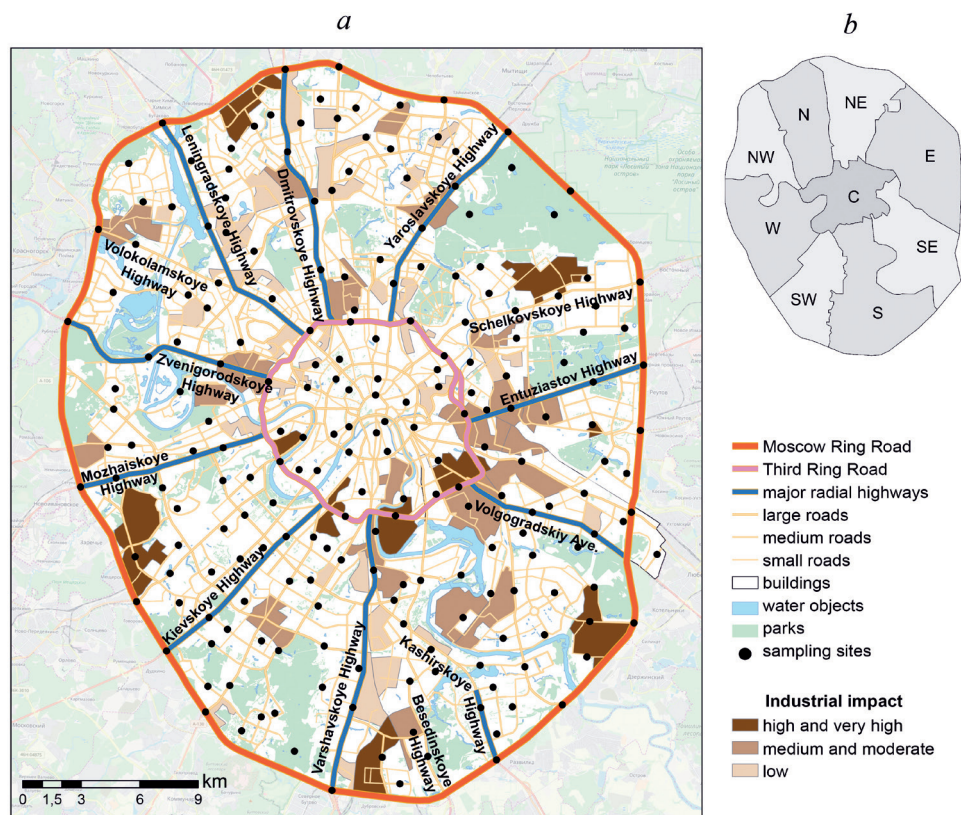
Fig. 1. Mobile and stationary sources of technogenic impact and road dust sampling locations in Moscow (a) and the administrative districts of Moscow within the Moscow Ring Road (b)
Impact levels of industrial zones are given according to Bityukova and Saulskaya (2017).
Capital letters indicate the names of administrative districts (okrugs): N – Northern,
NE – North-Eastern, E – Eastern, SE – South-Eastern, S – Southern, SW – South-Western,
W – Western, NW – North-Western, C – Central

Nikolay S. Kasimov, Natalia E. Kosheleva at al.   PHYSICOCHEMICAL PROPERTIES OF ...

04|2019

99 GES

et al. 2013). The particulate fraction PM_{10} is largely associated with emissions of diesel cargo transport (61%) and buses (29%), despite the fact that their number is much smaller than that of passenger transport; however, they have higher emission intensity and mileage and a smaller share of engines of high environmental classes. An apportionment of the sources of PM_{10} in Hatfield Tunnel (United Kingdom) showed that 60% of the particulate fraction is composed of particles originated from wear of road surfaces, tires, and brake pads, and re-suspension of the dust (i.e. non-exhaust emissions); while engine exhausts produce only 40% of PM_{10} (Lawrence et al. 2016).

The maximum concentrations of pollutants in the air are observed in close proximity to roads. Within a distance of 1 m from a roadway the average dust load is 1.77 g/m^2 per day and at a distance of 5 meters it is 0.47 g/m^2 per day, which is 262 and 67 times higher, respectively, than the background level (Achkasov et al. 2006). Even in the eastern industrial part of Moscow, the dust load near roads is 1.2–2 times more intensive than near industrial areas (Kasimov et al. 2012, 2017).

The generation of particles during braking of vehicles due to friction between parts of the brake system is one of the significant sources of road dust (Garg et al. 2000). Therefore, the contribution of the road dust loading to suspended PM in urban environment can be quantitatively assessed using markers of particles originated from brake and tire wear, which include Cu and Sb (Weckwerth 2001), as well as tracers of road wear – Ca, Al , Si, Ti, and Fe (Diapouli et al. 2017).

De-icing reagents. The DIAs used in Moscow are chloride-based. They comprise at least 93% of technical salt (sodium chloride). The salt is usually mixed with marble chips that after snowmelt mark the places where the DIAs were applied (Nikiforova et al. 2016). A single road treatment requires 80–200 g/m^2 of the DIA (Sister and Koretsky 2004). The total permitted salt load in Moscow reaches 420–500 thousand tons (as dry matter) during the winter season, or 37 kg of the DIAs per person (Khomyakov 2015). The

DIAs include combined (solid and liquid) agents. The municipal services of Moscow use liquid DIAs at temperatures higher 16ºC; at lower temperatures combined agents which include 50–60% of marble chips, crystals of calcium chloride, and formic acid salts are applied. The solubility of marble is low; with decreasing chip-size, it increases in the presence of dissolved calcium chloride and particles of road surface (Greinert et al. 2013). In the courtyards and adjacent areas, sidewalks, and pedestrian streets, only combined DIAs are allowed to be applied. Additionally, grains of crushed granite with a diameter of 2–5 mm can be used, mainly in yard areas and on dangerous road sections.

Industrial enterprises and construction. In Moscow, there are over 30,000 stationary sources of pollutant emissions concentrated in the industrial zones (Fig. 1 a). In different years, the total emission load ranged from 60 to 70 thousand tons per year with a contribution of solids of about 3%. Thirteen HPPs in Moscow account for almost 50–65% of atmospheric emissions from stationary sources, while 20–30% comes from oil refineries, 2–3% and about 2% are derived from engineering enterprises, and from food processing and building materials production, respectively (Bityukova and Saulskaya 2017).

The sources of aerosol emissions to the atmosphere also include about 700 objects of urban construction – residential buildings, urban infrastructure, road and transport facilities (Bityukova and Saulskaya 2017). Many stages of construction are accompanied by intense dust generation. In the near future, the number of construction projects in Moscow is expected to increase owing to the adoption of the law aimed at renovation the old housing stock. Accordingly, about 5,000 buildings needs to be demolished and rebuilt. Besides, in Moscow, some industrial zones are being redeveloped into residential areas.

Soil deflation. Dust contamination of roads increases due to wind erosion of poorly vegetated soils. Within the Moscow Ring Road (MRR), artificially created or highly transformed soils called urbanozems

(Prokofieva and Stroganova 2004) dominate; they have more alkaline pH, higher levels of C_{org} and readily soluble salts, increased accumulation potential and higher proportion of clay, which controls binding of HMMs in soils (Kosheleva et al. 2015). Extraneous material of anthropogenic origin, e.g., construction and household waste, are common in urban soils.

The composition of solid atmospheric fallout on the roadside areas of Moscow reflects its mixed origin. The coarse fractions consist mainly of quartz grains, feldspars, carbonates, and asphalt fragments; the fine fractions, in addition, carry carbon-containing matter, paint, glass, plastic, brick and other fragments (Prokofieva et al. 2015). The $PM_{2.5}$ fraction (particles with an aerodynamic diameter of 2.5 μm or smaller) is formed by soluble inorganic salts, mainly sulfates and nitrates (4–32% of the aerosol mass), insoluble mineral particles, carbon-containing material (1.2–48%) usually represented by elemental carbon (Privalenko and Bezuglova 2003; Da Costa and Oliveira 2009).

MATERIALS AND METHODS

The road dust was tested in Moscow within the MRR on roads with different traffic intensity in June–July 2017 in 9 administrative districts (Fig. 1), as well as inside courtyards with local driveways and parking lots. The courtyards protected from the winds often act as traps for inorganic pollutants which are accumulated in urban soils of residential areas (Kosheleva et al. 2018b). The sampling grid density was defined as one sample per approximately 4 km² (Demetriades and Birke 2015; Kasimov et al. 2016). The dust samples that represent geochemical background in urban environment were collected on pedestrian paths in natural forest parks (the Losiny Ostrov, the Izmaylovsky and Bitsevski parks), at the most remote locations from the highways. In total, 173 dust samples were collected on the roads, 36 – in the courtyards, and 5 – in the forest parks.

In terms of traffic intensity, all roads were divided into several types by the width of the roadway and the number of lanes: (1) MRR,

(2) the Third Ring Road (TRR), (3) major radial highways with more than four lanes in one direction, (4) large roads with three to four lanes, (5) medium roads with two lanes, and (6) small roads with one lane, and (7) local driveways and parking lots of courtyards. Table 1 shows the number of samples taken on different types of roads.

The fieldwork period was characterized by wet and rainy weather conditions; in June–July 2017 the precipitation norm for Moscow was exceeded nearly twice (Weather and Climate, 2017). The accumulation of the road dust was hampered by intensive surface drainage and daily road cleaning by public utilities. The sampling was carried out in days as dry as possible and no earlier than 24 hours after the rain and full road drying. Composite 300–500 g samples were collected along the curb on both sides of the road with a plastic scoop and brush, in 3–5 replications at a distance of 3–10 m from each other. On large and major radial roads, the samples were taken on the dividing strip; in the courtyards they were collected from the parking lots.

The main physicochemical properties of the dust samples were analyzed at the Ecological and Geochemical Center of the Faculty of Geography, Lomonosov Moscow State University. The pH values were measured in aqueous solutions (dust:water 1:2.5) by the potentiometric technique, the electrical conductivity (EC) – in aqueous solutions (dust:water 1:5) using EC meter,the content of organic carbon (C_{org}) was determined by the Tyurin (wet oxidation) method followed by titration, and the analysis of particle size distribution was performed by laser granulometry. The definition of particles is given according to the classification of N.A. Kachinsky adopted in Russia.

The obtained data were analyzed by statistical methods. For each district and road type, the following measures were calculated: sample averages (m), their errors, standard deviations σ, variation coefficients ($Cv = σ/m·100\%$), minimum and maximum values. The variation of the parameters depending on a set of factors (type of road, spatial

location of the sampling point in the city, particle size class, base-acid reaction, and C_{org} content) were estimated by the regression trees method in *S-Plus* package (MathSoft®). The visualization of the geochemical data was done in *ArcGIS 10* package.

RESULTS AND DISCUSSION

The physicochemical properties analyzed (Tables 1, 2), in general, fall into the range of values comparable to what has been found

in other cities of the world where pH, C_{org} content and EC varied between 7–9, 1–17%, and 100–2800 µS/cm, respectively (Wang and Qin 2007; Al-Khashman 2007; Ladonin and Plyaskina 2009; Acosta et al. 2011; Yisa et al. 2011; Hu et al. 2011; Sutherland et al. 2012).

The results of multivariate regression analysis (Fig. 2) revealed the leading factors determining the physicochemical properties of road dust.
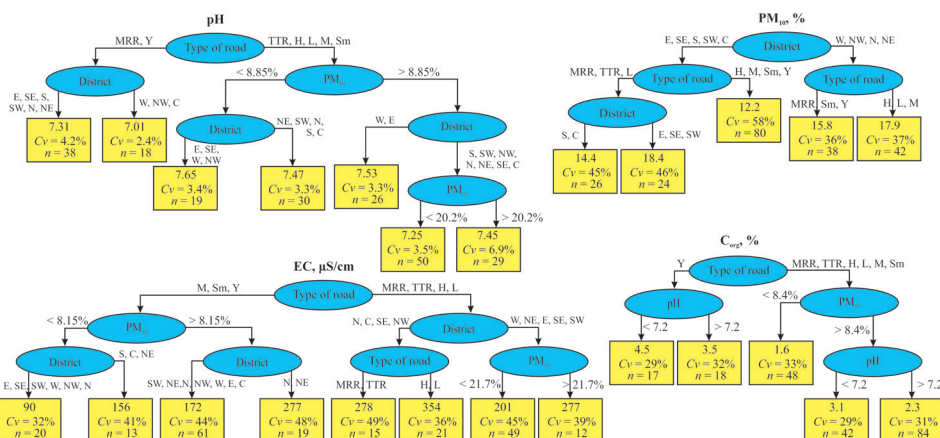
Table 1. Physicochemical properties of the dust collected from different road types

Roads (number of samples)	pH		EC, µS/cm		C_{org}, %		Share of PM_{10}, %	
	Average (min–max)	Cv,, %	Average (min–max)	Cv, %	Average (min–max)	Cv,, %	Average (min–max)	Cv,, %
forest parks (5)	7.1 (6.7–7.4)	3.2	70 (66–88)	17	4.1 (2.5–7.4)	42	13 (6.3–18)	37
MRR (20)	7.3 (6.8–7.9)	3.1	256 (98–521)	41	2.7 (1.5–4.9)	33	18 (5.4–31)	36
TRR (10)	7.4 (7.0–7.6)	2.4	277 (136–712)	57	2.8 (0.85–3.6)	29	18 (6.2–22)	25
major radial (19)	7.5 (7.1–8.0)	3.5	256 (118–537)	45	2.0 (1.0–4.0)	36	15 (4.1–29)	63
large (47)	7.4 (6.9–8.0)	3.9	257 (88–523)	49	2.1 (0.17–4.8)	41	16 (5.7–33)	44
medium (44)	7.4 (6.8–8.1)	3.7	174 (33–450)	55	2.3 (0.87–4.6)	38	13 (3.2–27)	52
small (34)	7.4 (6.4–8.1)	4.2	193 (47–525)	58	2.4 (0.91–4.8)	36	14 (4.0–39)	52
courtyards (36)	7.2 (6.6–8.1)	3.7	162 (63–483)	50	4.1 (1.1–6.7)	32	14 (5.2–28)	45

Note. Hereinafter, share of PM_{10} represents the share (%) of particles with a diameter of 10 µm and smaller in a bulk sample of the road dust (considering particles of all diameters).

Table 2. Physicochemical properties of the road dust collected in different administrative districts (okrugs) of Moscow

District (number of samples)	pH		EC, µS/cm		C_{org}, %		Share of PM_{10}, %	
	Average (min–max)	Cv, %	Average (min–max)	Cv,, %	Average (min–max)	Cv,, %	Average (min–max)	Cv,, %
Eastern (21)	7.4 (7.0–8.0)	3.8	174 (33–519)	67	2.2 (0.17–4.9)	51	14 (6.7–30)	46
Western (29)	7.4 (6.9–8.1)	4.0	183 (98–376)	40	2.5 (1.1–5.67)	45	16 (4.1–28)	41
Northern (12)	7.3 (7.1–7.9)	2.9	211 (97–537)	58	2.6 (1.4–3.8)	22	19 (6.9–28)	34
North-Eastern (23)	7.3 (6.4–7.7)	3.7	199 (65–352)	40	3.1 (1.6–5.1)	34	17 (6.7–29)	34
North-Western (16)	7.2 (6.7–8.0)	4.6	248 (90–459)	45	2.7 (0.85–5.1)	38	18 (7.2–29)	35
Central (32)	7.3 (6.8–8.1)	3.9	243 (80–712)	56	2.4 (0.85–4.8)	46	14 (4.2–24)	47
Southern (27)	7.4 (6.8–8.1)	4.2	214 (73–483)	42	2.8 (1.3–6.6)	49	12 (5–26)	55
South-Eastern (30)	7.4 (6.6–8.0)	4.3	242 (47–525)	64	2.7 (0.91–6.7)	46	15 (3.2–39)	62
South-Western (20)	7.4 (7.1–7.8)	2.4	176 (53–521)	61	2.4 (1.4–4.7)	38	14 (4.1–34)	55
Moscow (210)	7.4 (6.4–8.1)	3.9	211 (33–712)	56	2.6 (0.17–6.7)	44	15 (3.2–39)	48

Fig. 2. Differentiation of the physicochemical properties of the Moscow's road dust in relation to the type of the road, the administrative district, and the particle size distribution

For each terminal node, the average value of the parameter, the coefficient of its variation Cv, and the number of sampling points n are given. Types of roads: H – major radial highway, L – large, M – medium, Sm – small, Y – courtyards. For the names of the districts please see the footnote of Fig. 1
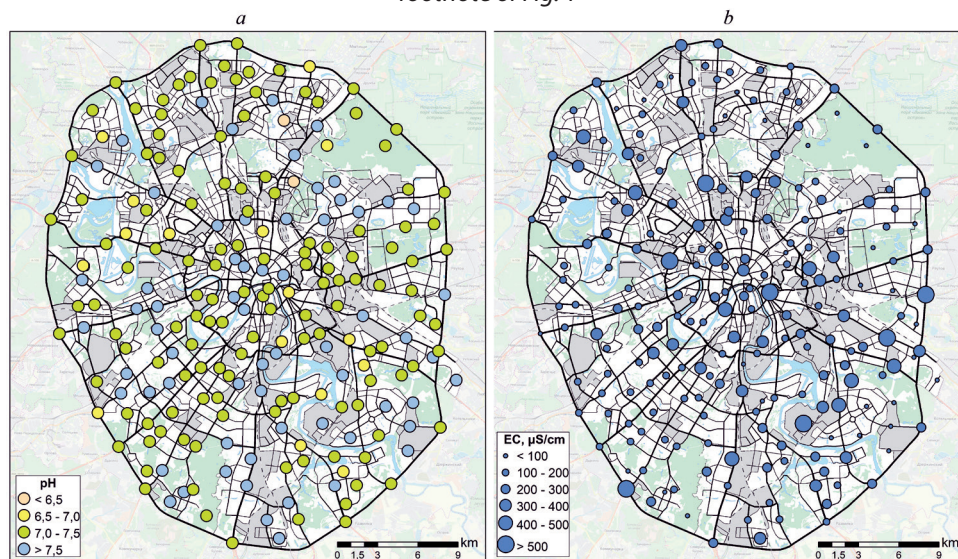
Fig. 3. Base-acid reaction (a) and the results of electrical conductivity measurements of the road dust in Moscow (b)

Urbanized background. The road dust in the urban forest parks (Table 1) had the lowest values of pH (7.1) and EC (70 µS/cm). The DIAs are not applied in these territories; there is no pollution by particles formed during mechanical deterioration of vehicle parts, and atmospheric deposition is hampered by vegetation. The main components of the dust in these background areas are plant residues and soil particles. In the forest parks,

natural sod-podzolic soils (Retisols) with slightly acidic reaction and the prevalence of fulvic acids in the surface horizon owing to plant litter (Prokofeva et al. 2013, Rozanova et al. 2016) are still present. Foliage residues serve as a natural source of C_{org}, which determined its increased concentrations – 4.1%, on average. Unlike the forest parks, fallen leaves are removed from the public gardens and parks, as well as in many
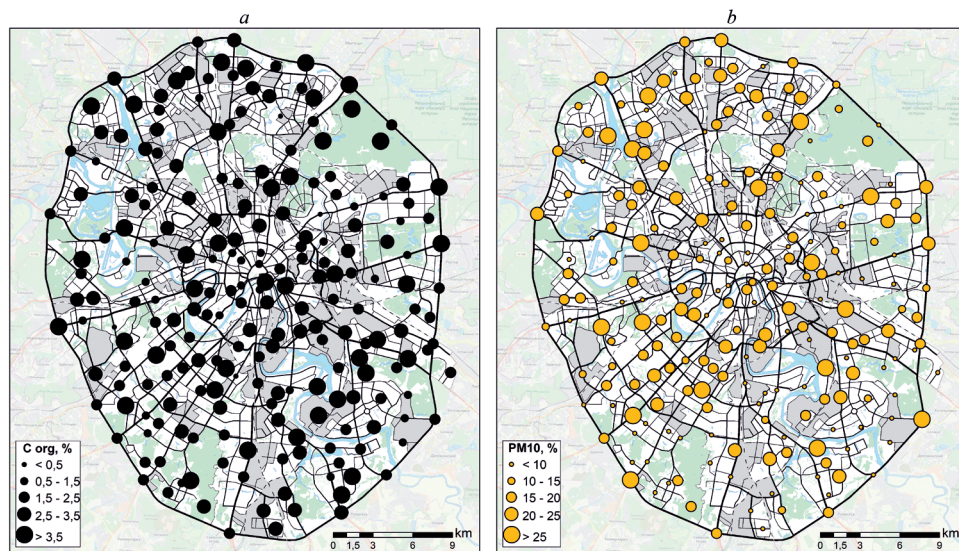
Fig. 4. The C_{org} content (a) and the proportions of PM_{10} fraction in the road dust samples in Moscow (b)

residential yards and green lawns, thereby reducing the new addition of organic matter into the soil. Also, the background dust had specific granulometric composition: in all 5 samples collected, a coarse particle size fraction 250–1000 μm prevailed (> 50%).

Base-acid reaction. The average pH of the dust sampled on the roads and in the courtyards is 7.4. The differences between the administrative districts were insignificant; the values that exceed the maximum and the average pH were typical of the western, southern and eastern parts of Moscow, while minimum values were observed in its northern part (Table 2, Fig. 3a). The lowest average pH of 7.2 was recorded in the North-Western district due to the prevailing northerly winds which contribute to the translocation of alkaline technogenic dust to the south of Moscow (Lokoshchenko 2015) – the road dust pH in the Southern, South-Eastern and South-Western districts, as well as in the Eastern and Western districts, exceeded the value of 7.4. The coarse sand fraction (particles with diameter >500 μm) is suspended at wind speeds exceeding 10 m/s; the coarse silt (with diameter 10–50 μm) and smaller particles may suspend in fairly weaker winds. Particles with diameter of 1–2 μm at wind speeds of 2–3 m/s are removed from

the soil surface, enter the surface aerosol, and remain suspended for quite a long time (Gendugov and Glazunov 2007). The particles' pH rises when their size decreases. Thus, in Western district, the pH in the aqueous extract of PM_{50} (with diameter ≤50 μm) was 0.6 units higher than that of $PM_{>50}$ (with diameter >50 μm); on large roads, this difference increased to almost 1 unit (Bityukova et al. 2016).

High pH values (≥8) in most cases are caused by the influx of alkalinizing substances during the repair of the roadway and laying paving slabs (Greinert et al. 2013). The maximum pH of 8.1 turned out to be lower than the average (8.2) and maximum (8.9) pH of road dust collected in the summer of 2013 for the eastern part of the city (Vlasov et al. 2015) when the weather was rather dry and hot. Low pH values in the summer of 2017 may be associated with intensive removal of carbonate dust by precipitation and surface runoff.

The pH values of the dust correlate well with the types of roads. The pH tends to increase in the following order: courtyards and small roads ➞ large and major radial roads. The exception is the road dust collected on the MRR which shows the intermediate pH values. The lowest average pH is restricted

to the inner yard territories (7.2), while the highest – is registered for the major radial highways (7.5); which supports the idea that pH increases with the increasing road width and intensity of traffic. Roadway abrasion is higher on large roads (even small ruts are formed here), the material of which has a slightly alkaline reaction with a pH of 7.4. The highest pH variability with both the minimum (6.4) and maximum (8.1) values was observed on small roads.

The pH rise with increasing road-size might be explained by a more active use of strong alkaline detergents on large roads. During summer period, roads are cleaned daily by sweeping dust and periodic washing of the road surface. Detergent products with high pH (9–11) are used ("Chistodor," "Tornado"). After deposition on road surfaces and drying they become one of the significant dust alkalinizing agents. The pH of the dust is minimal on parking lots in courtyards and on the MRR as they are not regularly washed (Fig. 2) while the road dust pH is much higher on the TRR, major radial, large, medium, and small roads, especially in Eastern, South-Eastern, Western and South-Western districts.

The predominance of the coarse particle size fractions in the road dust (Fig. 2) determines a more alkaline environment, which is associated with the input of slightly soluble particles of marble chips in winter season. The bulk of the DIAs used consists of particles with a diameter of 1–10 mm; the number of particles <1 mm does not exceed 15–20%.

Electrical conductivity. The Moscow's road dust has high EC, which is due to the presence of large quantities of soluble substances of technogenic and natural origin, detected in aqueous extracts. The average EC value of Moscow road dust was 211 µS/cm, which is about 3 times higher than the background value in the forest parks (70 µS/cm). The EC varies between the districts from 173 (Eastern district) to 248 µS/cm (North-Western district) and within the districts, where the EC variation coefficients are also significant (*Cv* 40–67%).

In winter time, the main source of readily soluble salts are the DIAs. With their excessive application, some of the reagents are not removed by the melt water, but remain in the solid form on the roadway, increasing the road dust EC. With decreasing particles' size, their EC rises: in Western district, the EC of PM_{50} is 2 times higher than that of $PM_{>50}$ (Bityukova et al. 2016).

The clear relationship between road-size and the EC was detected: the EC values on medium and small roads and in courtyards were 1.5 times lower than those on the MRR, TRR, major radial highways and large roads, especially in Northern, Central, South-Eastern and North-Western districts (Fig. 2) due to a high content of PM_{10} (Table 2). A similar effect was observed in Amman, Jordan (Al-Khashman 2007). The smallest average EC (161 µS/cm) was typical of courtyards with parking lots, while the highest (277 µS/cm) of the TRR. The minimum value was found on the medium-size roads in Eastern district (33 µS/cm), and the maximum (712), at the crossroad of the Zvenigorodskoye Highway and the TRR.

The map (Fig. 3b) shows that increased EC are confined to the area stretching from the North-West to South-East. Most likely, the high EC values in this area are associated with greater density of the road transport network and industrial facilities. Outside this area in the North-East of Moscow, there is a large forest park Losiny Ostrov, and in the South-West, the Bitsevski forest park.

Organic carbon. The pool of carbon in road dust is formed by soil particles containing humus and organic compounds of technogenic origin. In the traffic zone, the composition of organic matter is dominated by insoluble organic compounds, generally not susceptible to destruction by soil microorganisms, which increases their accumulation. Sources of these compounds are asphalt pavement and emissions from industries and motor vehicles (Faure et al. 2000). In the recreational and residential areas (forest parks and courtyards), the organic matter usually consists of natural fractions of humus (Lodygin et al. 2008); it is possible that in wet conditions (as it was

in summer 2017), the fungi mycelium was an additional source of organic carbon (Prokofieva et al. 2015). The increase in the C_{org} content in the forest parks is caused by the decomposition of plant litter as a natural source of C_{org}; in the courtyards, it is associated with the application of organic fertilizers (Vodyanitskii 2015).

The average content of C_{org} in road dust of Moscow was 2.6% ranging from 2.2% in Eastern district to 3.1% in North-Easterndistrict with the variation coefficient up to 50% (Table 1, Fig. 4a). In dust of different types of roads, the minimum content of C_{org} of 2.0% was associated with the major radial highways and large roads; the maximum of 4.0%, close to the background level of 4.1%, was observed in the courtyards (Fig. 2), where organic matter comes from soil particles that are blown out from lawns and carried on wheels of cars parked on bare ground. The lawn soils have a high content of C_{org} and nutrients, primarily nitrates (Kosheleva et al. 2018a). The addition of organic matter also occurs during idling of car engines responsible for increased emissions of soot and other organic compounds.

The C_{org} content in the road dust is positively correlated with PM_{10} fraction, which is partially derived from automobile exhaust containing various organic compounds,

including soot particles and lubricating oils (Grigoriev and Kissel 2002). The fine particle size fraction in the road dust also includes fine topsoil particles (1–2 μm), which are blown out by moving vehicles (Gendugov and Glazunov 2007). The smaller are the particles, the greater is the likelihood of them being blown out of the soil surface and getting into the dust. This explains the direct relationship between C_{org} and PM_{10}. The effect of pH on the C_{org} content (Fig. 2) relates to the contribution of soil particles, which, compared with technogenic material, have a more acidic reaction.

Particle size distribution. The granulometric composition of the Moscow's road dust was fairly uniform; it mainly contains sand (50–1000 μm) and coarse silt (10–50 μm) fractions, consisting predominantly of quartz and feldspar, respectively (Prokofieva et al. 2015). There were no significant differences in the particle size distributions between the road dust samples collected in different administrative districts and on different road types; the differences did not exceed 2–6% (Table 1, 2, Fig. 4b). Within the district groups, the share of PM_{10} in the road dust varied depending on the type of roads (Fig. 5). The road dust in Southern, South-Eastern and South-Western districts and on the large roads and the MRR was slightly dominated by $PM_{5–10}$ and $PM_{10–50}$ fractions (Fig. 5).
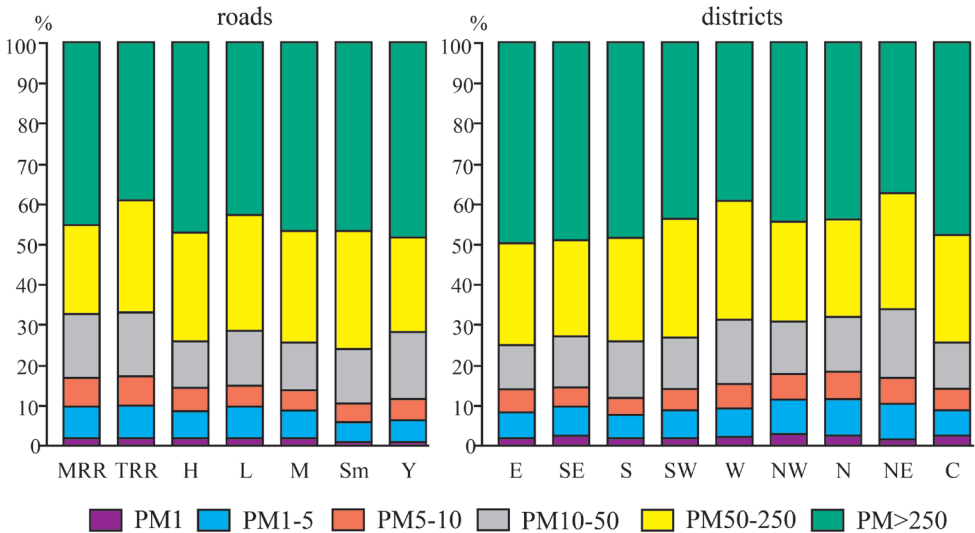

Fig. 5. The particle size composition of the road dust on various types of roads and in different administrative districts of Moscow. Types of roads are deciphered in Fig. 2.

The dust with a high content of the PM_{10} was typical for the Leningradskoye and Yaroslavskoye Highways, some of the busiest highways in Moscow, and for large roads at some distance from TRR and the city center. The PM_{10} content increases as a result of daily congestion of vehicles with long idling, which leads to an increase in emissions of fine particles and soot. This is especially pronounced in local depressions of the relief, where the most favorable conditions for the deposition of particles are formed.

The maximum content of coarse fractions was observed on the medium and small roads, as well as in Central, Eastern, South-Eastern and South-Western districts. The most likely reason for the predominance of coarse fractions in the road dust of the South-Eastern district is the coarse parent material of Meshchera lowland; there, a flat sandy plain is composed of fluvioglacial sands and sandy loam (Kasimov et al. 2016).

Technogenic transformation of the dust properties and the dust ability to accumulate pollutants.

Physicochemical properties of the road dust in the city are affected by technogenic sources. The comparison of the road dust with the dust sampled in the forest parks allowed us to estimate the intensity of the technogenic transformation of its properties (pH, EC, C_{org}, and the PM_{10} content) within Moscow. However, a comprehensive assessment of such transformation is difficult due to differences in the units of measurement and the variability of the parameters studied. To bring the heterogeneous data to a single scale, physicochemical properties of the road dust were normalized (Tikunov 1997):

$$X'_i = |X_i - X_b| / |X_{ex} - X_b|,$$

where X_i, X'_i are the initial and normalized values of a property at the i-th sampling point, respectively; X_b is the background value of the property in the dust of forest parks; X_{ex} is the extreme value of the property (X_{max} or X_{min}) most deviating from the background value X_b. As a rule, $X_{ex} = X_{max}$. If $|X_{min} - X_b| > |X_{max} - X_b|$, then $X_{ex} = X_{min}$. Then the *degree of technogenic transformation* (R) at the i-th sampling point can be defined as the total value of the normalized deviations of all parameters from the background values of $\Sigma X'_{ij}$, where j is the considered physicochemical property (in our case $j = 1, 2, 3, 4$). We set the approximate gradations of R depending on its range in the study area $\Delta R = R_{max} - R_{min}$ (Table 3).

Analysis of the spatial distribution of R (Fig. 6a) showed that the greatest transformation of the physicochemical properties of road dust was associated with the sections of major radial highways located near the industrial zones and bus depots: in Southern district – it was the Varshavskoye Highway (electrical substations, meat processing plant, bus and trolleybus depots, factory for the production of optoelectronic devices); in Eastern district – Schelkovskoye Highway (HPP-23); in Northern district – Dmitrovskoye Highway (bus depot, mechanical plants); in North-Western district – Volokolamskoye Highway (bus depot, reinforced-concrete plant) and

Table 3. Levels of technogenic transformation (R) of the road dust physicochemical properties

Level of technogenic transformation	Limit values of R	Ranking categories of R for Moscow
very low	$R \leq R_{min} + 0.1 \cdot \Delta R$	$R \leq 0.417$
low	$R_{min} + 0.1 \cdot \Delta R < R \leq R_{min} + 0.25 \cdot \Delta R$	$0.417 < R \leq 0.776$
medium	$R_{min} + 0.25 \cdot \Delta R < R \leq R_{min} + 0.5 \cdot \Delta R$	$0.776 < R \leq 1.374$
high	$R_{min} + 0.5 \cdot \Delta R < R \leq R_{min} + 0.75 \cdot \Delta R$	$1.374 < R \leq 1.972$
very high	$R_{min} + 0.75 \cdot \Delta R < R \leq R_{min} + 0.9 \cdot \Delta R$	$1.972 < R \leq 2.330$
extremely high	$R > R_{min} + 0.9 \cdot \Delta R$	$R > 2.330$

Zvenigorodskoye Highway (bus depot and HPP-16); in Western district – Mozhaiskoye Highway (HPP-25, wood processing plant, champagne wines plant, beer and non-alcoholic beverages plant); and in Central district – the Garden Ring road.

An increase in the pH, C_{org} and the PM_{10} contents in soils leads to the formation of technogenic alkaline, organo-mineral, and sorption-sedimentation geochemical barriers (Vodyanitskii 2008, 2015), whose capacity increases with the growth of these parameters (Kosheleva et al. 2015). Considering that roadside soils play an important role in the formation of the mineral part of road dust and supply

a significant amount of toxic chemical elements and compounds, an increase in pH, C_{org} and the PM_{10} content in the road dust, as in other mineral components of urban landscapes will contribute to the growth of its accumulation potential in relation to many HMMs.

To assess the spatial variability of the accumulation potential of the Moscow's road dust with respect to HMMs, the normalized index $Q = \Sigma X'_{ij}$ was calculated, with $j = 1, 2, 3$; $X'_i = (X_i - X_{min}) / (X_{max} - X_{min})$. The following ranking categories were adopted for the accumulation potential (Q) of road dust in Moscow taking into account its range in the study area $\Delta Q = Q_{max} - Q_{min}$ (Table 4).

Table 4. Ranking categories of the accumulation potential (Q) of the road dust

Accumulation potential	Limit values of Q	Ranking categories of Q for Moscow
very low	$Q \leq Q_{min} + 0.1 \cdot \Delta Q$	$Q \leq 0.796$
low	$Q_{min} + 0.1 \cdot \Delta Q < Q \leq Q_{min} + 0.25 \cdot \Delta Q$	$0.796 < Q \leq 1.052$
medium	$Q_{min} + 0.25 \cdot \Delta Q < Q \leq Q_{min} + 0.5 \cdot \Delta Q$	$1.052 < Q \leq 1.478$
high	$Q_{min} + 0.5 \cdot \Delta Q < Q \leq Q_{min} + 0.75 \cdot \Delta Q$	$1.478 < Q \leq 1.905$
very high	$Q_{min} + 0.75 \cdot \Delta Q < Q \leq Q_{min} + 0.9 \cdot \Delta Q$	$1.905 < Q \leq 2.160$
extremely high	$Q > Q_{min} + 0.9 \cdot \Delta Q$	$Q > 2.160$
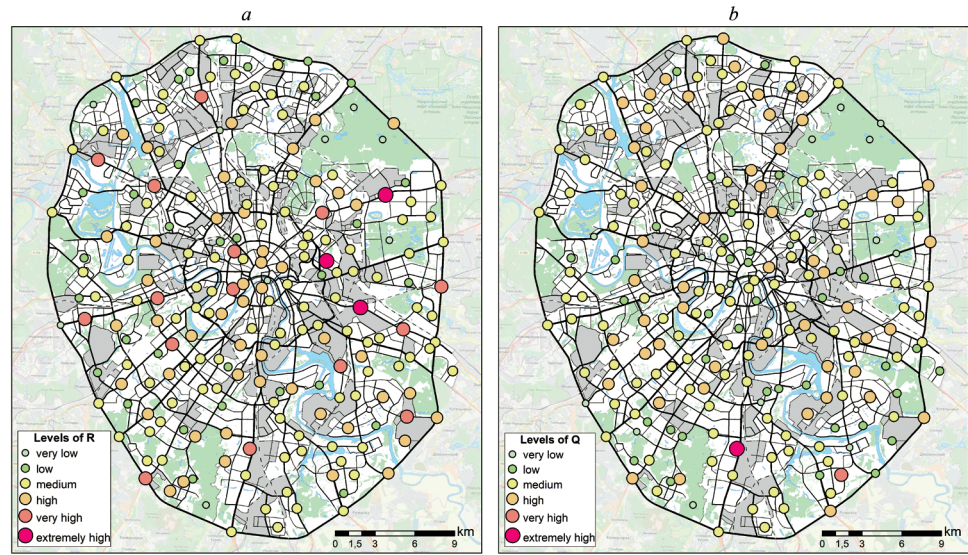
Fig. 6.The degree of technogenic transformation (R) of physicochemical properties (a) and the accumulation potential (Q) of the road dust (b)

The spatial distributions of the two indices – Q and R – differed for several reasons. First, the calculation of Q did not take into account the data on the EC of the aqueous extract of the road dust, since the EC's effect on the accumulation potential of mineral components has not been sufficiently studied. Secondly, the accumulation potential considers only the increase in pH values and the content of C_{org} and PM_{10}, whereas the index of technogenic transformation R summarizes both positive and negative deviations from the background conditions.

The analysis of the Q index distribution suggests the predominance of road dust with high and average accumulation potential in the traffic zone in all districts of the city. Medium levels of technogenic transformation and accumulation potential were typical of the MRR and the TRR, which is might be explained by rapid "regeneration" of dust material as a result of frequent road sweeping by municipal services. The largest accumulation potential of the road dust was detected in south of Moscow (along the Varshavskoye Highway), in the south-east (in courtyards and on medium-size streets between the Kashirskoye and Besedinskoye Highways), and in the north of Moscow (along the MRR and medium-size streets near the HPP-21, pipe plant, and fish and meat processing plants).

CONCLUSIONS

The dust in the urban forest parks of Moscow is mainly derived from the natural sources with minimal impact of anthropogenic fallout. Formed mainly by soil particles, it has the background properties most similar to those observed in the upper horizon of zonal sod-podzolic soils. It has neutral pH (average 7.1), low EC (70 µS/cm), high content of C_{org} (4.1%) and a significant amount of the coarse particle size fraction (> 250 µm). The high content of C_{org} in the forest parks is caused by decomposition of plant litter.

The dust on the roads has a more alkaline reaction (pH 7.4), high EC (211 µS/cm), and lower content of C_{org} (2.6%), which is explained by motor vehicles emissions and

the proximity to the industrial areas, as well as with a large volume of DIAs applied. The road dust is alkalinized by detergents and particles formed by abrasion of roadways and blown out from construction sites. A three-fold excess of the EC over the background values is mainly due to the use of the DIAs and roadway maintenance. The concentration of C_{org} in the Moscow's road dust is on average 2 times lower compared to the background values. In the courtyards, the increased content of C_{org} is associated with the application of organic fertilizers. In general, the road dust is composed mainly of sand-size particles (50–1000 µm) and coarse silt (10–50 µm) fraction. The variations in the share of particle size fractions by districts and different types of roads, as a rule, do not exceed 2–6%.

The most significant factor determining the physicochemical properties of the road dust is the type of road. The dust on large roads including TRR has higher pH, EC, and PM_{10} values, which is caused by the intense traffic and, as a result, the greater amount of particles formed through roadway and vehicle wear. The content of C_{org} in the road dust is reduced due to the lower contribution of soil particles. The spatial trends in the dust properties across the city territory are poorly expressed; to a large extent they are masked by other factors such as proximity to industrial zones and to large forest parks, the DIAs composition, frequency of the roadway cleaning and washing, and the contribution of soil particles of various genesis in different districts of Moscow.

The settling of airborne technogenic substances in the traffic zone increases the accumulation potential of the road dust with respect to pollutants binding compared to the dust of the forest parks. The most pronounced transformation of the road dust properties was found along some segments of the major radial highways that are located near the industrial areas and bus depots, especially in Southern, Eastern, Northern, North-Western, Western and Central districts. In Southern, South-Eastern and Central districts dust has the greatest accumulation potential. Cleaning roadways by municipal services reduces

Nikolay S. Kasimov, Natalia E. Kosheleva at al.   PHYSICOCHEMICAL PROPERTIES OF ...

04|2019

GES

109

technogenic transformation of the road dust properties and thereby diminish its ability to bind pollutants, what is most pronounced on MRR and TRR. Therefore, regular cleaning of all types of roads, including those in courtyards of residential areas, is an effective measure to improve the quality of urban environment by reducing the level of its contamination with dust and dust associated pollutants. Thus, these results and the approved methodology for studying the physicochemical properties of road dust can be useful in assessment of urban environmental pollution, as well as in planning and rationalizing activities for cleaning streets from road dust.

ACKNOWLEDGEMENTS

REFERENCES

Achkasov A., Basharkevich I., Varava K. and Samaev S. (2006). Pollution of snow cover under the influence of deicing agents. Exploration and protection of mineral resources, 9-10, pp. 132-137 (in Russian).

Acosta J., Faz A., Kalbitz K., Jansen B. and Martinez-Martinez S. (2011). Heavy metal concentrations in particle size fractions from street dust of Murcia (Spain) as the basis for risk assessment. Journal of Environmental Monitoring, 13, pp. 3087-3096. DOI: 10.1039/C1EM10364D

Al-Khashman O. (2007). Determination of metal accumulation in deposited street dusts in Amman, Jordan. Environmental Geochemistry and Health, 29, pp. 1-10. DOI: 10.1007/s10653-006-9067-8

Belis C., Karagulian F., Larsen B. and Hopke P. (2013). Critical review and meta-analysis of ambient particulate matter source apportionment using receptor models in Europe. Atmospheric Environment, 69, pp. 94-108. DOI: 10.1016/j.atmosenv.2012.11.009

Bityukova V. and Saulskaya T. (2017). Changes of the anthropogenic impact of Moscow industrial zones during the recent decades. Vestnik Moskovskogo Unviersiteta, Seriya Geografiya, 3, pp. 24-33 (in Russian with English summary).

Bityukova V., Vlasov D., Dorokhova M., Kasimov N., Kislyakova N., Kirillov P., Kosheleva N., Nikiforova E., Petukhova N., Ryzhov A., Savoskul M., Saulskaya T. and Shartova N. (2016). East – West of Moscow: a spatial analysis of social and environmental issues. Moscow: Faculty of Geography, Lomonosov Moscow State University (in Russian with English summary).

Da Costa D. and Oliveira D. (2009). Natural organic matter in atmospheric particles. In: Biophysico-chemical processes involving natural nonliving organic matter in environmental systems. New York: Wiley, pp. 451-485.

Demetriades A. and Birke M. (2015). Urban geochemical mapping manual: sampling, sample preparation, laboratory analysis, quality control check, statistical processing and map plotting. Brussels: EuroGeoSurveys.

Diapouli E., Manousakas M., Vratolis S., Vasilatou V., Maggos Th., Saraga D., Grigoratos Th., Argyropoulos G., Voutsa D., Samara C. and Eleftheriadis K. (2017). Evolution of air pollution source contributions over one decade, derived by PM_{10} and $PM_{2.5}$ source apportionment in two metropolitan urban areas in Greece. Atmospheric Environment, 164, pp. 416-430. DOI: 10.1016/j.atmosenv.2017.06.016

Faure P., Landais P., Schlepp L. and Michels R. (2000). Evidence for diffuse contamination of river sediments by road asphalt particles. Environmental Science & Technology, 34, pp. 1174-1181. DOI: 10.1021/es9909733

Fonova S. (2017). Scientific and methodological apparatus for assessing the geoecological risk of contamination by heavy metals in the area of roads of the first category. Ph.D. Thesis. Voronezh (in Russian).

Garg B., Cadle S., Mulawa P., Groblicki P., Laroo C. and Parr G. (2000). Brake wear particulate matter emissions. Environmental Science & Technology, 34, pp. 4463-4469. DOI: 10.1021/es001108h

Gendugov V. and Glazunov G. (2007). Wind erosion and dusting of air. Moscow: Fizmatlit (in Russian).

Greinert A., Fruzińska R. and Kostecki J. (2013). Urban soils in Zielona Góra. In: P. Charzyński, P. Hulisz and R. Bednarek, eds., Technogenic soils of Poland. Toruń: Polish Society of Soil Science, pp. 31-54.

Grigoriev V. and Kissel A. (2002). Handbook of methods and technical means of reducing emissions of pollutants into the atmosphere, used in the development of the draft MPE regulations. St. Petersburg: Atmosphere Research Institute (in Russian).

Hu X., Zhang Y., Luo J., Wang T., Lian H. and Ding. Z. (2011). Bioaccessibility and health risk of arsenic, mercury and other metals in urban street dusts from a mega-city, Nanjing, China. Environmental Pollution, 159, pp. 1215-1221. DOI: 10.1016/j.envpol.2011.01.037

Jayarathne A., Egodawatta P., Ayoko G. and Goonetilleke A. (2017). Geochemical phase and particle size relationships of metals in urban road dust. Environmental Pollution, 230, pp. 218-226. DOI: 10.1016/j.envpol.2017.06.059

Kasimov N., Kosheleva N., Vlasov D. and Terskaya E. (2012). Geochemistry of snow cover within the Eastern district of Moscow. Vestnik Moskovskogo Unviersiteta, Seriya Geografiya, 4, pp. 14-24 (in Russian with English summary).

Kasimov N., Vlasov D., Kosheleva N. and Nikiforova E. (2016). Landscape geochemistry of Eastern Moscow. Moscow: APR (in Russian).

Kasimov N., Kosheleva N., Nikiforova E. and Vlasov D. (2017). Benzo[a]pyrene in urban environments of eastern Moscow: pollution levels and critical loads. Atmospheric Chemistry and Physics. 2017, 17, pp. 2217-2227. DOI: 10.5194/acp-17-2217-2017

Khomyakov D. (2015). Moscow does not believe in salt. About deicing agents used in Moscow for the winter period, and their volume. Road Empire, 58, pp. 91-95 (in Russian).

Khusnullin M. (2013). The current state of the backbone of the street-road network [online] Urban Planning: The Transport Aspect. Russian and international experience. Available at: https://genplanmos.ru/event/transp_ap_2013_07_23 [Accessed 04 July 2017] (in Russian).

Kosheleva N., Kasimov N. and Vlasov D. (2015). Factors of the accumulation of heavy metals and metalloids at geochemical barriers in urban soils. Eurasian Soil Science, 5(48), pp. 476-492. DOI: 10.1134/S1064229315050038

Kosheleva N., Dorokhova M., Kuzminskaya N., Ryzhov A. and Kasimov N. (2018a). Impact of motor vehicles on the ecological state of soils in the Western District of Moscow. Vestnik Moskovskogo Unviersiteta, Seriya Geografiya, 2, pp. 16-27 (in Russian with English summary).

Kosheleva N., Vlasov D., Korlyakov I. and Kasimov N. (2018b). Contamination of urban soils with heavy metals in Moscow as affected by building development. Science of the Total Environment, 636, pp. 854-863. DOI: 10.1016/j.scitotenv.2018.04.308

Ladonin D. (2016). Forms of heavy metal compounds in technogenically polluted soils. Dr. of Biological Sciences Thesis, Moscow (in Russian).

Ladonin D. and Plyaskina O. (2009). Isotopic composition of lead in soils and street dust in the Southeastern administrative district of Moscow. Eurasian Soil Science, 1(42), pp. 93-104. DOI: 10.1134 / S1064229309010128

Lawrence S., Sokhi R. and Ravindra K. (2016). Quantification of vehicle fleet PM_{10} particulate matter emission factors from exhaust and non-exhaust sources using tunnel measurement techniques. Environmental Pollution, 210, pp. 419-428. DOI: 10.1016/j.envpol.2016.01.011

Lodygin E., Chukov S., Beznosikov V. and Gabov D. (2008). Polycyclic aromatic hydrocarbons in soils of Vasilievsky Island (St. Petersburg). Eurasian Soil Science, 12(41), pp. 1321-1326. DOI: 10.1134/S1064229308120107

Lokoshchenko M. (2015). Wind direction in Moscow. Russian Meteorology and Hydrology, 10(40), pp. 639-646. DOI: 10.3103/S1068373915100015

National Emissions Inventory. (2017). United States Environmental Protection Agency. [online]. Available at: https://www.epa.gov/air-emissions-inventories/2014-national-emissions-inventory-nei-data [Accessed 21 October 2017]

Nazzal Y., Rosen M. and Al-Rawabdeh A. (2013). Assessment of metal pollution in urban road dusts from selected highways of the Greater Toronto Area in Canada. Environmental Monitoring and Assessment, 185, pp. 1847-1858. DOI: 10.1007/s10661-012-2672-3

Nikiforova E., Kosheleva N. and Khaibrakhmanov T. (2016). Ecological impact of antiglaze treatment on soils of the Eastern district of Moscow. Vestnik Moskovskogo Unviersiteta, Seriya Geografiya, 3, pp. 40-49 (in Russian with English summary).

Privalenko V. and Bezuglova O. (2003). Ecological problems of anthropogenic landscapes of the Rostov region. Rostov-on-Don: Publishing House of North Caucasus Higher School Research Center (in Russian).

Prokofieva T. and Stroganova M. (2004). Soils of Moscow (soils in the urban environment, their features and ecological significance). Moscow: GEOS (in Russian).

Prokofieva T., Rozanova M. and Poputnikov V. (2013). Some features of soil organic matter in parks and adjacent residential areas of Moscow. Eurasian Soil Science, 3(46), pp. 273-283. DOI: 10.1134/S1064229313030071

Prokofieva T, Shishkov V., Kiryushin A. and Kalushin I. (2015). Properties of atmospheric solid fallouts in roadside areas of Moscow. Izvestiya Rossiiskoi akademii nauk, Seriya geograficheskaya, 3, pp. 107-120 (in Russian with English summary).

Report on the State of the Environment in the City of Moscow in 2016. Edited by Kulbachevsky A. (2017). Moscow: Department for Environmental Management and Protection; Institute of Urban Planning and System Design (in Russian).

Rozanova M., Prokofieva T., Lysak L. and Rakhleeva A. (2016). Soil organic matter in the Moscow State University botanical garden on the Leninskie Gori. Eurasian Soil Science, 9(49), p. 1013-1025. DOI: 10.1134/S106422931609012X

Sister V. and Koretsky V. (2004). Engineering-environmental protection of water system of the northern megapolis in winter period. Moscow: Center MSUIE (in Russian).

Sutherland R., Tack F. and Ziegler A. (2012). Road-deposited sediments in an urban environment: A first look at sequentially extracted element loads in grain size fractions. Journal of Hazardous Materials, 225-226, pp. 54-62. DOI: 10.1016/j.jhazmat.2012.04.066

Tager I. (2005). Health effects of aerosols: Mechanisms and epidemiology. In: Aerosols Handbook: Measurement, dosimetry, and health effects. Boca Raton: CRC Press, pp. 619-696.

Tikunov V. (1997). Modeling in cartography. Moscow: Publishing House of Moscow State University (in Russian).

Vlasov D. (2017). Metals and metalloids in PM_{10} fraction of the road dust of Eastern Moscow. RUDN Journal of Ecology and Life Safety, 4(25), pp. 529-539. DOI: 10.22363/2313-2310-2017-25-4-529-539 (in Russian with English summary).

Vlasov D., Kasimov N. and Kosheleva N. (2015). Geochemistry of the road dust in the Eastern district of Moscow. Vestnik Moskovskogo Unviersiteta, Seriya Geografiya, 1, pp. 23-33 (in Russian with English summary).

Vodyanitskii Yu. (2008). The affinity of heavy metals and metalloids to carrier phases in soils. Agrochemistry, 9, pp. 87-94 (in Russian with English summary).

Vodyanitskii Yu. (2015). Organic matter of urban soils: A review. Eurasian Soil Science, 8(48), pp. 802-811.

Wang X. and Qin Y. (2007). Leaching characteristics of heavy metals and As from two urban roadside soils. Environmental Monitoring and Assessment, 132, pp. 83-92. DOI: 10.1007/s10661-006-9504-2

Weather and Climate. (2017). Reference Information Portal "Weather and Climate". [online]. Available at: http://www.pogodaiklimat.ru [Accessed 21 July 2017] (in Russian).

Weckwerth G. (2001). Verification of traffic emitted aerosol components in the ambient air of Cologne (Germany). Atmospheric Environment, 35, pp. 5525-5536. DOI: 10.1016/S1352-2310(01)00234-5

Yang L., Zhu G., Pan H., Shi P., Li J., Liu Y. and Tong H. (2017). Surface dust heavy metals in the major cities, China. Environmental Earth Sciences, 76(757), pp. 1-4. DOI: 10.1007/s12665-017-7084-9

Yisa J., Jacob J. and Onoyima C. (2011). Identification of sources of heavy metals pollution in road deposited sediments using multivariate statistical analysis. Journal of Emerging Trends in Engineering and Applied Sciences, 2(4), pp. 658-663.

Natalia E. Chubarova[1*], Elizaveta E. Androsova[1], Alexandr A. Kirsanov[2], Bernhard Vogel[4], Heike Vogel[4], Olga B. Popovicheva[3], Gdali S. Rivin[2,1]

[1] Moscow State University, Faculty of Geography, 119991, Moscow, Russian Federation
[2] Hydrometeorological Centre of Russia, 11-13, B. Predtechensky per., Moscow, 123242, Russia
[3] Moscow State University, Faculty of Physics, 119991, P.O. Box 3640 76021, Moscow, Russian Federation
[4] Karlsruhe Institute of Technology, Karlsruhe, Germany
* Corresponding author: natalia.chubarova@gmail.com

AEROSOL AND ITS RADIATIVE EFFECTS DURING THE AERORADCITY 2018 MOSCOW EXPERIMENT

ABSTRACT. During the AeroRadCity-2018 spring aerosol experiment at the Moscow State University Meteorological Observatory the aerosol properties of the atmosphere and radiative aerosol effects were analyzed using a wide complex of measurements and model COSMO-ART simulations over Moscow domain. The program of measurements consisted of columnar aerosol AERONET retrievals, surface PM10, black carbon (BC) and aerosol gas precursors mass concentrations, as well as radiative measurements under various meteorological conditions. We obtained a positive statistically significant dependence of total and fine aerosol optical depth (AOD) mode ($R^2{\sim}0.4$) with PM concentrations. This dependence has revealed a pronounced bifurcation point around PM10=0.04 mgm^{-3}. The modelled BC concentration is in agreement with the observations and has a pronounced correlation with PM, but not with the AODs. The analysis of radiative effects of aerosol has revealed up to 30% loss for UV irradiance and 15% - for shortwave irradiance at high AOD in Moscow. Much intensive radiation attenuation is observed in the afternoon when remote pollution sources may affect solar fluxes at elevated boundary layer conditions. Negative (cooling) radiative forcing effect at the top of the atmosphere from -18 Wm^{-2} to -4 Wm^{-2} has been evaluated. Mean difference in visible AOD between urban and background conditions in Moscow and Zvenigorod was about 0.01 according to measurements and model simulations, while in some days the difference may increase up to 0.05. The generation of urban aerosol was shown to be more favorable in conditions with low intensity of pollutant dispersion, when mean deltaAOD550 was doubled from 0.01 to 0.02.

KEY WORDS: surface and columnar aerosol, black carbon, COSMO-ART, radiation, urban aerosol pollution, AERONET

INTRODUCTION

Atmospheric aerosol has a complex effect on the biosphere. It significantly affects the properties of the atmosphere, providing the uncertainty of climate change and directly affects human health increasing premature mortality and reduction of life (IPCC 2013; http://www.who.int/mediacentre/factsheets/fs313/en/). Depending on its optical and microphysical properties due to the processes of absorption and scattering of solar radiation, as well as through direct interaction with the cloud elements, the aerosol has different effects on temperature and humidity conditions of the atmosphere, thus determining the quality of the weather forecast and influencing regional climate. All these processes are exacerbated in the urban environment, where aerosol concentrations significantly increased and their optical properties changed dramatically. However, the estimates of the aerosol effects have large uncertainty, especially in the urban environment (Tegen et al. 1997; IPCC 2013). One of the most important components of an urban aerosol is black carbon (BC), a short-lived climate tracer, which stands on the second place in contributing atmospheric warming after carbon dioxide (IPCC 2013). Due to its properties BC significantly absorbs visible irradiance thus significantly affecting net shortwave radiation. Detailed studies of BC were carried out in IAP RAS (Kopeikin 1998; Golitsyn et al. 2015), in Western Siberia (Kozlov et al. 2016). There are several approaches (see, for example, Kozlov et al. 2008), in which BC measurements are used for retrieving aerosol single scattering albedo, which is one of the important aerosol parameters for radiative transfer (RT) modelling.

Different chemical, photochemical and meteorological processes play an important role in the urban aerosol formation affecting total columnar aerosol and, hence, further influencing the radiative and meteorological characteristics (Vogel et al. 2009, Chubarova et al. 2018). However, there are still gaps in understanding the reasons of various types of relationships between ground-based and columnar aerosol content. In addition, urban aerosol can change the absorbing properties of the atmosphere of large megacities (see for, example, Chubarova et al, 2011b). For studying these effects mesoscale atmospheric models with good temporal and spatial resolution can be used. One of them is the COSMO (COnsortium for Small-scale MOdelling) mesoscale model (http://www.cosmo-model.org/), which is currently an operational weather prediction model at the Hydrometeorological Centre of Russia. The ART (Aerosols and Reactive Trace gases) chemical model as a part of COSMO model (Vogel et al. 2010) allows a user to simulate the formation of secondary aerosol and gives the opportunity to quantify the rate of formation of new particles in the polluted urban atmosphere under different atmospheric conditions.

For understanding the physical processes of generating different aerosol types and their effects on solar irradiance, an intensive measurement campaign (AeroRadCity) has been carried out in spring 2018 at the Meteorological Observatory (MO), of Moscow State University. The AeroRadCity-2018 experiment included both experimental and model aerosol and radiation studies for better understanding the role of a large megacity in generating urban aerosol and evaluating its effects on solar irradiance.

In this paper we focus on the following tasks:

• Identification of the relationship between meteorological conditions with an additional characterization of the intensity of the particle dispersion (IPD) and different aerosol characteristics for quantifying the relation between surface and columnar aerosol loading.

• Evaluation of the aerosol radiative effects in different spectral regions.

• Assessment of the urban component of aerosol.

We analyze spring conditions since within a relatively short period we could test all

situations typical both for cold and warm seasons including important biomass burning episodes for studying a wide variety of different aerosol properties and their effects on solar radiation.

MATERIALS AND METHODS

The AeroRadCity-2018 experiment observational campaign included a large complex of measurements of different surface and columnar aerosol properties, aerosol gas precursors, as well as radiative and meteorological parameters at the Meteorological Observatory of Moscow State University (MO MSU), (55.707°N, 37.522°E, http://momsu.ru/english.html), which is located at the territory of the MSU Botanical Garden in the area of Vorobyovy Gory (Vorobyovy hills) far from local emission sources. MO MSU is qualified as an urban background site (Chubarova et al. 2014). The complex of aerosol measurements consisted of columnar aerosol characteristics from sun/sky CIMEL photometer installed at the MO MSU roof as a part of the AERONET program (Holben et al. 1998; Chubarova et al. 2011a). The AERONET aerosol retrievals included aerosol optical depth (AOD) within the spectral range from 340 nm to 1020 nm, Angstrom exponent, fine and coarse aerosol AOD modes at 500nm according to the retrieval method described in (O'Neill et al. 2001), single scattering albedo (SSA) and aerosol factor of asymmetry (ASYM) according to Dubovik and King (2000). The measurements of columnar aerosol characteristics were made in clear solar disk conditions using the additional cloud-screening filter described in (Chubarova et al. 2016). The data from the latest version 3 with final instrument calibration (level 2) were used for Moscow, and the data from version 3 at level 1.5– for Zvenigorod site, since no final data calibration is still available there. However, according to the experience, the correction usually does not exceed 0.01 AOD in a visible spectral region.

Setup of instruments for real-time equivalent black carbon mass concentration measurements and PM sampling was also installed at the MO MSU roof. Aerosol equivalent BC concentrations (marked as BC) were measured using the portable aethalometer developed by the MSU/CAO group (Popovicheva et al. 2019). In this instrument, the light attenuation caused by the particles depositing on a quartz fiber was measured at three wavelengths (450, 550, and 650 nm). BC concentrations were determined by converting the time-resolved light attenuation to BC mass concentration at 650 nm and characterized by a specific mean mass attenuation coefficient as described in (Popovicheva et al. 2017). The calibration parameter for the BC mass quantification was derived during parallel long-term measurements against an AE33 aethalometer (Magee Scientific) that operates at the same three wavelengths.

PM mass concentration with the diameter of aerosol particles smaller than 10 μm (PM10) and aerosol gas precursors were measured at the automatic station for air pollution monitoring with 20-minute resolution operated by the "Mosecomonitoring" State Environmental Protection Agency at the MO MSU. In particular, for the PM10 measurements, the TEOM 1400a instrument (Thermo Environmental Instruments Inc./ USA) has been applied. The description of other instrumentation can be found at the Mosecomonitoring site (http://mosecom.ru).

Standard meteorological observations (temperature, relative humidity, pressure, precipitation, wind speed, and wind direction) were taken from the automated Vaisala weather station with 1-minute resolution. Radiative measurements included global shortwave irradiance (less 4 μm) and ultraviolet (UV) irradiance over 300-380nm spectral interval. Global shortwave irradiance (Q) was obtained as a sum of horizontal direct (by the M-3 actinometer) and diffuse (by the M-10 pyranometer with a shadow ring) radiation components, that provided the best Q estimates. The measurements of UV irradiance were fulfilled by the UV-A-T Kipp&Zonen pyranometer calibrated for measuring global UV radiation over the 300-380nm spectral range (Q380) during the Second International UV Filter Radiometer Calibration Campaign UVC-II GAW regional UV calibration center at

PMOD/WRC in Davos, Switzerland (http://projects.pmodwrc.ch/bb2017/project.php). All data were collected in the database with 1-hour resolution. In some cases, we also analyzed instantaneous aerosol measurements. Figure 1 presents a view of the main instrumentation used in the experiment and the picture of MO MSU location.

During the period of the experimental studies the modelling of aerosol was carried out with the help of the COSMO-ART (Vogel et al. 2010; Vil'fand et al. 2017) model with a 7 km grid. The COSMO-ART model simulates chemical transformations of gaseous substances, taking into account for the aerosol chemistry. Chemical processes in the atmosphere are represented by 172 reactions. COSMO-Ru7 was used as initial and boundary conditions for meteorological simulations. The data from Global Land Cover 2000 project were used as land use input parameters. The TNO (Netherlands Organization for Applied Scientific Research) inventory data were utilized to specify anthropogenic emissions of polluting substances. We fulfilled the numerical experiments with different TNO emissions for 2010 and for the 2003-2007 inventory periods. Their spatial distribution for the aerosol gas-precursors emissions for April and May is shown in Fig. 2. It is clearly seen that the latest TNO2010 inventory data are much smaller than the old one. The main experiments in this study were fulfilled with the new TNO2010 emissions. However, some tests were also made with the old 2003-2007 TNO. We should note that only urban aerosol component was significant among other modelling aerosol components. Hence, in

our estimations, the simulated aerosol can be attributed as an urban aerosol. The 24-48-hour COSMO-ART model forecast was analyzed to have enough time for aerosol generation. Mainly we studied surface BC concentration, PM2.5 and AOD550 as well as the important aerosol gas precursors.

RESULTS

The description of weather and optical conditions during the experiment

The AeroRadCity-2018 experiment covered the period from April 1st to 31th of May 2018. During this period monthly mean air temperature was about 8.4^{0}C in April and 16.7^{0}C – in May, relative humidity comprised 54% and 51%, and precipitation - 34 and 45 mm, respectively. Their comparisons showed higher air temperature (+2-3^{0}C), and lower level of relative humidity (10%) and precipitation (7-10 mm) than climatological values over the 1954-2013 period (Chubarova et al. 2014).

Table 1 presents the statistics on the main gaseous and aerosol parameters in the atmosphere of Moscow during the experiment. One can see that AOD at 500 nm (AOD500) was 0.07-0.09 lower than typical AOD for Moscow for these months, while the PM10 concentrations (0.025 mgm^{-3}) were similar to climatological values (0.022 mgm^{-3}) during spring (Chubarova et al. 2014). On average, in Moscow, PM10 was found to be around 0.035 mgm^{-3} that is comparable with their level at European megacities (around 0.020-0.030 mg/m^3) and lower than in Asian megacities (0.05-0.1 mg/m^3) (Climate of Moscow.., 2017;

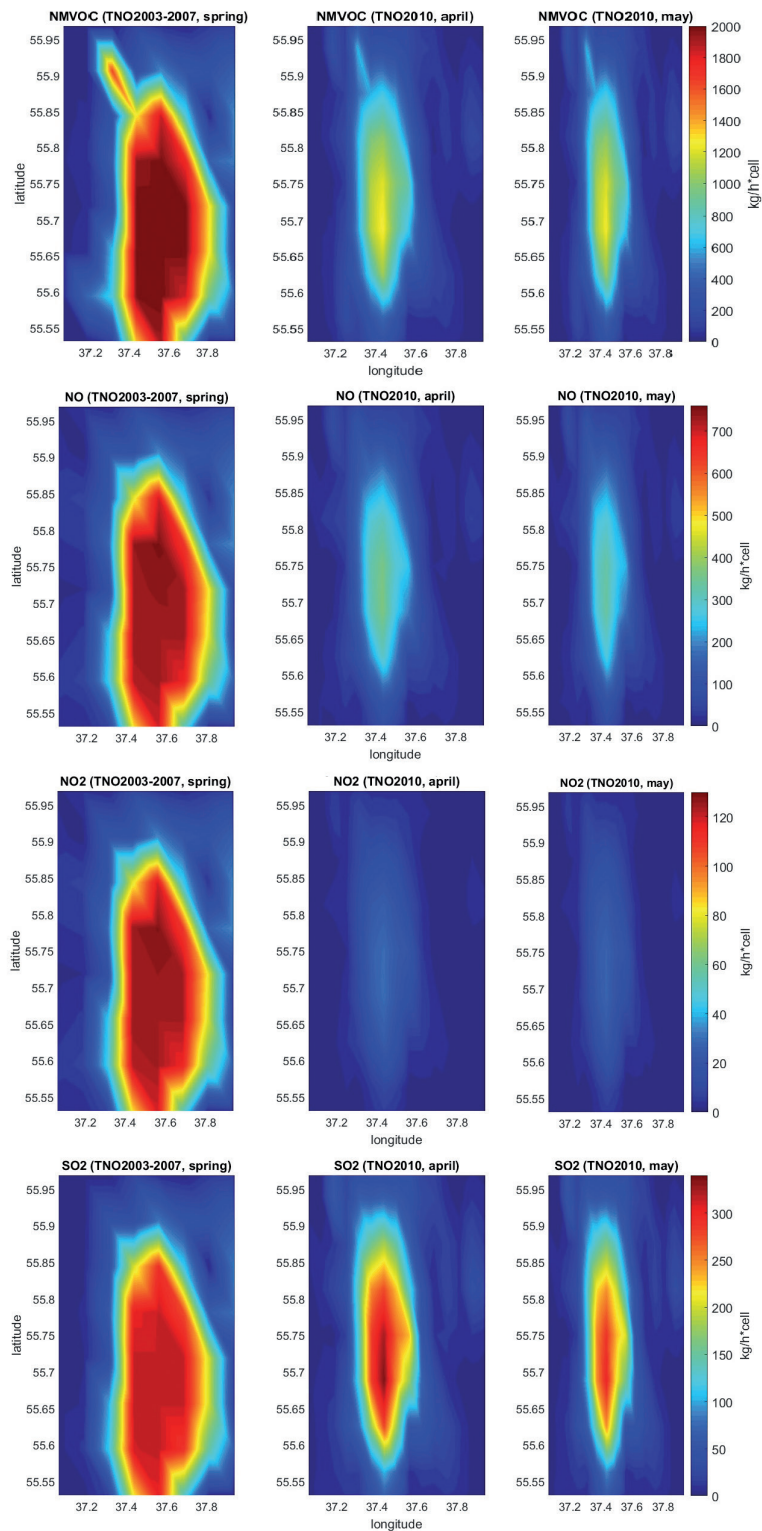**Fig. 1. Main instrumentation used in the AeroRadCity experiment and the picture of MO MSU**

Fig. 2. Emissions of gas-precursors according to the TNO 2010 and the TNO 2003-2007 inventory datasets

Table 1. Characteristics of gaseous and aerosol parameters in the atmosphere of Moscow during the period of the AeroRadCity experiment. April-May, 2018

	Average	50% quantile	Confidence intervals at P=95%	Minimum	Maximum	N case
AOD500	0.14	0.11	0.01	0.06	0.5	194
AOD_{coarse}/AOD, %	37.6	37.1	1.4	9.5	72.8	182
BC*, μgm^{-3}	1.16	0.9	0.07	0.01	8.1	712
PM10, mgm^{-3}	0.025	0.022	0.001	0.001	0.167	1458
BC/PM10*, %	5	4.43	0.27	0.06	61.8	708
SO_2, mgm^{-3}	0.003	0.003	0.0002	0	0.043	1440
NO, mgm^{-3}	0.044	0.032	0.002	0.008	0.33	1440
NO_2, mgm^{-3}	0.037	0.029	0.001	0.008	0.151	1440
CHx, mgm^{-3}	1.45	1.41	0.006	1.32	3.09	1390
CO, mgm^{-3}	0.23	0.2	0.007	0.11	1.31	1440
Angstrom exponent	1.17	1.18	0.031	0.35	1.56	194
Water vapor content, cm	1.22	1.17	0.066	0.35	2.33	194
SSA675	0.86	0.85	0.046	0.81	0.95	7
ASYM675	0.626	0.645	0.051	0.546	0.677	7
Ozone, DU	356.94	353.28	4.63	314.58	440.42	97

Note: statistics were obtained using hourly mean data for ground-based measurements (from initial time step of 20 minute) and direct sun photometer retrievals (with AERONET standard time step setup). Different case number is due to the absence of AERONET measurements in cloudy weather and restrictions on evaluation of SSA and ASYM parameters. Ozone was obtained from OMI satellite data.
*- averaging period from 19 of April to 23 of May 2019

Cheng et al. 2016; The Mosecomonitoring Report 2017). The mean BC concentrations (1.16 $mkgm^{-3}$) were similar to the typical BC for the Moscow region (1.1-1.3 $mkgm^{-3}$) according to (Koepke et al. 1997). However, in (Kopeikin et al. 2018) the Moscow BC concentration was found to be 3 times higher over the highways and central polluted area of Moscow. According to (Emilenko et al. 2018), by the end of 20 century the BC concentration reached 7 $mkgm^{-3}$ in the polluted urban areas. The average 5% BC/PM10 ratio obtained during the experiment was at the upper limit, which typically was smaller than 5%. Its ratio is higher (around 12%) in South America, parts of Africa, Europe, South East Asia, and Oceania due to anthropogenic influence, associated in some cases with biomass burning (IPCC 2007). On average, we can summarize that the analyzed period was characterized by lower total AOD and typical for urban background conditions levels of the surface BC and PM concentrations. The detailed analysis of BC in Moscow for spring conditions 2018 can be found in (Popovicheva et al. 2020).

In order to resolve the effects of aerosol advection and urban aerosol formation processes, the entire period of the AeroRadCity experiment was divided into 12 synoptic sub-periods with quasi-homogeneous atmospheric circulation and meteorological conditions with similar air mass advection according to the detailed analysis of synoptic conditions and 24-hour backward trajectories analysis. Since the concentrations of aerosol and gas composition of the atmosphere were also largely determined by the turbulent conditions in the boundary layer, in addition, the integral quantitative parameter of the intensity of the particle dispersion (IPD) was used in the analysis. The method of its calculation is described in (Kuznetsova et al. 2014). The intensity of air dispersion is classified from 1 to 3 using a number of characteristics including wind speed over 925-850 hPa layer (approximately 1-1.5 km), the type of atmospheric circulation, stratification of the atmosphere and precipitation conditions. For example, when the IPD=1, the atmospheric conditions are characterized by low wind speed, stable stratification, the absence of precipitation, that provides favorable conditions for the pollution accumulation. On contrary, high values of IPD=3 refers to unstable temperature stratification, high wind speed and possible intense precipitation in the zone of the atmospheric front, providing the atmosphere cleaning.

Fig. 3 presents the average values of several columnar and ground-based aerosol characteristics as well as the IPD indices for the 12 sub-periods during the experiment. One can see that the average IPD index is higher than 2 for all sub-periods, that indicates a rather rare frequency of unfavorable meteorological conditions. However, during the two periods –– April 11-16 and May 13-17 we observed statistically significant smaller IPD values due to the prevalence of conditions with stable stratifications and low wind speed in the boundary layer at the elevated atmospheric pressure. One can see that during these periods we have elevated levels of both surface and columnar aerosol including BC component. Note, that during the period with low IPD index the coarse/total aerosol ratio is getting smaller possibly due to the favorable processes of additional accumulation of fine aerosol mode in urban conditions (see Fig. 3). However, during the April 30-May 5 sub-period elevated aerosol values occurred in conditions with a high intensity of particle dispersion. This happened due to air advection from the South-West with elevated levels of aerosol and biomass burning aerosol loading from agricultural fires during the May 1st holiday period.
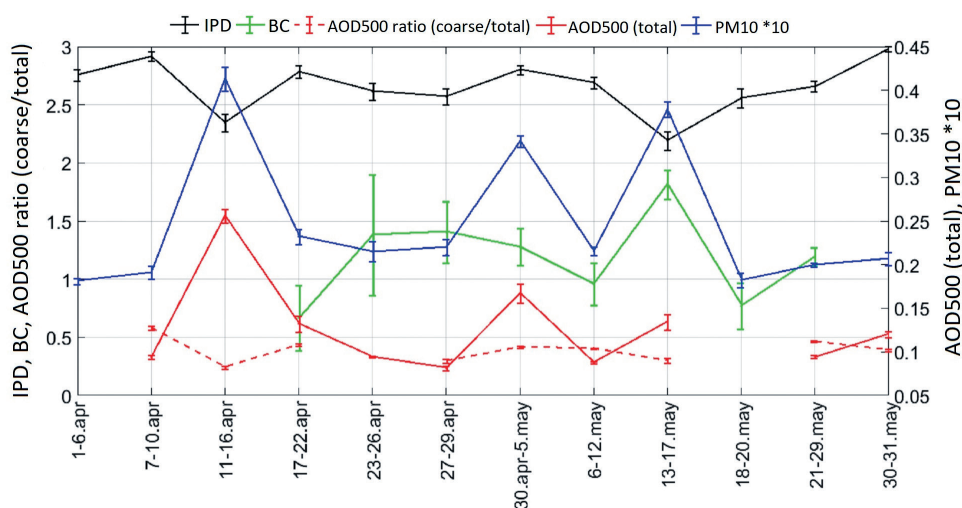
Fig. 3. Average values of AOD at 500 nm, coarse/total aerosol AOD ratio, PM$_{10}$ (mgm^{-3}) and BC (mkgm^{-3}) concentrations as well as the index of intensity of particle dispersion (IPD) over the sub-periods of the AeroRadCity experiment

The relationship between different aerosol and gas aerosol precursors

The dependence of columnar AOD500 on PM_{10} and BC values for different classes of the intensity of pollutant dispersion is shown in Fig. 4. One can see that for the dependence of AOD500 versus PM10 (Fig. 4 A, B, C) the two types of relationships with a bifurcation point around PM10=0.04 mgm^{-3} are observed. At high surface PM10 concentrations usually there is an increase in AOD500, but in conditions with IPD=1, low AOD500 can be also observed. This happens due to the conditions of very stable stratification of the atmosphere with accumulation of urban secondary generated aerosol particles near the surface. That means that in such conditions if we analyze the climate effects, even the effective generation of aerosol near the surface will not play any role for radiation and, hence, temperature changes. However, when the AOD500 growth is observed due to the process of the advection from the regions with elevated columnar aerosol loading the stable stratification (i.e. low IPD index=1) does not play a vital role. On average, we have a statistically significant dependence of AOD500 changes on PM10 for total and fine AOD500 mode (R^2=0.4 in both cases), while no dependence is obtained for coarse mode aerosol (Fig. 4C), since the coarse mode is mainly located near the surface due to larger mass of the particles.

There is no statistically significant AOD dependence on BC concentrations. However, we can see some small sub-visible bifurcation point for total AOD500 at BC=1.5 mkgm^{-3}. Since the size of the BC sample is not large and is smaller than for other components, the studies should be continued before making conclusions.

In order to understand the efficiency of PM_{10} generation, we made comparisons of surface BC dependencies on PM concentration. The increase in PM10 due to BC was obtained according to both the model and experimental
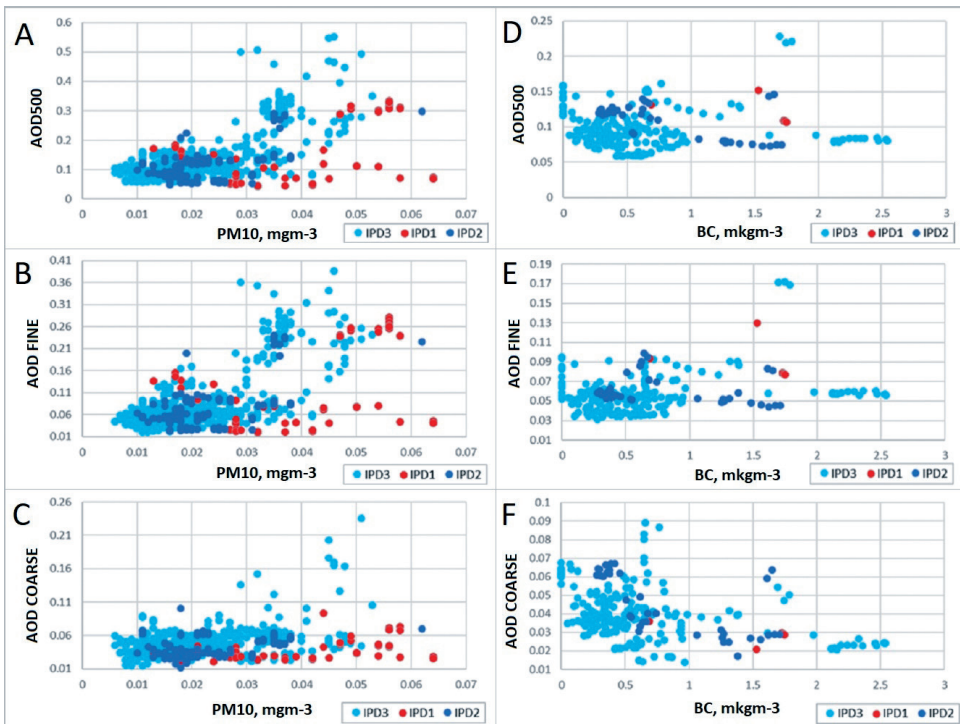

Fig. 4. Columnar AOD500 and AOD500 fine and coarse modes versus PM10 (left panel) and BC (right panel), for different classes of intensity of pollutant dispersion (IPD)

datasets (Fig. 5 A, D). There is also a high correlation between modelled BC and SO_2 concentrations (Fig. 5E). However, according to the measurements, the real SO2 concentrations are much lower and no dependence is seen (see Fig. 5B). This difference can be explained by the overestimation of TNO SO_2 emissions in Moscow. The main source of SO_2 is coal fuel in power plants which is not usually used in Moscow. A high correlation between BC and NO_2 concentrations obtained both in model and experiment demonstrated similar sources of emissions from diesel fuel in motor vehicle transport (Fig. 5 C, F).

Radiative effects of aerosol

In order to reveal the sensitivity of solar irradiance to aerosol, we analyzed the dependence of ultraviolet and global shortwave irradiance on aerosol optical thickness for clear sky conditions. To exclude the solar angle dependence and to evaluate the aerosol effects, radiation was normalized on the corresponding values in the molecular atmosphere. We added the analysis for the UV spectral region 300-380 nm with the effective wavelength at 345 nm, since it is more sensitive to the effects of aerosol and urban gas absorption and at this wavelength, is not practically sensitive to ozone. However, we made the account
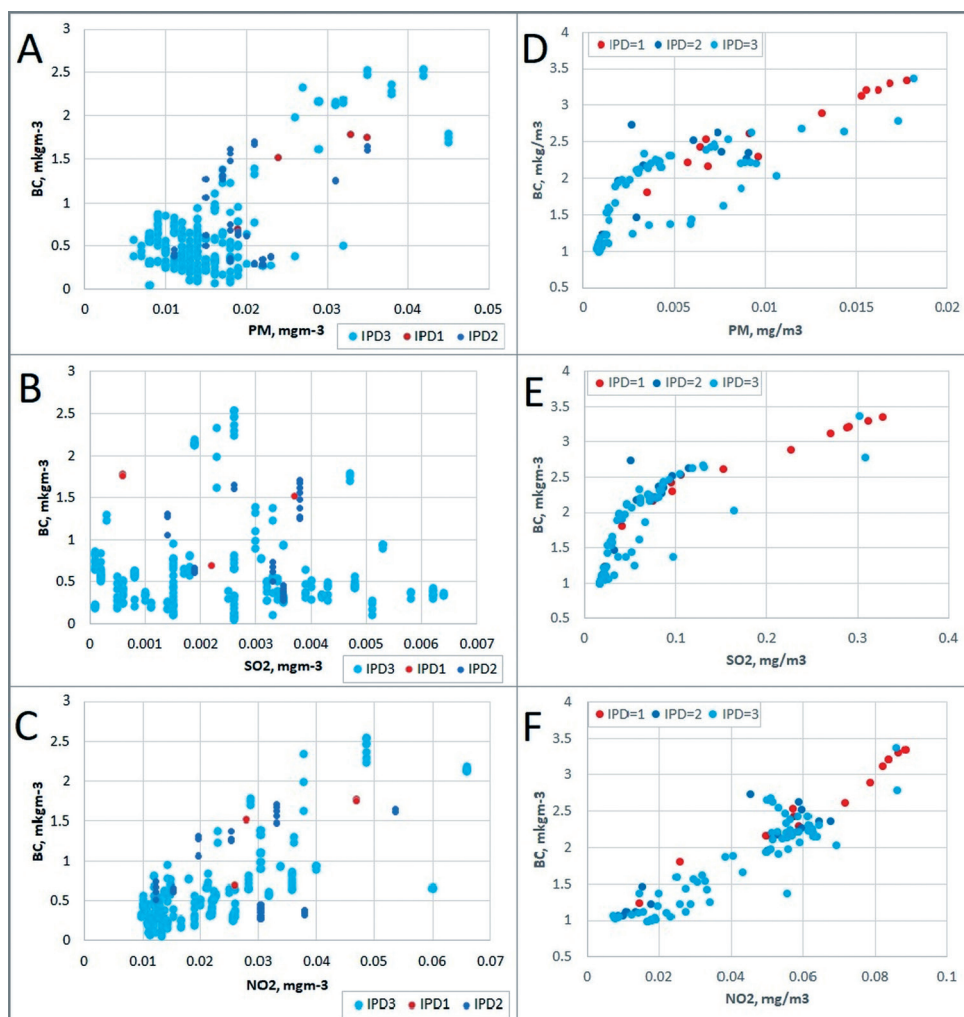

Fig. 5. The BC concentrations versus PM$_{10}$ at different IPD conditions according to measurements (left panel) and COSMO-ART modelling (right panel)

for ozone for UV irradiance according to OMI satellite dataset, which is of few percents, and to water vapor content for shortwave irradiance according to the standard AERONET retrievals. Figure 6 presents the dependence of normalized global shortwave and UV irradiance Qaer/Qmol, % on AOD according to observations and simulations using radiative transfer (RT) DISORT model with different single scattering albedo (SSA). One can see a pronounced dependence with up to 30% loss for UV irradiance and 15% for shortwave irradiance. However, this strong attenuation, especially for UV irradiance, was not reproduced by the RT modelling. When dividing the dataset into morning (before 13:00) and daytime (after 13:00) samples, all low observed values were found in the daytime sample. This result may be due to the fact that the MO MSU is a fairly "clean" site located far from the sources of local pollutant emissions, which are mainly observed at highways and near local points of pollution. In the morning, convective mixing is very weak, so the pollutants are near the earth's surface and do not affect irradiance, while

in the afternoon the convection increases and the polluted air with stronger absorption reaches higher levels affecting even urban background sites. We should mention that AERONET data provide all aerosol properties for visible and near infrared range but no retrievals on single scattering albedo are available for UV spectral region, where these effects are most strong. In addition to black carbon, there can be other types of urban aerosol, i.e., organic carbon aerosols, which have effective absorption in UV (Kirchstetter et al. 2004; Kazadzis et al. 2012). For example, during forest fires in 2010, we have a dramatic decrease in UV irradiance due to high emissions of organic aerosol matter (Chubarova et al. 2012). In addition, we examined the dependence of the SSA retrievals in a visible part of the spectrum on the BC/PM ratio according to our observations. However, due to lack of statistics we were not able to find any dependence, which had been obtained in the previous work (Kozlov et al. 2008).

For different sub-periods, where clear sky conditions were observed, we evaluated
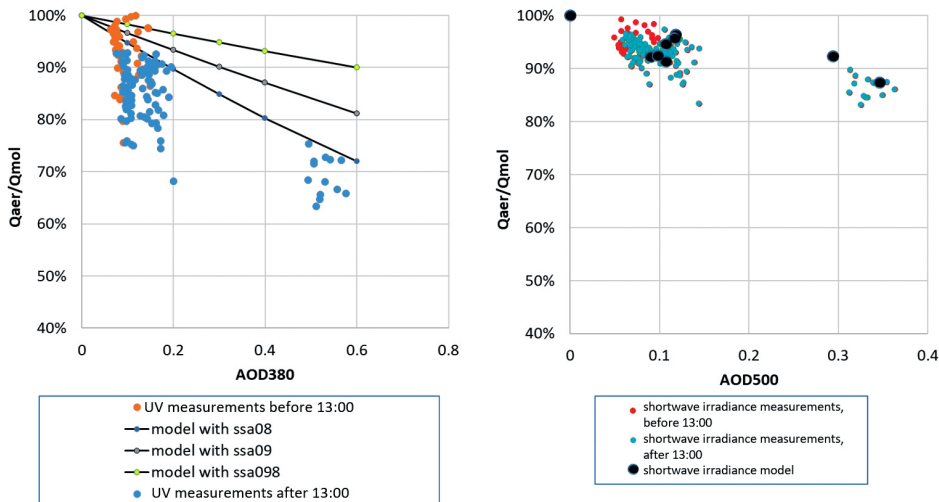
Fig. 6. The dependence of normalized UV (left) and shortwave (right) irradiance (Qaer/Qmol, %) on aerosol optical depth according to observations and radiative transfer DISORT model. Clear sky conditions

Note. The UV model values were simulated taking into account for the ozone using the OMI satellite data. For shortwave irradiance we accounted for the same water vapor content which was inferred from AERONET standard retrievals. All values were corrected to mean solar-earth distance. The measurements during the first part of the day before 13:00 are shown by orange (left panel) and red (right panel) dots

aerosol radiation forcing effects (RFE) at the top (TOA) of the atmosphere. The RFE is determined following the equation:

$$RFE_{TOA} = - (F_{net,a,TOA} \downarrow\uparrow - F_{net,o,TOA} \downarrow\uparrow) \quad (1)$$

where $F_{net,a}$ and $Fn_{et,o}$ are the net radiation at TOA with and without aerosols, respectively.

Fig. 7 presents RFE at TOA and columnar aerosol characteristics (AOD at 500 nm, single scattering albedo (SSA at 675nm) and aerosol factor of asymmetry (ASYM at 675nm) for different sub-periods in clear sky conditions. The RFE is negative for all periods that provides a cooling effect. It varies from -18 Wm^{-2} during 11-16 April, 2018 to -4 Wm^{-2} during May 6-12, 2018 period due to a substantial decrease in AOD and the conditions with slightly absorbing aerosol (SSA is higher 0.8 for all cases). We also should mention that due to prevalence of smaller aerosol particles we have a smaller factor of asymmetry which can lead to additional cooling effect. Our previous studies we also demonstrated the decrease in surface temperature due to such kind of aerosol is about -0.1…-0.2^{0}C (Chubarova et al, 2018).

Urban aerosol effects over Moscow domain area

We also analyzed, how the modelled urban PM concentrations contribute to the difference in AOD values on the example of Moscow and Zvenigorod (Moscow suburb, background conditions) sites. The Zvenigorod site is located 55 km to the west of Moscow in the upwind direction. This point was chosen since long-term AERONET measurements have been in operation there at the Zvenigorod Scientific Station of Institute of Atmospheric Physics RAS. The comparisons were made for 4 days (15/04, 3/05, 8/05 and 9/05) with different meteorological conditions, when we have large AOD statistics from measurements.

Fig. 8 shows the difference in AOD550 and in PM concentrations between Moscow and Zvenigorod only due to urban aerosol generation for different meteorological regimes according to the COSMO-ART modelling. One can see that according to model results, we have a substantial increase in AOD550 up to 0.05 due to an urban component with an increase in urban PM. No dependence on IPD regimes is seen. The comparison
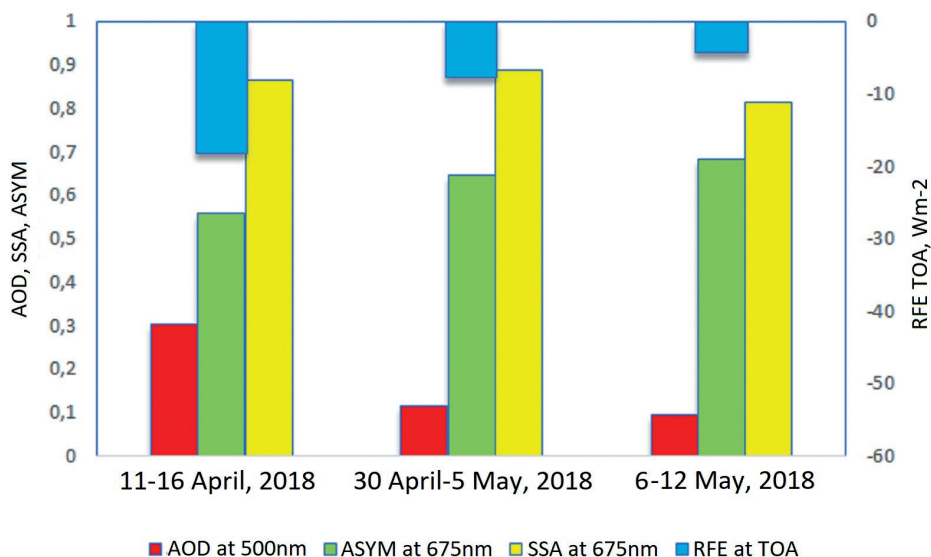
Fig. 7. Aerosol radiative forcing effect (RFE) at the top of the atmosphere and aerosol characteristics (aerosol optical thickness – AOD, ASYM – factor of asymmetry, SSA – single scattering albedo) in clear sky conditions

of modelled and experimental data are presented in Fig. 9, where the deltaAOD550 difference is shown between Moscow and Zvenigorod versus observed PM concentration in Moscow for different meteorological conditions. We clearly see the effects of stable IPD=1 regime on positive urban bias in the observed AOD550. In other IPD regimes, experimental data show both positive and negative differences in AOD550 due to variations in natural aerosol advection. According to modelled data, we see in all cases the increase in AOD in Moscow since we do not take into account natural aerosol in these experiments. In addition,

we should mention that the level of modelled PM concentrations in Moscow is only of urban origin and, hence, is significantly lower than the observed ones.

The application of different emission inventories provides some differences in AOD550 simulations. We made the estimates for two days (8 and 9 of May, 2018), which have revealed that on May 8th the old TNO2003-2007 inventory provided an overestimation of AOD550 difference between Moscow and Zvenigorod (deltaAOD550$_{model}$= 0.055 against deltaAOD550$_{observ}$=0.03),

Fig. 8. The dependence of difference in AOD550 (delta AOD550) on difference in PM concentrations (delta PM) between Moscow (MOMSU, urban conditions) and Zvenigorod (background Moscow suburb conditions) for different meteorological regimes according to the COSMO-ART modelling
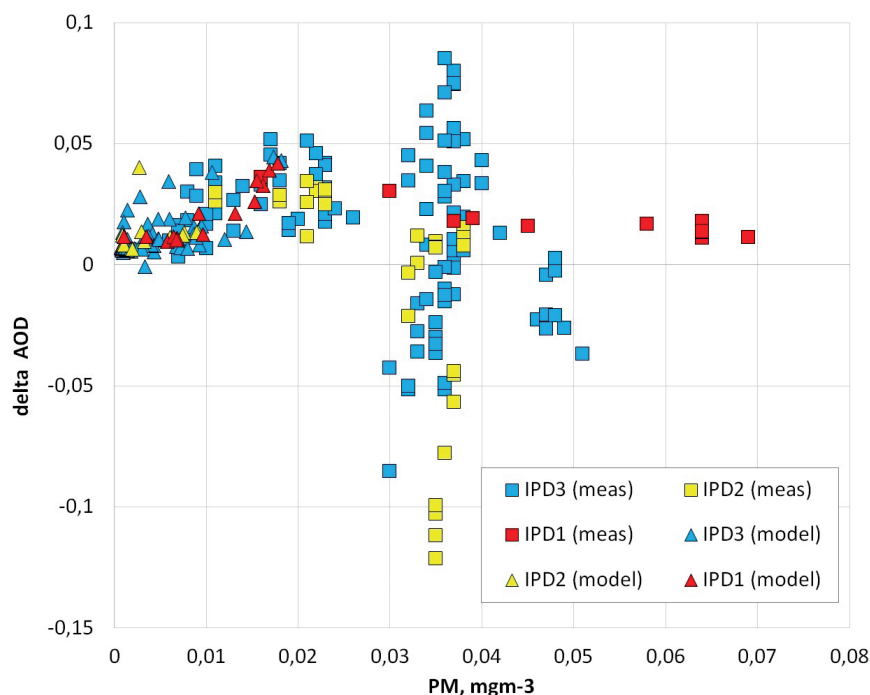
Fig. 9. The difference in AOD550 between Moscow and Zvenigorod (Moscow suburb) as a function of PM concentrations in Moscow for different meteorological IPD regimes according to the COSMO-ART modelling and experimental data

while a new TNO2010 was much closer to measurements (deltaAOD550$_{model}$=0.023). For May 9th the old TNO demonstrated a better agreement (deltaAOD550$_{model}$=0.019 against deltaAOD$_{observ}$=0.017) compared with the new TNO2010 inventory (deltaAOD550$_{model}$=0.007). However, the difference is rather small and lies within the uncertainty of measurements and modelling.

On average, the observed difference between Moscow and Zvenigorod delta AOD550 comprises 0.01 reaching 0.02 at IPD=1 for both the results of modelling and observations (Fig. 10). A smaller range of changes in modelled delta AOD550 is observed since no natural variation of aerosol is taken into account in these numerical COSMO-ART experiments, when mainly urban component of the AOD was calculated with negligible contribution of biogenic aerosol (Fig. 10A). The simulated BC concentration is in agreement with the observed

concentration for urban background conditions over the MO MSU (Fig. 10B). The modeled PM concentrations are much lower than the results obtained from observations since they do not account for natural aerosol components (Fig. 10C). We should emphasize that similar results of about 0.02 for delta AOT500 were obtained in our previous direct comparisons between Moscow and Zvenigorod (Chubarova et al. 2011b). However, in Berlin, much higher difference was obtained when deltaAOD= 0.08 (Li et al. 2018) according to MODIS (MYD04_3K and MYD11_A1) dataset, which might be explained by not full accounting for higher reflectance over the city in the MODIS algorithm. For Warsaw (Poland) conditions, despite much smaller size of the city, the difference is also about 0.02 according to ground based sun photometer measurements (Zawadzka et al. 2013), possibly due to much higher emissions of SO$_2$, which are negligible in Moscow. We should also mention that the level of anthropogenic emission in
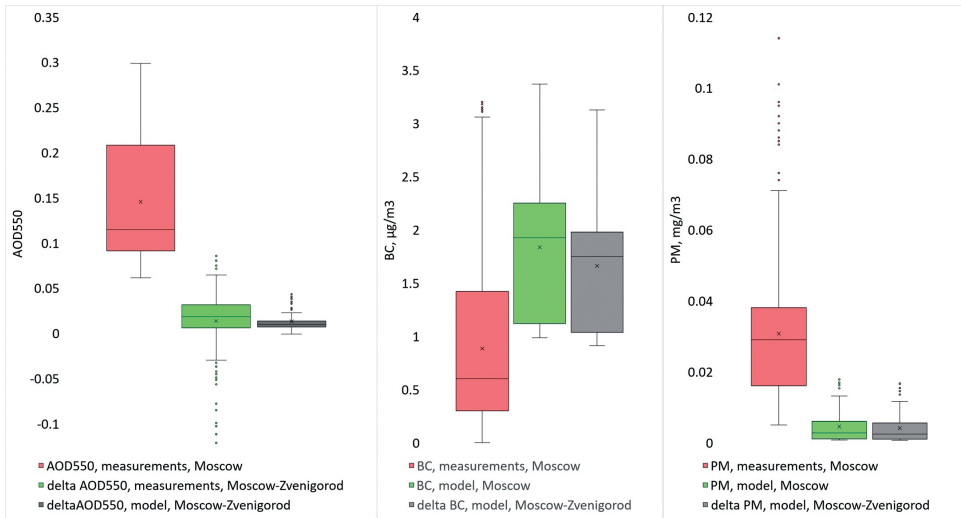
Fig. 10. A box and whisker charts for AOD550(A), BC(B) and PM(C) aerosol characteristics according to measurements and modelling and their difference between Moscow (urban) and Zvenigorod (background conditions). Simulations were made with TNO2010 inventory dataset

Note. Distribution of data is shown in quartiles (interquartile range, IQR), highlighting the mean (sign "X") and outliers (circle signs). The lines extending vertically are error bars. The median (second quartile) is the horizontal line inside the box

Moscow is getting lower during the last decade (Bityukova and Saulskaya, 2017), that causes relatively small AOD increase over the city.

In order to analyze the distribution of urban aerosol over Moscow area, the charts with 7 km grid were made for different days over the whole Moscow district. As an example, Fig. 11 shows the urban aerosol spatial variation for April 15th, 2018 for 10[h] local time. One can see a pronounced high PM concentration over central Moscow with an aerosol plume towards North-East due to

wind predominant direction shown in Fig. 11B. One can see much higher BC concentrations simulated along the highways and over the center of Moscow. The simulated urban AOD550 has also the maximum over the center of Moscow with some plumes over local south-eastern and east areas due to aerosol effective generation over these areas.

DISCUSSION AND CONCLUSIONS

The AeroRadCity-2018 spring experiment, organized at the MO MSU and accompanied by COSMO-ART numerical experiments,
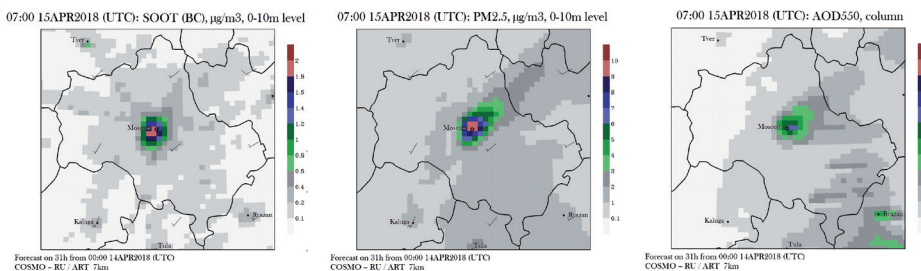
Fig. 11. The spatial distribution of surface BC concentration (A), PM concentrations (B), and AOD550 (C) over Moscow and Moscow suburbs according to the COSMO-ART model simulations. April 15, 7[h] GMT (10h local time)

provided data which joint analysis helps in understanding the processes of aerosol pollution over Moscow megacity. With a large complex of measurements including surface and columnar aerosol characteristics as well as BC concentrations and radiative measurements in different spectral ranges, a detailed study of the observed variations in aerosol and their radiative feedback has been performed.

The analysis of the dependence between AOD500 and PM_{10} has revealed the two types of relationships with a bifurcation point around PM10=0.04 mgm^{-3}. We showed that usually at high PM10 the elevated AOD500 values are observed due to both natural and urban aerosol, but at specific meteorological conditions (IPD=1) the increase in PM can be observed at very low AOD500 level due to conditions of very stable stratification and urban aerosol accumulation near the surface. The detailed analysis of AOD500 relationship with PM_{10} concentrations revealed a positive statistically significant dependence for total and fine AOD500 mode (R^2=0.4 in both cases) while no dependence is obtained for coarse mode aerosol. No statistically significant AOD dependence was obtained with BC concentration and BC/PM10 ratio.

However, high correlation was obtained between PM and BC concentrations according to both model and experimental data, which can be attributed to the important role of BC in PM formation. We also obtain a high correlation between modelled BC and SO_2 concentration, which was not confirmed by measurements with much lower observed SO_2 concentrations. The main source of SO_2 is coal fuel for power plants, which is not usually used in Moscow. Hence, this difference can be explained by the overestimation of TNO2010 inventory on SO_2 emissions in Moscow. A high correlation between BC and NO_2 concentrations demonstrated similar sources of emissions from diesel fuel in motor vehicle transport.

The analysis of radiative effects of aerosol has revealed up to 30% loss for UV irradiance and 15% for shortwave irradiance at high AOD500 in Moscow. However, this strong attenuation, especially for UV irradiance, was not reproduced by RT modelling. We show that situations with strong attenuation relate to the daytime sample, which can be explained by additional effects of more effective afternoon convection at higher level affecting solar irradiance due to increasing absorption. However, the revealed dependence should be studied more on larger statistics at different meteorological conditions. We also obtained a negative radiative forcing effect at TOA for clear sky conditions which lead to the cooling of the atmosphere and earth surface. The significant decrease in its absolute values from -18 Wm^{-2} to -4 Wm^{-2} is explained by the decrease in AOD500 and, to some extent, by aerosol factor of asymmetry due to decrease in aerosol particle size.

On average, the modelled and observed difference in AOD550 during the period of experiment was about 0.01, but in some days deltaAOD550 may increase up to 0.05. We have shown that the generation of urban aerosol is more favorable in conditions with IPD=1, when from both measurements and modelling we obtained deltaAOD550 of about 0.02. The modelled BC concentrations were in agreement with the observed data, however, the PM concentrations were much lower due to not accounting for natural aerosol contribution.

ACKNOWLEDGEMENTS

Natalia E. Chubarova, Elizaveta E. Androsova et al.   AEROSOL AND ITS RADIATIVE EFFECTS ...

04|2019

GES

129

REFERENCES

Bityukova V.R., Saulskaya T.D. (2017). Changes of the anthropogenic impact of Moscow industrial zones during the recent decades. Vestnik Moskovskogo Unviersiteta, Seriya Geografiya, 3, pp. 24-33. (In Russian with English summary)

Cheng Z., Luo L., Wang S., Wang Y., Sharma S., Shimadera H., Wang X., Bressi M., de Miranda R.M., Jiang J., Zhou W., Fajardo O., Yan N., and Hao J. (2016). Status and characteristics of ambient PM2.5 pollution in global megacities. Environment International, vol. 89-90, pp. 212-221. DOI:10.1016/j.envint.2016.02.003.

Chubarova N., Smirnov A., Holben B.N. (2011a). Aerosol properties in Moscow according to 10 years of AERONET measurements at the Meteorological Observatory of Moscow State University. Geography, Environment, Sustainability, vol. 4, № 1, pp. 19-32.

Chubarova N. Y., Sviridenkov M.A., Smirnov A., and Holben B.N. (2011b). Assessments of urban aerosol pollution in Moscow and its radiative effects. Atmospheric Measurement Techniques, vol. 4, № 2, pp. 367–378. DOI:10.5194/amt-4-367-2011.

Chubarova N., Nezval' Ye, Sviridenkov I., Smirnov A., and Slutsker I. (2012). Smoke aerosol and its radiative effects during extreme fire event over Central Russia in summer 2010. Atmospheric Measurement Techniques, vol. 5, pp. 557-568. DOI:10.5194/amt-5-557-2012.

Chubarova N., Belikov I., Gorbarenko E., Eremina I., Zhdanova E.Y., Korneva I., Konstantinov P., Lokoshchenko M., Skorokhod A., and Shilovtseva O. (2014). Climatic and environmental characteristics of Moscow megalopolis according to the data of the Moscow State University Meteorological Observatory over 60 years. Russian Meteorology and Hydrology, vol. 39, pp. 602-613. DOI:10.3103/S1068373914090052.

Chubarova N., Poliukhov A., and Gorlova I. (2016). Long-term variability of aerosol optical thickness in eastern Europe over 2001–2014 according to the measurements at the Moscow MSU MO AERONET site with additional cloud and NO2 correction. Atmospheric Measurement Techniques, vol. 9, № 2., pp. 313–334. DOI:10.5194/amt-9-313-2016.

Chubarova N., Poliukhov A., Shatunova M., Rivin G., Becker R., and Kinne S. (2018). Clear-sky radiative and temperature effects of different aerosol climatologies in the Cosmo model. Geography, Environment, Sustainability, vol. 11, № 1, pp. 74-84. DOI:10.24057/2071-9388-2018-11-1-74-84.

Climate of Moscow in global warming conditions (2017). Edited by Kislov A.V. Moscow: Moscow University Press (in Russian).

Dubovik O. and King M.D. (2000). A flexible inversion algorithm for retrieval of aerosol optical properties from sun and sky radiance measurements. J. Geophys. Res., vol. 105, № D16, pp. 20673-20696. DOI:10.1029/2000JD900282.

Emilenko A.C., Geng-Chen W., Kopeikin V.M., and Isakov A.A. (2018). Urban and regional classes of aerosol taking Beijing and Moscow as examples. Proc. SPIE 10833, 24th International Symposium on Atmospheric and Ocean Optics: Atmospheric Physics, 108334T. DOI:10.1117/12.2504379.

Golitsyn G.S., Grechko E.I., Wang G., Wang P., Dzhola A.V., Emilenko A.S., Kopeikin V.M., Rakitin V.S., Safronov A.N., and Fokeeva E.V. (2015). Studying the pollution of Moscow and Beijing atmospheres with carbon monoxide and aerosol. Izvestiya, Atmospheric and Oceanic Physics, vol. 51, № 1, pp. 1-11. DOI:10.1134/S0001433815010041.

Gubanova D.P., Belikov I.B., Elansky N.F., Skorokhod A.I., and Chubarova N.E. (2018). Variations in PM 2.5 Surface Concentration in Moscow according to Observations at MSU Meteorological Observatory. Atmospheric and Oceanic Optics, vol. 31, pp. 290-299. DOI:10.1134/S1024856018030065.

Holben B.N., Eck T.F., Slutsker I., Tanre D., Buis J.P., Setzer A., Vermote E., Reagan J.A., Kaufman Y.J., Nakajima T., Lavenu F., Jankowiak I., and Smirnov A. (1998). AERONET – A federated instrument network and data archive for aerosol characterization. Remote Sensing of Environment, vol. 66, № 1, pp. 1-16. DOI:10.1016/S0034-4257(98)00031-5.

IPCC (2007): Climate Change 2007: The Physical Science Basis. Contribution of Working Group I to the Fourth Assessment Report of the Intergovernmental Panel on Climate Change. Solomon S., Qin D., Manning M., Chen Z., Marquis M., Averyt K.B., Tignor M., and Miller H.L. (eds.) Cambridge University Press, Cambridge, United Kingdom and New York, NY, USA, 996 pp.

IPCC (2013): Climate Change 2013: The Physical Science Basis. Contribution of Working Group I to the Fifth Assessment Report of the Intergovernmental Panel on Climate Change. Stocker T.F., Qin D., Plattner G.-K., Tignor M., Allen S.K., Boschung J., Nauels A., Xia Y., Bex V., and Midgley P.M. (eds.) Cambridge University Press, Cambridge, UK and New York, NY, USA, 1535 pp.

Kazadzis S., Amiridis V., Kouremeti N. (2013). The Effect of Aerosol Absorption in Solar UV Radiation. In: Helmis C., Nastos P. (eds.) Advances in Meteorology, Climatology and Atmospheric Physics. Springer Atmospheric Sciences. Springer, Berlin, Heidelberg, pp. 1041-1047. DOI:10.1007/978-3-642-29172-2.

Kirchstetter T.W., Novakov T., and Hobbs P.V. (2004). Evidence that the spectral dependence of light absorption by aerosols is affected by organic carbon. J.Geophys.Res., vol. 109, № D21208, pp. 1-12. DOI:10.1029/2004JD004999.

Koepke P., Hess M., Schult I., and Shettle E.P. (1997). Global Aerosol Data Set. Report No. 243, Max-Planck-Institut für Meteorologie, Hamburg.

Kopeikin V.M., Emilenko A.S., Isakov A.A., Loskutova O.V., and Ponomareva T.Ya. (2018). Variations in soot and submicron aerosols in the Moscow region in 2014-2016. Atmospheric and Ocean Optics, vol. 31, № 1, pp. 5-10 (in Russian).

Kozlov V.S., Panchenko M.V., and Yausheva E.P. (2008). Mass fraction of Black Carbon in submicron aerosol as an indicator of influence of smokes from remote forest fires in Siberia. Atmospheric Environment, vol. 42, №. 11, pp. 2611-2620.

Kozlov V.S., Panchenko M.V. Pol'kin V.V., and Terpugova S.A. (2016). Technique for determination of the single scattering albedo of submicron aerosol in the approximation of lognormal size distribution of black carbon. Proc. SPIE 10035, 22nd International Symposium on Atmospheric and Ocean Optics: Atmospheric Physics, DOI: 10.1117/12.2247992

Kuznetsova I., Shalygina I., Nakhaev M., et al. (2014). Unfavorable meteorological factors for air quality Russian Hydrometeocenter Proceedings, vol. 351, pp. 154-172 (in Russian).

Natalia E. Chubarova, Elizaveta E. Androsova et al.   AEROSOL AND ITS RADIATIVE EFFECTS ...

04|2019

GES

131

Li H., Meier F., Lee X., Chakraborty T., Liu J., Schaap M., Sodoudi S. (2018). Interaction between urban heat island and urban pollution island during summer in Berlin. Science of The Total Environment, vol. 636, pp. 818-828. DOI:10.1016/j.scitotenv.2018.04.254

Mosecomonitoring, 2017 (2016). Environment report in Moscow city. Ed. Kulbachevsky A.O., 363 (in Russian).

O'Neill N.T., Dubovik O., Eck T.F. (2001). Modified Ångström exponent for the characterization of submicrometer aerosols. App. Opt., vol. 40, № 15, pp. 2368-2374. DOI:10.1364/AO.40.002368.

Popovicheva O., Ivanov A., Sitnikov N., Volpert E. (2020). Black carbon in spring aerosols of Moscow urban background. DOI: DOI-10.24057/2071-9388-2019-90. 2020.

Rivin G.S., Rozinkina I.A., Vil'fand R.M., et al. (2015). The COSMO-Ru system of nonhydrostatic mesoscale short-range weather forecasting of the Hydrometcenter of Russia: The second stage of implementation and development. Russian Meteorology and Hydrology, vol. 40, № 6, pp. 400-410. DOI:10.3103/S1068373915060060.

Tegen I., Hollrig P., Chin M., Fung I., Jacob D., and Penner J. (1997). Contribution of different aerosol species to the global aerosol extinction optical thickness: Estimates from model results. J. Geophys. Res., vol. 102, pp. 23895-23915. DOI:10.1029/97JD01864.

Vil'fand R.M., Kirsanov A.A., Revokatova A.P., Rivin G.S., Surkova G.V. (2017), Forecasting the Transport and Transformation of Atmospheric Pollutants with the COSMO-ART Model. Russian Meteorology and Hydrology, vol. 42, № 5, pp. 292–298. DOI:10.3103/S106837391705003X.

Vogel B., Vogel H., Bäumer D., Bangert M., Lundgren K., Rinke R., and Stanelle T. (2009). The comprehensive model system COSMO-ART – Radiative impact of aerosol on the state of the atmosphere on the regional scale. Atmos. Chem. Phys., vol. 9, pp. 8661–8680. DOI:10.5194/acp-9-8661-2009.

Vogel B., Bäumer D., et al. (2010). COSMO-ART: Aerosols and Reactive Trace Gases within the COSMO Model. In: Baklanov A., Mahura A., Sokhi R. (eds.) Integrated Systems of Meso-meteorological and Chemical Transport Models, Springer, pp. 75-80.

Zawadzka O., Markowicz K. M., Pietruczuk A., Zielinski T., and Jaroslawski J. (2013). Impact of urban pollution emitted in Warsaw on aerosol properties. Atmos. Environ., vol. 69, pp. 15–28. DOI:10.1016/j.atmosenv.2012.11.065.

Physikalisch-Meteorologisches Observatorium Davos World Radiation Center (2017). Project, World Calibration Center – Ultraviolet. [online] Available at: http://projects.pmodwrc.ch/bb2017/project.php [Accessed 19 Jun. 2019].

World Health Organization (2019). Ambient (outdoor) air quality and health. [online] Available at: http://www.who.int/mediacentre/factsheets/fs313/en/ [Accessed 19 Jun. 2019].

Anna V. Talovskaya[1], Egor G. Yazikov[1], Nina A. Osipova[1], Elena E. Lyapina[2], Victoria V. Litay[3], George Metreveli[4], Junbeum Kim[5]

[1] School of Earth Sciences and Engineering, National Research Tomsk Polytechnic University, 30 Lenin Ave., 634050, Tomsk, Russia

[2] Laboratory of Physics of Climatic Systems, Institute of Monitoring of Climatic and Ecological Systems of the Siberian Branch of the RAS, 10/3 Academichesky Ave., 634055, Tomsk, Russia

[3] Siberian Geotechnical Service, 40 Korolev, 630015, Novosibirsk, Russia

[4] Group of Environmental and Soil Chemistry, Institute for Environmental Sciences, University of Koblenz-Landau, Fortstrasse 7, D-76829 Landau, Germany

[5] CREIDD Research Centre on Environmental Studies & Sustainability, Department of Humanities, Environment & Information Technology (HETIC), University of Technology of Troyes, UMR 6281, France

* Corresponding author: talovskaj@yandex.ru

MERCURY POLLUTION IN SNOW COVER AROUND THERMAL POWER PLANTS IN CITIES (OMSK, KEMEROVO, TOMSK REGIONS, RUSSIA)

ABSTRACT. Although snow cover is studied as an efficient scavenger for atmospheric mercury (Hg), up to now little is known about Hg behaviour in urban snow cover impacted by thermal power plants (TPPs) during the winter heating season. This study is focused on quantification of Hg in the particulate phase in snow cover and estimation of atmospheric particulate Hg (Hg^p) depositional fluxes around urban TPPs in cities of Omsk, Kemerovo, Yurga, Tomsk (the south part of Western Siberia, Russia) to provide new insight into Hg occurrence in urban snow. The results demonstrate that the mean Hg content in the particulate phase of snow varied from 0.139 to 0.205mg kg^{-1}, possibly depending on thermal power of TPPs and fuel type used. The estimated mean atmospheric Hg^p depositional fluxes ranged from 6.6 to 73.1 mg km^{-2} d^{-1}. Around thermal power plants atmospheric Hg^p depositional flux was controlled by particulate load. Higher Hg contents in the particulate phase of snow and higher atmospheric Hg^p depositional fluxes observed in relation to the background values, as well as high enrichment factors determined for Hg in the particulate phase of snow relative to the mean Hg content in the Earth's crust showed that the snow pollution with Hg is of anthropogenic origin. The coexistence of Hg and S observed for the particulate phase of snow indicated the possible presence of mercury sulfide in this phase. The parameters like Hg content in the particulate phase of snow and Hg^p atmospheric flux can be used as markers for the identification of coal combustion emission sources.

Anna V. Talovskaya, Egor G. Yazikov et al.   MERCURY POLLUTION IN SNOW ...

04|2019   GES   133

INTRODUCTION

Snow cover is a natural ground cover in the winter season in several regions (e.g. Siberia, Russian Far East, southern Canada, central and northern Europe) and it is an efficient scavenger of air pollutants caused by fuel combustion, emissions of industries, vehicle exhaust as well as by long-range transport events. Wet and dry deposition of contaminants results in snow cover pollution (Davidson et al. 1996). Therefore, snow cover is the subject of many studies as a reliable indicator of air pollution, and it can provide information on sources of air pollutants (Raputa et al. 2010; Baltrėnaitė et al. 2014; Yanchenko et al. 2015; Gao et al. 2018).

Mercury (Hg), as one of the greatest toxic trace elements (Tchounwou et al. 2003), can be accumulated in snow cover (Ferrari et al. 2002; Siudek et al. 2014; Douglas et al. 2017), both in inorganic (Ferrari et al. 2002) and organic form (Maruszczak et al. 2011) impacting negatively the aquatic and terrestrial ecosystems after snow melting (Wiener et al. 2003). Up to date, many studies have paid attention to Hg content and speciation in polar (Fitzgerald et al. 1991; Douglas et al. 2017) and mountain snow (Ferrari et al. 2002; Huang et al. 2014) to identify Hg sources and to obtain the information on the past and recent changes in the global cycle of this element. Some researchers (Boutron et al. 1998; Gratz and Keeler 2011) indicated that Hg deposition in snow cover in polar and mountain regions could be due to long-range transport of compounds emitted from coal combustion.

The total mercury concentration in urban snow was evaluated within several studies in Toronto (Brzezinska-Paudyn et al. 1986), Maine (Nelson et al. 2007), Shanghai (Zhang et al. 2013), Gdynia (Siudek et al. 2014), Svirsk (Grebenshchikova et al. 2017), Ursk (Gustaytis et al. 2018) and Moscow (Galitskaya and Rumyantseva 2012). Some researchers (Nelson et al. 2007; Galitskaya and Rumyantseva 2012; Zhang et al. 2013; Siudek et al. 2014) revealed that during winter season the combustion of coal, which is still applied in numerous countries for the energy generation irrespective of negative impact on the climate, caused high Hg contents in snow cover within the urban areas. Additionally, Zhang et al. (2013) indicated that biomass combustion, heavy local traffic emissions and secondary aerosols also contributed to Hg deposition in snow cover. However, much less is known about Hg speciation and behavior in snow cover around urban coal-fired thermal power plants (TPP), being the main emission source of anthropogenic Hg in the world (UNEP 2013). Coal combustion emissions include three forms of Hg: (i) gaseous elemental mercury (Hg^0) representing much frequently ($\geq$ 95%) occurring form of Hg; (ii) bivalent reactive gaseous mercury (Hg^{2+}) and (iii) particulate mercury (Hg^P) (Galbreath and Zygarlicke 2000). Generally, emissions can be transported locally, regionally, and globally and then deposited at any distance from its sources (Nelson et al. 2010; Raputa et al. 2010; Antonova et al. 2019). Emissions of Hg into the air significantly affect snow cover chemical composition (Siudek et al. 2014; Siudek 2016). It is important to assess snow pollution by Hg with great clarity at regional and local scales. Chemistry of Hg during wintertime is of crucial interest (Siudek et al. 2014), particularly in cold climatic regions with long wintertime heating season. According to Kim et al. (2012), after emission, gaseous mercury can adsorb onto

the fine particles in the air. It is expected that the association with particulate phase can facilitate the deposition of Hg, e.g. in snow cover.

Anthropogenic Hg emission increases during the winter season since TPPs operate more intensively in this period (Siudek et al. 2014). This is especially relevant for urban areas of Western Siberia, where more than 30% of Hg emissions originate from coal-fired TPPs (Arbuzov et al. 2015) and Hg is accumulated in snow cover during a long winter season. Although the large amounts of fine Hg^p were observed in the ambient air during the winter season in urban and rural areas (Kim et al. 2012) and most of Hg in snow cover was associated with particulate matter (Huang et al. 2014), there are still some gaps with respect to quantification of Hg^p in snow cover, particularly near to the emission sources (Nelson et al. 2010) such as TPPs.

Systematic studies on Hg^p in snow cover within urban areas impacted by TPPs are necessary to understand better the chemistry of emitted and deposited Hg, to obtain knowledge about atmospheric Hg^p depositional fluxes during winter season, and finally to assess potential human health risk. The importance of further studies on Hg^p in snow cover is also supported by our earlier research finding showing that around fossil fuel TPP (Tomsk, Western Siberia) Hg was predominantly associated with the particulate phase in snow cover, representing 78 % of total Hg (Talovskaya et al. 2014).

The aim of this study is to provide new insight into the occurrence of Hg^p deposited in snow cover around urban thermal power plants representing the predominant source for Hg emissions in such cold climatic region as Western Siberia (Russia). The more specific objectives are (i) quantification of Hg contents in the particulate phase of snow cover, (ii) estimation of atmospheric Hg^p depositional fluxes, (iii) identification of Hg-bearing particles in snow cover, and (iv) assessment of TPP contribution to the Hg^p snow cover pollution.

MATERIALS AND METHODS

Description of study area

As shown in Fig. 1, the study area included the following large cities: Omsk, Kemerovo, Tomsk and small city of Yurga, located in the south part of Western Siberia, Russia. These

Fig. 1. Location of studied cities (Western Siberia, Russia; source: maps open source, modified)

cities belong to the industrially-impacted areas where thermal power plants are working during whole year operating more intensively in the wintertime heating season. Moreover, TPP areas are embraced inside a dense urban network, indicating that TPP emissions can diffuse over the urban areas and reach residential districts. The climate varies from a moderate (Omsk) to humid (Kemerovo, Yurga and Tomsk) (open source: Wikipedia). The air temperature ranges from −9 to −40°C in the winter season. The prevailing winds through the year come from both the South-West and South. Snow typically covers the ground from November to mid-April (about 6 months), and its depth is 60–70 cm.

Thermal power plants

For this study, we selected four urban thermal power plants close to the community infrastructure and residential districts: (i) Omsk coal-fired (TPP-1), (ii) Kemerovo coal-fired (TPP-2), (iii) Yurga coal-fired (TPP-3), and (iv) Tomsk fossil fuel (TPP-4) thermal power plants. The characteristics of these thermal power plants are summarized in Table 1, showing operating conditions, stack heights and specification of the fuel type used (open access Internet data). Each TPP has two stacks of different heights (except TPP-4 having the

same heights) that can disperse pollutants around TPPs and over large areas with the main wind direction.

The coal used at the studied TPPs contains Hg as a trace element (Table 1). It is necessary to note that the Russian coal classification system used in this study is based on the technical grade of the coal applied in the energy industry (Russian State Standard 25543-88). The coal of grade D from Kuznetsk Basin (Russia) is used at the TPP-2, TPP-3, and TPP-4, and the coal of grade SS from Ekibastuz Basin (Kazakhstan) is applied at TPP-1. The coal of grade D is used as high-reactivity power fuel, while the coal of grade SS belongs to low-reactivity high-ash coals. The predominant energy fuel for the TPP-4 is coal (75–90 %) and natural gas (10–25 %).

Sampling and sample preparation

To identify the impact of TPPs on the ambient air quality, the sampling sites were selected in the North-East and the North areas surrounding each plant, according to the prevalent wind direction (Table 2). In these areas, the sampling sites were located at a distance of 0.6 to 4.5 km from the plant. Additionally, for the selection of sampling locations following factors were considered: (i) extension of emissions depending on

Table 1. Characteristics of urban thermal power plants and fuel type used (large cities in Western Siberia)

Thermal power plant in large cities	Thermal power, Gcal/hour	Capacity, MW	Two stack heights, m	Fuel type	Specification of coal (Zharov et al. 1996)			
					Grade	Deposit	A^d, %	Hg content, mg kg^{-1}
Omsk (TPP-1)	1763	695	180 and 275	coal	SS	Ekibastuz Basin	36–52	0.12
Kemerovo (TPP-2)	1540	485	180 and 210	coal	D	Kuznetsk Basin	7–20	0.08
Yurga (TPP-3)	91	614	58 and 100	coal	D	Kuznetsk Basin	7–20	0.08
Tomsk (TPP-4)	815	331	100 of each stack	coal, natural gas	D	Kuznetsk Basin	7–20	0.08

Note: source: data open source; A^d – fuel ash content on dry basis

the operating conditions and stack heights (Russian State Standard for air pollution control RD 52.04.186-89); (ii) flat terrain; (iii) sampling site accessibility; (iv) vicinity of community infrastructure and residential areas; (v) distance from roads and other emission sources; (vi) high snow pollution with deposited airborne particles (Osipova et al. 2015). Table 2 demonstrates the sampling site distances from the studied TPPs. In total, samples from 28 sampling sites were collected around the studied plants.

Samples were collected and prepared in accordance with the Russian State Standard for air pollution control (RD 52.04.186-89) and several studies (Williamson et al. 2008; Galitskaya and Rumyantseva 2012; Kasimov et al. 2012; Filimonova et al. 2015; Yanchenko et al. 2015; Grebenshchikova et al. 2017; Taraškevičius et al. 2017; Gustaytis et al. 2018). To obtain the representative data on atmospheric Hg snow cover deposition rates during the winter season, snow sampling was performed at the end of February, before the beginning of the snowmelt period.

Snow samples were collected from a snow pit, along the vertical profile from the top of the snow pack to at least 5 cm above the ground in order to avoid sample contamination with soil. Pit size was 45×50 cm. The snow samples were stored in polyethylene bags. Sample weights varied from 17 to 18 kg. This amount of snow was necessary to obtain a sufficient amount of particulate matter deposited in snow. The samples were melted inside of clean closed plastic containers at room temperature. After melting, meltwater was immediately filtered through pre-weighed

1-2.5 μm Blue Line cellulose non-ashen filters (Russian State Standard 12026-76 for laboratory filter paper) retaining the solid particles bigger than filter cut-off. Then, the filters with particulate phase were dried at room temperature and, finally weighed. The fraction isolated by this method is called in this work as 'the particulate phase of snow'. The weighing of filter before and after filtering of samples enabled the calculation of particulate load (P_n) (mg m^{-2} d^{-1}).

Hg analysis in the samples

The particulate phase of snow was analyzed by atomic absorption spectrometry (AAS) with pyrolytic volatilization and scanning electron microscopy (SEM) equipped with an energy dispersive X-ray spectroscopy (EDX) in the laboratories of the Uranium Geology International Centre, Tomsk Polytechnic University (TPU), Russia. The Hg analysis was carried out under dust free conditions.

AAS with pyrolytic volatilization

The content of Hg^P in the samples was measured by AAS with pyrolytic volatilization using an atomic absorption spectrometer RA-915+ with pyrolyzer PYRO-915 (Lumex, Russia) and software package RA915R. In samples, Hg compounds were atomized at 850°C in a cuvette connected with an open absorption cell. For each sample, 150 mg of particulate phase obtained by filtration method described above was taken for Hg detection. Three replicate measurements were performed for each sample. From replicates, average contents of Hg in each sample of the particulate phase of snow (mg

Table 2. Sampling site distances around urban thermal power plants located in cities (Omsk, Tomsk, Kemerovo region, Western Siberia)

Thermal power plant	North-east area, km						North area, km					Number of sampling sites
TPP-1	0.75	1.5	3.5	4.5	-	-	0.75	1.5	2.0	-	-	7
TPP-2	0.6	1.1	1.8	2.3	2.7	3.9	-	-	-	-	-	6
TPP-3	0.6	1.1	-	-	-	-	0.6	1.2	1.8	-	-	5
TPP-4	0.73	1.0	1.3	1.6	2	-	0.6	0.9	1.4	1.8	2.1	10

Note: description of TPPs are given in Table 1

kg^{-1}) were calculated. The detection limit of the method for Hg quantification in the particulate phase of snow was 0.005 mg kg^{-1} and analytical precision was within 20–28%.

SEM-EDX

SEM-EDX analysis was used to determine Hg-bearing particles in the samples collected at ca. 1 km to the North-East and the North of each TPP. The selection of the sampling distance is based on the results of our previous study where we observed an accumulation of physically and chemically absorbed mercury in a particulate phase of snow sampled in 1.3 km from Tomsk fossil fuel thermal power plant (Filimonenko at al. 2014).

Morphological characteristics, size, and element analysis of individual particles were performed by SEM (Hitachi S-3400N SEM, Japan) equipped with an EDX (XFlash 4010 detector, Bruker AXS Microanalysis GmbH, Germany). First, each sample was fixed on a carbon tape with a surface area of 25 mm^2 for carbon coating. Then, a very thin film of carbon was deposited on the surface of each sample using the high vacuum method, resulting in electrically conductive samples. The working conditions of SEM measurements were: 20 kV accelerating voltage, 30 s spectral acquisition time, and 10 mm working distance. SEM images were acquired at a magnification of 500x. EDAX Esprit software was used for the quantitative analysis of individual particles. The weight percent of each element was determined from the EDX spectrum. To reveal Hg-bearing particles, approximately 150 particles were analyzed in each sample.

Data analysis

STATISTICA 8.0 software was used to calculate the mean values and standard deviations as well as to reveal the statistically significant differences between groups applying the Kruskal-Wallis non-parametric test (when comparing more than two groups).

Following indexes were calculated to assess Hg^p snow cover pollution:

The concentration coefficient representing the level of element enrichment in the particulate phase of snow in relation to the background content was determined using equation 1 (Galitskaya and Rumyantseva 2012; Kasimov et al. 2012; Filimonova et al. 2015; Taraškevičius et al. 2017; Gustaytis et al. 2018):

$$K_c = \frac{C_i}{C_b} \quad (1)$$

where, K_c is the concentration coefficient; C_i is the element content in the particulate phase of snow (mg kg^{-1}); C_b is the background element content in the particulate phase of snow (mg kg^{-1}). The background content of Hg in the particulate phase under Western Siberia conditions (IAO SB RAS at Fonovaya Observatory (Antonovich et al. 2018)) equals 0.08 mg kg^{-1} (Talovskaya et al. 2012).

The element load was calculated to evaluate the atmospheric Hg^p depositional flux (equations 2–3) (Galitskaya and Rumyantseva 2012; Kasimov et al. 2012; Filimonova et al. 2015; Taraškevičius et al. 2017; Gustaytis et al. 2018):

$$E_l = C_i \times P_n \quad (2)$$

$$P_n = \frac{P_o}{S \times t} \quad (3)$$

where, E_l is the element load (mg km^{-2} d^{-1}); C_i is the element content in the particulate phase of snow (mg kg^{-1}); P_n is the particulate load (mg m^{-2} d^{-1}); P_o is the mass of the particulate phase (mg); S is the square of snow pit (m^2); t is the time representing the stable snow cover formation duration up to sampling day (d).

The coefficient of element load is shown as the ratio of element load to the background element load (equation 4) (Kasimov et al. 2012):

$$K_p = \frac{E_l}{E_{lb}} \quad (4)$$

where, K_p is the coefficient of element load; E_{lb} is the background element load. The background Hg load under Western Siberia conditions (IAO SB RAS at Fonovaya Observatory (Antonovich et al. 2018)) equals 1.2 mg km^{-2} d^{-1} (Talovskaya et al. 2012).

The enrichment factor (EF) of element in particulate phase of snow relative to the Earth's crust (Shevchenko et al. 2003), was calculated using equation 5:

$$EF = \frac{(C_i / C_{Sc})\,particulate\,phase\,of\,snow}{(C_i / C_{Sc})} \quad (5)$$

where, C_i is the element content (mg kg^{-1}); C_{Sc} is the scandium content (mg kg^{-1}).

Usually, Al, Si, Ti, Sc or Fe are used as reference elements, since crustal material contains these elements in high amounts, they are characterized by low occurrence variability, and are not significantly affected by contamination (Saur and Juste 1994). In this study, Sc was chosen as the reference element for the EF calculation. The content of Sc (15.6 mg kg^{-1}) and Hg (0.065 mg kg^{-1}) in Earth's crust was chosen from the study of Grigor'ev (2009). The content of Sc in the particulate phase of snow was measured by instrumental neutron activation analysis (neutron research reactor IRT-T in the Physical-Technical Institute of TPU, γ-spectrometer Canberra with Ge-detector, USA) in the laboratory of Uranium Geology International Centre, TPU.

It can be stated that, if K_c, K_p, and EF values are higher than 1, mercury could be of anthropogenic origin.

RESULTS

Hg in the particulate phase of snow samples

Table 3 shows the statistical evaluation for Hg content in the particulate phase of snow. The contents of Hg in the samples collected around TPP-1, TPP-2 and TPP-4 were statistically compared with each other (Kruskal-Wallis test, p≥0.1). However, statistically slightly higher Hg contents were observed in the samples around TPP-1 than in those around TPP-3 (Kruskal-Wallis test, 0.1>p≥0.05). Moreover, Hg contents were significantly higher within the studied area of TPP-4 than in those within the studied area of TPP-3 (Kruskal-Wallis test, 0.05>p≥0.01). Furthermore, Hg contents did not significantly differ in the samples from TPP-2 and TPP-3 areas.

Calculation of K_c showed that Hg contents exceeded background value more than two for the samples collected at the studied TPP-1, TPP-2 and TPP-4 areas, whereas Hg contents were about two times higher than the background value in the samples from TPP-3 area (Table 4).

Table 4 also demonstrates the mean values and range of EFs for Hg in the particulate phase of snow. EF values for Hg were higher than one, indicating that this element was enriched relative to the Earth's crust. In addition, EF of Hg was higher for the samples collected around TPP-4 than for those around other plants.

Atmospheric Hg^P depositional flux

Fig 2. presents the variations of mean Hg load, E_i, indicating the rates of atmospheric Hg depositional fluxes. The Hg load around TPP-3 ranged from 17.2 to 191 mg km^{-2} d^{-1} with a mean 73.1±32.2 mg km^{-2} d^{-1},

Table 3. Statistical summary of Hg content in particulate phase of snow around urban thermal power plants located in large cities of Western Siberia

Thermal power plant	Hg content in particulate phase of snow (mg kg^{-1})			
	Mean±SD	Median	Min	Max
TPP-1	0.205±0.028	0.196	0.179	0.246
TPP-2	0.173±0.019	0.165	0.156	0.203
TPP-3	0.139±0.045	0.125	0.098	0.210
TPP-4	0.194±0.032	0.199	0.126	0.238

Note: SD – standard deviation; description of TPPs are given in Table 1

Table 4. Concentration coefficient (K_c), coefficient load (K_p) and enrichment factor (*EF*) of Hg in the particulate phase of snow around urban thermal power plants located in large cities of Western Siberia

Thermal power plant	K_c			K_p			*EF*		
	Mean	Min	Max	Mean	Min	Max	Mean	Min	Max
TPP-1	2.5	2.2	3.1	34.1	22.5	62.9	2.3	1.8	2.9
TPP-2	2.1	1.9	2.5	35.8	20.0	46.2	2.6	2.2	3.1
TPP-3	1.7	1.2	2.6	60.9	14.3	159	1.6	1.1	3.7
TPP-4	2.4	1.6	3.0	5.5	2.5	8.4	4.3	3.3	5.1

Note: description of TPPs are given in Table 1

which was higher than the mean Hg load determined within the studied area of other plants. The lowest value for El (range: 3.0–10.1 mg km^{-2} d^{-1}, mean: 6.6±2.0 mg km^{-2} d^{-1}) was observed around TPP-4 which was significantly lower than the values determined for other studied TPP areas (Kruskal-Wallis test, 0.01>p≥0.001). The Hg load around TPP-1 ranged from 20.8 to 75.5 mg km^{-2} d^{-1}, with mean value of 41.5 ±20.0 mg km^{-2} d^{-1}. The

Hg load within the studied area of TPP-2 varied from 24.0 to 55.4 mg km^{-2} d^{-1}, with a mean value of 42.9 ±11.5 mg km^{-2} d^{-1}.

The coefficients of Hg load, K_p, calculated according to equation 4, are given in Table 4. The K_p values showed that the Hg load determined for the areas around the studied TPPs exceeded the background values several times. The mean values of K_p increased in the following order: TPP-4
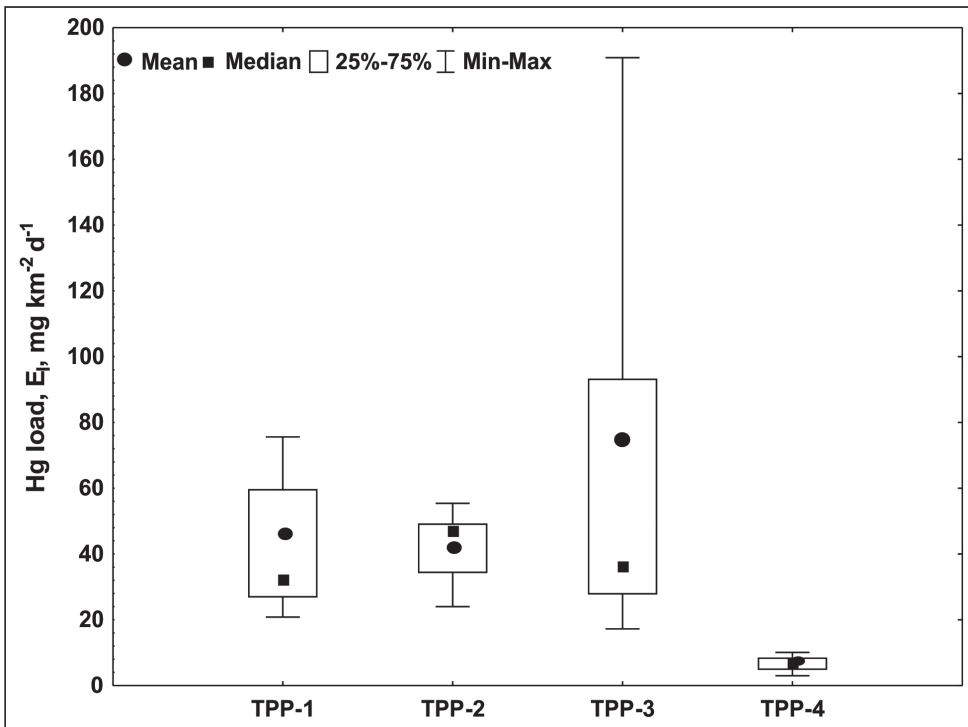
Fig. 2. Box plot of Hg load around urban thermal power plants located in large cities of Western Siberia (note: description of TPPs are given in Table 1)

< TPP-1 ≈ TPP-2 < TPP-3. This indicates that the Hg load around TPP-3, relative to the background value, was higher than in the areas around other plants.

The Hg load mainly depends on the value of particulate load, P_n (Fig. 3). The mean values of P_n increased in the following order: TPP-4 (34.2 mg m^{-2} d^{-1}) < TPP-1 (201 mg m^{-2} d^{-1}) < TPP-2 (248 mg m^{-2} d^{-1}) < TPP-3 (555 mg m^{-2} d^{-1}). This shows that the largest P_n was identified around TPP-3, while the smallest one was found around TPP-4. Additionally, the values of particulate load within the studied area of TPP-3 varied stronger (133–1527 mg m^{-2} d^{-1}) compared to other TPPs.

Hg-bearing particles in the particulate phase of snow samples

SEM-EDX measurements revealed the presence of Hg-bearing particle only in the particulate phase of snow sample collected at 0.5 km from TPP-3 (Fig. 4). Such particles were not detected in the samples collected around other studied TPPs.

Fig. 4 demonstrates the SEM photomicrograph (a) and EDX spectra (b) of the identified Hg-bearing particle. This particle exhibited uneven shape with 1.2×0.7 µm size. Based on the chemical information derived from EDX (Fig. 4, b), the identified particle was composed of Hg and S. Furthermore, the emission spectrum of elements showed a high content of O and traces of Si, Al, Na, K, Fe, and Ca which most likely originated from the nearby large particle. The presence of these elements in the large particle indicates that this particle represents an aggregate of alumosilicate minerals (Fig. 4, c).

DISCUSSION

The Hg content determined in the particulate phase of snow samples and atmospheric Hg depositional fluxes showed that Hg can be present in the snow cover around the urban thermal power plants irrespective of their operating conditions (capacity and thermal power) and fuel type used. The calculated indexes (K_c, K_p and EF) were higher than one, indicating the anthropogenic origin of Hg in the studied areas.

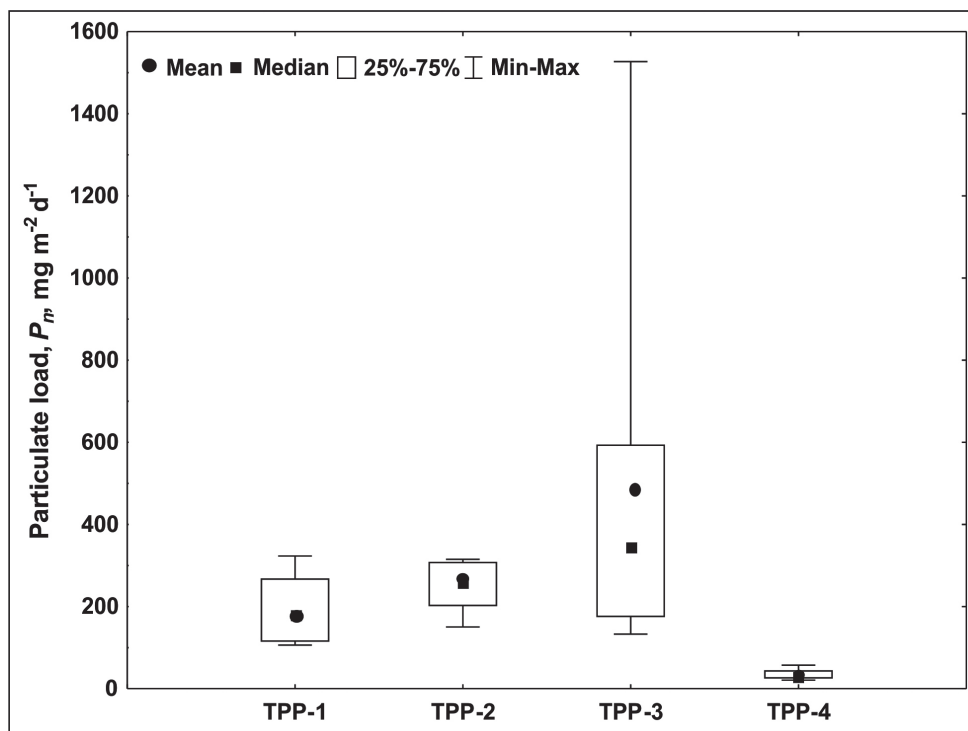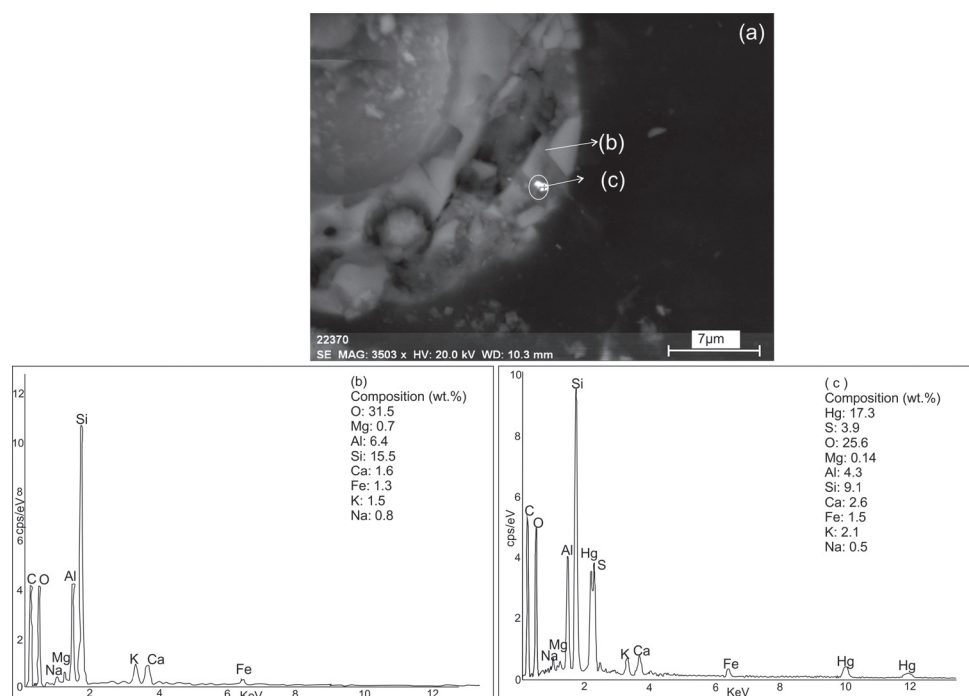**Fig. 3. Box plot of particulate load around urban thermal power plants located in large cities of Western Siberia (note: description of TPPs are given in Table 1)**

Fig. 4. SEM photomicrograph (a) and EDX spectra of alumosilicate particle (b) and Hg-bearing particle (c) in particulate phase of snow collected around the coal-fired thermal power plant

Mercury exists in the air in one of three states, which are gaseous elemental mercury (Hg^0), reactive gaseous mercury in divalent form (Hg^{2+}) and particulate mercury (Hg^P). The elemental Hg^0 can remain in the air longer (0.5–2 years) and can be transported over long distances, transforming later into soluble divalent forms, and then deposited (Schroeder and Munthe 1998).

The content of Hg in the particulate phase of snow determined in this study could confirm the suggestions about high sorption of gaseous Hg species, Hg^{2+}, and Hg^P on airborne particles at low ambient temperatures (Kim et al. 2012), effective scavenging by winter precipitation, and finally deposition in snow (Siudek et al. 2014). In addition, Kim et al. (2012) demonstrated that the fine particles (< 1.8 μm) of atmospheric Hg^P were dominated in the winter season.

It was surprising to identify that there were no statistically significant differences of Hg content in the samples collected in the areas around TPP-1, TPP-2 and TPP-4,

despite their different operating conditions and fuel type used. This fact may indicate that high thermal power (815–1763 Gcal/hour) characteristic for these three TPPs influences the high Hg content in the particulate phase of snow (0.173–0.205 mg kg^{-1}), regardless of different capacity, stack heights, and coal origin (Table 1). The low Hg content, identified in the samples around TPP-3, could be explained by smaller thermal power (91 Gcal/hour) than those for other studied TPPs.

Although Hg content in the coal is low (Table 1), this element could be released during coal combustion with the exhaust gases from the stacks into the air. From the literature it is known that 98% of Hg in similar exhaust gases appears as Hg^0, HgO, and CH_3Hg (Xu et al. 2003). Additionally, in the flue gas, Hg^0 is partly converted to Hg^{2+} by oxidation and is also partly associated with fly ash particles (Hg^P). After emission, Hg^P and Hg^{2+} can be deposited around their anthropogenic emission sources (Galbreath and Zygarlicke 2000), i.e. thermal power plants. Results of Hg measurements in the

air within Tomsk indicated that one of total Hg sources was the emissions of fossil fuel thermal power plant (Lyapina et al. 2009).

High *EF* values of Hg determined for the particulate phase of snow around TPP-4 could be affected not only by combustion of coal representing 75–90% of total fuel used in this TPP but also by natural gas corresponding to the rest of 10–25%. Mercury is often presented in natural gas as a trace element and can be emitted during high temperature combustion (Wilhelm 2001).

Open coal warehouses located in the territory of each studied thermal power plant could be considered as an additional source of Hg^P mainly due to the possible transport of coal aggregates from these warehouses by the wind at long distances. Considering the locations of studied TPPs in urban areas, close to residential districts, the exhausts of Hg from vehicle traffic cannot be excluded. Some studies have indicated that vehicle exhausts slightly contribute to Hg deposition in snow cover (Siudek et al. 2014; Zhang et al. 2013).

Based on the results obtained, the Hg contents measured in the particulate phase of snow samples and atmospheric Hg^P depositional fluxes can be used as markers for Hg source identification, specifically for combustion of coal from the Kuznetsk Basin. However, more investigations are needed to determine content markers in the samples collected around TPPs using coal from the Ekibastuz Basin and from other origins.

In addition, the correlation between the Hg load and characteristics of TPPs (Table 1) was not observed. The data indicated that the Hg load is predominantly affected by values of particulate load than by Hg content in the samples. The following correlation was observed: (1) the lower value of the particulate load and the higher value of the Hg content formed the lower value of the Hg load; (2) the higher value of the particulate load and the lower value of the Hg content formed the higher value of the Hg load. The first observed dependence could indicate a

significant Hg accumulation in a small mass of particulate phase of snow, while the second dependence could be a result of Hg spread in a large mass of particulate phase. The highest values of particulate load is due to the low efficiency of the capture systems to retain emitted gases and particulate matter, as well as due to the extended coal dust distribution in the main wind direction from the open coal warehouses located in the plant territory.

Individual particle analysis by SEM-EDX identified anthropogenic Hg-bearing particle in the form of HgS in the particulate phase of snow collected in the vicinity of TPP-3. Most likely the HgS was originated from coal and was emitted during combustion into the atmosphere. The HgS was already observed as a minor phase in Siberian coal (Arbuzov et al. 2015). The fact that the Hg containing particle was observed only in one sample can be explained by the generally low Hg contents in the particulate phase of snow. The concentration range of 0.139 – 0.205 mg kg^{-1} or 139 – 205 ng g^{-1} determined for Hg contents in the particulate phase of snow is too low to find enough Hg-bearing particles in the samples using SEM measurements. At this content range, a lot of SEM photos and consequently large measurement times are needed. An attachment of the Hg-bearing particles to the aluminosilicate phases during the filtration of snow melting water cannot be fully excluded. Due to the small size of the Hg-bearing particle, it belongs to the fine particulate matter (Pope and Dockery 2006). If this Hg-bearing particle was suspended in the air as an individual particle not bound to the aluminosilicates, it could be in this case inhaled and remained in respiratory organs such as lungs.

CONCLUSIONS

The presence of mercury in the particulate phase of snow cover around the thermal power plants determined in this study allowed new insights on Hg occurrence. Higher Hg concentration coefficient and coefficient of load observed in relation to the background values, as well as high Hg enrichment factors determined relative to the mean Hg content in the Earth's crust

indicated the clear contribution of thermal power plants to the pollution of snow by anthropogenic Hg[p]. Furthermore, our results clearly indicated the importance of Hg monitoring in the particulate phase of snow in the areas impacted by the thermal power plant for the evaluation of particulate Hg budget in such urban areas in the winter season.

The results showed that the mean Hg content in the particulate phase of snow samples was similar for the areas surrounding TPPs, which have high thermal power and use different fuel types. TPP with low thermal power contributed to low Hg contents in particulate matter deposits. Furthermore, we did not observe any correlation between Hg content in the samples and the capacity of TPPs. It was found that particulate load was a key factor for the variability of atmospheric Hg deposition fluxes determined in the areas around urban TPPs. The relationship between atmospheric Hg depositional fluxes and thermal power plant characteristics was not observed.

The obtained data showed that Hg was derived from anthropogenic sources, including emissions from TPPs and possibly long-range transport from open coal warehouses located in the territory of the plants.

Based on the size, shape, and element composition, the Hg-bearing particle identified by SEM-EDX measurements can be considered as non-mineral type, possibly of anthropogenic origin. The Hg content in the particulate phase of snow and the atmospheric Hg depositional fluxes can be considered as effective pollution markers for the identification of coal combustion emission sources.

The results obtained in the present study providing reliable data for human health risk assessment are essential for further environmental studies, and can also be applicable to other urban areas worldwide, being impacted by coal-fired thermal power plants.

ACKNOWLEDGEMENTS

REFERENCES

Antonova A.M., Vorobev A.V., Vorobev V.A., Dutova E.M., Pokrovskiy V.D. (2019). Modelling distribution of contaminating substances of electric power emissions in the atmosphere on the basis of the SKAT programming complex. Bulletin of the Tomsk Polytechnic University, Geo Assets Engineering, 330(6), pp. 174–186.

Antonovich V.V., Antokhin P.N., Arshinov M.Y., Belan B.D., Balin Y.S., Davydov D.K., Ivlev G.A., Kozlov A.V., Kozlov V.S., Kokhanenko G.P., Novoselov M.M., Panchenko M.V., Penner I.E., Pestunov D.A., Savkin D.E., Simonenkov D.V., Tolmachev G.N., Fofonov A.V., Chernov D.G., Smargunov V.P., Yausheva E.P., Paris J.-D., Ancellet G., Law K.S., Pelon J., Machida T., and Sasakawa M. (2018). Station for the comprehensive monitoring of the atmosphere at Fonovaya Observatory, West Siberia: Current status and future needs. In: Proc. of SPIE, 24th International Symposium on Atmospheric and Ocean Optics: Atmospheric Physics, Volume 10833. Available at: https://doi.org/10.1117/12.2504388

Arduzov S.I., Osipova N.A., Zaitseva O.P. and Belaya E.V. (2015). Geochemistry of Hg in Siberian coals. In: Proc. of 2d International symposium on mercury in biosphere: Ecological and geochemical approach, held 21–25 September 2015 in Novosibirsk, Russia, pp. 27–31 (in Russian)

Baltrénaité E., Baltrénas P., Lietuvninkas A., Šerevičiené V. and Zuokaité E. (2014). Integrated evaluation of aerogenic pollution by air-transported heavy metals (Pb, Cd, Ni, Zn, Mn and Cu) in the analysis of the main deposit media. Environmental Science and Pollution Research, 21, pp. 299–313.

Boutron C.F., Vandal G.M., Fitzgerald W.F. and Ferrari C.P. (1998). A forty year record of mercury in central Greenland snow. Geophysical Research Letters, 25, pp. 3315–3318.

Brzezinska-Paudyn A., Van Loon J.C. and Balicki M.R. (1986). Multielement analysis and mercury speciation in atmospheric samples from the Toronto area. Water, Air, & Soil Pollution, 27, pp. 45–56.

Davidson C.I., Bergin M.H., and Kuhn H.D. (1996). The deposition of particles and gases to ice sheets. In: E.R. Wolff, R.C. Bales, ed., Chemical exchange between the atmosphere and polar snow, Berlin: Springer. NATO ASI Series I, 43, pp. 275–306.

Douglas T.A., Sturm M., Blum J.D., Polashenski C., Stuefer S., Hiemstra C., Steffen A., Filhol S. and Prevost R. (2017). A pulse of mercury and major ions in snowmelt runoff from a small Arctic Alaska Watershed. Environmental Science & Technology, 51, pp. 11145–11155.

Ferrari C.P., Dommergue A., Veysseyre A., Planchon F. and Boutron C.F. (2002). Mercury speciation in the French seasonal snow cover. Science of the Total Environment, 287(1–2), pp. 61–69.

Filimonenko E.A., Lyapina E.E., Talovskaya A.V. and Parygina I.A. (2014). Eco-geochemical peculiarities of mercury content in solid residue of snow in the industrial enterprises impacted areas of Tomsk. In: Proc. of SPIE 9292, 20th International Symposium on Atmospheric and Ocean Optics: Atmospheric Physics, Volume 929231. Available at: https://doi.org/10.1117/12.2075637

Filimonova L.M., Parshin A.V., and Bychinskii V.A. (2015) Air pollution assessment in the area of aluminum production by snow geochemical survey. Russian Meteorology and Hydrology, 40 (10), pp. 691–698.

Fitzgerald W.F., Mason R.P., and Vandal G.M. (1991). Atmospheric cycling and air-water exchange of mercury over mid-continental lacustrine regions. Water, Air, & Soil Pollution, 56, pp. 745–764.

Galbreath K.C. and Zygarlicke C.J. (2000). Mercury transformation in coal combustion flue gas. Fuel Processing Technology, 65–66, pp. 289–310.

Galitskaya I.V. and Rumyantseva N.A. (2012). Snow-cover contamination in urban territories (Lefortovo district Moscow). Annals Glaciology, 53 (61), pp. 23–26.

Gao Y., Yang C., Maa J. and Yinc M. (2018). Characteristics of the trace elements and arsenic, iodine and bromine species in snow in east-central China. Atmospheric Environment, 174, pp.43–53.

Gratz L.E. and Keeler G.J. (2011). Sources of mercury in precipitation to Underhill, VT. Atmospheric Environment, 45, pp. 5440–5449.

Grebenshchikova V.I., Efimova N.V., and Doroshkov A.A. (2017). Chemical composition of snow and soil in Svirsk city (Irkutsk Region, Pribaikal'e). Environmental Earth Sciences, 76 (20), pp. 712.

Grigor'ev N.A. (2009). Distribution of chemical elements in the upper continental crust. Yekaterinburg: UrO RAN (in Russian)

Gustaytis M.A., Myagkaya I.N., and Chumbaev A.S. (2018.) Hg in snow cover and snowmelt waters in high-sulfide tailing regions (Ursk tailing dump site, Kemerovo region, Russia). Chemosphere, 202, pp. 446–459.

Huang J., Kang S., Guo J., Sillanpaa M., Zhang Q., Qin X., Du W. and Tripathee L. (2014). Mercury distribution and variation on a high-elevation mountain glacier on the northern boundary of the Tibetan Plateau. Atmospheric Environment, 96, pp. 27–36.

Kasimov N.S., Kosheleva N.E., Vlasov D.V. and Terskaya E.V. (2012). Geochemistry of snow cover within the eastern district of Moscow. Vestnik Moskovskogo Unviersiteta, Seriya Geografiya. 4, pp. 14–24 (in Russian with English summary)

Kim P-R., Han Y-J., Holsen T.M. and Yic S-M. (2012). Atmospheric particulate mercury: Concentrations and size distributions. Atmospheric Environment, 61, pp. 94–102.

Lyapina E.E., Golovatskaya E.A., Ippolitov I.I. (2009). Investigation of mercury content in natural objects of West Siberia. Contemporary Problems of Ecology, 2(1), pp. 1–5.

Marusczak N., Larose C., Dommergue D., Yumvihoze E., Lean D., Nedjai R. and Ferrari C. (2011). Total mercury and methylmercury in high altitude surface snow from the French Alps. Sci. Science of the Total Environment, 409, pp. 3949–3954.

Nelson S.J., Fernandez I.J., and Kahl J.S. (2010). A review of mercury concentration and deposition in snow in eastern temperate North America. In: Hydrological Processes Special Issue: Eastern Snow Conference, 24 (14), pp. 1971–1980. Available at: https://doi.org/10.1002/hyp.7660

Nelson S.J., Johnson K.B., Kahl J.S., Haines T.A. and Fernandez I.J. (2007). Mass balances of mercury and nitrogen in burned and unburned forested watersheds at Acadia National Park, Maine, USA. Environmental Monitoring and Assessment, 126, pp. 69–80.

Osipova N.A., Filimonenko K.A., Talovskaya A.V. and Yazikov E.G. (2015). Geochemical approach to human health risk assessment of inhaled trace elements in the vicinity of industrial enterprises in Tomsk, Russia. Human and Ecological Risk Assessment, 21, pp. 1664–1685.

Pope C.A. and Dockery D.W. (2006). Health effects of fine particulate air pollution: Lines that connect. Journal of the Air & Waste Management Association, 56(6), pp. 709–742.

Raputa V.F., Kokovkin V.V., Shuvaeva O.V. and Morozov S.V. (2010). Experimental study and numerical analysis of the pollution in the area of highway according to the snow cover composistion. In: Proc. of International Conference on Energy and Development, Environment and Biomedicine, pp. 104–108.

Russian State Standard 12026-76 for Laboratory filter paper. Specifications. Available at: http://meganorm.ru/Data2/1/4294838/4294838884.pdf [Accessed 15 January 2013] (in Russian)

Russian State Standard 25543-88. Brown coals, hard coals and anthracites. Classification according to genetic and technological parameters. Available at: http://www.internet-law.ru/gosts/gost/7460 [Accessed 15 July 2018] (in Russian)

Russian State Standard for air pollution control. RD 52.04.186-89. Available at: http://docs.cntd.ru/document/1200036406 [Accessed 15 Dec. 2012] (in Russian)

Saur E. and Juste C. (1994). Enrichment of trace elements from long-range aerosol transport in sandy podzolic soils of Southwest France. Water, Air, & Soil Pollution, 73, pp. 235–246.

Schroeder W.H. and Munthe J. (1998). Atmospheric mercury an overview. Atmospheric Environment, 32, pp. 809–822.

Shevchenko V., Lisitzin A., Vinogradova A. and Stein R. (2003). Heavy metals in aerosols over the seas of the Russian Arctic. Science of the Total Environment, 306 (1–3), pp. 11–25.

Siudek P. (2016). Distribution and variability of total mercury in snow cover – a case study from a semi-urban site in Poznan. Poland. Environmental Science and Pollution Research, 23, pp. 24316–24326.

Siudek P., Falkowska L., Frankowski M. and Siepak J. (2014). An investigation of atmospheric mercury accumulated in the snow cover from the urbanized coastal zone of the Baltic Sea, Poland. Atmospheric Environment, 95, pp. 10–19.

Talovskaya A.V., Filimonenko E.A., Osipova N.A., Lyapina E.E. and Yazikov E.G. (2014). Toxic elements (As, Se, Cd, Hg, Pb) and their mineral and technogenic formations in the snow cover in the vicinity of the industrial enterprises of Tomsk. XVIII International Scientific Symposium in Honour of Academician M. A. Usov: PGON2014 IOP Publishing IOP Conference Series of Earth Environment Scicience, Volume 21, 012042. Available at: https://doi.org/10.1088/1755e1315/21/1/012042

Talovskaya A.V., Filimonenko E.A., Osipova N.A. and Yazikov E.G. (2012). Mercury in dust aerosols in the territory of Tomsk. Safety in Technosphere, 2, pp. 30–34 (in Russian with English summary).

Taraškevičius R., Zinkut R., Gedminien L., Stankevičius Z. (2018). Hair geochemical composition of children from Vilnius kindergartens as an indicator of environmental conditions. Environmental Geochemistry and Health, 40(5), pp. 1817–1840.

Tchounwou P.B., Ayensu W.K., Ninashvili N. and Sutton D. (2003). Review: environmental exposure to mercury and its toxicopathologic implications for public health. Environmental toxicology, 18 (3), pp. 149–175.

UNEP. (2013). Global mercury assessment 2013: sources, emissions, releases and environmental transport, UNEP Chemicals Branch, Geneva, Switzerland

Wiener J.G., Krabbenhoft D.P., Heinz G.H. and Scheuhammer A.M. (2003). Ecotoxicology of mercury. In: Hoffman DJ, Rattner BA, Burton GA, Cairns JS, ed., Handbook of ecotoxicology, Lewis Publ, Boca Raton, pp. 409–463.

Wilhelm S.M. (2001). Mercury in petroleum and natural gas: estimation of emissions from production, processing, and combustion. In: EPA/600/R-01/066 (NTIS PB2001-109026), U.S. Environmental Protection Agency, Washington

Williamson B.J., Purvis O.W., Mikhailova I.N., Spiro B. and Udachin V. (2008). The lichen transplant methodology in the source apportionment of metal deposition around a copper smelter in the former mining town of Karabash, Russia. Environmental Monitoring and Assessment, 141 (1–3), pp. 227–236.

Xu M., Yan R., Zheng C., Qiao Y., Han J. and Sheng C. (2003). Status of trace element emission in a coal combustion process: a review. Fuel Processing Technology, 85, pp. 215– 237.

Yanchenko N.I., Slutskii S.L., Baranov A.N. and Verkhoturov V.V. (2015). Dynamics of fluoride atmospheric fallouts in the Baikal region. Russian Meteorology and Hydrology, 40 (11), pp. 766–771.

Zhang Y., Xiu G., Wu X., Moore C.W., Wang J., Cai J., Zhang D., Shi C. and Zhang R. (2013). Characterization of mercury contents in snow and potential sources, Shanghai, China. Science of the Total Environment, 449, pp. 434–442.

Zharov Yu.N., Meitov E.S. and Sharova I.G .(1996). Valuable and toxic elements in traded coal of Russia. Handbook. Moscow: Nedra (in Russian)

Irina D. Eremina*, Jessica Yu. Vasil'chuk

Lomonosov Moscow State University, Len GSP-1, Leninskie Gory, Moscow, 119991, Russia

* Corresponding author: meteo@rambler.ru

TEMPORAL VARIATIONS IN CHEMICAL COMPOSITION OF SNOW COVER IN MOSCOW

ABSTRACT. This article summarizes the data of the chemical composition and the acidity of the seasonal snow precipitation for the cold periods 1999-2006 (n=180), 2010-2013 (n=82) and 2018-2019 (n=18) in different parts of Moscow. Major ions content was measured, such as SO_4^{2-}, HCO_3^-, Cl^-, NO_3^-, Ca^{2+}, Mg^{2+}, Na^+, K^+ and NH_4^+, also pH and sum of ions (mg/L) were measured. During the 2018-2019 season, snowpack samples were taken twice at 4 sites in Moscow: two in the North-East Administrative Okrug (NEAO) near the road and in the park at the distance of 3 km from each other, and two in the South-Western Administrative Okrug (SWAO) and in the Western Administrative Okrug (WAO) near the road and in the park at the distance of 6 km from each other. Samples were taken with a break of 5 days to determine the dynamics of the chemical composition within the beginning of the snow-melting. In each pair of sampling sites there was one that is located in the park and one located near the road. This experiment showed a slight variability of the chemical composition of snow during 5 days under the influence of the new snowfall. In general, there is a trend of changing the composition of snow from calcium carbonate to calcium chloride, which is mainly connected to the use of anti-icing reagents; for the same reason, the areas that are closer to the roads are the most polluted.

INTRODUCTION

The study of the chemical composition of snow cover is an important part in the research of the air pollution processes. The study of the pollution of the snow cover is widely used to control atmospheric input. The snow cover is a depositary for pollutants and is an informative object in identifying anthropogenic air pollution. The chemical composition of melting snow is formed as a result of the input of various chemical elements with precipitation, the absorption of gases by the snow, water-soluble aerosols, and the interaction of the dust particles deposited from the atmosphere with the snow cover. Snow cover pollution occurs in two stages. Firstly, it is the pollution of snow during its formation in the cloud and falling on the location which is wet deposition of pollutants with snow, secondly, the pollution of the snow which has already fallen as a result

of the dry sedimentation of pollutants from the atmosphere, as well as their input from the underlying soils and rocks (Vasilenko et al. 1985).

The study of the chemistry of snow cover is carried out intensively in Russia as well as in other countries of the world. Yakhnin and his co-workers (2003) provide data of the content of major components and trace elements in the atmospheric precipitation of Leningrad Area and Finland. It is showed that the content of sulfates in the snow in Finland was decreasing, and in Leningrad Area was increasing through the period from 1999 to 2001. Comparison of the composition of samples of snow cover and wet fallout during the winter period provide comparable results. Yakhnin et al (2002) also studied the level of the contamination of snow cover in Estonia and in the west of Leningrad Area near industrial zones considering the connection between the structure of technogenic atmospheric fallout and the main sources of emissions into the atmosphere. Negrobov et al. (2005) proposes to use data on snow cover to determine the level of the pollution and the composition and emission rates of enterprises. Yanchenko (2014) notes an increase of alkalinity of snow in industrial areas of Bratsk. Belozertseva et al. (2017) studied chemical composition of snow in lake Baikal area and showed the difference between contaminating compounds for different hollows in this area: the northern part is contaminated mostly by SO_4^{2-}, HCO_3^-, Cl^-, Ca^{2+}, while the southern receives NO_3^-, NH_4^+ and Na^+. Analysis of the chemical composition of snow cover in Komi (Vasilevich et al. 2011) showed low salinity and acid pH values – EC varies from 9.4 to 10.02 μS/cm that is approximately 6.0 −6.4 mg/L, pH varies from 4.6 to 4.8. Prozhorina et al. (2014) and Prozhorina and Yakunina (2014) studied the snow cover of Voronezh in 2013 and 2014. The authors have shown that nitrates, nitrites, and chlorides predominate in technogenic emissions in Voronezh, and that motor transport and industrial enterprises are the main sources of pollution. Shumilova et al. (2012) investigated the pollution of snow cover in Izhevsk; the authors obtained high values of the snow salinity (up to 1247.5 mg /L) in the industrial zone.

Studies of snow cover in Moscow Area in 2009–2013 (Yermakov et al. 2014) revealed relatively high salinity of snow in several districts (up to 46 mg/L) in comparison to Sergiyevo-Posadsky District (where salinity reaches 9.6 mg/L) and a pH value is close to neutral, indicating the high dust content of the atmosphere.

A study held in the United States (Ingersoll, et all, 2008) compares the composition of snow cover with the results of analysis of the wet deposition samples. Interesting conclusions were obtained that the content of calcium, magnesium and potassium in snow cover is much higher than in wet precipitations, and the concentrations of sulfates and nitrates are comparable in both types of samples and have been decreasing in recent years. Nawrot et al. (2016) studied the chemical composition and the acidity of the snow cover of the Hans Glacier in the South of Svalbard during the season 2005-2006. This season was both the warmest (the mean January temperature was −1.7 ° C in January) and with the highest level of in precipitation since 1988, also, within this season 1.3 m of snow accumulated on the Hans Glacier. The authors noted the high contamination of the snow with sulfates and nitrates, according to their analysis of the reverse trajectories, agricultural fires in Eastern Europe (Stohl et al. 2007) were the source of the contamination.

Jacobi et al. (2012) investigated the snow cover of the coast of Alaska, mainly high contents of sodium, chloride, sulfate and potassium were found due to the influence of sea salts, also high content of magnesium and calcium were found due to the combination of dust and sea salts. Similar studies were conducted in other regions of the United States (Rocky Mountains), as well as for the highlands of Europe and the Himalayas, and were summarized in (Hidy 2003). In the Rocky Mountains thermal power plants are the main source of sulfates and nitrates in the snow cover. Jarzina et al. (2017) investigated physical and chemical properties of melting snow in Poland. The results indicate a significant contribution of pollutants produced by the local metallurgical plant to the chemical composition of snow melt. Kępski et al. (2016) conducted the research on snowmelt snow in the Sudetes and showed

that 50-76% of pollutants are added to the soil in first two weeks of snowmelt. Curtis et al. (2018) analyzed the spatial patterns of nitrate distribution in western Greenland and found that nitrate content significantly declined from inland to the coast. Williams et al. (1992) conducted a study of the sources and spatial variations of the chemical composition of snow in eastern Tien Shan, China. According to their data, the average concentration of sulfates in the snow was three times higher than background concentrations in other remote areas of the world.

The relationship between dry and wet deposition depends on many factors, the main of which are: the duration of the cold period, the frequency of snowfalls and their intensity, the physical and chemical properties of pollutants, the size of aerosols.
Due to the high intensity of wet leaching processes the proportion of dry deposition for regional and global pollution in the Northern Hemisphere is usually 10–30%. However, near the local sources with large emissions of coarse aerosols, the picture is reversed, i.e. dry deposition can be from 70 to 90%.

The aim of the research is to determine long-term changes in pH and ionic composition of seasonal snowpack in Moscow within the period from 1999 to 2019. Also, we examined the variability of snow chemical composition within the period of snow melt to be able to find out if the variation during one season is significant.

MATERIALS AND METHODS

The collection and analysis of winter snow samples in Moscow and Moscow Area (Moscow Oblast) were carried out from 1999 to 2006 (Eremina and Grigoriev 2010), as well as in winter in 2010-2011, 2011-2012 and 2012-2013 (Belikov et al. 2012; 2013; 2014), also, sampling took place in 2018-2019 (Fig. 1). In winter season of 2018-2019, samples were taken at 4 sites in the North-East Administrative Okrug (NEAO), South-Western Administrative Okrug (SWAO) and Western Administrative Okrug (WAO) with a break of 5 days to determine the dynamics of the chemical composition within the beginning of the snow-melting period. Also, the sites sampled in 2018-2019 winter

season were located in 2 main directions (South-West and North-East), in each direction two sites were sampled: one near the road (88 km MKAD and Stoletova Street) and one in the park (Narodny Park and Kotlovka floodplain) to show the difference between two types of anthropogenic influence. Winter snow samples were also taken in the end of winter and annually analyzed the territory of Meteorological Observatory of Lomonosov Moscow State University (MSU MO). Therefore, it is possible to trace the dynamics of the chemical composition of snow cover over last 20 years.

Sampling was carried out in the period of maximum liquid water content (LWC) in the snow, in the end of February – beginning of March. All sampling was held mostly in places, that are not influenced by human activity (parks, forests) more than in 100-200 meters from the roads, with exception of two sites sampled in season 2018-2019: at 88 km of MKAD and Stoletova street, that were located near roads. Such sampling was conducted in order to compare sites that are relatively close to each other, but experience different levels of anthropogenic influence. Samples taken from 1999 to 2013 were taken in parks, the sites were chosen in such a way to cover different directions and distance from the center of Moscow (Fig.1). The one column of the entire thickness of snow cover was sampled with a standard snow sampler 60 cm long and with a cross-section area of 50 cm^2. Then the snow was transferred to plastic cuvettes. The sampling protocol used in this study is similar to the sampling standard for ionic composition study used in USA (Snow-survey sampling guide, 1967). A study to determine the representativeness of one sample was conducted in 2010 (Eremina and Grigoriev 2010). For this purpose, 10 seasonal snowpack samples were taken at a site with total area of 100 m^2. After full chemical analysis, it was found that the content of all components, with the exception of the hydrocarbonate ion, differs slightly in these samples (standard deviation S = 0.06–0.10). For the HCO_3^- ion, the scatter was slightly higher, probably due to the plant of building materials, that was close to the sampling site and which gave alkaline emissions (Eremina and Grigoriev 2010).
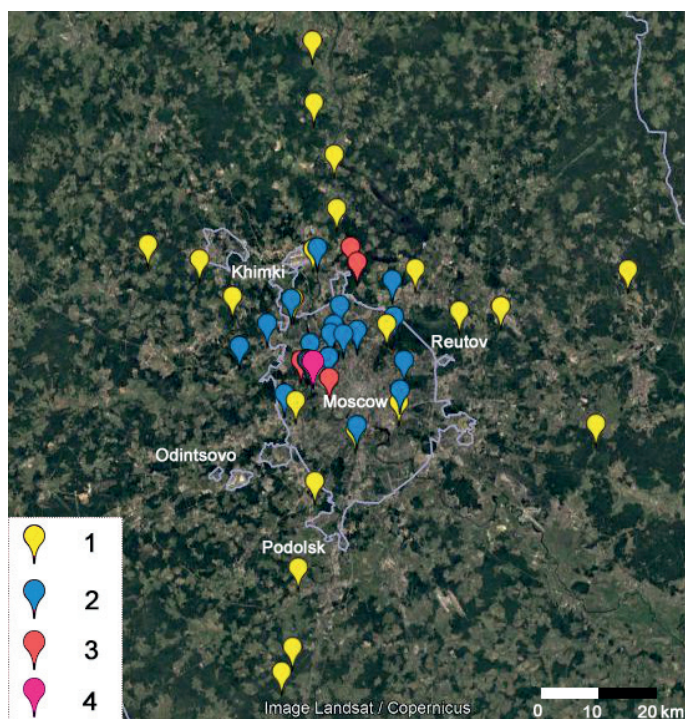
Fig. 1. Sampling points: 1 – 1999 – 2006; 2 – 2011 – 2013; 3 – 2018 – 2019 ; 4 – MSU MO 1999 – 2006, 2011 – 2013, 2018 – 2019

Melting of snow samples was conducted at a temperature of 20°C±2°C (the standard temperature in a laboratory room) without additional heating during 24 hours. The samples were closed in cuvettes during the melting procedure. Chemical analysis of snow samples was carried out in the chemical laboratory of Moscow State University. Preparation for sample analysis included thawing to room temperature and filtration. Major ions content was measured, that are anions: sulfate (SO_4^{2-}), bicarbonate (HCO_3^-), chloride (Cl^-), nitrate (NO_3^-): as well as cations: calcium (Ca^{2+}), magnesium (Mg^{2+}), sodium (Na^+), potassium (K^+) and ammonium (NH_4^+). The ion concentration is expressed in mg /L, microeq/L and %-eq. Concentration of HCO_3^- and the pH of samples were measured immediately after the sample preparation, since the pH value and the concentration of HCO_3^- ions can change quite significantly during long-term storage of the sample. The pH value and the concentration of bicarbonate (by titration with hydrochloric acid) were determined on an Expert -001 ion meter (Ekoniks, RF). The content of cations and anions was determined by ion chromatography on a JetChrom instrument

(PortLab, RF). The ionic composition is studied as it the most reliable analysis that can show the contamination of atmosphere air through the dissolved compounds.

RESULTS AND DISCUSSION

Studies of snow samples on the territory of MSU MO showed no significant change in their acidity (Table 1). The average value of pH for all 20 years of observations at MSU MO is around 6.3. A slight increase in the acidity of seasonal snow was observed during the cold periods of 2006–2007, 2008–2009, and 2009–2010 (average values from 5.5 to 5.8). In other years, the pH of seasonal snow samples varied in the range of 6.2 - 7.1.

To observe the trends in the ionic composition, we divided the entire study period into 2 parts,10 years each. Concentrations of some ions in recent years have decreased the comparing with the first period, while others have increased. Thus, the decrease in the content of the following ions: HCO_3^-, SO_4^{2-} and Ca^{2+} in the second period (Table 1) is noted. The total sum of ions (mineralization, salinity) of the samples also decreased. The HCO_3^-

content decreased by 2 times from 4.7 mg /L to 2.3 mg /L. The lowest value of bicarbonate ion was obtained in the winter of 2009-2010 (1.1 mg/L), and the maximum in 2007-2008. (12.0 mg/L). The content of SO_4^{2-} also decreased from 2.0 to 1.2 mg/L, and the highest average content of sulphate ion 3.6 mg/L was noted in 2005-2006. In the second observation period, the content of the main cation calcium (Ca^{2+}) decreased slightly from 2.6 to 1.8 mg /L.

The concentrations of the other ions in the second period have increased. Comparing with the first period, the content of chloride and sodium ions increased remarkably. In the snow of the first period from 1999 to 2008 the mean content of Cl^- was 1.4 mg/L, and in 2009-2018 2.4 mg/L. The maximum amount of chloride obtained in the winter season 2012-2013 (3.8 mg/L). In the second period, the content of sodium ion increased from 0.4 to 0.9 mg /L. Apparently, this is due to the active use of anti-icing reagents, the main components of which are chloride and sodium ions (Eremina et al. 2015). Anti-icing reagents in Moscow are used not only on the roads, but also in parks, so the short distance aeolian transport of their components is possible. The content of the other ions has not changed significantly. The values of confidence interval show that the increase of contamination is not significant, only Cl^- and Na^+ content increase significantly.

In Table 1 the concentrations are presented not only in mg/L, but also in the %-eq. From these data, the contribution of each ion to the total mineralization of the sample can be estimated. Among the cations, calcium is the predominant ion (in all the years of observation), and the share of sodium has greatly increased in the second period (12.3%-eq). In the first period, the bicarbonate was the predominant anion (21.3 %-eq.) and in the last decade the chloride ion became the predominant one. So, if in the first period the seasonal samples of snow cover belonged to the bicarbonate-calcium class, now it is the chloride-calcium one. Chloride prevails not only in seasonal snow samples, but also in daily samples. (Eremina 2013, 2019).

Considering general data for Moscow sampling sites, the ion content is significantly higher here, because the MSU MO is located on the territory of the Botanical Garden of Moscow State University and is protected by trees from major highways, and there are no industrial enterprises close to it.

Results of snow study for 1999 - 2006 are presented in (Eremina and Grigoriev 2010). However, during these years, samples were taken mainly in the park zone near Moscow Ring Road (MKAD) and there were practically no samples in the center of Moscow. And in winter seasons 2010-2011, 2011-2012 and 2012-2013 samples were taken in the center of Moscow (Fig. 1).

Table 1. Chemical composition and pH of snow samples from the territory of MSU MO in different years, CI – confidence interval

MSU MO, sampling period	pH	HCO_3^-	SO_4^{2-}	Cl^-	NO_3^-	Ca^{2+}	Mg^{2+}	Na^+	K^+	NH_4^+	Sum of ions
		Concentration, mg/L									
1999-2008 n=23	6.30	4.7	2.0	1.4	1.3	2.6	0.1	0.4	0.1	0.4	13.0
2009-2018 n=22	6.25	2.3	1.2	2.4	1.2	1.8	0.1	0.9	0.2	0.3	10.4
CI	±0.12	±0.8	±0.3	±0.3	±0.1	±0.3	±0.01	±0.2	±0.03	±0.1	±1.2
		Concentration, %-eq..									
1999-2008		21.3	11.9	11.5	5.8	35.8	2.5	4.7	0.7	5.7	
2009-2018		12.4	8.4	21.7	6.5	28.7	2.5	12.3	1.5	5.8	

All collected samples of the snow cover of these three seasons can be divided into 4 groups by the sampling site: 1) Moscow Center (approximately within the third transport ring (TTK); 2) Parks (squares, forest parks, etc. near MKAD); 3) Moscow Area - suburbs (4 samples at a distance of 5, 15, 25, and 40 km from MKAD in 4 main directions); 4) MO MSU (for comparison).

Table. 2 shows the mean salinity values for all groups of sampling sites for each of the 3 seasons. The trend of decreasing of snow contamination from the center to the suburbs of Moscow is stable over years. Therefore, it is possible to average all values for each group (more than 100 samples in total), and the mean and range of salinity values are also shown in table 2. The most polluted samples of snow were collected in the center of Moscow (average salinity 61.2 mg/L), the less polluted in Moscow Area and MSU MO. Moreover, in

Moscow parks near MKAD, seasonal snow mineralization is 3 times less, and in Moscow Area and MSU MO - almost 5 times less than in the center of Moscow. MSU MO may be considered as "background" station compared with other sampling sites in the city.

Figure 2 shows the average content of the main anions and cations for the same 4 sampling sites. A decrease in the concentrations of all ions from Moscow Center to Moscow Area is observed. High concentrations of chloride, calcium and sodium ions in the city center is noted. These are the main components of anti-icing agents, which in recent years have been used in large quantities on the roads of Moscow. In large parks and in outskirts of Moscow this influence is not significant, however, in small parks, surrounded by roads this influence is obvious.

Table 2. Salinity of snow in different sampling sites in 2011-2013 (n=82)

	Salinity, mg/L			
	Moscow Center	Parks near MKAD	Moscow Oblast	MSU MO
2010-2011	60.2	19.6	16.1	12.8
2011-2012	71.1	18.8	15.1	13.4
2012-2013	46.8	24.0	12.4	13.9
Mean	61.2	20.6	14.5	13.4
Min.	24.3	5.6	4.7	5.6
Max.	199.1	53.3	41.8	25.3
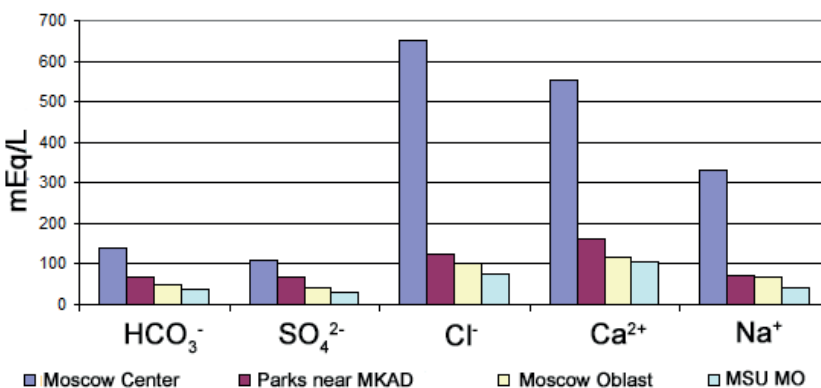
Fig. 2. Ionic composition of snow in different sampling sites

Table 3 shows the average values and the range of pH of snow in 4 sites. The acidity of all collected samples of snow cover varied from 5.1 to 7.9 i.e. there no acidic samples (pH <5.0).

However single (daily) snowfalls are sometimes acidic, especially in winter of 2009-2010 (more than 20%). Usually there are 60-80 single samples during the winter, each sample is taken and analyzed as it falls. However, our analysis of seasonal snow includes all the snow that accumulates from the beginning of the formation of snow cover to the beginning of its melting. Deposition of alkaline particles on the surface of an urban aerosol neutralizes the acidity of individual samples, so seasonal snow has a pH> 5. The lack of acidity is an important environmental indicator, since it means that acid does not enter the soil and rivers with the snow melt.

The composition of the snow in 2018-2019 was also studied at 4 points in different parts of Moscow: Narodny Park and 88 km of the Moscow Ring Road - MKAD in the north-eastern part of Moscow, Nakhimovsky Av. near the floodplain of Kotlovka River in the south-western part of Moscow and Stoletova Str. in western part of Moscow. Samples were taken twice with a break of 5 days at the beginning of the period of snow melt (Fig. 3.). Samples taken at 88 km of MKAD show the highest salinity of 41.8-57.4 mg /L and the most alkaline pH values of 6.75-7.10. Calcium chlorides predominate in these samples. In Narodny Park, located in the same part of Moscow, calcium and bicarbonate ions predominate, pH varies in range of 6.55-6.70. Salinity here is 2 times lower than in snow from Moscow Ring Road and varies in range of 19.4-21.1 mg/L. In samples near Stoletova Street in the west of Moscow, the pH is 7.05-

7.15, and salinity is 18.6-28.4 mg/L. On the floodplain of the Kotlovka River near Nakhimov Avenue in the south-west of Moscow, the pH is 6.35-6.75, the salinity is 11.1-19.1 mg /L, and snow samples had of calcium - chloride composition. In general, the comparison of the sites located in the parks (Narodny Park and floodplain of Kotlovka river) with the sites in 3-6 km, but located near the roads (88 km MKAD and Stoletova street), show not only the obvious higher mineralization of samples and higher pH due to the influence of the roads, but also more intensive change in an ionic composition. Near the roads the increase of HCO_3^- content in 5 days is higher from 9%-eq. to 19%-eq. in NEAO and from 18%-eq. to 25%-eq. in WAO, while in parks the difference in HCO_3^- content within 5 days is not higher than 2-3%-eq. (Fig. 3).

The predominantly calcium and chloride composition of snow indicates pollution with anti-icing agents (Gladkov et al. 2016)

The samples were taken twice: on 3 March and 8 March 2019. An increase in pH, an increase in the concentration of Ca^{2+} is observed in samples, that were taken later. At the sites in the West and South-West, an increase in salinity, and decrease in the content of Cl^- is observed.

Comparing the composition snow of 2018-2019 (Table 4) to the results of previous years shows, in the last season, slightly higher values of salinity, pH, as well as concentrations of some ions (HCO_3^-, Cl^-, Ca^{2+} and Na^+) were obtained. These samples were collected in other sites, then in previous years, thus the influence of other sources of pollution could have an effect.

Table 3. pH values of snow

	pH			
	Moscow Center	Parks near MKAD	Moscow Oblast	MSU MO
Mean	6.96	6.46	6.00	6.56
Min.	6.70	6.00	5.10	5.45
Max.	7.55	7.85	6.85	7.20
Δ	0.85	1.85	1.75	1.75
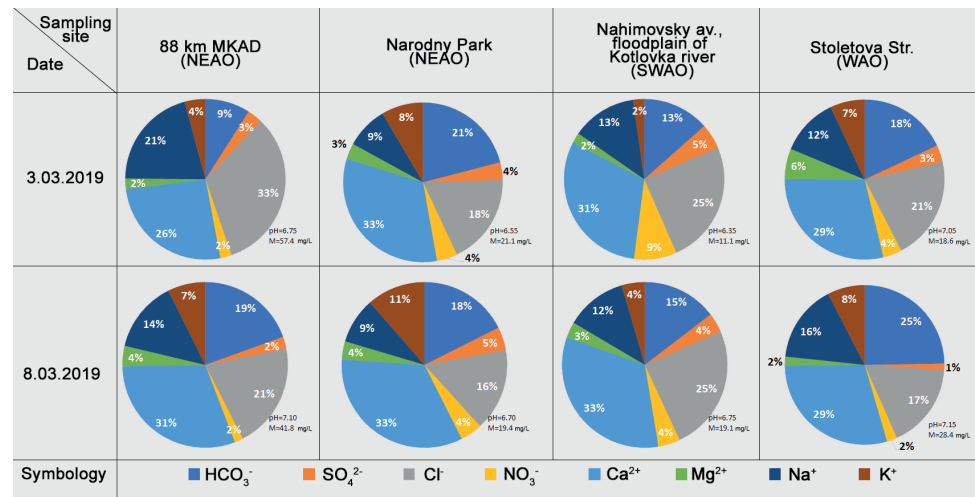
Fig. 3. Chemical composition of snow in 4 sampling sites for 3.03.19 and 8.03.19

In recent years, there is a decrease in sulfates in the snow cover (Table 4), and a noticeable increase in chlorides and sodium. Concentrations of other ions do not change significantly.

The composition of the snow cover in Moscow can be compared to one in Izhevsk in the same winter season of 2010-2011 (Shumilova et al. 2012). The pH of snow in Izhevsk varied from 6.63 to 7.25, in Moscow in the same period pH was 6.30-6.70. The content of chlorides in Izhevsk varied from 1.78 to 40.12 mg /L, in Moscow suburbs according to our data during this period the chloride concentrations were in a range of 1.6-6.1 mg /L, and in the center

Table 4. Comparison of mean values in snow in Moscow over 20 years, CI – confidence interval

Sampling period	pH	Ion concentration, mg/L									Sum of ions, mg/L
		HCO_3^-	SO_4^{2-}	Cl^-	NO_3^-	Ca^{2+}	Mg^{2+}	Na^+	K^+	NH_4^+	
1999-2006 (Eremina and Grigoriev 2010) n=84	6.1	3.9	3.0	2.7	1.7	2.6	0.2	0.8	0.3	0.6	15.8
CI	±0.02	±0.6	±0.6	±0.7	±0.2	±0.4	±0.04	±0.4	±0.1	±0.1	±2.4
2010-2011 (Belikov et al. 2012) n=9	6.5	4.4	4.3	2.9	2.2	2.8	0.4	0.9	0.8	0.9	19.6
CI	±0.1	±1.6	±1.3	±0.9	±0.5	±0.7	±0.1	±0.2	±0.6	±0.2	±4.7
2011-2012 (Belikov et al.. 2013) n=9	6.4	4.1	2.4	3.7	3.1	3.4	0.3	1.2	0.2	0.4	18.8
CI	±0.1	±1.2	±1.0	±1.0	±1.3	±0.9	±0.1	±0.4	±0.02	±0.3	±4.5
2012-2013 (Belikov et al. 2014) n=11	6.6	3.8	2.7	7.5	2.0	3.5	0.3	3.1	0.7	0.4	24.0
CI	±0.1	±0.8	±0.6	±1.9	±0.2	±0.8	±0.1	±0.7	±0.2	±0.1	±5.1
2018-2019 (this study) n=18	6.7	6.2	2.2	8.6	1.5	4.7	0.3	3.4	0.8	0.5	28.2
CI	±0.1	±1.6	±0.6	±2.9	±0.3	±1.2	±0.1	±1.2	±0.3	±0.2	±7.1

of Moscow from 6.8 to 75.0 mg/L. Sulfate ion in Izhevsk was detected with a concentration of 3.37-5.55 mg/ L, in Moscow the range is slightly wider from 2.2 to 7.7 mg/L, and in the center of Moscow values reach 19.5 mg /L. Snow in Izhevsk contains nitrate ion in amount of 0.5-5 mg/L, in Moscow the average content was 2.38 mg /L (the range is 0.7-4.7 mg /L). The snow in Moscow is more polluted than in Izhevsk, but the patterns are the same. High content of chlorides is also associated with anti-icing reagents, since the main pollution with chlorides is associated with large highways, which are regularly influenced by reagents in winter. The concentration of sulfate in the snow of Izhevsk is marked as relatively low, as in Moscow. (Shumilova et al. 2012).

CONCLUSIONS

1. In the snow cover in the MSU MO, there is a tendency of a change of snow chemical composition from 1999 to 2019 from bicarbonate-calcium to chloride-calcium, which is associated with the use of anti-icing reagents.

2. For mean values in Moscow the significant increase of sodium and chloride ions content as well as the increase of mineralization in general is shown for the period of 20 years, pH values of snow increased by 0.6 from 1999 to 2019.

3. The comparison of snow samples in the center of Moscow and Moscow suburbs showed a decrease in pollution in this sequence, but the least polluted samples are collected at MSU MO.

4. The ionic composition and the pH of snow samples at 4 sites in Moscow, twice taken in the interval of 5 days, showed significant difference and, therefore, high sensitivity to single events of rain and snow. In general, the comparison of the sites located in the parks (Narodny Park and floodplain of Kotlovka river) with the sites in 3-6 km, but located near the roads (88 km MKAD and Stoletova street) show not only the obvious higher mineralization of samples and higher pH due to the influence of the roads, but also a more intensive change in an ionic composition. Near the roads the increase of HCO_3^- content in 5 days is higher from 9%-eq. to 19%-eq. in NEAO and from 18%-eq. to 25%-eq.in WAO, while in parks the difference in HCO_3^-content within 5 days is not higher than 2-3%-eq. It can be assumed that with the regular snow sampling during one winter, the result of the analysis of the entire snow layer will differ significantly.

ACKNOWLEDGEMENTS

REFERENCES

Belikov I., Gorbarenko E., Elokhov A., Eremina I., Ivanov V. Konstantinov P., Lokoshchenko M., Nezval E., Postylyakov O., Chubarova N., Shilovtseva O. and Shumsky R. (2012) The chemical composition of precipitation in 2011. In: N.Chubarova, ed., Ecological and climatic characteristics of the atmosphere in 2011 according to the meteorological observatory of Moscow State University. Moscow: MAKS Press. (in Russian).

Belikov I, Gorbarenko E., Eremina I., Zhdanova E., Konstantinov P., Korneva I., Lokoshchenko M., Nezval E., Skorohod A., Chubarova N., Shilovtseva O., Shumsky R., Akhiyarova K. and Remizov A. (2013) The chemical composition of precipitation in 2012. In: N.Chubarova, ed., Ecological and climatic characteristics of the atmosphere in 2012 according to the meteorological observatory of Moscow State University. Moscow: MAKS Press. (in Russian).

Belikov I., Gorbarenko E., Eremina I., Zhdanova E., Konstantinov P., Korneva I., Lokoshchenko M., Nezval E., Skorohod A., Sokratov S., Chubarova N., Shilovtseva O., Polyukhov A., Gorlova I., Seliverstov Yu. and Grebennikov P. (2014) The chemical composition of precipitation in 2013. In: N.Chubarova, ed., Ecological and climatic characteristics of the atmosphere in 2013 according to the meteorological observatory of Moscow State University. Moscow: MAKS Press. (in Russian).

Irina D. Eremina and Jessica Yu. Vasil'chuk.   TEMPORAL VARIATIONS IN ...

04|2019   GES

157

Belozertseva I., Vorobyeva I., Vlasova N., Yanchuk M. and Lopatina D. (2017) Chemical composition of snow in the water area of lake Baikal and on the adjacent territory. Geography and natural resources, 1, 90–99. (in Russian with English summary), DOI: 10.21782/GIPR0206-1619-2017-1(90-99).

Curtis C., Kaiser J., Marca A., Anderson J., Simpson G., Jones V. and Whiteford E. (2018) Spatial variations in snowpack chemistry, isotopic composition of NO_3^- and nitrogen deposition from the ice sheet margin to the coast of western Greenland. Biogeosciences, 15, 529–550. DOI: 10.5194/bg-15-529-2018.

Eremina I. (2013). Monitoring chemical composition of atmospheric precipitation according to observations in meteorological observatory of Moscow State University. International Scientific Journal for Alternative Energy and Ecology, 6(2), 10–17.

Eremina I. (2019) The chemical composition of precipitation in Moscow and the tendencies of its long-term changes. Vestnik Moskovskogo Universiteta. Seria 5, Geografia. 3, 1-10. (in Russian with English summary).

Eremina I., Aloyan A., Arutyunyan V., Larin I., Chubarova N. and Yermakov A. (2015) Acidity and Mineral Composition of Precipitation in Moscow: Influence of Deicing Salts. Izvestiya, Atmospheric and Oceanic Physics, 2015, 51 (6), 624–632, DOI: 10.1134/S0001433815050047.

Eremina I. and Grigoriev A. (2010), Acidity and chemical composition of snow cover in the city of Moscow and the Moscow region during 1999-2006. Vestnik Moskovskogo Universiteta. Seria 5, Geografia, 3, 55-60. (in Russian with English summary).

Gladkov E., Evsyukov S., Shevyakova N., Dolgikh Yu., Gladkova O. and Glushetskaya L. (2016). Effect of anti-icing reagents on lawn grasses. Izvestia of Samara Scientific Center of the Russian Academy of Sciences, 5 (1), 157-159. (in Russian with English summary).

Hidy G. (2003) Snowpack and precipitation chemistry at high altitudes. Atmospheric Environment., 37 (9–10), 1231–1242, DOI: 10.1016/S1352-2310(02)01024-5.

Ingersoll G., Mast M., Campbell D., Clow D., Nanus L. and Turk J. (2008) Trends in snowpack chemistry and comparison to National Atmospheric Deposition Program results for the Rocky Mountains, US, 1993–2004. Atmospheric Environment., 42(24), 6098–6113, DOI: 10.1016/j.atmosenv.2008.02.030.

Jakobi H., Voisin D., Jaffrezo J., Cozic J. and Douglas T. (2012) Chemical composition of the snowpack during the OASIS campaign 2009 at Barrow, Alaska. Journal of geophysical research, 117, D00R13. DOI: 10.1029/2011JD016654.

Jarzyna K., Kozłowski R. and Szwed M. (2017). Chemical properties of snow cover as an impact indicator for local air pollution sources. Infrastructure and Ecology of Rural Areas, 4(2), 1591–1607. DOI: http://dx.medra.org/10.14597/infraeco.2017.4.2.120.

Kępski, D., Błaś, M., Sobik, M., Polkowska Ż. and Grudzińska K. (2016) Progressing Pollutant Elution from Snowpack and Evolution of its Physicochemical Properties During Melting Period – a Case Study From the Sudetes, Poland. Water Air Soil Pollution, 227, 112. DOI: 10.1007/s11270-016-2797-z.

Nawrot A., Migala K., Luks B., Pakszys P. and Giowacky P. (2016) Chemistry of snow cover and acidic snowfall during a season with a high level of air pollution on the Hans Glacier, Spibergen. Polar Science, 10(3), 249–261. DOI: 10.1016/j.polar.2016.06.003.
Negrobov O, Astanin I., Starodubtsev V. and Astanina N. (2005). Snow cover as the indicator of the condition of atmospheric air in system of socially-hygienic monitoring. Vestnik VGU. Seria Humiya. Biologiya. Farmaciya, 2, pp. 149–153. (in Russian with English summary)

Prozhorina T., Bespalova E. and Yakunina N. (2014) Estimation of the condition of snow cover in Voronezh according to the chemical analysis of water from melted snow. Principy ecologii, 3(1), 53–58 (in Russian with English summary).

Prozhorina T. and Yakunina N. (2014). Assesment of pollution of atmospheric air of the city of Voronezh on a condition of snow cover. Astrahanskij vestnik ekologicheskogo obrazovaniya, 1 (27), 111–114. (in Russian with English summary)

Shumilova M. Saidulina O. and Petrov V. (2012). Study of snow cover contamination by example of Izhevsk. Vestnik Udmurtskogo universiteta, 2, 83–89. (in Russian with English summary).

Snow-survey sampling guide (1967) Soil Conservation Service. USDA, Agriculture Handbook No. 169, Washington, D.C.

Stohl, A., Berg, T., Burkhart, J., Fjǽraa, A., Forster C., Herber A., Hov Ø., Lunder C., McMillan W., Oltmans S., Shiobara M., Simpson D., Solberg S., Stebel K., Ström J., Tørseth K., Treffeisen R., Virkkunen K. and Yttri K. (2007). Arctic smoke – record high air pollution levels in the European Arctic due to agricultural fires in Eastern Europe in spring 2006. Atmospheric Chemistry and Physics, 7, 511–534. DOI: 10.5194/acp-7-511-2007.

Vasilenko V., Nazarov I. and Fridman M. (1985). Monitoring of snow pollution. Leningrad.: Gidrometeoizdat (in Russian).

Vasilevich M., Beznosikod V. and Kondratenok B. (2011) Chemical composition of snow cover in the Taiga Zone of the Komi Republic. Water Resources, 38(4), 530–542. DOI: 10.1134/S0097807811040130.

Williams M., Tonnessen K., Melack J. and Daqing Y. (1992) Sources and spatial variation of the chemical composition of snow in the Tien Shan, China. Annals of Glaciology, 16, 5–32. DOI: 10.3189/1992AoG16-1-25-32.

Yakhnin E., Goltsova N., Tomilina O., Kaasik M., Syukand Yu. and Hongisto M. (2002). Atmospheric depositions in the north-eastern regions of Estonia and in the west of the Leningrad Region (according to data on snow cover pollution). Russian journal of general chemistry, 11(3), 145–156. (In Russian).

Yakhnin E., Tomilina O, Chekushin V. and Salminen R. (2003). Comparative analysis of data on the composition of precipitation and snow cover on the territory of the Leningrad Region and South-Eastern Finland and specification of the parameters of atmospheric deposition of heavy metals. Russian journal of general chemistry, 12(1), 1–12. (In Russian).

Yanchenko N. (2014). Features of changing pH value and conductivity of snow cover in Bratsk. Bulletin of the Tomsk Polytechnic University. Geo.Assets Engineering, 325 (3), 23–30. (in Russian with English summary).

Yermakov A., Karpova E., Malysheva A., Mikhaylova R. and Ryzhova I. (2014). Monitoring of the chemical composition of snow cover pollution in Moscow Region. Hygiene and sanitation, 5, 88–94. (in Russian with English summary).

Irina V. Kozliakova, Olga N.Eremina*, Nadezhda G. Anisimova, Irina A. Kozhevnikova

Sergeev Institute of Environmental Geoscience, Russian Academy of Sciences (IEG RAS) Ulansky per. 13, str.2, Moscow,101000 Russia
* Corresponding author: sci-council@geoenv.ru

SPECIFIC FEATURES OF GEOLOGICAL RISK ASSESSMENT IN MOSCOW

ABSTRACT. The paper describes approaches to assessing geohazards and georisk of economic losses in Moscow. It is shown that for surface construction, the principle geohazards in Moscow are karst-suffosion sinkholes, land subsidence, landslides, and waterlogging. The subsurface construction is endangered by karstification and fracturing of limestone, decompaction, and swelling of clay, quicksand phenomena, and groundwater breakthrough to tunnels. The different procedures for the assessment of geological risk in Moscow have been suggested for already existing urban infrastructure and for future planned construction. For existing surface urban infrastructure, geological risk is considered to be an integral parameter of probable damage caused by geohazards and the anthropogenic load on the specific territories. The main aim of risk mapping in this case is outlining the territories, for which restrictions and prohibitions should be imposed for further urban engineering development. For future subsurface urban construction, the risk-analysis consists in assessing the impact of geohazards on the engineering structure by comparing the future expenditures for the construction and operation under different engineering geological conditions. The procedures of risk mapping elaborated for both approaches are described; the typification schemes are listed; and the relevant risk maps built for the Moscow territory are provided. The risk maps will help planners to compare and make alternative project decisions in order to minimize the cost in future economic expenditures. Both approaches are successfully approved in Moscow.

KEY WORDS: Exogenous geohazards, risk analysis, urban areas, mapping, urban environment vulnerability

INTRODUCTION

Urban Infrastructure And Subsurface Development In Moscow

Sustainable urban development of Moscow is based on the balance between ecological and socio-economic demands, rational nature use and improvement of ecological situation.

The Moscow megacity area has reached 2511 km² lately, whereas as long as 7 years ago it approximated 1100 km². In 2012, the Moscow area grew significantly by adding a part of Moscow outskirts to the city. The present-day urban development of Moscow city is uneven. The most densely built-up part of the city of about 800 km² is enclosed within the Moscow ring highway. It consists

of the historical part of the city (about 18 km^2 in area), where the bulk of architectural and historical monuments are concentrated. The historical city centre still operates as its administrative centre, where the modern downtown business district with the highly developed subsurface is located. This part of Moscow appears to be the most vulnerable to geological hazards. Outwards the historical centre, towards the Moscow ring highway, different city belt zones are distinguished differing in the prevailing age and type of buildings. Five-eight-story buildings with strip foundations constructed before mid-1960s prevail in the immediate vicinity to the historical centre. Farther from the centre, the area is built-up with more modern buildings of 9 and more stories usually with piles and plate foundations. These are mainly the residential districts with apartment houses.

Lately, the urban subsurface is being intensely developed in Moscow megacity. New metro lines are under construction, as well as motorway tunnels and buildings with underground stories. In Moscow, metro has been operating since 1930s; however, until recently the density of metro facilities was much lower in the distant part of the city than in its central part. As proceeds from the international experience in running megacities like Moscow, the optimal conditions for sustainable development and comfortable living in a city are achieved upon the share of subsurface facilities no less than 20-25% of the entire number of urban engineering structures. In the central district of Moscow, this ratio averages to 30%, whereas, it does exceed 1-2% in the peripheral dwelling districts (Merkin et al 2013).

At present, many research projects are focused on finding the efficient and promising ways for ensuring the sustainable development of urban areas and enclosing the underground space in urban planning. A major EU project on the European COST Sub-Urban Action (TU1206) that was carried out in 2013-2017 and involved more than 30 countries was just one of the recent examples of collaborative efforts of scientists and urban decision-makers in overcoming

the knowledge gap between the experts and potential users aimed at the sustainable use of urban subsurface (Campbell et al 2017). As a rule, these projects are based on the interdisciplinary approach taking into consideration many aspects and criteria of comfortable human living ranging from the social and cultural infrastructure to favourable natural environment (Admiraal and Cornaro 2016; Bobylev 2009; Bobylev and Sterling 2016; Li et al 2016; Sterling et al 2012; Wende et al 2010). Geological hazards and their possible effect on urban infrastructure appears to be one of these criteria.

Exogenous geological processes exert a significant impact on the geoecological condition of urban area, because of being widespread they complicate both surface and underground engineering construction as well as the operation of existing buildings and other engineering structures. Intensification of exogenous geological processes may pose immediate danger to urban infrastructure stability and even to human health and loss of lives. Now it is commonly recognized among urban geologists that the assessment of geohazards alone is not enough for urban planning. In order to ensure the sustainable development of cities, it is necessary to start with the estimation of geohazards and pass to the assessment of geological risk. Actually, it is risk analysis that provides an adequate idea about the size of possible economic loss caused by geohazards in an urban area. The development of technology and working procedure of assessing risk caused by the hazardous geological processes is the most important task for urban geologists. Due to geodata uncertainties, this problem seems to be hardly solved on a quantitative level (Clayton 2009; Kalsnes et al 2010; Knill 2003). Almost all researchers involved in risk assessment in urban areas agree that the combination of geohazard maps with the maps of urban environment vulnerability is the most promising approach to the georisk assessment in cities (Marchiori-Faria et al 2006; Mora 2010; Price et al 2018; Zhang et al 2006). So far, assessment and mapping of exogenous geological hazards is the first step in georisk analysis in urban areas. In

our research, we made an attempt to show the possibilities of using mapping methods for the geological risk assessment in the form of possible losses from geohazard manifestation by the example of Moscow megacity.

Engineering Geological Conditions In Moscow

As applied to Moscow area, the exogenous geohazards that affect the urban geoenvironment originate from its peculiar geological setting and engineering geological conditions. Engineering geological conditions in the Moscow region have been comprehensively studied before by many previous researchers (Bolysov et al 2017; Golodkovskaya and Lebedeva 1984; Koff et al 2006; Kozlyakova et al 2015; 2016; Kutepov et al 2011; Osipov and Medvedev 1997; Osipov 2008; 2014; Sergeev 1982). Geomorphologically, Moscow is located within three natural geographical regions, i.e., Smolensk-Moscow upland in the Northwest, Meshchera lowland in the East, and Teplyi Stan upland in the South-Southwest. These regions are divided by the valleys of the Moscow and the Yauza rivers. Within the city territory, the Moscow River valley consists of the floodplain and three alluvial terraces lying above the floodplain. The surface topography has been transformed substantially in the city by technogenic impact. Many minor rivers and creeks were removed from the surface to flow in underground pipes. Gullies were backfilled; the outlines of river banks were modified, as well as the depth and width of the Moscow and the Yauza river channels; the water level in the Moscow river was raised. The absolute elevations of the terrace and floodplain surfaces were altered by levelling and backfilling by human activities. The floodplain was partially flooded.

In terms of geology, Moscow is located within a vast syncline in the centre of the East European platform covered by a thick mantle of sedimentary deposits. Within the depth of technogenic impact, the sedimentary mantle in Moscow area consists of stratified Carboniferous, Jurassic, Cretaceous, and Quaternary deposits of various genesis.

Geological structure of Moscow is extremely variable (Fig. 1). This variability arises mainly due to the river erosion and it is pronounced in abrupt fluctuations of thickness and lithological composition of soil and rock complexes.

The mid- and upper Carboniferous limestone, marl and clay occur at a depth 5-150 m. Carbonate deposits are intensely fractured and karstified. Limestone, dolomite, marl and clay of Carboniferous age are overlain by Meso-Cenozoic sandy-clayey deposits. Carboniferous deposits underlie immediately the Quaternary deposits in thalwegs and slopes of preglacial and modern river valleys. Mesozoic deposits consist of mid-Jurassic continental deposits of Bathonian and Callovian stages, marine sandy-clayey mid- and upper Jurassic deposits, marine sandy-clayey mid- and upper Jurassic deposits of Callovian, Oxfordian and Tithonian stages, as well as marine mainly sandy deposits of Cretaceous system. Bathonian and Callovian deposits are represented by interlayers and lenses of dark grey and brown sand, loam and sandy loam with coal inclusions and interlayers and lenses of sand. Bluish grey and brown dense clay with sandy interlayers also occur locally. The thickness of Bathonian-Callovian strata rarely exceeds 10 m. These deposits are preserved in the local depressions of the Carboniferous massif roof. They are overlain by middle and upper Jurassic Callovian and Oxfordian clay, or sporadically, by Quaternary sand, sandy loam and loam. Callovian and Oxfordian clay were deposited during the Jurassic sea, which spread over the entire Moscow territory. Once the sea retreated, the continuous mantle of these deposits overlying the Carboniferous massif covered the entire territory of Moscow. They were eroded later in Cenozoic era by the rivers. The preserved thickness of Jurassic clay varies significantly. It depends on the preJurassic subcrop topography, with maximum thickness (50 m) in the central part of the Main Moscow depression in the south of the city; whereas this thickness rarely exceeds 10 m at the preJurassic watersheds in the north of the city. These are dark grey and black homogenous dense micaceous clay with few fossil fragments.

On the preglacial watersheds, Callovian and Oxfordian clay are overlapped by marine sandy-clayey Tithonian deposits; whereas in the preglacial valleys, this clay underlies the lower and middle Quaternary alluvial and fluvioglacial sands.

Marine sand and clay of Tithonian age are preserved only on the preglacial watersheds, where they overlie discordantly the Callovian-Oxfordian clay. The thickness of the Tithonian strata ranges from 0-1 to 10-30 m depending on the preglacial topography, with the maximal thickness being registered in the southwest of Moscow (within the Teply Stan elevation). Cretaceous deposits are preserved and uneroded predominantly in the south and southwest of Moscow, where they compose preQuaternary and modern interfluves. They are represented by up to 40 m thick marine deposits overlying the Tithonian upper Jurassic strata. The bottom of the Cretaceous massif is composed of brown, dark grey and greenish grey sands and sandstones with pebbly phosphorite layer at the basement. Upward by the cross-section, they are replaced by black and dark grey clay, which is overlain by light yellow and yellow-grey fine-grained sand with very few thin interlayers of loose sandstone. Cretaceous deposits are overlain by the Quaternary strata.

Quaternary deposits are represented by moraine loam of three glaciation periods; interfluvial (mainly sandy) deposits; alluvial sands of three terraces above the floodplain of the Moscow River and its tributaries, as well as technogenous deposits. The thickness of the Quaternary deposits ranges from few meters to 50 m. It's maximum is registered in the south and southwest of Moscow, where the erosion activity of the modern river network was the weakest. The Quaternary strata are very thick within the deep preglacial valleys filled with fluvioglacial sand (Fig. 1). Technogenous deposits cover almost the entire city territory, with their thickness reaching 15-20 m.

Groundwater aquifers in Moscow area are confined to the Quaternary and Mesozoic sandy and sandy-loamy deposits, as well as to Carboniferous limestone massif. In the areas, where low-permeable moraine loam strata occur, the following aquifers are distinguished: (a) above-moraine unconfined aquifer, and (b) intra-moraine and under-moraine (often confined) aquifers. In the areas, where moraine is absent, the Quaternary groundwater aquifer is unconfined as a rule. Mesozoic aquifers may be both unconfined and confined. Fractured karstic aquifers in Carboniferous limestone showed a high hydraulic head in Moscow in the early 20th century. However, intense water extraction in the 20th century lowered their head significantly, and at present, the upper water horizons in Carboniferous limestone massif are mainly unconfined. However, the deep Carboniferous aquifers may show the hydraulic head up to 25 m.

Due to the specific engineering geological structure of Moscow, the city territory is subjected to a number of exogenous geological processes (EGP). The principle exogenous geohazards in Moscow are karst-suffosion sinkholes, land subsidence, landslides, and waterlogging. Karst and suffusion most often develop in thalwegs and on slopes of preglacial valleys, where the upper Jurassic clay is partially or completely eroded (Kutepov et al 2009; 2011). Upon certain hydrodynamic conditions, the clay stratum may be destroyed, and the suffosional downward flow of sand to karstic caverns and fractures in limestones may be triggered. This process results in sinkhole formation on the surface. Karst and suffusion develop most intensively in the northwest of Moscow, were the preJurassic and preglacial channels have eroded partially or completely the overlying Mesozoic deposits. Limestone is highly karsitified there, and more than 40 karst sinkholes are registered in that area (Kozlyakova 2016).

Landslides are mostly confined to the slopes of the Moscow river valley and its tributaries. One can distinguish deep landslides with a slipping surface confined to the Jurassic clay and shallow landslides confined in Quaternary deposits only. Deep landslides affect 15 slopes in the Moscow river valley within the city boundaries. Surface landslides are more widespread. They are registered both in the areas disturbed by

major landslides and in the valleys of minor rivers, brooks, and gullies. Waterlogging development is controlled by the modern topography in Moscow. The areas, within which the uppermost aquifer occurs at a depth of less than 3 m are considered to be waterlogged. These are mainly floodplains of the Moscow River and its tributaries. The perched groundwater horizons may form in watershed areas, where moraine loam is preserved. The areas, within which the groundwater level occurs at a depth 3-5 m, are considered as potentially prone to waterlogging. Permanently waterlogged areas occupy about 30% of Moscow;

and 25% of territory may be classified as potentially prone to waterlogging (Osipov 2014).

The above-mentioned EGPs exert a significant impact on Moscow geoenvironment affecting the urban infrastructure. They should be taken into consideration upon both surface and subsurface construction. The subsurface construction is endangered by karstification and fracturing of crystalline limestone, decompaction and swelling of clay, quicksand phenomena, and groundwater breakthrough to the tunnels.
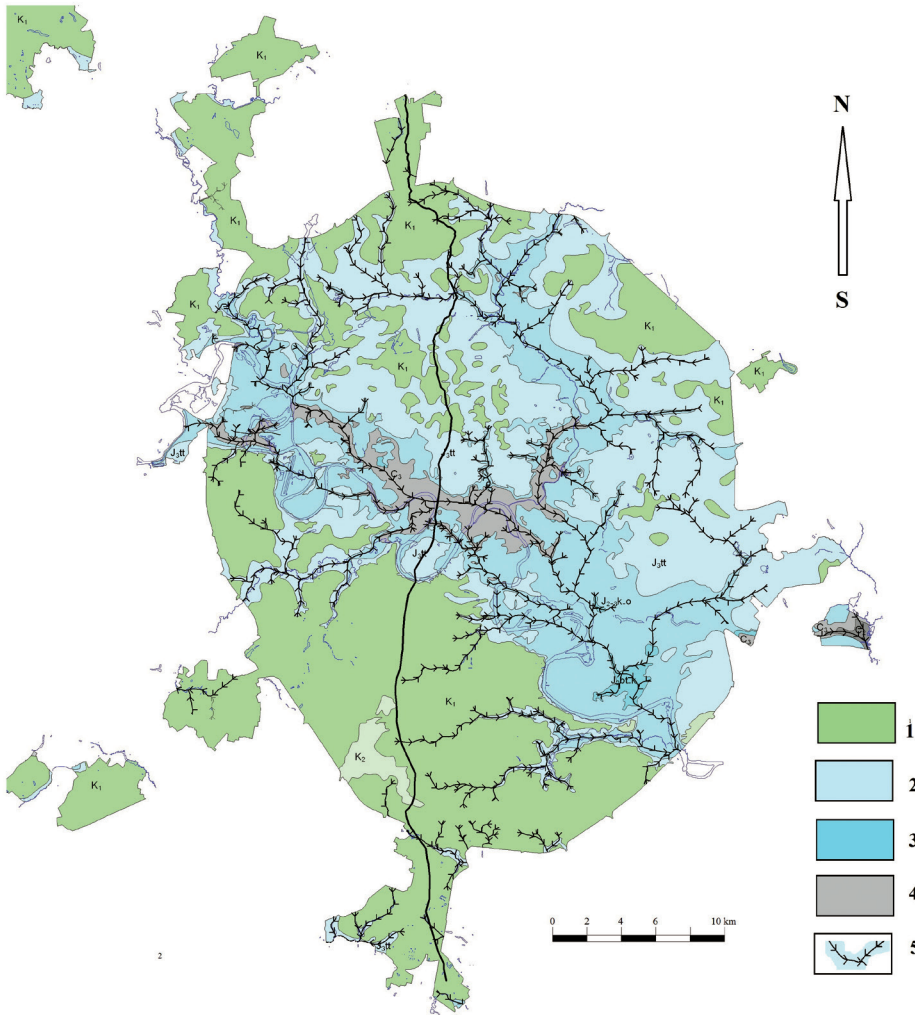
Fig. 1. Geological map and geological cross-section of the Moscow territory. Designations: 1 – Cretaceous deposits, 2 – upper Jurassic deposits, Tithonian stage, 3 – mid- and upper Jurassic deposits (Oxfordian, Callovian, and Bathonian stages), 4 – Carboniferous deposits, 5 – thalwegs of preglacial erosional cuttings

Approaches To Geohazard And Risk Assessment In Moscow

In western countries, urban geology has developed as a special field of geological science, and its role is becoming more important in the last decades (Bell et al 2009; Brennard 1998; Culshaw and Price 2011; Legget 1973; 1987; Marker 2009; 2016; Pereyra 2003; Tan 2009). Lately, urban geologists including engineering geologists have gained huge experience in assessing hazardous geological processes in cities, with one of the principal methods being engineering geological zoning and GIS-based special mapping of urban areas (Burns, 2015; Cavaleiro et al 2009; Chatterjee 2006). It is commonly recognized now that spatial planning with consideration of natural hazards maps laying restrictions on the territory use appears to be the most efficient economic tool for providing sustainable urban development (Price et al 2016; Taselaar 2008; Tsangaratos et al., 2014). The development of geohazard risk assessment procedure is now the most acute issue for urban sustainable development (Rauh et al 2008). The most common way is combining the maps of hazardous geological processes with the maps of urban environment vulnerability (Blong 2003; Cormonias et al 2014; Thierry 2001; Torok 2006). However, due to geodata uncertainties, this problem cannot be considered to be solved on a quantitative level anywhere in the world (Clayton 2001).

Geological risk is defined as the qualitative or quantitative measure of a geological hazard or a number of hazards determined for a particular object or particular territory in the form of possible absolute or relative economic losses (damage) (Cascini 2014; Ragozin 2003; Ragozin and Yolkin 2006; Osipov et al 2017; Recommendations... 2002). This definition suggests that risk is a function of the hazard impact value and the engineering structure (territory) vulnerability.

The authors applied different methods for the study of geohazards operating in Moscow depending on the purpose and the scale of the study. For the preliminary stage of investigation, to a small scale, special mapping and zoning of city surface or subsurface environment appears to be the most appropriate; whereas, at the follow up stages of survey, mapping is combined with the calculation and analytical methods.

In authors' view point, the risk of economical loss caused by exogenous geological hazards in cities should be assessed separately for already existing urban infrastructure and for future planned construction. In both cases, upon mapping the qualitative comparative assessment of geological risk is made (Fig.2). For existing infrastructure, the main aim of risk mapping is to outline the territories, for which special requirements should be laid on engineering survey, as well as restrictions and prohibitions should be introduced on urban engineering development. For future construction, the risk maps permit comparing alternative project decision variants in order to minimize economic losses from geological hazards upon the construction and operation of buildings and other engineering structures. Both approaches have been tested in Moscow.

Assessing Geohazards And Georisk For The Existing Urban Infrastructure

For assessing georisk that is caused by exogenous geohazards for the existing infrastructure, we have developed the mapping procedure that involves the following steps:

- assessment and mapping of exogenous geological processes (EGPs) according to the degree of hazard;

-assessment and mapping of urban environment vulnerability to EGPs (where the urban environment is taken to mean the city territory with buildings and on-surface engineering facilities);

-distinguishing risk categories by the analysis of the hazardous geological processes affecting the city territory and surface urban infrastructure;

- compilation of the risk map by superposition of the integral map of EGPs hazard and the map of urban environment vulnerability.

The qualitative comparative assessment and geological risk mapping were performed on the basis of integral assessment of EGP hazard and the functional zoning of city territory. The
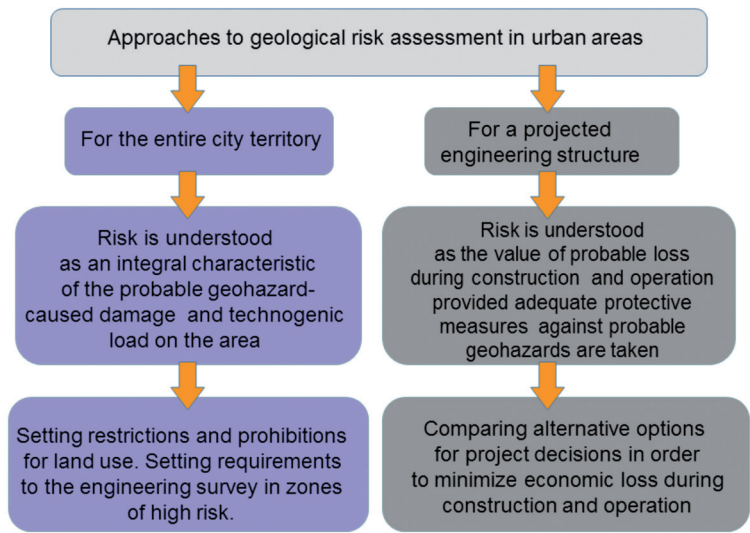
Approaches to geological risk assessment in urban areas

For the entire city territory

For a projected engineering structure

Risk is understood as an integral characteristic of the probable geohazard-caused damage and technogenic load on the area

Risk is understood as the value of probable loss during construction and operation provided adequate protective measures against probable geohazards are taken

Setting restrictions and prohibitions for land use. Setting requirements to the engineering survey in zones of high risk.

Comparing alternative options for project decisions in order to minimize economic loss during construction and operation

Fig. 2. Two approaches to the georisk assessment in urban areas

integral hazard assessment implies revealing the possible adverse changes in urban environment and obstacles to construction and operation of buildings and engineering structures in the areas of EGPs development and the subsequent typification of the territory by its favorability. The "Map of geoecological state of the Moscow territory (assessment of hazardous exogenous geological processes) prepared in a scale 1 : 50 000, is taken as the basis of this assessment (Kozlyakova et al, 2015). Here, the object at risk is the urban environment, which includes the city territory with the surface infrastructure.

As was mentioned above, the most hazardous EGPs in Moscow are landslides (deep, above all), as well as karst and suffosion collapses and surface subsidence (Kutepov et al., 2009; 2011). These processes cause damage or ruining of buildings, leading sometimes to catastrophic consequences. Waterlogging is another geological process developing in Moscow, which is less hazardous to buildings and engineering structures. However, being a permanently acting factor widespread by the area, waterlogging may cause substantial economic damage to the city. Five categories of geoecological state are distinguished in the Moscow territory from the comprehensive analysis of the above-mentioned EGPs, i.e., favorable, conventionally favorable, conventionally unfavorable, unfavorable, and very unfavorable (Fig. 3).

Geoecological state (assessment of geohazards) \ Vulnerability	Low (recreational zones)	Moderate (industrial and transport zones)	High (public and residential zones)
Favorable	No risk		
Conventionally favorable	Low risk		Moderate risk
Conventionally unfavorable			
Unfavorable	Moderate risk	High risk	Very high risk
Very unfavorable			

Fig. 3. The schematic state and functional zones of geological risk map in Moscow

The functional zoning of Moscow territory includes 5 types of functional zones: transport, recreational, industrial, social (public), and residential (Fig. 3). In this way, this zoning gives us a tentative idea about the vulnerability of separate parts of the city to the hazardous EGPs. The density of territory building-up with on-surface permanent engineering structures usually increases in the row: recreational - transport - industrial - public - residential zones. These parameters appear to be one of the most vivid and reliable characteristics of urban territory vulnerability. The classification is based on the density of territory building-up with on-surface permanent engineering structures as well as on the degree and type of EGPs' impact on urban environment. Risk categories are distinguished depending on the level of possible loss caused by the manifestation of individual processes or their combinations.

Therefore, to the first approximation, the idea about the geological risk in Moscow can be obtained from the superposition and the analysis of geoecological conditions (hazardous EGP), the functional zoning of the territory and the distinguished risk categories.

In this analysis, estimation and mapping of vulnerability of urban territory and its infrastructure seems to be the most difficult problem (Osipov et al, 2017). Functional zoning surely gives only tentative and rough index of vulnerability. Therefore, now one can only speak about the schematic risk map for the existing urban infrastructure. The comprehensive procedure of vulnerability analysis should include the estimation of density, type, and age of housing development as well as the assessment of geohazard impact on the urban environment.

On the basis of the developed georisk assessment procedure, the authors have compiled the schematic geological risk map for the existing infrastructure in Moscow arising from EGPs to a scale of 1:50000. This map shows the risk as a comparative integral characteristics of the probable damage caused by the geological hazards as well as the level and type of the technogenic load of the territory (Fig. 4).

Assessing Geohazards And Georisk For The Future Subsurface Construction

The risk of losses for a particular engineering structure at the stage of its construction may be analyzed only qualitatively by assessing the impact of geohazards on this engineering structure, since the value of engineering structure vulnerability will be the same in this case. Assuming that this engineering structure may be built in different engineering geological conditions, the risk will be characterized by the possible damage caused by geohazards within the areas of a certain type of engineering geological conditions. Upon this approach, the qualitative risk-analysis in this case may be reduced to assessing the impact of geohazards on the given engineering structure by comparing the future expenditures for its construction and operation under different engineering geological conditions.

For instance, for a projected metro tunnel driven at a shallow depth by an open-pit method, we propose the following risk-assessment procedure. It consists of the following steps:

1. To know the geological structure and hydrogeological conditions in the foot and walls of the tunnel at the planned construction depth proceeding from the 3D model of geoenvironment.

2. To typify the engineering geological conditions and the analysis of geohazard impact on the engineering structure for each type of engineering geological conditions;

3. To determine the possible losses (expenditures) during the construction and operation of the facility;
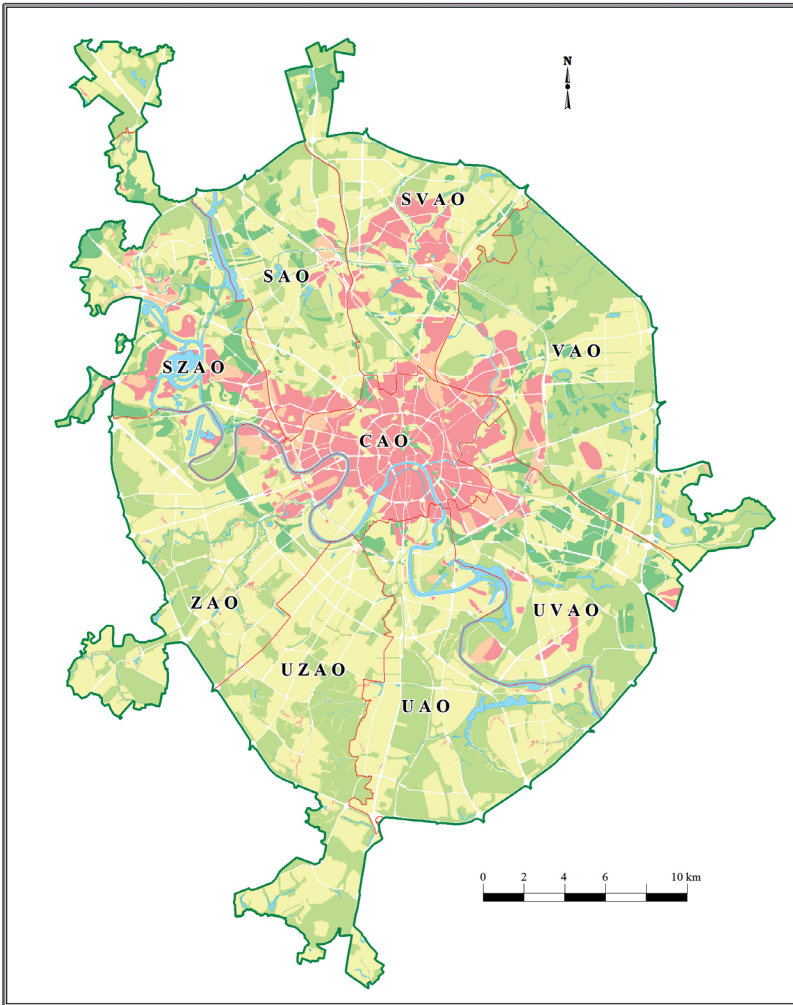
Fig. 4. The schematic map of geological risk for existing urban infrastructure in Moscow. See Fig. 3 for designations

4. To distinguish and substantiate the comparative qualitative categories of risk;

5. To build the map of geological risk.

During present study, the authors distinguish three main groups of ground conditions that one can come across in the bottom and walls of the shallow metro tunnel driven by an open-pit method in Moscow subsurface:

- Meso-Cenozoic sand with interlayers and lenses of sandy loam and loam (Quaternary, Cretaceous and Jurassic). For the most part, soils are water-saturated. Aquifers are confined and unconfined.

-Jurassic clay, weakly permeable.

-Carboniferous terrigenic and carbonate deposits: limestone, dolomite, marl, and clay. Unevenly watered with confined aquifers.

The combinations of these types in the walls and in the bottom of the tunnel result in 7 types of possible engineering geological conditions along the tunnel route (Fig. 6). The possible damage for the tunnel under construction was assessed proceeding from the analysis of the impact on it of such geohazards as groundwater and quicksand breakout to the construction pit, suffusion, and karst-suffosion processes. As a result, we distinguished and substantiated four

risk categories: very high, high, moderate, and low. (Fig. 6). Very high geological risk is recognized for the construction and operation of tunnels in Meso-Cenozoic water-saturated sand, which is proved by many unfortunate cases of the shallow tunnel construction on Moscow. Meso-Cenozoic sand outcropping in the tunnel's walls gives rise to a high risk for an engineering structure irrespectively of the deposit types in the tunnel foot. Running a tunnel in the karstified Carboniferous deposits (limestone, dolomite, marl, and clay), due to their karstification and uneven watering with confined groundwater aquifers produces a

moderate risk to engineering structures. A low risk is usually identified for the tunnels drawn in the low permeable Jurassic clay horizon.

According to this procedure, we have compiled the map of geological risk for the construction and operation of shallow tunnels (a depth of 20 m) to a scale of 1: 100 000 . The representative city territory within the Moscow ring highway was taken for this purpose, for which the 3D model of geoenvironment has been built, permitting us to analyse the geological structure of the area at any desired level to a depth of 100

Deposits in the tunnel walls / Deposits in the tunnel foot	Meso-Cenozoic sand with interlayers and lenses of sandy loam and loam; mainly water-saturated; confined and unconfined aquifers	Weakly permeable Jurassic clay	Carboniferous terrigenic and carbonate deposits: limestone, dolomite, marl, and clay. Unevenly watered with confined aquifers .
Meso-Cenozoic sand with interlayers and lenses of sandy loam and loam; mainly water-saturated; confined and unconfined aquifers	Very high risk	Moderate risk	
Weakly permeable Jurassic clay	High risk	Low risk	
Carboniferous terrigenic and carbonate deposits: limestone, dolomite, marl, and clay. Unevenly watered with confined aquifers.	High risk	Moderate risk	Moderate risk

Fig. 5. The geological map risk for the construction and operation of shallow tunnels (at a depth of 20 m)

m from the surface. These maps may be compiled for different tunnel depth, which permits to compare the alternative project options in the viewpoint of their safety and economic efficiency at the investment stage.

The task of further studies is to develop mapping technologies and to substantiate scientifically the compilation of the integral map of geological risk for the future subsurface construction. This map may be compiled by superposition and the analysis of the risk maps for two or three levels of subsurface development. The principal aim of this map is to reveal the zones at geological risk, within which a considerable damage may arise at any depth of laying engineering facility, and recommendations on special protective measures should be given. The three-dimensional model of Moscow geoenvironment permits obtaining actual data necessary for solving this problem.
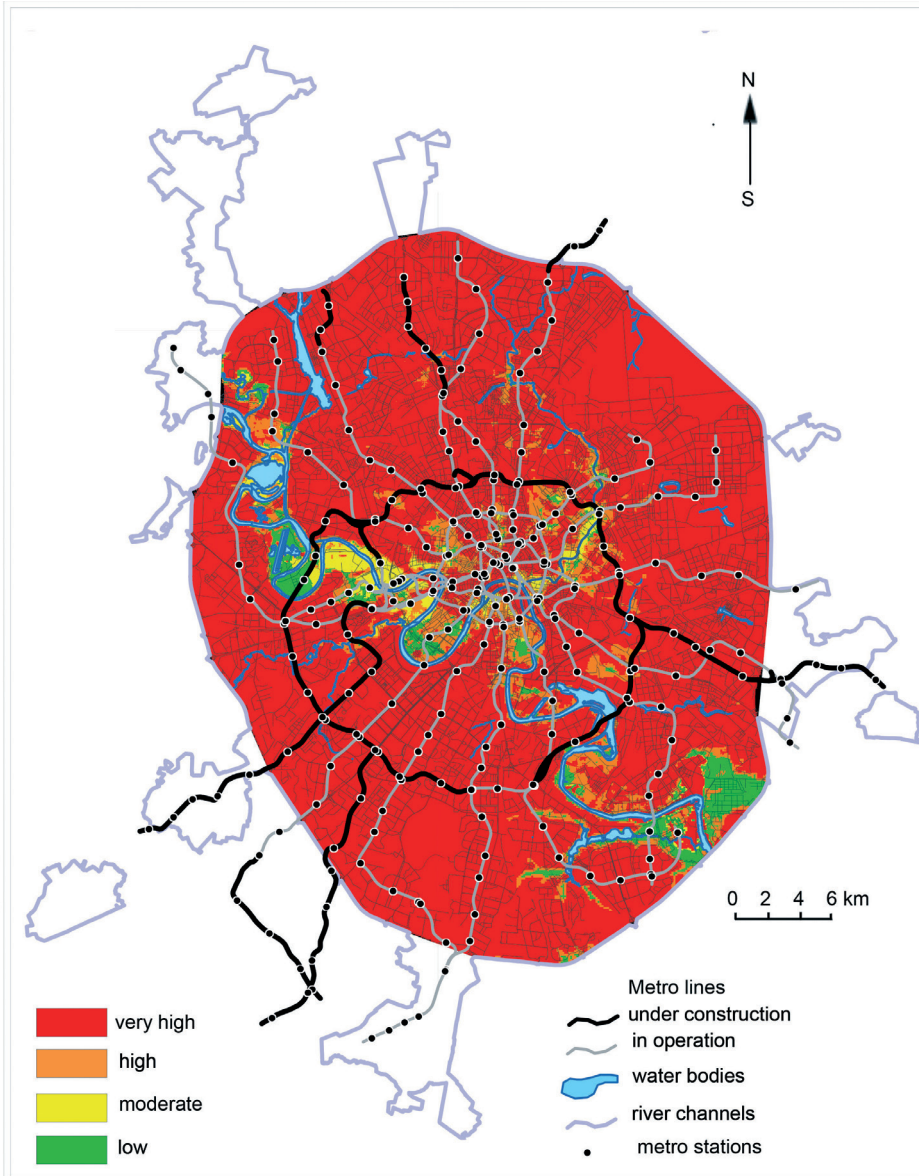
Fig. 6. The geological risk map for the construction of a metro tunnel at a depth of 20 m in Moscow. See Fig. 5 for designations

CONCLUSION

Geological risk mapping is the principal method in risk analysis at the initial stages of projecting urban development. The performed studies in assessment and mapping of geological risk in Moscow attests to the diverse possibilities in the risk-analysis tool application to engineering geology of urban areas. Approaches to risk assessment differ depending on the purpose and scale of research. For the city territory, the result of risk-analysis most often consists in zoning the city territory on the basis of the risk level. It is hard to estimate quantitatively the level of geological risk, the more so, for the entire city territory. However, the qualitative comparative risk assessment also appears to be very important. For the entire city territory, geological risk is estimated as an integral characteristic of probable damage caused by geohazards and of technogenic load in this area. For a particular projected engineering structure, its risk is estimated as the value of probable expenses during its construction and operation. Geological risk mapping for future construction in cities appears to be a new approach in risk analysis. Application of this approach permits us to compare the alternative variants for driving linear engineering facilities (e.g., metro) in order to avoid substantial economic losses caused by geohazards. In cities, it is often difficult to change project decisions by moving construction to less risky geoenvironment. The purpose of the risk maps is to manage risks by predicting geohazard manifestations in the construction area and by giving recommendations on special protective measures for substantiating construction costs.

ACKNOWLEDGEMENTS

REFERENCES

Admiraal H. and Cornaro A. (2016). Why underground space should be included in urban planning policy – And how this will enhance an urban underground future, Tunnelling and Underground Space Technology, 55, pp. 214-220.

Bell F.G., Culshaw M.G., Forster A., and Nathanail C.P. (2009). The engineering geology of the Nottingham area, UK. In: Culshaw, M.G., Reeves H.J., Jefferson, I., and Spink, T.W. (eds.) 2009. Engineering geology for tomorrow's cities. Geological Society, London, Engineering Geology Special Publications, 22, pp. 1-24.

Blong R. (2003). A new damage index. Natural Hazards, 30(1), pp.1–23

Bobylev N. (2009). Mainstreaming sustainable development into a City's Master Plan: a Case of Urban Underground Space Use. Land Use Policy, 26 (4), pp. 1128-1137.

Bobylev N. and Sterling R. (2016). Urban underground space: a growing imperative. Perspectives and current research in planning and design for underground space Use. Tunnelling and Underground Space Technology, vol. 55, pp. 1 – 5.

Bolysov S.I., Nekhodtsev V.A., and Kharchenko S.V. (2017) Subsurface relief of Moscow. Vestnik Moskovskogo universiteta. Ser.5. Geografiya, no. 2, pp. 59-71 (in Russian)

Brennard T.A. (1998). Urban geology note: Oshawa Ontario. In: P.F. Karrow & O.L. White (eds.), Geological Association of Canada, special paper 42: Urban Geology of Canadian Cities, pp. 353-364.

Irina V. Kozliakova, Olga N.Eremina et al.   SPECIFIC FEATURES OF GEOLOGICAL RISK …

04|2019

GES

171

Burns S. (2015). Urban landslides: challenges for forensic engineering geologists and engineers. In: Lollino G., et al (Eds.), Engineering geology for society and territory, Vol. 5, Springer International Publishing, Switzerland, pp. 3-11.

Campbell D. et al. (2017). Transforming the relationships between geoscientists and urban decision-makers: European cost sub-urban action (TU1206). Procedia Engineering, no. 209, pp. 4–11.

Cascini L. and Ferlisi S. (2014). Introduction to the thematic set of papers on the quantitative analysis of landslide risk. Bull. Eng. Geol. Environmn, vol. 73, no. 2, pp. 207-208.

Cavaleiro V.M., Rodrigues-Carvalho J.H.A. and Gomes L.F. (2009). Geotechnical mapping in the area of Covilha, Portugal. A method using GIS. In: Culshaw, M.G., Reeves, H.J. Jefferson, I. and Spink, T.W (eds.) Engineering Geology for Tomorrow's Cities. Geological Society, London, Engineering Geology Special Publication, 22, on CD-rom insert, paper 211

Chatterjee B. (2006). Engineering geological aspect for urban development in three capital cities in North Eastern India. In: Engineering Geology for Tomorrow's Cities. IAEG 2006, 6-10 Sept., CD-rom, paper no. 3-833.

Clayton C.R.I. (2001). Managing geotechnical risk. London: Thomas Telford.

Clayton C.R.I. (2009). Urban site investigation. In: Culshaw, M.G., Reeves, H.J. Jefferson, I. and Spink, T.W (eds.) Engineering Geology for Tomorrow's Cities. London: Geological Society, Engineering Geology Special Publication, vol. 22, pp. 15-–141.

Cormonias J. et al. (2014). Recommendations for the quantitative analysis of landslide risk. Bulletin of Engineering Geology and the Environment, vol. 73, no. 2, pp. 209-263.

Culshaw M.G. and Price S.J. (2011). The 2010 Hans Cloos Lecture. The contribution of urban geology to the development, regeneration and conservation of cities. Bulletin of Engineering Geology and the Environment, vol. 70, no. 3, pp. 333-376

Golodkovskaya G.A. and Lebedeva N.I. (1984). Engineering geological zoning of Moscow. Inzhenernaya geologiya (Engineering geology), no. 3, pp. 87-–102. (in Russian)

Kalsnes B., Nadim F., and Lacasse, S. (2010). Managing geological risk. In: Geologically active, Williams, A.L., Pinches, G.M., Chin, C.Y., McMorran, T.J., and Massey, C.I. (Eds.). Proceedings of the 11th IAEG Congress, Auckland, New Zealand, 5-10 September 2010, London: Taylor & Francis group, pp.111-126.

Knill J. (2003). Core values: the first Hans-Cloos lecture. Bulletin of Engineering Geology and the Environment, vol. 62 (1), pp. 1-–34.

Koff G.L., Likhacheva E.A., and Timofeev D.A. (2006). Geoecology of Moscow: methodology and methods of assessing the urban environment state. Moscow: Media-Press (in Russian).

Kozlyakova I., Eremina O., Anisimova N., and Kozhevnikova I. (2016). Study of geology and Carboniferous roof topography upon engineering geological mapping of Moscow territory. In.: Developments in Engineering Geology. Eggers, M.J., Griffiths, J.S., Parry, S., Culshaw, M.G. Eds., London: Geological Society, Engineering Geology Special Publication, v. 27, pp. 45-–53, http://doi.org/10.1144/EGSP27.4

Kozlyakova I.V., Mironov O.K., and Eremina O.N. (2015). Engineering geological zoning of Moscow by the conditions for subsurface construction. In: Proceedings 12th IAEG Congress, Turin, Italy: Springer, 2015, vol. 5, pp. 923-–926.

Kutepov V.M., Anisimova N.G., Eremina O.N., Kozhevnikova I.A. and Kozlyakova I.V. (2011). The map of pre-Quaternary deposits as a base for large-scale geological mapping of Moscow territory. Geoekologiya (Environmental Geoscience), no. 5, pp. 399–411. (in Russian)

Kutepov V.M., Anisimova N.G., Eremina O.N., Kozlyakova I.V., and Kozhevnikova I.A. (2009). Hazardous geological processes and geoecological conditions in Moscow. In: Proc. Second Sci.-Practical Conference on Ecological and Geological Problems in Urbanized Areas, November 26-27, 2009, Yekaterinburg. Yekaterinburg, pp. 194-196. (in Russian)

Kutepov, V.M., Kozlyakova, I.V., Anisimova, N.G., Eremina, O.N., and Kozhevnikova, I.A. (2011). Assessment of karst and karst-suffosion hazard in the project of large-scale geological mapping in Moscow. Geoekologiya, no. 3, pp. 215-226. (in Russian)

Li X, Hui Xu, Congcong Li, Liping Sun, Rui Wang (2016). Study on the demand and driving factors of urban underground space use, Tunnelling and Underground Space Technology, vol. 55, pp. 52-58,

Legget R.F. (1973). Cities and geology, New York: McGraw-Hill Book Co.

Legget R.F. (1987). The value of geology in planning. In: Culshaw, M.G., Bell, F.G. Cropps, J.C., & O'Hara, M. (eds.) Planning and Engineering geology. London: Geological Society, Engineering Geology Special Publications, issue 4, pp. 53-58.

Marchiori-Faria D.G. and Ferreira C.J. (2006). Hazard mapping as part of civil defense preventive and contingency actions: a case study from Diadema, Brazil. In: Engineering Geology for Tomorrow's Cities. IAEG 2006, 6-10 Sept. 2006, CD-rom, paper no. 154.

Marker B.R. (2009). Geology of megacitites and urban areas. Engineering Geology for Tomorrow's Cities. Culshaw, M.G., Reeves, H.J. Jefferson, I. and Spink, T.W., Eds., Geological Society, London, Engineering Geology Special Publication, no. 22, pp. 33-48

Marker B.R. (2016). Urban planning: the geoscience input. In: In: Eggers, M.J., Griffiths, J.S., Parry, S & Culshgaw, M. G. (Eds.), Developments in Engineering Geology. Geological Society, London. Engineering Geology Special Publication, 27, pp. 35-43,

Merkin V.E., Zertsalov, M.G., Konyukhov, D.S. (2013) The concept of complex development of the Moscow subsurface at the present stage. Available at: https://undergroundexpert. info/issledovaniya-i-tehnologii/nauchnye-stati/kontseptsiya-osvoeniya-podzemnogo-prostranstva-moskvy/print/ (in Russian)

Mora S. (2010). Disasters should not be protagonists of Disaster Risk. In: Geologically active, Williams, A.L., Pinches, G.M., Chin, C.Y., McMorran, T.J., and Massey, C.I. (Eds.). Proceedings of the 11th IAEG Congress, Auckland, New Zealand, 5-10 September 2010, London: Taylor & Francis group, pp.89-–110.

Osipov V.I. (2014). Large-scale thematic geological mapping of Moscow area. In: G. Lollino et. al. (Eds.) Engineering Geology for Society and Territory. Vol. 5, Springer International Publishing Switzerland, pp. 11–16.

Osipov V.I. (2008). Geological conditions of Moscow urban development. Moscow: ZAO Mir, 36 p. (in Russian)

Osipov V.I. and Medvedev O.P. (Eds.). (1997). Moscow. Geology and the City. Moscow: Moskovskie uchebniki i kartolitografiya Publ., 400 p. (in Russian)

Osipov V.I., Burova V.N., and Karfidova E.A. (2017). Methodological principles of geohazard vulnerability evaluation of capital construction assets in urbanized areas. Soil mechanics and foundation engineering, vol. 53, no. 6, pp. 420–425

Pereyra F.X. and Rimoldi H. (2003). Geological and environmental aspects of the development of megacities: the case of Buenos Aires metropolitan area (AMBA), Argentina. Bulletin of Engineering Geology and the Environment, 62(4), pp. 431-351

Price S.J., Ford J.R., Campbell S.D.G., and Jefferson I. (2016). Urban futures: the sustainable management of the ground beneath cities. In: Eggers, M.J., Griffiths, J.S., Parry, S & Culshaw, M. G. (Eds.). Developments in Engineering Geology. Geological Society, London. Engineering Geology Special Publication, 27, pp. 19-33,

Price S.J., Terrington R.L., Busby J., Bricker S., Berry T. (2018). 3D ground-use optimisation for sustainable urban development planning: A case-study from Earls Court, London, UK. Tunnelling and Underground Space Technology, no. 81, pp. 144–164

Ragozin A.L. (ed.). (2003). Natural hazards of Russia. Assessment and management of natural risks. Topical vol., Moscow: KRUK, 320 p.(in Russian)

Ragozin A.L. and Yolkin V.A. (2006). Geological risks, formation and assessment in urbanized areas in Russia. In.: Engineering Geology for Tomorrow's Cities. IAEG 2006, 6-10 Sept., CD-rom, paper no. 282.

Rauh F. Neumann P., and Bauer, M. (2008). Practical experience with geological and geotechnical risks in urban areas – insights from case studies. In: Proceedings of II European Conference of IAEG, Madrid, Spain, 15-19 September 2008 "Cities and their Underground Environment", paper no. 124.

Recommendations on geological risk assessment in Moscow territory. (2002). Ragozin A.L., Ed., Moskomarkhitektura, GU GO ChS g. Moskvy. Moscow: GUP NIATs Publ. (in Russian)

Sergeev E.M. (1982). Geological basement of Moscow. Gorod, priroda, chelovek [City, nature, man]. Moscow: Mysl, pp. 109-142 (in Russian)

Sterling R., Admiraal, H., Bobylev, N., Parker, H., Godard, J.P., Vähäaho, I., Rogers, C.D.F., Shi, X., Hanamura T. (2012) Sustainability Issues for Underground Space in Urban Areas. Proceedings of the ICE - Urban Design and Planning, vol. 165, issue 4, December 2012. pp. 241–254 (14).

Tan B.K. (2009). Urban Geology of Kuala Lumpur and Ipoh, Malaysia. In: Culshaw, M.G., Reeves, H.J. Jefferson, I. and Spink, T.W (eds.) Engineering Geology for Tomorrow's Cities. Geological Society, London, Engineering Geology Special Publication, 2009, 22, on CD-rom insert, paper 24

Taselaar F.M. and Kamphuis A. (2008). Spatial planning and the use of the underground in The Netherlands In: Proceedings of II European Conference of IAEG, Madrid, Spain, 15-19 September 2008 "Cities and their Underground Environment" CD-rom, paper no.070.

Thierry P. and Vinet L. (2001). Mapping an urban area prone to slope instability: Greater Lyons. Bulletin of Engineering Geology and the Environment. 2001, vol. 62, no. 2, pp. 135-143.

Torok Akos, Xeidakis G., Kleb B., and Marinos P.G. (2006). Karst-related engineering geological hazards, a comparative study of Hungary and Greece In: Engineering Geology for Tomorrow's Cities. IAEG 2006, 6-10 Sept. 2006, CD-rom, paper no. 4-353.

Tsangaratos P., Rozos D., Ilia I., and Markantonis K. (2014). The use of a spatial multi—criteria technique for urban suitability assessment, due to extensive mass movements. The case study of Vitala village, Kimi, Euboea, Greece. In: Proceedings XII IAEG Congress, Torino, vol. 5, pp. 339-345.

Wende W., Huelsmann W., Marty M., Penn-Bressel G., Bobylev N. (2010). Climate protection and compact urban structures in spatial planning and local construction plans in Germany. Land Use Policy, vol. 27, issue 3, pp. 864-868.

Zhang F., Yang Q., Jia X., Liu J., and Wang B. (2006). Land-use optimization by geological hazard assessment in Nanjing City, China. In: Engineering Geology for Tomorrow's Cities. IAEG 2006, 6-10 Sept. 2006, CD-rom, paper no. 324.

Thanh Tien Nguyen

Faculty of Surveying, Mapping and Geographic Information, Hanoi University of Natural Resources and Environment, Vietnam

* Corresponding author: tdgis_ntthanh@163.com

FRACTIONAL VEGETATION COVER CHANGE DETECTION IN MEGACITIES USING LANDSAT TIME-SERIES IMAGES: A CASE STUDY OF HANOI CITY (VIETNAM) DURING 1986-2019

ABSTRACT. The objective of the study is to assess changes of fractional vegetation cover (FVC) in Hanoi megacity in period of 33 years from 1986 to 2016 based on a two endmember spectral mixture analysis (SMA) model using multi-spectral and multi-temporal Landsat-5 TM and -8 OLI images. Landsat TM/OLI images were first radiometrically corrected. FVC was then estimated by means of a combination of Normalized Difference Vegetation Index (NDVI) and classification method. The estimated FVC results were validated using the field survey data. The assessment of FVC changes was finally carried out using spatial analysis in GIS. A case study from Hanoi city shows that: (i) the proposed approach performed well in estimating the FVC retrieved from the Landsat-8 OLI data and had good consistency with in situ measurements with the statistically achieved root mean square error (RMSE) of 0.02 (R^2=0.935); (ii) total FVC area of 321.6 km^2 (accounting for 9.61% of the total area) was slightly reduced in the center of the city, whereas, FVC increased markedly with an area of 1163.6 km^2 (accounting for 34.78% of the total area) in suburban and rural areas. The results from this study demonstrate the combination of NDVI and classification method using Landsat images are promising for assessing FVC change in megacities.

KEY WORDS: Fractional vegetation cover; Landsat images; Change assessment; Megacities; Hanoi, Vietnam

INTRODUCTION

Vegetation is a general term for the plant community on the ground surface, such as forests, shrubs, grassland and agricultural crops, and it can intercept rainfall, alleviate runoffs, prevent desertification and conserve soil and water (Zhang et al.

2013a). Vegetation plays an important role in the exchanges of carbon, water, and energy at the land surface (Hoffmann and Jackson 2000). Fractional vegetation cover (FVC) refers to the percentage taken by the vertical projected area of vegetation (including leafs, stem and branches) in the total statistical area (Godínez-Alvarez et

al. 2009; Jing et al. 2011). FVC is not only one of the main biophysical parameters involved in the surface processes, which is also a necessary requirement for Numerical Weather Prediction, regional and global climate modelling, and global change monitoring (Avissar and Pielke 1989; Trimble 1990), but also an important parameter for describing the surface vegetation, a comprehensive quantitative variable for plant community on ground surface, and a basic data for characterizing ecosystems, playing an extremely crucial role in the study of regional ecosystems (Godínez-Alvarez et al. 2009; Jing et al. 2011). In addition, it can be also a key parameter in thermal remote sensing, since it is a basic parameter from which surface emissivities can be estimated (Jiménez-Muñoz et al. 2009). In terms of the state-of-art and development trend in the research on the FVC estimation, Zhang et al. (2013a) indicated the three main methods including: field measurement, remote sensing and a combination of the two. The former is a traditional method for the estimation of FVC, which includes visual estimation method, sampling method and instrument method according to different measuring modes (Zhang et al. 2013a) and plays an major role in survey of land surface vegetation. With the help of a digital camera and image processing software packages (e.g. Photoshop and ERDAS Imagine), Zhou and Robson (2001) estimated FVC faster and more accurate. However, the main advantage of these methods is that measurement is nearly impossible to gather enough data over a large area (Zhang et al. 2013a). The occurrences of remotely sensed imageries overcome most of these limitations of conventional methods. Remote sensing can be considered as an effective tool for observing the distribution and evolution of the FVC. The characteristics of large scale and periodic detection with remote sensing data make it possible to obtain vegetation coverage and its dynamic change in a large area (Chen et al. 2010; Xing et al. 2009). Particularly, since remotely sensed imageries of high spatial resolution satellite sensors such as Landsat Thematic Mapper (TM), Enhanced Thematic Mapper Plus (ETM+) and most recently the Operational Land Imager (OLI) started to become available, the FVC estimation and monitoring from space became easier (Alejandro and Omasa 2007; Zhang et al. 2013b). Several methods for the FVC estimation from remotely sensed data have been developed, and the main ones include empirical model (Zhou and Robson 2001), vegetation index (Choudhury 1987), sub-pixel unmixing models (Asner and Heidebrecht 2002) and linear spectral mixture models (Li 2003; Li 2008; Wu and Peng 2010). When comparing these methods, Zhang et al. (2013a) indicated that the shortcoming of the empirical model is the rely on in situ measurement data in specific regions, and the measured result is fairly accurate only if the study area is small. Whereas, the vegetation index method may be less accurate than the empirical model in estimating the FVC in certain localities. In addition, an accurate conversion relationship between vegetation index and the FVC is usually difficult to obtain (Zhang et al. 2013a). The linear mixed model combining four bands was more effective than the simple vegetation index in estimating the FVC. Particularly, for Landsat data, a maximum of four endmembers are usually used because the three visible bands are strongly correlated with each other (Small 2001; Theseira et al. 2002). The term endmember has been used by Xiao and Moody (2005) to refer to a pure surface material or land-cover type that is assumed to have a unique spectral signature. However, when applying this approach, Zhang et al. (2013a) indicated the serious weakness is the correct identification of $NDVI_{soil}$ and $NDVI_{veg}$ values. It is therefore, in this study, a method based on a combination of NDVI and classification method is proposed to identify these $NDVI_{soil}$ and $NDVI_{veg}$ values. In this method, NDVI provides a measure of vegetation density, whereas, the classification method classifies land cover into various types. Additionally, this study attempts to discuss how FVC changes in megacities are detected through Landsat images using the two endmember SMA model. At the same time, an assessment is conducted concerning the usability of the proposed method in vegetation monitoring.

MATERIALS AND METHODS

STUDY AREA

The city of Hanoi (latitudinally from 20°35'28.2"N to 21°24'15"N and longitudinally from 105°18'28.21"E to 106°02'15"E), the capital of Socialist Republic of Vietnam is the political, economic, cultural, scientific and technological center of the whole country. It is located in the center of the Northern Delta, northern Vietnam (Fig. 1.). After the new economic policies were approved in 1986, the Communist Party and national and municipal governments attracted international investments for urban development projects in Hanoi (Logan 2005). Particularly, Hatay province, Vinhphuc province's Melinh district and 4 communes of Hoabinh province's Luongson district were merged into the metropolitan area of Hanoi from August 2008 (Hiep 2014). Rapid urban development displaced vegetation in many areas in central Hanoi. Covering an area of 3,328.9 square kilometers, Hanoi is now the largest city in Vietnam by area. With an estimated population of 8.05 million and a population density of 2,300 people for every square kilometer in 2019, Hanoi satisfies criteria of being a megacity. It is therefore Hanoi is selected for this study, exhibiting rapid population growth and urban expansion in the form of encroachment to the limited agricultural areas in limited directions at the cost of destruction of vegetation coverage. The study of FVC changes plays an important role in integration of knowledge in decision-making process for future development of the city.

MATERIALS

In this study, a total of four daytime Landsat-5 TM and Landsat-8 OLI scenes acquired in July 1986 and June 2019 with 30-m spatial resolution were collected (Tab. 1.). All the daytime Landsat TM/OLI datasets were the standard terrain correction (L1TP) products, downloaded from the U.S. Geological Survey (USGS) website, which provides systematic radiometric and geometric accuracy estimates by incorporating ground control points (GCPs) from the global land survey of 2000 (GLS2000) and employing a digital elevation model (DEM) for topographic accuracy. DEM sources include the Shuttle Radar Topography Mission (SRTM), the National Elevation Dataset (NED), Canadian Digital Elevation Data (CDED), Digital Terrain Elevation Data (DTED), and GTOPO 30 (a global DEM from the USGS). All the datasets were projected in the UTM Zone N48 and WGS 1984 ellipsoid datum. In addition, the field survey data were also collected and used to validate FVC estimated from 2019 June Landsat image.
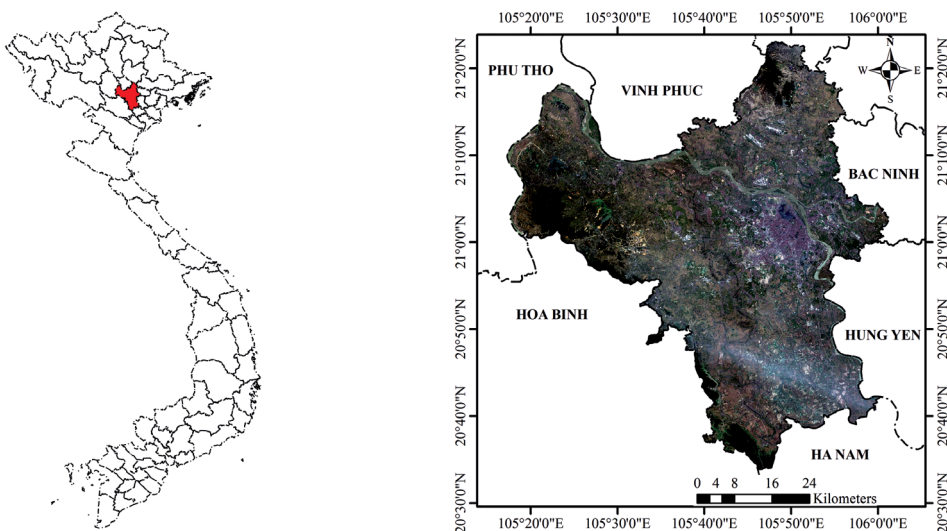
Fig. 1. A true color RGB composite from Landsat-8 OLI image collected on June 26, 2019 in Hanoi city (right), northern Vietnam (left)

Table 1. Details of the Landsat datasets used for FVC change detection in Hanoi city

Landsat sensors	Path/row	Acquisition date (yy-mm-dd)	Acquisition time (hh:mm:ss)	Spatial resolution (m)	Image quality
TM	127/045	01-7-1986	02:46:39	30	9/9
TM	127/046	01-7-1986	02:47:03	30	9/9
OLI	127/045	26-6-2019	03:23:18	30	9/9
OLI	127/046	26-6-2019	03:23:42	30	9/9

METHODS

Image pre-processing

This process involved two steps. The Landsat instruments have aged, and their characteristics have changed since launch (Chander and Markham 2003), therefore, the first step of this process involved the conversion of calibrated digital numbers (Q_{cal}) to top of atmosphere radiance ($L_{at-sensor,\lambda}$) using inflight sensor calibration parameters. The equation (1) and (2) are used to perform the (Q_{cal})-to-$L_{at-sensor,\lambda}$ conversion for Landsat-5 TM (Chander et al. 2009; Vu and Nguyen 2018a) and Landsat-8 OLI data (Nguyen and Vu 2019; Vu and Nguyen 2018b; Zanter 2015), respectively:

$$L_{\lambda} = \left(\frac{L\max_{\lambda} - L\min_{\lambda}}{Q_{cal\_max} - Q_{cal\_min}} \right) \times (Q_{cal} -$$

$$- Q_{cal\_min}) + L\min_{\lambda} \qquad (1)$$

where: L_{λ} is spectral radiance at the sensor's aperture [W/m².sr.μm]; Q_{cal} is quantized calibrated pixel values (DN values); Q_{cal_min} and Q_{cal_max} are minimum quantized calibrated pixel values corresponding to $L_{min\lambda}$ and $L_{min\lambda}$ respectively; $L_{min\lambda}$ and $L_{max\lambda}$ are spectral at-sensor radiance, scaled to and respectively [W/m².sr.μm].

$$L_{at-sensor,\lambda} = M_L Q_{cal} + \Delta_L \qquad (2)$$

where: $L_{at-sensor,\lambda}$ is the at-sensor radiance or Top of Atmospheric (TOA) radiance [W/(m²·sr·μm)] at the wavelength λ (μm); M_L is the radiance multiplicative scaling factor for the band (RADIANCE_MULT_BAND_n from the metadata); Q_{cal} is the the quantized calibrated pixel value; Δ_L is the radiance additive scaling factor for the band (RADIANCE_ADD_BAND_n from the metadata)

The second step involves compensating for atmospheric effects for Landsat reflective bands using FLAASH algorithm developed by the Air Force Phillips Laboratory, Hanscom AFB and Spectral Sciences, Inc (SSI) (Adler-Golden et al. 1999). The spectral radiance is calculated using equation (3) (Adler-Golden et al. 1998; Adler-Golden et al. 1999):

$$L^* = \left(\frac{Ap}{1 - p_e S} \right) + \left(\frac{Bp_e}{1 - p_e S} \right) + L_a^* \qquad (3)$$

where: ρ is the pixel surface reflectance; ρ_e is an average surface reflectance for the pixel and a surrounding region; S is the spherical albedo of the atmosphere; L_a^* is the radiance back scattered by the atmosphere; A and B are coefficients that depend on atmospheric and geometric conditions but not on the surface.

The values of A, B, S and L_a^* are determined from MODTRAN4 calculations that use the viewing and solar angles and the mean surface elevation of 10m. These atmospheric characteristics quantities assume a certain model atmosphere, urban aerosol type, and initial visible range of 40km. All of the Landsat sensors do not have the appropriate bands to perform the water retrieval (Flaash 2009). Therefore, in this study, the water retrieval was performed using a constant column water vapor amount for all pixels in the image which is determined according to the standard column water vapor amount for the tropical atmosphere model. After the water retrieval is performed, the spatially averaged reflectance ρ_e is estimated using equation (4) (Adler-Golden et al. 1998; Adler-Golden et al. 1999):

$$L_e = \left(\frac{(A+B)p_e}{1 - p_e S} \right) + L_a^* \qquad (4)$$

The FLAASH model includes a method for retrieving an estimated aerosol/haze amount from selected dark land pixels in the scene. The method is based on observations by Kaufman et al. (1997) of a nearly fixed ratio between the reflectances for such pixels at 660 nm and 2100 nm.

Estimation of fractional vegetation cover

The form of the linear spectral mixture analysis is (Jiménez-Muñoz et al. 2009; Li 2003; Small 2001):

$$R_k = \sum_{i=1}^{n} f_i r_{i,k} + e_k \qquad (5)$$

where: R_k is the reflectance for each band (k), n is the number of endmembers in a pixel, f_i is the fraction of endmember i, $r_{i,k}$ is the reflectance of endmember i at band k, and e_k is the residual term at band k.

The derived fractions of endmembers are often subject to the unity constraint:

$$\sum_{i=1}^{n} f_i = 1 \qquad (6)$$

Deardorff (1978) expressed heat and moisture coefficients as linear functions of fractional vegetation cover. The general form of the linear relation is written as:

$$\Phi = (1 - \sigma) \times \Phi_{\sigma=0} + \sigma \times \Phi_{\sigma=1} \qquad (7)$$

where: Φ is the heat or moisture coefficient, $\Phi_{\sigma=0}$ and $\Phi_{\sigma=1}$ are contributions from vegetated ground and bare soil, respectively, and σ is fractional vegetation cover. Wittich and Hansing (1995) applied this general formulation to NDVI for the approximation of FVC using the two endmember SMA model:

$$NDVI = f^* NDVI_{veg} + (1 - f)^* NDVI_{soil} \qquad (8)$$

which can be rewritten as:

$$f = \frac{NDVI - NDVI_{soil}}{NDVI_{veg} - NDVI_{soil}} \qquad (9)$$

where: $NDVI_{veg}$ is the NDVI value of a pure green vegetation pixel, $NDVI_{soil}$ is the NDVI of bare soil, NDVI is the value of NDVI, given by:

$$NDVI = \frac{\rho_{nir} - \rho_{red}}{\rho_{nir} - \rho_{red}} \qquad (10)$$

where: ρ_{nir} and ρ_{red} are the at-surface reflectivities obtained from sensor bands located in the near infrared (NIR) and red spectral regions.

The main problem when applying equation (7) is the correct identification of $NDVI_{soil}$ and $NDVI_{veg}$ values. This is a critical task, so these values are region- and season-specific. Hence, for global studies with very low spatial resolution data (0.15º x 0.15º), Gutman and Ignatov (1998) proposed $NDVI_{soil}$=0.04 ± 0.03 and $NDVI_{veg}$=0.52 ± 0.03, which correspond to minimum and maximum values of the desert and evergreen clusters, respectively. Sobrino and Raissouni (2000) considered a similar value for $NDVI_{veg}$ (0.5), but a $NDVI_{soil}$ value of 0.2. In this study, the land surface coverage was mainly composed of vegetation, residential area, surface water (rivers, lakes and small ponds), bare soil and sand. To accurately estimate $NDVI_{veg}$ and $NDVI_{soil}$, the land cover in the study area was first classified into five categories of vegetation, residential area, surface water (rivers, lakes and small ponds), bare soil and sand on a Supervised Maximum Likelihood (ML) Classification method, which calculated the discriminant functions for each pixel in the image (Richards and Richards 1999). The 5% and 95% confidence levels of NDVI values corresponding to each land cover type, $NDVI_{5\%}$ and $NDVI_{95\%}$, were then computed. $NDVI_{soil}$ and $NDVI_{veg}$ of each pixel were then calculated for each image using the following equations:

$$NDVI_{soil} = \sum_{i}^{n} NDVI_{5\%} {}^* P_i \qquad (11)$$

$$NDVI_{veg} = \sum_{i}^{n} NDVI_{95\%} {}^* P_i \qquad (12)$$

where: P_i is the pixel values in the ith binary images with 0 and 1 representing none and one of the above classified land cover type pixels, respectively; n is the number of land cover types.

Fractional vegetation cover change detection

The change of FVC at pixel i is computed using the following equation:

$$f_{change\_1} = f_{time\_2i} - f_{time\_1i} \qquad (13)$$

where: f_{time_1i} and f_{time_2i} are FVC of the ith pixel estimated in the first and second year. In this study, five levels of FVC changes are obtained and were ranked accordingly: (i) high decrease, if $-1 \leq f_{change} \leq -0.6$; (ii) low decrease, if $-0.6 < f_{change} \leq -0.2$; (iii) no change, if $-0.2 < f_{change} \leq 0.2$; (iv) low increase, $0.2 < f_{change} \leq 0.6$ and (v) high increase, if $0.6 < f_{change} \leq 1.0$.

RESULTS AND DISCUSSIONS

Accuracy assessment

In this study, in order to assess the accuracy of the Landsat-8 OLI data in FVC estimation, a validation of ground quadratic data and the FVC results retrieved from the Landsat-8 OLI data was made. A total of 32 in situ measurements in forest, grassland, farming land, building and surface water were used to do the fitting analysis for accuracy assessment. Data from Fig. 2 shows the result of validation of the FVC as retrieved from the Landsat-8 OLI against the 32 in situ measurements. Obviously the FVC retrieved from the June 2019 Landsat-8 OLI data fits well with the field survey results. The root mean square error (RMSE) of the FVC values retrieved from June 2019 Landsat-8 OLI with reference to the in situ data is 0.02 with R square = 0.935. Data in Figure 2 shows that there

are 2 points in the upper right corner which are located quite far away from the regression line and can be considered outliers. The measured and estimated FVC values of these points were [0.98; 0.79] and [0.7; 1.0], respectively. The value difference of the first pair shows that there was not much difference between measured and estimated FVC of 0.19 in this area. The second pair had a bigger difference in value of 0.3. Uncertainties may have affected the accuracy of the proposed method. The main uncertainty was the inconsistencies in the spatial resolution between in situ samples of (40 m × 40 m for a large area; 30 m × 30 m for a small area) and Landsat TM/OLI images (30 m × 30 m). In addition, the effects of leaf area index under different vegetation types and land cover types were also not taken into consideration in the FVC estimation. These uncertainties may have caused the fractional vegetation cover estimation results to have the above-mentioned outliers. However, these outliers only account for 6.2% of total in situ samples (2/32). More importantly, a low value of RMSE of 0.02 and a relatively high R squared ($R^2 = 0.935$) indicate the reliability of the predicted model. The results show that the proposed approach performed well in estimating FVC and had good consistency with in situ measurements.
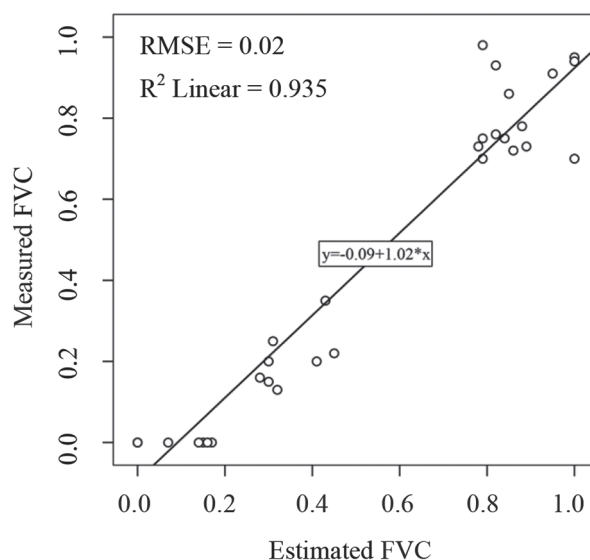

RMSE = 0.02
R^2 Linear = 0.935

$y=-0.09+1.02*x$

Fig. 2. Scatter plot of measured FVC and FVC estimated from Landsat imagery

Fractional vegetation cover

The FVC determined from Landsat TM and OLI images is shown in Fig. 3 and 4. Data in Fig. 3 shows that, in general, the FVC obtained in 2019 was higher than that of 1986, especially in suburban areas. Data from histograms in Fig. 4 shows that, when comparing to the FVC in 2019, the total area of low FVC (approximately 0) in 1986 accounts for larger area. Meanwhile the FVC ranging from 0.4 to 0.8 in 2019 had more area than that of 1986. Data from the histogram in Fig. 4. (left) and Tab. 2. obtained in 1996 demonstrates that the largest area of 964.4 km^2 was detected with low-density vegetation cover (0.2<FVC≤0.4) which accounting for 28.8% of the total area, followed by 825.0 km^2 (24.7%) of very low-density vegetation cover

(0.0<FVC≤0.2), 678.8 km^2 (16.2%) of medium-density vegetation cover (0.4<FVC≤0.6), 542.0 km^2 (20.3%) of high-density vegetation cover (0.6<FVC≤0.8), and 335.5 km^2 (10.0%) of very high-density vegetation cover (0.8<FVC≤1.0). The density line in Fig. 4. (left) shows a fairly uniform distribution among FVC intervals. The bell-shaped curve at about 0.3 indicates that the FVC in the range of from 0.2 to 0.3 takes up a larger area than the other intervals. Meanwhile, data from the histogram in Fig. 4. (right) and Tab. 2. obtained in 2019 demonstrates that the FVC area in the range of 0.0 to 0.2 had decreased to 229 km^2 (accounting for only 6.8% of the study area), low-density vegetation cover (0.2<FVC≤0.4) accounted for 616.2 km^2 (18.4%), medium-density vegetation cover (0.4<FVC≤0.6) accounted for a larger area of 1277.9 km^2
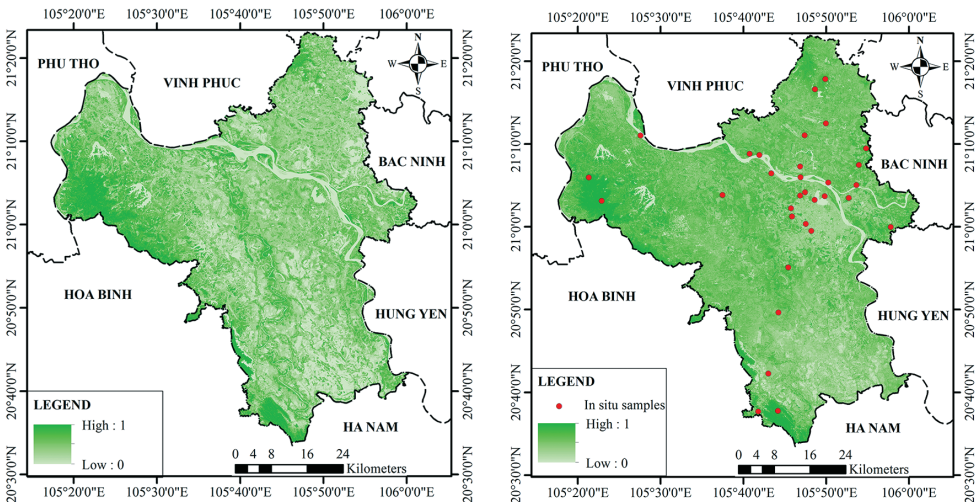
Fig. 3. Maps of FVC estimated from Landsat-5 TM images in 1986 (left) and Landsat-8 OLI images in 2019 (right) in Hanoi, Vietnam
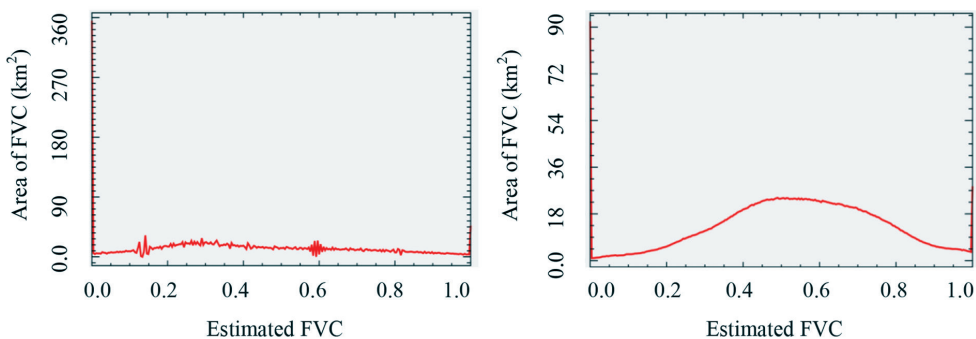
Fig. 4. Histograms of FVC estimated from Landsat-5 TM images in 1986 (left) and from Landsat-8 OLI images in 2019 (right) in Hanoi, Vietnam

Table 2. Summary of FVC areas in 1986 and 2019 in Hanoi, Vietnam

FVC	Levels	1986		2019	
		Area (km²)	Percentage (%)	Area (km²)	Percentage (%)
[0.0, 0.2]	Very low	825.0	24.7	229.0	6.8
[0.2, 0.4]	Low	964.4	28.8	616.2	18.4
[0.4, 0.6]	Medium	678.8	20.3	1277.9	38.2
[0.6, 0.8]	High	542.0	16.2	982.4	29.4
[0.8, 1.0]	Very high	335.5	10.0	240.1	7.2
Total		3345.7	100.0	3345.7	100.0

(38.2%), high-density vegetation cover (0.6<FVC≤0.8) with 982.4 km² (29.4%), and very high-density vegetation cover (0.8<FVC ≤1.0) with only 240.1 km² (7.2%). The density line in Fig. 4. (right) shows the bell-shaped curve was at in the range of 0.4-0.6 and 0.6-0.8 indicating that the FVC areas distributed mainly in the range of 0.4 to 0.8.

Fractional vegetation cover changes

The results of FVC changes during the period of from 1986 to 2019 in the area of Hanoi are shown in Fig. 5 and 6, and are statistically summarized in Tab. 3. Data from Tab. 3 demonstrates that FVC has been significantly reduced to an insignificant area of 0.9 km² (accounting for 0.03% of the Hanoi surface area) mainly occurring in the city center (Fig. 5). FVC slightly reduced an area of 321.6 km² (accounting for 9.61% of the total area). These areas were mainly detected in densely populated areas in the center of the city. No change of FVC covered an area of 1724.8 km² (accounting for 51.55%). Data from the histogram in Fig. 6 also shows that FVC change peaks at about 0.0 which occupies a very large area of 126 km² (3.8% of total area). This indicates the vegetation density in these areas remained unchanged after 33 years. Meanwhile, FVC in the range of from 0.2 to 0.6 had increased markedly with an area of 1163.6 km² (accounting for 34.78% of the total area). In addition, some areas of FVC high increase were

also detected with an area of 134.8 km² (equivalent to 4.03% of the total area). It can be seen that FVC in the Hanoi city increased mainly in suburban districts and strongly decreased in urban districts in period of 33 years from 1986 to 2019.

The results showed that fractional vegetation cover has dramatically decreased in urban districts such as Tayho, Badinh, Caugiay, Dongda, Hoankiem, Thanhxuan, Haibatrung, Hoangmai and Longbien and some areas of Donganh suburban district because of the incessant urbanization process in the central urban areas and some sub-urban areas of the Hanoi city, especially after the Doi Moi Policy started in 1986 (Logan 2005) which has greatly contributed to the rapid urbanization process in Hanoi city (Tsunoda et al. 2014). The rapid development in these urban areas has brought the replacement of among land cover types especially vegetation cover replaced with urban built-up land (Nguyen et al. 2019). These findings were similar to those reported in previous studies (Hoang 2016; Hoang 2017). Particularly, the emergence of Hatay province, Vinhphuc province's Melinh district and 4 communes of Hoabinh province's Luongson district into the metropolitan area of Hanoi in August 2008 (Hiep 2014) has led the rapid urban development displaced vegetation in many areas, especially in urban districts. The increase of FVC was mainly detected in sub-urban districts such as Socson,
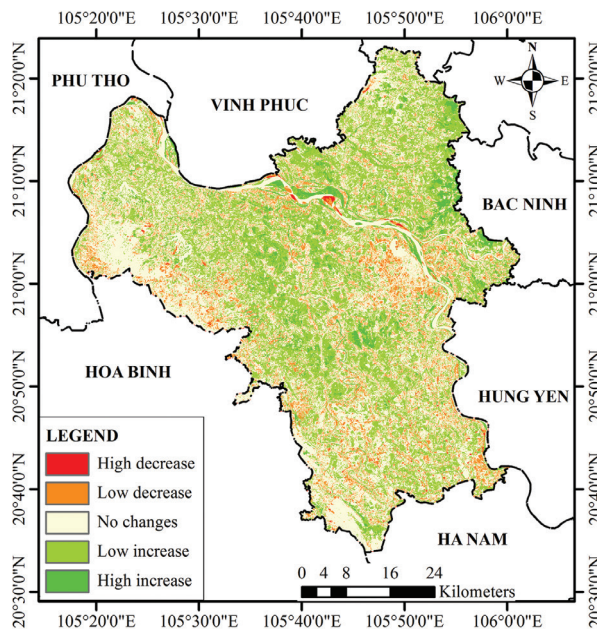
Fig. 5. Map of FVC changes in Hanoi city from 1986 to 2019
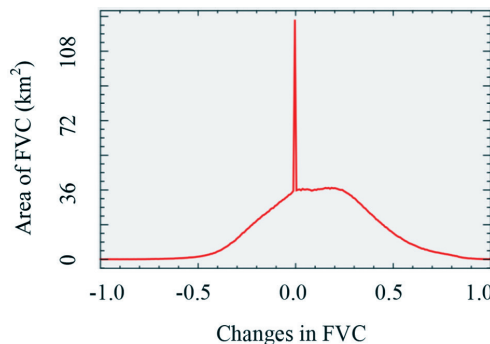
Fig. 6. Histograms of FVC estimated from Landsat-5 TM images in 1986 (left) and from Landsat-8 OLI images in 2019 (right) in Hanoi, Vietnam

Myduc, Sontay, Chuongmy, Quocoai, Thachthat and Bavi. This increase of FVC was mainly due to afforestation policies to increase the forest cover in Bavi National Park (Thinh 2006) and forests in these sub-urban districts (Clement and Amezaga 2009; Clement et al. 2009).

CONCLUSIONS

In this study, fractional vegetation cover changes in Hanoi city (Vietnam) during the period of 1986-2019 were assessed using the two endmember spectral mixture analysis model which is

based on the combination of NDVI and classification method from Landsat-5 TM and -8 OLI images. Landsat remotely sensed images were first pre-processed. FVC was then estimated by NDVI and Maximum likelihood (ML) classification algorithm. The estimated FVC results were validated using 32 in situ measurements. The assessment of FVC changes was finally carried out with the help of GIS. It was found that the combination of NDVI and ML method allows for an improved estimation of FVC with the statistically achieved root mean square error (RMSE) of 0.02 (R^2=0.935). Total FVC area of 321.6 km^2

Table 3. Summary of the FVC changes in Hanoi city from 1986 to 2019

FVC change	Levels of change	Area (km²)	Percentage (%)	Zones
[-1.0; -0.6]	High decrease	0.9	0.03	Small areas of urban districts such as Tayho and Donganh.
[-0.6; -0.2]	Low decrease	321.6	9.61	Some areas of urban districts: Tayho, Badinh, Caugiay, Dongda, Hoankiem, Thanhxuan, Haibatrung, Hoangmai and Longbien.
[-0.2; 0.2]	No change	1724.8	51.55	Areas of sub-urban districts such as Bavi, Myduc, Sontay and of urban district such as Tayho, Badinh, Hoankiem, and Haibatrung.
[0.2; 0.6]	Low increase	1163.6	34.78	Outer-city districts such as Socson, Myduc, Sontay, Chuongmy, Quocoai, Thachthat and Bavi.
[0.6; 1.0]	High increase	134.8	4.03	Outer-city districts such as east of Dong Anh, north of Gialam and Thanhoai, north of Danphuong and south of Melinh.
Total		3345.7	100.0	

(accounting for 9.61% of the total area) was reduced in the center of the city, whereas, FVC increased markedly with an area of 1163.6 km² (accounting for 34.78% of the total area) in suburban and rural areas. The results from this study support the combination of NDVI and ML classification method from Landsat images in FVC change detection in megacities. ▪

REFERENCES

Adler-Golden S. et al. (1999). FLAASH, a MODTRAN4 atmospheric correction package for hyperspectral data retrievals and simulations. In: Proc. 7th Ann. JPL Airborne Earth Science Workshop, 1998. JPL Publication Pasadena, CA, 9-14.

Adler-Golden S.M. et al. (1999). Atmospheric correction for shortwave spectral imagery based on MODTRAN4. In: Imaging Spectrometry V, 1999. International Society for Optics and Photonics, 61-70. http://dx.doi.org/10.1117/12.366315

Alejandro M., Omasa K. (2007). Estimation of vegetation parameter for modeling soil erosion using linear Spectral Mixture Analysis of Landsat ETM data ISPRS Journal of Photogrammetry and Remote Sensing 62. 309-324.

Asner G.P., Heidebrecht K.B. (2002). Spectral unmixing of vegetation, soil and dry carbon cover in arid regions: comparing multispectral and hyperspectral observations International Journal of Remote Sensing, 23, 3939-3958.

Avissar R., Pielke R.A. (1989). A parameterization of heterogeneous land surfaces for atmospheric numerical models and its impact on regional meteorology Monthly Weather Review, 117, 2113-2136.

04|2019

GES

185

Chander G., Markham B. (2003). Revised Landsat-5 TM radiometric calibration procedures and postcalibration dynamic ranges IEEE Transactions on geoscience and remote sensing, 41, 2674-2677.

Chander G., Markham B.L., Helder D.L. (2009). Summary of current radiometric calibration coefficients for Landsat MSS, TM, ETM+, and EO-1 ALI sensors Remote sensing of environment, 113, 893-903. https://dx.doi.org/10.1016/j.rse.2009.01.007

Chen F., Qiu Q, Xiong Y., Huang S. (2010). Pixel unmixing based on linear spectral mixture model: methods and comparison Remote Sens Info, 4, 22-28.

Choudhury B.J. (1987). Relationships between vegetation indices, radiation absorption, and net photosynthesis evaluated by a sensitivity analysis Remote Sensing of Environment, 22, 209-233.

Clement F., Amezaga JM (2009). Afforestation and forestry land allocation in northern Vietnam: analysing the gap between policy intentions and outcomes Land Use Policy, 26, 458-470.

Clement F., Orange D., Williams M., Mulley C., Epprecht M. (2009). Drivers of afforestation in Northern Vietnam: assessing local variations using geographically weighted regression Applied Geography, 29, 561-576.

Deardorff J.W. (1978). Efficient prediction of ground surface temperature and moisture, with inclusion of a layer of vegetation Journal of Geophysical Research: Oceans, 83, 1889-1903.

Flaash Us.G. (2009). Atmospheric Correction Module: QUAC and Flaash User Guide v. 4.7 ITT Visual Information Solutions Inc: Boulder, CO, USA.

Godínez-Alvarez H., Herrick J., Mattocks M., Toledo D., Van Zee J. (2009). Comparison of three vegetation monitoring methods: their relative utility for ecological assessment and monitoring Ecological indicators, 9, 1001-1008.

Gutman G., Ignatov A. (1998). The derivation of the green vegetation fraction from NOAA/AVHRR data for use in numerical weather prediction models International Journal of remote sensing, 19, 1533-1543.

Hiep N.T. (2014). Economic Evaluation of Transportation Infrastructure Science, 47, 415-455.

Hoang A.H. (2016). Fractional Vegetation Cover Estimation in Urban Area of Hanoi City using Landsat 8 OLI Images VNU Journal of Science: Earth and Environmental Sciences, 32, 8.

Hoang A.H. (2017). Assessment of Fractional Vegetation Cover Changes in some Urban and Sub-urban Areas of Hanoi Using Multi-spectral and Multi-temporal LANDSAT Images VNU Journal of Science: Earth and Environmental Sciences, 33, 8.

Hoffmann W.A., Jackson R.B. (2000) Vegetation–climate feedbacks in the conversion of tropical savanna to grassland Journal of Climate, 13, 1593-1602.

Jiménez-Muñoz J., Sobrino J., Plaza A., Guanter L., Moreno J., Martínez P. (2009). Comparison between fractional vegetation cover retrievals from vegetation indices and spectral mixture analysis: Case study of PROBA/CHRIS data over an agricultural area Sensors, 9, 768-793.

Jing X., Yao W-Q., Wang J-H., Song X-Y. (2011). A study on the relationship between dynamic change of vegetation coverage and precipitation in Beijing's mountainous areas during the last 20 years Mathematical and Computer Modelling, 54, 1079-1085.

Kaufman Y., Wald A., Remer L., Gao B., Li R., Flynn L. (1997). Remote sensing of aerosol over the continents with the aid of a 2.2 m channel IEEE Trans Geosci Remote Sens, 35, 1286-1298.

Li M. (2003). The method of vegetation fraction estimation by remote sensing Beijing: Chinese Academy of Sciences.

Li X. (2008). Quantitive retrieval of sparse vegetation cover in arid regions using hyperspectral data Beijing: Chinese Acanemy of Forestry.

Logan W.S. (2005). The cultural role of capital cities: Hanoi and Hue, Vietnam Pacific Affairs, 78, 559-575.

Nguyen T.M., Lin T-H., Chan H-P. (2019). The Environmental Effects of Urban Development in Hanoi, Vietnam from Satellite and Meteorological Observations from 1999–2016 Sustainability 11, 1768.

Nguyen T.T., Vu T.D. (2019). Use of Hot Spot Analysis to Detect Underground Coal Fires from Landsat-8 TIRS Data: A Case Study in the Khanh Hoa Coal Field, North-East of Vietnam Environment and Natural Resources Journal, 17, 1-10; DOI: 10.32526/ennrj. 32517.32523. 32019.32517.

Richards J.A., Richards J. (1999). Remote sensing digital image analysis - An Introduction vol 3. Springer, Berlin, Heidelberg

Small C. (2001). Estimation of urban vegetation abundance by spectral mixture analysis International journal of remote sensing 22, 1305-1334.

Sobrino J., Raissouni N. (2000). Toward remote sensing methods for land cover dynamic monitoring: Application to Morocco International journal of remote sensing 21, 353-366.

Theseira M., Thomas G., Sannier C. (2002). An evaluation of spectral mixture modelling applied to a semi-arid environment International Journal of Remote Sensing, 23, 687-700.

Thinh V.T. (2006). Bird species richness and diversity in relation to vegetation in Bavi National Park, Vietnam Ornithological Science, 5, 121-125.

Trimble S. (1990). Geomorphic effects of vegetation cover and management: some time and space considerations in prediction of erosion and sediment yield Vegetation and erosion Processes and environments, 55-65.

Tsunoda T., Cuong T.C., Dong T.D., Yen N.T., Le N.H., Phong T.V., Minakawa N. (2014). Winter refuge for Aedes aegypti and Ae. albopictus mosquitoes in Hanoi during Winter PloS one 9:e95606.

Vu T.D., Nguyen T.T. (2018a). Remote Sensing and GIS-based River Bank Accretion/Erosion Assessment in the Confluence of Thao-Da-Lo Rivers, North East of Vietnam EnvironmentAsia 11.

Vu T.D., Nguyen T.T. (2018b). Spatio-temporal changes of underground coal fires during 2008–2016 in Khanh Hoa coal field (North-east of Viet Nam) using Landsat time-series data Journal of Mountain Science, 15, 2703-2720.

Wittich K., Hansing O. (1995). Area-averaged vegetative cover fraction estimated from satellite data International Journal of Biometeorology, 38, 209-215.

Wu J., Peng D-l. (2010). A research on extracting information of the arid regions' vegetation coverage using improved model of spectral mixture analysis. In: 2010 International Conference on Multimedia Technology, IEEE, 1-5.

Xiao J., Moody A. (2005). A comparison of methods for estimating fractional green vegetation cover within a desert-to-upland transition zone in central New Mexico, USA Remote sensing of environment, 98, 237-250.

Xing Z., Feng Y., Yang G., Wang P., Huang W-j. (2009). Method of estimating vegetation coverage based on remote sensing Remote Sens Tech Appl, 24, 849-854.

Zanter K. (2015). Landsat 8 (L8) data users handbook Survey, Department of the Interior US Geological.

Zhang X., Liao C., Li J., Sun Q. (2013a). Fractional vegetation cover estimation in arid and semi-arid environments using HJ-1 satellite hyperspectral data International Journal of Applied Earth Observation and Geoinformation, 21, 506-512.

Zhang Y., Odeh I.O., Ramadan E. (2013b). Assessment of land surface temperature in relation to landscape metrics and fractional vegetation cover in an urban/peri-urban region using Landsat data International Journal of Remote Sensing, 34, 168-189.

Zhou Q., Robson M. (2001). Automated rangeland vegetation cover and density estimation using ground digital images and a spectral-contextual classifier International Journal of Remote Sensing, 22, 3457-3470.

Elena Yu. Novenko[1,2], Andrey N. Tsyganov[2,3], Kirill V. Babeshko[3], Richard J. Payne[4], Jinlin Li[5], Yuri A. Mazei[1,3], Alexander V. Olchev[1,6]

[1] Lomonosov Moscow State University, Moscow, Russia
[2] Institute of Geography Russian Academy of Science, Moscow, Russia
[3] Penza State University, Penza, Russia
[4] Environment and Geography, University of York, York YO105DD, United Kingdom.
[5] Shenzhen MSU-BIT University, Shenzhen, Guangdong province, China
[6] A.N. Severtsov Institute of Ecology and Evolution, Russian Academy of Sciences, Moscow, Russia
*Corresponding author: lenanov@mail.ru

CLIMATIC MOISTURE CONDITIONS IN THE NORTH-WEST OF THE MID-RUSSIAN UPLAND DURING THE HOLOCENE

ABSTRACT. This study aimed to reconstruct the climatic moisture conditions of the Mid-Russian Upland through the Holocene. Surface moisture conditions in the study region were inferred from published pollen records from the Klukva peatland, in the north-west of the Mid-Russian Upland. Three climatic indices were derived from previously-published reconstructions of mean annual temperature and precipitation: the Climate Moisture Index, the Aridity Index and the Budyko Dryness Index. A simple modeling approach to reconstruct annual potential evapotranspiration and net radiation was developed and used to estimate the indices for different periods of the Holocene. The moisture indices were compared with independent proxies of climate moisture such as peatland surface wetness, reconstructed from testate amoebae and regional fire activity, reconstructed from charcoal. Results show that the surface moisture conditions in the study region were characterized by large variability. Periods of mild temperature and moderately wet conditions were followed by dry periods, which resulted in significant changes in palaeoenvironments. The method developed for calculation of potential evapotranspiration and indices of surface moisture conditions could be a useful tool for climate reconstructions. Our results demonstrate the detailed and nuanced palaeoclimate data which can be derived from pollen data.

KEY WORDS: paleoenvironmental reconstruction, Mid-Russian Upland, climate moisture conditions, potential evapotranspiration, precipitation, Best Modern Analogue technique

INTRODUCTION

Information about spatial and temporal variability of climate and vegetation in past epochs is important for better understanding of climate-vegetation interactions and prediction of possible vegetation changes under future climate change scenarios. During recent decades various proxy methods have been developed and applied for reconstructions of plant species composition and regional climatic conditions (Khotinsky 1977; Zagwijn 1994; Isarin, Bohncke 1999; Krementski et al. 2000; Barber et al. 2004). Many methods are based on analysis of pollen data in order to reconstruct long-term temperature variability. While pollen-based temperature reconstructions often perform well, reconstructions of climatic moisture conditions are largely limited to assessing major changes between wetter and drier phases (Velichko et al. 2002; Stančikaite et al. 2008; Inisheva et al. 2013; Kalnina et al. 2015). Precipitation amount has been considered as key factor influencing surface moisture conditions in these studies (Khotinsky and Klimanov 1997; Nakagawa et al. 2002; Davis et al. 2003; Tarasov et al. 2009; Mauri et al. 2015). Surface evapotranspiration (potential and actual evapotranspiration) has been either ignored, or parameterized using simplified regression functions and modeling approaches (Prentice et al. 1992; Olchev and Novenko 2012; Novenko and Olchev 2015). Other studies have compared pollen-based moisture reconstructions to independent reconstructions of local surface moisture based on methods such as plant macrofossil and testate amoeba analysis from peatlands (Lamentowicz et al. 2008; Bunbury et al. 2012; Gałka et al. 2017; Tsyganov et al. 2017).

Boreal and temperate forests cover large areas of Northern Eurasia and are expected to be very sensitive to projected climate warming (Olchev et al. 2009, 2013; Novenko et al. 2014). Despite numerous studies of past temperature variability, temporal change in surface moisture conditions and effects on vegetation cover are poorly-constrained. According to the classical paradigm (the so-called 'Blytt-Sernander

scheme with Khotinsky modification' (Khotinsky 1977), the climate conditions of the Holocene in the East European Plain can be classified as follows: a cold and relatively dry Boreal (10.3 – 8.8 ka BP), a wet and warm Atlantic (the Holocene thermal maximum, 8.8-5.7 ka BP), a cool and dry Subboreal (5.7-2.6 ka BP) with a warm phase in its middle part, and a wetter Subatlantic (2.6 ka BP – present). Recent studies have however demonstrated that the Holocene climate conditions in the East European Plain were characterised by greater variability than was previously supposed. Specifically, it has been shown that the Boreal period included a humid phase between 9.3 and 9.1 ka BP (Fleitmann et al. 2008; Novenko and Olchev 2015). The early Atlantic warming period was interrupted by a short-term but abrupt cooling, the so-called '8.2 ka event', which has been traced, almost simultaneously, in northwestern Europe (Alley et al. 1997; Allen et al. 2007; Thomson et al. 2007). The late Atlantic (7.0-5.5 ka BP) may have been relatively dry in Eastern Europe as studies have shown decreased river discharge in Central European Russia (e.g. Sidorchuk et al. 2012) and very high fire frequency in some regions of the East European Plain (Novenko et al. 2016, 2017).

In this study we attempt to develop a detailed reconstruction of Holocene climate moisture conditions in the north-west of the Mid-Russian Upland. The study area is situated close to the southern boundary of the mixed coniferous-broad leaved forest zone, in the ecotone between forest and steppe zones (Fig. 1). This combination makes the vegetation of the area very sensitive to changes in regional thermal and moisture conditions. To reconstruct moisture conditions through the Holocene we use several different surface moisture indices: the Aridity Index, the Budyko Dryness Index and the Climate Moisture Index. All of these indices classify moisture conditions as the difference between available annual precipitation and potential land surface evapotranspiration. For the reconstruction of these parameters we use previously-published pollen-based reconstructions of the mean annual temperature and precipitation from a small peat

bog (Klukva) situated in the northwestern part of the Mid-Russian Upland (Novenko et al. 2015). To verify reconstructed mois-ture conditions of the study area through the Holocene we compare pollen-based reconstructions to independent proxy data on peatland surface wetness inferred from testate amoebae (Tsyganov et al. 2017) and to reconstructed regional fire activity, based on charcoal (Novenko et al. 2018).

MATERIALS AND METHODS

Study area

The Klukva peatbog (53.834°N, 36.252°E) is located on the sandy fluvio-glacial plain ad-jacent to the right bank of the Upper Oka River, near the town of Belyov (Tula region) in the north-western part of the Mid-Rus-sian Upland (Fig. 1). Early-to-Middle Pleis-tocene fluvio-glacial sands are underlain by Lower Carboniferous limestones, resulting in active karst processes. Previous studies by Novenko et al. (2015) have shown that the Klukva peatbog was formed in a sink

hole (280 cm depth) around 10.0 ka BP. An age-depth model of the peat core has been developed based on 6 radiocarbon dates using the "clam 2.2" package (classical age-depth modelling; Blaauw 2010).

The climate of the study area is temperate and moderately continental with a mean annual air temperature +5.5°C and mean January and July temperatures of -9.7°C and +19°C, respectively. The mean annual precipitation is about 600 mm [http://www.meteo.ru]. The vegetation cover of Klukva peatbog largely consists of ombrotrophic species with *Pinus sylvestris, Oxycoccus pa-lustris, Eriophorum vaginatum* and *Sphag-num* mosses particularly abundant (Volkova 2011). The peatbog is surrounded by very diverse mesophytic and hygromesophytic coniferous and mixed broadleaf-coniferous forests (Bohn et al. 2003). The main forest forming species in the area are *Picea abies, Tilia cordata, Quercus robur, Ulmus laevis, Ul-mus glabra* and *Acer platanoides.* Scots Pine (*Pinus sylvestris*) forests are also present in areas of sandy soils (Fig. 1).
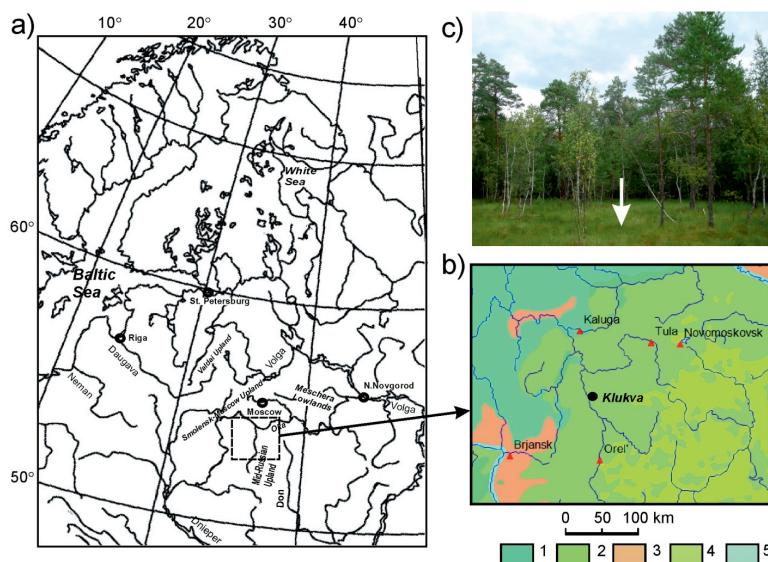
Fig. 1. Location of the study area
a) Location of the Mid-Russian Upland within the East European Plain
b) Vegetation map of the Mid-Russian Upland (after Bohn et al., 2003) and location of the Klukva peatland. Vegetation units: 1 – Mesophytic and hygromesophytic coniferous and mixed broadleaf-coniferous forests; 2 – Mesophytic deciduous broadleaf and mixed coniferous-broadleaf forests; 3 – Boreal and hemiboreal pine forests, 4 – Forest steppe; 5 – Vegetation of flood-plains and other moist or wet sites. c) Klukva peatland and location of the coring site

Reconstruction of the air temperature and precipitation

Mean annual temperature and precipitation were reconstructed using the Best Modern Analogue (BMA) technique, based on pollen data. Details of the BMA approach have been described in many previous publications (e.g. Nakagawa et al. 2002; Williams and Shuman 2008) and the implementation applied here has been described and tested in several studies in various regions of the East European Plain (Novenko et al. 2015; 2016; 2017). The main principles of this technique can be summarized as follows: (*i*) comparing the fossil pollen assemblages with modern pollen assemblages using squared-chord distance (SCD) as the index of dissimilarity between pollen spectra (two spectra are considered analogous if their SCDs are less than a threshold "T" value); (*ii*) for each fossil assemblage selecting the closest modern pollen assemblages (the best modern analogues). The climatic characteristics (temperature, precipitation, etc.) of these selected best analogues are then averaged to estimate the environmental conditions represented by the fossil assemblage. The threshold value used in our study is 0.1. We kept eight best modern analogues for data analysis as recommended by Nakagawa et al. (2002). BMA calculations were undertaken using Polygon 1.5 software (http://polsystems.rits-palaeo.com).

As modern analogues for our reconstruction we used 720 pollen spectra originating from a wide diversity of landscapes in Northern Eurasia, including European Russia and Siberia (Novenko et al. 2014). All modern surface samples were extracted from the European Pollen Database (Davis et al. 2014). Climatic information was taken from the BRIDGE Earth System Modelling dataset (https://www.paleo.bristol.ac.uk). Analogue selection was geographically constrained (Williams and Shuman 2008). We used surface pollen spectra only from the places in which the modern vegetation and environmental conditions could be considered potentially analogous for Holocene paleoenvironments in the forest zone of the East European Plain. Therefore we re-

stricted the area of calibration datasets to the northern and eastern parts of Europe, and Western Siberia (30–55°N, 45–65°E).

To test the accuracy of climate reconstructions based on the BMA approach, a leave-one-out cross-validation was applied to the modern training set (Ter Braak 1995). One modern pollen spectrum was sequentially removed from the total modern data set and mean annual temperature and precipitation were calculated for our site on the basis of the remaining data.

Comparisons of pollen-based reconstructions of mean annual temperature with observed values in the sites show a strong correlation ($R^2 = 0.81$, RMSEP = 1.5 °C). Correlation between reconstructed and observed values of annual precipitation are somewhat lower ($R^2 = 0.51$ and RMSEP = 101 mm); however we assume that they are nevertheless adequate for the reconstruction of prevailing climatic changes in the area.

It is clear that climatic reconstructions provided by the BMA approach are reliable only in the case of undisturbed vegetation not affected by human activity. In our pollen records from the Klukva peatbog, three periods of human impact were identified: the Neolithic occupation (5.2 – 4.3 ka BP), the Middle Ages (about 1.2-0.9 ka BP) and the last 300 years (Novenko et al. 2015). These periods with pollen assemblages representing vegetation disturbance were therefore excluded from our data analysis.

Indices of surface moisture conditions

To quantify change in surface moisture conditions through the Holocene we re-analysed the results of published paleo-reconstructions of annual temperature and precipitation. From the pollen-based reconstructions we calculated three indices characterizing surface moisture conditions: the Aridity Index, the Budyko Dryness Index and the Climate Moisture Index (Fig. 2).

The Aridity Index (AI) is calculated as (UNEP 1992):

$$AI = P / PET \qquad (1)$$

where *PET* is the annual potential evapo-transpiration (mm/yr), and *P* is the annual precipitation (mm/yr). For humid and sub-humid areas *AI* is typically greater than 0.65, while for dry sub-humid areas *AI* is typically between 0.50 and 0.65 and for semi-arid and arid areas *AI* is typically lower than 0.50 (UNEP 1992).

The Budyko Dryness Index (DI) can be calculated as (Budyko 1958):

$$DI = Rn / \lambda P \qquad (2)$$

where *Rn* is mean annual net radiation at ground surface (MJ m^{-2} yr^{-1}) and λ is latent heat of vaporization (MJ kg^{-1}). The ratio of *Rn* and λ can be considered as a rough equivalent to potential evapotranspiration rate. The *Rn* value in our study is calculated as a sum of mean daily net radiations estimated taking into account the annual variability of incoming solar radiation, surface albedo, air temperature, etc. For excessively wet areas *DI* is typically lower than 0.45, for wet areas it ranges between 0.45 and 1.0, for insufficiently wet areas *DI* varies between 1.0 and 3.0 and dry areas are characterized by *DI* > 3.0 (Giese 1969).

An Annual Average Climate Moisture Index (CMI) has been suggested by Willmott and Feddema (1992) and compared to other dryness and moisture indexes it is well adapted to evaluating moisture conditions in both dry and humid regions. The *CMI* indicator ranges from -1 to +1 and can be computed as:

$$CMI = \begin{cases} (P/PET)-1 \ when \ P < PET \\ 1-(PET/P) \ when \ P \geq PET \end{cases} \qquad (3)$$

Wet climates are characterized by positive *CMI*, and dry climates by negative *CMI*, respectively. To quantify the various surface moisture conditions we used the nine categories described in Table 1.

These categories were determined according to the drought index classification suggested by Rind and Lebedeff (1984). Annual *P* is obtained by the BMA technique and annual *PET* is assumed to be equal to potential evaporation (*PE*), is simulated based on the well-known Priestley-Taylor equation (Priestley, Taylor 1972) from mean daily *PE* values (*PE$_d$*) as:

$$PET = PE = \int_1^{N_d} PE_d \cdot dt = \alpha_{PT} \cdot \int_1^{N_d} \left(\frac{\Delta}{\Delta+\gamma} \cdot \frac{Rn_d}{\lambda} \right) \cdot dt \qquad (4)$$

where N_d is the number of the days per year, γ is the psychrometric constant (γ=0.0665 kPa °C^{-1}), α_{PT} is the Priestley-Taylor constant (α_{PT}=1.26 mm day^{-1}) and Δ is the slope of the relationship between saturation vapor pressure and the air temperature (Δ, kPa °C^{-1}). Δ can be parameterized as:

Table 1.The main categories applied to describe the surface moisture conditions using the Climate Moisture Index

CMI ranges	Categories of surface moisture conditions
0.8 to 1.0	Extremely wet
0.6 to 0.8	Severely wet
0.2 to 0.6	Moderately wet
0 to 0.2	Mildly wet
0.0	Normal
-0.2 to -0.0	Mildly dry
-0.6 to -0.2	Moderately dry
-0.8 to -0.6	Severely dry
-1.0 to -0.8	Extremely dry

$$\Delta = \frac{4098.0 \cdot \left[0.6108 \cdot \exp\left(\dfrac{17.27 \cdot T}{T + 237.3} \right) \right]}{(T + 237.3)^2} \quad (5)$$

where T is the mean daily air temperature on the sequential day of the year. This is approximated by a sine function using reconstructed mean annual temperature and annual temperature range.

The daily net radiation at ground surface is derived as a sum of short-wave (Rn_s) and long-wave (Rn_l) radiation balances:

$$Rn = Rn_s + Rn_l = Q \cdot (1 - \alpha) + (R_{il} - R_{ol}) \quad (6)$$

where Q is the incoming daily solar radiation, α is the surface albedo and R_{il} and R_{ol} are the incoming and outgoing long-wave radiation, respectively. Surface albedo depends on vegetation types (e.g. coniferous forest, deciduous forest, mixed forest, grassland), soil properties and forest cover percentage.

Following to McMahon et al (2013) the equation for Q can be written as:

$$Q = Q_S \cdot (0.85 - 0.047 \cdot N) \quad (7)$$

where N is the number of tenths of the sky covered by clouds and Q_S is mean daily solar radiation on a horizontal surface at the top of the Earth's atmosphere, which can be calculated as:

$$Q_S = 86400 / \pi \cdot Q_{S0} \cdot d_r^2 \cdot (\omega_s \cdot \sin\varphi \cdot \sin\delta + \quad (8)$$
$$+ \cos\varphi \cdot \cos\delta \cdot \sin\omega_s)$$

where Q_{S0} is the solar constant (Q_{S0}=0.001367 MJ m^{-2} s^{-1}), φ is latitude, d_r is the inverse relative distance between the Earth and the Sun, δ is the solar declination angle, and ω_s is the sunset hour angle.

Equations for d^r can be written as (McMahon et al. 2013):

$$d_r = 1 + 0.033 \cdot \cos(2\pi \cdot doy / 365), \quad (9)$$

for ω_s as:

$$\omega_s = \arccos(-\tan\varphi \cdot \tan\delta) \quad (10)$$

and for δ as:

$$\delta = 0.409 \cdot \sin(2\pi \cdot doy / 365 - 1.39) \quad (11)$$

where doy is the sequential day number of the year.

The equations for R_{il} and R_{ol} are written as:

$$R_{ol} = 0.97 \cdot \sigma \cdot (T + 273.16)^4 \quad (12)$$
$$R_{il} = (C_f + (1 - C_f) \cdot (1 - (0.261 \cdot \exp(-7.77 \times$$
$$\times 10^{-4} \cdot T^2)))) \cdot \sigma \cdot (T + 273.16)^4$$

where σ is the Stefan-Bolzmann constant (σ=4.903x10^{-9} MJ m^{-2} K^{-4} day^{-1}) and C_f the fraction of cloud cover that is derived empirically as a function of mean daily precipitation (McMahon et al. 2013).

Reconstruction of peatland surface wetness

Peatland surface wetness in terms of the water table depth (WTD, cm), has been suggested to be a useful proxy for climate moisture conditions. WTD was reconstructed from palaeoecological data (Novenko et al. 2015) using a testate amoeba-based transfer function (inverse weighted averaging regression model) which was specifically developed for the forest zone of European Russia (Tsyganov et al. 2017). The transfer function included 80 samples from 18 peatlands located in the taiga, mixed and broadleaf forest, and forest-steppe zones of European Russia. Leave-one-out cross-validation showed reasonably strong model performance (R^2 = 0.74; RMSEP = 5.5 cm). In ombrotrophic peatlands, water-table depths inferred from testate amoebae generally reflect the length and severity of the summer moisture deficit, which may correspond to rate of summer precipitation and evapotranspiration (Charman 2007).

Reconstruction of fire activity

As an additional independent proxy for climate moisture conditions we used the macro-charcoal record from the Mochulya peatland in the "Kaluzhskie Zaseki" Natural Reserve, located 70 km to the north-west of the Klukva peatbog. The results of macro-charcoal analysis were expressed as charcoal concentration (pieces cm^{-3}). The chrononology for the cores is based on 5 radiocarbon dates with an age-depth model produced by the "clam 2.2" package (Blaauw, 2010). The main source of macroscopic charcoal particles (>125 µm)
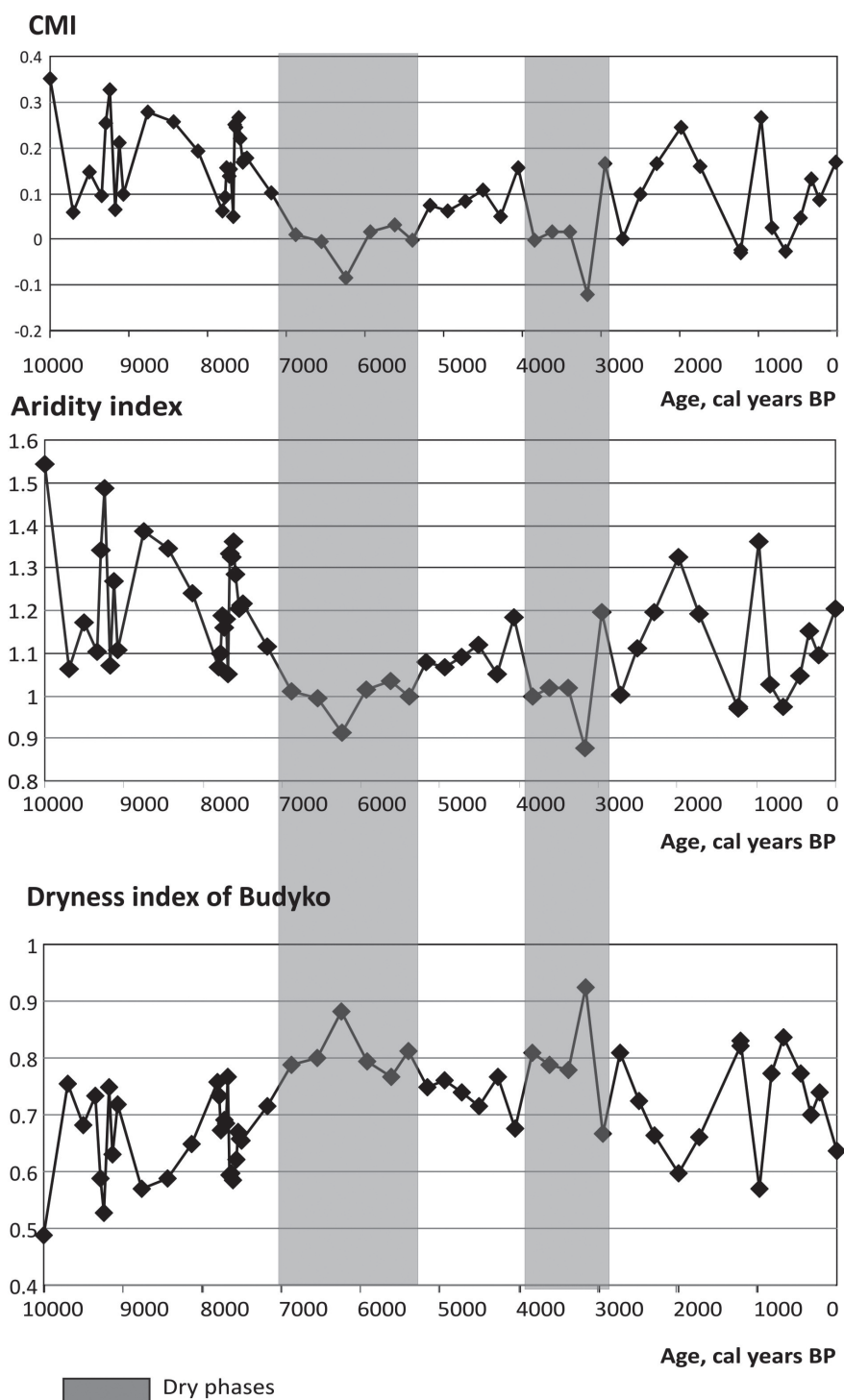
Fig. 2. Indices of surface moisture conditions: Climate Moisture Index, Aridity Index and Budyko Dryness Index. Grey bands indicate dry periods

in peat deposits is assumed to be atmospheric deposition as a result of convective processes arising from the thermal effects of fires (Mooney and Tinner 2011). Fire occurrence and intensity can be assumed to represent climatic aridity in the absence of human activity. Macro-charcoal records are available for the last 4200 cal years only.

RESULTS AND DISCUSSION

We reconstructed variability in environmental conditions over the last 10.0 ka BP (Fig. 2) using pollen-based modeling approaches for the reconstruction of changes in surface moisture indices, and compared them with independent proxy data (Fig. 3). Pollen data showed that the study area was occupied mainly by pine-birch forests with minor admixture of Quercus, Tilia and *Ulmus* between 10.0 and 8.5 ka BP (the second part of the Boreal period). During this period the climate was colder than today with the mean annual temperature around 3-4ºC, 2-3ºC lower than at present. The annual precipitation was close to modern val-

ues (about 600 mm per year). Overall, the climate in the period was relatively humid: CMI reached 0.3-0.4 (moderately wet); the Aridity Index was around 1.5 and the Budyko Dryness Index varied from 0.5 to 0.8 (Fig. 2). WTD reconstructed from testate amoeba data was not lower than 5 cm, indicating a relatively high water table and a wet peatland surface environment.

During the period 10.0-8.5 ka BP, climatic fluctuations with a duration of several centuries were identified. A cooling phase detected at 9.3-9.2 ka BP correlates with the 9.2 ka event (Fleitmann et al. 2008). This cooling was associated with increased precipitation (by about 100 mm), and reduced potential evapotranspiration. As result, the CMI in the period declines to 0.1, corresponding to moderately wet surface moisture conditions (Fig. 3).

Between 8.5 and 6.7 ka BP climate was warm and moderately wet. The mean annual temperatures reached 6-7.5°C, 1.0-2.5°C higher than at present. The mean annual precip-
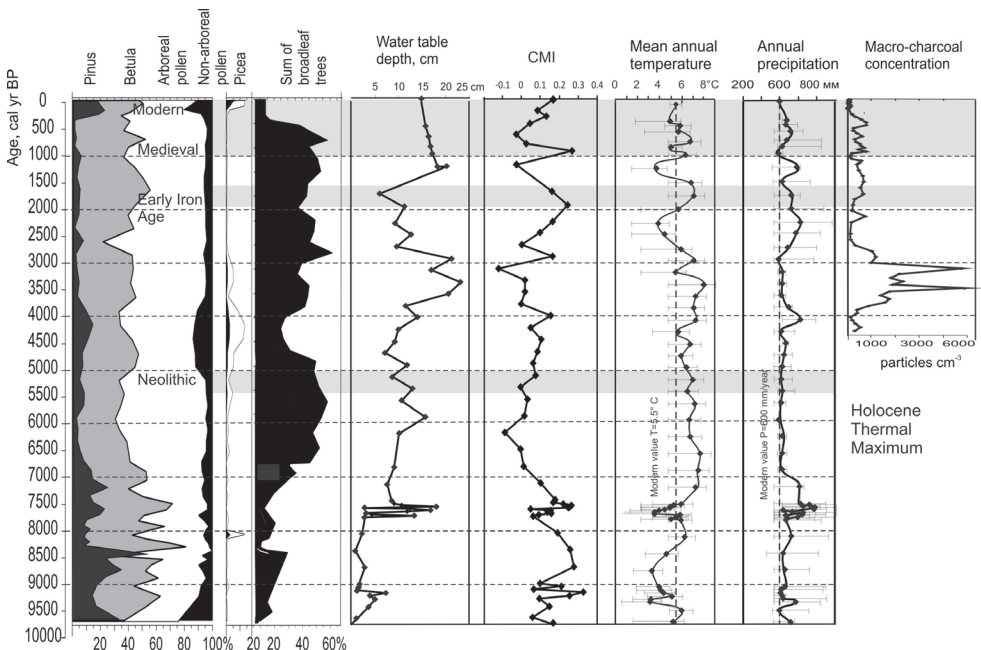
Fig. 3. Summary of pollen records from the Klukva peatland, reconstruction of climatic conditions and water table depth inferred from pollen and testate amoeba data; macro-charcoal data from the Mochulya peatland, located in the Kaluzhskie Zaseki Natural Reserve. Grey bands indicate periods of probable vegetation disturbance due to human impact

itation increased to 800 mm and exceeded modern values by 200 mm. CMI increased up to 0.3 (around 7.5 ka BP); the Aridity Index decreased to 1.3-1.4 and the Budyko Dryness Index was close to 0.6 (Fig. 2) Reconstructed WTDs varied from 5 to 10 cm, indicating a moderately wet peatland surface environment (Fig. 3). Vegetation cover was represented by Quercus forests with an admixture of *Ulmus, Tilia, Fraxinus* and *Corylus* in the understory (Novenko et al. 2015). This species composition persisted in the study area during the middle and late Holocene, until disturbance by humans in historical time.

In the period 6.7-5.5 ka BP, the mean annual precipitation decreased to modern values while the temperatures remained somewhat higher than at present. Climate conditions became somewhat drier than present, as demonstrated by surface moisture indices (Fig. 2): CMI decreased to -0.1 (mildly dry) and the Aridity Index dropped to 0.9-1.0 while the Budyko Dryness Index increased to 0.8-0.9. Reconstructed WTDs fell to 15 cm, probably due to reduced summer precipitation and/or greater evapotranspiration. These findings agree well with evidence for decreased river discharge in the Don and Dnieper Rivers basins during this time (Sidorchuk et al. 2012), and evidence for very high frequencies of forest fires in the Meschera Lowlands (Novenko et al. 2016; Dyakonov et al. 2017).

During the next phase, 5.5-3.7 ka BP, mean annual temperatures decreased to modern values, and mean annual precipitation varied around 600 mm. CMI rose up to 0.2, indicating increased climate humidity. The Aridity Index varied from 1.1 to 1.2 and the Budyko Dryness Index was 0.7-0.8 (Fig. 2). WTD increased to 10-12 cm, suggesting slightly wetter surface conditions as compared to the previous period. This climate deterioration and increased surface wetness coincided with global climate cooling (Davis et al. 2003; Mauri et al. 2015) and glacier advances in the Northern Hemisphere (Solomina et al. 2015) after 5.7 ka BP. General circulation model simulations show a clear tendency for climate cooling in Northern and Central Europe during the period, primarily driven by decreased air temperatures in the summer (Wanner et al. 2008).

A warm and extremely dry phase was detected between 3.7 and 2.7 ka BP. Mean annual temperatures increased to 7-8°C, 1.5-2.5°C higher than at present, while precipitation was similar to modern values. An increase in surface dryness was also shown in the dynamics of the moisture indices considered here. The CMI was about -0.1 (mildly dry) and reached its minimum for the entire period under consideration; the Aridity Index decreased to 0.9-1.0 and the Budyko Dryness Index was 0.8-0.9. WTD in the peatland fell to a depth of 20-25 cm, the maximum water table depth in the Klukva mire for the entire Holocene indicative of very dry conditions.

Indirect evidence for dry climate conditions during this period is provided by a large amount of macro-charcoal in the Mochulya peatland in the "Kaluzhskie Zaseki" Natural Reserve (Novenko et al. 2018). It is well known that the frequency and severity of forest fires depends on various factors such as climate conditions, vegetation type, soil water availability and human impact (Whitlock et al. 2010; Dyakonov et al. 2017). In the areas where human activity was relatively low, fire events occur more frequently during dry climatic periods, while fire frequency typically declines with increasing climatic moisture (Clear et al. 2014). In the time interval 3.7-2.7 ka BP macro-charcoal accumulation rates in peat cores from the Mochulua peatland were an order of magnitude higher than in subsequent periods (Fig. 3). In the absence of any human impact, the high fire activity is likely to have been caused by summer drought.

Climatic reconstructions in the south taiga vegetation zone have also shown warm and dry phases during the same time interval (Novenko et al. 2017). Based on pollen and testate amoeba data taken from the Staroselsky Moch peatbog, in the south of Valdai Hills the mean annual temperature exceeded modern-day values by 1–2°C between 3.4 and 2.5 ka BP, while the CMI decreased to its minimum values. The WTD in the Staroselsky Moch peatbog dropped to 20–25 cm during this time period and reached the deepest level for the entire Holocene (Payne et al. 2016).

During the period 2.7-2.0 ka BP, climate in the study area became cooler and wetter. The mean annual temperature dropped to 4°C and the mean annual precipitation reached 700 mm (Fig. 3). The CMI increased to 0.1-0.2 (mildly wet), the Aridity Index ranged between 1.0 and 1.1 and the Budyko Dryness Index decreased to 0.7-0.6 (Fig. 2). In this period, WTD was 7–12 cm, which is typical for relatively humid climate conditions. This cooling was superimposed on the global temperature decline in Europe, mainly due to summer cooling from 2.7-2.6 ka BP (Wanner et al. 2011; Mauri et al. 2014). An increase in climate moisture in Eastern Europe after 2.6 ka BP was accompanied by increased rates of peat accumulation in ombrotrophic peatbogs in the forest zone of the East European Plain (Klimanov, Sirin 1997; Inisheva et al. 2013; Kalnina et al. 2013; Novenko et al. 2017), by decreased water table depth in the peatlands of Poland (Gałka et al. 2017) and reduced fire frequencies in different regions of European Russia and Eastern Europe (Clear et al. 2014; Novenko et al. 2016, 2017; Dyakonov et al. 2017).

The next warm phase in the study area was identified between 2.0 and 1.7 ka BP. The mean annual temperatures rose to 7°C and precipitation varied from 600 to 700 mm per year (Fig. 3) implying relatively wet climatic conditions. The CMI in the period exceeded 0.2 (moderately wet), the Aridity Index was 1.3 and the Budyko Dryness Index was 0.6 (Fig. 2). WTD moved to 5-10 cm, indicating high surface wetness in the peatbog. This phase with relatively warm climate could correlate with the Roman Warm Period (~200 BC-600 AD/ 2.2 – 1.4 ka BP; Davis et al. 2003). This warming was followed by cooling between 1.4 and 1.0 ka BP with the mean annual temperature declining to 4°C and precipitation around 700 mm per year. Probably, this period corresponded to the European cooling of the 'Dark Ages' (Helama et al. 2017). However, this cooling was represented in the peat core from the Klukva mire by a single sample that is not sufficient for any accurate conclusions. Climate dynamics during the last millennium were characterized by a series of short-term warm and cool intervals (Mauri et al. 2015). Surface moisture conditions varied between moderately wet and mildly dry (Fig. 2). Low

sampling resolution due to low peat accumulation rate or, probably, loss of part of the peat profile due to a fire, and the probability for human impacts on the vegetation, did not allow us to make reliable climatic reconstructions for the last 1000 years.

CONCLUSIONS

The results of climatic reconstructions based on pollen data from the Klukva peatbog show clear temporal variability in surface moisture conditions, derived by the modelling approaches applied here. This study shows that in the study area during the Holocene, the CMI index reached -0.13 in the period 3.7-2.7 ka BP and -0.09 in the period 6.7-5.5 ka BP which corresponded to mildly dry conditions, to 0.30-0.35 in the period between 10.0 and 8.5 ka BP, indicating a moderately wet climate. The Aridity Index ranged between 0.88 and 1.6 (humid and sub-humid climate) through the Holocene, and the Budyko Dryness Index from 0.49 to 0.93 (wet climate). The temporal variability of surface moisture conditions agreed well with indirect estimation of climate wetness using testate amoeba data and macro-charcoal analysis.

Our research is the first reconstruction of the moisture characteristics for the Central European Russia. It is clear that fully representative reconstructions of the climatic conditions in the study region require additional data showing, in particular, the spatial variability of temperature and moisture conditions along meridional and zonal profiles crossing the Mid-Russian Upland from the south to the north and the west to the east. This study provides new data and methodological insights towards this aim.

ACKNOWLEDGEMENTS

REFERENCES

Allen J.R.M., Long A.J., Chris J. Ottle C.J., Pearson D.G. and Huntley B. (2007). Holocene climate variability in northernmost Europe. Quaternary Science Reviews, 26, pp. 1432–1453.

Alley R.B. and Ágústsdóttir M.A. (2005). The 8k event: cause and consequences of a major Holocene. Quaternary Science Reviews 24, pp. 1123–1149.

Barber K., Zolitschka B., Tarasov P. and Lotter A.F. (2004). Atlantic to Urals—the Holocene climatic record of mid-latitude Europe. In: R.W. Battarbee et al. eds. Past Climate Variability through Europe and Africa. Dordrecht, Kluwer Academic Publishers, pp. 417-442.

Blaauw M. (2010). Methods and code for 'classical' age-modelling of radiocarbon sequences. Quaternary Geochronology, 5, pp. 512-518.

Bohn U., Neuhäusl R., Gollub G., Hettwer C., Neuhäuslová Z., Schlüter H. and Weber H. (2003). Map of the Natural Vegetation of Europe. Münster: Landwirtschaftsverlag.

Budyko M.I. (1958) The Heat Balance of the Earth's Surface, US Department of Commerce, Washington, D.D., 259 p.

Bunbury J., Sarah A., Finkelstein S. A. and Bollmann J. (2012). Holocene hydro-climatic change and effects on carbon accumulation inferred from a peat bog in the Attawapiskat River watershed, Hudson Bay Lowlands, Canada, Quaternary Research, 78, pp. 275–284.

Charman D.J. (2007). Summer water deficit variability controls on peatland water-table changes: implications for Holocene palaeoclimate reconstructions. The Holocene, 17 (2), pp. 217-227.

Clear J.L., Molinari C. and Bradshaw R.H.W. (2014). Holocene fire in Fennoscandia and Denmark. International Journal of Wildland Fire, 23 (6)., pp.781-789.

Davis B.A.S, Zanon M., Collins P., Mauri A. et al. (2014). The European modern pollen database (EMPD). Project. Vegetation History and Archaeobotany, 22 (6)., pp. 521-530.

Dyakonov K., Novenko E., Mironenko I., Kuprijanov D. and Bobrovsky M. (2017). The Role of Fires in the Holocene Landscape Dynamics of the Southeastern Part of Meshchera Lowlands. Doklady Earth Sciences, 477 (1), pp. 1336-1342.

Isarin R.F.B. and Bohncke S.J.P. (1999). Mean July Temperatures during the Younger Dryas in Northwestern and Central Europe as Inferred from Climate Indicator Plant Species. Quaternary Research, 51, pp. 158–173.

Fleitmann D., Mudelsee M., Burns S.J., Bradley R.S., Kramers J. and Matter A. Evidence for a widespread climatic anomaly at around 9.2 ka before present (2008). Paleoceanography and Paleoclimatology [online] Volume 23 (1), Available at: https://agupubs.onlinelibrary.wiley.com/doi/abs/10.1029/2007PA001519. [Accessed 2 Oct. 2018].

Gałka M., Tobolski K., Lamentowicz Ł., Ersek V., Jassey, V.E.J., van der Knaap W.O. and Lamentowicz M. (2017). Unveiling exceptional Baltic bog ecohydrology, autogenic succession and climate change during the last 2000 years in CE Europe using replicate cores, multi-proxy data and functional traits of testate amoebae. Quaternary Science Reviews, 156, pp. 90–106.

Giese E. (1969). Die Klimaklassifikation von Budyko und Grigor'ev. Erdkunde, XXIII(4): pp. 317-325.

Hansen M., Townshend J., De Fries R. and Carroll M. (2005). Estimation of tree cover using MODIS data at global, continental and regional/local scales. International Journal of Remote Sensing, 26(19), pp. 4359-4380.

Inisheva L.I., Kobak K.I. and Turchinovich I.E. (2013). The development process of waterlogging and rate of accumulation of carbon in wetland ecosystems Russia. Geography and Natural Resources, 3, pp. 60–68 (in Russian).

Kalnina L., Stivrins N., Kuske E., Ozola I., Pujate A., Zeimule S., Grudzinska I. and Ratniece V. (2015). Peat stratigraphy and changes in peat formation during the Holocene in Latvia. Quaternary International, 383, pp. 186–195.

Khotinski N.A. (1977). Holocene of the Northern Eurasia. Moscow: Nauka (in Russian).

Khotinski N.A. and Klimanov V.A. (1997). Alleröd, Younger Dryas and early Holocene Palaeo-Environmental Stratigraphy. Quaternary International, 41/42, pp. 67–70.

Klimanov V.A. and Sirin A.A. (1997). Dynamics of peat accumulation in peatbogs of the Northern Eurasia during the last 3000 years. Doklady Earth Science, 354 (5), pp. 683–686.

Krementski K.V., Borisova O.K., Zelikson E.M. (2000). The Late Glacial and Holocene history of vegetation in the Moscow region. Paleontological Journal, 34 (1), pp. 67–74.

Lamentowicz M., Cedro A., Gałka M., Miotk-Szpiganowicz G., Mitchell E.A.D., Pawlyta J. and Goslar T. (2008). Last millennium palaeoenvironmental changes from a Baltic bog (Poland), inferred from stable isotopes, pollen, plant macrofossils and testate amoeba. Palaeogeography, Palaeoclimatology, Palaeoecology, 265, pp. 93-106.

McMahon T.A., Peel M.C., Lowe L., Srikanthan R., McVicar T.R. (2013). Estimating actual, potential, reference crop and pan evaporation using standard meteorological data: A pragmatic synthesis. Hydrol. Earth Syst. Sci. 17, pp. 1331–1363.

Mauri A., Davis B.A.S., Collins P.M. and Kaplan J.O. (2015). The climate of Europe during the Holocene: a gridded pollen-based reconstruction and its multi-proxy evaluation. Quaternary Science Reviews, 112, pp. 109-127.

Mooney S.D. and Tinner W. (2011). The analysis of charcoal in peat and organic sediments. Mires and Peat, 7, pp. 1-18.

Nakagawa T., Tarasov P., Kotoba N., Gotanda K. and Yasuda Y. (2002). Quantitative pollen-based climate reconstruction in Japan: application to surface and late Quaternary spectra. Quaternary Science Reviews, 21, pp. 2099–2113.

Novenko E.Y., Zyuganova I.S., Olchev A.V. (2014) Application of the paleoanalog method for prediction of vegetation dynamics under climate changes. Doklady Biological Sciences 457(1), pp. 228-232.

Novenko E., Tsyganov A., Volkova E., Babeshko K., Lavrentiev N., Payne R. and Mazei Yu. (2015). The Holocene palaeoenvironmental history of Central European Russia reconstructed from pollen, plant macrofossil and testate amoeba analyses of the Klukva peatland, Tula region. Quaternary Research, 83, pp. 459-468.

Novenko E., Tsyganov A., Payne R., Mazei N., Volkova E., Chernyshov V., Kupriyanov D., and Mazei Yu. (2018). Vegetation dynamics and fire history at the southern boundary of the forest vegetation zone in European Russia during the middle and late Holocene. Holocene, 28(2), pp. 308–322.

Novenko E., Tsyganov A., Volkova E., Kupriyanov D., Mironenko I., Babeshko K., Utkina A., Popov V. and Mazei, Yu. (2016). Mid- and Late Holocene vegetation dynamics and fire history in the boreal forest of European Russia: A case study from Meshchera Lowlands. Palaeogeography, Palaeoclimatology, Palaeoecology, 459, pp. 570-584.

Novenko E.Yu., Eremeeva A.P. and Chepurnaya A.A. (2014). Reconstruction of Holocene vegetation, tree cover dynamics and human disturbances in central European Russia, using pollen and satellite data sets. Vegetation History and Archaeobotany, 23, pp. 109-119.

Novenko E.Yu, Tsyganov A.N., Mazei N.G., Kupriyanov D.A., Rudenko O.V., Bobrovsky M.V., Erman N.M. and Nizovtsev V.A. (2018). Palaeoecological evidence for climatic and human impacts on vegetation in the temperate deciduous forest zone of European Russia during the last 4200 years: A case study from the Kaluzhskiye Zaseki Nature Reserve. Quaternary International (in press). doi:10.1016/j.quaint.2018.06.028.

Novenko E.Yu. and Olchev A.V. (2015). Early Holocene vegetation and climate dynamics in the central part of the East European Plain (Russia). Quaternary International, 388, pp. 12-22.

Novenko E.Yu., Tsyganov A.N. and Olchev A.V. (2018). Palaeoecological data as a tool to predict possible future vegetation changes in the boreal forest zone of European Russia: a case study from the Central Forest Biosphere Reserve. IOP Conf. Series: Earth and Environmental Science, 107 (2017). 012104.

Olchev A. and Novenko E. (2011). Estimation of potential and actual evapotranspiration of boreal forest ecosystems in the European part of Russia during the Holocene. Environmental Research Letters, 6, 045213.

Olchev A., Novenko E., Desherevskaya O., Krasnorutskaya K., Kurbatova J. (2009). Effects of climatic changes on carbon dioxide and water vapor fluxes in boreal forest ecosystems of European part of Russia. Environmental Research Letters 4 045007 (8pp).

Olchev A. and Novenko E. (2012) Evaporation of forest ecosystems in the Central part of European Russia during the Holocene. Mathematical Biology and Bioinformatics, 7(1), pp. 284-298.

Olchev A.V., Deshcherevskaya O.A., Kurbatova Y.A., Molchanov A.G., Novenko E.Y., Pridacha V.B., Sazonova T.A. (2013). CO2 and H2O exchange in the forest ecosystems of Southern Taiga under climate changes. Doklady Biological Sciences 450(1), pp. 173-176.

Payne R.J., Malysheva E., Tsyganov A., Pampura T., Novenko E., Volkova E., Babeshko K. and Mazei Y. (2016). A multi-proxy record of Holocene environmental change, peatland development and carbon accumulation from Staroselsky Moch peatland, Russia. The Holocene, 26(2), pp. 314-326.

Prentice I.C., Cramer W., Harrison S.P., Leemans R., Monserud R.A. and Solomon A.M. (1992). A global biome model based on plant physiology and dominance, soil properties and climate. Journal of Biogeography, 19, pp. 117–134.

Priestley C.H.B., Taylor R.J. (1972). On the assessment of surface heat flux and evaporation using large-scale parameters. Monthly Weather Review, 100(2), pp. 81-92.

Rind D. and Lebedeff S. (1984) Potential Climatic Impacts of Increasing Atmospheric CO2 with Emphasis on Water Availability and Hydrology in the United States'. Report, Strategic Studies Staff, Office of Policy Anal., Office of Policy, Plann. and Eval., Washington D.C., 96 pp.

Sidorchuk A.Yu., Panin A.V. and Borisova O.K. (2012). River runoff decrease in North-Eurasian Plains during the Holocene Optimum. Water Resources, 39, pp. 69-81.

Solomina O.N., Bradley R.S., Hodgson D.A. et al. (2015). Holocene glacier fluctuations. Quaternary Science Reviews, 111, pp. 9-34.

Stančikaite M., Šinkŭnas P., Šeiriene V., Kisieliene D. (2008). Patterns and chronology of the Lateglacial environmental development at Pamerkiai and Kašučiai, Lithuania. Quaternary Science Reviews, 27, pp. 127–147.

Tarasov P.E., Bezrukova E.V. and Krivonogov S.K. (2009). Late Glacial and Holocene changes in vegetation cover and climate in southern Siberia derived from a 15 kyr long pollen record from Lake Kotokel. Climate of the Past, 5, pp. 285–295.

Ter Braak C. (1995). Ordination. In: Jongman R., Ter Braak C., Van Tongeren O., eds. Data analysis in community and landscape ecology. Wageningen: Pudoc, pp 91-173.

Thomas E.R., Wolff E.W., Mulvaney, R. et al. (2007). The 8.2 ka event from Greenland ice cores. Quaternary Science Reviews, 26, pp. 70–81.

Tsyganov A.N., Babeshko K.V., Novenko E.Yu, Malysheva E.A., Payne R.J. and Mazei Y.A. (2017). Quantitative Reconstruction of Peatland Hydrological Regime with Fossil Testate Amoebae Communities. Russian Journal of Ecology, 48 (2), pp. 191-198.

Velichko A.A., Catto N., Drenova A.N. et al. (2002). Climate changes in East Europe and Siberia at the late glacial-Holocene transition. Quaternary International, 91, pp. 75–99.

Volkova E.M. (2011). Rare mires of the north-western Mid Russia Upland: vegetation and genesis. Botanical Journal, 96, pp. 55–70 (in Russian).

Wanner H., Beer J., Bütikofer J. et al. (2008). Mid- to Late Holocene climate change: an overview. Quaternary Science Reviews, 27, pp. 1791-1828.

Whitlock C. and Bartlein P.J. (2003). Holocene fire activity as a record of past environmental change. In: Gillespie A.R., Porter S.C., Atwater B.F., eds. The Quaternary period in the United States. Amsterdam: Elsevier, pp. 479-490.

Williams J.W. and Shuman B. (2008). Obtaining accurate and precise environmental reconstructions from the modern analog technique and North American surface pollen dataset. Quaternary Science Reviews, 27, pp. 669-687.

Willmott C.J. and Feddema J.J. (1992) A more rational climatic moisture index. Professional Geographer, 44, pp. 84-88.

UNEP (1992). World Atlas of Desertification. Edward Arnold, London.

Zagwijn W.H. (1994). Reconstruction of climate change during the Holocene in western and central Europe based on pollen records of indicator species. Vegetation History and Archaeobotany, 3, pp. 65-88.

Nikolay N. Klyuev
Institute of Geography, Russian Academy of Sciences
Corresponding author: klyuev@igras.ru

THE SPATIAL ANALYSES OF NATURAL RESOURCES USE IN RUSSIA FOR 1990-2017

ABSTRACT. Trends in the development of natural resources use in Russia for 1991-2017 are presented. The role of industries based on mineral resources has increased over the post-Soviet years. The use of renewable natural resources is increasingly shrinking into compact areas near "central sites" and main transportation routes. The inventory of implemented investment projects was used as the basis for compiling a small-scale map to display the main features of industrial and transport development of the territory of post-Soviet Russia. The article states that topical changes in the natural-resource sphere do not match the criteria of sustainable development.

INTRODUCTION

Natural resources, for which the territory of Russia has long been famous, are still providing Russia with survival and even development (however, very unstable development) in the conditions of the continuing crisis of recent decades. The contribution of the export of mineral resources alone to the country's hard currency proceeds 65–70% (40–54% in the Soviet Union in the 1980s) and at least half of the income of the federal budget (Klyuev 2015).

The high demand for Russian natural resources in the global market preconditions Russia's place as a resource-providing zone on the planet; the strategic significance of the natural resource complex[1] in the country's economy; and the priority of the earth sciences, including geography, in the Russian scientific sphere.

Development trends of the Russian natural resource complex as a whole in the post-Soviet period were considered in domestic and foreign literature (Doroshenko et al. 2014; Bradshaw and Connolly 2016; et al.). However, we are not aware of studies of the spatial patterns of these trends.

The purpose of the article is to determine the post-Soviet trends in the development of the Russian natural resource complex and their compliance with the criteria for sustainable development. For the first time, an attempt is made to map the post-Soviet industrial and transport development of Russian territory.

[1] Natural resource complex is a set of industries that extract and primary processing of natural resources: extractive industry, agriculture, forestry, water industry, fishery, etc.

MATERIALS AND METHODS

The materials for the study were official statistics (Russian Statistical Yearbook 2017; 1994). The mapping is based on materials from business journalism gathered by this author, and regional, sectoral and corporate Internet websites as well as data reported by separate researchers (Litvinenko 2014; Makhrova et al. 2008; Savelyeva 2012). A total of 1040 projects were taken into account: 981 point objects (industrial enterprises and their facilities) located in 600 settlements as well as in uninhabited areas, and 59 objects of linear transport infrastructure (pipelines, railroads, and power lines)[2]. Because of the specific nature of information, the map (Fig. 1) displays only a representative sample of the largest investment projects implemented to date.

The main research method is integrated small-scale thematic mapping.

RESULTS AND DISCUSSION

After a significant drop in the 1990s, the production of non-renewable mineral resources in Russia practically reached the Soviet level by the 2010s and even exceeded it in some positions (Table 1). An exception is the extraction of nonmetallic building materials, which has shrunk by a third. This was caused by a drastic reduction in industrial, transport, and residential construction, since the industry of construction materials works for the domestic market. On the contrary, the extraction of fuel and energy resources, ferrous and nonferrous metal ores, and chemical raw materials are largely export oriented, which predetermines Russia's status as a warehouse of the world's mineral resources.

Table 1. Dynamics of the extraction of mineral resources and production based on renewable resources in Russia over 1990–2017 (1990 = 100%)

Product / Year	1990	2000	2017
Coal	100	65	104
Oil	100	63	106
Natural gas	100	91	108
Iron ore	100	81	89
Nonmetallic building materials	100	27	68
Fertilizers	100	76	141
Peat	100	39	50
Commercial wood	100	31	53
Fish	100	47	58
Grains	100	62	107
Cattle and poultry	100	49	98
Milk	100	62	57
Eggs	100	68	89
Wool	100	24	25

[2] We made the first attempt at the inventory and mapping of the new construction projects in (Klyuev 2018): we compiled the map displaying about 950 projects.
Source: Russian Statistical Yearbook 2017; 1994.
Note. Five-year averages for agricultural products: 1990 for 1986–1990; 2000 for 1996–2000; and 2017 for 2013–2017.

The export orientation of the mining industry significantly increased during the years of restoration of capitalism in Russia (Table 2). Russia is the world's largest exporter of natural gas, while the gasification of, for example, Sakhalin region (a gas-producing region) is 14.2% (2017); in rural districts this index is much lower. Russia exports most (up to 90%) of the aluminum, copper, nickel, and zinc it produces as the domestic consumption of the non-ferrous metallurgy products, which refines the economy and makes its structure more progressive, has dropped drastically. The Soviet Union consumed over 10% of the world's aluminum; contemporary Russia consumes 10 times less; copper consumption has decreased by 8 times, and nickel consumption has decreased by 12 times (Kashin 2009).

Against the backdrop of the increasing exploitation of the subsurface, renewable resource–based industries have drastically reduced the production over the post-Soviet period. It is noteworthy that sustainable development implies the gradual replacement of non-renewable mineral resources with renewable ones. It is clear that this problem cannot be solved overnight. However, it is hard to rely on solving it if we move in the opposite direction.

A distinctive geographical feature of the Russian natural-resource complex has been the almost full spatial incongruity of human and resource distribution (an exception is the soil–climatic resources). Siberia and the Far East, inhabited by 20% of the population, have 70% of the

Table 2. Extraction and export of oil, gas, coal, and iron ore in Russia

Mineral resources / Year	1993	2000	2005	2011	2017
Oil, million tons					
Extraction	354	324	470	512	546
Export	80	145	253	244	253
Export share on extraction, %	22.6	44.7	53.8	47.7	46.3
Natural gas, billion cubic meters					
Extraction	618	584	641	671	691
Export	96	194	207	187	210
Export share on extraction, %	15.5	33.2	32.3	27.9	30.4
Coal, million tons					
Extraction	306	258	299	335	410
Export	20	44	80	111	181
Export share on extraction, %	6.5	17.1	26.8	33.1	44.1
Iron ore, million tons					
Extraction	76	87	95	104	95
Export	10	19	18	28	21
Export share on extraction, %	13.2	21.8	18.9	26.9	22.1

Source: Russian Statistical Yearbook 2017; 1994.

natural-resource potential, excluding agricultural resources. This circumstance predetermines the key problems of developing the country's natural resources: expensive extraction in the conditions of "ice isotherms"; the absence of roads, infrastructure, and labor; and the high price of the transportation of extracted raw materials to consumers. All these problems only worsen with time.

The agrarian profile of the regions has changed, shifting toward crop production. In the 1980s, it prevailed only in several southwestern regions, and now it already dominates most of the country's territory, from the dry steppes to the tundra. The relation between crop production and livestock production is of high environmental, in addition to economic, importance. It predetermines the type and intensity of agrarian loads on nature and the proportions between farmland types (plow land, hay land, and pastureland) and, thus, the face of contemporary rural landscapes.

The characteristic features of the current period are the preferred shrinkage of the Russian resource space, the concentration of natural resource use in "central parts," and the economic desolation of the periphery. This is indicated by the distribution of industrial investments, which are, in fact, future anthropogenic loads, by the country's regions. There is a concentration of the use of natural resources in relatively well (by Russian standards) developed territories, where the pressure on nature has previously been high. Beyond the Urals, only the Khanty–Mansi and Yamalo–Nenets autonomous districts in Tyumen' region are noticeably distinguished by the level of investment concentration.

The inventory of implemented investment projects was used as the basis for compiling a small-scale map to display the main features of industrial and transport development of the territory of post-Soviet Russia (Fig 1). An exceptional spatial differentiation of industrial construction is revealed, expressed primarily in its superconcentration in the Moscow region, as well as in the north-west (St. Petersburg and Leningrad region). The northern and eastern regions of the country are characterized by focal industrial development and the dominance of mining enterprises. In Asiatic Russia large-scale industrial construction is allocated to Kuzbas, Khanty–Mansi, and Yamalo–Nenets autonomous districts, but the "density" of development is small (Fig 2). The resulting map reveals new foci and areas of change in the natural environment and its large-scale transformation. The analysis of the structure of new industrial construction did not reveal any signs of its greening. 2/3 of new facilities are related to basic, environmentally "aggressive" industries.

The key cause and, simultaneously, indicator of the desolation of northern and eastern regions of the country is the reduction of their population. Between 1991 and 2017, the reduction amounted to 35% in Murmansk region, 61% in Magadan region, and almost 68% in Chukotka autonomous district.

The rate of drawdown in forest harvesting in the main forestry regions is higher than in other regions of the country. Remote wood cutting areas are abandoned, and forest extraction is concentrated near thoroughfares. In forest deficient regions, where the forests are heavily disturbed, increased felling is observed. In mountainous regions, especially in the North Caucasus, mid-mountain and low-mountain forests and shrubs are felled intensively for firewood, thus increasing the areas of mudflow sites.

At the same time, the 2000s witnessed patchy involvement of export-oriented resources in newly developed regions, mainly in the north and east of the country. Among large subsurface development projects in post-Soviet Russia, we should note oil and gas extraction at the Vankor oil and gas, Yurobcheno–Tokhomsk oil and gas condensate (Krasnoyarsk krai), and Talakan oil (Yakutia); fields on the

shelves of the Okhotsk, Caspian, Baltic, Black, and Pechora seas; the advance of gas extraction in the Yamalo–Nenets autonomous district to the north; the preparation of the development of Timan bauxites; etc.

The focal development of resources is becoming more deconcentrated. Now there are no giant deposits like Samotlor, Urengoy, and Medvezh'e. In the early 1970s, the average size of reserves at newly discovered oil deposits in Western Siberia was 77 million tons (30 million tons in the Russian Soviet Federative Socialist Republic); now it is 1 million tons. What we see now are the signs of a late stage in the life cycle in the country's main "hard currency shop"—the Western Siberian oil and gas province. An increasing number of infield and interfield pipelines is needed for each unit of resources extracted. This increases the environmental risks, since

such pipelines spill at least 1% of the oil produced.

Against the background of the significant reduction in transportation, which reduced the effects of hazardous transport on roadside landscapes on territories between populated localities, a pipeline–port boom is observed, causing the transfer of transport–environmental threats to offshore zones and their approach to the Russian borders. Here we may single out the Blue Stream, Nord Stream, and Yamal–Europe gas pipelines; the Turkish Stream and Power of Siberia gas pipeline projects; the Eastern Siberia–Pacific Ocean oil pipeline; the Baltic pipeline system (Kirishi–Primorsk); the Primorsk oil transshipment terminal; the Vitino (Murmansk region) and Privodino (Arkhangelsk region) oil terminals; etc. The export-oriented raw-stock model of the Russian economy is secured in new investments.


Fig. 1. Industrial and transport projects on the territory of Russia in the post-Soviet period

Projects: 1 – industrial enterprises, 2 – gas pipelines (the project under construction is shown as a dashed line), 3 – oil pipelines, 4 – petroleum product pipelines, 5 – railroad (the railroad under construction is shown as a dashed line), 6 – power transmission line.
Sectors of the economy: I – extractive industry, II – electricity, III – metallurgy, IV – oil refining industry, V – chemical and petrochemical industry, VI – mechanical engineering and metalworking, VII – timber, forest product and pulp and paper industry, VIII – building materials industry, IX – food industry, X – light industry, XI – ports and terminals.
The size of the circle indicates the number of projects.
Cartographer – A.N. Vasiltsova.
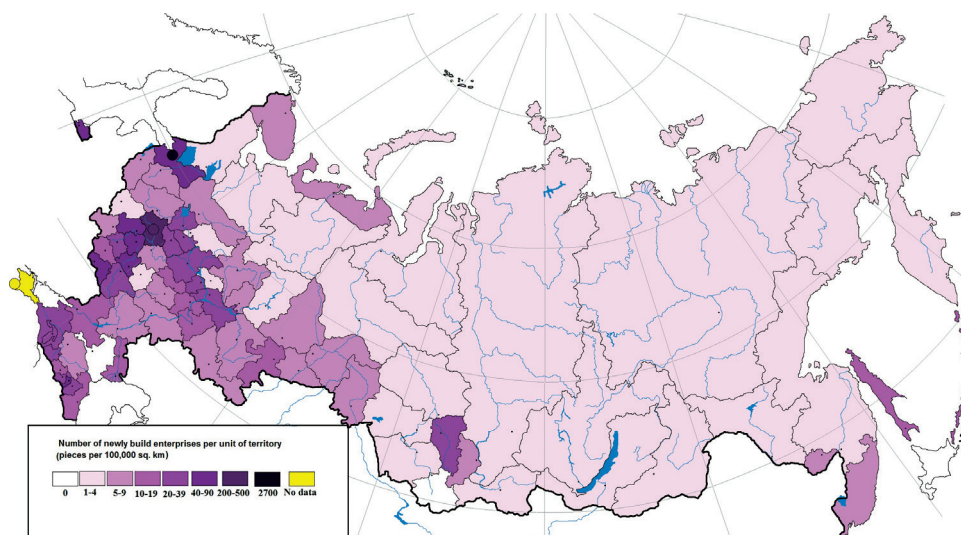
Fig. 2. Industrial construction in Russia in the post-Soviet period

"The whole history of Russia is related to the development of vast land . . . . This is its function and, if you like, mission" (Sysoeva 2007). Therefore, the development of new natural resources follows the main path of the country's development, but with an important reservation. The key innovation of the contemporary world is the environmental imperative. The unique diversity of Russian landscapes should be developed carefully, with account for the spatiotemporal characteristics of their resistance to technogenesis. Development is not just the expansion of mining facilities, which leave behind an anthropogenic desert. Environmental development implies the arrangement of a territory, the organization of tourist and recreation zones on it, territories of different security levels, organic agriculture, progressive means of transportation and communications, traditional crafts of small nations, etc.

Thus far, unfortunately, the principles of sustainable development have not become a regular fixture in domestic natural resources use. At first sight, new mining facilities should show a high degree of environmental friendliness. However, this is not always the case. New oil extraction fields in the Khanty–Mansi autonomous district are not included into the network of operations that utilize

the associated petroleum gas. Newly commissioned oil fields have a very low degree of gas utilization. Only at old and well-developed fields it can reach 60–90%. Russian oil and gas deposits on the Arctic shelf should be viewed as a resource for future generations. Their frontal development in the next 10–20 years is unwarranted for several reasons, including those related to climate transformation. Changes are manifested, in particular, in the acceleration of extremely hazardous phenomena, fraught with environmental emergencies. Severe but stable natural conditions are very costly; however, they do not involve readily predictable consequences. At the same time, the "efficient presence" on a territory is needed for geopolitical reasons— infrastructural development of navigation in Arctic regions, the intensification of the information stage of their development (exploration, monitoring, etc.), and colossal capital investments, required for new shelf projects, must be channeled to improve the recovery of oil and gas resources at already developed deposits.

Unfavorable features of the geographical position of our country hinder its frontal inclusion into international labor division. A scientifically justified territorial policy can and should strengthen the merits of Russia's location and smooth out its

drawbacks. This can be done by organizing railroad and marine super-thoroughfares "from the English to the Japanese" and a central link of a single integral infrastructure of Eurasia on Russian land and in Russian waters.

The years of perestroika, crises, and reforms have escalated the problem of information support for the country's natural resource complex. The development of mineral riches has still been mainly based on reserves explored by Soviet geologists, which betokens an imminent resource crisis. The reduction of things to order in the "book accounting" of natural values is an important task of national administration, and geographers can and should contribute to its solution. Knowledge obtained by the earth sciences is of strategic importance for the country's sustainable development. It is necessary to intensify the scientific investigation of Russian territory – the most environmentally friendly and geopolitically essential form of its development.

CONCLUSION

In the post-Soviet years, the Russian economy has seen the strengthening of the role of the natural resource complex, and the importance of industries based on mineral resources has increased in its structure. In addition, gaps between the extraction and processing of mineral resources, as well as between extraction and internal consumption, are increasing. The export orientation of the natural resource sphere is growing. This dynamics does not correspond to the objectives of the country's innovative, informational, and environmentally oriented development.

The export-oriented mineral resource complex is experiencing an expansion of the resource space: the focal involvement of new resources of Eastern Siberia, the Far East, the North, and the shelf regions into exploitation. As opposed to this, the use of renewable (biological, forest, soil, agroclimatic, aquatic) resources, as well as non-ore construction materials consumed

inside the country, is concentrated in compact areas near central parts and main thoroughfares and is oriented at the use of the "best lands". Topical changes in the natural resource sphere do not match the criteria of sustainable development.

It is important to undertake efforts to reanimate industries that are based on renewable resources and that have suffered severely during the crisis and reforms: agriculture, forestry, water industry, fishery, etc. In addition to economic and environmental effects, their restoration and development will also yield a geopolitical result. These industries are crucial in "rebuilding" the country's territory.

The small-scale map, compiled on the basis of a selective inventory of the investment projects thus far implemented reflects the main features of industrial and transport development of post-Soviet Russia. The study revealed an exceptionally high territorial differentiation of industrial construction which implies primarily its overconcentration in the Moscow region as well as in the North-West (the city of St. Petersburg and Leingrad region). The northern and eastern areas of the country are distinguished by focal industrial development, and by a predominance of extractive enterprises. No shift of productive forces to the east, which is necessary for ensuring geopolitical stability of the country and leveling off the industrial load on the environment over the territory, has been observed at all.

The analysis of the structure of new industrial construction did not reveal any signs of its "greening". Two thirds of the new projects refer to the basic, environmentally "aggressive" sectors.

The newly constructed transport infrastructure facilities (pipelines, railroads, ports, and terminals) are largely export-oriented rather than enhancing the connectivity of its territory.

The compiled map of industrial and transport construction reveals new

foci and areas of changes in the natural environment and its large-scale transformation. The growing concentration of economic life in sparse areas of economic activity is the main vector of Russia's spatial development. Having developed in the conditions of market chaos, it is of poor quality from both the environmental and geopolitical positions

REFERENCES

Doroshenko S.V., Shelomentsev A.G., Sirotkina N.V., and Khusainov B.D. (2014). Paradoxes of the "natural resource curse" regional development in the post-Soviet space. Regional Economy, 4, pp. 81-93. DOI: 10.17059/2014-4-6.

Bradshaw M. and Connolly R. (2016). Russia's Natural Resources in the World Economy: history, review and reassessment. Eurasian Geography and Economics, (57), pp. 1-27. DOI: 10.1080/15387216.2016.1254055.

Kashin V.I. (2009). Natural Resources as Part of Russia's National Riches. The Use and Protection of Natural Resources in Russia, (5), pp. 3-7 (in Russian)

Klyuev N. N. (2018). Industrial and Transport Development of the Territory of Russia in the Post-Soviet Period. Geography and Natural Resources, 39(1), pp. 1-9. DOI: 10.1134/S1875372818010018

Klyuev N.N. (2015). Russia's Natural-Resource Sphere and Trends in Its Development. Herald of the Russian Academy of Sciences, 85(4), pp. 303–315. DOI: 10.1134/S1019331615030016

Litvinenko T.V. (2014). Post-Soviet Transformation of Resource Management and Its Social-Environmental Consequences in Eastern Regions of Russia. In: I.N. Volkova and N.N. Klyuev, ed., Environmental Management in Territorial Development of Modern Russia, Moscow: Media-Press, pp. 251–283. (in Russian with English summary)

Makhrova A.G., Nefedova T.G., and Treivish A.I. (2008). Moscow Oblast Today and Tomorrow: Tendencies and Prospects of Spatial Development. Moscow: Novyi Khronograf (in Russian)

Russian Statistical Yearbook. 2017. [online] Available at: http://www.gks.ru/bgd/regl/b17_13/Main.htm [Accessed 07 Nov. 2018].

Russian Statistical Yearbook. 1994. Moscow: Goskomstat (in Russian)

Savelyeva I.L. (2012). Eastern Siberia: The Formation Potential of the TPC of Polyresource Nature Management. In: Russia and Its Regions: Integration Potential, Risks and Avenues for the Transition to Sustainable Development. Moscow: KMK, pp. 380–399 (in Russian with English summary)

Sysoeva N.M. (2007). The Processes of Economic Development of Siberia, and the Current Problems of Territorial Development. Geography and Natural Resources, (3), pp. 37-41. (in Russian with English summary)

Hovsepyan Azatuhi¹*, Tepanosyan Garegin¹, Muradyan Vahagn¹, Asmaryan Shushanik¹, Medvedev Andrey², Koshkarev Alexander²

¹ Center for Ecological – Noosphere Studies NAS RA, GIS & Remote sensing department, Abovyan str. 68, Yerevan, 0025, Armenia

² Institute of Geography Russian Academy of Sciences, Laboratory of Cartography, Staromonetny line 29, Moscow, 119017, Russia

* Corresponding author: aza.hovsepyan@cens.am

LAKE SEVAN SHORELINE CHANGE ASSESSMENT USING MULTI-TEMPORAL LANDSAT IMAGES

ABSTRACT. Shoreline changes are important indicators of natural and manmade impacts on inland waters and particularly lakes. Man-induced changes in Lake Sevan water level during the 20th century affected not only the ecological status of the Sevan water but also near-shore areas. This article considers a long-term study of changes in Lake Sevan shoreline that occurred between 1973 and 2015. The Normalized Difference Water Index (NDWI) was applied to delineate the Sevan shoreline changes according to periods of lake water fluctuation from multi-temporal Landsat images and Historical changes in shorelines were analyzed with help of the Digital Shoreline Analysis System (DSAS) toolbox. Data obtained from the analysis have indicated that changes in the lake shoreline that occurred in different periods are similar to those in the lake water balance. Areas with the greatest shoreline changes have comparatively flat relief, so in the result of the lake water level raise vast forested areas were submerged. This study shows that application of multi-temporal spatial imagery and GIS methods can provide valuable information on time-and-space changes in the Sevan shoreline. Such information is important for monitoring Lake Sevan shoreline and nearshore changes.

INTRODUCTION

Shoreline is the line between water and land. Shoreline changes are the best visible indicators that give information about changes in lake water and surrounding environment. However, geographical position of a shoreline should be considered in the view of temporal resolution and time scale used when assessing changes. Shorelines delineation and assessment of multi-year changes allow visualizing shorelines and changes, getting a better understanding of causes, rate and effects of such changes (Boak & Turner, 2006).

Hovsepyan Azatuhi, Tepanosyan Garegin et al.   LAKE SEVAN SHORELINE CHANGE ...

04|2019

GES

213

The shoreline delineation methods include a coastal survey, GPS survey, aerial photography and satellite imagery (remote sensing (RS)). Each of these methods has its advantages and disadvantages. The choice of method should be based on the purpose and objectives of the research, spatial and temporal resolution of data, economic accessibility, and so on (Samanta & Paul, 2016). A RS-supported delineation of shorelines is important for erosion monitoring, shoreline areas management, flood prediction, evaluation of water resources, and so on (Bagli, Soille, & Fermi, 2004).

RS imagery and GIS are widely used for identification of inland water bodies, delineation of shorelines and coastlines of estuaries, lakes, reservoirs etc., for assessing changes on local, regional and global levels. One of best examples of application of RS for inland water bodies change detection on the global level is the work of Pekel et al. (2016), who used three million Landsat images (Landsat 5, 7, 8) between 1984-2015 for mapping the global surface water and changes in it (Pekel et al., 2016). Application of RS is an important tool supporting compilation the Pan-European coastline and lake database (Vogt et al., 2007). Agyemang et al. used Landsat images and GIS techniques to assess historical development of area of Lake Sevan from 1933 to 2005 (Agyemang et al., 2017).

There are many RS and GIS applications for coastline delineation in different regions of the world. Qiao et al. (2018) used declassified intelligence satellite images (CORONA) and Landsat images, for analyzing the 55-year shoreline changes in Shanghai (Qiao et al., 2018). Bai et al. (2011) applied Landsat images to assess the change of lake areas for the Central Asia region during 30 years (Bai et al., 2011). Oyedotum (2017) used historical maps and Digital Shoreline Analysis System (DSAS) to assess shoreline changes for the period of 1845-2010 and 1881-2010 respectively in St. Ives-Hayle Bay and Padstow-Camel Bay in Southwest England (Oyedotun, 2017).

Lakes are known to be more vulnerable to natural and anthropogenic impacts which affect both the quality and quantity of lake water and the surrounding environment (Aladin et al., 2005; Timoshkin et al., 2016; Babich et al., 2016).

Climate change and its consequences are among the important factors that impact on quantity and quality of water bodies, especially on inland waters. Because of climate change extremal weather conditions, such as floods and droughts became more frequent. As a result, water level in lakes and rivers fluctuate in more significant ranges. As for the lake Sevan, according to "First National Communication of the Republic of Armenia on Climate Change" reduction of annual river flow by 15%, and increase of evaporation from the surface of Lake Sevan by 13-14% is expected (Dokulil, 2014)(Ministry of Nature Protection of the Republic of Armenia, 1998).

Thus, shoreline delineation of individual lakes and detection and assessment of changes in such water bodies are essential on the local and regional scale. As an example: El-Asmar et al. (2013) applied Landsat images for Burlus Lagoon between 1973 and 2011 (El-Asmar, Hereher, & Kafrawy, 2013). Du et al. (2014) used Landsat 8 OLI images to map surface water bodies in the Yangtze River basin and the Huanghe River basin in China (Du et al., 2014). Landsat images were used in Armenia's neighbouring countries, too. Thus, in Iran, Alesheikh et al. (2007) applied RS methods for studying Lake Urmia shoreline changes (Alesheikh, Ghorbanali, & Nouri, 2007).

For this research, the RS method with application of Landsat images was selected as the most appropriate for Lake Sevan because Landsat images have longest retrospective data series, are free of charge, give periodic information, have a reasonable spatial, temporal and radiometric resolution. Due to these advantages, Landsat images are widely used in various studies as well (Feyisa et al., 2014; Wulder et al., 2016).

The importance of this research can be ensured by the several reasons: (i) the study object is Lake Sevan. The one of the largest alpine lakes in the world and the biggest freshwater reservoir in Armenia and the South Caucasus, the Sevan has a huge ecological and economic importance for the whole of the region, (ii) dramatic shoreline changes caused by dramatic drop in the lake water level in the result of manmade intervention were triggered in the 1930s. At present, lots of ecological problems emerged as a result of short-sighted management decisions, establishing an ecological monitoring system with a RS component is required, (iii) this study is an exceptional experience for Armenia and for the whole of the South Caucasian region in application of RS methods and GIS technologies and particularly the Digital Shoreline Detection System (DSAS) for determining the shoreline and its modifications over a long period of time (1973-2015).

A similar research in region was implemented in Turkey by Duru (2017) who used remote sensing data (Landsat imagery) and DSAS tool for the assessing shoreline displacement for Lake Sapanca between 1975 through 2016 (Duru, 2017). However, the present research is unique as it involved combination of these methods for a much more bigger water body – Lake Sevan.

MATERIALS AND METHODS

Study Site

Lake Sevan (40°23'N, 45°21'E) resides in Gegharkunik region in Armenia at an altitude of 1900 m a. s. l. Sevan is Armenia's largest water body and the largest freshwater resource for the whole of the South Caucasian region.

Morphologically, Lake Sevan is divided into two basins– Big and Small Sevan. Its surface area is 1278.13 km^2, according to the data as of January 1, 2017 (Hydrological regime of Lake Sevan, 2017). In natural conditions Sevan covered an area of 1416.km^2 at an altitude of 1915m a.s.l.

28 rivers empty into the lake and only one river, the Hrazdan, runs out of it, due to which Sevan is a freshwater lake.

The main inflow sources of the lake water balance are water inflow from rivers, water inflow from the Vorotan-Arpa-Sevan tunnel, groundwater flow.

Main outflow components are the Hrazdan river, evaporation from the water surface, water discharge, groundwater outflow (Ogannesian, 1994).

It is necessary to give a brief history of the so-called "Sevan Problem" to understand dramatic changes that took place in Lake Sevan from the 1930 onward. At the beginning of XX century it was decided to use centuries-old resources of the lake for energetic and agricultural needs. The result has been a drop in the lake water level, eutrophication of the lake, activation of erosion processes and so forth. (Pavlov et al., 2010).

The fluctuation of Lake Sevan water level can be divided into three main periods:

I. 1933 – 1981. A drop of lake water level associated with exploitation of centuries-old water resources and a water level drop by almost 18.8m.

II. 1981-2002. Relative stabilization due to Arpa-Sevan tunnel was put into operation in 1981 and annually conveying more than 200 mln. m3 of River Arpa water to Lake Sevan.

III. From 2002 onward. A raise of lake water level in 2002. Since then, water balance has been mainly positive and the water level has been rising steadily. This is mainly due to Vorotan-Arpa tunnel was put into operation in 2004 and the inflow of additional 165 mln. m3 of water to the Sevan annually. To have the lake ecosystem stabilized and prevent its further pollution, it is planned to increase Sevan water level to 1905m by 2013 after massif clean-up of shoreline zones from trees and other sources of pollution (Law of RA on Lake Sevan-https://www.arlis.am/) (Lake Sevan drainage basin planning project, 2013).

One should mention an intermediate period related to mismanaged release of the Sevan water for energetic needs in the 1990s during the energetic crisis in the country.

Since the early 1930s, the lake water level has been changing with different intensity (fig. 1) mainly due to overuse of century old resources of lake, and to a lesser degree due to climate change. As a result, shoreline changes have been affecting the ecological status of Lake Sevan and nearshore area. This all makes it urgent to study the shoreline changes and effects these produce on the nearshore belt   (Babayan et al., 2013; Baghdasaryan, Abrahamyan, & Aleksandryan, 1971).

Data collection

Remote sensing data

Landsat images applied in this study are provided in Tab. 1. Landsat imagery used for shoreline delineation was selected for August or days as close to August as possible to avoid seasonal fluctuations of lake water because it is in August when the river inflow to Lake Sevan is minimal. Images which are used to verify the accuracy of the results are selected as close as possible to January 1, which corresponds to the data of the measurements of the lake water level and the surface area (Hydrological regime of Lake Sevan, 2017).

This research employs Landsat imagery in open access through USGS online service (USGS-https://earthexplorer.usgs.gov/); Landsat TM, Landsat 8 OLI data are available in the World Geodetic System (WGS84) Datum and are projected using Universal Transverse Mercator system (USGS-https://landsat.usgs.gov).

National Aeronautics and Space Administration (NASA) provides images which have already been geometrically corrected and orthorectified to the so-called Landsat Level 1 (L1T) (Gutman et al., 2013). All Landsat images used in this research are Level 1 products from Landsat Collection 1. All images besides Landsat 1 MSS for 1973, correspond to Tier 1 category and are eligible for time series analysis. Image-to-image registration accuracy threshold is Root-Mean-Square-Error (RMSE) ≤12m (LANDSAT COLLECTION 1 LEVEL 1, 2017). For the image-to-image registration, Landsat 5 TM for 1985 was selected as a basic image. This image was georeferenced using a topographic map for 1984.

Ancillary data

Hydrological data – inflow and outflow components of water balance for the period of 1927-2015 necessary for this research were obtained from published sources and reference material published by the Service of the Hydrometeorology and Active Influence on Atmospheric Phenomena
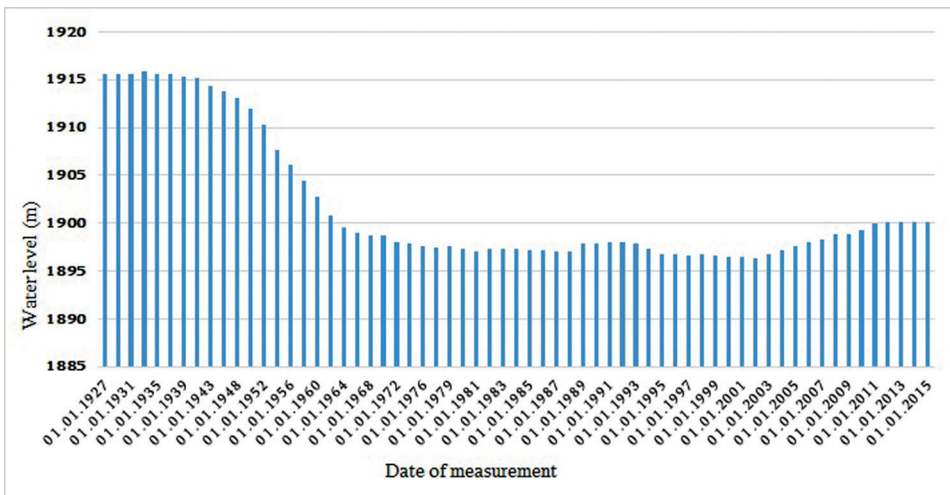

Fig. 1. Changes in Lake Sevan water level from 1927 to 2015

SNCO , Ministry of Emergency Situations RA (hereafter referred to as the Service) (Hydrological regime of Lake Sevan, 2017; Papikyan, 2011).

"Sevan" national park provided a GIS database on land use (protected areas, forested areas, species composition of trees and bushes, etc.) of Lake Sevan nearshore sites ("Sevan" national park- http://sevanpark.am/).

Methods

The shoreline delineation and shoreline change assessment methodology used in this research is given in Figure 2 and is discussed in detail below.

Shoreline delineation

The most applicable RS methods for water objects identification and classification and shoreline detection include classification (supervised and unsupervised) and spectral signature feature analysis, which in turn is divided into single-band and multi-band methods (Li et al., 2013).

A single–band method is based on selection of bands and thresholds, which show a water-to-land transition in a more precise way. A multi-band method is based on band ratio or on spectral indices. This method provides more precise information as it is based on the analysis of signature differences between

water and other surfaces. In the case of a simple band ratio, the ratio of one of visible bands, e.g., green, and NIR is calculated. On a productive image reflective properties of water objects are expressed stronger as compared to non-water objects (Qiao et al., 2012).

A spectral index most frequently used for detecting water bodies and assessing shoreline changes is Normalized Difference Water Index (NDWI) derived by McFeeters (1996). NDWI ranges from -1 to 1, where water has values above 0 and non-water objects have values below 0 (McFeeters, 1996). Later Xu (2006) proposed a Modified Normalized Difference Water Index, where MIR band is used instead of NIR band. According to Xu (2006), MNDWI as compared to NDWI is more acceptable for water bodies with larger amounts of built-up land on the background in nearshore sites, since it can effectively reduce and/or remove noise resulted from built-up land, bare soil and vegetation (Xu, 2006). Nonetheless, as the research advanced, all the above-mentioned methods were employed in order to find the most appropriate method for Lake Sevan.

DSAS is applied for assessing changes in shoreline position along the whole of the lake in selected time intervals between 1973 to 2015 (1973-1985, 1985-1990, 1990-1995, 1995-2002, 2002-2015 (the selection of time slots was based on Lake Sevan water level change periods and RS data availability).

Table 1. The applied Landsat images and their properties

RS data	Date	Resolution, m	Geometric RMSE model, m
Landsat 1MSS	July 13, 1973	80	17.159
Landsat 5 TM	August 21, 1985	30	4.666
Landsat 5 TM	September 20, 1990	30	4.587
Landsat 5 TM	September 02, 1995	30	4.261
Landsat 5 TM	December 20, 2001	30	6.473
Landsat 5 TM	August 04, 2002	30	4.102
Landsat 5 TM	December 16, 2010	30	6.604
Landsat 8 OLI	January 12, 2015	30	9.264
Landsat 8 OLI	September 09, 2015	30	7.001

As an example of a single-band method application, the NIR band was selected due to better absorption by water and reflection by vegetation and land. As a threshold value for water and non-water bodies, 0.1 is selected based on the values of visual differentiation between water and non-water on a space image histogram. Thus, reflectance values > 0.1 and <0.1 indicate land and water, respectively.

The Green/NIR band ratio is used to define the lake shoreline as an example of the band ratio method. In this case, a threshold value=1 is selected for water - non-water differentiation. Values > 1 and < 1 correspond to water and land, respectively. For NDWI and MNDWI, the aforesaid threshold value=0 was selected. The accuracy of shoreline delineation method was assessed through Root Mean Square Error.

Shoreline change assessment

 In order to implement Lake Sevan shoreline change assessment a DSAS tool developed by the United States Geological Survey (USGS) was used. This tool computes rate-of-change statistics for a time series of shoreline data. The statistics are represented by Net Shoreline Movement (NSM), which shows a distance between the oldest and youngest

shorelines for each transect. End Point Rate (EPR) denoting NMS divided into the number of years elapsed and showing the "velocity" of shoreline change, whereas Shoreline Change Envelop (SCE) is the distance between the shorelines farthest and closest to the baseline (Himmelstoss, 2009).

RESULTS AND DISSCUSION

Shoreline delineation and accuracy assessment

It should be stressed that the all the shoreline delineation methods tested when conducting this research gave good results. However, the best results were achieved when applying NDWI, and it was the reason for which subsequent shoreline delineation for all dates was conducted using NDWI alone. (Fig. 4 a-e). Correlation of data of surface area of Lake Sevan provided by Service (Table 2) (Kireev, 1933) with surface area data derived using NDWI gives (shows) RMSE value of 8.15.

Analysis of GIS database provided by "Sevan" national park shows that almost 1900 ha of forests (trees and shrubs) were watered as a result of Lake Sevan water level rise between 2002-2015 as the main water level rise took place on that period.
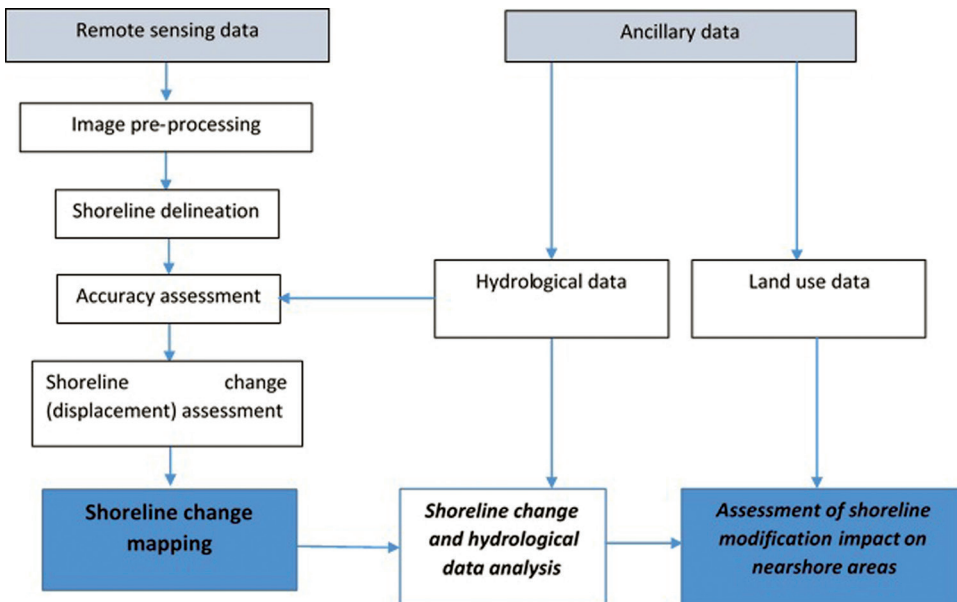

Fig. 2. A summarized methodology of delineation of shorelines and assessment of their spatiotemporal changes

Table 2. The area of Lake Sevan according to Service and NDWI

Date (Space image/Service)	Area, sq.km (Service)	Area sq.km (NDWI)
23.12.2001/01.01.2002	1236.2	1231.13
16.12.2010/01.01.2011	1272.8	1263.32
12.01.2015/01.01.2015	1274.99	1265.83

Total shoreline change analysis for each time period

The onshore baseline shapefile was created at a distance of 200 m from the last shoreline position (2015). The selected transects spacing was 300 m for the whole of the lake. All the transects which intersected the shorelines more than once, were manually deleted in order to avoid computational errors, a confidence interval being set within 90%.

DSAS statistics NSM, EPR describe a change in shoreline from the first to the last date (1793-2015 in this case), whereas SCE describes the overall change in shoreline position. These statistics cannot fully reflect a real picture of shoreline changes because Lake Sevan shoreline changes on different time periods had different directions. In order to understand the cause of changes, DSAS was applied for each period of time and data were compared with hydrological data on water balance (Fig. 3a) (The Digital Shoreline Analysis System (DSAS) Version 4.0 - An ArcGIS extension for calculating shoreline change, 2009). The data of almost 750 transects for each period were analysed. Minimum and maximum transect lengths are given in Figure 3b, which corresponds to NSM for each of transects. As baseline location is selected "Onshore" in DSAS, negative values of NSM correspond to shoreline (water) movement towards land.

The period between 1973 and 1985 is selected because the first available Landsat image for Lake Sevan is for 1973 and the image of 1985 is the nearest available image to 1981 when intensive lowering of Lake Sevan water level stopped and a water level stabilization period started. The average annual water balance is negative for that period as seen from Fig. 3a. As a result, shoreline moved towards the water.

The period between 1985 and 1990 was a lake water level stabilization period, when Arpa river water via the Arpa-Sevan tunnel was inflowing to Lake. Water balance was positive and as a result, shoreline moved towards the land.

The period between 1990 and 1995 corresponds to that of energetic crisis in Armenia, when additional volumes of lake water released for energetic purposes resulted in water level lowering and subsequent shoreline movement toward the water.

According to the water balance data for the period of 1995-2002, water inflow slightly exceeds outflow but the shoreline moves in the opposite direction.

The last considered period is 2002-2015. 2002 corresponds to the beginning of Lake Sevan restoration consistent with the RA Government Program (World Bank Technical Paper, 2001) (Parliament-http://parliament.am/legislation.php?sel=show&ID=1676&lang=arm).

As a result, the water inflow to Lake Sevan has increased due to the operation of Vorotan-Arpa tunnel. As seen from Figure 3b, the absolute NSM value is higher in this period and the direction of the shoreline movement is towards land.

Besides, Fig. 3b shows that basic shoreline changes exceed 30 m – the pixel size of most of Landsat images used in this study. This is robust evidence of changes that occurred in shoreline positions, even if accounting for a problem of mixed pixels and misclassification.

a

b
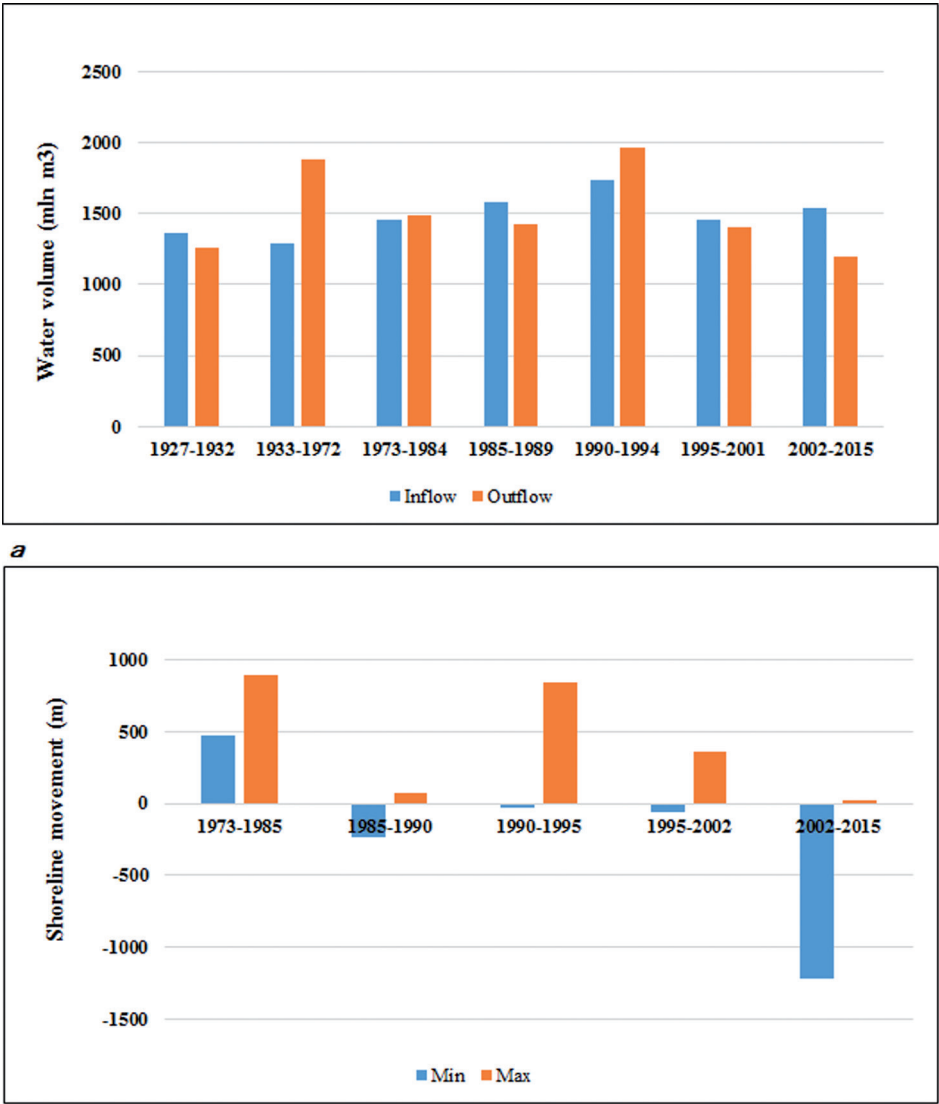
Fig. 3. The averaged values of water inflow and outflow for the period of 1927-2015 (a) and Shoreline changes for each period of time (1973-2015) represented by NSM (b)
(first two time periods on Fig. 3.a are included in order to visualize the lake water balance in natural conditions (1927-1932) and after water level lowering (1933-1972))

Shoreline change analysis for each region

Because of the variety of forms and complexity of relief of Lake Sevan and its shores, the shoreline changes are dissimilar in different parts along the entire shoreline. In the areas with relatively plane relief shorelines were changed significantly. Five regions were distinguished based on more significant changes. In those regions, DSAS was applied for a period of 1973-2015. For the Regions 1 to 4 Onshore baseline and transect spacing 300 m were selected. Shoreline in Region 5 is more complicated and Onshore/Offshore baseline and transect spacing 50 m was set. In this case the confidence interval has also been set within 90%.

The shores of Small Sevan are steeper than those of Big Sevan especially on sections where the shore is edged by steep slopes

of Areguni mountain range, and partly the western shore. So, lake water fluctuation does not cause more changes in shoreline in these areas. The shores near Lchashen village and town of Sevan (Region-1) and Gavaraget estuary (Region-3) are changed significantly. Changes in the eastern shore of Big Sevan and that located close to Artanish peninsula are not significant. The southern (Region-1) and western (Region-2) shorelines are changed significantly. The statistics of change rates are provided in Table 3.

Region 1 is a shoreline of almost 1400 km. As seen from Fig. 4a, the shoreline transformations in this region are similar to transformations of entire shoreline for the period of 1973-2015. As it can be seen from Table 3, the shoreline mean movement rate is 2.26 ± 0.15 m/year for the period of 1973-2015. In the case of Lake Sevan, this figure cannot reflect the real picture of changes, because shoreline movements for different periods had a different direction. DSAS gives statistics (in particular EPR and NSM) for the period of 1973-2015. The longest shoreline displacement for this period (NSM) is towards land and is almost 244 m. But the largest displacement of shoreline (SCE) – some 610 m - occurred between 2002 and 2015. Table 3 and Figure 4a show that shoreline movement direction is not the same for the entire region. In some parts of shoreline, there is a movement opposite to the main direction. The causes may be both cartographic errors and natural and manmade processes. In the case of Region 1, the main reason is the land assertion in the estuary of the Masrik river. Region 1 is on the territory of Gili reserves, and partly on the territory of Vardenis and Tsovak forests. In the result of a water level rise, part of these forests covering some 420 ha and consisting mainly of poplar and willow trees are completely submerged by the lake.

Table 3. Statistics of Lake Sevan shoreline in different regions (segments) from 1973-2015

Regions	Statistics	EPR (m/yr)	LMS (m/yr)	LRR (m/yr)	SCE (m)	NSM (m)
R-1	Min	-6.1	2.76	-5.18	172.22	-244.99
	Max	1.11	14.71	1.62	610.03	44.71
	Mean	-2.26	10.18	-1.16	376.22	-90.84
R-2	Min	-8.25	3.06	-4.76	174.4	-347.9
	Max	-1.04	19.82	0.04	755.77	-43.94
	Mean	-3.72	9.81	-1.56	454.11	-156.78
R-3	Min	-12.67	-0.96	-10.56	42.2	-534.13
	Max	-0.21	13.88	-0.15	691.94	-8.85
	Mean	-4.85	3.83	-3.66	328.22	-204.66
R-4	Min	-5.93	-1.87	-4.21	22.68	-250.06
	Max	-0.47	5.73	0.11	413.62	-19.79
	Mean	-2.9	2.87	-1.92	218.52	-122.28
R-5	Min	-15.75	-13.92	-13	6.95	664.15
	Max	0.87	19.73	4.57	814.8	36.59
	Mean	-2.53	2.65	-1.46	268.95	-106.88

Region 2 is an almost 7600 m long shoreline (Fig. 4b). The shoreline movement in this region reflects the movement along the entire shoreline for all periods. The mean shoreline movement rate between 1973 and 2015 is 3.72 ± 0.15 m/year. From 1973 to 2015, shoreline maximum displacement is almost 348 m, but the longest change occurred between 2002 and 2015 - almost 755 m. This region is partly on the territory of Gavaraget sanctuary, and partly on the territory of Noraduz forest. Today, almost 100 ha of forested and sea-buckthorn –planted area is also submerged by the lake as a consequence of the Sevan water level rise.

Shoreline in Region 3 has almost 9200 m length (Fig. 4c). Mean shoreline movement towards land is 4.85 ± 0.15 m/year from 1973 to 2015. From 1973 to 2015, shoreline displacement is almost 692 m. The longest displacement - some 534 m - occurred between 2002 and 2015. This region partly lies on the territory of Gavaraget sanctuary. It also occupies part of territories of Noraduz and Ajrivank forests. The area submerged by the lake is almost 160 ha, main submerged species being poplar, willow and sea buckthorn.

Region 4 has almost 3700 m length shoreline (Fig. 4d). The mean shoreline movement from 1973 to 2015 is 2.9±0.15 m/year. In this Region, the longest shoreline movement towards land (250 m) occurred between 1973 and 2015; the longest distance between these shorelines in this Region was recorded between 2002 and 2015. The mean and maximum movement from that point (SCE) is 218 and 413, respectively. This Region is on the territory of Sevan forest, where some 25 ha of poplar trees and sea buckthorn bushes are submerged by the lake.

Region 5 is the most complicated region (Fig. 4e). Shoreline in this region is very complex. Even transect spacing of 50 m instead of 300 m set for other regions could not give the real picture of this region. This region is on the territory of Norashen reserves. Its relief is flat and the shore rugged. In the Norashen reserves, there are three small lakes (black circled in Fig. 4e Region 5 a) (IRTEK-http://www.irtek.am/views/act.aspx?aid=41347).

DSAS cannot give the real picture of changes in this area even if it shows that shoreline maximum displacement is almost 815 m. As seen from the map of the Region, the shorelines of small lakes in this area are not always separated from Lake Sevan. Presumably, shoreline movement by 815 m is the perimeter of one of small lakes (upper left side) rather than the shoreline real displacement. Sources of error can be both differences in spatial resolution (80 m for 1973 and 30 m for 2015) and seasonal changes in water level. As soon as this area is flat, it can be affected by seasonal water level rising.

CONCLUSIONS

The application of RS methods and particularly Landsat image-based delineation of shorelines using NDWI spectral index gives sufficiently reliable results for Lake Sevan. This method is used not only for shoreline delineation, but also for visualizing changes in Lake Sevan shoreline. Applying DSAS in its turn helps make statistical and quantitative spatiotemporal analyses of shoreline changes.

The shoreline change analyses show that these changes correspond to water balance changes. Because of different landforms, the consequences of shoreline changes are different along the whole length of shore. In the areas where the shore is edged by gentle slopes the shoreline displacement can even reach 600-700 m, on a steep slope edging areas shoreline changes being insignificant.
 A water index NDWI is a reliable method for shoreline delineation, nonetheless in some cases DSAS calculations indicate some inconsistencies with the direction of the main shoreline course. Most of these are within one-pixel size (30 m) and are supposed to be cartographic or computational errors. In the larger areas, the causes can include natural phenomena as it was in the case of Region 1, or man-made impacts (sprawls, etc.).

Shoreline displacements, especially when occurring on larger territories, affect nearshore areas and the land use in Lake Sevan region. After Lake Sevan water level had lowered, water-free places were planted by trees and shrubs. However, since 2002 water level has been rising steadily, and these areas

Fig. 4a. Lake Sevan with outlined Region 1, shoreline positions in each date and shorelines displacements

Fig. 4b. Lake Sevan with outlined Region 2, shoreline positions in each date and shorelines displacements

Fig. 4c. Lake Sevan with outlined Region 3, shoreline positions in each date and shorelines displacements
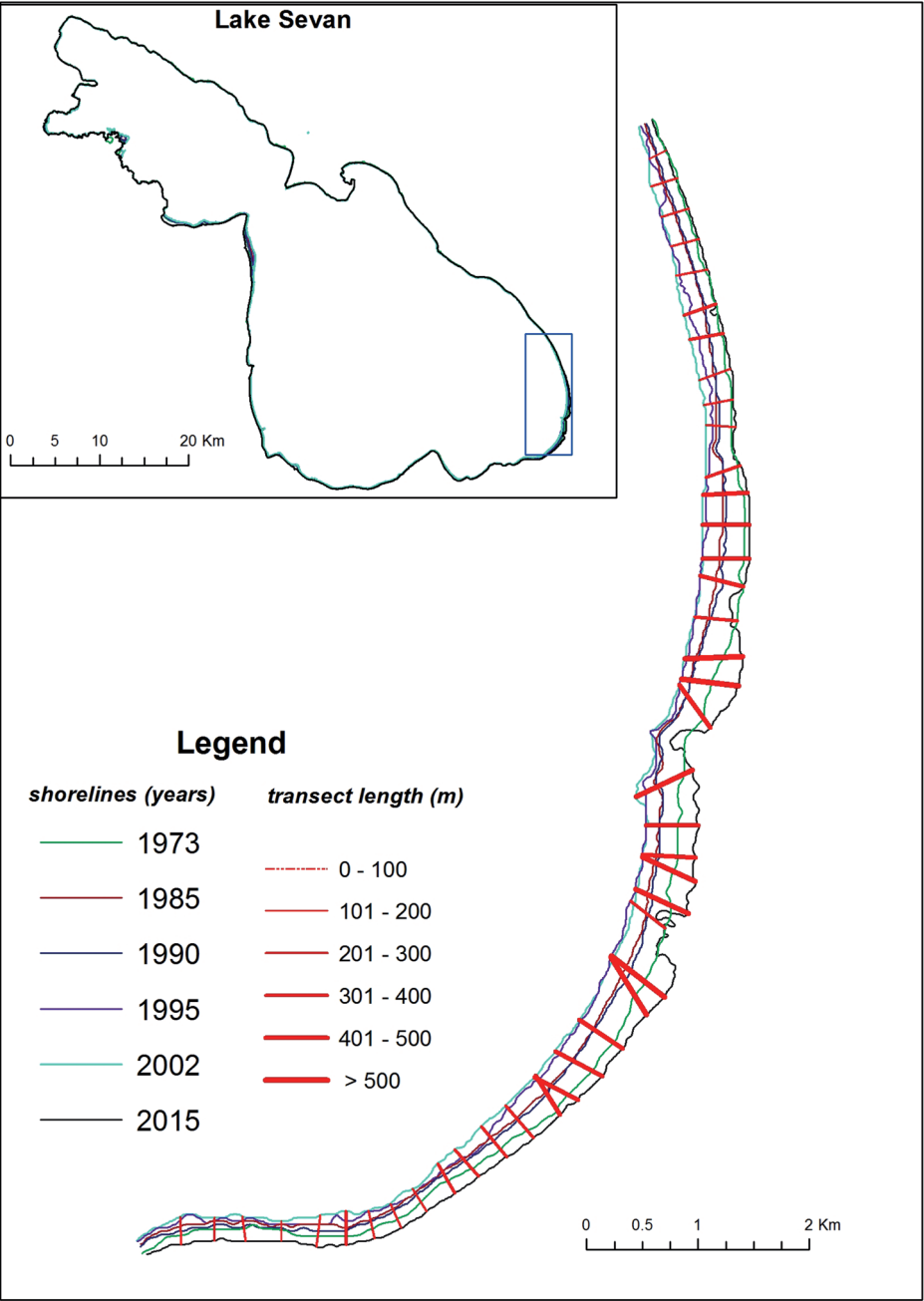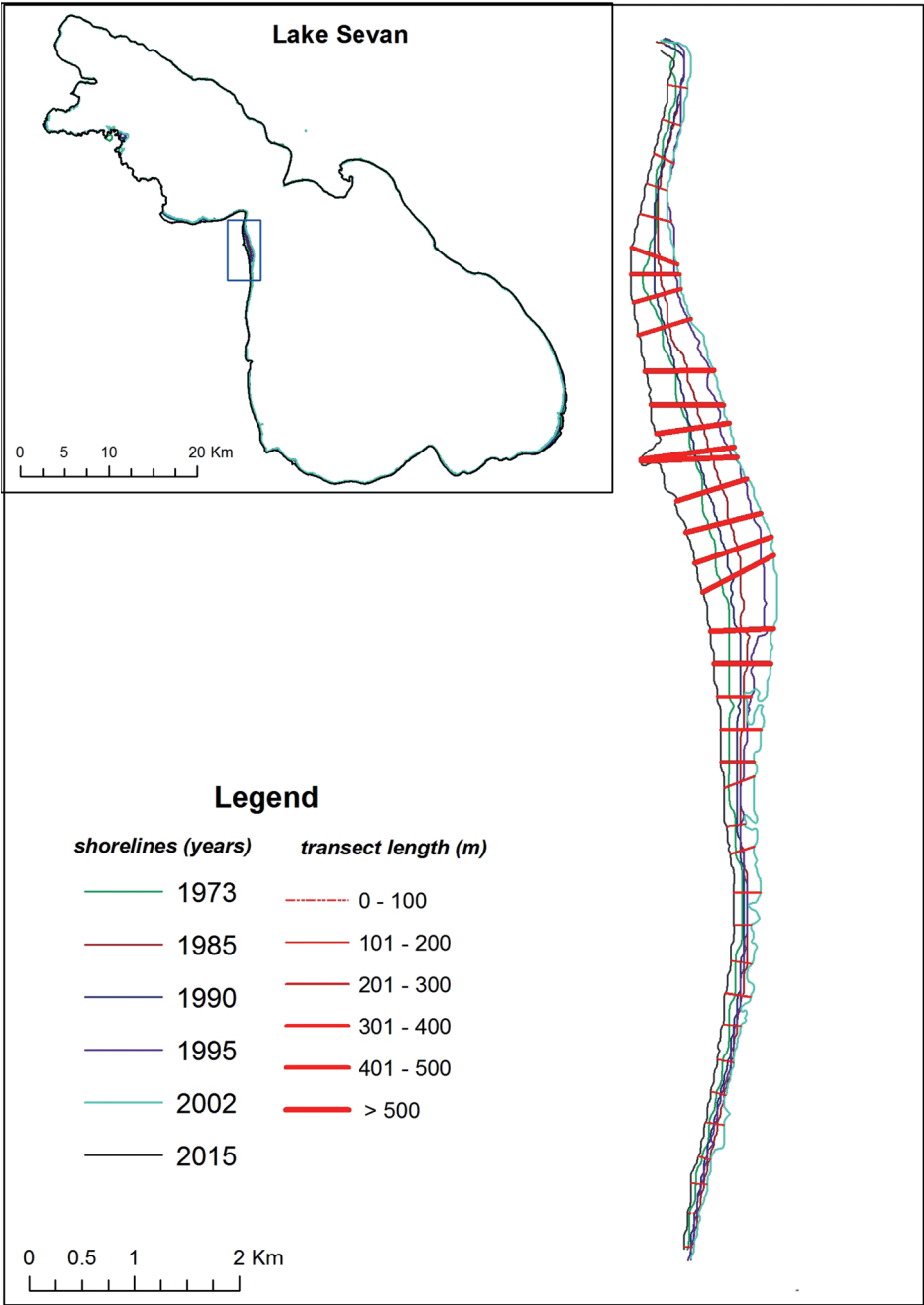
Fig. 4d. Lake Sevan with outlined Region 4, shoreline positions in each date and shorelines displacements

Fig. 4e. Lake Sevan with outlined Region 4, shoreline positions in each date and shorelines displacements
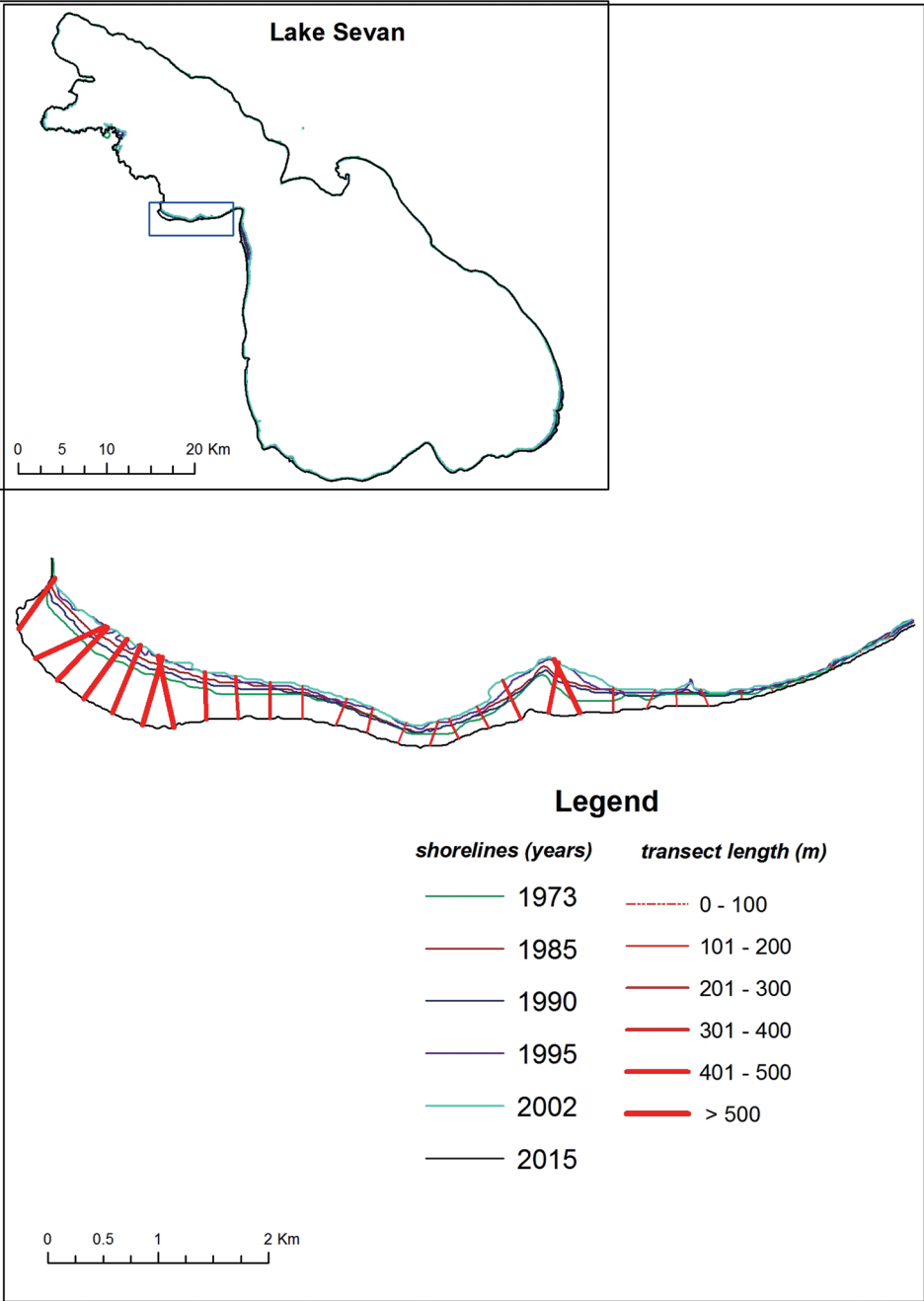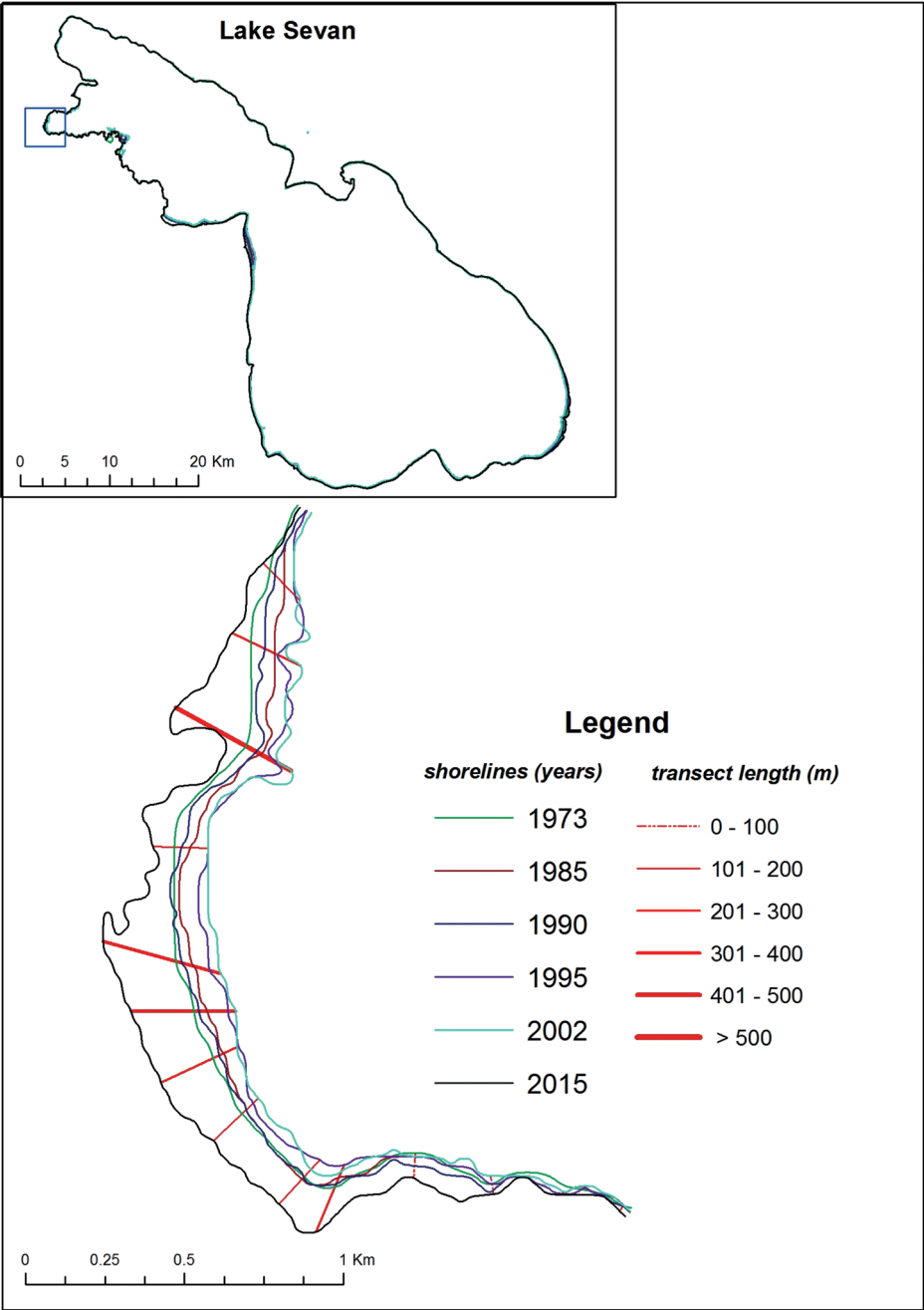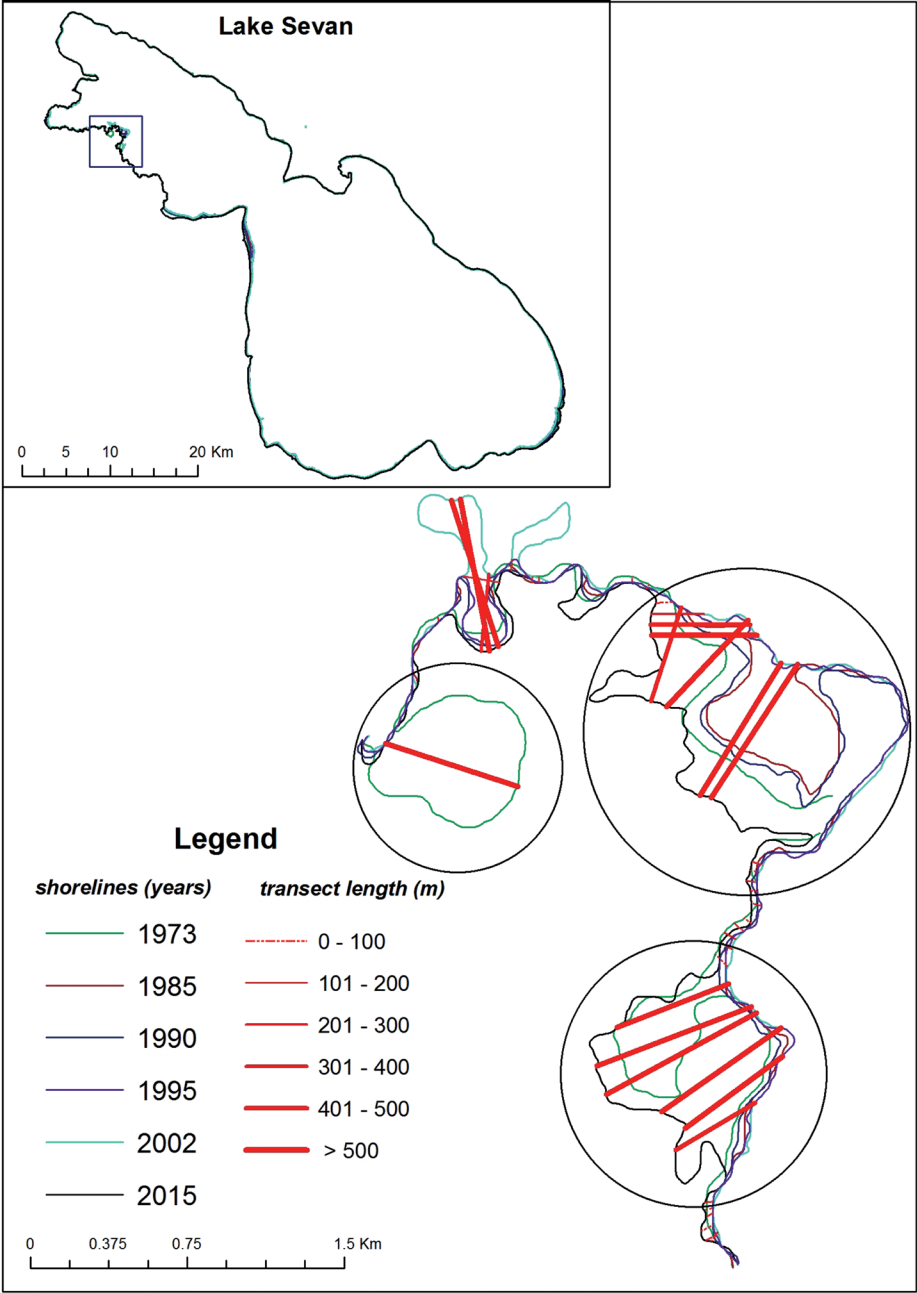
are submerged by the lake. To avoid further eutrophication of the lake in consequence of water level rise to the 1905 m it is necessary to properly clean nearshore areas.

REFERENCES

Agyemang, T. K., Schmieder, K., Heege, T., Heblinski, J., Sajadyan, H., Vardanyan, L., & Böcker, R. (2017). Reviewing Lake Sevan's surface area using remote sensing & GIS techniques. SIL Proceedings, 1922-2010, 30(8), 1264–1266. https://doi.org/10.1080/03680770.2009.11923926

Aladin, N., Crétaux, J. F., Plotnikov, I. S., Kouraev, A. V., Smurov, A. O., Cazenave, A., … Papa, F. (2005). Modern hydro-biological state of the Small Aral sea. Environmetrics, 16(4), 375–392. https://doi.org/10.1002/env.709

Alesheikh, A. A., Ghorbanali, A., & Nouri, N. (2007). Coastline change detection using remote sensing. International Journal of Environmental Science and Technology, 4(1), 61–66. https://doi.org/10.1007/BF03325962

Babayan A., Hakobyan S., Jenderjyan K., Muradyan S., (2013). Lake Sevan: Experience and Lessons learned Brief. Experience and Lessons Learned Brief, 6, 347–362. Retrieved from http://www.ndr.mw:8080/xmlui/handle/123456789/384

Babich D.B., Vinogradov N.N., Ivanov V.V., Korotaev V.N., Chalova E.R. (2015). DELTAS OF THE RIVERS RUNNING IN TO LAKES AND RESERVOIRS: MORPHOGENETIC TYPES AND RECENT DYNAMICS. Vestnik Moskovskogo Unviersiteta, Seriya Geografiya, 4, 18-26. (In Russian with English summary)

Baghdasaryan, A. B., Abrahamyan, S. B., & Aleksandryan, G. A. (1971). Physical geography of Armenian SSR. (A. Baghdasaryan (editor-in-chief), Ed.). Yerevan: AS ArmSSR.

Bagli, S., Soille, P., & Fermi, E. (2004). Automatic delineation of shoreline and lake boundaries from Landsat satellite images. Proceedings of Initial ECO-IMAGINE GI and GIS for Integragted Coastal Management, (May), 13–16. Retrieved from http://www.gisig.it/eco-imagine/full papers/bagli-soille2004eipaper.pdf

Bai, J., Chen, X., Li, J., Yang, L., & Fang, H. (2011). Changes in the area of inland lakes in arid regions of central Asia during the past 30 years. Environmental Monitoring and Assessment, 178(1–4), 247–256. https://doi.org/10.1007/s10661-010-1686-y

Boak, E. H., & Turner, I. L. (2006). Shoreline Definition and Detection: A Review. Journal of Coastal Research, 214, 688–703. https://doi.org/10.2112/03-0071.1

Dokulil, M. T. (2014). Impact of climate warming on European inland waters. Inland Waters, 4(1), 27–40. https://doi.org/10.5268/IW-4.1.705

Du, Z., Li, W., Zhou, D., Tian, L., Ling, F., Wang, H., … Sun, B. (2014). Analysis of Landsat-8 OLI imagery for land surface water mapping. Remote Sensing Letters, 5(7), 672–681. https://doi.org/10.1080/2150704X.2014.960606

Duru, U. (2017). Shoreline change assessment using multi-temporal satellite images : a case study of Lake Sapanca , NW Turkey. https://doi.org/10.1007/s10661-017-6112-2

El-asmar, H. M., Hereher, M. E., & Kafrawy, S. B. El. (2013). Surface area change detection of the Burullus Lagoon , North of the Nile Delta , Egypt , using water indices : A remote sensing approach. The Egyptian Journal of Remote Sensing and Space Sciences, 16(1), 119–123. https://doi.org/10.1016/j.ejrs.2013.04.004

Feyisa, G. L., Meilby, H., Fensholt, R., & Proud, S. R. (2014). Automated Water Extraction Index: A new technique for surface water mapping using Landsat imagery. Remote Sensing of Environment, 140(January), 23–35. https://doi.org/10.1016/j.rse.2013.08.029

Gutman, G., Huang, C., Chander, G., Noojipady, P., & Masek, J. G. (2013). Assessment of the NASA-USGS Global Land Survey (GLS) datasets. Remote Sensing of Environment, 134, 249–265. https://doi.org/10.1016/j.rse.2013.02.026

Hydrological regime of Lake Sevan. (2017). Yerevan.

Kireev, V. (1933). Materials on the investigation of Sevan its basin. (V. Davydov, Ed.). Leningrad.

Lake Sevan drainage basin planning project, Pub. L. No. 746- ǔ (2013). Armenia.

Li, W., Du, Z., Ling, F., Zhou, D., Wang, H., Gui, Y., … Zhang, X. (2013). A comparison of land surface water mapping using the normalized difference water index from TM, ETM+ and ALI. Remote Sensing, 5(11), 5530–5549. https://doi.org/10.3390/rs5115530

McFeeters, S. K. (1996). The use of the Normalized Difference Water Index (NDWI) in the delineation of open water features. International Journal of Remote Sensing, 17(7), 1425–1432. https://doi.org/10.1080/01431169608948714

Ministry of Nature Protection of the Republic of Armenia. (1998). First national communication of the Republic of Armenia under the United Nations Framework Convention on Climate Change.

Ogannesian R. (1994). Lake Sevan yesterday, today... Yerevan.

Oyedotun, T. D. T. (2017). Historical Shoreline Changes as Indication of Geomorphic Phases in St Ives and Padstow Bays of Southwest England. Environmental Processes, 4(1), 273–282. https://doi.org/10.1007/s40710-017-0213-3

Papikyan, S. (2011). Sevan Problem. Yerevan.

Pavlov, D. S., Kopylov, A. I., Poddubny, S. A., Gabrielyan, B. K., Chilingaryan, L. A., Mnatsakanyan, B. P., … Krylov, A. V. (2010). Ecology of Lake Sevan during a raise of its level. The Results of Russian-Armenian Biological Expedition for Hydroecological Survey of Lake Sevan (Armenia) (2005–2009). (K. A. Pavlov D., Poddubniy S., Gabrielyan B., Ed.). Makhachkala.

Pekel, J.-F., Cottam, A., Gorelick, N., & Belward, A. S. (2016). High-resolution mapping of global surface water and its long-term changes. Nature, 540(7633), 418–422. https://doi.org/10.1038/nature20584

Qiao, C., Luo, J., Sheng, Y., Shen, Z., Zhu, Z., & Ming, D. (2012). An Adaptive Water Extraction Method from Remote Sensing Image Based on NDWI. Journal of the Indian Society of Remote Sensing, 40(3), 421–433. https://doi.org/10.1007/s12524-011-0162-7

Qiao, G., Mi, H., Wang, W., Tong, X., Li, Z., Li, T., … Hong, Y. (2018). 55-year (1960–2015) spatiotemporal shoreline change analysis using historical DISP and Landsat time series data in Shanghai. International Journal of Applied Earth Observation and Geoinformation, 68(February), 238–251. https://doi.org/10.1016/j.jag.2018.02.009

Samanta, S., & Paul, S. K. (2016). Geospatial analysis of shoreline and land use/land cover changes through remote sensing and GIS techniques. Modeling Earth Systems and Environment, 2(3), 108. https://doi.org/10.1007/s40808-016-0180-0

The Digital Shoreline Analysis System (DSAS) Version 4.0 - An ArcGIS extension for calculating shoreline change. (2009).

Timoshkin, O. A., Samsonov, D. P., Yamamuro, M., Moore, M. V., Belykh, O. I., Malnik, V. V., … Bukshuk, N. A. (2016). Rapid ecological change in the coastal zone of Lake Baikal (East Siberia): Is the site of the world's greatest freshwater biodiversity in danger? Journal of Great Lakes Research, 42(3), 487–497. https://doi.org/10.1016/j.jglr.2016.02.011

USGS EROS. (2017). Landsat Collection 1 Level 1 Product Definition. Retrieved from https://landsat.usgs.gov/sites/default/files/documents/LSDS-1656_Landsat_Level-1_Product_Collection_Definition.pdf

Vogt, J., Soille, P., De Jager, A., Rimavičiūtė, E., Mehl, W., Foisneau, S., … Bamps, C. (2007). A pan-European river and catchment database. JRC Reference Reports. https://doi.org/10.2788/35907

Wulder, M. A., White, J. C., Loveland, T. R., Woodcock, C. E., Belward, A. S., Cohen, W. B., … Roy, D. P. (2016). Remote Sensing of Environment The global Landsat archive : Status , consolidation , and direction. Remote Sensing of Environment, 185, 271–283. https://doi.org/10.1016/j.rse.2015.11.032

Xu, H. (2006). Modification of normalised difference water index (NDWI) to enhance open water features in remotely sensed imagery. International Journal of Remote Sensing, 27(14), 3025–3033. https://doi.org/10.1080/01431160600589179

USGS, (2019). USGS Landsat missions [online] Available at: https://landsat.usgs.gov [Accessed 22 January 2019]

Nikolay S. Yasinskiy[1*], Oksana N. Erina[2], Dmitry I. Sokolov[2],
Alexander I. Belolubtsev[3]

[1] MapMakers Group Ltd., Novovagankovskiy In., 5, bld. 1, 123242, Moscow, Russia
[2] The Department of Land Hydrology, Faculty of Geography, Lomonosov Moscow State University, Vorobiovy Gory, 1, 119991, Moscow, Russia
[3] The Department of Meteorology and Climatology, Faculty of Agronomy and Biotechnology, Timiryazev State Agrarian University, Pryanishnikova str., 12, 127550, Moscow, Russia
* Corresponding author: jasen.y@mail.ru

MODELLING PHOSPHORUS INFLOW TO THE MOZHAYSKOE RESERVOIR WITH THE HYPE HYDROLOGICAL MODEL

ABSTRACT. Biogenic flow is the determining factor of ecological well-being of water bodies. It depends on a number of factors, such as weather conditions, soil and vegetation cover, agricultural use of the catchment area. Its simulation is possible based on a complex water quality model with parameters distribution. In this paper, we show that the model calculates the water flow with satisfactory accuracy and gives reliable values of phosphorus flow in the investigated river outlet. The influence of dryness of the year on the phosphorus flow is important and reduces dissolved phosphorus flow several times. The results of experiments with the model show a decrease of dissolved phosphorus flow subsequent to cease of fertilizing in range from 5 to 11%. The values of the surface and groundwater genetic components of phosphorus flow are comparable, while soil component amounts 65% of local phosphorus flow.

KEY WORDS: Phosphorus, HYPE, river flow modeling, nutrients, eutrophication, Mozhayskoe reservoir

INTRODUCTION

Biogenic flow is an essential factor for hydroecological condition of water bodies. The influence of meteorological conditions, topography, agricultural development of the catchment area, soil and vegetation should be taken into account while modelling it. It should be much emphasized in our opinion, that the very models with distributed or semi-distributed parameters are the most adequate tool for assessment of agricultural development impact on biogenic flow. While choosing an appropriate model, the physical validity of the parameters, the flexibility of settings, volume, and complexity of obtaining input data hit the first place.

In this study, we have shown that the HYPE model could provide phosphorus

flow simulation for a small river with an agricultural watershed, that can be used for analysis of phosphorus flow and its genetic components. The first part of the article presents the results of survey of the Mozhayskoe reservoir catchment area, used to configure the HYPE water quality model of the Swedish hydrometeorological Institute (SHMI) and hydrological and geographical features of the modeling object. The second part discusses the results of modelling the phosphorus flow and concentrations for the catchment of the upper Moskva river upstream the Mozhayskoe reservoir. The phosphorus annual and seasonal flow for dry and wet years was calculated from the simulation as well as its genetic components. The HYPE (HYdrologic Predictions in the Environment) is a dynamic, semi-distributed, physically based, watershed scale hydrological model for continuous simulation (Lindström 2010). The model has been being developed from 2005 at SMHI (Swedish Hydrometeorology Institute) and successfully used there for river flow forecasting. As for Russian Federation, the model was used in the research of great Siberian watersheds (Gelfan et al. 2017). Simple format of the input files, flexible customization, series of alternative built-in models for the calculation of main components of water and chemical balance, and transport processes of water and chemicals are the main advantages of HYPE.

Object of study

We have chosen the upper Moskva river catchment upstream of the Mozhayskoe reservoir as an object due to its natural and water management features, as well as to higher degree of knowledge of its territory, chemical and water runoff in common as compared with other watersheds of water reservoirs. It forms an inflow into the Mozhayskoe reservoir, which is a part of the drinking water supply system of the Moscow city.

The catchment area is situated in the central part of the Smolensk-Moscow upland and belongs to the province of glacial hilly and flat plains. The height of the catchment varies from 160 to 311 m. The highest point

of the watershed, which divides catchments of the Moskva, the Ugra and the Protva rivers, is located within the Gzhatsko-Mozhaysky ridge of the Smolensk-Moscow upland being also the highest point of the Moscow region. The width of the Moskva River in the upper reaches is 2–15 m. The climate of the basin of the Mozhayskoe reservoir is moderately continental with cold winters and moderately warm summers.

The catchment area has a high degree of agricultural development. According to our estimates, the share of agricultural land in the total catchment area is 31%, 2% - floodplain meadows, 2% - rural settlements and household plots, the rest of the area - 65% is occupied by mixed forests. The land includes: intensively used arable land with growing potatoes, corn, feeding root crops with annual distribution of a large amount of organic and mineral fertilizers; moderately used arable land with grains and perennial grasses cultivation with occasional cattle grazing and fertilization in the part of the area; least intensively used arable land is the one with the predominant perennial grasses cultivation and regular fertilization in small quantities; pastures; hayfields which include floodplain water meadows.

The landuse data used in the work represents the situation of 1984-1985 (see Figure 1). Comparison of the landuse pattern of that period with modern satellite images indicates a slight change in the outlines of the fields. On the other hand, field studies have shown that about 2/3 of the land that was used as arable land in the 80s is now abandoned.

Currently, a number of enterprises of the agro-industrial complex, such as CJSC "Shinichino", CJSC "Uvarovsky" kolkhoz", CJSC "Porechye" and others, engaged in plant growing and animal husbandry, operate on the territory of the studied watershed. Also, in the catchment area there are several farms and peasant farms engaged in plant growing, animal husbandry, and poultry farming.
Fig. 1. Maps of the catchment of the upper Moskva river (left) and landuse with survey points (right).
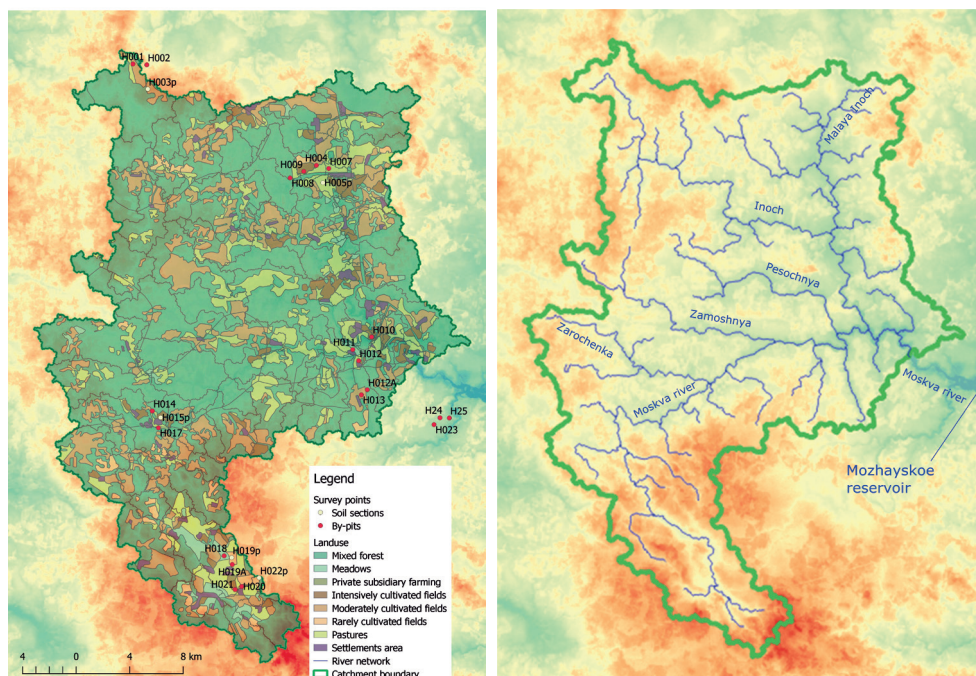
Fig. 1. Maps of the catchment of the upper Moskva river (left) and landuse with survey points (right)

The Mozhayskoe reservoir is experiencing a significant nutrient load almost since its creation, which is confirmed by studies of the primary production growth rate in the spring and summer period. In the 70s, the reservoir was second among all reservoirs of the Moskva River basin by average values of permanganate index in summer period (Edelshtein K. et al. 1978). Studies of the phosphorus flow from river bed sediments conducted in 1979 (Martynova 1979) and 1995 (Edelshtein 1995) indicate its increase. In 2009 year, under conditions of increasing water turnover, decreasing dryness of the year and low reservoir level high values of primary phytoplankton production and a slight predominance of destruction over primary production were observed (Kremenetskaya et al. 2015).

Due to the variability of ratio of the nutrient balance components during the year depending on weather conditions, stratification of the water column and the regime of water inflow into the reservoir, researchers note the importance of treating the components of the reservoir nutrient balance separately (Datsenko 2007). In this view modeling of nutrient runoff from the reservoir catchment becomes especially relevant.

Previous research

The observations of biogenic flow in the Moscow region have been being conducted from 1970s till now based on the Krasnovidovo laboratory of Moscow State University. They included biogenes, suspended materials, consumed oxygen water sampling at the outlets of the Moskva river and its tributaries. There were no trials of modelling the biogenic inflow into the Mozhayskoe reservoir, but several studies illustrate water inflow simulations made with ECOMAG model (Antokhina and Zhuk 2011; Motovilov et al. 2018) and GR4J model (Ayzel et al. 2019). Also, there are series of studies that are aimed at evaluating a modelling methodology of water masses transfer (the case of Uchinskoe reservoir (Datsenko 2019)) or characterize the variability of phosphorus and other hydrochemical parameters in the waters of Mozhayskoe reservoir (Sokolov et al. 2016).

Obtained data and methods used in the research

The series of temperature and precipitation at the meteorological stations of Mozhaysk, Gagarin, Volokolamsk, Staritsa, Klin, Maloyaroslavets for the period from 1997 to 2018 were used as meteorological information. Discharges, waterlevels and other hydrological information at the gauge Barsuki on the Moskva river were used for model calibration and verification.

We used the results of field research of the catchment, conducted by Yasinskiy N. in August - September 2017, for parameterization of the model (Yasinskiy and Belolyubtsev 2019). This comprised the initial level of phosphorus in soil, its distribution through the soil profile. Rates of residues degradation and mineralization as well as density of the soil solid phase were based on common values taken from academic books, study guides and some studies concerning in-stream chemical processes (Datsenko and Puklakov 2010; Kremenetskaya et al. 2015). Soil samples were studied in the laboratory of the Testing Center for Soil and Ecological Research of the Faculty of Soil Science at the K.A. Timiryazev University (RSAU-MAA).

The data on the phosphorus concentrations in the Moskva river, obtained by the authors and others in different years during the period from 1983 to 2012 at the Krasnovidovo Laboratory for Water Reservoirs Research, was used for calibration of the model's chemical block.

The map of agricultural land of the the Mozhayskiy Site (the territory of upper influents of the Mozhayskoe water reservoir) was developed at the Department of Physical Geography and Landscape Studies of the Geographical Faculty of Moscow State University in the 1980s by I.A. Gorbunova. It characterizes the landuse in the period before the general decline in agricultural production in the 1990s. For the purposes of our study, the map was georeferenced, digitized and corrected using modern satellite images for the period of 2015 - 2017, published in open sources. Digital elevation models with a resolution of 1 minute (30 m),

formed with SRTM Mission Data, were taken from open sources (USGS). For some farms, we obtained statistical information on the amount and timing of fertilizer application.

The HYPE spatial approach is based on dividing the catchment area into sub-catchments with an arbitrary degree of detalization and identifying non-localized landscape-landuse classes defined as an area fraction for each subcatchment (Pers 2014). Therein lies the core sense of parameters semidistribution (Xu 2002). Within each sub-basin snow cover formation, movement of water and substances in different soil horizons (up to three) and movement of groundwater are modelled. The water runoff formed within a subwatershed comes first to the local and then to the main river network. Both networks have parameters independent of each other. The transport of nutrients in the model is divided into groups of processes related to fertilizer input, plant consumption, transformation in soil cover, removal with suspended solids and water runoff and transformations during its movement along the river network. Fertilizer supply is set explicitly, depending on the crop and alternation of agricultural activities. Plant growth is simulated according to the timing of plowing, planting and harvesting and is set for each class. The complex of processes occurring in the soil cover comes to the movement of substances between pools. So, for phosphorus, a pool of humus organic phosphorus, organic phosphorus, dissolved organic and dissolved inorganic phosphorus, as well as phosphorus adsorbed on soil particles can be distinguished.

The HYPE model, which is a hydrological model of water quality, makes part of the HYSS modeling system, which comprises loading input files, optimizing parameters and recording results. At the preliminary stage, text files with subwatersheds data and river network characteristics, and a file with classes description should be generated. We developed them in the GRASS GIS environment, so a digital river network, a layer of 86 subcatchments, a corrected landuse map and a soil map were created on the basis of the digital elevation model. Based on available landuse and soil types,

a classification of 27 classes was compiled. After that, in the QGIS environment, GIS layers were superimposed on each other, the shares of the area occupied by each class in the area of each sub-collection were calculated. The final processing of the files was carried out in Excel and the RHYPE package written in R, designed by HYPE model developers to prepare, analyze and graphically display simulation results.

We have distinguished arable land with intensive, medium and low intensity of agriculture activity; meadows; pastures; kitchen gardens and territories of rural settlements among the landuse types. Mixed forest with undergrowth of deciduous trees, shrubs and grass cover was identified as a background type of vegetation. Meteorological series of air temperature and precipitation observations were interpolated into centroids of subwatersheds by kriging using variograms (Ly et al. 2013). The method development resulted in a Python program, which includes data preparation, error checking, filling in data gaps, interpolation using the PyKrige package (PyKrige, 2018) and time series generation in centroids. For the period of 1968 - 1980, the algorithm was simplified: now we have only to assign the values of precipitation and temperature at the meteorological station point located closer to the centroid, since for this period data only for Mozhaysk and Gagarin stations was used. Other input data such as hydrological series were converted to HYPE formats directly or used in parameterization files.

The evapotranspiration can be calculated in HYPE with 5 models, including Jensen-Haise, Hargreaves–Samani and FAO Penman-Monteith methods. Most of these models need additional data such as wind velocity, solar radiation, water vapor pressure etc, so we used the simplest model among those above, where the base potential evaporation is calculated when the air temperature is higher than corresponding threshold and then distributed exponentially between two upper soil layers. Potential evaporation depends on evaporation rate which is calibrated for each landuse type. The resulting evaporation depends on soil water content.

HYSS provides several different algorithms of parameter optimization, but the developers themselves recommend a method of differential evolution of parameters. The method consists in generating parameter vectors based on the latest values, choosing the best of the vectors, and accepting new parameter values with a given probability (Arsenault and Alcan 2019).

RESULTS AND DISCUSSION

At the first stage, the hydrological part of the model has been manually calibrated to determine the most sensitive parameters. The study has revealed two parameter groups that fundamentally affect the quality of modeling. The first group includes porosity of the upper soil horizons, coefficients and threshold values of infiltration and recession coefficients of the groundwater runoff; the second group includes the temperatures and snowmelt rates specified for each landuse type. At the second stage, these parameters were used in the process of automatic calibration by the method of differential evolution with the generation of 15 vectors in each of the 60 generations. At the final stage, the phosphorus concentrations calculated by the model were compared with those measured at the outlet gauge.

The simulation has been carried out for periods from 1966 to 1980, 1982 – 1987 and 1998 - 2015. The results for the first two-three years haven't been recorded for the model to warm-up. The period of 2002 - 2012 was used for calibration of the hydrological block. The need of dividing the period of 1966 – 1987 into two parts arose due to the absence of data for some rain gauges. So, we used different periods for validation in order to make sure that the model simulated waterflow satisfactorily acceptable. According to the results of manual calibration, the parameters that characterize the infiltration and leakage through the deep soil horizons, as well as the parameters characterizing the process of snowmelt, turned out to be the most sensitive parameters in the calculation of the water flow as variations of these parameters within the limits of 5 – 10% can result variations of output values by 50% and more.

The comparison of the optimal soil hydrology values and snowmelt parameters, and field measurements and data taken from literature has shown good agreement. The optimal value of melting rate ranged this way: for forest areas from 1.3 to 1.8 mm/°C day, for open areas from 1.5 to 2.2 mm/°C day and that agrees with the values given in literature (Alyushinskaya 1962; Zhidikov and Nechaeva 1982). The porosity of the upper soil horizons was 0.04 – 0.06. This value as a parameter does not take into account the presence of macropores, and rather corresponds to mesoporosity (Levkovskiy and Guber 2008). The measured water conductivity of soil ranged within the catchment from 100 to 500 mm/day and corresponded to the value of the mactrinf parameter (infiltration threshold), whose optimal value ranged from 90 to 120 for different catchment areas.

Within the watershed area according to FAO classification we have identified two soil types – Luvisols and Gleysols. The Gleysols occupied depressions and shadowed areas. The density of the upper soil horizon averaged was 1,430 kg / m³ over the catchment area. In studied sections, soil included the following set of horizons: AY (or P – arable horizon on agricultural land) with a capacity of 30–40 cm gray and dusty (or brown and dense in case of horizon P), in most cases under a sod of 5–7 cm thick, whitish podzolic horizon EL with a capacity

of 15–20 cm, light brown subeluvial horizon BEL and darker textural horizon BT with nutty structure with a common capacity of 40 - 50 cm, smoothly passing at a depth of 80 - 100 cm to the parent rock C, represented by heavy loam. The loam without inclusions belongs in this area to the Dnieper-Moscow and the Moscow region of water-glacial deposits. The indexes of soil horizons are given corresponding to the new Russian soil classification (Gerasimova 2019).

In total, there were carried out about 200 manual model launches and about 1500 launches during the automatic calibration, that together amounted to 56.6 machine-hours.

The model has shown satisfactory simulation accuracy in comparison with the water discharges observed at the outlet, which is confirmed by the values of the quality criteria given in Table 1. The result of the water flow simulation for the validation period is shown in Figure 2. The analysis of the graph shows a good accuracy of simulation, both the total volume of the flood and its maximum values. The values of the parameters in the above calculation give a sufficient basis for simulation of the biogenic flow.

The values of parameters related to the balance of nutrients, such as their content in various soil pools and fertilizer intake

Table 1. Simulation quality criteria for optimal values of model parameters for simulation of water flow

	r	KGE	NSE	PBIAS%	SDobs/2*	MAE
Acceptable value (Gupta et al. 2009; Moriasi et al. 2007; Waseem et al. 2017)	> 0.5	> 0.5	> 0.5	-10 < PBIAS< 10		SDobs/2
2002 – 2012	0.77	0.68	0.6	-9.3	5.51	3.42
2013 – 2015	0.93	0.75	0.85	-10.4	5.91	2.35
1968 – 1980	0.83	0.64	0.67	8	6.37	3.43
1983 – 1987	0.65	0.52	0.41	11.5	6.12	3.19

*less than a half of the standard deviation of the series
r – Pearson correlation coefficient, KGE – Kling-Gupta efficiency, NSE – Nash-Sutcliff efficiency, PBIAS – percent bias, MAE – mean absolute error

were identified on the basis of chemical analysis of the catchment soils, standard fertilizer application rates and statistical data on fertilization in specific farms. Table 2 presents the average content of biogenic elements in the upper soil layer in areas with different land use types.

According to the data in Table 2 and distribution of landuse areas, phosphorus content generally corresponds to the intensity of landuse (moderate, medium or intensive), the distribution of nitrogen is opposite. Significantly higher levels of nutrient elements are observed at the sample points located on floodplains of the Moskva river due to high concentrations of phosphorus during floods and migration of elements to the depressions. On abandoned lands, the content of total phosphorus and nitrogen is 15–20% higher than on the used ones, the content of mobile phosphorus — 50–70% higher. It is not possible to establish the relationship of the content of nutrients with the altitude of land.

The formation of phosphorus runoff in the HYPE model is regulated by a number of parameters, among which one group concerns the transformation of soil phosphorus, including the initial levels of the element in different pools, the specific transition rates between pools, the Freundlich isotherm parameters. These parameters can be set based on the results of the analysis of the phosphorus content in soil samples. Another group of parameters relates to in-stream processes. These include specific rates of transition between different phosphorus forms in the water, half-saturation concentrations, and a production parameter. This parameter is the basic primary production, relative to which phosphorus degradation or production in a watercourse is calculated depending on the above

Table 2. Mean phosphorus content, P2O5, organic matter and nitrogen resulting from the watershed survey for different types of land-use

Landuse	Total phosphorus, g/kg		Mobile phosphorus, mg/kg		Organic matter (OM), g/kg		Total nitrogen, g/kg (conversion OM/20)	
	AY/P *	BEL	AY/P *	BEL	AY/P *	BEL	AY/P *	BEL
Fallow:	1980-e (landuse according to the map)							
Moderate	1,34	1,18	41,33	43,77	16,40	11,30	0,82	0,57
Medium	1,58	0,99	42,80	26,04	14,22	10,26	0,71	0,51
Intensive	2,30	1,38	57,00	32,58	12,84	9,42	0,64	0,47
Pasture	1,81	1,49	57,74	41,92	15,84	11,64	0,79	0,58
	2017 (landuse resulting from the survey)							
Non used	1,98	1,37	67,19	39,74	16,68	11,12	0,83	0,56
Used	1,74	1,12	35,44	26,63	12,34	9,49	0,62	0,47
	Not changed							
Meadow	3,44	2,27	54,70	63,40	18,60	12,45	0,93	0,62
Forest	1,19	1,08	23,87	23,90	17,40	9,50	0,87	0,48

* Soil horizons are given according to the New Russian Soil Classification: AY – gray-humic (soddy) – corresponds to layer H of FAO classification, P – agrohumic – corresponds to layer H, BEL – subeluvial – corresponds to layer E.
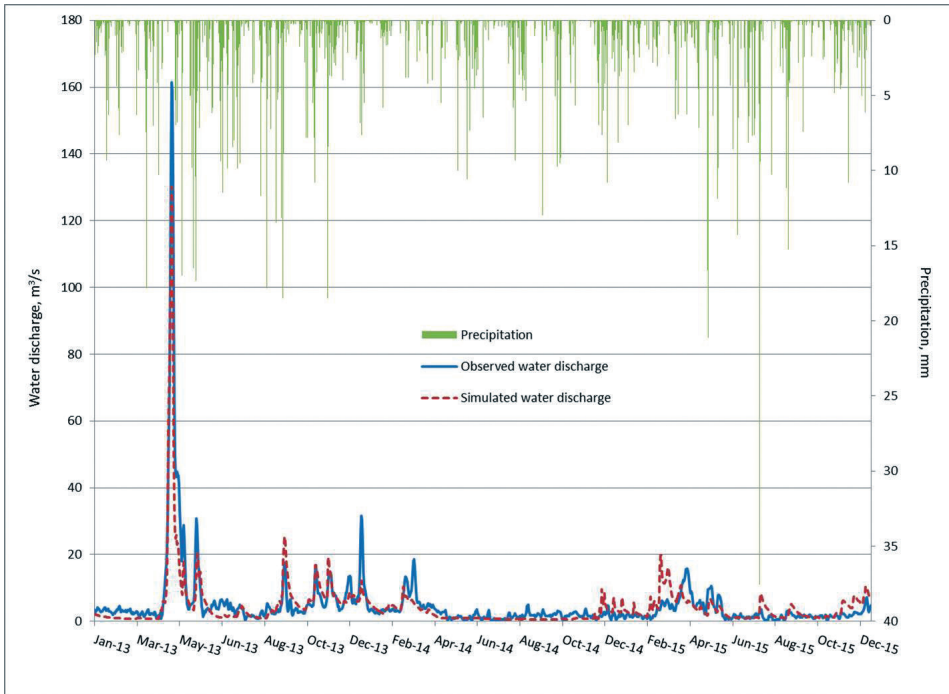
Fig. 2. Results of water flow simulation at the outlet of Moscow river in Barsuki village, compared to the observed flow and combined with the precipitation for validation period

mentioned parameters and temperature. The parameter values for the in-stream block can be refined based on those proposed in the literature. For example, in the research of Lindenshmidt (2006) and documentation concerning simulations with QUAL-2E (Cole and Wells 2013). When simulating phosphorus runoff, it is also essential to take into account the mode of mineral and organic fertilizers application, since they are the main sources of biogenic elements in catchments with intensive agriculture. In the HYPE model, it is possible to adjust the amount of fertilizer applied for each type of land use separately and the schedule of application of each type of fertilizer throughout the year.

Among parameters characterizing a specific catchment, it is worth paying special attention to those which are set separately for different types of landuse and the initial concentrations of elements in the soil. For flood periods, it becomes important to tune the parameters of soil erosion, since during these periods its transport with suspended matter contributes significantly to the phosphorus runoff (Yasinskiy and Datsenko 2018).

For simulation of phosphorus, the following initial contents were agreed: in slow phosphorus pool 100 g/m^3 for forested areas, 195 g/m^3 for open areas; in particulated phosphorus pool 80 g/m3 for forested, 150 g/m^3 for open areas. For initial phosphorus content in the pool with rapid turnover, 5 g/m^3 was agreed. The field survey findings about biogenic elements content in soils were also used for setting up parameters depending on distribution of elements in the soil profile and transition rates between pools.

Simulation of phosphorus concentrations was performed for the same periods, as the water flow simulation, but calibration and validation were made only for the years with data about phosphorus concentrations in the outlet: 1984 was used for calibration and 2010 and 2012 for validation. The values of the calculation quality criteria for the results of modeling the concentrations of phosphorus are given in Table 3. To assess the simulation quality of biogenic flow, a different set of indicators is used, since the time series of concentrations has a different statistical nature, and the observed values are available for comparison with a much greater discreteness. The results satisfy our standard error

value only for 1984 for dissolved phosphorus, the correlation coefficient value for dissolved phosphorus in 2012 and 1984, and for total phosphorus in 2012. It is important to note that using of quality criteria for daily concentrations gives too detailed result and can be treated as additional information. When we compared annual and seasonal phosphorus flow, calculated from modelling results, observed data the relative error fell inside the limits of 0 – 76%. The essential point to remember is that the error of water sample analysis, which attains sometimes tens of percent, is comprised by the error of model calibration.

Combining the phosphorus concentrations hydrograph for total and dissolved phosphorus (Figure 3) shows the partial coincidence of peaks and accordance of simulated and observed concentrations in general. Concentrations overestimation within the region of summer and autumn floods and underestimation of spring hydrograph region can be explained for the most part by similar discrepancies in the simulation of water flow, since the form of concentration hydrographs is very sensitive to changes in flow. Important deviations of total concentrations are due to underestimation of suspended phosphorus. The suspended phosphorus flow mainly depends on suspended solids. So, during the calibration, the values of the parameters concerning soil erosion have been set to correspond the values, which were measured on the outlet gauge in 2016, which is the fact that the flow of suspended solids should not exceed 500 – 600 tons per day. We don't discuss the results for suspended phosphorus flow here a lot because on the current stage of

the model calibration, we consider them as less reliable than the results for dissolved phosphorus due to the lack of the data on suspended solids concentrations in river water.

For 1984, we have performed an experiment to make an increase of the amount of fertilizer applied. Thus, before the experiment, the model was adjusted to apply mineral fertilizers only on arable lands with intensive use and kitchen gardens (48 and 60 kg / ha per year, respectively, in spring and 32 kg / ha at the end of summer only for arable lands). The experiment suggested that fertilizers are applied on all the fallows with proportional diminution by landuse intensity. This caused slightly worse values of simulation quality criteria, but, as a result, concentrations corresponded better to the extreme values of phosphorus concentrations observed. The common area of fertilized land for the experiment was three times bigger, since for current period it's three times smaller than during 1980 – 1985 years. It arises from the results of the field survey.

The parameterization of the latter experiment was used for the following research because it complies the most with the real situation in the watershed area. Based on it, the influence of mineral fertilizers on phosphorus flow has been studied. We have been divided years from 2000 to 2018 into groups of wet, medium and dry years using subtractive-cumulative curves method. For dry and wet groups, phosphorus flow has been calculated from the results of simulation. Dissolved phosphorus average flow in wet years was 24440 kg/year, in dry years it didn't exceed 6550 kg/year.

Table 3. Simulation quality criteria for optimal values of model parameters for simulation of phosphorus concentrations for separate years. SP – dissolved phosphorus, TP – total phosphorus

	RMSE		MAE		r		TEIL		SDobs/2	
	SP	TP	SP	TP	SP	TP	SP	TP	SP	TP
2010	57.3	76.4	41.6	61.2	0.28	0.22	0.33	0.23	29.1	28.6
2012	67.5	82.5	42.5	51.7	0.56	0.73	0.28	0.39	23.5	15.3
1984	82.2	98.7	43.5	56.8	0.50	0.30	0.43	0.37	39.3	26.2
1984**	85.3	105.2	47.4	63.0	0.50	0.31	0.42	0.38	39.3	26.2

RMSE - root mean square error, TEIL – Teil criterion
*** simulation with an increase of fertilized area*
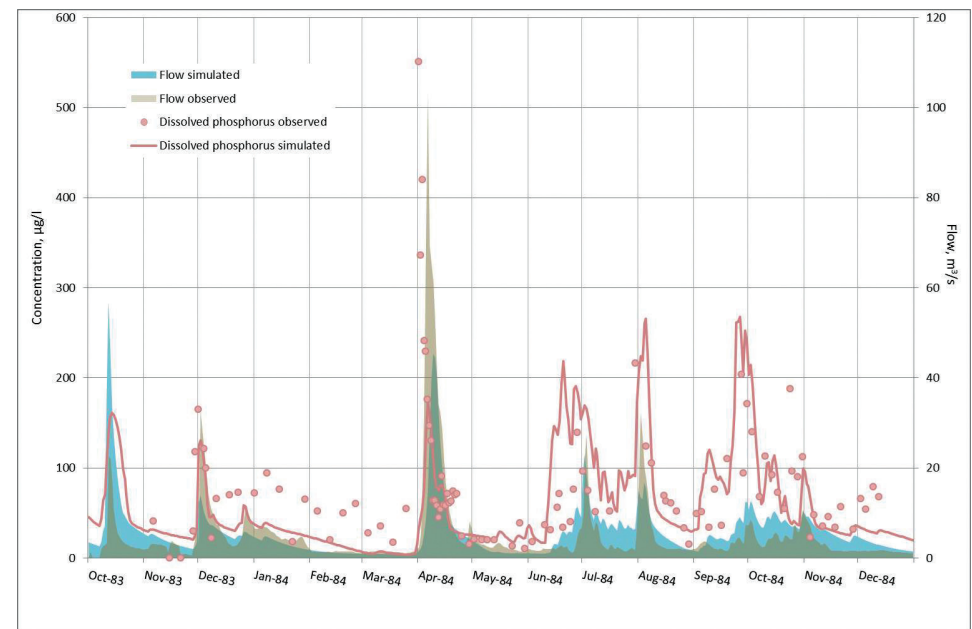
Fig. 3. Combining results of dissolved phosphorus concentration and water flow simulation at the outlet of the Moskva river (Barsuki village) in 1984

Then, we have performed another simulation having set values of mineral fertilization for every landuse to zero. The results of this simulation have been compared with the basic simulations for 1984 and 2012 years. This experiment has shown that applying no fertilizers results in decreasing of the dissolved phosphorus flow during spring flood by 5% (360 kg) in wet and by 11%

(410 kg) in dry years. Average annual total phosphorus flow is decreasing then by 7 – 8%.

The genetic components of the phosphorus flow have been analyzed for 1984 and 2012 years, as they are both rather well covered with data.

Table 4. Total phosphorus average monthly flows with genetic components of water flow in 1984 compared with 2012 for summer and spring periods, kg/km²

Components	1984		2012	
	Spring	Summer	Spring	Summer
Average				
Surface	0.51	0.40	1.94	0.02
Subsurface	3.22	5.90	4.29	1.94
Groundwater	0.39	0.44	0.33	0.29
Summary	4.12	6.74	6.56	2.25
Maximum				
Surface	1.57	3.73	6.06	0.29
Groundwater	0.49	0.60	0.46	0.38

The phosphorus loads on 3 soil layer is rather constant, 0.65 kg/km^2 average and 1.4 maximum. It corresponds to 10 – 30% of local phosphorus flow for average and to 4 – 12% for maximum values. As it follows from the table 4, the surface and the groundwater components of phosphorus flow are comparable and the subsurface component in comparison is greater by value. It was estimated as 65% of summary flow. This corresponds well to the water flow by different soil layers, as in 1984 the surface component of water flow was 12% of total local flow, the groundwater was 21%. During the wet 2012 year, the surface component runs up to 25%. The analysis of different components of the phosphorus flow mapped for the watershed area shows higher groundwater flow for forested areas and higher surface flow for agricultural areas with intensive landuse.

CONCLUSION

The amount of unused land has increased 3 times since the 1980s. On abandoned lands, the content of total phosphorus and nitrogen is 15–20% higher than that of used ones, while mobile phosphorus is 50–70% higher. The highest content of all forms of phosphorus and nitrogen is observed on floodplain meadows.

Model HYPE satisfactorily reproduces water runoff from the catchment area of the Moscow river. Phosphorus concentrations have been simulated in conformity with observed phosphorus concentration changes, but some quantitative criteria of simulation quality yet are not satisfactory. However, the model can be used for calculations of phosphorus loads at the current stage of calibration on condition of good water flow simulation. Errors in phosphorus simulation are caused by extremely poor data on observed concentrations in water, by complexity and large errors of phosphorus observation methods themselves and high sensitivity of the shape of concentration plots to changes in water flow hydrograph.

The results of experiments with the model show a decrease of dissolved phosphorus flow subsequent to cease of fertilizing in range from 5 to 11%.

The values of the surface and groundwater components of phosphorus flow are comparable, while soil component amounts 65% of local phosphorus flow. It mainly corresponds to the distribution of components of the water flow.

It should be emphasized that the simulation of nutrient runoff with distributed or semi-distributed parameters is one of the best way to gain knowledge about the influence of the location and landuse, as well as of the change in forest area, on phosphorus flow. Further work with the involvement of more data could allow to get a more detailed analysis of nutrient concentrations carried out on the basis of the model. ■

REFERENCES

Alyushinskaya N., Aniskina L., Ivashintsova L. (1962). Spring flow of the rivers of the Northern Dvina Basin and its forecasts. Leningrad: Gidrometeoizdat. (in Russian).

Antokhina E., Zhuk V. (2011). IMC ECOMAG application for flow modelling from watersheds with different areas. Water management in Russia: problems, technologies, management, № 4, 17–32. (in Russian).

Arsenault R., Alcan R.T. (2014). A Comparison of Stochastic Optimization Algorithms in Hydrological Model Calibration. Journal of Hydrologic Engineering, № 7 (19), 17–32, DOI:10.1061/(asce)he.1943-5584.0000938

Ayzel G, Varentsova N, Erina O, Sokolov D, Kurochkina L, Moreydo V. (2019). OpenForecast: The First Open-Source Operational Runoff Forecasting System in Russia. Water, 11(8), 1546, DOI: 10.3390/w11081546.

Cole T. and Wells S. (2006). "CE-QUAL-W2: A two-dimensional, laterally averaged, Hydrodynamic and Water Quality Model,Version 3.5," Instruction Report EL-06-1, US Army Engineering and Research Development Center, Vicksburg, MS.

Datsenko Y. (2007) Eutrophication of reservoirs. Hydrological and hydrochemical aspects. Moscow: GEOS. (in Russian).

Datsenko Y. (2019). The reservoir water quality modeling using the function of water masses residence time distribution. Moscow University Bulletin, Series 5, Geography, № 1, 93–96. (in Russian with English summary).

Datsenko Y., Puklakov V. (2010). Phytoplankton growth modelling in Mozhayskoe water reservoir. Moscow University Bulletin, Series 5, Geography, № 3, 1–7. (in Russian with English summary).

Edelshtein K. (1995) Phosphorus mode modeling in a valley reservoir. Moscow University Publishing. (in Russian).

Edelshtein K., Sokolova T., Bykov V. (1978). Reservoirs of the Moscow River Water System. Complex studies of reservoirs, Issue 4. Moscow: Moscow University Publishing. (in Russian).

Gelfan A. Gustafsson, D, Motovilov Y., Arheimer B., Kalugin A., Krylenko I., Lavrenov A. (2017). Climate change impact on the water regime of two great Arctic rivers: modeling and uncertainty issues. Climatic Change, № 3 (141), 499–515, DOI 10.1007/s10584-016-1710-5.

Gerasimova M. (2019). Russian Soil Classification System: Towards the Next Approximation. Eurasian Soil Science, (52), 25–33. (in Russian).

Gupta H., Kling H.,Yilmaz K., Martinez G. (2009). Decomposition of the mean squared error and NSE performance criteria: Implications for improving hydrological modelling. Journal of Hydrology, № 1–2 (377), 80–91, DOI: 10.1016/j.jhydrol.2009.08.003.

Kremenetskaya E., Belova D., Sokolov D., Lomova D. (2015). Features of production and transformation of organic matter in Mozhaisk reservoir at low water level. Water Resources, № 1 (42), 71–84. (in Russian with English summary).

Levkovskiy E., Guber A. (2008). Differential porosity calculation based on soil solid phase properties. OSU Bulletin, № 85, 108–113. (in Russian with English summary).

Lindenschmidt K. (2006). The effect of complexity on parameter sensitivity and model uncertainty in river water quality modelling. Ecological Modelling, № 1–2 (190), 72–86, DOI: 10.1016/j.ecolmodel.2005.04.016

Lindström G., Pers C., Rosberg J., Strömqvist J.,Arheimer B. (2010). Development and testing of the HYPE (Hydrological Predictions for the Environment) water quality model for different spatial scales. Hydrology Research, № 3–4 (41), 295–319, DOI: 10.2166/nh.2010.007.

Ly S., Charles C., Degré A. (2013). Different methods for spatial interpolation of rainfall data for operational hydrology and hydrological modeling at watershed scale: a review. Biotechnologie, Agronomie, Société et Environnement, № 2 (17), 392–406.

Martynova M.V. (1979) The role of bottom sediments in the cycle of nitrogen and phosphorus in the Mozhayskoe Reservoir. In: Water quality formation processes in water supply reservoirs. Moscow: MSU, 49–65. (in Russian).

Moriasi D., Arnold J., Liew M., Bingner R., Harmel R., Veith, T. (2007) Model evaluation guidelines for systematic quantification of accuracy in watershed simulations. Transactions of the ASABE, № 3 (50), 885–900.

Motovilov Y., Suchkova K., Edelshtein K., Puklakov V., Erina O., Sokolov D. (2018). Modeling of genetic components of river runoff using hydrochemical method of identification of water masses. Water Resources, (45), 135–145. (in Russian with English summary).

Pers C. (2014). The code of HYSS and HYPE - overview HYSS – Hydrological Simulation System HYPE – Hydrological Predictions for the Environment Part 1 Introduction to the HYSS and HYPE code. [online] Available at: https://hypeweb.smhi.se/wp-content/uploads/2019/04/HYSS_HYPE_code_overview.pdf [Accessed 13.12.2019]

PyKrige develpers. (2018). PyKrige Documentation. Release 1.4.0 2018. [online] Avalable at: https://buildmedia.readthedocs.org/media/pdf/pykrige/latest/pykrige.pdf [Accessed 14.12.2019]

Sokolov D., Erina O., Edelshtein K. (2016). Variability of hydrological and hydrochemical characteristics in a stratified reservoir. Moscow University Bulletin, Series 5, Geography, № 5, 61–68. (in Russian with English summary).

USGS Space Shuttle Radar Topography Mission (SRTM) [online]. Avalable at: https://earthexplorer.usgs.gov/. [Accessed 12.12.2019]

Waseem M., Mani N., Andiego G., Usman, M. (2017). A review of criteria of fit for hydrological models. International Research Journal of Engineering and Technology (IRJET), 11 (04), 1765–1772.

Xu C. (2002). Textbook of Hydrologic Models. Uppsala University, Sweden.

Yasinskiy N., Belolyubtsev A. (2019). Determination of hydrophysical characteristics of soils for modeling of basic hydrological processes at the catchment area of the Mozhaiskoe Reservoir. Natural and technical sciences, № 3, 134–143. (in Russian with English summary).

Yasinskiy N., Datsenko Y. (2018). Patterns of phosphorus river runoff formation for hydrological modeling purposes. Environmental management, 1, 25–33. (in Russian with English summary).

Zhidikov A., Nechaeva N. (1982). Guidelines for the development of schemes for short-term forecasts of river water discharge and reservoirs water inflow. Leningrad: Gidrometeoizdat. (in Russian).

Myagmardorj Oyunchimeg[1], Badrakh Burmaajav[2], Altangerel Enkhjargal[3], Sambuu Tsegmed[1], Batbaatar Suvd[1], Otgonbyamba Oyun-Erdene[1], Davaadorj Zolzaya[1], Demberel Otgonbayar[1], Dovdon-Ulzii Oyunchimeg[1], Lkhagvasuren Azjargal[1], Ganchimeg Soyombo[1], Khishigt Byambasuren[1], Baldandorj Dorjkhand[1], Sandag Enkh-Amgalan[4], Svetlana M. Malkhazova[5], Byambaa Tsogtbaatar[1]

[1]National Center for Public Health, 13381 Peace Avenue 17, 3 khoroo Bayanzurkh district, Ulaanbaatar, Mongolia, email: oyunchimeg_myagmardorj@yahoo.com
[2]Ach Medical University, Peace Avenue-11, Songino-Khairkhan district-18, Ulaanbaatar 18080, Mongolia, email: burmaajav55@gmail.com
[3]Academy of Medical Professionals, Capital Tower, Khudaldaany street, 3 khoroo, Chingeltei district, Ulaanbaatar, Mongolia, email: ajargal8@gmail.com
[4]Institute of Geography & Geo ecology MAS, Social Economic Division; Erkhuu street, Chingeltei district, Ulaanbaatar, 14192, Mongolia.
[5]Lomonosov Moscow State University, Faculty of Geography, Department of Biogeography, Leninskie Gory 1, 119992 Moscow, Russia.
* Corresponding author: amgalan69@yahoo.com

SOIL MICROBIAL CONTAMINATION AND ITS IMPACT ON CHILD DIARRHEAL DISEASE INCIDENCE IN ULAANBAATAR

ABSTRACT. Air and soil contamination in developing countries exacerbates due to poor management of waste collection and serves as a morbidity and mortality factor. This study aimed to conduct an assessment of soil pollution level in Ulaanbaatar and establish a correlation between microbial contamination and registered occurrences of contagious diarrheal diseases among children (0-5 years old). This is a cross-sectional study conducted in Ulaanbaatar in June-September of 2016. Samples of soil and contagious diarrheal disease morbidity data in 0-5-year-old children were used. Samples were taken from the sites three times, in July, August, and September. The data analysis was done in the SPSS-21 program and relevant parametric and non-parametric tests were used. The highest level microorganisms were found in the samples taken from sites near major markets and then in the samples from ger areas. The analysis of the samples revealed that 111.78 microorganisms exceed the standard level 1.1 times in summer. The *Escherichia coli (E.Coli)* and Proteus also contaminated the ground water. All diarrhea occasions in Ulaanbaatar were analyzed by seasons and months, the prevalence was peaking in August. A correlation was found with the soil *E.Coli* titers and infectious diarrheal disease children under five years old morbidity. The number of microorganisms in soil tends to increase in summer. Diarrheal disease infections among children under five increase most in summer and autumn and correlate with soil contamination with pathogenic microorganisms.

KEY WORDS: ger area, diarrheal diseases, soil microbial contamination

INTRODUCTION

The United Nations defines soil as a basis for agricultural development, ecosystem services, and food security and highlights its importance for the sustainability of life on the planet. Moreover, the 68th Session of the UN General Assembly announced the year of 2015 as an international year of soil (Gomiero 2016). Soil is considered a non-recoverable natural resource. Fertile soils play an essential role in the provision of livelihood and needs for millions of people and support food production, provide ecosystem services and regulate the climate (Stringer 2011).

Air and soil pollution in developing countries exacerbates because of poor management of waste collection, storage and processing, and serves as a morbidity and mortality factor.

Soil is a dynamic, natural body occurring on the surface of the Earth. It is a medium for plant growth. Soil pollution is defined as a phenomenon characterized by the loss of structural and biological properties by the soil layers as a result of numerous human and natural factors, such as wind, deforestation, chemical use, etc. Developmental activities such as construction, transportation and manufacturing not only deplete the natural resources but also produce large amount of waste that leads to pollution of air, water, soil, and oceans, global warming and acid rains (Gangadhar 2014). Soil pollution is a condition of excessive concentration of substances (fertilizers, pesticides, organic chemical compounds, acidic and alkali compounds) surpassing their normal level in nature negatively affecting the

aqua systems, atmosphere, ecosystems, and organisms. Local soil contamination occurs where intensive industrial activities, inadequate waste disposal, mining, military activities or accidents have introduced excessive amounts of contaminants. Soils only have a limited ability to process these contaminants, through filtering or transformation, for example. Once this ability is exceeded, issues such as water pollution, human contact with polluted soil, plants taking up contaminants and dangers from landfill gases become more significant (Liedekerke et al 2014). Multiple kinds of research have confirmed that the main source of soil pollution in Ulaanbaatar is the pit latrines of the ger areas (Narantuya L et al 1991; Urantsetseg et al 2001). In 2013, the pathogenic microbial contamination of the soil in Ulaanbaatar reached a severe level for 20.6% of the territory of the city, medium level for 74.5% and at a mild level for only 5% of the territory (CGA 2013).

According to the data of the National Statistics Office of Mongolia for 2015, Ulaanbaatar was inhabited by 1.4 million people and over 60% of them lived in ger districts. Moreover, 97.3% of all households in ger areas used pit latrines. The city also hosts 314 car repair shops, tire repair shops, car oil and spare parts sales points, 166 gas stations and oil storage facilities, 4 asphalt factories, 19 brick factories, 32 gravel extraction sites and 76 hides processing factories which also serve as factors negatively affecting the environment and population health (Government of Mongolia 2009).

According to the World Health Organization report, three million children dies every year due to diarrheal disease and most of

them are children from the developing world. The occurrence of diarrhea among the general population not exclusively in ger district dwellers has been increasing recently presenting an issue of urgency to the health sector (Avaandorj 2014). Multiple studies of chemical and microbial contamination of the soil in Ulaanbaatar have been undertaken, however, a scarce amount of works devoted to exploring the soil pollution in ger districts is available (Kasimov et al 2011, 2016). Therefore, it is vitally important to study the chemical and microbial contamination level in ger areas (living area of the city which are not connected to the central heating and sewage system) of Ulaanbaatar hosting more than half of the population of Ulaanbaatar.

This study aims to conduct an assessment of soil microbial pollution levels in Ulaanbaatar and establish a correlation between such contamination and registered occurrences of contagious diarrheal diseases among children (0-5 years old).

MATERIALS AND METHODS

This is a cross-sectional study conducted in 9 districts of Ulaanbaatar in June-September, 2016. Samples for laboratory tests (microbiological) were collected from the soil at various locations and the data of contagious diarrheal disease morbidity of children under five years old in the 73 khoroos (the smallest unit of community in the city) adjacent to these locations were analyzed. For the study of the level of soil bacterial contamination, samples were taken from 111 sites in ger areas of 9 districts of Ulaanbaatar and 1 site was used for a reference site (Fig 1). Samples for microbiological tests were taken from the sites three times, in July, August, and September. The soil microbial contamination characteristics were studied in the laboratory of the National Centre for Public Health (MSO 2008).

Soil sampling area. The soil sampling was arranged in 9 districts of Ulaanbaatar with consideration of the areas of the ger suburbs. However, to improve the scope of the study and avoid sampling errors,
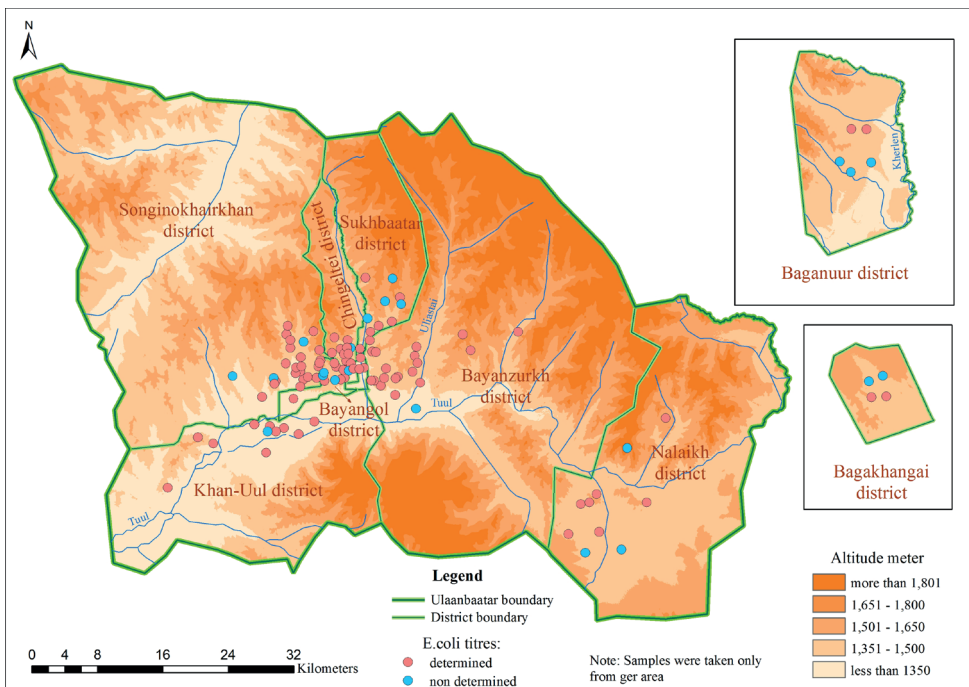
Fig. 1. Map of soil sampling location and existence of E.Coli titers by districts of Ulaanbaatar city

we increased the number of sites and took samples from 111 sites. For identification of the sampling sites, the ger area of Ulaanbaatar was divided into 10 segments to pick up 10 sites from each segment. A site at a sufficient distance from sources of contamination was chosen as a reference site and the data of the analysis of the other samples were compared against it. Also, samples were taken from the drinking water sources in the vicinity of 20 m from the sampled sites to examine the transmission of contamination and assess their risk effects.

Soil sampling methodology. An "envelope" method was used to perform soil morphological recording in conformance with the documents: "Environmental preservation. General requirements for taking a sample for soil research MNS 3298-1990"; "Soil Procedures of taking samples; using containers and transporting MNS 2305-1994 in extracting the samples (MSO 1994)". According to the national standard, microbiological contamination was divided by "low degree", "medium degree" and "high degree" contamination, based on titers of microorganisms.

Establishing effects of soil pollution on underground water. To establish whether the soil pollution affects the underground water, samples of water were taken from the underground water from the proximity of the soil sampling sites. 20 water points were selected and 60 samples were taken in three repetitions. Tests for contamination with pathogenic bacteria were done at the reference laboratory of the National Public Health Centre.

Diarrheal disease. We had a diarrheal disease record of children under four years old from the National center for Combinable disease of Ulaanbaatar city. Those are the whole year record of all diarrheal disease records of 2016. For the correlation between soil contamination and diarrheal disease, we selected the incidence of the outbreak during the data collection period (July-September, 2016).

Statistical analysis. For the quantitative data analysis, we used Statistical Package for the Social Sciences-21 (SPSS-21). The relevant parametric and non-parametric tests were used for calculation. For testing the differences of the results, appropriate non-parametric tests were used: Kruskal-Wallis one way analysis of variance, Mann-Whitney U test and paired T-tests. The Kolmogorov-Smirnoff test has been used to check the normality of data distribution. Pearson's correlation coefficient also has been used and linear regression was calculated for estimating soil microbiological influence on diarrheal diseases.

RESULTS

The morphological study of the selected sites showed that 29.4% of the ger area soil near service centers has brown colored soil, 10.3% has the color of black one, 52.9% features high density, 72.1% is sand-rock and 70% has been severely eroded. 80% of the brown soils were around the service centers in the ger areas. The morphological records of the soil sampled near car and bike repairs, and car washing services showed that 35.7% of the soil is light brown, 64.3% has high density, and 71.4% is heavily eroded. At the sample sites, 31.5% of the soil was light brown, 70.8% has sand-rock mechanic structure, and 53.9% has high density. The percentage of soil humus was 7.89 at the reference site. The average percentage of humus compared with the reference site was 1.80 times lower.

Soil bacterial contamination level is defined as the total number of microbes, titers of E.coli, Proteusand bacteria, Clostridium Perfringens and thermophilic bacteria per 1 gram of soil.

The number of microbes in the soil of the ger areas in Ulaanbaatar was high at all sites in July-September. Microbes increase trend was observed during the summer months. The level of microbiological titers of samples taken in September was twice as higher (42.56% [95%CI 31.74-60.1]) than the July samples (21.51% [95%CI 16.56-27.53]), and 1.3 times higher than the August samples (p=0.003).

In categorizing the sample sites by locations, as shops, hair stylists locations, bathhouses, schools and kindergartens, major market places were defined as service centers (Fig 2).

The number of microorganisms from sample location sites showed the highest level in the samples taken from sites near major markets amounting to 37.63 million organisms, then in the samples from ger areas amounting to 37.24 million and in the samples taken near service centers.

Titration of E.Coli. Detection of *E.Coli* titers in any laboratory test indicates comparatively fresh contamination with human or animal feces. Titer corresponds to the least amount of soil expressed in grams in which the microorganisms are still found. Of the total 333 soil samples, 85.3% (284) were yielded by E.Coli titers while 14.7% (49) were clean. Most 79.2% (225) of the sites where *E.Coli* titers were detected had a low degree of contamination, 18.3% (52) had a medium degree and 2.1% (7) had a high degree of contamination.

Proteus. It does not serve as a soil contamination indicator but it is positive along with *E.Coli* while *Clostridium perfringens* indicates contamination. The average content of *Proteus* bacteria in July, August, and September in the ger areas soil samples was highest amongst the other locations and fit in the high contamination degree

of the standard. The contamination degree was medium (100-1000) in the samples from major market areas, roads, and gas stations. Proteus was detected in 65.1% (217) of all samples of which 38.1% had a low degree, 22.5% (75) had a medium degree and 4.5% (15) had a high degree of contamination.

C.Perfringens titers. The soil analysis was negative for *C.Perfringens* titers in the samples from Bayangol, Khan-Uul, Nalaikh, Baganuur, and Bagakhangai districts. It was positive in Songinokhairhan (14.7%) and Bayanzurh (11.7%) districts in the category of low degree of contamination.

Soil and water contamination. To confirm whether soil contamination affects underground water, water samples were taken from the household yards adjacent to the soil sampling sites and from households that have deep wells in those areas. The analysis of the samples revealed that 111.78 microorganisms exceeding the standard level 1.1 times in summer. The presence of *E.Coli* and Proteus in summer and autumn confirms that the water is contaminated. Microbial contamination is 1.56 times higher in autumn than in summer and E. coli titers are 1.3 times more in autumn (T=4.6, p=0.004). Among all water samples used in the course of the study, 47.8% (27) contained more than 100 microorganisms while *E.Coli* was detected in 24.7% (17) and *Proteus* was detected in 27.5% (19) of the samples (Table 1).
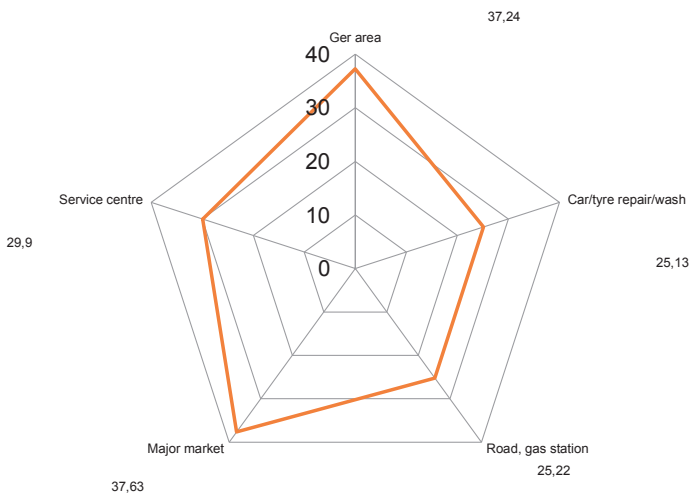

Fig. 2. Average microbial level in Ulaanbaatar, July-September 2016

Table 1. Microbial contamination of the soil and water by seasons

Indicators	N	Summer		N	Autumn		N	Total	
		Mean	95%CI		Mean	95%CI		Mean	95%CI
Soil microbial indicators									
Microorganisms (mln)	222	27.25	21.76-34.16	111	42.56	29.53-55.49	333	32.35	26.44-39.04
E.Coli	222	370.41	205.97-529.1	111	488.83	225.75-820.07	333	409.88	281.32-575.63
Proteus	222	702.52	453.7-1012.9	111	719.37	348.12-1205.43	333	708.14	493.21-961.10
Perfringens	222	10.36	6.9-14.05	111	757	3.93-11.75	333	9.43	6.72-12.13
Microbial indicators of water									
Microorganisms	19	111.78	102.5-121.49	9	95.1	85.95-55.49	28	32.35	26.44-39.04
E.Coli	19	346.32	166.54-576.6	9	30	10-55	28	244.64	104.38-420.27
Proteus	18	270.0	110.0-447.32	7	74.29	33.66-100	25	215.20	100-359.2

We calculated the number of microorganisms in the soil, where *E.Coli, Proteus, Enterococci, anaerobic microorganisms, Perfringens* and *Salmonella* serve as indicators of soil microbial contamination against the number of microorganisms in the water samples from adjacent underground water sources, and the *E.Coli, Proteus, Enterococci, anaerobic microorganisms,* perfringens and salmonella correlation using the Spearman correlation coefficient was applied. The total number of microorganisms is in a positive weak correlation with soil *E.Coli* (r=0.252, p=0.019) and also in a positive weak correlation with soil proteus (r=0.266, p=0.013). The water *E.coli* titers are positively medium correlated with the soil *Clostridium Perfringers* (r=0.544, p=0.003) and salmonella (r=0.398, p=0.03) level. The water *Proteus* level had a strong positive correlation with the soil nitrates level (NO$_3$) (r=0.717, p=0.45).

Sources and factors of soil pollution. The effect of the ger area households, solid and liquid waste disposed in ravines by the households, their latrines, the number of latrines in the area of the sampling site, their distance, bus stations, service centers, and others on soil pollution was also computed. There is a weak correlation of the presence of roads in the ger areas with the number of soil microorganisms and medium correlation with water *Proteus* (r=0.546, p=0.005), and a weak correlation of the number of latrines at soil sampling sites with E.Coli titers (r=0.133, p=0.01) and *Proteus* (r=0.124, p=0.02). The correlation between soil *E.Coli* titers and water microorganism population numbers is weak and direct (r=0.252, p=0.01). The number of soil microorganisms is in direct but weak correlation with the distance to a pit latrine of the sampling site (r=0.1, p=0.05).

Soil contamination and diarrheal diseases in children under five years old. Among the population of Ulaanbaatar, 4023 occurrences of contagious diarrheal diseases were registered in 2016 indicating an increase by 181 against the previous year. There are 2336 occurrences of dysentery or the rate of 18.1 per 10,000 population which shows an increase by 2.7 compared with the previous year.

As of the cases of dysentery infections analyzed by the sources, 7.4% are from sick persons, 0.1% are from asymptomatic carriers and 92.5% are from unknown sources. As for the routes of infection, 10.2% are via domestic contacts while 89.8% are via unknown routes (MOH 2016).

In a whole year, the occurrence of intestinal infections (AO2-AO5) in January-December 2016 analyzed by districts reveals the diarrheal diseases prevalence in two districts of Ulaanbaatar city — the occurrence in Bayazurkh and Chingeltei is higher than in the other 7 districts. The pick of diarrheal disease incidences in Ulaanbaatar was during August and September which was in line with the soil data collection period. The tendency of diarrheal disease infections in the population and under-five years old children in the khoroos in the ger areas of the city exhibit increase from June reaching the highest number of registered cases in September. A correlation was found in which an increase in the soil E.Coli titers is accompanied by an increase in the infectious diarrheal disease morbidity in children under five per 10,000 children. Regression analysis demonstrated that 1% of the causes of infectious diarrheal disease morbidity of considered children are due to the number of *E.Coli* in the surface soil, and 2.1% of them were caused by all number of bacteria in surface soil.

DISCUSSION

The current research was undertaken in the ger areas of nine districts of Ulaanbaatar in June-September 2016. We performed the tests of soil microbial tests (total number of microorganisms (per 1 gram), intestinal pathogens (per 100 ml), *Clostridium Perfringers titers, E.Coli*, anaerobic microorganisms) in corresponding laboratories and assessed the pollution and contamination situations. Also, we established the effect of soil microbial contamination on the prevalence of diarrheal disease infections among children under 5 years old registered at the khoroo health centers adjacent to the soil sampling sites.

Study of 2001 "Hygiene assessment of the soil microbial contamination and chemical pollution level in Ulaanbaatar" established that the city's soil microbiological contamination was at the III degree (Public Health Institute 2001). Research on the "Soil microbiological contamination level in major cities" of 2005 found the content of lead exceeding the maximum permissible level 2.4-2.8 times. This study also established that the level of microbiological contamination of the city is as the III degree as the preceding studies. Public Health Institute (2001, 2009) "Soil microbiological study of in cities" showed soil *E.Coli* titers as 0.004 on average, anaerobic titers as 0.001 and the number of thermophilic bacteria as 28.8x103 cells/g. A study of 2010 in Ulaanbaatar found that soil microbiological contamination was 10-16 times higher than the permissible level. And another survey finding of 2011 defined that Ulaanbaatar soil had a high level of fungi content besides pathogens such as *E.coli* and *Salmonella*. Also, Batkhishig et al has found that 31% of soil in Ulaanbaatar had a high degree of contamination, 45.5% had medium and 23.5% had a low degree of contamination of *E.Coli* titers (Batkhishig et al 2016).

The results of our research confirm the outcomes of the above studies. The number of microorganisms in July-September was at a contaminated level at all sites selected for the study. A tendency for an increase in several microbes was observed during the months when the samples were taken with a twice higher degree in September against July, 1.3 times against August. However, it is notable that microbial contamination was highest in the samples taken near major markets, ger areas and service centers.

Detection of *E.Coli* titers in any laboratory test indicates comparatively fresh contamination with human or animal feces. The findings of our study demonstrate that the surface soil in the ger areas has continually been contaminated with human and animal feces. Contamination at levels higher than the medium degree is found in 20% of the contaminated soil samples. These are observed at sites near pit latrines in the ger areas.

Drinking water standard Mongolian National Standard 900:2005 provides that the total number of microorganisms in drinking water should be less than 100 and there should be no *E.Coli* and other pathogenic bacteria. To study the effect of soil contamination on underground water, samples were taken from households that have deep wells in their yards and the analyses revealed that the number of microorganisms in the water increased 1.1 times in summer. The detection of *E.Coli* and Proteus indicates that the water is contaminated.

The main point is that *E.Coli* titers are in direct correlation with the numbers of microorganisms and Salmonella in water. The correlation between *E.Coli* titers and water microorganism quantities is also indicating that soil contamination directly affects the safety of underground water. Besides, there is a strong correlation between the number of pit latrines in the proximity of the soil sampling site and soil *E.Coli* and *Proteus.*

Soil contamination and morbidity. In total, 4023 intestinal infections cases were registered among a population of Ulaanbaatar in 2015, an increase of 181 cases compared with the previous year. In these cases, 58.1% were dysentery, 9.4% were food poisoning, 2.6% salmonellosis and 29.9% were hand foot and mouth diseases. The dynamics of diarrheal disease infections among a population of the khoroos in the ger areas of Ulaanbaatar, especially children under five years old, showed an increase starting in June and reaching its peak in September with the registration of the highest number of cases. According to the regression analysis, about 1% of the causes of infectious diarrheal disease children morbidity in the ger areas could be caused by *E.Coli* in the surface soil pollution and 2.1% of them are caused by all bacteriological contamination of the soil.

CONCLUSION

The number of microorganisms in the ger area soil in Ulaanbaatar is high in July-September indicating severe contamination. The number of microorganisms in soil tends to increase in summer. Major markets, pit latrines in the ger areas and the major service centers are the direct sources of microbiological contamination. The surface soil in the ger areas of Ulaanbaatar is polluted with human and animal feces, and the influence of substandard pit latrines further leads to contamination of the underground water with pathogenic microorganisms. Diarrheal disease infections in the population of the khoroos of the ger areas of Ulaanbaatar, especially children under five years old, increase most in summer and autumn. Soil contamination with pathogenic microorganisms directly affects the occurrence of intestinal diseases in children of the ger areas of Ulaanbaatar.

REFERENCES

Avaandorj D. (2014). Some geoecological issues in Mongolia, Ulaanbaatar. Soil Science, 376-383.

Batkhishig O., Oyunbat P., Bolormaa Ts. (2016). Microbiological contamination of soil in Ulaanbaatar. In: Discussion book on soil protection and reduction of land degradation, Ulaanbaatar, Institute of Geography and Geoecology, 265-282.

Gangadhar Z. (2014). Environmental Impact Assessment on Soil Pollution Issue about Human Health. Int. Res. J. Environment Sci. International Science, Vol. 3(11), 78-81.

CGA. (2013). Amendments to the General Plan of Development of Ulaanbaatar till 2020, Development tendency till 2030, Study of the current situation in Ulaanbaatar, 1, 21-24.

Government of Mongolia (2009). Millennium Development Goals of Ulaanbaatar, Ulaanbaatar.

Gomiero (2016). Soil Degradation, Land Scarcity, and Food Security: Reviewing a Complex Challenge.

Kasimov N., Kosheleva N. E., Sorokina O. I., Bazha S.N., Gunin P. D., and Enkh-Amgalan S. (2011). Ecological-geochemical state of soils in Ulaanbaatar (Mongolia). Eurasian Soil Science, 44 (7), 709–721, DOI 10.1134/S106422931107009X

Kasimov N., Kosheleva N., Gunin P., Korlyakov I., Sorokina O., and Timofeev I. (2016). State of the environment of urban and mining areas in the Selenga transboundary river basin (Mongolia Russia) // Environmental Earth Sciences, 75(1283), 1–20, DOI 10.1007/s12665-0166088-1

Liedekerke M., Prokop G., Rabl-Berger S., Kibblewhite M. and Louwagie G. (2014). Progress in the management of Contaminated Sites in Europe. Luxembourg: Publications Office of the European Union. DOI:10.2788/4658

MSO. (2008). Soil quality. Highest permissible levels of soil contaminating substances and elements. MNS 5850:2008, Ulaanbaatar, 4-5.

MSO. (1994). MNS 3298-1990" and "Soil Procedures of taking samples; use containers and transporting MNS 2305-1994, 1-7.

MOH, CHD, (2016). Communicable diseases, In: Health indicators, 2016. Ulaanbaatar: Center for Health Development, 60-67.

Narantuya L., B. Burmaa, S. Bumaa, J. Kupul, Sh. Uranstegeg (1991). Content of heavy metals in the surface soil of Ulaanbaatar, mapping of the sources of pollution, Study report, National Center for Public Health.

Public Health Institute (2001). "Soil microbiological contamination level in major cities", Study report, Public Health Institute, Ulaanbaatar.

Public Health Institute (2009). Soil microbiological study in major cities, survey report, Ulaanbaatar, Study report, Public Health Institute, Ulaanbaatar.

Stringer Lindsay C. (2011). Global land and soil degradation: challenges to soil Sustainability Research Institute, School of Earth and Environment, University of Leeds, Survey report, West Yorkshire, UK.

Urantsetseg Sh., B.Burmaa., S.Bumaa., J.Kupul. (2001). The level of soil microbiological contamination and chemical pollution in Ulaanbaatar and hygiene assessment, Survey report, Ulaanbaatar.

Lilit Sahakyan, Gevorg Tepanosyan, Gayane Melkonyan*,
Nairuhi Maghakyan, Armen Saghatelyan

The Center for Ecological-Noosphere Studies, NAS, Abovyan str. 68, Yerevan, 0025
Republic of Armenia
* Corresponding author: gayane.melkonyan@cens.am

MERCURY SOIL CONTENTS AND ASSOCIATED ECOLOGICAL AND HEALTH RISKS IN KINDERGARTENS AND FUNCTIONAL AREAS OF THE CITY OF VANADZOR (ARMENIA)

ABSTRACT. Mercury is a widespread environmental pollutant becoming a crucial health concern as a result of natural and anthropogenic releases. Understanding Hg distribution pattern between different functional urban areas is needed for urban pollution control and health impact assessment. Therefore, in this paper urban soil Hg spatial distribution, pollution level evaluation, and mercury-induced health risks were studied, for different urban functional areas (355 samples) and kindergartens (18 samples) of Vanadzor. Geospatial mapping and the geostatistical analysis suggest that Hg concentration in the entire area of Vanadzor and its kindergartens has a natural origin, besides a certain anthropogenic impact on some urban sites. According to geoaccumulation index (Igeo), uncontaminated or moderately contaminated levels were detected only in 2 samples from industrial area and 5 samples from residential area, the remaining samples were classified as uncontaminated. In all kindergartens and the 22.15 sq.km of the city (270 samples) are characterized by low level potential ecological risk, whereas 3.85 sq.km (85 samples) correspond to moderate and for 1 sampling site high level of potential ecological risk. A non-carcinogenic health risk assessed for children and adults indicates health hazards neither in Vanadzor entire areas nor in kindergartens. The hazard index (HI) in each urban functional area is less than allowable level (HI <1) for children and adults. Obtained results are indicative and offer the ability for better management of urban soil and urban planning in terms of Hg pollution regulation in different functional areas.

KEY WORDS: Mercury, Soil pollution, Urban functional area, health risk, kindergartens

INTRODUCTION

Mercury is one of the metals which pose a grave environmental threat worldwide (Yanin 1992; B.J. Alloway 2013; Driscoll et al. 2013). Due to its chemical and ecotoxicological properties, this element is listed among persistent bioaccumulative toxic elements (PBTs) producing negative effects on both living organisms and the environment (Yanin 1992).

On a global scale, the mercury contamination issue is determined primarily by a complex geochemical cycle of this element (Li et al. 2009; Rice et al. 2014) which includes accumulation of naturally occurring mercury in the earth crust, its emission to the atmosphere (Beckers and Rinklebe 2017), deposition in soil and water, evaporation from these environments (Selin 2009) and consequent accumulation in soil substrates (AMAP/UNEP 2013). In biogeochemical cycle of mercury, soil has an essential part in distribution and accumulation of this element in different environments (Nezhad 2014; Kelepertzis and Argyraki 2015) thus serving as a key indicator of environmental contamination with mercury (Szymon Różański 2015). In soil, mercury is most commonly encountered in organic (Hg^{-C}) and inorganic (Hg^{2+}) forms (Lymberidi 2005; UNEP 2013), the presence of which affects the soil quality characteristics including natural soil profile and soil fertility values (Laker 2005). Since recent years the mercury contamination issue has become increasingly topical in regard to urban soils (Li et al. 2010; Szymon Różański 2015; Gray et al. 2015; Wan et al. 2016; Kumar et al. 2017; Moller et al. 2018).

Globally, Hg concentrations in the soil range between 0.01 and 0.2 mg/kg, with a mean of 0.03 mg/kg (Reimann and de Caritat 1998). According to Pan et al. 2018, in urban soils from 32 Chinese cities, Hg concentration ranges from 0.02-0.93 mg/kg, with the median of 12.05 mg/kg, and in all studied cities non-carcinogenic health risks of Hg were within threshold values (HI < 1) (Pan et al. 2018). In the case of European cities, according to Rodrigues et al. 2006, measured total Hg contents in 6 cities (Aveiro (Portugal), Glasgow (Scotland), Ljubljana (Slovenia), Sevilla (Spain), Torino (Italy) and Uppsala (Sweden)) varied from 0.015 to 6.3 mg kg^{-1}. The lowest median value was found in Aveiro (0.055 mg/kg), and the highest- in Glasgow (1.2 mg/kg) (Rodrigues et al. 2006).

The issue of urban soil contamination with mercury is prioritized due to serious risks this element poses to human health (Ajmone-Marsan and Biasioli 2010; Wip et al. 2013; Kotova et al. 2017; Li et al. 2017).

Through direct or indirect ingestion, inhalation or skin absorption mercury and its compounds travel from soil into the organism (Steffan et al. 2018), causing thus acute and chronic diseases including dysfunction of locomotive and nervous systems, toxic effects on the respiratory system (Bernhoft 2012; AMAP/UNEP 2013) and in some severe cases kidney and liver failure.

Different groups of the population depending on physiological, biological and social conditions respond to mercury contamination in different ways (Mamtani et al. 2011). In this respect, a special emphasis is placed on children since their organisms and immune system are still immature. Another fact to explain the sensitivity of children is that for them is more likely to come into contact with soils/soil-derived materials and that due to low stature they inhale topsoil weathering-induced contaminants more intensively than adults (Mielke 2011; Kumpiene and Brännvall 2011; Tepanosyan et al. 2017a). Also, it needs to take into consideration so-called main venues, which for children commonly are kindergartens (Sun et al. 2013; Zheng et al. 2015), for adults – certain functional urban areas (Jing et al. 2012).

Since targeting careful studies with regard to mercury pollution in soils havenot been performed in Armenia, in 2016 the Center for Ecological-Noosphere Studies of the National Academy of the Republic of Armenia (CENS) implemented a first-ever complex research aimed at mercury contamination in city of Vanadzor (former Kirovakan)- one of Armenia's biggest industrial centers. Although according to Vanadzor's geological base, Hg natural concentrations are not typical for the city, however, due to intense industrial activity of Vanadzor 's Kimprom chemical plants, hydroelectric power stations, an electrotechnical plant, a number of

chemicals and chemical fiber manufacturing enterprises ,the city was notable for mercury pollution of its environment. At present, the major contamination source to the city is the Vanadzor-Kimprom (Nazaryan 2009). In 1978 as the result of an accident at the chemical plant, significant amounts of mercury were emitted into the city environment. Afterward, massive destruction of thousands of structures during the catastrophic Spitak earthquake of 1988 led to the origination of huge quantities of debris and toxic leakage from the plant's tailing dump (Karakhanian et al. 2004)

Thus, to understand the current city state of Hg pollution, this particular research was initiated with a purpose of 1. detecting mercury contents in Vanadzor's functional areas and kindergartens, 2. establishing regularities of mercury distribution and 3. assessing mercury-induced health risks.

MATERIAL AND METHODS

Study area

Vanadzor (40°48´46´´N,44°29´18´´E) is Armenia's third-biggest city located in the north of the country in intermountain basin at a height of 1350 m a.s.l. The city covers an area of 26 sq.km and has a population of 80.7 thousand inhabitants. Vanadzor city is surrounded by

wooded slopes. The central part of the city mainly occupied by residential, public and industrial buildings while on the outskirts of the city the abandoned manufacturing buildings and small houses (sometimes metal made) for low-income families are located.

The climate is temperate: hot, moderately mild summer and mild winter. The average annual precipitation is 600mm, the average temperature in summer varies from +4°C to +24°C, in winter -3.2 °C to -18°C. The cardinal direction of the Vanadzor wind rose is southerly and (State Committee of the Real Estate Cadastre 2007). To the city carbonate rocks and debris, forest cinnamon and limestone loam and black soils are common. The city sits in the forest-steppe landscape belt. The geological structure of the city is complex and involves alluvial, diluvial sediments and basalts, tuffs and other conglomerates (State Committee of the Real Estate Cadastre 2007).

Soil sampling and pretreatment of soil samples

In the frames of this research in August-September 2016 18 soil samples were collected from Vanadzors' kindergartens as well 355 soil samples were collected from the entire area of Vanadzor (Fig. 1), of which 64 were spatially located within industrial area, 19-
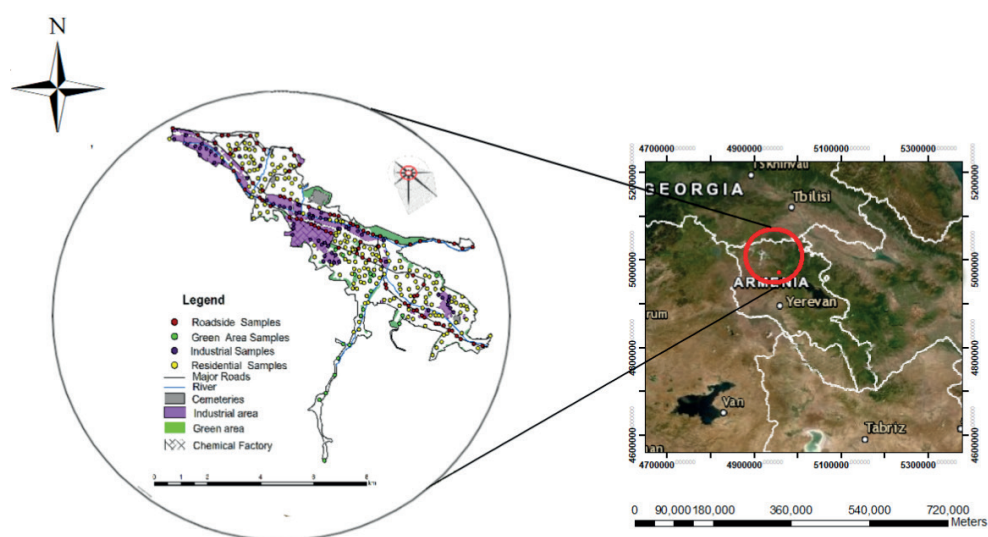
Fig. 1. A map of spatial distribution of soil samples in different functional areas in Vanadzor

in the green belt, 82- on a roadside section, 184- in the residential area of the city (6 samples overlapped). In order to determine a local geochemical background of Hg, 20 soil samples were collected from a background plot (about high of 1750m) in 17km away to the west of the city which can be regarded as being uncontaminated. Background soils are mainly characterized by forest cinnamon and limestone loam and black soils, which are also similar to the city soils. In order to obtain a bulk soil sample, 3-5 subsamples were collected with a stainless steel spade from 0-5 cm deep soil layer, then labeled, placed into plastic zip-lock containers and transported to the CENS lab. Then the samples were air-dried at 20°C, sieved through a 2mm sieve, then crushed and homogenized in compliance with standard operation procedures (SOPs) developed at CENS in compliance with international ISO (ISO 10381-2 2002), US EPA (US EPA 2001), and other international standards (Stauffer 2008).

Analytical method and QA/QC

Total mercury in the soil samples was determined by X-ray fluorescent spectrometry (Olympus Innov-X-5000 (USA)) consistent with the US EPA 6200 method. Detection limit for Hg in the soil is 0.0003 mg/kg. The quality of analytical work was assured based on a SiO2 blank sample certified by the National Institute of Standards and Technologies USA and reference substances NIST 2710a and NIST 2711a.

Statistical treatment and geochemical mapping

Statistical treatment of data was performed (IBM SPSS 21). Normal distribution of data was tested by the Shapiro-Wilk test. In order to visualize mercury contents in different urban functional areas, respective box plots were constructed. The geochemical background of mercury was calculated in compliance with an integral method of determining the background contents of chemical elements in soil (Tepanosyan et al. 2017b). Geochemical mapping of data was implemented in ArcGIS 10.1 program environment by the IDW interpolation method of mapping.

Contamination level assessment

The concentration coefficient (Kc) is a criteria of abnormality of an element denoting an excess of the substance against the background and determined through the ratio between its actual contents (Kosheleva et al. 2003). The concentration coefficient is calculated by a formula (1)

$$K_c = C_{Hg} / C_f \tag{1}$$

where K_c is the concentration coefficient;
C_{Hg} - mercury contents in the study environment (mg/kg);
C_f – background contents of mercury. Different soil contamination levels are determined by Kc values as follows: Kc<4 corresponds to allowable, 4-8 to moderately hazardous, 8-16 hazardous, 16-32 highly hazardous, >32 extremely hazardous level (Golovin 2000).

Assessment of geoaccumulation index

The geoaccumulation index (Igeo) employed for assessing the intensity of manmade contamination, was first suggested by Müller (Müller 1969) as a method for determining metal contamination of soils through collation between background contents and detected concentrations of the element (Barbieri 2016). Igeo is determined by the following formula (2):

$$I_{geo} = Log_2 \left(\frac{C_{Hg}}{1.5 \times B_{Hg}} \right) \tag{2}$$

where C_{Hg} is mercury content of soils, B_{Hg} -background contents of mercury (Tepanosyan et al. 2017b). The 1.5 factor is used because of possible variations of the background data due to lithological variations and it helps analyze natural fluctuations of mercury in the environment and determine small anthropogenic impacts (Müller 1969). A descriptive classification of I_{geo} values suggested by Müller is provided in Table 1.

Assessment of potential ecological risk

In order to describe a potential hazard caused by toxicity of mercury assessment was done of the ecological risk of Vanadzor soils. This risk was identified in compliance with the Potential Ecological Risk Index (PERI) suggested by

Table 1. Classification of Igeo index (Müller 1969)

Class	Value	Classification
0	$I_{geo} \leq 0$	Uncontaminated
1	$0 < I_{geo} < 1$	Uncontaminated to moderately contaminated
2	$1 < I_{geo} < 2$	Moderately contaminated
3	$2 < I_{geo} < 3$	Moderately to heavily contaminated
4	$3 < I_{geo} < 4$	Heavily contaminated
5	$4 < I_{geo} < 5$	Heavily to extremely contaminated
6	$I_{geo} \geq 5$	Extremely contaminated

Hakanson (Hakanson 1980) and intended for contamination assessment in sedimentology. However, many researchers widely employ this method for assessing ecological risks of soil and dust as well (Sun et al. 2010; Yuan et al. 2014; Soliman et al. 2015; Zhao et al. 2015). PERI (E_r^{Hg}) is determined by the formula (3) and (4) as follows:

$$C_r^{Hg} = \frac{C_x^{Hg}}{C_n^{Hg}} \qquad (3)$$

$$E_r^{Hg} = T_r^{Hg} \times C_r^{Hg} \qquad (4)$$

where T_r^{Hg} is a mercury toxicity-response factor ($T_r^{Hg} = 40$); C_r^{Hg} – contamination factor; C_x^{Hg} mercury content of soil; C_n^{Hg} background content of mercury.

Non-carcinogenic risk assessment

Non-carcinogenic health risk was assessed by the formula suggested by US EPA, according to which non-carcinogenic risk assessment can be done through calculation of three mercury exposure routes: inhalation, ingestion, skin absorption (US EPA 2002a). Based on the three routes of exposure chronic daily intake (CDI) for mercury was calculated by formulae 5-7 (RAIS 2018):

$$CDI_{ing} = \frac{C \times IngR \times CF \times EF \times ED}{BW \times AT} \qquad (5)$$

$$CDI_{inh} = \frac{C \times IngR \times EF \times ED}{BW \times AT \times PEF} \qquad (6)$$

A whole set of CDI calculation parameters is given in Table 2. Hazard Quotient (HQ) for non-carcinogenic risk is calculated through an

$$CDI_{dermal} = \frac{C \times SA \times CF \times AF \times}{BW \times} \\ \frac{\times ABF \times EF \times ED}{\times AT} \qquad (7)$$

RfD (referent dose) ratio (8) (Saleem 2014). RfD value for ingestion is $3.0 \cdot 10^{-4}$ (we used RfD for inorganic mercury (RAIS 2018), as in soil, water and sediments inorganic mercury salts are prevalent (Lymberidi 2005)). RfD values for skin absorption and inhalation are $2.10 \cdot 10^{-5}$ and $8.57 \cdot 10^{-5}$, respectively (Nazarpour et al. 2017);

HQ<1 denotes the absence of non-carcinogenic risk, whereas HQ>1 means a hazardous effect to human health (US EPA 2002a; RAIS 2018)

$$HQ = \frac{CDI}{RfD} \qquad (8)$$

where CDI is daily intake from i –route: the sum of HQ value calculated for each of three routes represents HI – a hazard index, $HI = \sum HQ$ (US EPA 1989).

RESULTS AND DISCUSSION

The entire area of Vanadzor

Mercury content of soil samples collected from the entire area of Vanadzor varies from 0.001mg/kg to 0.29 mg/kg, with a mean value of 0.043 mg/kg. A map of spatial distribution of mercury contents of Vanadzor soils provided in Fig.3 shows that the city area is dominated by a field of 50-75% mercury contents ranging between 0.039

Table 2. Parameters of descriptive statistics, MAC and geochemical background of mercury contents(mg/kg) of soils in different functional areas in Vanadzor

Index	Parameters of exposure	Unit	Value		Published source
			Children	Adults	
IngR	Ingestion rate of soil	mg/day	100	200	(US EPA 2011; RAIS 2018)
EF	Exposure frequency	days/year	350	350	(US EPA, 1989; RAIS 2018)
ED	Exposure duration	years	6	30	(US EPA 2002b; USEPA 2004)
BW	Average body weight	kg	15	70	(U.S. EPA 2011)
AT	Average time	days	365 ED		(RAIS 2018)
CF	Conversion factor	kg/mg	10-6	10-6	(US EPA 1989)
InhR	Inhalation rate	m^3 /kg	7.63	12.8	(US EPA 1989; Nazarpour et al. 2017)
PEF	Particle emission factor	m^3 /kg	1.36 109	1.36 109	(Nazarpour et al. 2017)
SA	Surface area of the skin that contacts the soil	cm^3	2670	5800	(DEQ 2015)
AF	Skin adherence factor		0.2	0.7	(Nazarpour et al. 2017)
ABF	Dermal absorption factor		0.001	0.001	(Nazarpour et al. 2017)

and 0.05 mg/kg. Relatively high content of mercury (95%, 0.064 mg/kg) exceeds the local background value (0.05 mg/kg) and is characterized by patch-like distribution in form of point-source anomalies throughout the city, whereas the most intensive of these anomalies are spatially located close to the chemical plant and once active but presently inactive industrial centers in the northwest and north of the city. In the entire area of the city, Hg content does not exceed MAC (2.1 mg/kg).

According to descriptive statistics parameters (Table 3) as well as box-plots (Fig. 2) the mean value of mercury contents throughout the city is higher than the median, while the skewness differs from 0, being thus indicative of right asymmetry (<1) and deviation from normal distribution. According to the Shapiro-Wilk test, mercury contents are abnormally distributed, which can possibly be due to presence of outlier values, and after their excluding abnormal distribution is observable again. However, after logarithmic transformation of data and

exclusion of outliers, consistent with the Shapiro-Wilk test log-normal distribution is derived.

In 83.9% of Vanadzor area (21.81 sq.km-305samples) the detected Hg contents of soil do not reach the background values. In 16% of the city area (4. 16sq.km – 49 samples) the detected Hg contents exceed the background 1.2 -2.15 times. Calculated contamination coefficient (Kc) is less than 4, which is indicative of low-level mercury contamination; however, for the only sample (0.086% of the city area, 0.02 sq.km) which exceed the background 5.8 times, Kc is 4-8, corresponding to a moderate mercury contamination level.

Mercury contents detected in Vanadzor are typical of other cities of the world (McGrath 1995; Birke and Rauch 2000; Manta et al. 2002; Tijhuis 2002; Crnković et al. 2006; Szymon Różański 2015). For instance, in Berlin and Tallinn, where the local background value is close to that in Vanadzor (0.05 mg/kg), mean mercury contents of soils are assessed to be

Table 3. Parameters of descriptive statistics, MAC and geochemical background of mercury contents(mg/kg) of soils in different functional areas in Vanadzor

Descriptive statistics	Entire area	Industrial area	Green area	Residential area	Roadside area	Kindergartens
Mean	0.043	0.0423	0.044	0.043	0.041	0.037
Median	0.039	0.042	0.047	0.038	0.038	0.034
Standard deviation	0.019	0.013	0.013	0.023	0.013	0.010
Min.	0.0015	0.024	0.025	0.0015	0.024	0.025
Max.	0.290	0.095	0.064	0.290	0.080	0.049
Coefficient of variation %	44.22	31.14	29.14	53.4	31.65	26.73
Skew	6.60	1.528	-0.298	6.929	0.830	0.205
Quantity of samples	355	64	19	184	82	18
MAC	2.1					
Background	0.05					
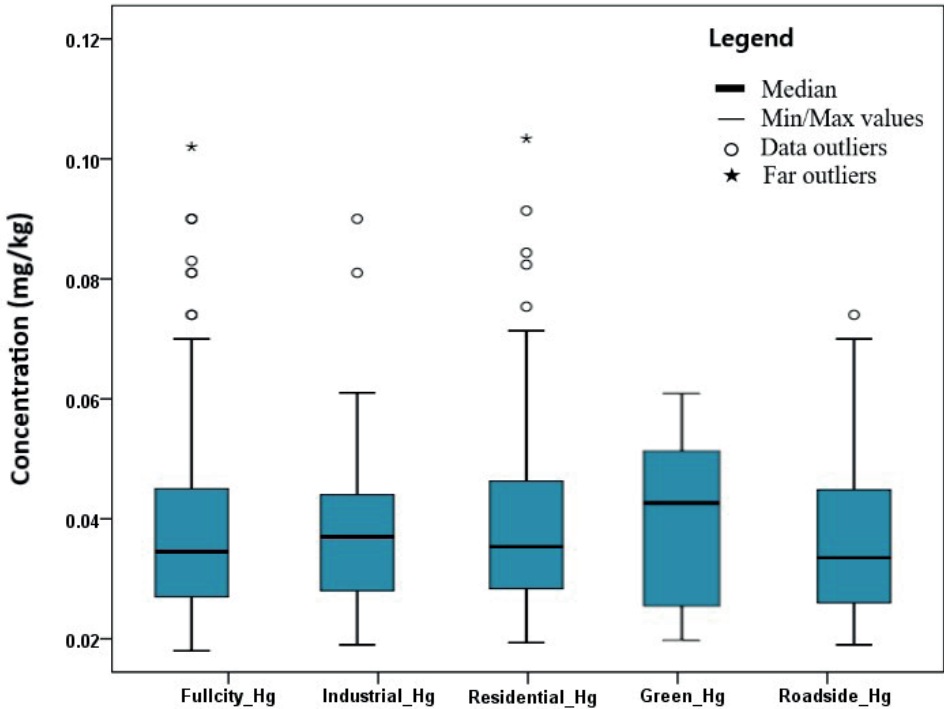
Fig. 2. Box-plots of mercury contents in industrial, green, residential, roadside areas and kindergartens in Vanadzor

0.42 mg/kg and 0.24 mg/kg, respectively (Birke and Rauch 2000; Bityukova et al. 2000). In Palermo, where the local background content (0.06 mg/kg) is similar to Vanadzor, Hg mean content is 0.68mg/kg (Manta et al. 2002). In Warsaw, where the local background value is twice as higher as it is in Vanadzor (0.1 mg/kg), Hg mean content is 0.13 mg/kg. The same contents are typical for Oslo, where the local background is 0.03 mg/kg (Tijhuis 2002). So, mean Hg contents of soils in Berlin, Tallin, Oslo (where the local background is lower than it is in Vanadzor (0.05 mg/kg)), max 8 times (Berlin) and min 2.5 times (Oslo) are higher than in Vanadzor.

I_{geo} values are provided in Table 4, which shows that Igeo for Vanadzor varies from 1.56 to 1.9, with a mean value of – 0.9. For 96.9% of samples (344 samples). I_{geo} corresponds to uncontaminated level (I_{geo}≤0), for 2.81% of samples (10 samples) – to uncontaminated or moderately contaminated level (0<I_{geo}<1) and for the only sample – to the moderately contaminated level (1<I_{geo}<2). Summarizing the descriptive statistic data as well as Kc and I_{geo} values allows to conclude that in different parts of Vanadzor ambiguous contents of mercury are found, the origin and potential sources of which were identified through determining mercury contents of soils in separate functional urban areas.

Industrial area

Mercury contents of 64 soil samples collected from the Vanadzor industrial area range between 0.024 and 0.095 mg/kg, with a mean value of 0.042 mg/kg. The mean mercury contents of these samples are almost identical to the mean value obtained for almost the entire area of the city (0.043 mg/kg). As seen from Table 3 and the diagram (Fig. 2), mean and median values are similar (0.0423 and 0.0420), however, the skewness differs from 0, which is indicative of some deviation from normal distribution. According to the Shapiro-Wilk test, in the industrial area of the city abnormal distribution of mercury (p<0.05) is observable, whereas after logarithmic transformation (p=0.061>0.05) lognormal distribution is derived. Having regard to low values of the coefficient of variation (31.14%) as well as lognormal distribution of mercury, one may suppose that mercury contents in this area of the city are mainly of natural origin. Nonetheless, according to the box-plots (Fig. 2) in the industrial area of the city two mercury outliers are found which are 1.7 and 1.9 times higher against the background value. One of two mentioned samples is spatially adjacent to a welding plant site which accommodates huge amounts of domestic garbage and waste

Table 4. I_{geo} values for different functional areas in Vanadzor

I_{geo} value		Entire area	Industrial area	Green area	Residential area	Roadside area	Kindergartens
Mean		-0.903	-0.885	-0.821	-0.923	-0.928	-1.044
Min		-5.640	-1.64	-1.580	-5.640	-1.64	-1.580
Max		1.950	0.340	-0.22	1.950	0.070	-0.600
SD		0.574	0.413	0.462	0.679	0.438	0.353
I_{geo} classes							
I_{geo}≤0	Uncontaminated	97.18%	96.8%	100%	96.2%	100%	100%
0<I_{geo}<1	Uncontaminated to moderately contaminated	2.53%	3.12%	-	3.26%	-	-
1<I_{geo}<2	Moderately contaminated	0.281%	-	-	0.54%	-	-

metals; the second sample is spatially located on the abandoned industrial site with survived metal warehouses. Hence, high mercury contents of these samples could presumably be due to large amounts of metals on the mentioned sites (Sastry et al. 2001) 14% of samples (9 samples) exceed the background value 1.1-1.9 times (0.05 mg/kg), whereas the contamination coefficient varies 0.48 to 1.9, with a mean value of 0.84. For all the samples Kc is less than 4, which corresponds to the allowable level of mercury contamination on these urban sites. I_{geo} values range between 1.67 - 0.34, with a mean value of -0.88. Only for two samples $I_{geo} > 0$ which, according to I_{geo} classification (Table 1), corresponds to uncontaminated or moderately contaminated level. Considering the value of the coefficient of variation (31.14%) as well as lognormal distribution of mercury, one may suppose that mercury detected in these parts of the city is mainly of natural origin. In comparison with Hg concentrations from different areas of various cities (Table 6), Hg mean value in Vanadzor industrial area is 5.4 and 5 times lower than in Zima(Russia) and Changchun(China) cities respectively, Hg Max content is 4 and 5.8 times, min content - 8 and 5 times lower than in above cities, respectively.
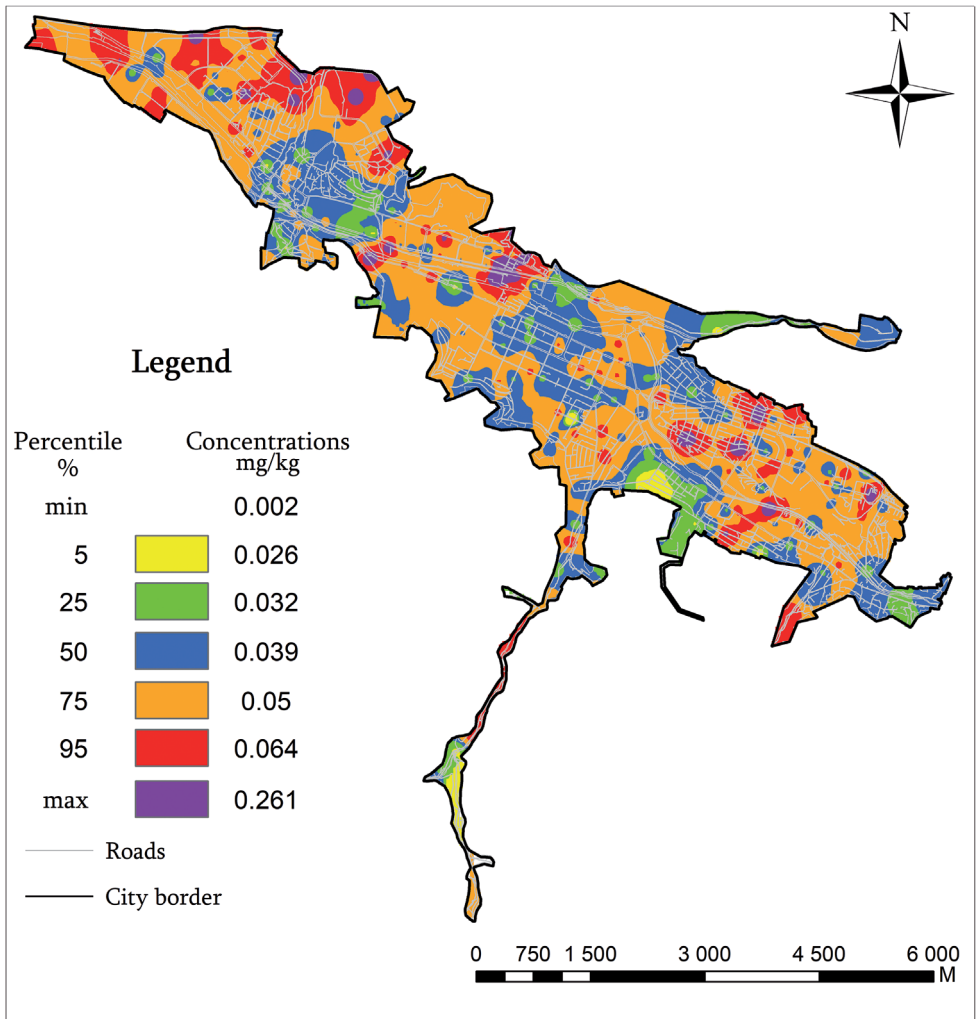
Green area

Mercury contents of 19 soil samples collected from the green area of the city vary 0.025 to 0.064 mg/kg, with a mean value of 0.044 mg/kg, which insignificantly exceeds the mean value obtained for the entire area of the city (0.043 mg/kg). The skewness value for this part of the city is negative, mean value is lower than median, thus pointing to left-side deviation from normal distribution. However, according to the Shapiro-Wilk test, the green area of the city is characterized by normal distribution of mercury. 36.8% of samples (7 samples) exceed the background contents (0.05 mg/kg) 1.1.05 to 1.29 times (Table 3). The contamination coefficient Kc varies from 0.5 to 1.29, with a mean value of 0.8. For all the samples Kc<4, corresponding to the allowable level of mercury contamination, whereas I_{geo} value ranges between -158 and 0.21, with a mean value of -0.82, which is indicative of the absence of contamination.

Hence, collation between statistical parameters, insignificant excess against the background contents and the low coefficient of variation (29.14%) points to the natural origin of mercury in the green area of Vanadzor.

Table 6. Literature data on Hg concentrations (mg/kg) in urban different areas from various cities around the world

City	Urban area	Min	Max	Mean	Reference
Mexico(Mexico)	Residential	0.017	0.061	-	(Morton-Bermea et al. 2016)
Bydgoszcz(Poland)	Green	0.009	1.114	0.210	(Szymon Różański 2015)
Palermo(Italy)	Green	0.040	5.600	0.070	(Manta et al. 2002)
Kavalas(Greece)	Roadside	Not detected	3.300	0.100	(Christoforidis and Stamatis 2009)
Changchun (China)	Industrial	0.140	0.479	0.208	(Fang et al. 2004)
Beijing(China)	Roadside	0.022	1.500	0.210	(Chen et al. 2010)
Beijing(China)	Residential	0.034	2.800	0.350	(Chen et al. 2010)
Beijing(China)	Green	1.100	9.400	2.900	(Chen et al. 2010)
Zima city(Russia)	Industrial	0.100	0.810	0.230	(Butakov et al. 2017)

Fig. 3. Spatial distribution of mercury content in Vanadzor soils

In comparison with Hg concentrations from different areas of various cities (Table 6), we can conclude, that in Vanadzor's green area Hg mean content is 72, 5 and 1.75 times lower than the mean reported for Beijing(China), Bydgoszcz(Poland) and Palermo(Italy), respectively. Hg max content is 146, 17.8 and 87.5 times lower than in above cities respectively, Hg min content - 44 and 1.6 times lower than in Beijing (China) and Palermo (Italy), but approximately the same with Bydgoszcz(Poland).

Residential area

As evidenced by descriptive statistic data (Table 3), mercury contents of 184 soil samples collected from Vanadzor residential area vary from 0.0015 to 0.29 mg/kg, with a mean value of 0.043 mg/kg, which is equal to mean values obtained for the entire area of the city. Of all soil samples collected throughout the city, minimal and maximal contents of mercury were established for those taken from the residential area. In this area mean contents of mercury are higher than median, this being indicative of skewness, which, as visualized by a box plot (Fig 2), is right-sided. The skewness value differs from 0, this fact pointing to the presence of some deviation from normal distribution as evidenced by a large amount of outlier values. The Shapiro-Wilk test shows abnormal distribution and even after exclusion of outliers and log transformation of data the pattern does not change.

22.8% of samples (42 samples) exceed the background contents (0.05 mg/kg) 1.5-5.8 times. According to the coefficient of contamination varying within 0.03-5.8 in this area with the exception of the only sample, Kc<4, which corresponds to the allowable level of mercury contamination. Only for one sample Kc value is in the range of 4-8 (Kc=5.8), thus corresponding to moderate contamination level. The sample was taken from the surroundings of private houses located close to one of the main roads. As such a high content of mercury was not detected in the rest of samples taken from this area (VS-220 =0.051 mg/kg, VS-217=0.036 mg/kg), so one may conclude that mercury contents in the mentioned sample can possibly be due to manmade point-source contamination: combustion of fuel, broken thermometers, or other anthropogenic activities.

I_{geo} values vary from -5.64 to 1.95, with a mean value of -0.92. Only 5 out of 185 samples taken from this area have I_{geo}>5, corresponding thus to uncontaminated or moderately contaminated level (0<I_{geo}<1), while moderately contaminated level (1<I_{geo}<2) was established for a single sample only.

According to Hg concentrations in different areas of various cities (Table 6), in Vanadzor's residential area Hg mean content is 8 times lower than the mean reported for Beijing(China), but 4.8 times higher than Hg max content in Mexico(Mexico). Hg Min content is 15 and 22 times lower than in Beijing(China) and Mexico(Mexico), respectively.

Roadside area

Mercury contents of the roadside samples vary 0.024 - 0.08 mg/kg, with a mean value of 0.041 mg/kg, which is lower than mean contents throughout the city (0.043 mg/kg). As seen in Table 3, the skewness value differs from zero, which is indicative of a certain deviation from normal distribution. The Shapiro-Wilk test points to abnormal distribution, but after log transformation of data lognormal distribution is derived. A conclusion drawn from this is that roadside

mercury is naturally occurring. However, mercury contents in these roadside area samples exceed the background, which can possibly be due to heavy road traffic.

18.3% of samples (15 samples) exceed the background (0.05 mg/kg) 1.2-1.6 times. The concentration coefficient (Kc) ranges between 0.48-1.58, therefore Kc<4, thus corresponding to the allowable level of mercury contamination. In the roadside area, I_{geo} values vary from -1.64 to 0.075, with a mean value of 0.92. For all the samples I_{geo} values are below zero, this corresponding to the absence of mercury contamination in the given area.

In comparison with Hg concentrations from various city areas (Table 6), in Vanadzor's roadside area Hg mean content is 2.5 and 5.2 times lower than in Kavalas (Greece) and Beijing (China), respectively. The max content is 41 and 30 times lower than in the above cities respectively, but Hg min content is approximately the same with Beijing(China).

Kindergartens

Mercury contents of soil samples collected from 18 kindergartens in Vanadzor vary 0.025 to 0.049 mg/kg, with a mean value of 0.037 mg/kg, which is lower than mean contents of the element throughout the city (0.043 mg/kg). As visualized in Table 3 and Fig. 2, mean and median values differ insignificantly (0.037 and 0.034, respectively), whereas the skewness value differs from zero, which points to right-side asymmetry (<1) and deviation from normal distribution. According to the Shapiro-Wilk test, kindergarten soils exhibit normal distribution of mercury, but after log transformation of data and exclusion of outlier values log normal distribution is derived.

Considering a low value of the coefficient of variation (26.73-24.5%) as well as lognormal distribution of mercury, one may suppose that the detected mercury contents in the given area are mainly of natural origin.

In Vanadzor kindergartens no MAC and

background exceeding contents were established. According to the concentration coefficient (Kc) which varies 0.5 to 0.98, Kc<4 correspondings to the low level of Hg contamination. I_{geo} values for the mentioned kindergartens range between -1.58-0.6, with a mean value of -1.04. I_{geo} values for all the samples are below zero, which is indicative of the absence of contamination.

Assessing potential ecological risk

The index of potential ecological risk of mercury exposure from Vanadzor soils including classification of ecological risk levels is given in Fig 4. E_r^{Hg} value for Vanadzor soils varies from 1.2 to 85.6, with a mean value of 33.73. Only one out of 355 samples exhibits E_r^{Hg}=232, thus corresponding to high potential ecological risk. For 76.05% of samples (270 samples) E_r^{Hg} value is below 40, which corresponds to low level potential ecological risk; however, the remaining 23.38% of samples (83 samples) correspond to moderate and the only sample to high potential ecological risk (Fig. 4). The sample exhibiting high contamination level was collected from the residential area, at the intersection of main roads close to private houses. It is noteworthy that as compared with this sample Er values for other samples collected from the given area are relatively low (VS-218- 39.2; VS-217-28.8). Hence, one may concludethat high mercury contents of the mentioned sample can presumably
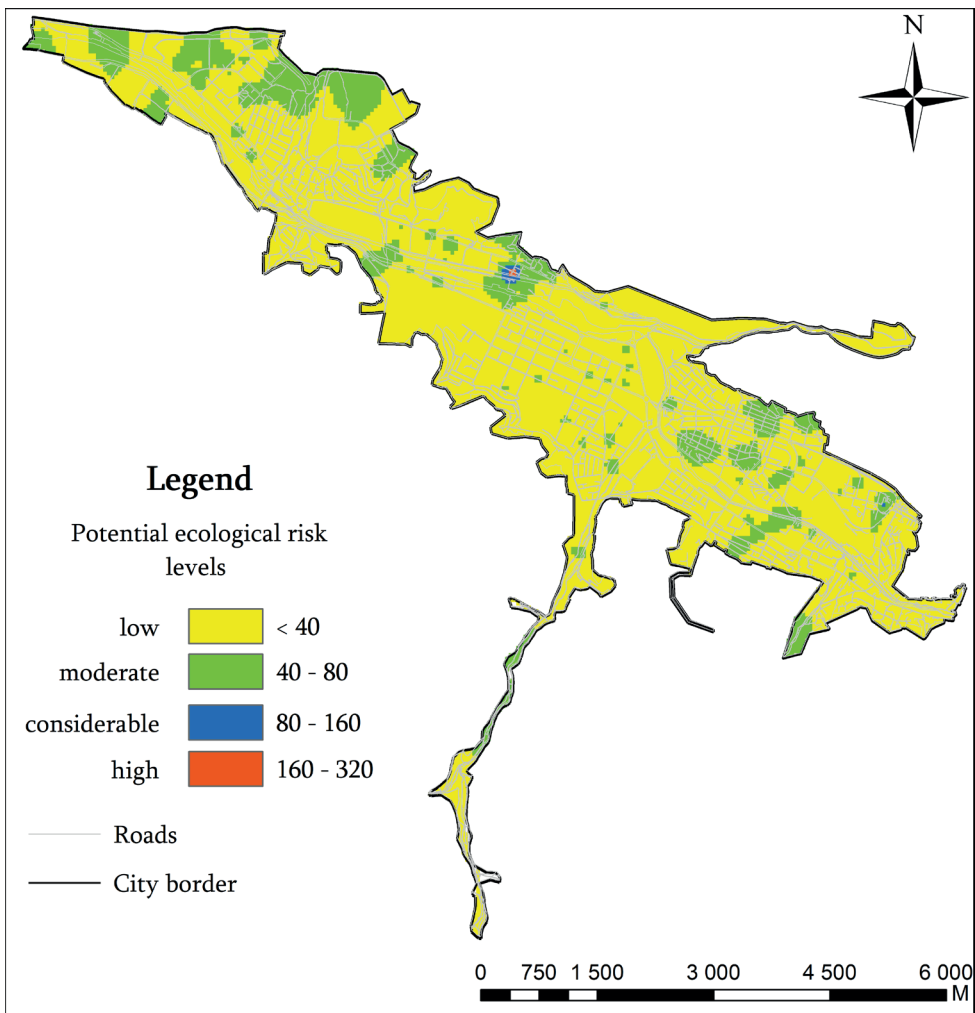
Fig. 4. Spatial distribution of mercury potential ecological risk levels (Er) in Vanadzor soils

be due to point-source contamination: broken thermometers, combustion of fuel, or can result from other activities of a man. Contrastingly, for all Vanadzor kindergartens a mean value of E_r^{Hg} is 29.92, which is <40 i.e. corresponds to low level potential ecological risk.

Assessing non-carcinogenic risk of mercury exposure

Assessment data on non-carcinogenic risk of mercury exposure from Vanadzor soils are provided in Table 5. HQ values for children and adults were calculated in respect of main mercury exposure routes: ingestion, inhalation, dermal absorption. Ingestion risk to Vanadzor adult population ranges between $1.37 \cdot 10^{-5}$ and $2.64 \cdot 10^{-3}$, with a mean value of $3.91 \cdot 10^{-4}$. HQ for inhalation varies $2.25 \cdot 10^{-9}$ to $4.36 \cdot 10^{-7}$, with a mean value of $6.45 \cdot 10^{-8}$, HQ for dermal absorption - $3.97 \cdot 10^{-6}$ to $7.6 \cdot 10^{-4}$, with a mean value of $1.13 \cdot 10^{-4}$. In general, a mean value of HI is $5.04 \cdot 10^{-4}$, minimal $1.77 \cdot 10^{-5}$, maximal $3.4 \cdot 10^{-3}$ (Table 5). In adults and children, alike HQ values for all functional urban areas have the following decreasing order $HQ_{ing} > HQ_{dermal} > HQ_{inh}$, according to which the major route of non-carcinogenic risk of mercury exposure is ingestion.

Ingestion risk in Vanadzor kindergarteners varies within $5.3 \cdot 10^{-4}$ to $1.05 \cdot 10^{-3}$, with a mean value of $7.97 \cdot 10^{-4}$. HQ for inhalation is $1.04 \cdot 10^{-7}$ to $2.06 \cdot 10^{-7}$, mean $1.56 \cdot 10^{-7}$; HQ for dermal absorption $4.06 \cdot 10^{-5}$ to $8.03 \cdot 10^{-5}$, with a mean value of $7 \cdot 10^{-5}$. In general, a mean value of HI is $8.58 \cdot 10^{-4}$, minimal $5.73 \cdot 10^{-4}$, maximal $1.13 \cdot 10^{-3}$. In contrast to the functional areas of Vanadzor, in kindergartens HQ values have the following decreasing order: $HQ_{inh} > HQ_{ing} > HQ_{dermal}$, according to which the major route of non-carcinogenic risk of mercury exposure is inhalation.

As evidenced by research results, in the entire area of Vanadzor and its kindergartens HQ value is below the safe level (HQ<1), which is indicative of the absence of non-carcinogenic risk in Vanadzor soils.

Conclusion

The mean contents of soil samples throughout Vanadzor city range from 0.025-0.04 mg/kg which are common to urban soils. However, in comparison with Hg concentrations from different areas of various cities, the mean value of Hg in Vanadzor's functional areas is much lower than reported data.

Collating between mean contents of mercury in different areas of Vanadzor has indicated that the difference between mean values is insignificant, so no mercury distribution regularity can be established.

Mercury content of kindergarten soil does not exceed MAC and the background; that of city soils does not exceed MAC, however, the contents of this element in 50 soil samples collected from separate functional urban areas exceed the background in the range from 1.2 to 5.8. According to research outcomes, after the exclusion of 2 samples collected from the industrial area, 1 sample – from the roadside area and 6 samples – from residential area normal distribution was derived for the entire area of Vanadzor, this being indicative of the natural origin of mercury. However, mercury contents on excluded sites can probably be due to a certain anthropogenic impact.

The natural origin of mercury in Vanadzor kindergartens and the entire area of the city is also evidenced by I_{geo} values below zero for the majority of samples. According to geoaccumulation index, uncontaminated or moderately contaminated levels in the city soils were detected only in industrial (2 samples, 3.12%) and residential (5 samples, 3.2%) areas. The kindergartens and the major portion of the city (76.05%, 270 samples) are characterized by low level potential ecological risk.

23.38% of Vanadzor soil samples (83 samples) correspond to moderate potential ecological risk. Those samples were mosaically distributed mainly in the industrial and residential areas, close to the welding plant site, near chemical plant

Table 5. Hazard quotient (HQ) of non-carcinogenic risk in children and adults in Vanadzor kindergartens and different functional areas

Functional area	Value	Adults			Children		
		HQ_{ing}	HQ_{inh}	HQ_{derm}	HQ_{ing}	HQ_{inh}	HQ_{derm}
Industrial area	Min	$2.19 \cdot 10^{-4}$	$3.61 \cdot 10^{-8}$	$6.35 \cdot 10^{-5}$	$1.02 \cdot 10^{-3}$	$1 \cdot 10^{-7}$	$3.90 \cdot 10^{-5}$
	Max	$8.67 \cdot 10^{-4}$	$1.43 \cdot 10^{-7}$	$2.5 \cdot 10^{-4}$	$4.04 \cdot 10^{-3}$	$3.97 \cdot 10^{-7}$	$15 \cdot 10^{-5}$
	Mean	$3.86 \cdot 10^{-4}$	$6.37 \cdot 10^{-8}$	$1.12 \cdot 10^{-4}$	$1.8 \cdot 10^{-3}$	$1.77 \cdot 10^{-7}$	$6.88 \cdot 10^{-5}$
Residential area	Min	$1.37 \cdot 10^{-5}$	$2.25 \cdot 10^{-9}$	$3.97 \cdot 10^{-6}$	$3.19 \cdot 10^{-5}$	$6.27 \cdot 10^{-9}$	$2.43 \cdot 10^{-6}$
	Max	$2.64 \cdot 10^{-3}$	$4.36 \cdot 10^{-7}$	$7.6 \cdot 10^{-4}$	$6.17 \cdot 10^{-3}$	$1.21 \cdot 10^{-6}$	$4.7 \cdot 10^{-4}$
	Mean	$3.95 \cdot 10^{-4}$	$6.51 \cdot 10^{-8}$	$1.14 \cdot 10^{-4}$	$9.22 \cdot 10^{-4}$	$1.81 \cdot 10^{-7}$	$7.03 \cdot 10^{-5}$
Roadside area	Min	$2.19 \cdot 10^{-4}$	$3.61 \cdot 10^{-8}$	$6.35 \cdot 10^{-5}$	$5.1 \cdot 10^{-4}$	$1 \cdot 10^{-7}$	$3.9 \cdot 10^{-5}$
	Max	$7.21 \cdot 10^{-4}$	$1.18 \cdot 10^{-7}$	$2.09 \cdot 10^{-4}$	$1.6 \cdot 10^{-3}$	$3.3 \cdot 10^{-7}$	$1.28 \cdot 10^{-4}$
	Mean	$3.77 \cdot 10^{-4}$	$6.21 \cdot 10^{-8}$	$1.09 \cdot 10^{-4}$	$8.8 \cdot 10^{-4}$	$1.72 \cdot 10^{-7}$	$6.71 \cdot 10^{-5}$
Green area	Min	$2.28 \cdot 10^{-4}$	$3.76 \cdot 10^{-8}$	$6.62 \cdot 10^{-5}$	$5.3 \cdot 10^{-4}$	$1.04 \cdot 10^{-7}$	$4.06 \cdot 10^{-5}$
	Max	$5.89 \cdot 10^{-4}$	$9.7 \cdot 10^{-8}$	$1.7 \cdot 10^{-4}$	$1.37 \cdot 10^{-3}$	$2.7 \cdot 10^{-7}$	$1.04 \cdot 10^{-4}$
	Mean	$4.05 \cdot 10^{-4}$	$6.68 \cdot 10^{-8}$	$1.17 \cdot 10^{-4}$	$9.4 \cdot 10^{-4}$	$1.86 \cdot 10^{-7}$	$7.22 \cdot 10^{-5}$
Entire area of Vanadzor	Min	$1.37 \cdot 10^{-5}$	$2.25 \cdot 10^{-9}$	$3.97 \cdot 10^{-6}$	$3.19 \cdot 10^{-5}$	$6.27 \cdot 10^{-9}$	$2.43 \cdot 10^{-6}$
	Max	$2.64 \cdot 10^{-3}$	$4.36 \cdot 10^{-7}$	$7.6 \cdot 10^{-4}$	$6.17 \cdot 10^{-3}$	$1.21 \cdot 10^{-6}$	$4.7 \cdot 10^{-4}$
	Mean	$3.91 \cdot 10^{-4}$	$6.45 \cdot 10^{-8}$	$1.13 \cdot 10^{-4}$	$9.14 \cdot 10^{-4}$	$1.79 \cdot 10^{-7}$	$6.97 \cdot 10^{-5}$
Kindergartens	Min	-			$5.3E \cdot 10^{-4}$	$1.05 \cdot 10^{-3}$	$4.06 \cdot 10^{-5}$
	Max	-			$1.04 \cdot 10^{-7}$	$2.06 \cdot 10^{-7}$	$8.03 \cdot 10^{-5}$
	Mean	-			$7.97 \cdot 10^{-4}$	$1.56 \cdot 10^{-7}$	$6.07 \cdot 10^{-5}$
HI	Min	$1.77 \cdot 10^{-5}$			$3.43 \cdot 10^{-5}$		
	Max	$3.4 \cdot 10^{-3}$			$6.64 \cdot 10^{-3}$		
	Mean	$5.04 \cdot 10^{-4}$			$9.84 \cdot 10^{-4}$		
HI (kindergartens)	Min	$5.73 \cdot 10^{-4}$					
	Max	$1.13 \cdot 10^{-3}$					
	Mean	$8.58 \cdot 10^{-4}$					

surroundings and abandoned an industrial site. Only 1 sample taken from the residential area's private house surroundings, located close to one of the main roads, corresponds to high potential ecological risk.

The obtained non-carcinogenic risk assessment data have indicated that mercury content detected in both kindergartens and Vanadzor soils is not a health risk factor in adults and children.

Finally, data generated from this research support the conclusion that mercury found in all of Vanadzor and its kindergartens has a natural origin, not excepting, however, a certain anthropogenic impact on some urban sites.

ACKNOWLEDGMENTS

REFERENCES

Ajmone-Marsan F. and Biasioli M. (2010). Trace elements in soils of urban areas. Water Air Soil Pollut 1(4), 121–143, DOI: 10.1007/s11270-010-0372-6

AMAP/UNEP (2013). Technical Background Report for the Global Mercury Assessment. Arctic Monitoringand Assessment Programme Oslo, Norway/UNEP ChemicalsBranch.

Alloway B. (2013). Heavy Metals in Soils Trace Metals and Metalloids in Soils and their Bioavailability Chapter 15 Mercury. In: Environmental Pollution 411-428, DOI: 10.1007/978-94-007-4470-7_15

Barbieri M. (2016). The Importance of Enrichment Factor (EF) and Geoaccumulation Index (Igeo) to Evaluate the Soil Contamination. J Geol Geophys 5(1) 1-4, DOI: 10.4172/2381-8719.1000237

Beckers F., Rinklebe J. (2017). Cycling of Mercury in the Environment: Sources, Fate, and Human Health Implications -A Review. Crit Rev Environ Sci Technol 3389, DOI: 10.1080/10643389.2017.1326277

Bernhoft R. (2012). Mercury toxicity and treatment: A review of the literature. J Environ Public Health 10., DOI: 10.1155/2012/460508

Birke M. and Rauch U. (2000). Urban geochemistry: Investigations in the Berlin metropolitan area. Environ Geochem Health (22) 233–248. DOI: 10.1023/A:1026554308673

Bityukova L., Shogenova A., Birke M. (2000). Urban geochemistry: A study of element distributions in the soils of Tallinn (Estonia). Environ Geochem Health 22, 173–193. DOI: 10.1023/A:1006754326260

Butakov E V., Kuznetsov P V., Kholodova MS, Grebenshchikova VI (2017). Mercury in soils of the agro-industrial zone of Zima city (Irkutsk oblast). Eurasian Soil Sci 50, 1354–1361. DOI: 10.1134/S1064229317110035

Chen X., Xia X., Wu S. et al (2010). Mercury in urban soils with various types of land use in Beijing, China. Environ Pollut 158, 48–54. DOI: 10.1016/j.envpol.2009.08.028

Christoforidis A. and Stamatis N. (2009). Heavy metal contamination in street dust and roadside soil along the major national road in Kavala's region, Greece. Geoderma 151, 257–263. DOI: 10.1016/j.geoderma.2009.04.016

Crnković D., Ristić M., Antonović D. (2006). Distribution of heavy metals and arsenic in soils of Belgrade (Serbia and Montenegro). Soil Sediment Contam 15, 581–589. DOI: 10.1080/15320380600959073

DEQ (2015). Remediation and Redevelopment Division Michigan Department of Environmental Quality Part 201 Generic Exposure Assumption Values Update Subjects:Technical support document. Michigan.

Driscoll T., Mason P., Chan M. et al (2013). Mercury as a Global Pollutant: Sources, Pathways, and Effects. Environ Sci Technol 47, 4967–4983. DOI: 10.1021/es305071v

Fang F, Wang Q, Li J (2004). Urban environmental mercury in Changchun, a metropolitan city in Northeastern China: Source, cycle, and fate. Sci Total Environ 330, 159–170. DOI: 10.1016/j.scitotenv.2004.04.006

Golovin A. (2000). Assessment of damage to the environment from pollution by toxic metals. IMGRE (34):

Gray E, Theodorakos M, Fey L, Krabbenhoft P (2015). Mercury concentrations and distribution in soil, water, mine waste leachates, and air in and around mercury mines in the Big Bend region, Texas, USA. Environ Geochem Health 37, 35–48. DOI: 10.1007/s10653-014-9628-1

Hakanson L (1980). An ecological risk index for aquatic pollution control, a sedimentological approach. Water Res 14, 975–1001. DOI: 10.1016/0043-1354(80)90143-8

Karakhanian A., Trifonov V, Philip H. et al (2004). Active faulting and natural hazards in Armenia, eastern Turkey and northwestern Iran, Tectonophysics 380 (3-4) 189–219, DOI: 10.1016/j.tecto.2003.09.020

Kelepertzis E, Argyraki A (2015). Mercury in the urban topsoil of Athens, Greece. Sustain. 7(4), 4049–4062. DOI: 10.3390/su7044049

Kosheleva N, Kasimov N, Dorjgotov D et al (2010). Assessment of Heavy Metal Pollution of Soils in Industrial Cities of Mongolia, Geography, Environment, Sustainability; 3(2) 51-65. DOI: 10.24057/2071-9388-2010-3-2-51-65

Kotova T.V., Malkhazova S.M., Tikunov V.S., Bandrova T (2017). Visualization of public health dynamics. Geography Environment Sustainability, 10 (4), 27–42. DOI: 10.24057/2071-9388-2017-10-4-27-42

Kumar M, Gogoi A, Kumari D, et al (2017). Review of Perspective, Problems, Challenges, and Future Scenario of Metal Contamination in the Urban Environment. J Hazardous, Toxic, Radioact Waste, 21(4) 04017007-7, DOI: 10.1061/(ASCE)HZ.2153-5515.0000351

Kumpiene J, Brännvall E (2011). Spatial variability of topsoil contamination with trace elements in preschools in Vilnius, Lithuania. J Geochemical Explor 108(1) 15–20. DOI: 10.1016/J.GEXPLO.2010.08.003

Laker M. (2005). Urban soils: Land use, Land Cover and Land Sciences. In: Encyclopedia of Life Support Systems (EOLSS)

Li F, Zhang J, Jiang W, et al (2017). Spatial health risk assessment and hierarchical risk management for mercury in soils from a typical contaminated site, China. Environ Geochem Health, 39 (4), 923–934. DOI: 10.1007/s10653-016-9864-7.

Li P, Feng XB, Qiu GL, et al (2009). Mercury pollution in Asia: A review of the contaminated sites. J Hazard Mater 168, 591–601. DOI: 10.1016/j.jhazmat.2009.03.031.

Li XH, Cheng HX, Zhao CD, Xu XB (2010). Mercury contamination in the topsoil and subsoil of urban areas of Beijing, China. Bull Environ Contam Toxicol. 85, 224–228 DOI: 10.1007/s00128-010-0042-9

Lymberidi E (2005). Zero Mercury Key issues and policy recommendations for the EU Strategy on Mercury. European Environmental Bureau,UK,133.

Mamtani R, Stern P, Dawood I, Cheema S (2011). Metals and disease: a global primary health care perspective. J Toxicol 1-10, DOI: 10.1155/2011/319136.

Manta D, Angelone M, Bellanca A (2002). Heavy metals in urban soils: a case study from the city of Palermo (Sicily), Italy. Sci Total Environ, 300, 229–243.

McGrath D (1995) Organic micropollutant and trace element pollution of Irish soils. Sci Total Environ, 164(2), 125–133. DOI: 10.1016/0048-9697(95)04451-6.

Mielke, H., Alexander J (2011). Children, soils, and health: how do polluted soils influence children's health? In: Mapping the Chemical Environment of Urban Areas. Wiley-Blackwell, 134–150.

Moller K.M., Hartwell J.G., Simon-friedt B.R., et al (2018). Soil contaminant concentrations at urban agricultural sites in New Orleans , Louisiana : A comparison of two analytical methods. J Agric Food Syst Community Dev, 8(2), 139–149, DOI: 10.5304/jafscd.2018.082.010.

Morton-Bermea O, Hernández-Álvarez E, Ordoñez-Godinez SL (2016). Mercury and other trace elements contamination of the urban area of Mexico City: Use of ficus benjamina as biomonitor.

Müller G. (1969). Index of geoaccumulation in sediments of the Rhine River. Geo J 2, 108–118.

Nazarpour A, Ghanavati N, Watts MJ (2017). Spatial distribution and human health risk assessment of mercury in street dust resulting from various land-use in Ahvaz, Iran. Environ Geochem Health 1–12. DOI: 10.1007/s10653-017-0016-5.

Nazaryan G. (2009). Geo Alaverdi, Environment and development of the city. Yerevan.

Nezhad K.(2014). Cadmium and mercury in topsoils of Babagorogor watershed, western Iran. In: Distribution, relationship with soil characteristics and multivariate analysis of contamination sources. Geoderma, 177–185. DOI: 10.1016/j.geoderma.2013.12.021.

Pan L, Wang Y, Ma J, et al (2018). A review of heavy metal pollution levels and health risk assessment of urban soils in Chinese cities. Environ Sci Pollut Res, (25), 1055–1069. DOI: 10.1007/s11356-017-0513-1.

RAIS (2018) The Risk Assessment Information System Risk Exposure Models for Chemicals User's Guide. Available at: https://rais.ornl.gov/tools/rais_chemical_risk_guide.html [Accessed 25 Nov. 2019]

Reimann C, de Caritat P (1998). Chemical Elements in the Environment. Springer Berlin Heidelberg.

Rice K, Walker E, Wu M. et al (2014). Environmental mercury and its toxic effects. J. Prev. Med. Public Heal. 47.

Rodrigues S, Pereira M. Duarte A. et al (2006) Mercury in urban soils: A comparison of local spatial variability in six European cities. Sci Total Environ 368 (2-3), 926–936. DOI: 10.1016/j.scitotenv.2006.04.008

Saleem M (2014). Non-carcinogenic and carcinogenic health risk assessment of selected metals in soil around a natural water reservoir, Pakistan. Ecotoxicol Environ Saf, 108, 42–51. DOI: 10.1016/j.ecoenv.2014.06.017.

Sastry R, Orlemann J, Koval P. (2001). Mercury Contamination from Metal Scrap Processing Facilities – A Study by Ohio EPA.

Selin NE (2009). Global Biogeochemical Cycling of Mercury: A Review Methylmercury: the toxic form of mercury, CH 3 Hg +. Annu. Rev. Environ. Resour 34, 43–63 DOI: 10.1146/annurev.environ.051308.084314.

Soliman N, Nasr S, Okbah M. (2015). Potential ecological risk of heavy metals in sediments from the Mediterranean coast, Egypt. J Environ Heal Sci Eng 13, 70. DOI: 10.1186/s40201-015-0223-x.

State Committee of the Real Estate Cadastre (2007). Center of Geodesy and Cartography National Atlas of Armenia. Yerevan.

Stauffer E. (2008). Field Sampling Procedures Manual ,Chapter 6 - Sample Collection. Fire Debris Anal 188, 163–197. DOI: 10.1016/B978-012663971-1.50010-5

Steffan JJ, Brevik EC, Burgess LC, Cerdà A (2018). The effect of soil on human health: an overview. Eur J Soil Sci 69:159–171. DOI: 10.1111/ejss.12451

Sun, Y., Zhou, Q., Xie, X., Liu R (2010). Spatial, sources and risk assessment of heavy metal contamination of urban soils in typical regions of Shenyang, China. J Hazard Mater 174, 455–462. DOI: 10.1016/J.JHAZMAT.2009.09.074

Sun G, Li Z, Bi X, et al (2013). Distribution, sources and health risk assessment of mercury in kindergarten dust. Atmos Environ 73, 169–176. DOI: 10.1016/j.atmosenv.2013.03.017.

Różański S at al. (2015). Profile distribution of mercury in selected urban soils. Environ Prot Nat Resour 26, 1–5. DOI: 10.1515/OSZN-2015-0016.

Tepanosyan G, Maghakyan N, Sahakyan L, Saghatelyan A (2017a) Heavy metals pollution levels and children health risk assessment of Yerevan kindergartens soils. Ecotoxicol Environ Saf 142, 257–265. DOI: 10.1016/j.ecoenv.2017.04.013.

Tepanosyan G.O., Belyaeva O.A,. Saakyan L.V., Sagatelyan AK (2017b). Integrated approach to determine background concentrations of chemical elements in soils. Geochemistry Int 55, 581–588. DOI: 10.1134/S0016702917060106.

Tijhuis L. (2002). A geochemical survay of topsoil in the city of Oslo, Norway, Environmental Geochemistry and Health 24, 67–94.

U.S. EPA (2011) Exposure Factors Handbook (2011 Final Report) - Chapter 8. 25–26

UNEP (2013) Global Mercury Assessment 2013: Sources, Emissions, Releases and Environmental Transport. Geneva, Switzerland.

US EPA (2002a) Supplemental Guidance for Developing Soil Screening Levels for Superfund Sites. United States Environmental Protection Agency.

US EPA (1989) Risk Assessment Guidance for Superfund. Volume I Human Health Evaluation Manual (Part A). United States Environmental Protection Agency, Washington.

US EPA (2011) Soil and dust ingestion. Expo Factors Handb. United States Environmental Protection Agency, Washington.

US EPA Risk Assessment Guidance for Superfund (RAGS): Part A. EPA/540/1-89/002: United States Environmental Protection Agency, Washington.

US EPA (2002b) Child-Specific Exposure Factors Handbook, 448, United States Environmental Protection Agency, Washington.

USEPA (2004) Risk assessment guidance for superfund (RAGS). Volume I. Human health evaluation manual (HHEM). Part E. Supplemental guidance for dermal risk assessmentUSEPA, 2004. Risk assessment guidance for superfund (RAGS). Volume I. Human health evaluation manual (H. US Epa 1:1–156. DOI: EPA/540/1-89/002.

Wan D, Han Z, Yang J. et al (2016). Heavy metal pollution in settled dust associated with different urban functional areas in a heavily air-polluted city in North China. Int J Environ Res Public Health 13, DOI: 10.3390/ijerph13111119.

Wip D, Warneke T, Petersen A. et al (2013). Urban mercury pollution in the City of Paramaribo, Suriname. Air Qual Atmos Heal 6, 205–213. DOI: 10.1007/s11869-011-0162-3.

Yanin E. (1992). Mercury in the environment of an industrial city, IMGRE. Moscow.

Yuan G-L, Sun T-H, Han P. (2014). Source identification and ecological risk assessment of heavy metals in topsoil using environmental geochemical mapping: Typical urban renewal area in Beijing, China. J Geochemical Explor 136, 40–47. DOI: 10.1016/J.GEXPLO.2013.10.002

Zhao W, Ding L, Gu X, et al (2015). Levels and ecological risk assessment of metals in soils from a typical e-waste recycling region in southeast China. Ecotoxicology 24, 1947–1960. DOI: 10.1007/s10646-015-1532-7.

Zheng L, Tang Q, Fan J, et al (2015). Distribution and health risk assessment of mercury in urban street dust from coal energy dominant Huainan City, China. Environ Sci Pollut Res. DOI: 10.1007/s11356-015-4089-3.

Tatyana V. Sapelko[1*], Vladimir R. Boynagryan[2], Mikhail A. Naumenko[1], Dmitry V. Sevastyanov[3], Ivan G. Gabrielyan[4], Artak S. Piloyan[2], Liana A. Margaryan[2], Mikhail Yu Aleksandrin[5], Anton V. Terekhov[1]

[1]Institute of Limnology RAS, St. Petersburg, Russia,
[2]Yerevan State University, Yerevan, Armenia
[3]St. Petersburg State University, St. Petersburg, Russia
[4]Institute of Botany of NAS RA, Yerevan, Armenia
[5]Institute of Geography RAS, Moscow, Russia
* Corresponding author: tsapelko@mail.ru

FIRST MULTY-PROXY STUDIES OF HIGH-MOUNTAIN LAKES IN ARMENIA: PRELIMINARY RESULTS

ABSTRACT. Within the framework of the Russian-Armenian project "The Paleolimnological Aspect of Studying the Evolution of Ecosystems of High-Mountain Lakes of Russia and Armenia" in July-August 2018, we investigated four high-mountain lakes of Armenia. The research focuses on the lakes Kari, Umroi, Akna and Sev. All investigated lakes are located at the altitudes about 3000 m above sea level. We first time these lakes were investigated using a multi-proxy method that includes paleolimnological, geomorphological, hydrological, geochemical and biogeographic studies. The research offers the first statistical characteristics of lake depth distribution, water volume and other morphometrics. Lake sediments sequences and radiocarbon dates were received and analyzed for Armenian small lakes for the first time. We determined that all the studied lakes were formed during the Holocene. Sediments of Lake Kari were deposited in the last 4000 years, sediments of Lake Umroi – within the last 8000 years, while maximum thickness of sediments is around 1 m in both lakes. Hence, we assume low deposition rate in Armenian high-mountain lakes, however, it varied significantly in different periods of lake history.

KEY WORDS: mountain lakes, Armenian plateau, geomorphology, paleolimnology, Holocene

INTRODUCTION

Almost all the data concerning the history of Armenian lakes are associated with the studies of Lake Sevan. Evolution of this lake, the largest in Armenia, was reconstructed based on small outcrops of buried peat and archeological sites (Sayadyan 2000; Ollivier et al. 2010; 2011; Joannin et al. 2014). Reported Holocene radiocarbon ages were obtained either from Lake Sevan or on its watershed. Analysis of peat located on the shore of Lake Sevan, near Vanevan village (Leroyer

et al. 2016), shows that the climate of the Early Holocene was dry (precipitation rate was below 180 mm per year), and steppe landscapes prevailed. In the Mid Holocene (between 7800 and 5100 cal BP) precipitation became higher by 28%, climate got to be milder, the water level in Lake Sevan rose and the forest vegetation spread over lake watershed. Around 5700 cal BP climate started to turn drier and after 5100 cal BP arid conditions are dominating.

First research of high-mountain lakes situated on Armenian plateau was reported by L. Arnoldi (1931) in the beginning of the XX century. The research covered hydrological, hydrochemical, biogeographical studies of lake sediments of Lake Akna (western slope of Gegham mountains). In 1930s, the first data on chemical composition of Lake Kari lake water (southern slope of Mount Aragats massif), its sediments and phytoplankton (Kireeva 1933) were published. The other high-mountain lakes located in Armenia were hardly studied (Boynagryan et al. 2018). Paleolimnological investigations are carried out for the first time. The main purpose of this research is to study the history of lakes in different spatial and temporal scales, which allows discovering the main patterns of the variations of environmental conditions (Sevastyanov et al. 2014; Subetto et al 2017).

STUDY AREA

The Caucasus is part of the Alpine-Himalayan mountainous belt that was created by the collision of the Arabian and Eurasian continental plates during the Neogene (Sayadian et al. 1983). This tectonic activity resulted in the formation the Lesser Caucasus ranges.

The research was carried out in the reference points of the lakes Kari, Umroi, Akna and Sev in July-August 2018 (Fig. 1). Studied lakes are situated in different parts of Armenian Highlands at elevations around 3000 m above sea level (m a.s.l.). Aragats is a volcano massif, the most elevated part of

Armenian plateau. Slopes of Aragats show the traces of ancient glaciations like cirques and moraine fields with water-filled depressions. Southern slopes of Aragats are made of andesite-basalt lava outflows during mid- and late Oligocene and possess a typical block surface topography. South-western and south-eastern slopes are made of andesite-basalt lava flows. Northern slopes consist of pyroxene-andesites, which create here knob topography. From north-east Aragats is surrounded by block lavas, descending towards river Kasakh valley. These lavas superimpose fluvio-glacial and lake sediments of Riss glaciation age. At the contact of these geological formations, springs are outflowing. Lava-made surfaces are rugged, knobs and hills covered with blocks, are interleaved by depressions, filled with small seasonal lakes and bogs. Western slopes of Aragats are similar to south-eastern ones. Their surface is shaped by tuffs and lavas, significantly changing their thickness due to ruggedness of underlying rocks. Here most widespread is the landscape of plateau, hills and ridges (Balian 1969). Blister volcanic cones are presented at the western and south-western slopes. Lots of small lakes are situated on Aragats, mostly between 2900 and 3500 meters. Lakes are situated inside depressions of glacial relief, being moraine-dammed or cirque-situated. Only several lakes are located near north-eastern foot of Aragats, in the pits inside lava-made surface, and they could be considered as volcanic. The largest lakes among high-mountain ones are moraine-dammed Kari (3187 m, southern slope) and Umroi (3050 m).

Lake Kari is located at the southern macroslope of Mount Aragats at 3200 m a.s.l. Kari catchment presents a glacial knob-and-basin topography on volcanic rocks having the traces of the mountain glaciation. Lake itself is moraine-dammed. Trench-shaped lake Umroi lies in an intermorainal depression at the eastern macroslope of Mount Aragats at 3050 ma.s.l. The topography of its watershed territory is mountainous and glacial.

Large number of lakes is possessed by high-mountain lanscapes of Gegham massif. The largest lake – Akna, is located 122 meters below the water divide at 3031 m a.s.l. It is surrounded by ancient volcanic cones, which consists of tuff and slags. The outflow is controlled by a human-made dam.

Lots of lakes are situated in the tundra belt of Syunik volcanic plateau, being originated inside depressions of volcanic and glacial relief. Enclosed lake Sev is situated at the southeastern slope of Ishkhansar Mountain, Syunik highlands, at 2660 m a.s.l. in a trough valley with volcanic cones besides it. From north and south lake is surrounded by steep slopes, other slopes are relatively shallow. On the steep slopes the numerous stone fields are located, moving downwards up to 4-8 cm per year (Boynagryan 2007). According to weather station located near Lake Kari, mean annual temperature in the region is around 6.7°C while mean annual precipitation is 560.7 mm. Watersheds of lakes Kari, Umroi and Akna are covered with alpine meadows, and also with mountain meadows for Lake Sev.

Present-day vegetation of lakes and their watersheds was described by S. Baloyan (2005) as well as during our studies (Gabrielyan and Sapelko 2018). A detailed investigation of the flora around the studied four lakes revealed the presence of 323 species of higher vascular plants. Aquatic plants of **Lake Kari** are mainly presented by rare species of Characeae. In the surroundings *Anthriscus nemorosa* (Bieb.) *Spreng.*, *Bupleurum polyphyllum Ledeb.*, *Chamaesciadium acaule* (Bieb.) Boiss., *Aster alpinus L.*, *Jurinea moschus* (Habl.) *Bobr.*, *Chamaenerion angustifolium* (L.) Scop., *Draba bruniifolia Stev., Campanula tridentata Schreb., Cerastium cerastoides* (L.) Britt. and other species are found.

Rare species of Characeae exist in **Lake Umroi** as well. In the surroundings *Allium szovitsii* Regel, *Carum caucasicum* (Bieb.) Boiss., *Bupleurum persicum* Boiss.,

Chamaesciadium acaule (Bieb.) Boiss., *Erigeron caucasicus Stev., Jurinea moschus* (Habl.) Bobr., *Taraxacum bessarabicum* (Hornem.) Hand., *Campanula aucheri* A. DC., *Silene ruprechtii Schischk.* and other species are widespread.

During underwater survey in **Lake Akna**, we discovered a dense thicket species from Characeae family. Around the lake *Allium schoenoprasum* L. var *alpinum* Lam., *Allium szovitsii* Regel, *Bupleurum persicum* Boiss., *Chamaesciadium acaule* (Bieb.) Boiss., *Aster alpinus* L., *Jurinea moschus* (Habl.) Bobr., *Coluteocarpus vesicaria* (L.) Holmboe, *Vavilovia formosa* (Steven) Fed., *Draba bruniifolia* Stev., *Campanula tridentata* Schreb., Cerastium cerastoides (L.) Britt. and other species could be found.

On the date of our fieldwork, the water of **Lake Sev** was muddy green due to the presence of microbial algae communities. *Persicaria amphibia* (L.) Delarbre, *Carex caucasica* Stev., *Carex huetiana* Boiss. and other *Carex* grow inside the lake and on its shores. Alpine meadows and mountain meadows around Sev consist of: *Allium szovitsii* Regel, *Carum caucasicum* (Bieb.) Boiss., *Chamaesciadium acaule* (Bieb.) Boiss., *Dryopteris oreades* Fomin, *Aster alpinus* L., *Erigeron caucasicus* Stev., *Tanacetum chiliophyllum* (Fisch. et C.A. Mey. ex DC.) Sch. Bip., *Taraxacum bessarabicum* (Hornem.) Hand., *Hordeum violaceum* Boiss. et Huet, *Chamaenerion angustifolium* (L.) Scop., *Draba bruniifolia* Stev., *Urtica dioica* L., *Polygonum hydropiper* L., *Rumex crispus* L., *Papaver orientale* L., *Campanula aucheri* A. DC., *Silene ruprechtii Schischk.* and of other species. Unlike the other lakes, the coastal zone of Sev is covered with bushes of Rosa spinosissima L. Nearby Lake Sev, within the distance of 270-300 m, a small and shallow nameless lake is situated at 2667 m a.s.l. In contrast to Lake Sev, aquatic vegetation here is more widespread and presented by *Potamogeton gramineus* L. and other species. The shore is covered with *Sparganium neglectum Beeby.*, etc.
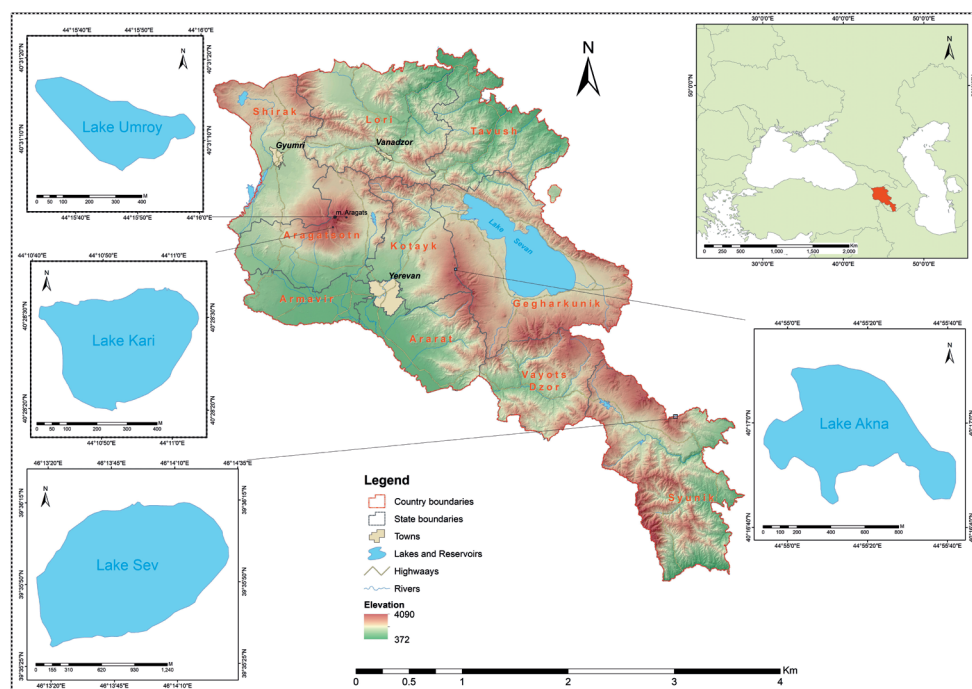
Fig. 1. Map of Armenia with studied lakes

METHODS

Multi-proxy investigations of four mentioned lakes included paleolimnological, geomorphological, hydrological, hydrochemical and biogeographical studies. Sediments of all the lakes were sampled for paleobotanical, carpological, diatom, geochemical and radiocarbon analyses. Bathymetric surveys allowed to obtain depth maps and 3D models of Lake Floor. We have also compiled geomorphological maps for watershed territories. Reconstruction of lake history is conducted in different spatial and temporal scales based on bottom relief and sediments, which allows discovering the main patterns of environmental conditions change.

Depth measurements were made with 0.1 m accuracy using echo-sounding device «Lowrance», equipped with a GPS receiver, for digital bathymetric elevation model creation. Total number of measured points is over 60000. A horizontal spatial resolution of derived DEM is 10 m.

Water samples were collected from at depth of 0.5m, near shore. Water sampling was done according to ISO 5667 and the requirements of the developed protocols and forms (ISO 5567-1:2006). Water temperature, dissolved oxygen, turbidity and pH were measured in-situ by advanced test kits (Hanna pH-meter, WTW 320i multi parameter device).

The collected water samples were labeled and transported to the laboratory in the special cooler box (under the <6°C) for the further test. In the laboratory, water samples were stored in the refrigerator for no more than a day.

In all sampling points we performed hydrochemical measures of the lakes for general ions, mineralization, conductivity, total hardness, BOD_5, COD, nutrients and 20 metals (Manual 1977; Standard methods for the examination of water and wastewater 1998). The mineralization of lake water was assessed as the sum of general ions (calcium, manganese, potassium, sodium, sulphate, chloride, bicarbonate) (Guidance… 1977; Standard methods for the examination of water and wastewater 1998). Total hardness of water was assessed as the sum of calcium and manganese equivalents amount. Concentrations of calcium, manganese, potassium, sodium, total phosphorus, as

well as 20 metals (Li, Al, Ti, V, Cr, Fe, Mn, Co, Ni, Cu, Zn, As, Se, Sr, Mo, Cd, Sn, Sb, Ba, Pb) were determined by ICP-mass spectrometric methods on ISO 17294-2:2005 via Elan 9000 device. Concentrations of sulphate, chloride and nitrate were determined by ion-chromatography method on ISO 10304-1:2007 via Dionex 1000 device. Concentrations of bicarbonate in water samples were measured by Turbidimetric method on GOST 20806-228:069 (02)-77.

Lake sediments were sampled using Russian corer with 5 cm chamber diameter from a platform mounted on a catamaran. The corers consist of single 1 m length corers, sampled with overlapping to provide a continuous sediment sequence. Radiocarbon dating (AMS) was performed by Institute of Geography, Russian Academy of Sciences. The calibrated age ranges were calculated using CALIB REV7.1.0 and the Intcal 13 dataset (Stuiver et al. 2019; Reimer et al. 2013). The range represents the 2-sigma values, and the median ages are in parentheses (Table 1). We performed preliminary lithological

description and photography during the fieldwork. Then, in the laboratory, in the process of core splitting, we refined the borders between stratigraphic units, as well as their lithological composition. Further correlation of overlapping cores was made based on lithostratigraphy.

RESULTS

Lithostratigrsphy and chronology

Lake sediment thickness for all the studied lakes is relatively low and cored successions length does not exceed 2 m. Cores mainly consist of loam, sand, gyttja and, in some of the lakes, peat (Fig. 2). Seven cores were retrieved from different parts of Lake *Kari*. Cores 1-3 were retrieved at the sampling point 1 (40°17'6" N; 44°6'26"E), cores 4-7 – at the sampling point 2 (40°17'1" N; 44°6'35"E). Cores 3 (water depth 2.28 m), 5 (water depth 1.2 m) and 7 (water depth 1.9 m) were split for carpological analysis soon after coring. The longest ones are the cores 2, 4 and 6, they are about 50-55 cm long. Apparently

**Table 1. Radiocarbon ages (AMS) for sediments of Kari and Umroi lakes**

Lake, core number	Depth, m	Lab Number	Material Dated	Radiocarbon Age, ^{14}C yr BP	Calibrated Age, cal yr BP (2σ range, median)
Kari-6	2.43	IGAN-6540	plant macrofossils	3730±30	3981–4154 (4080)
Kari-6	2.19-2.21	IGAN-6541	plant macrofossils	1430±35	1291–1382 (1329)
Kari-6	2.07-2.09	IGAN-6542	plant macrofossils	1055±30	926–1051 (960)
Kari-6	2.00-2.01	IGAN-6543	plant macrofossils	585±30	535–651 (604)
Kari-6	1.96-1.97	IGAN-6544	TOC	680±35	559–683 (648)
Umroi-4	4.42-4.44	IGAN-6545	TOC	6285±40	7156–7313 (7216)
Umroi-4	4.15-4.17	IGAN-6546	TOC	2915±40	2945–3179 (3057)
Umroi-4	4.03-4.05	IGAN-6547	TOC	2925±30	2973–3163 (3072)
Umroi-4	3.84-3.86	IGAN-6548	TOC	2415±20	2348–2700 (2455)
Umroi-4	3.40-3.42	IGAN-6549	TOC	650±20	560–666 (591)

these sediment sequences represent all the history of the lake. According to AMS-dating, these sediments have been accumulated within 4000 cal years BP. Underlying formation is a dense sandy loam. Cores number 1, 3, 5 and 7 are 22-39 cm long.

Sediment sequences of Lake *Umroi* were sampled at one point (40°18'46"N; 44º9'21"E) with water depth 3.35 m, six cores were retrieved (Fig. 2). Maximum sediment thickness is 1.17 m. Lithostratigraphical analysis and radiocarbon dating were performed. Lithological unit borders are the same in primary and secondary sediment sequences, except well-distinguished layer of coarse sand located at 4.05-4.06 depth in the primary sediment sequence and not presented in the secondary. Laminated loam thickness is significant in the bottom part of sediment sequences. Thickness of organic sediments is low. According to radiocarbon dating, sediments of Lake Umroi were formed within 8000 cal years BP (Table 1).

At the Lake *Akna*, four sediment sequences were retrieved at one sampling point (40°16'47"N; 44°55'38"E). All four successions are duplicative for different analyses (Fig. 2). Maximum sediment thickness is 0.92 m. Bottom part of the sediment sequences contains gravel or pebbles. Above the interbedding of dark and lighter interlayer of the clay gyttja begins. Then gyttja becomes more organic and liquid. Upper parts contain a significant number of non-decomposed organic remains. Sediments from all the lithological units were sampled for radiocarbon dating.

At Lake *Sev*, 3 sediment sequences were retrieved, each composed of 3 single cores, from one sampling point (39°35'47" N 46°13'25" E). Maximum sediment thickness is 2.52 m (from cores 1, 2 and 3). Other cores are duplicative. Bottom part of sediment sequences consists of densely laminated loam with presence of seeds, loam is gradually becoming homogenous. Above there is the clayey gyttja, which is periodically substituted by peat gyttja with
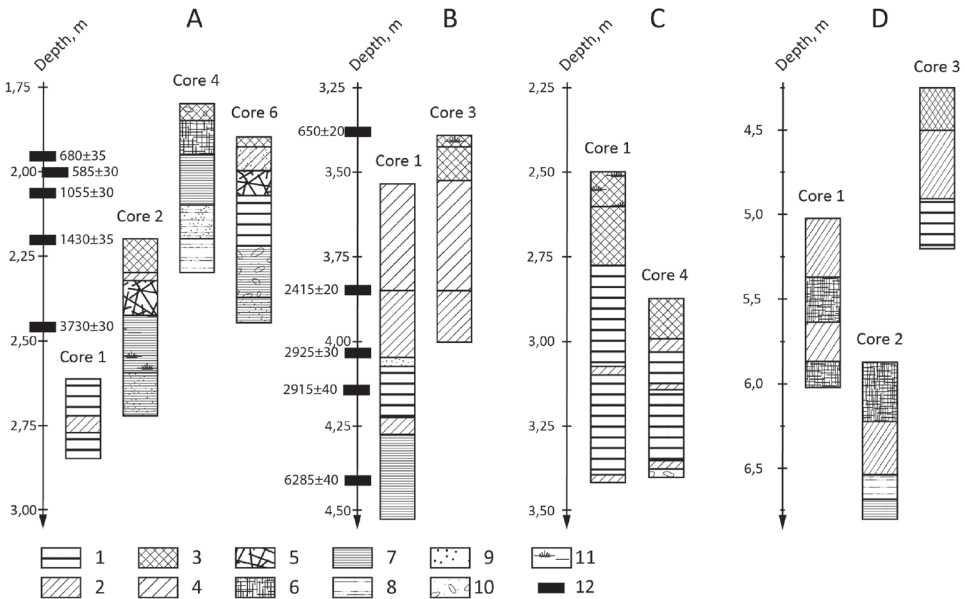
Fig. 2. Lithostratigraphy of lake sediments: A – Lake Kari, B – Lake Umroi, C – Lake Akna, D – Lake Sev. Legend: 1 – brown and dark-brown clayey laminated gyttja; 2 – brown and dark-brown clayey homogenous gyttja; 3 – liquid organic gyttja; 4 – light-brown homogenous gyttja; 5 – peat with organic remains; 6 – black peat gyttja with organic remains; 7 – laminated loam; 8 – homogenous loam; 9 – sand; 10 – gravel and/or pebble; 11 – organic remains; 12 - Radiocarbon Age, 14C yr BP.

a significant number of non-decomposed organic remains. Upper part of sediment sequences is liquid organic gyttja without visible remains, some ruptures present. Samples for radiocarbon analysis were collected from all lithological units, mostly near unit borders.

According to radiocarbon ages age-depth models for Kari and Umroi lakes were constructed (Fig. 3). As it is shown, sedimentation rates varied in time during the Holocene. It is intended to refine these models based on pollen analysis results in the future.

Geomophology and the lakes morphometry

Geomorphological data were obtained for the four studied lake basins and their watersheds. Relief of lake basins was investigated on the base of created digital models (Naumenko et al. 2014). Digital models of underwater relief allowed studying basins carefully and therefore to obtain morphometric values for Kari, Umroi, Akna and Sev lakes (Fig. 4). Direct depth measurements were made by echo-sounding device with GPS positioning which allowed to create digital morphometric models. It should be noted that values of a lake water volume and coastline length depend on water level and they are determined by seasonal dynamics of water balance components: precipitation, evaporation and snow amount on watershed territory.

Prior to our research, only topographic maps (Boynagryan 2007) and direct measurements (Arnoldi 1931) supplied morphometric values of the lakes. In this study, for the first time we created a digital model with 10 × 10 m spatial resolution offering statistical characteristics for depth distribution, water volume and other parameters. The model allowed to refine lake surface areas and maximum depths reported before (Table 2).

Lake Umroi lies in an intermorainal depression, is oviform and oriented along NW-SE direction. There is a shallow bay in the south-east part of the lake, which is separated from the main basin by rock ridge during low water level. Lake Basin is trench-shaped with hogbacked bottom and large boulders. Maximum depths are situated in the north-western part of the lake and exceed 10 m according to our measurements (Fig. 4). Coast is mainly steep, consist of coarse colluvial material. Swampy sites exist near the three inlets flowing from north-west, north and east. Lake Umroi is fed primarily by snow and snowfields melt. Relief of watershed territory is mountain and glacial. In the south and in the north-west, the lake is surrounded by steep slopes of a cirque-shaped rock fold, exposed in a north-eastern direction. Altitudes of its ridge are 3283-3372 m. A thick moraine field lies between the lake and a wide corrie in a rock ridge to the North. Three terminal moraines are well-distinguished here. Smaller lakes are situated in the lows between these moraine ridges according
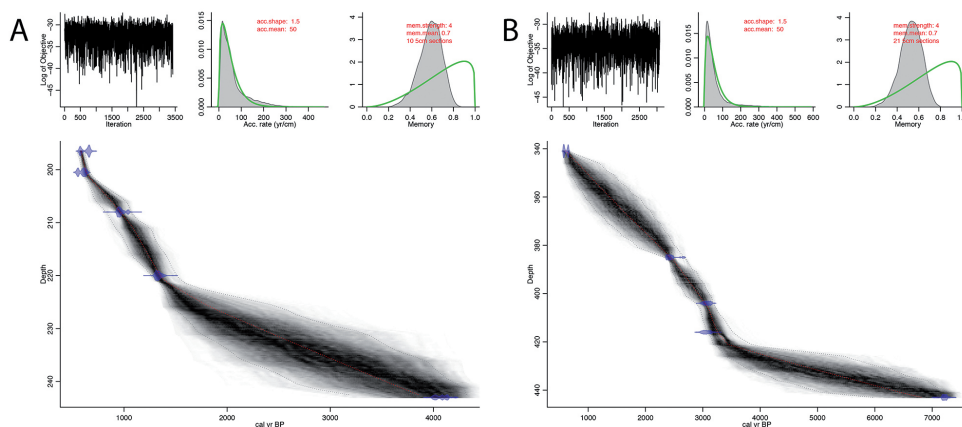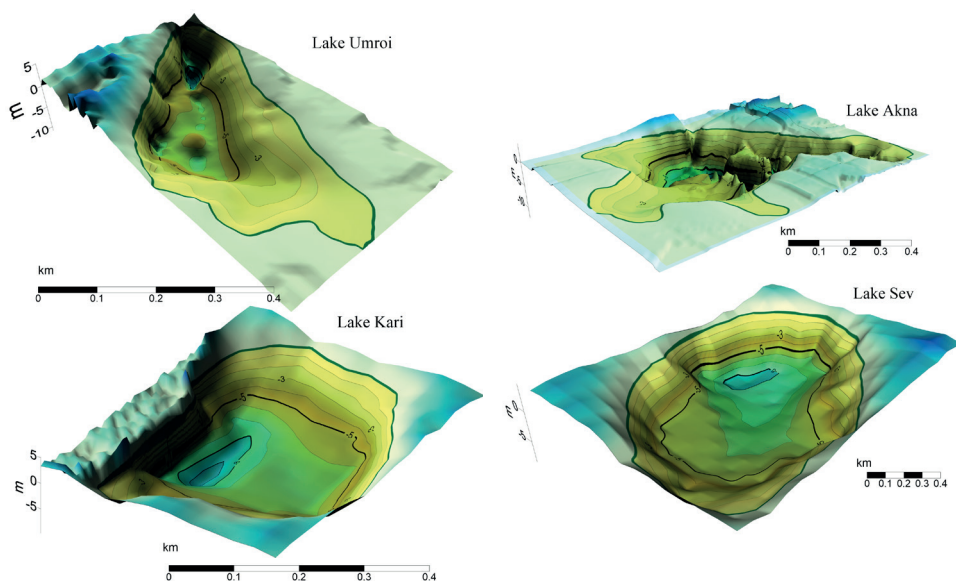

Fig. 3. Age-depth models for Kari (left) and Umroi lakes (right)

Fig. 4. 3D-view of studied lakes floor from Lake Umroi, Lake Kari, Lake Akna and Lake Sev

to topographic maps. It could be assumed that these moraines correspond to stationary termini positions of a retreating glacier in the Holocene during the last phase of Caucasus glaciation decline (Shnitnikov 1985). Retreat of the glacier to the North probably led to a formation of moraine-dammed Lake Umroi.

Coastline of Lake *Kari* is not indented. Watershed territory is made up of volcanic rocks and possesses a knob-and-basin topography, having traces of last glaciations, which existed on the Armenian plateau in the Late Pleistocene and Holocene. Altitudinal range of a relief is 50-250 m. Lake basin is dammed by ancient moraine remains, significantly eroded. Lake is fed mainly by snow and snowfields melt, and groundwater inflow. North-eastern bank is swampy, spring-water outflows are observed. Present-day water level is controlled by human-made dam with a spillway. Outflow takes place in spring and in summer, during ablation season. Coastline is rocky, made of colluvial boulders and pebble, partly swampy with light-grey sand and silt. Bottom is flat, saucer-shaped (Fig. 4). Maximum depth 9.8 m was discovered in the central part of Lake Basin, closer to the northern side of the shore, which adjoins the steepest mountain slope.

Lake *Akna* basin is made up of volcanic rocks and lies in a depression surrounded by ancient volcanic cones, consisting of tuff and slags, elevated for 50-450 m above the lake. Coastline is indented with small bays and gulfs. According to the studies of the 30s of XX century (Arnoldi 1931), interannual water level change is more than 2 m. Thus, lake surface area and depth vary significantly. The highest water level is observed in summer, while the lowest – in February and March. During our fieldworks in August 2018, water level was 0.3-0.5 m below maximum judging by coastal terraces. Several smaller shallow lakes were isolated from the south-eastern gulf of the Lake Akna, as the bathymetric map created by Arnoldi (Arnoldi 1931) shows. Lake Akna is mainly fed by snow melt. Snowfields of the surrounding slopes ensure the level rise of the several temporal watercourses in the warm season. Outflow from the lake takes place by a canal in the north-western part of a basin, controlled by a human-made dam and used for pasture irrigation. Relief of lake bottom is complex: bathymetric survey revealed two depressions separated by a slight ridge (Fig. 4). Lake sediments vary in grain size and in material and depend on depth. Nearby lake shore, in the East and the South, coarse sediments, consisting of andesite-basalt and rusty-brown tuff,

Table 2. Morphometric values from digital lake floor models

Morphometric value	Lake			
	Umroi	Kari	Akna	Sev
Number of pixels	1152	1465	3790	12105
Area, km^2	0.117	0.146	0.496	1.747
Volume, m^3	365.1.10^3	661.9.10^3	1843.1.10^3	7791.3.10^3
Average depth, h$_{mean}$, m	3.2	4.5	3.7	4.5
Median, m	2.6	5.0	3.2	5.0
25% quartile, m	1.0	2.4	1.6	2.5
75% quartile, m	5.5	6.5	5.3	6.3
Max. depth, h$_{max}$, m	10.9	9.8	12.4	8.5
Standard deviation, δ_h, m	2.46	2.40	2.75	2.31
Coefficient of variation, δ_h / h$_{mean}$	0.77	0.53	0.74	0.52
h$_{mean}$ / h$_{max}$ ratio	0.29	0.46	0.30	0.53
Perimeter, km	1.55	1.52	3.86	5.01
Shoreline development	1.28	1.12	1.55	1.07

dominate. In the shallow parts fine sand and light-grey or yellow silt are widespread.

The basin of Lake **Sev** is situated in a trough valley with volcanic cones besides; elevated from 3073 to 3550 m. Lake is oviform and elongated from South-West to North-East. According to our measurements, lake surface area is 1.77 sq km and maximum depth is 8 m (Fig. 4). Lake is fed primarily by liquid precipitation and snowfields located on volcanic slopes. High water surface temperature (18-20°C) observed at the moment of fieldwork (August 2018) could be explained by relative shallowness of the lake, intensive water overturn and water warm-up. It is notable that the water is turbid and green due to presence of algae. No outflows were discovered. Bottom sediments are presented by light-grey silt and sand. The steepest northern bank is made up of coarse colluvial material.

Hydrochemistry

The hydrochemical study results showed that the water of lakes Kari, Umroi, Akna and Sev has hydrocarbonate-calcium-sulphate nature with low mineralization and hardness. Water in lakes Umroi, Akna and Sev has light alkalinity pH, whereas water in Lake Kari has neutral environment. The oxygen regime in lakes Umroi and Akna was normal for the functioning of the lake's biodiversity, compared to the other two lakes where dissolved oxygen was dissatisfied. These two lakes Kari and Sev were also distinguished by comparatively high turbidity. The concentrations of V, Cr, Co, Ni, Cu, Zn, As, Se, Mo, Cd, Sn, Sb, Pb were below 5×10-5 mg/l. Despite some similarities, all the four observed lakes differed in their unique hydrochemical regimes, which did not correspond to each other.

DISCUSSION

Depth distributions for the three lakes (Kari, Umroi and Sev) are relatively simple, as well as the shapes of their basins. In each basin only one depression with a maximum depth exists. Maximum depths are located not exactly in the center, but closer to the shore. Mean depth to the maximum depth rate varies from 0.29 (Lake Umroi) to 0.52 (Lake Sev). Lake Akna is the deepest of the studied lakes and possesses a highly dissected bottom relief and an indented shoreline.

Lake Kari: the water of lake distinguished by the lowest mineralization and concentration of main ions, low content of organic pollutants, as well as low content of nutrients (nitrate, phosphate and ammonium ions). However, the lake had relatively high turbidity, water temperature and low oxygen content, which might be a result of the source of the lake feed (mainly surface flows, melting waters) and water depth. Sediment thickness is the lowest among the studied lakes. The longest

core retrieved is 0.55 m. However, large amount of described lithostratigraphic units indicates significant changes of sedimentary conditions during the 4000-year period of Lake Kari existence. Low sediment thickness may be determined by severe environmental conditions: according to our botanical descriptions, the vegetation cover on Lake Kari catchment is the sparsest and poor as compared to the three other lakes.

Lake Umroi: the water of the lake distinguished by the highest concentration of sulphate and nitrate ions. The limiting nutrient is phosphorus. This may be the result of the presence of an underground water flow at the bottom of the lake. The lake was formed 3000 years earlier than Lake Kari and the sediment thickness here is higher. The longest succession sampled is 1.17 m. Maximum depth is relatively large – 10.9 m, this promotes more inorganic sedimentation as compared with the other lakes. Here, the thickest mineral sediments were found, while organic gyttja layer is the thinnest. However, according to heterogeneity of

Table 3. Hydrochemical characteristics for the studied lakes

	Lake			
	Kari	Umroi	Akna	Sev
pH	7.72	8.02	8.96	8.67
Cond. µS/cm	22	27	24	116
Ca µeq/l	135.90	187.31	183.81	961.72
Mg µeq/l	31.76	39.53	44.93	197.52
Na µeq/l	29.83	21.12	15.70	71.70
K µeq/l	15.28	28.80	16.71	107.25
HCO_3^- µeq/l	250.08	300.10	350.11	1200.39
SO_4^{2-} µeq/l	41.08	51.57	36.21	45.55
Cl^- µeq/l	27.01	28.09	24.61	67.35
NO_3^- µgN/l	1.76	3.28	0.64	0.27
NH_4^+ µgN/l	1.98	0.99	2.97	0.74
TP µg/l	0.1–1ppb	0.1–1ppb	13.24	92.25

lithostratigraphy, during the last 7000 years lake sediments were forming under changing environmental conditions.

Lake Akna: the water of the lake distinguished by a relatively high level of BOD and COD, which indicates the existence of the high level of organic compounds. However, the dissolved oxygen was 7 mg/l, which is favorable for aquatic biodiversity. Lake Akna revealed the most intensive Charophyceae bloom. The normal oxygen regime can be caused by the periodic flow of surface water into the lake. Lake Akna is the deepest among the studied lakes; maximum depth measured is 12.4 m. Sediment thickness does not exceed 1 m. Basing on lithology, it could be assumed that deposition environment was the most stable. Transition to the organic gyttja in the upper part of the sediment cores is the clearest.

Lake Sev: the lake has a completely different hydrochemical regime compared to the three other lakes. The lake is characterized by the highest concentrations of the hydrocarbonate, chloride, phosphate, sodium, magnesium, potassium and calcium ions, as well as iron, strontium and barium. The Lake distinguished by the high content of phosphorus except for the nitrogen, which was a limited nutrient for the lake. In addition to the content of nutrients, the lake water also showed the high content of organic compounds and turbidity. These indicate the existence of the active eutrophication processes in the lakes. Lake Sev is located at a lower altitude than the other lakes and hence the vegetation of its catchment is the most diverse. It is covered with alpine and mountain meadows, the latter are not present within the catchments of the other three lakes. Lake is the shallowest (maximum depth around 8.5 m), while sediment thickness (2.52 m) is the highest. Basing on lithology, we assume that depositional settings had changed drastically: there are thick layers of peat gyttja indicating sudden water level decrease.

CONCLUSION

The results of the multi-proxy research allowed to obtain data on poorly studied high-mountain Armenian lakes. The research provided the first-time statistical characteristics of depth distribution, water volume and other morphometric values. The deepest lake among the studied is Lake Akna, the shallowest and the largest is Lake Sev. The hydrochemical results are important for further paleolimnological reconstructions. All the samples were collected while the fieldwork with the time of sampling. So, the hydrochemical results can be intercompared. The first time, the hydrochemical regime was studied for 41 parameters for four target lakes. The hydrochemical study results showed that the water of the Umroy, Kari, Akna and Sev Lakes has hydrocarbonate-calcium-sulphate nature with low mineralization and hardness. Water in the lakes Umroy, Akna and Sev has light alkalinity pH, as well as water in Kari Lake has neutral environment. The oxygen regime in the lakes Umroy and Akna was normal for the functioning of the lake's biodiversity, compared to the other two lakes where dissolved oxygen was dissatisfied. These two lakes (Kari and Sev) were also distinguished by comparatively high turbidity. The concentrations of V, Cr, Co, Ni, Cu, Zn, As, Se, Mo, Cd, Sn, Sb, Pb were low of the $5*10-5$ mg/l. Despite some similarities, all four observed lakes differed in their unique hydrochemical regimes, which did not correspond to each other. According to hydrochemical analysis, Lake Sev has the most eutrophic water. The smallest surface area belongs to Lake Umroi, though its depth is relatively high exceeding 10 m. Kari lies at the highest altitudes, and therefore the water and coastal vegetation of lake is poor.   1.   Lake sediments sequence and radiocarbon dates were sampled and analyzed for the first time, none of small Armenian lakes were sampled for radiocarbon dating before the described ones. According to our results, all the studied lakes were formed during the Holocene. Sediments of Lake Kari were deposited in the last 4000 years, of Lake Umroi – within the last 7000 years, while maximum thickness of sediments is around 1 m in both lakes. We assume low deposition rate in Armenian high-mountain lakes, however it varied significantly in different periods of lake history.

REFERENCES

Arnoldi L.V. (1931). Lake Kanly-gel //Watershed of Sevan Lake, 2(2), pp. 255-264 (In Russian).

Balian S.P. (1969). Structural geomorphology of the Armenian highlands and bordering areas. Yerevan: EHU.

Baloyan S. (2005). Alpine vegetation cover of Armenia. Yerevan (Ayastani alpiakan busakan cackuytn - In Armenian).

Boynagryan V. R. (2007). Lakes of Armenian Highlands. Erevan: YSU (In Russian).

Boynagryan V.R., Sapelko T.V., Gabrielyan I.G., Sevast'yanov D.V., (2018). Present-day knowledge on history of high-mountain lakes of Armenia. Proceedings of the Russian Geographical Society 6(150), pp. 88-103 (In Russian).

Gabrielyan I.G., Sapelko T.V. (2018). Comparison between present and fossil lacustrine vegetation of Armenia //Topical issues of biogeography. Proceedings of International conference. St. Petersburg, pp. 91-93 (In Russian).

Guidance on chemical analysis of surface waters: Main Administration of Hydrometeorology under the USSR Council of Ministers (1977). Leningrad

ISO 5667-1:2006, Water quality -Sampling -Part 1: Guidance on the design of sampling programmes and sampling techniques

Joannin, S., Ali, A.A., Ollivier, V., Roiron, P., Peyron, O., Chevaux, S., Nahapetyan, S., Tozalakyan, P., Karakhanyan, A., Chataigner, C. (2014). Vegetation, fire and climate history of the Lesser Caucasus: a new Holocene record from Zarishat fen (Armenia) // Journal of Quaternary Science. 29. pp. 70-82.

Kireeva M.S. (1933). Lake Kara-gel at Aragats massif. Studies of Caucasian lakes and their ichthyofauna //Proceedings of Sevan Lake Station, 3(2). pp.3-34 (In Russian).

Leroyer C., Joannin S., Aoustin D., Ali A., Peyron O., Ollivier V., Tozalakyan P., Karakhanyan A., Jude F. (2016). Mid Holocene vegetation reconstruction from Vanevan peat (south-eastern shore of Lake Sevan, Armenia) // Quaternary International. 395. pp. 5-18.
Naumenko M.A. Guzivatyj V.V., Sapelko T.V. (2014). Digital morphometric models of small lakes//Proceedings of Russian State Hydrometeorological University, 34. pp.26-32 (In Russian).

Ollivier V., Nahapetyan S., Roiron P., Gabrielyan I., Gasparyan B., Chataigner C., Joannin S., Cornee J.-J., Guillou H., Scaillet S., Munch P. and Krijgsman W. (2010). Quaternary volcano-lacustrine patterns and paleobotanical data in South Armenia //Quaternary International. 223-224. pp. 312-326.

Ollivier, V., Joannin, S., Roiron, P., Nahapetyan, S., Chataigner, C. (2011).Travertinization and Holocene morphogenesis in Armenia: a reading grid of rapid climatic changes impact on the landscape and societies between 9500-4000 cal. BP in the Circumcaspian regions? // European Archaeologist. 36. pp. 26-31.

Sayadian, J.V., Aleshinskaja, Z.V., Pirumova, L.G., Rybakova, N.O. (1983). On the Age, Interrelations and Conditions of the Formation of Pliocene continental deposits of the Syunik plateau // Problems of geology of Quaternary period of Armenia. Yerevan, pp. 45–59 (in Russian).

Sayadyan YU.V. (2000). Changes of Sevan lake shoreline in Holocene //Proceedings of the Russian Geographical Society/ 3(132). pp.37-47 (In Russian).

Sevastyanov D., Sapelko T., Subetto D., Boynagryan V.R. (2014). Paleolimnology of Northern Eurasia // Proceeding of the International conference. Petrozavodsk. pp. 24-25.

Shnitnikov A.V. (1985). Theoretical basis of centuries-long changes of moisturization and condition of lakes – present-day and future state //Problems of large lakes studies. Leningrad, pp. 5-22. (In Russian).

Standard methods for the examination of water and wastewater, (1998). 20th edition USA. Edited by Lenore S. Clesceri, Arnold E. Greenberg, Andrew D. Eaton. pp.1.27-3.52.

Stuiver, M., Reimer, P.J., and Reimer, R.W. (2019). CALIB 7.1 [WWW program] at http://calib.org, accessed, pp. 5-28.

Subetto D.A., Sevast'yanov D.V., Sapelko T.V., Grekov I.M., Bojnagryan V.R. (2017). Lakes as accumulative information systems and climate indicators //Herald of Astrakhan ecological education. Earth Sciences. 4(42) pp.4-14 (In Russian).

Reimer, P. J., Bard, E., Bayliss, A., Beck, J. W., Blackwell, P. G., Ramsey, C. B. & Grootes, P. M. (2013). IntCal13 and Marine13 radiocarbon age calibration curves 0–50,000 years cal BP. Radiocarbon, 55(4), pp.1869-1887.

AUTHOR GUIDELINES

1. Authors are encouraged to submit high-quality, original work: scientific papers according to the scope of the Journal. reviews (only solicited) and brief articles.

2. Papers are accepted in English. Either British or American English spelling and punctuation may be used.

3. All authors of an article are asked to indicate their names (with one forename in full for each author, other forenames being given as initials followed by the surname) and the name and full postal address (including postal code) of the affiliation where the work was done. If there is more than one institution involved in the work, authors' names should be linked to the appropriate institutions by the use of 1, 2, 3 etc superscript. Telephone and fax numbers and e-mail addresses of the authors could be published as well. One author should be identified as a Corresponding Author. The e-mail address of the corresponding author will be published, unless requested otherwise.

EXAMPLE:

Ivan I. Ivanov[1], Anton A. Petrov[1*], David H. Smith[2]
[1]University/Organization name, Street, City, ZIP-code, Country
[2]University/Organization name, Street, City, ZIP-code, Country
* Corresponding author: example@example.com

4. The GES Journal style is to include information about the author(s) of an article. Therefore we encourage the authors to submit their portrait photos and short CVs (up to 100 words).

5. Article structure should contain further sections:
   • Abstract.
   • Keywords (Immediately after the abstract, provide a maximum of 6 keywords, avoiding general and plural terms and multiple concepts (avoid, for example, 'and', 'of'). Be sparing with abbreviations: only abbreviations firmly established in the field may be eligible. These keywords will be used for indexing purposes.).
   • Introduction (State the objectives of the work and provide an adequate background, avoiding a detailed literature survey or a summary of the results.).
   • Material and methods (Provide sufficient details to allow the work to be reproduced by an independent researcher. Methods that are already published should be summarized, and indicated by a reference. If quoting directly from a previously published method, use quotation marks and also cite the source. Any modifications to existing methods should also be described.
   • Results (Results should be clear and concise.).
   • Discussion (This should explore the significance of the results of the work, not repeat them. A combined Results and Discussion section is often appropriate. Avoid extensive citations and discussion of published literature.).
   • Conclusions (The main conclusions of the study may be presented in a short Conclusions section, which may stand alone or form a subsection of a Discussion or Results and Discussion section.).
   • Acknowledgements (List here those individuals who provided help during the research and funds which provided financial support of your research.).
   • References (Make a list of references according to guidance provided below).
   • Appendices (If there is more than one appendix, they should be identified as A, B, etc.

Formulae and equations in appendices should be given separate numbering: Eq. (A.1), Eq. (A.2), etc.; in a subsequent appendix, Eq. (B.1) and so on. Similarly for tables and figures: Table A.1; Fig. A.1, etc.).

6. Sections and sub-sections shouldn't be numbered, but divided into sub-levels. If you would like to refer to a particular section, name it without any numbers (for example: see "Materials and methods")

7. Math equations should be submitted as editable text and not as images (use appropriate tool in text editor). Present simple formulae in line with normal text where possible and use the solidus (/) instead of a horizontal line for small fractional terms, e.g., X/Y. In principle, variables are to be presented in italics. Number consecutively any equations that have to be displayed separately from the text (if referred to explicitly in the text).

8. Figures and figure captions. Number the illustrations according to their sequence in the text. Regardless of the application used, when your figure is finalized, please 'save as' or convert the images to one of the following formats: TIFF, JPG. Supply files that are optimized for screen use. **The resolution should be at least 300 dpi**. Besides inserting figures into your manuscript, you must also upload appropriate files during paper submission. Ensure that each illustration has a caption. A caption should comprise a brief title (not on the figure itself) and a description of the illustration beginning from "Fig. 1…" (note: no any dots in the end of the capture!). Keep text in the illustrations themselves to a minimum but explain all symbols and abbreviations used.

Example of referring to the figure in text: (Fig. 1)
Example of figure caption: Fig. 1. The distribution of the family Monimiaceae

9. Tables. Please submit tables as editable text and not as images. Tables can be placed either next to the relevant text in the article, or on separate page(s) at the end. Number tables consecutively in accordance with their appearance in the text, place table caption above the table body and place any table notes below the body. Be sparing in the use of tables and ensure that the data presented in them do not duplicate results described elsewhere in the article. Please avoid using vertical rules and shading in table cells.

Example of table caption: Table 1. Case studies and used methods

10. The optimum size of a manuscript is about 3,000–5,000 words. Under the decision (or request) of the Editorial Board methodological and problem articles or reviews up to 8,000–10,000 words long can be accepted.

11. To facilitate the editorial assessment and reviewing process authors should submit "full" electronic version of their manuscript with embedded figures of "screen" quality as a **PDF or DOC file.**

12. We encourage authors to list three potential expert reviewers in their field. The Editorial Board will view these names as suggestions only.

13. Original reviews of submitted manuscripts remain deposited for 3 years.